Conception, synthèse, caractérisation chimique et évaluation biologique de nouveaux agents anticancéreux ciblant les microtubules et les mécanismes de réparation et de réplication de l'ADN

Thèse

Mathieu Gagné-Boulet

Doctorat en sciences pharmaceutiques
Philosophiæ doctor (Ph. D.)

Québec, Canada

Conception, synthèse, caractérisation chimique et évaluation biologique de nouveaux agents anticancéreux ciblant les microtubules et les mécanismes de réparation et de réplication de l'ADN

Thèse

Mathieu Gagné-Boulet

Sous la direction de :

Sébastien Fortin, directeur de recherche

Résumé

Le cancer est une maladie majeure ayant un taux de mortalité élevé dans le monde et au Canada. C'est pourquoi notre équipe de recherche développe de nouvelles classes d'agents anticancéreux, notamment les phényl 4-(2-oxoimidazolidin-1-yl)benzènesulfonates (PIB-SOs) et les *N*-phényl ureidobenzènesulfonates (PUB-SOs). Les PIB-SOs et les PUB-SOs sont constitués de deux cycles aromatiques identifiés A et B reliés entre eux par un pont sulfonate. Les PIB-SOs sont principalement caractérisés par un groupement imidazolidin-2-one sur le cycle aromatique A alors que les PUB-SOs possèdent un groupement 2-chloroéthylurée ou éthylurée sur ce cycle. D'un côté, les PIB-SOs montrent une activité antiproliférative sur des cellules cancéreuses de l'ordre du nanomolaire, arrêtent le cycle cellulaire en phase G2/M et ciblent les microtubules dans le site de liaison de la colchicine (C-BS). D'un autre côté, les PUB-SOs ont une activité antiproliférative de l'ordre du bas micromolaire sur des lignées cellulaires cancéreuses. Selon leur structure, ils peuvent soit arrêter le cycle cellulaire en phase G2/M et cibler le C-BS des microtubules lorsqu'ils sont substitués en position 3, 4 et/ou 5 sur le cycle aromatique B ou soit arrêter le cycle cellulaire en phase S et cibler les mécanismes de réparation et de réplication de l'ADN lorsque le cycle aromatique B est substitué en position 2 par des halogènes ou de courtes chaînes alkyles. Les travaux de mon doctorat avaient pour objectif général d'optimiser les propriétés physicochimiques, pharmacologiques et pharmacocinétiques des PIB-SOs et des PUB-SOs. À cet effet, 187 nouveaux dérivés et analogues des PIB-SOs et des PUB-SOs ont été préparés, purifiés, caractérisés et évalués biologiquement. Les nouveaux dérivés et analogues des PIB-SOs sont divisés en neuf familles principales caractérisées par la substitution du groupement imidazolidin-2-one par un groupement lactame, imidazolidin-2,4-dione, imidazolidin-2,5-dione, éthyl 2-uréidoacétate, butyramide, éthylurée, 2-chloroéthylurée, éthylthiourée ou phénylurée. L'activité antiproliférative des familles peuvent être divisée en trois catégories : (1) très active (ordre du nanomolaire), (2) modérément active (ordre du micromolaire) et (3) peu ou non active (supérieure à 100 µM). Les familles de composés possédant le groupement lactame, imidazolidin-2,4-dione ou imidazolidin-2-one intègrent la catégorie très active. Les familles de composés ayant les groupements butyramide, éthylurée, 2-chloroéthylurée, éthylthiourée ou phénylurée sont dans la catégorie modérément active et finalement, ceux

portant les groupements imidazolidin-2,5-dione ou éthyl 2-uréidoacétate sont dans la catégorie peu ou non active. Les composés les plus puissants des familles très actives et modérément actives arrêtent la progression du cycle cellulaire en phase G2/M, inhibent la polymérisation des microtubules et perturbent le cytosquelette en se liant au C-BS. Ils sont aussi actifs sur des lignées cellulaires résistantes au paclitaxel, à la vinblastine et sur une lignée cellulaire surexprimant la glycoprotéine P. Ils ne sont pas ou seulement faiblement toxiques sur le modèle d'embryons de poulet et ils montrent des propriétés physicochimiques et pharmacocinétiques théoriques prometteuses en plus de respecter les filtres de biodisponibilité *per os*. Les dérivés et analogues des PUB-SOs sont divisés en deux familles principales en remplaçant le groupement 2-chloroéthylurée soit par différents groupements amides ou soit par différents groupements urées. L'activité antiprolifération de ces nouveaux dérivés et analogues des PUB-SOs est généralement plus puissante avec les groupements urées qu'avec les groupements amides et elle se situe entre la centaine de nanomolaire et le bas micromolaire. Les relations structure-activité des composés les plus puissants montrent que l'arrêt de la progression du cycle cellulaire en phase S survient seulement lorsque le cycle aromatique B est substitué en position 2 par des halogènes ou de courtes chaînes alkyles ; les composés ayant un autre patron de substitution sur le cycle aromatique B arrêtent la progression du cycle cellulaire en phase G2/M et perturbent les microtubules. Les composés les plus puissants arrêtant le cycle cellulaire en phase S induisent la phosphorylation de l'histone 2AX, un marqueur de stress réplicatifs. Des essais de cinétique d'alkylation démontrent que leur activité biologique n'est pas causée par leur potentiel alkylant. Les nouveaux analogues ne sont pas ou seulement faiblement toxiques sur le modèle d'embryons de poulet et ont également des propriétés physicochimiques et pharmacocinétiques théoriques prometteuses tout en respectant les filtres biodisponibilité *per os*. Les dérivés et analogues des PIB-SOs et des PUB-SOs composent donc de nouvelles familles d'agents anticancéreux prometteurs pour des études précliniques plus poussées.

Abstract

Cancer is a major disease leading to a high mortality rate worldwide and in Canada. As a result, our research team develops new anticancer agent classes notably phenyl 4-(2-oxoimidazolidin-1-yl)benzenesulfonates (PIB-SOs) and phenyl ureidobenzenesulfonates (PUB-SOs). PIB-SOs and PUB-SOs consist of two aromatic rings named A and B connected together by a sulfonate bridge. PIB-SOs are mainly characterized by an imidazolidin-2-one moiety on the aromatic ring A while PUB-SOs bear a 2-chloroethylurea or an ethylurea on this ring. On the one hand, PIB-SOs show antiproliferative activity in the nanomolar range towards cancer cells, block cell cycle progression in G2/M phase and target microtubules in the colchicine-binding site (C-BS). On the other hand, PUB-SOs exhibit antiproliferative activity in the low micromolar on cancer cell lines. Depending on their structures, they either stop the cell cycle progression in the G2/M phase and target the C-BS of microtubules when they bear substituents at position 3, 4 and/or 5 on the aromatic ring B or they arrest the cell cycle progression in the S phase and target the DNA repair and replication mechanisms when they bear halogens or short alkyl chains at position 2 on the aromatic ring B. The general objective of my doctoral work was to optimize the physicochemical, pharmacological and pharmacokinetic properties of PIB-SOs and PUB-SOs. To this end, 187 new derivatives and analogues of PIB-SOs and PUB-SOs were prepared, purified, characterized and biologically evaluated. New PIB-SOs are divided into nine families of compounds characterized by the replacement of the imidazolidin-2-one moiety by lactam, imidazolidin-2,4-dione, imidazolidin-2,5-dione, ethyl 2-ureidoacetate, butyramide, ethylurea, 2-chloroethylurea, thioethylurea or phenylurea group. The antiproliferative activity of these families can be divided into 3 categories: (1) very active (nanomolar range), (2) moderately active (micromolar range) and (3) weakly or not active (over 100 µM). Families of compounds having a lactam, an imidazolidin-2,4-dione or an imidazolidin-2-one are in the very active category. Families bearing a butyramide, an ethylurea, a 2-chloroethylurea, a thioethylurea or a phenylurea group are in the moderately active category while those bearing an imidazolidin-2,5-dione or an ethyl 2-ureidoacetate are in the weakly or not active category. The most potent compounds of the most and moderately active families arrest the cell cycle progression in G2/M phase, inhibit microtubule polymerization and disrupt the cytoskeleton

by binding to the C-BS. They are also active in paclitaxel- and vinblastine-resistant cell lines and on a cell line overexpressing the P-glycoprotein. Moreover, they are not or only weakly toxic on the chick embryos model and they exhibit promising theoretical physicochemical and pharmacokinetic properties in addition to respecting oral bioavailability filters. Derivatives and analogues of PUB-SOs are divided into two main families by replacing the 2-chloroethylurea moiety either by various amide groups or by different urea moieties. The antiproliferative activity of these new derivatives and analogues of PUB-SOs is generally more potent when they are substituted with a urea group than by an amide group and is between the hundred nanomolar to low micromolar. The structure-activity relationships with the most potent derivatives show that the arrest of the cell cycle progression in S phase occurs only when the aromatic ring B is substituted at position 2 by halogens or short alkyl chains; compounds bearing other substitution patterns on the aromatic ring B arrest the cell cycle progression in G2/M phase and disrupt microtubules. Moreover, the most potent compounds blocking the cell cycle progression in S phase induce the phosphorylation of the histone 2AX, a marker of the replicative stress. Alkylation kinetic assays show that their biological activity is not related to their alkylating potency. Moreover, they are not or only weakly toxic on the chick embryos model and they exhibit promising theoretical physicochemical and pharmacokinetic properties in addition to complying oral bioavailability filters. The derivatives and analogues of PIB-SOs and PUB-SO constitute new families of anticancer agents promising for further preclinical studies.

Table des matières

Liste des figures

Liste des tableaux

Liste des abréviations, sigles, acronymes

Produits chimiques, groupements chimiques et solvants

Acr : Acrylamide

CA : 2-Chloroacétamide

CA-4 : Combrétastatine A-4

CAU : 2-Chloroacétylurée

CBA : 4-Chlorobutyramide

CBL : Chlorambucil

CCNU : Lomustine

CENU : Phénylchloroéthylnitrosourée

CEU : *N*-Phényl-*N'*-(2-chloroéthyl)urée

CoQ : Ubiquinone

CPA : 3-Chloropropionamide

CPU : 3-Chloropropylurée

DDT : Dichlorodiphényltrichloroéthane

DMAP : 4-Diméthylaminopyridine

DMSO : Diméthylsulfoxyde

EBI : *N*,*N'*-Éthylènebis(iodoacétamide)

EDTA : Acide éthylènediaminetétracétique

EU : Éthylurée

FMN : Flavine mononucléotide

GTP : Guanosine triphosphate

GDP : Guanosine diphosphate

IMZ : Imidazolidin-2-one

CH_3CN : Acétonitrile

MeOH : Méthanol

OXA : 4,5-Dihydro-*N*-phényloxazol-2-amine

PIB-SO : Phényl 4-(2-oxoimidazolidin-1-yl)benzènesulfonate

PPB-SO : Tétrahydro-2-oxopyrimidin-1(2H)-yl

PUB-SO : *N*-Phényl uréidobenzènesulfonate

SDS : Dodécylsulfate de sodium

tBCEU : 4-*tert*-Butyl-(3-(2-chloroéthyl)uréido)benzène

TBST : Tris-buffered saline with 0.1% (V/V) Tween 20

TBSTM : Tris-buffered saline with 0.1% (V/V) Tween-20 and 5% fat-free dry milk

TEA : Triéthylamine

THF : Tétrahydrofurane

Tris : Tris(hydroxyméthyl)aminométhane

Unités

°C : Degré Celcius

Eq. : Équivalent

g : Gramme

h : Heure

M : Molaire

mg : Milligramme

min : Minute

mL : Millilitre

µL : Microlitre

mmol : Millimole

mol : Mole

m/z : Rapport masse/charge

nm : Nanomètre

V : Volume

δ : Déplacement chimique

µm : Micromètre

Å : Ångström

Méthodes d'analyses et appareils

ESI : Ionisation par électronébuliseur

FACS : Tri cellulaire par cytofluorométrie

HPLC : Chromatographie en phase liquide à haute performance

HRMS : Spectrométrie de masse à haute résolution

RMN : Résonance magnétique nucléaire

SDS-PAGE : Électrophorèse sur gel de polyacrylamide en présence de dodécylsulfate de sodium

UHPLC : Chromatographie en phase liquide à très haute performance

Termes biologiques

ADN : Acide désoxyribonucléique

ARN : Acide ribonucléique

BBBP : Perméabilité de la barrière hémato-encéphalique

CAM : Membrane chorioallantoïque

C-BS : Site de liaison de la colchicine

DMEM : Milieu Eagle modifié de Dulbecco

GIA : Absorption gastrointestinal

GnRH : Hormone de libération de la gonadotrophine

H2AX : Histone de la famille des H2A (membre X)

*h*DHODH : Dihydroorotate déshydrogénase humaine

HT-1080 : Lignée cellulaire de fibrosarcome humain

HT-29 : Lignée cellulaire d'adénocarcinome du côlon

IC_{50} : Concentration nécessaire pour inhiber 50% de la croissance cellulaire

LH-RH : Hormone de libération de la lutéinostimuline

LMA : Leucémie myéloïde aiguë

M21 : Lignée cellulaire du mélanome de la peau

MCF-7 : Lignée cellulaire du carcinome du sein

PBS : Tampon phosphate salin

Autres

ATCC : American Type Culture Collection

CLogP : Coefficient de partage octanol/eau

FDA : Food and Drug Administration

Log P : Coefficient de partage octanol/eau

Log S : Logarithme de la solubilité molaire dans l'eau

N/A : Non applicable

NCI : National Cancer Institute

N.E. : Non évalué

NIH : National Institute of Health

OMS : Organisation mondiale de la Santé

PDB : Protein Data Bank

PSA : Surface polaire

RSA ou SAR : Relations structure-activité

SVM : Modèle de machines vectorielles de soutien

TPSA : Surface polaire topologique

UV : Ultraviolet

"What can be asserted without evidence can also be dismissed without evidence."

- Christopher Hitchens

Remerciements

Je tiens à transmettre mes plus sincères remerciements à mon directeur de recherche, le Dr Sébastien Fortin pour sa supervision depuis l'été 2013, lors de mon premier stage de recherche. Merci pour ton soutien lors des moments difficiles, pour ton enseignement des notions relatives aux différents projets du laboratoire et de la confiance que tu m'as accordée tout au long de mes stages de recherche, de ma maîtrise et de mon doctorat. Si c'était à recommencer, je referais le même choix.

Je remercie le Dr René C.-Gaudreault, qui m'a initié à la chimie médicinale et qui m'a aidé à pousser mon raisonnement toujours plus loin, tout en me transmettant sa passion pour la recherche lors de nos discussions.

Je remercie également Marie-France Côté pour ses judicieux conseils et ses formations en biologie moléculaire et en culture cellulaire, M. Pierre Audet pour son expertise en RMN, en HPLC et en HRMS. J'aimerais aussi remercier Charahzed Bouzriba, Atziri Corin Chavez Alvarez, Vincent Ouellet et l'ensemble des étudiants que j'ai côtoyés tout au long de mes études graduées.

Je veux aussi remercier les organismes subventionnaires qui ont permis la réalisation de ma formation aux études graduées : le Fonds de recherche du Québec - Santé (FRQS), le centre de recherche du Centre hospitalier universitaire de Québec-Université Laval (CRCHUQ-UL) en collaboration avec Desjardins et le Fonds d'enseignement et de recherche (FER) de l'Université Laval.

Et sans oublier ma famille, mes amis et ma conjointe Catherine, qui m'ont aidé et m'ont supporté durant l'ensemble de mon parcours universitaire.

Avant-propos

Cette thèse de doctorat intitulée : « *Conception, synthèse, caractérisation chimique et évaluation biologique de nouveaux agents anticancéreux ciblant les microtubules et les mécanismes de réparation et de réplication de l'ADN* » est présentée à la Faculté des études supérieures et postdoctorales de l'Université Laval pour l'obtention du grade de *Philosophiae doctor* (Ph.D.) et est rédigée sous la forme de thèse par articles. Les manuscrits scientifiques sont rédigés en anglais selon les normes et exigences des journaux internationaux à comité de pairs dans lesquels ils ont été publiés ou soumis aux Éditeurs pour leur évaluation. Les manuscrits insérés sont accompagnés d'un résumé en français introduit au début des chapitres. Les articles ont été insérés selon les classes d'agents anticancéreux présentées et non selon la chronologie de leurs dates de publication. À cet effet, les articles de la première section de cette thèse traitent des nouvelles familles d'agents antimicrotubules conçues et préparées alors que les articles de la deuxième section traitent des inhibiteurs des mécanismes de réparation et de réplication de l'ADN. Finalement, l'introduction et la conclusion sont rédigées afin de faire ressortir la cohérence entre les différentes sections de cette thèse.

Le premier chapitre de cet ouvrage consiste en une introduction sur le cancer, tout en incluant des concepts de pharmacologie moléculaire et de chimie médicinale. Cette section se veut être un rappel des connaissances générales nécessaires pour apprécier pleinement les travaux présentés dans cette thèse.

Le deuxième chapitre de cette thèse fait l'objet de l'article scientifique intitulé : « *Phenyl 4-(2-oxopyrrolidin-1-yl)benzenesulfonates and phenyl 4-(2-oxopyrrolidin-1-yl)benzenesulfonamides as new antimicrotubule agents targeting the colchicine-binding site* » publié le 6 janvier 2021 dans le *European Journal of Medicinal Chemistry* (*213*, 113136). Chahrazed Bouzriba et Atziri Corin Chavez Alvarez ont participé à la réalisation de cet article sous la supervision du Dr Sébastien Fortin. Je suis l'auteur principal de cet article, ma contribution est estimée à 75%. J'ai synthétisé, purifié et caractérisé tous les composés étudiés de cet article. J'ai effectué les essais antiprolifératifs, la cytométrie en flux, l'essai de polymérisation des microtubules et l'essai d'immunofluorescence des microtubules. J'ai fait la modélisation moléculaire et utilisé l'outil SwissADME pour évaluer

les propriétés pharmacocinétiques et physicochimiques théoriques des composés étudiés. J'ai rédigé l'article et la réponse aux évaluateurs.

Le troisième chapitre fait l'objet du manuscrit scientifique intitulé : « *Preparation, biological evaluation and structure-activity relationships of new phenyl 4-(dioxoimidazolidin-1-yl)benzenesulfonate and ethyl 2-(3-(4-(phenoxysulfonyl)phenyl)ureido)acetate analogs to phenyl 4-(2-oxoimidazolidin-1-yl)benzenesulfonate: study of the imidazolidin-2-one moiety* » soumis le 14 mai 2021 dans le journal *Chemical Biology & drug Design*. Chahrazed Bouzriba et Atziri Corin Chavez Alvarez ont contribué à la réalisation de ces travaux qui ont été effectués sous la supervision du Dr Sébastien Fortin. Ma contribution à cet article est d'environ 65%. J'ai effectué les synthèses, les purifications et les caractérisations chimiques des molécules étudiées. J'ai également réalisé les essais antiprolifératifs, les expériences de cytométrie en flux, d'immunofluorescence, de modélisation moléculaire et d'inhibition de polymérisation des microtubules. J'ai aussi évalué avec l'outil SwissADME les propriétés pharmacocinétiques et physicochimiques théoriques des molécules étudiées. J'ai participé à l'expérience des essais de compétition de ligands avec le *N,N'*-éthylènebis(iodoacétamide) (EBI) et j'ai rédigé l'article.

Le quatrième chapitre fait l'objet du manuscrit scientifique intitulé : « *Rationale, synthesis and biological evaluation of substituted 1-(4-(phenylthio)phenyl)imidazolidin-2-one, urea, thiourea and amide analogs and derivatives designed to target the colchicine-binding site* » soumis le 26 mai 2021 dans le journal *Bioorganic & Medicinal Chemistry*. Chahrazed Bouzriba et Atziri Corin Chavez Alvarez ont participé à la réalisation des travaux qui ont été effectués sous la direction du Dr Sébastien Fortin. Ma contribution à cet article est d'environ 65%. J'ai effectué l'ensemble des synthèses, purifié et caractérisé les dérivés étudiés et j'ai effectué les essais antiprolifératifs, de cytométrie en flux et d'immunofluorescence des microtubules. J'ai aussi réalisé une section des essais de compétition de ligands, des essais de polymérisation des microtubules et j'ai utilisé l'outil SwissADME pour évaluer les propriétés pharmacocinétiques et physicochimiques théoriques des composés étudiés. J'ai rédigé l'article.

Le cinquième chapitre comprend le manuscrit scientifique intitulé : « *Synthesis and biological evaluation of novel N-phenyl ureidobenzenesulfonate derivatives as potential anticancer agents. Part 2. Modulation of the ring B* » publié le 10 septembre 2015 dans l'*European Journal of Medicinal Chemistry* (*103*, 563-573). Je suis premier auteur de cet article. Hanane Moussa, Jacques Lacroix et Marie-France Côté ont également participé à la réalisation de cet article sous la supervision du Dr Jean-Yves Masson et du Dr Sébastien Fortin. Ma contribution à cet article est d'environ 45%. J'ai synthétisé, purifié et caractérisé les composés étudiés. J'ai effectué les essais antiprolifératifs, les essais de cytométrie en flux et participé aux essais d'immunocytochimie. J'ai rédigé une partie du manuscrit et participé à la rédaction de la réponse aux évaluateurs.

Le sixième chapitre comprend le manuscrit scientifique intitulé : « *Preparation, characterisation and biological evaluation of new phenyl amidobenzenesulfonates and N-phenyl ureidobenzenesulfonates inducing DNA double-strand breaks. Part 3. Modulation of ring A* » publié le 21 juin 2018 dans l'*European Journal of Medicinal Chemistry* (*155*, 681-694). Je suis premier auteur de cet article. Chahrazed Bouzriba et Marvin Godard ont également participé à la réalisation de cet article sous la supervision du Dr Sébastien Fortin. Ma contribution à cet article est d'environ 60%. J'ai synthétisé, purifié et caractérisé les composés étudiés. J'ai réalisé les essais antiprolifératifs, les essais de cytométrie en flux et j'ai utilisé l'outil SwissADME pour déterminer les propriétés pharmacocinétiques et physicochimiques théoriques des molécules étudiées. J'ai finalement rédigé le manuscrit et participé à la rédaction de la réponse aux évaluateurs.

Autres publications scientifiques ne faisant pas partie de la présente thèse :

C. Bouzriba, L. Larcher, **M. Gagné-Boulet**, S. Fortin. *N-phenyl ureidobenzenesulfonates, a novel class of promising human dihydroorotate dehydrogenase inhibitors*. Bioorganic & Medicinal Chemistry **2020**, 28, 115739.

M. Zarifi Khosroshahi, A.C. Chavez Alvarez, **M. Gagné-Boulet**, R. C.-Gaudreault, S. Gobeil et S. Fortin. *Evaluation of the time-dependent antiproliferative activity and liver microsome stability of 3 phenyl 4-(2-oxo-3-alkylimidazolidin-1-yl)benzenesulfonates as*

promising CYP1A1-dependent antimicrotubule prodrugs. Journal of Pharmacy and Pharmacology **2019**, 72, 249-258.

A.C. Chavez Alvarez, M. Zarifi Khosroshahi, M.-F. Côté, **M. Gagné-Boulet** et S. Fortin. *4-(3-Alkyl-2-oxoimidazolidin-1-yl)-N-phenylbenzenesulfonamides as new antimitotic prodrugs activated by cytochrome P450 1A1 in breast cancer cells. Part 2. Modulation of the ring B*. Bioorganic & Medicinal Chemistry **2018**, 103, 563-73.

M. Gagné-Boulet, S. Fortin, J. Lacroix, C.-A. Lefebvre, M.-F. Côté et R. C.-Gaudreault. *Styryl-N-phenyl-N'-(2-chloroethyl)ureas and styrylphenylimidazolidin-2-ones as new potent microtubule-disrupting agents using combretastatin A-4 as model*. European Journal of Medicinal Chemistry **2015**, 100, 34-43.

Introduction

1.1. Le cancer

1.1.1. Étymologie

Le mot cancer tient son origine du mot latin *karkinos*, qui signifie écrevisse ou crabe [1]. C'est grâce à Hippocrate (460-377 avant l'ère commune) qui remarqua pour la première fois une analogie entre un crabe et les tumeurs du sein. En effet, ce type de tumeur est caractérisé par une forme arrondie et entourée de prolongements sur les côtés ressemblant aux pattes d'un crabe. Cette comparaison a été reprise avec davantage de précisions par Galien (131-201 après l'ère commune) décrivant le cancer du sein. Galien a aussi introduit le mot d'origine grec *onkos* signifiant « masse » et désignant une tumeur ayant un aspect malin. Finalement, le mot grecque *karkinôma* est devenu au 19^{e} siècle le terme officiel pour désigner des lésions cancéreuses. De nos jours, le terme cancer est utilisé par les professionnels de la santé pour désigner toutes les formes de la maladie [2].

1.1.2. Historique

Le cancer est probablement apparu peu de temps après l'émergence de la vie sur terre. Il est présent chez toutes les espèces animales et végétales [3]. D'ailleurs, des preuves confirmant la présence de cancers chez les dinosaures ont été trouvées dans le passé [4]. La première description du cancer de l'histoire de l'humanité a été réalisée durant la civilisation égyptienne quelques milliers d'années avant l'ère commune. En effet, un cancer du col utérin et un cancer du sein ont été décrits grossièrement sur des papyrus datant de cette époque. Toutefois, c'est plusieurs centaines d'années plus tard durant l'antiquité qu'Hippocrate donna une première définition du cancer et fournit une description relativement détaillée de plusieurs cancers [5]. Leonide, Aulus Cornelius Celsus, Aretaeus et Galien firent aussi leur propre description de cancers et mirent sur pieds leur propre théorie sur la maladie. On retrouve notamment la fameuse théorie du médecin grec Galien des « humeurs ». Cette théorie évoque un déséquilibre de quatre humeurs du corps qui contribuerait à l'apparition du cancer. Le patient se voyait alors administrer une purge ou des saignées afin de dissoudre ou vider le corps d'une bile solidifiée (humeur noire) ou excédentaire. La théorie des humeurs

resta de mise pour une longue période et peu de progrès furent réalisés jusqu'à la renaissance [6]. C'est au 16e siècle que des avancées significatives dans la compréhension du cancer survinrent. Ces avancées ont été entre autres catalysées par la découverte du système lymphatique par Gaspard Asselli, système jouant un rôle primordial dans la dissémination du cancer. De plus, les médecins Falloppius, Pecquet et plusieurs autres profitèrent de la levée de l'interdiction de pratique d'autopsie présente dans de nombreux pays pour approfondir leurs connaissances et rédiger des descriptions précises et détaillées des cancers et de techniques chirurgicales utilisées à l'époque.

Malheureusement, une recrudescence des notions « d'humeurs » avancées par Galien s'échelonnant entre le 18e et le 19e siècle retarda le développement de nouveaux traitements efficaces. Durant ces années, différentes théories basées sur des concepts non fondés existaient par rapport au cancer, dont la théorie du trauma selon laquelle le cancer serait causé par des blessures [7]. En revanche, le médecin allemand Rudulf Virchow proposa en 1858 l'idée selon laquelle les pathologies seraient causées par des altérations des cellules du corps. Il affirma d'ailleurs « *omnis cellula a cellula* » qui signifie que toute cellule naît d'une autre cellule. Sa conception de l'origine des maladies promut l'excision des tumeurs par chirurgie pour traiter les patients atteints d'un cancer [8]. D'ailleurs, plusieurs médecins connurent des succès thérapeutiques grâce à la chirurgie vers la fin du 19e siècle. Par exemple, Theodor Billroth exécuta avec succès la première ablation d'un cancer de l'estomac. William Halsted prévint l'apparition de métastases avec une mastectomie radicale et Ernst Wertheim réalisa pour la première fois une hystérectomie radicale pour traiter un cancer du col utérin [9]. La radiothérapie se développa en parallèle, notamment grâce à Victor Despeignes qui traita pour la première fois un patient atteint d'un cancer de l'estomac à l'aide de rayons X.

Le début du 20e siècle fut marqué par la multiplication des centres de traitement pour les patients atteints d'un cancer et le regroupement de plusieurs spécialités scientifiques (chirurgien, physicien, chimiste, etc.) pour combattre la maladie. C'est grâce à leurs efforts combinés qu'un nouveau mode de traitement fut mis au point pour traiter les patients atteints de cancers disséminés (métastases) : la chimiothérapie cytotoxique [10]. Les travaux des chercheurs Louis S. Goodman et Alfred Zack Gilman sur les effets cytotoxiques du gaz moutarde, gaz utilisé lors de la Première Guerre mondiale, ont contribué à la mise en marché

du premier agent chimiothérapeutique anticancéreux de l'histoire médicale [11]. C'est cependant en 1948 que Sidney Farber fut considéré comme le « père » de la chimiothérapie lorsqu'il traita des enfants atteints de leucémie avec l'aminoptérine. Il aura fallu attendre les années 50 avant de voir apparaître la polychimiothérapie, c'est-à-dire l'utilisation de plusieurs médicaments afin de traiter plus efficacement le cancer [12]. C'est en 1956 que le premier traitement officiel contre les cancers métastatiques fut utilisé au National Cancer Institute (NCI) pour traiter un choriocarcinome. Depuis, plusieurs nouvelles thérapies telles que la chimiothérapie, l'immunothérapie et l'hormonothérapie se sont développées et font maintenant partie intégrante de l'arsenal utilisé par les oncologues pour traiter les patients atteints du cancer. De plus, les techniques chirurgicales et radiothérapeutiques se perfectionnent continuellement afin d'améliorer le taux de succès des traitements. Néanmoins, bien que les progrès réalisés dans la lutte contre le cancer sont considérables depuis le début du 20^{e} siècle, il y a encore énormément de gens qui succombent aux cancers de nos jours. C'est pourquoi le développement et l'optimisation de nouvelles technologies allant de la prévention aux traitements sont essentiels pour améliorer l'espérance et la qualité de vie des patients atteints de cancer. Actuellement, l'approche préconisée pour traiter les patients atteints de cancer est de « personnaliser » leur traitement en fonction du profil génétique des tumeurs, rendant ainsi les traitements optimisés pour chaque patient [13-15].

1.1.3. Causes

L'origine des cancers est multifactorielle et est associée à plusieurs facteurs de risque. Les facteurs de risque sont généralement divisés en trois catégories : comportementaux, environnementaux et liés à l'individu et son histoire. Les facteurs de risque comportementaux sont responsables d'environ un cancer sur trois. Les cinq principaux comprennent : le tabagisme, un indice de masse corporelle élevée, la sédentarité, la faible consommation de fruits et légumes et la consommation d'alcool. Il est estimé que 70% des cancers pulmonaires et 22% de l'ensemble des décès causés par le cancer sont associés au tabagisme [16]. Lorsqu'une substance provoque, aggrave ou favorise l'apparition du cancer, elle est alors nommée cancérigène, cancérogène ou carcinogène. Une exposition répétée aux cancérigènes peut entraîner la génération de dégâts et de mutations à l'ADN résultant au processus de cancérogenèse [17]. Selon l'Organisation mondiale de la Santé (OMS), une proportion

importante des cancers chez l'humain peut être associée à l'exposition aux cancérigènes, soit volontairement comme la fumée du tabac ou soit de façon involontaire qui constitue les facteurs de risque dit environnementaux. L'exposition involontaire aux cancérigènes peut se faire par trois voies distinctes, soit par la voie digestive (arsenic dans l'eau, nitrites, etc.), soit par les voies respiratoires (amiante, polluants atmosphériques, etc.) ou soit par la voie cutanée (contact direct avec certains produits nettoyants, solvants, etc.). De plus, l'exposition aux cancérigènes peut provenir de différentes sources telles que l'environnement (rayonnement solaire, radioactivité du radon, etc.), l'alimentation (nitrite, nitrate, etc.), les infections (VIH, VPH, etc.) et bien d'autres [18]. Les facteurs de risques liés aux infections sont souvent associés aux infections virales. L'hypothèse mise de l'avant quant à leur mécanisme d'induction du cancer est qu'ils insèrent des proto-oncogènes ou oncogènes dans la cellule hôte ce qui a pour effet de promouvoir l'apparition du cancer [19, 20]. Les facteurs de risque liés à l'individu et à son histoire comprennent notamment l'avancée en âge, les hormones, certaines maladies comme les maladies inflammatoires ou auto-immunes, les traitements antérieurs, les antécédents personnels de cancer et l'hérédité. Beaucoup de progrès ont été réalisés au cours des dernières années pour l'identification de facteurs de risques associés à l'hérédité et aux gènes défectueux, particulièrement sur les sections d'ADN mutés responsables de l'apparition des cancers. Les gènes favorisant la survenue des cancers sont nommés oncogènes. Ces gènes participent à la transformation d'une cellule saine en cellule cancéreuse [21]. En résumé, l'étiologie du cancer est complexe et est majoritairement causée par un ensemble de facteurs de risque.

1.1.4. Incidences

1.1.4.1. Dans le monde

Selon l'OMS, le cancer est la deuxième cause de mortalité dans le monde avec près de 9.6 millions de morts en 2018, représentant environ un décès sur six [16]. Parmi les 9,6 millions de décès, 70% proviennent de pays à faible revenu ou à revenu intermédiaire. Les cinq cancers causant le plus grand nombre de décès étaient en 2015 le cancer du poumon (1 690 000), le cancer du foie (788 000), les cancers colorectaux (774 000), le cancer de l'estomac (754 000) et le cancer du sein (571 000) [16]. Les hommes et les femmes ne sont

pas affectés pareillement par le cancer. En effet, l'incidence est légèrement plus élevée chez les hommes que chez les femmes. En 2018, les cancers les plus fréquents chez les hommes incluaient le cancer du poumon (1 368 524), le cancer de la prostate (1 276 106), les cancers colorectaux (1 026 215), le cancer de l'estomac (683 754) et le cancer du foie (596 574). Les cancers les plus fréquents chez la femme pour la même année étaient le cancer du sein (2 088 849), les cancers colorectaux (823 303), le cancer du poumon (725 352), le cancer du col de l'utérus (569 847) et le cancer de la thyroïde (436 344) [22]. Finalement, il est estimé qu'en 2040, l'incidence mondiale passera de 18 078 957 à 29 532 994, une augmentation de plus de 63%. Le nombre de décès mondial estimé en 2018 par type de cancer est représenté à la Figure 1.1 [23].

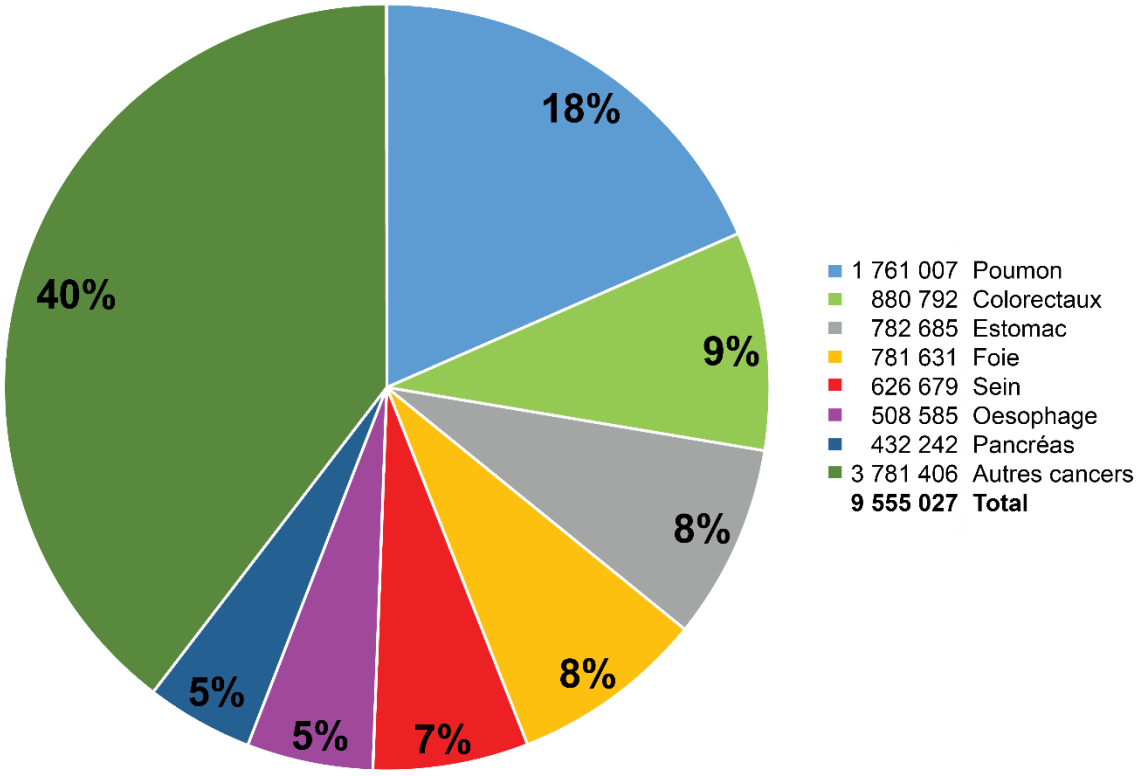

Figure 1.1. Nombre estimé de décès causés dans le monde en 2018 par type de cancer [16].

1.1.4.2. Au Canada

Le cancer est la première cause de mortalité au Canada (Figure 1.2). Il est estimé qu'environ un Canadien sur deux sera atteint du cancer au cours de sa vie, ce qui se traduit

par 25 diagnostics de cancer pancanadien par heure. En 2019, 82 100 Canadiens sont décédés du cancer et il était estimé qu'environ un Canadien sur quatre décédera du cancer [24]. Le cancer du poumon est le cancer ayant le plus grand nombre de décès suivi des cancers colorectaux, du pancréas et du sein. La survie nette à cinq ans au cancer du poumon est de seulement 19% au Canada, bien qu'elle soit une des plus élevée au monde. Les cancers les plus diagnostiqués chez les hommes sont les cancers de la prostate, du poumon, colorectaux, de la vessie et les lymphomes non hodgkinien alors que chez la femme, le cancer du sein, du poumon, colorectal, de l'utérus et de la glande thyroïde sont les plus fréquents [24]. C'est pourquoi le développement de nouveaux traitements anticancéreux est essentiel.

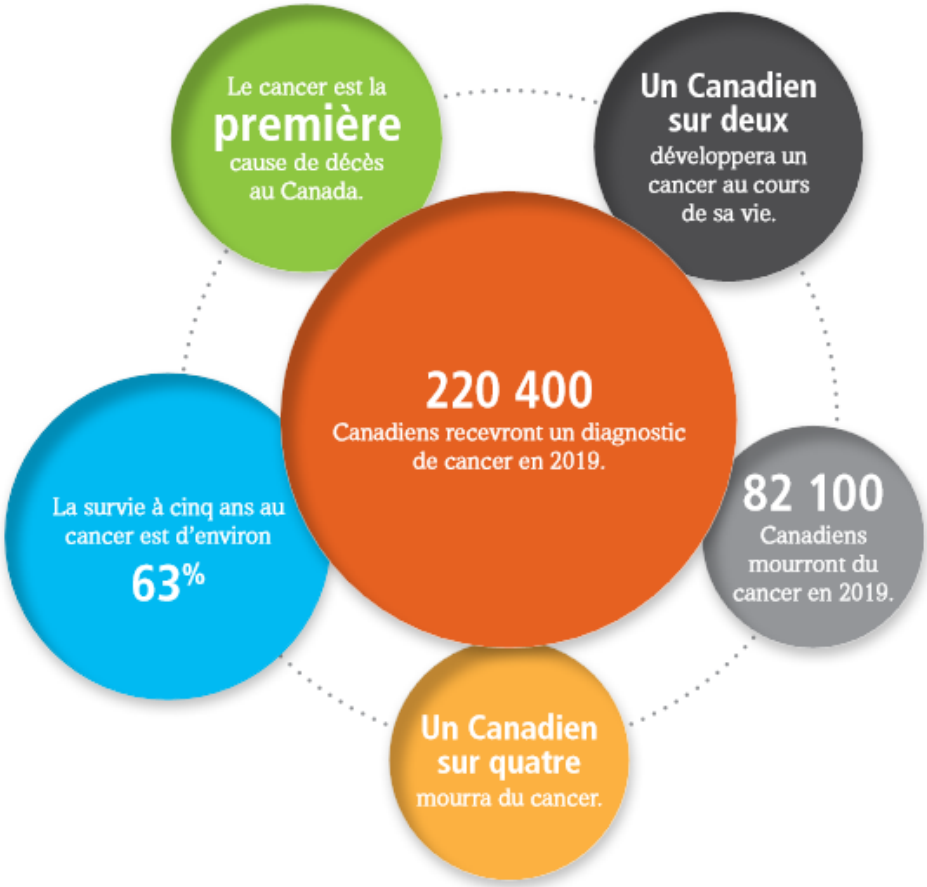

Figure 1.2. Résumé des statistiques canadiennes du cancer en 2019 tiré du Comité consultatif des statistiques canadiennes sur le cancer [25].

1.2. La division cellulaire

La division cellulaire est le processus de multiplication de toutes les cellules. Ce processus cyclique nommé cycle cellulaire est essentiel à la vie, car il permet la croissance, la régénération des tissus et la reproduction des organismes vivants. La division cellulaire somatique comprend deux étapes principales : l'interphase et la mitose.

L'interphase est caractérisée par une augmentation du volume cellulaire, une transcription importante des gènes et la duplication des chromosomes. Lorsque la cellule est en processus de division, elle se retrouve dans l'interphase 90% du temps alors qu'elle se retrouve 10% du temps dans la phase mitotique [26]. Toutefois, ces pourcentages peuvent varier significativement d'un type cellulaire à l'autre. Lorsque la cellule ne se divise pas et accomplit ses fonctions usuelles prédéterminées, la cellule se retrouve dans la phase G_0 dite de quiescence, un état de repos. Lorsque le processus de division cellulaire débute, la cellule entre dans l'interphase. Cette phase se divise en trois étapes, soit la phase G_1 (intervalle de croissance 1), S (synthèse de l'ADN) et G_2 (intervalle de croissance 2). La phase G_1 est la phase où la cellule prend de l'expansion, croît et fabrique la quasi-totalité des glucides, lipides et protéines nécessaire à sa division. Pour une cellule se divisant en 24 h, cette phase dure approximativement entre 5 et 6 h [27]. Pour passer en phase S, la cellule effectue des points de contrôle pour vérifier l'intégrité structurelle de l'ADN, entre autres avec la protéine p53. Si l'ADN est endommagé, la cellule enclenche des réparations ou le processus de mort cellulaire (apoptose) si les lésions sont irréparables. Il est aussi possible que la cellule retourne en phase G_0 aux points de contrôle G_1. Des facteurs de croissance peuvent alors réenclencher le processus de division cellulaire. La phase S est associée à la duplication de l'ADN ainsi qu'à la copie des histones et des autres protéines impliquées au niveau de l'ADN. Au début de cette phase, le chromosome est constitué d'une seule chromatide alors qu'en fin de phase, le chromosome sera constitué de deux chromatides reliées par un centrosome [26]. La copie de l'ADN est accompagnée du dédoublement et du positionnement opposé des centrosomes qui sont cruciaux à la migration. Selon une division cellulaire de 24 h, cette phase dure environ entre 10 et 12 h [27]. La phase G_2 est une seconde phase de croissance où la cellule produit les protéines nécessaires pour effectuer la mitose. Au cours de cette phase, la cellule procède principalement à une vérification du bon fonctionnement

de la réplication de l'ADN et de son intégrité structurelle. Cette phase est d'une durée comparable à la phase G_1 (approximativement 4 à 6 h). Si des dommages sont détectés par des points de contrôle en fin de phase G_2, la cellule peut entrer en apoptose. Si l'ADN est intact, la cellule entre en mitose [26, 27].

La mitose est la division d'une cellule mère en deux cellules filles génétiquement identiques. Elle se divise en six étapes, soit la prophase, la prométaphase, la métaphase, l'anaphase, la télophase et la cytodiérèse. L'ensemble de ces étapes dure environ 1 h pour une division cellulaire de 24 h [27]. La prophase est initiée par la formation du fuseau de division et de la condensation de l'ADN en chromosomes dans un noyau encore intact. Les centrosomes se séparent, se positionnent et génèrent des microtubules très actifs qui vont former les pôles du fuseau mitotique [28]. La membrane du nucléole s'affaiblit. La prométaphase suit avec la fragmentation de la membrane du noyau et l'envahissement des microtubules du fuseau dans le noyau. Les chromosomes se condensent encore et les microtubules s'attachent à leurs kinétochores [29]. La métaphase débute avec la condensation complète des chromosomes et leur alignement à équidistance des pôles du fuseau sur le plan équatorial (métaphasique) de la cellule. Les microtubules radiaires, ou encore astériens sont alors en contact avec la membrane cellulaire et forment le fuseau mitotique dans son entièreté. L'anaphase suit avec la séparation des chromatides sœurs en deux groupes de chromosomes identiques. Ces deux lots migrent ensuite vers leurs pôles respectifs du fuseau mitotique grâce au raccourcissement des microtubules kinétochoriens [26]. Dans un même temps, les pôles s'éloignent d'eux-mêmes et un anneau contractile d'actine commence à se former à l'équateur alors que les chromosomes commencent à se décondenser. Par la suite, la télophase s'amorce et l'anneau d'actine se contracte induisant la séparation de la cellule mère en deux cellules filles. Les chromosomes finissent de se décondenser et deviennent une chromatine diffuse [27]. Une enveloppe nucléaire se forme à chaque extrémité de la cellule englobant la chromatine filamenteuse et les microtubules kinétochoriens disparaissent. Finalement, lors de la dernière étape (cytodiérèse), les organites manquants sont à nouveau synthétisés et l'anneau contractile de microfilaments d'actine termine la séparation des 2 cellules filles qui retournent en phase G_0 [26, 27].

1.3. La cancérogenèse et la nomenclature

La cancérogenèse est le processus de formation du cancer. Ce terme est utilisé au sens large comme étant la formation de néoplasmes qui sont anormaux et qui croissent de manière incontrôlée. La néoplasie est décrite comme la formation de nouveaux tissus (néoplasmes) ou comme « nouvelle croissance » [21]. Les néoplasmes sont classés et nommés selon l'origine de la cellule ou du tissu et selon les caractéristiques de croissance bénigne ou maligne. D'ailleurs, les termes « tumeur » et « cancer » sont souvent utilisés de manière interchangeable par la communauté scientifique. Néanmoins, une tumeur est caractérisée par la prolifération de cellules constituant un nouveau tissu et peut être bénigne ou maligne [30].

Le grade et le stade d'un cancer sont des échelles d'évaluation des cellules cancéreuses servant aux oncologues pour proposer aux patients le plan de traitement le mieux adapté à leur maladie. Le grade décrit les caractéristiques malignes du cancer. Il est obtenu par une évaluation subjective de ses caractéristiques morphologiques basée sur la prépondérance d'anaplasie et du degré de prolifération observé par microscopie. Le grade du cancer est généralement représenté sur une échelle de 1 à 4. En bref, plus la différence entre les cellules saines et les cellules cancéreuses est élevée, plus le grade aura une valeur élevée et sera associé à un mauvais pronostic. Le stade du cancer quant à lui est une notion indépendante de sa gradation. Elle tient compte de la quantité, la localisation et la propagation du cancer. Un chiffre de 1 à 4 est attribué selon les paramètres mentionnés précédemment. Un cancer de petite taille, essentiellement localisé à un seul endroit est associé à un score de 1, alors qu'un chiffre plus élevé implique une taille tumorale supérieure et/ou une plus grande dissémination. La combinaison du grade et du stade du cancer d'un patient influencera l'approche thérapeutique recommandée par les oncologues [21].

Le processus de carcinogenèse peut prendre des années, voir des décennies avant de se réaliser. Différentes théories sur la carcinogenèse ont été élaborées, notamment la théorie des mutations génétiques, la théorie de la différenciation aberrante et la théorie virale. Toutefois, la théorie acceptée par la communauté scientifique est la théorie à plusieurs étapes. Cette théorie stipule que la cancérogenèse est un processus constitué de plusieurs étapes entre le

premier contact avec un carcinogène et l'apparition du cancer. Ces étapes comprennent le stade d'initiation, le stade de promotion et le stade de progression.

Le stade d'initiation s'amorce lorsqu'un carcinogène interagit avec l'ADN, induisant une lésion. Si cette lésion échappe aux mécanismes de réparation de l'ADN de la cellule, elle peut être reproduite ultérieurement et transmise à de nouvelles cellules filles. Cette altération génétique irréversible permet à la cellule initiée de former des cellules prénéoplasiques clones et de ne pas être reconnue et éliminée par le système immunitaire de l'organisme. Le stade d'initiation est un processus rapide qui dure quelques minutes à quelques heures. Ces cellules initiées peuvent rester indéfiniment dans ce stade ou entrer dans le stade de promotion [21].

Le stade de promotion correspond à la sélection clonale des cellules initiées par l'agent carcinogène. Lorsque l'ADN d'une cellule a été modifié par un carcinogène, la cellule devient vulnérable aux agents promoteurs. Ces agents stimulent la prolifération de la cellule ayant subi les dégâts causés par le carcinogène. Contrairement aux agents responsables du stade d'initiation, les agents promoteurs ne sont généralement pas mutagènes ou carcinogènes. Ils se lient habituellement à la membrane cellulaire et affectent les sentiers signalétiques intracellulaires reliés à la prolifération cellulaire. Les cellules initiées auront un avantage de croissance par rapport aux cellules normales environnantes ce qui augmentera leur proportion par rapport aux cellules saines [21].

Le stade de progression est caractérisé par le début de la malignité, une hétérogénéité cellulaire substantielle et l'induction de changements qui peuvent ultimement causer la mort de l'organisme hôte. À cette étape, les cellules sont pourvues de multiples altérations génétiques, allant jusqu'à la modification du caryotype et de son instabilité. Les tumeurs sont en prolifération rapide et les cellules ont des propriétés métastatiques. Un des mécanismes les plus probables du stade de progression implique la sélection d'une partie de la population néoplasique ayant des caractéristiques de croissance augmentée. Ayant une division cellulaire accentuée, cette population cellulaire deviendra majoritaire dans le tissu tumoral [21].

1.4. Les traitements

Les premiers traitements contre le cancer remontent à l'époque de l'Égypte ancienne. Depuis ce temps, les traitements se sont grandement améliorés et ne sont plus uniquement d'usage palliatif, mais peuvent désormais guérir le patient. Ces traitements font partie d'un vaste arsenal d'outils thérapeutiques à la disposition des oncologues contemporains. Les traitements pour les patients atteints d'un cancer peuvent être divisés en trois grandes classes : la chirurgie, la radiothérapie et la chimiothérapie. Étant donné la nature différente de chacun de ces traitements, leur utilisation n'est pas appropriée pour tous les types de cancer. Une combinaison de ces traitements peut être envisagée pour améliorer les chances de rémission. Le choix du ou des traitements qui seront employés pour traiter un patient dépend de plusieurs paramètres, notamment, le type, le stade, le grade, sa localisation dans l'organisme, l'état de santé général du patient, la présence de comorbidité, etc. [7].

1.4.1. La chirurgie

La chirurgie fut le premier traitement utilisé pour les patients atteints d'un cancer. Le médecin Romain Celsus a écrit : « après l'excision, même lorsqu'une cicatrice est formée, la maladie est réapparue » [31]. Les chirurgies effectuées avant le 19^{e} siècle étaient primitives en plus de présenter fréquemment plusieurs complications comme des infections et des pertes de sang importantes. C'est à partir du 19^{e} siècle que des avancées majeures ont été réalisées. Le début de l'anesthésie en 1846 a créé une avancée spectaculaire en chirurgie, au point que le siècle suivant fut appelé « le siècle du chirurgien ». Trois chirurgiens se sont démarqués pour leurs contributions à la chirurgie des patients atteints du cancer : W. Sampson Handley en Angleterre, Theodor Bilroth en Allemagne et W. Stewart Halsted aux États-Unis. L'expertise technique des chirurgiens acquise lors du 20^{e} siècle a permis de minimiser la quantité de tissus sains enlevés durant les opérations. Par exemple, des tumeurs osseuses des bras et des jambes ne nécessitaient plus d'amputation dans la majorité des cas. Aujourd'hui, les technologies comme la fibre optique et la miniaturisation des caméras permettent de limiter les chirurgies très invasives. Les chirurgies servent aussi à prévenir et diagnostiquer les cancers, par exemple en effectuant des biopsies incisionnelles (retrait d'une fraction d'une masse ou d'une section anormale) ou excisionnelles (retrait de l'entièreté d'une masse ou

d'une section anormale). Dans certains cas de cancers avec une tumeur localisée et avancée, l'ablation partielle de la tumeur est de mise pour améliorer les probabilités de réussite des traitements subséquents comme la radiothérapie et la chimiothérapie. Finalement, la chirurgie peut servir de traitement palliatif pour regagner une fonctionnalité perdue ou diminuer la douleur afin d'améliorer la qualité de vie du patient [32-34].

1.4.2. La radiothérapie

La radiothérapie est un traitement utilisant la radiation pour tuer les cellules cancéreuses. Cette radiation est de nature ionisante, c'est-à-dire qu'elle possède suffisamment d'énergie pour arracher les électrons des molécules. Elle se retrouve soit sous forme de rayons X ou de rayons γ. Cette énergie radiative génère des radicaux libres qui sont extrêmement réactifs et qui vont réagir avec les composantes de la cellule. Il en résulte des lésions à l'ADN induisant des cascades biochimiques de signalisations cellulaires entraînant à la fois la mort cellulaire et une diminution de la taille de la tumeur [35, 36].

Selon la disposition de la tumeur et les caractéristiques du cancer, la radiothérapie peut être curative, palliative ou prophylactique. La radiothérapie curative a pour but d'éliminer complètement la tumeur et de guérir le patient. La radiothérapie palliative a pour but de soulager le patient des douleurs et multiples symptômes associés à son cancer, sans intention de guérison. Finalement, la radiothérapie prophylactique est un traitement par radiation ayant pour but la prévention du développement de la maladie. Par exemple, une irradiation prophylactique crânienne permet de prévenir des métastases au cerveau causées par un cancer localisé ailleurs dans le corps [37]. La radiothérapie peut être utilisée seule, mais est fréquemment utilisée en association avec d'autres traitements. Lorsque la radiothérapie est utilisée avant la chirurgie pour réduire la taille de la tumeur pour qu'elle soit plus facile à exciser, on parle de radiothérapie néo-adjuvante. La radiothérapie adjuvante réfère à l'utilisation de la radiothérapie suite à l'ablation chirurgicale d'une tumeur. Finalement, certains agents chimiothérapeutiques sont radiosensibilisants et peuvent être donnés en même temps que la radiothérapie pour augmenter l'efficacité des rayons sur les cellules cancéreuses. Cette radiothérapie particulière réfère à la chimioradiothérapie et est utilisée dans le traitement des cancers bronchiques localement avancés, de l'œsophage ou du col de l'utérus [38].

La radiothérapie est soit sous forme externe ou interne. La radiothérapie externe est sans douleur et la plupart des patients peuvent reprendre leurs activités quotidiennes la journée même journée du traitement. Cette forme de radiothérapie comprend de nombreuses variantes telles que la radiothérapie stéréotaxique, la radiothérapie conformationnelle tridimensionnelle, la protonthérapie et l'irradiation corporelle totale. La radiothérapie stéréotaxique est un traitement qui focalise une très haute dose de radiation dans un petit volume. Afin de limiter la toxicité aux cellules saines, plusieurs angles de faisceaux de radiations convergent sur la tumeur. Ce type de radiothérapie permet de délivrer une dose de radiation importante et avec précision à la tumeur. La radiothérapie conformationnelle tridimensionnelle utilise la modélisation 3D de la forme de la tumeur ou de la zone de traitement afin de focaliser les faisceaux de radiation. Cette technique permet d'optimiser la dose de radiation sur la tumeur où les faisceaux se croisent. La protonthérapie utilise des faisceaux de protons contrairement aux rayons X. L'utilisation des protons a pour avantage de causer moins de dommages aux tissus normaux voisins, car l'énergie libérée par les protons est davantage concentrée alors que les rayons X libèrent une quantité importante d'énergie avant et après avoir atteint la section visée. Pour terminer, l'irradiation corporelle totale correspond à une radiothérapie administrée à l'entièreté du corps. Elle peut être utilisée lors de la préparation à une greffe de cellules souches [39]. La radiothérapie interne est appelée brachythérapie ou curiethérapie. Elle consiste à insérer une source de radioactivité à proximité ou à l'intérieur de la zone à traiter. Cette technique a été mise au point par l'Institut Curie. La radiothérapie interne comprend aussi la curiethérapie interstitielle qui consiste en l'implantation d'aiguilles radioactives dans la section tumorale. La radiothérapie intracavitaire est une méthode de radiothérapie interne insérant une source radioactive dans une cavité corporelle (e.g. utérus, vagin). Elle se distingue de la radiothérapie intraluminale qui consiste à insérer un tube ou un applicateur pour des organes creux comme les intestins. De plus, la radiothérapie par plaque ou curiethérapie de surface consiste à utiliser un petit implant radioactif qui est déposé à la surface de la tumeur. Finalement, l'utilisation de molécules radioactives injectées par voie intraveineuse comme la radiothérapie interne vectorisée et l'immunocuriethérapie sont d'autres exemples de radiothérapie interne [40]. Bien que la radiothérapie présente beaucoup d'avantages thérapeutiques, elle possède aussi

des limitations, notamment lorsque le patient traité est atteint de cancers radiorésistants et non localisés [41, 42].

1.4.3. L'immunothérapie

L'immunothérapie ou immuno-oncologie est un traitement visant à augmenter la réponse du système immunitaire envers des cellules malignes pour traiter le cancer. L'immunothérapie est un type de thérapie biologique. En d'autres mots, c'est un type de traitement qui utilise des molécules synthétisées à partir d'organismes vivants pour traiter la maladie. Ces substances peuvent être présentes naturellement dans le corps ou peuvent être synthétisées en laboratoire. L'immunothérapie est divisée en différentes classes : les anticorps monoclonaux, les inhibiteurs de points de contrôles immunitaires, les anticorps monoclonaux conjugués, l'immunothérapie non spécifique (interférons, interleukines, etc.), les médicaments immunomodulateurs, les vaccins anticancéreux et la virothérapie oncolytique [43, 44].

1.4.4. L'hormonothérapie

L'hormonothérapie consiste en la modification du système endocrinien. Elle peut être utilisée dans les traitements des patients atteints du cancer en ajoutant, en bloquant ou en enlevant des hormones dans le but de faire ralentir ou d'arrêter la croissance des cellules cancéreuses qui dépendent des hormones pour leur prolifération. L'hormonothérapie peut être administrée seule ou en concomitance avec d'autres traitements. Par exemple, l'hormonothérapie peut diminuer la taille d'une tumeur afin de faciliter une chirurgie subséquente ou encore réduire le risque de récidive lors de traitements avec des agents chimiothérapeutiques. L'hormonothérapie est divisée en plusieurs types, on y retrouve notamment les anti-estrogènes, les anti-androgènes, les anti-aromatases, les analogues de l'hormone de libération de la lutéinostimuline (LHRH) et les antagonistes de l'hormone de libération de la gonadotrophine (GnRH) [45-47].

1.4.5. Les thérapies ciblées

Les thérapies ciblées ou traitements ciblés sont des traitements conçus pour interférer avec des mécanismes biologiques ou des molécules spécifiques nécessaires à la croissance et

à la progression de la tumeur. Ils servent à limiter la croissance du cancer, tuer les cellules cancéreuses ou soulager les symptômes causés par le cancer. Il existe différents types de thérapies ciblées. Certaines thérapies ciblées visent des protéines uniquement présentes chez les cellules cancéreuses, alors que d'autres ciblent des protéines ou gènes mutés des cellules cancéreuses. Les thérapies ciblées sont d'ailleurs un outil important en médecine personnalisée. En effet, l'un des principaux objectifs des thérapies ciblées est de tuer les cellules cancéreuses avec plus de précision et potentiellement moins d'effets secondaires. Les thérapies ciblées sont généralement divisées en deux groupes, soit les anticorps monoclonaux et les médicaments à petites molécules. Les thérapies peuvent être notamment des inhibiteurs de tyrosine kinases, des inducteurs d'apoptoses, des inhibiteurs de l'angiogenèse et des inhibiteurs de la protéine mTOR.

1.4.6. La chimiothérapie

1.4.6.1. Généralités

Le terme « chimiothérapie » était décrit historiquement comme l'utilisation de molécules pour traiter les maladies, sans nécessairement référer au cancer. Le terme a été inventé au début du 20^{e} siècle par le médecin allemand Paul Ehrlich, l'inventeur de l'arsphénamine, un composé à base d'arsenic pour traiter les patients atteints de la syphilis. Les années suivantes, il y a eu la découverte des sulfamidés (molécules antibactériennes à large spectre d'activité) par Gerhard Domagk, un pathologiste allemand qui commercialisa le Prontosil comme premier antibactérien. En 1928, Alexander Fleming a découvert la pénicilline à partir du champignon *Penicillium notatum* ce qui lui a valu le prix Nobel de médecine en 1945. Beaucoup de progrès ont été réalisés depuis cette époque [48]. De nos jours, le terme « chimiothérapie » est remplacé par « pharmacothérapie » lorsqu'on traite une maladie avec un médicament. Le terme « chimiothérapie » est majoritairement employé pour la pharmacothérapie anticancéreuse. Cette dernière sera explorée plus en profondeur dans la prochaine section.

1.4.6.2. Historique

Les observations médicales sur des soldats en contact avec le gaz moutarde lors de la Première Guerre mondiale ont montré une importante toxicité sur leur moelle osseuse et leurs ganglions lymphatiques au point d'empêcher l'hématopoïèse. Ces observations ont mené aux travaux d'Alfred Gilman et Louis Goodman sur le développement des moutardes à l'azote, des agents alkylants utilisés dans le traitement d'un certain nombre de cancers. Peu de temps après la Seconde Guerre mondiale, Sidney Farber, un pathologiste de Harvard, découvrit l'acide folique et son action stimulante pour la prolifération de cellules de leucémies lymphoblastiques aiguës. Ainsi, Farber sera un des premiers à mettre au point la conception rationnelle d'un médicament lorsqu'il prépara des analogues de l'acide folique. Un de ces analogues était le méthotrexate (améthoptérine), un inhibiteur de la dihydrofolate réductase. Cette enzyme catalyse la conversion du dihydrofolate en tétrahydrofolate. Elle est cruciale pour la synthèse des purines, qui mène ultimement à la synthèse de l'ADN. Ces antagonistes furent les premiers agents anticancéreux à induire une rémission chez les enfants atteints de leucémies lymphoblastiques aiguës. Joseph Burchenal, un oncologiste américain a suivi la même approche que Farber en modifiant légèrement la purine, une base azotée, composante nécessaire à la division cellulaire. Avec l'aide de George Hitchings et Gertrude Elion, Burchenal découvrit la 6-mercaptopurine, un composé aux propriétés immunosuppressives et cytostatiques ayant une puissante activité sur les leucémies. Après la découverte et le développement de ces agents anticancéreux par ces pionniers, maints autres agents anticancéreux ont été découverts et développés. De nos jours, une panoplie de nouveaux agents chimiothérapeutiques ont été étudiés permettant la commercialisation de plusieurs nouveaux médicaments. Les prochaines sections présentent un résumé des principaux agents anticancéreux utilisés en clinique.

1.5. Les agents anticancéreux

Puisque les travaux de cet ouvrage traitent principalement de la chimiothérapie cytotoxique, seulement cette approche sera approfondie. La classification de ces traitements peut s'avérer complexe étant donné leurs cibles biologiques variées. Néanmoins, différentes approches de classification de ces médicaments ont été mises au point afin de résoudre ce

problème. Une des méthodes traditionnellement employées est la classification par mécanisme d'action. Cette classification comprend les agents alkylants, les antimétabolites, les antibiotiques antitumoraux, les inhibiteurs des topoisomérases I et II, les enzymes, les antimicrotubules et les autres.

1.5.1. Les agents alkylants

Les agents alkylants sont caractérisés par leur capacité à ajouter des groupements alkyles à divers groupes nucléophiles au sein de la cellule comme notamment les groupements purine, pyrimidine, phosphate, thiol, carboxyle, hydroxyle, amino et imidazole. La réactivité des agents alkylants leur permet d'interagir avec l'ADN, l'ARN et les protéines essentielles à la survie et à la réplication de la cellule. Ils ne sont pas spécifiquement actifs dans une des phases du cycle cellulaire. Par contre, ces agents semblent induire l'apoptose majoritairement aux cellules qui se divisent, ce qui les rend plus toxiques aux tissus qui prolifèrent rapidement [49]. Par ailleurs, ils produisent des modifications chimiques irréversibles à l'ADN ce qui peut les rendre tératogènes, mutagènes et carcinogènes. Ils sont aussi radiomimétiques puisqu'ils produisent des lésions biochimiques similaires à des radiations ionisantes [49]. Les patients traités avec les agents alkylants souffrent couramment d'infections causées par les effets myélosuppresseurs et immunosuppresseurs [49]. Les agents alkylants se divisent généralement en quatre familles : les moutardes à l'azote, les nitrosourées, les sels de platine et les autres. Une liste non exhaustive d'agents alkylants est présentée au Tableau 1.1.

Tableau 1.1. Classes, noms génériques et structures moléculaires d'agents alkylants utilisés en clinique.

Classe	Nom générique	Structure moléculaire
Moutardes à l'azote	Chlorambucil	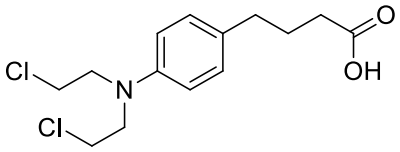
	Melphalan	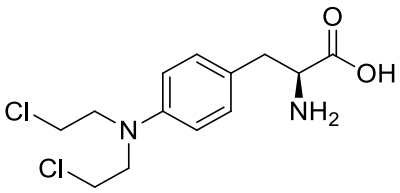
	Cyclophosphamide	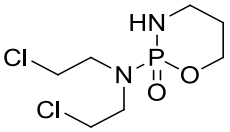
	Ifosfamide	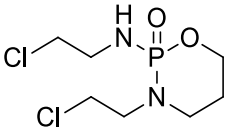
Nitrosourées	Carmustine	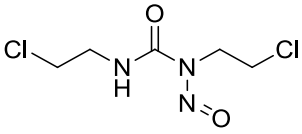
	Streptozotocine	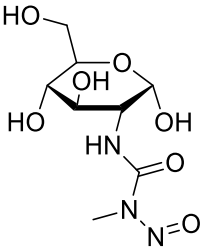
Sels de platine	Cisplatine	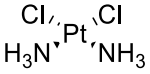
	Carboplatine	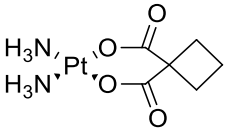

	Oxaliplatine	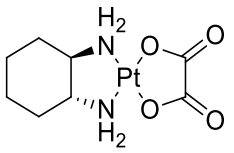
Autres	Busulfan	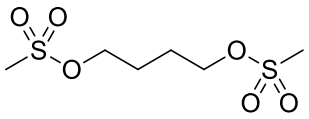
	Thiotépa	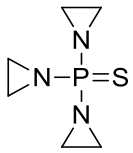
	Dacarbazine	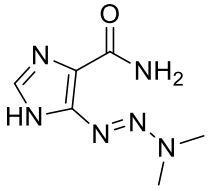
	Témozolomide	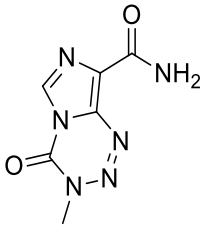

1.5.2. Les antimétabolites

Les antimétabolites possèdent une structure similaire aux purines, aux pyrimidines ou à l'acide folique. Ces derniers sont impliqués dans la synthèse de l'ADN, de l'ARN et de coenzymes. Il existe trois classes d'agents antimétabolites : les analogues de l'acide folique, les analogues des purines et les analogues des pyrimidines. La similarité structurelle des antimétabolites peut permettre leur incorporation dans l'ADN et l'ARN. Ils peuvent également inhiber les cascades métaboliques des nucléotides ou entraver la biosynthèse de précurseurs cruciaux aux fonctions cellulaires normales. Ces différents bouleversements mèneront ultimement la cellule à l'apoptose. L'effet des antimétabolites est majoritairement réalisé dans la phase de synthèse de l'ADN (phase S) du cycle cellulaire. Les tissus ou organes nécessitant une division cellulaire rapide tels que la moelle osseuse et les muqueuses du tube digestif sont particulièrement affectés par ces agents, notamment au niveau de la muqueuse orale [49]. Des exemples d'agents antimétabolites sont illustrés au Tableau 1.2.

Tableau 1.2. Classes, noms génériques et structures moléculaires d'antimétabolites utilisés en clinique.

Classe	Nom générique	Structure moléculaire
Analogues de l'acide folique	Méthotrexate	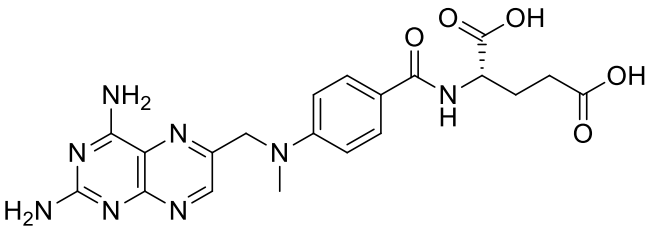
	Pémétrexed	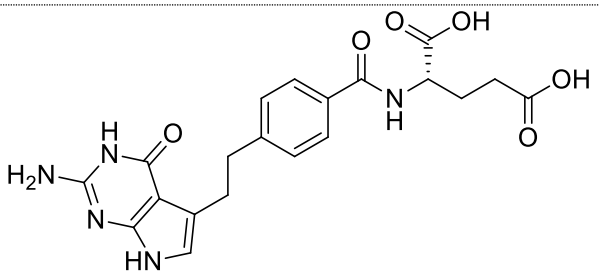
Analogues des purines	6-Mercaptopurine	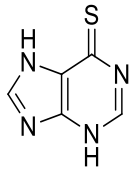
	6-Thioguanine	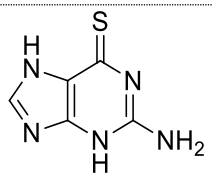
	Nélarabine	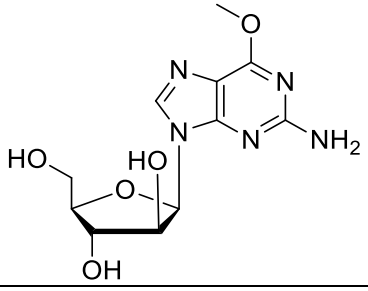
Analogues des pyrimidines	Cytarabine	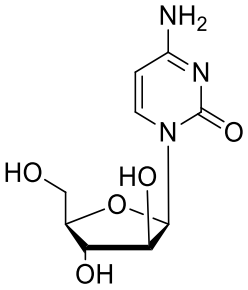

Gemcitabine	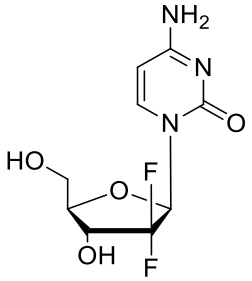
Capécitabine	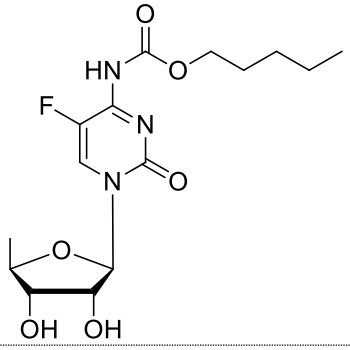
5-Fluorouracile	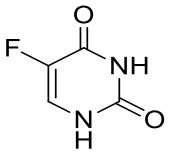

1.5.3. Les antibiotiques antitumoraux

Les antibiotiques antitumoraux sont des molécules découvertes originairement comme antibiotiques et qui ont été requalifiées comme agents anticancéreux. Ces substances sont produites naturellement par une variété de *Streptomyces*, soit des bactéries filamenteuses à Gram positif non pathogènes appartenant à l'ordre des Actinomycètes [50]. Leur mécanisme d'action constitue d'une part une liaison irréversible avec l'ADN produisant des complexes qui inhibent la division cellulaire, mais d'autres mécanismes d'actions ont été proposés pour expliquer leur toxicité. Particulièrement, des ions oxygénés et métalliques seraient impliqués. Les antibiotiques anticancéreux induisent des lésions à la cellule dans l'ensemble des phases du cycle cellulaire. Des effets indésirables comme des stomatites, de la myélosuppression et des vomissements sont associés à cette classe d'agents sauf dans le cas de la bléomycine (myélosuppression et nausée très faible) [49]. Des exemples d'antibiotiques antitumoraux sont présentés au Tableau 1.3.

Tableau 1.3. Classes, noms génériques et structures moléculaires d'antibiotiques antitumoraux utilisés en clinique.

Classe	Nom générique	Structure moléculaire
Antibiotiques antitumoraux	Bléomycine	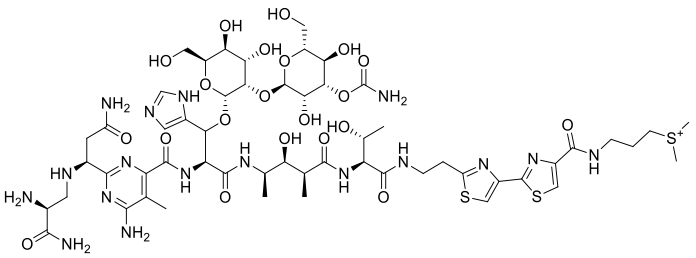
	Mitomycine C	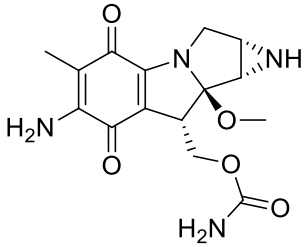
	Mithramycine	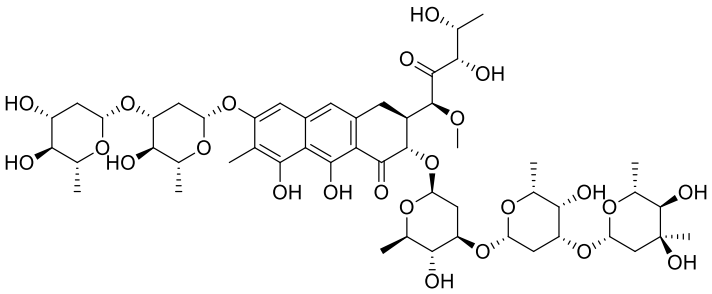

1.5.4. Les inhibiteurs des topoisomérases I et II

Les inhibiteurs des topoisomérases, comme leur nom l'indique, sont des agents conçus pour inhiber l'activité des topoisomérases, des enzymes contrôlant la structure topologique de l'ADN notamment lors de sa réplication et de sa transcription. Les inhibiteurs des topoisomérases incluent la famille des anthracyclines, des épipodophyllotoxines, des anthracènes et des camptothécines. Les anthracyclines sont des antibiotiques antitumoraux ayant une structure de quatre cycles fusionnés (deux phényles, une benzoquinone et un cyclohexyle). Différents mécanismes d'actions pour cette famille d'agents sont proposés. En premier lieu, ils agissent en générant des radicaux libres au niveau de la membrane cellulaire.

En second lieu, leur structure planaire permet leur intercalation entre les paires de bases azotées de l'ADN, affectant ainsi la synthèse de l'ADN et de l'ARN. En dernier lieu, ils agissent comme des inhibiteurs de la topoisomérase II qui sont connus pour induire des bris double-brins à l'ADN lors de la division cellulaire. Les effets secondaires associés à ces composés incluent la myélosuppression, un effet vésicant, des mucosites, de la cardiotoxicité et le syndrome d'érythème palmo-plantaire [51]. Les épipodophyllotoxines sont des composés caractérisés une fois de plus par quatre cycles fusionnés composés des groupements dioxine, phényle, cyclohexyle et lactone. Ces molécules se retrouvent dans les racines de l'espèce *Podophyllum peltatum* et forment un complexe tertiaire avec la topoisomérase II et l'ADN. Cette famille cause principalement de la myélosuppression et des nausées comme effets secondaires [52]. Les anthracènes sont constitués de trois cycles fusionnés formant un noyau hydroxyanthraquinone. La mitoxantrone est produite par synthèse totale. Son activité antinéoplasique est causée par l'inhibition de la topoisomérase II, résultant en des bris double-brins à l'ADN. Contrairement aux anthracyclines, la mitoxantrone a un risque beaucoup plus faible de générer des radicaux libres associés à une toxicité cardiovasculaire [49]. Les camptothécines proviennent de l'arbre *Camptotheca acuminata* originaire du sud de la Chine. Leur cytotoxicité est causée par l'inhibition de la topoisomérase I, entraînant des bris simple-brin à l'ADN et ultimement la mort cellulaire. Les effets secondaires majeurs de cette famille sont la myélosuppression, une diarrhée nécessitant une attention médicale soutenue et des symptômes d'excès cholinergique (salivation, crampes abdominales, etc.) [53]. Une liste d'inhibiteurs des topoisomérases I et II est présentée au Tableau 1.4.

Tableau 1.4. Classes, noms génériques et structures moléculaires d'inhibiteurs des topoisomérases I et II utilisés en clinique.

Classe	Nom générique	Structure moléculaire
Anthracyclines	Idarubucine	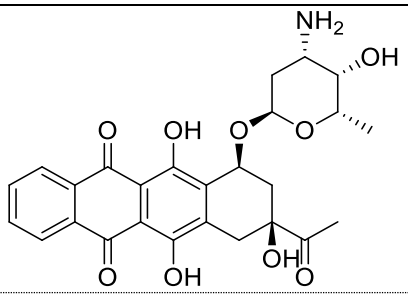
	Doxorubicine	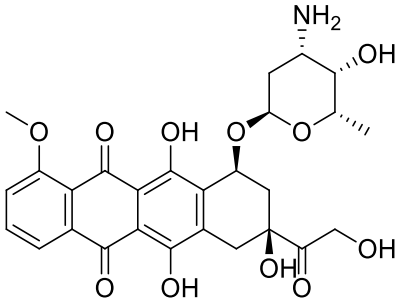
	Épirubicine	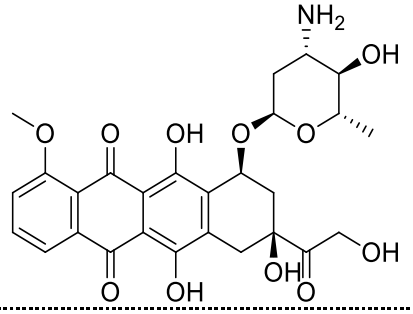
Épipodophyllotoxines	Étoposide	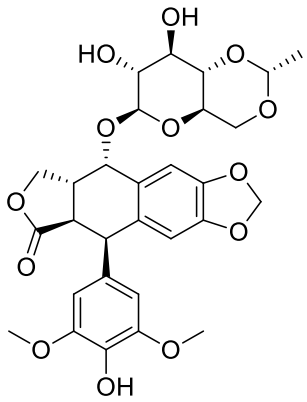

	Téniposide	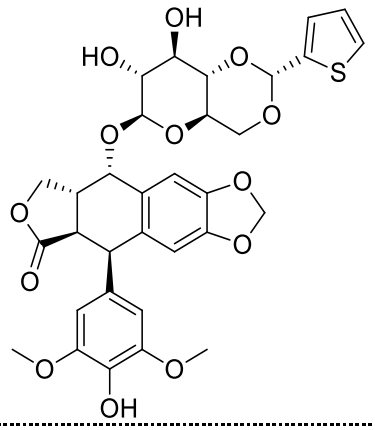
Anthracène	Mitoxantrone	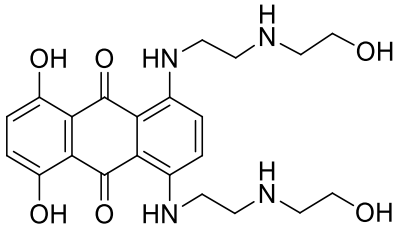
Camptothécines	Irinotécan	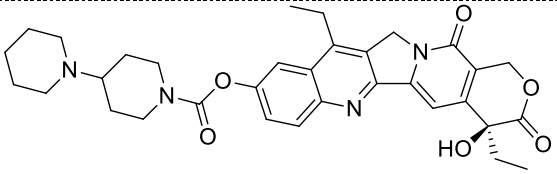
	Topotécan	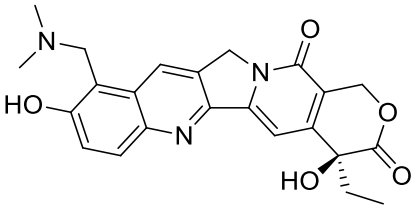

1.5.5. Les enzymes

L'utilisation d'enzymes pour traiter des patients atteints d'un cancer est une avenue encore peu exploitée de nos jours. En effet, une seule enzyme est disponible en clinique comme traitement contre le cancer, soit la L-asparaginase. Certaines cellules tumorales ne peuvent produire leur propre acide aminé asparagine contrairement aux cellules saines. Puisque la croissance et la survie des cellules tumorales dépendent de l'asparagine, la L-asparaginase épuise les réserves de cet acide aminé en catalysant son hydrolyse en acide aspartique et en ammoniac. Les cellules tumorales ayant alors épuisé leur réserve d'asparagine entrent en apoptose. L'activité de cette enzyme est principalement dans la phase G_1 du cycle cellulaire. Des réactions anaphylactiques, des réactions d'hypersensibilité, des

thromboses, des pancréatites et des intolérances au glucose sont associées à l'utilisation de ce traitement [49].

1.5.6. Les agents antimicrotubules

Les agents antimicrotubules sont des agents ciblant les microtubules, une des trois fibres du cytosquelette. Ils peuvent agir selon deux mécanismes d'action généraux, soit hyperstabiliser les microtubules ou soit inhiber leur polymérisation. Les principales familles d'agents antimicrotubules comprennent les vinca-alcaloïdes, l'analogue du macrolide halichondrine B et les taxanes. Les vinca-alcaloïdes et l'analogue du macrolide halichondrine B sont des agents inhibiteurs de la polymérisation des microtubules alors que les taxanes sont des hyperstabilisateurs des microtubules. Les vinca-alcaloïdes ont été isolés notamment de la Pervenche de Madagascar. L'activité antinéoplasique des vinca-alcaloïdes est attribuée à leur capacité à arrêter le cycle cellulaire lors de la métaphase en inhibant la formation du fuseau mitotique. Le profil toxicologique de cette famille varie de manière importante malgré la similarité structurelle de ces molécules. De la neurotoxicité, de la neutropénie, des mucosites, de l'alopécie et de puissants effets vésicants sont associés à l'utilisation de ces molécules [49]. L'analogue du macrolide halichondrine B est l'éribuline. Ce composé est extrait d'éponges marines (*Phakellia carteri, Axinella sp.*). Il présente une structure chimique simplifiée par rapport à l'halichondrine B. L'éribuline se lie uniquement aux extrémités positives de la tubuline, inhibant la polymérisation des microtubules. Une perte de globules blancs, des neuropathies, des cardiopathies et des lésions foetales ont été notées avec l'utilisation de l'éribuline [54]. Les taxanes sont constitués de deux médicaments, le paclitaxel et le docétaxel. Le paclitaxel est un produit isolé à partir des extraits d'écorce d'if de l'Ouest ou d'if du Pacifique (*Taxus brevifolia*) tandis que le docétaxel est un composé semi-synthétique dérivant du paclitaxel. La faible solubilité dans l'eau des taxanes nécessite des formulations particulières. L'utilisation du Kolliphor® EL (Cremophor® EL) dans ces formulations est responsable de plusieurs effets indésirables des taxanes tels que la dyspnée, l'hypotension et les réactions d'hypersensibilité [55]. Les effets indésirables associés aux taxanes incluent de la neurotoxicité, de la myélosuppression et des effets vésicants [49]. Des exemples de médicaments de chacune de ces familles sont illustrés au Tableau 1.5.

Tableau 1.5. Classes, noms génériques et structures moléculaires d'agents antimicrotubules utilisés en clinique.

Classe	Nom générique	Structure chimique
Vinca-alcaloïdes	Vinblastine	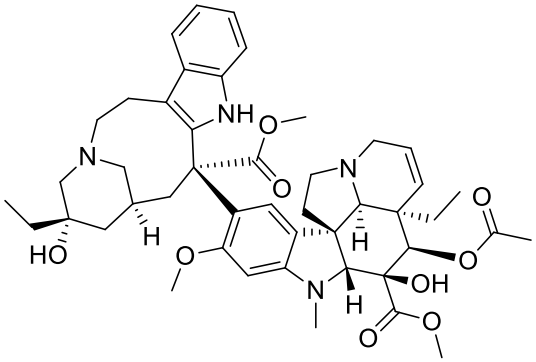
	Vincristine	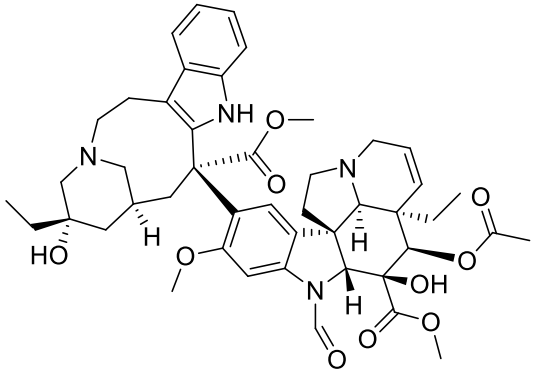
	Vinorelbine	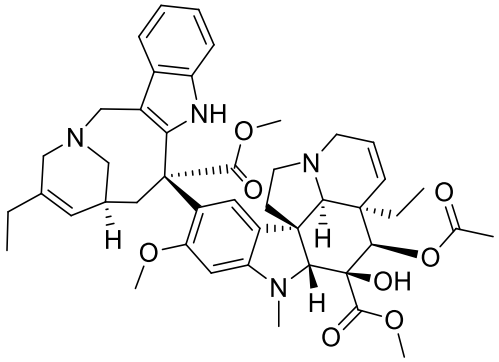
Halichondrine	Éribuline	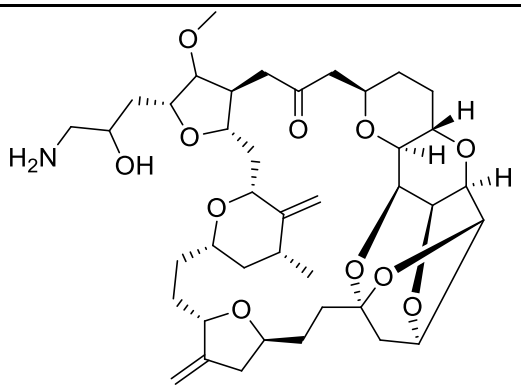

Taxanes	Paclitaxel	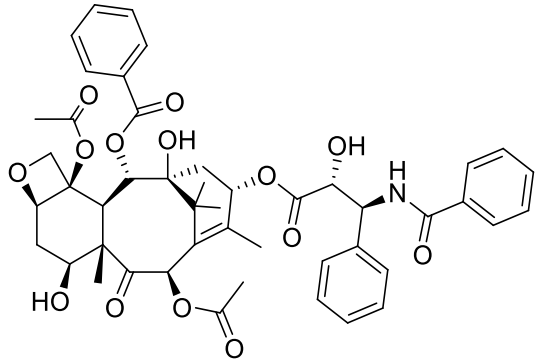
	Docétaxel	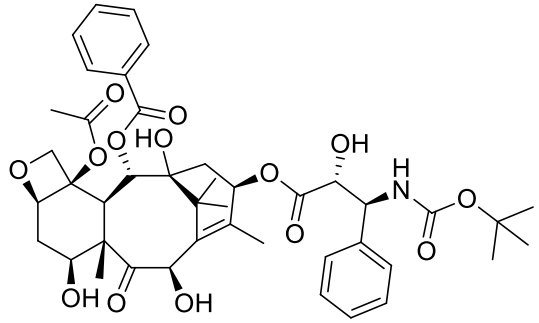

1.5.7. Les autres

La classe « autres » contient les différents médicaments ayant des mécanismes d'actions ne pouvant pas être regroupés dans les classes présentées précédemment. L'hydroxyurée, la thalidomide et le mitotane sont présentés comme exemples dans cette section. L'hydroxyurée a été synthétisée pour la première fois en 1869, mais son utilisation dans le traitement du cancer n'a débuté qu'à partir de 1960. Cette molécule est métabolisée en radical libre nitroxide qui diffuse dans la cellule pour inhiber la ribonucléotide réductase, une enzyme jouant un rôle clé dans la transformation des ribonucléotides en désoxyribonucléotides, molécules essentielles à la synthèse de l'ADN. De la myélosuppression, des nausées et des irritations cutanées font partie de la liste des effets indésirables [49]. La thalidomide a été utilisée chez les femmes enceintes en Europe et au Canada dans les années 50 comme anxiolytique, antiémétique et sédatif. Elle a été retirée du marché quelques années plus tard et a engendré une polémique majeure après que ses effets tératogènes ont été découverts. Néanmoins, la thalidomide a été réintroduite et approuvée pour le traitement de la maladie de Hansen (lèpre) et plusieurs autres maladies (stomatite ulcéreuse associée au SIDA, polyarthrite rhumatoïde et chronique, etc.) vers la fin des années 90. Depuis, la thalidomide est devenue un traitement pour plusieurs myélomes. Le

mécanisme d'action de la thalidomide est complexe et mal compris, mais il mène ultimement à l'anti-angiogenèse et à la modulation du système immunitaire. Les effets secondaires incluent des irritations cutanées, des neuropathies, un effet sédatif en plus d'augmenter le risque de développer de la thrombose veineuse [49]. Le mitotane est un composé analogue à l'insecticide dichlorodiphényltrichloroéthane aussi connu sous le nom DDT. Il cible les cellules saines et cancéreuses des glandes surrénales. Son mécanisme n'est pas complètement connu. C'est un médicament orphelin puisque l'incidence du cancer visé est très faible (une à deux personnes par millions d'habitants). Il génère de la neurotoxicité, des nausées, des démangeaisons, de la gynécomastie et des pertes de mémoire chez les patients traités [49]. Le Tableau 1.6 présente les exemples de médicaments de la classe autres mentionnés précédemment.

Tableau 1.6. Classes, noms génériques et structures moléculaires d'agents anticancéreux appartenant à la classe « autres » utilisés en clinique.

Nom générique	Structure moléculaire
Hydroxyurée	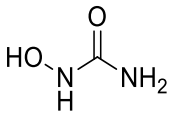
Thalidomide	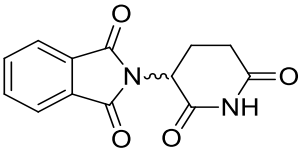
Mitotane	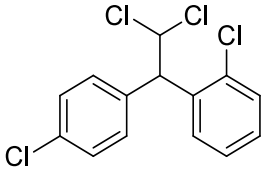

1.6. Le cytosquelette et les microtubules

Le cytosquelette est un ensemble de polymères biologiques qui confère à la cellule la majorité de ses propriétés structurelles et mécaniques. Malgré le mot « squelette », le cytosquelette n'est pas une structure fixe. Au contraire, c'est une structure dynamique qui s'adapte à son milieu et qui requiert une multitude de protéines pour accomplir ses rôles

biologiques. Le cytosquelette possède trois fonctions principales. Il relie physiquement et biochimiquement la cellule à son environnement, il est responsable de l'organisation dans l'espace du contenu cellulaire et il génère des forces coordonnées capables de déplacer la cellule et modifier sa forme. Le cytosquelette est constitué de filaments d'actines (microfilaments), de filaments intermédiaires et des microtubules.

Les filaments d'actines sont composés de deux brins d'actine de 7 nm de diamètre. Ils possèdent une rigidité mitoyenne comparativement aux filaments intermédiaires et aux microtubules. L'actine peut se retrouver sous une forme assemblée en filaments d'actine (forme fibrillaire) ou sous forme monomérique libre dans le cytosol (forme globulaire). Les filaments d'actine jouent des rôles importants dans la motilité cellulaire, la contraction musculaire, le maintien de la structure de la cellule et la formation du sillon de division cellulaire [56].

Les filaments intermédiaires sont les fibres les plus massives du cytosquelette, mais ce sont les plus souples. Ils sont formés de plusieurs protéines organisées en superhélices avec un diamètre de 8 à 12 nm. Ces filaments peuvent faire des liens entre eux et avec les filaments d'actines et les microtubules avec des protéines appelées plectines. Ils possèdent des rôles dans le maintien de la structure et la forme de la cellule en plus de fixer des organites comme les mitochondries et l'appareil de Golgi. Généralement, la cellule assemble les filaments intermédiaires en réponse à des stress mécaniques. En comparaison aux filaments d'actine et aux microtubules, les filaments intermédiaires ne sont pas polarisés et sont plus stables [57].

Les microtubules sont les composantes les plus rigides du cytosquelette. Ces tubes rectilignes mesurent environ 25 nm de diamètre et peuvent varier entre 200 et 2 500 nm de longueur. Les microtubules sont formés par polymérisation de l'α, β-tubuline. Cet hétérodimère peut se retrouver sous forme libre (soluble) dans le cytosol ou sous forme assemblé, formant ainsi des protofilaments qui par association vont former le microtubule (Figure 1.3). Les protofilaments sont des polymères rectilignes alignés parallèlement formant des contacts latéraux pour créer un cylindre creux généralement de 13 protofilaments chez l'humain formant ainsi un microtubule [58]. Les microtubules sont organisés d'une manière polaire exposant l'α-tubuline d'un bout (terminaison « - ») alors que la β-tubuline est exposée du côté opposé (terminaison « + », Figure 1.3). La tubuline libre possède une guanosine

triphosphate (GTP) située sur l'α- et sur la β-tubuline. La GTP associée à l'α-tubuline ne peut pas faire d'échange avec son milieu, elle est piégée dans la protéine. En contrepartie, la GTP de la β-tubuline est interchangeable et est responsable de la polymérisation de l'hétérodimère α, β-tubuline au sein des microtubules lors de son hydrolyse en guanosine diphosphate (GDP). L'ajout de nouvelles sous unités se fait majoritairement à l'extrémité « + », du côté de la β-tubuline alors que la dépolymérisation se fait majoritairement à l'extrémité « - », du côté de l'α-tubuline [58]. La structure de l'hétérodimère d'α, β-tubuline-GDP est non favorisée, mais stabilisée par les protofilaments. Afin d'empêcher la dépolymérisation spontanée du microtubule, l'extrémité « + » du microtubule doit être stabilisée par un « bouchon de GTP », c'est-à-dire un anneau d'α, β-tubuline-GTP ayant le côté β-tubuline exposé au cytoplasme [56].

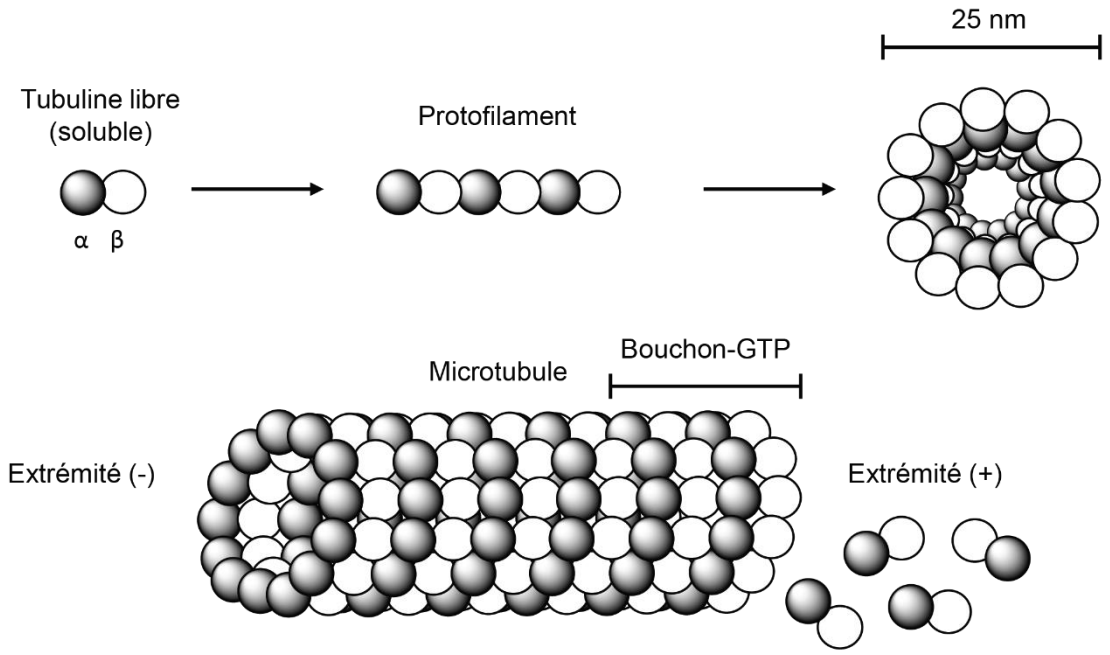

Figure 1.3. Structure et nomenclature des composantes des microtubules.

1.7. La dihydroorotate déshydrogénase

La dihydroorotate déshydrogénase humaine (*h*DHODH) est une oxydoréductase catalysant la transformation de l'acide 4,5-dihydroorotique ([*S*]-dihydroorotate) en acide orotique (orotate), un précurseur des pyrimidines. Les pyrimidines sont requises pour la

biosynthèse de l'ADN, de l'ARN, des glycoprotéines et des phospholipides. La *h*DHODH possède plusieurs fonctions cellulaires. Elle joue un rôle déterminant dans la chaîne de transport d'électrons et l'apoptose dans certains types cellulaires. Le mécanisme d'action de la *h*DHODH est du type « ping-pong » d'où la similitude des mouvements que l'on exécute en pratiquant ce sport. Elle nécessite la flavine mononucléotide (FMN) et l'ubiquinone (CoQ) pour effectuer sa catalyse. Les réactions d'oxydoréductions impliquées sont illustrées dans la Figure 1.4.

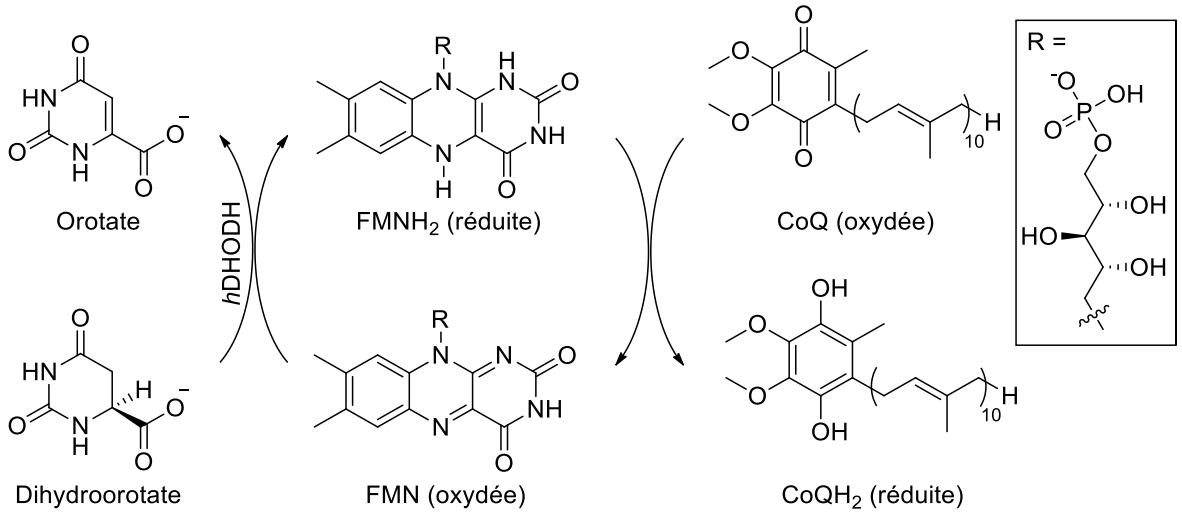

Figure 1.4. Mécanisme d'oxydoréduction de la *h*DHODH de type « ping-pong » transformant la dihydoorotate en orotate et impliquant la flavine mononucléotide (FMN) et l'ubiquinone (CoQ) [59].

Les pyrimidines peuvent être biosynthétisées selon deux voies de synthèse : la voie *de novo* qui implique la *h*DHODH et la voie de sauvetage qui n'implique pas la *h*DHODH [59]. Les cellules complètement différenciées ou quiescentes requièrent peu de pyrimidines et ces cellules emploient principalement la voie de sauvetage. Cette voie recycle les bases azotées et les nucléosides lors de la dégradation de l'ARN et de l'ADN. Les composantes récupérées peuvent alors être transformées en nucléotides et être incorporées à nouveau dans l'ARN et l'ADN. La *h*DHODH n'est donc pas essentielle pour les cellules ayant un rythme normal de prolifération. En opposition, les cellules ayant une prolifération soutenue ont besoin d'un apport important en pyrimidines et dépendent fortement de la voie *de novo*. La transformation

de la dihydroorotate en orotate par la *h*DHODH est l'étape limitante de la cascade métabolique de la voie *de novo*. Par conséquent, l'inhibition de la *h*DHODH diminue les réserves intracellulaires de pyrimidines dans les cellules ayant une prolifération soutenue engendrant un arrêt de leur division cellulaire et ultimement leur mort cellulaire. La voie *de novo* est représentée à la Figure 1.5.

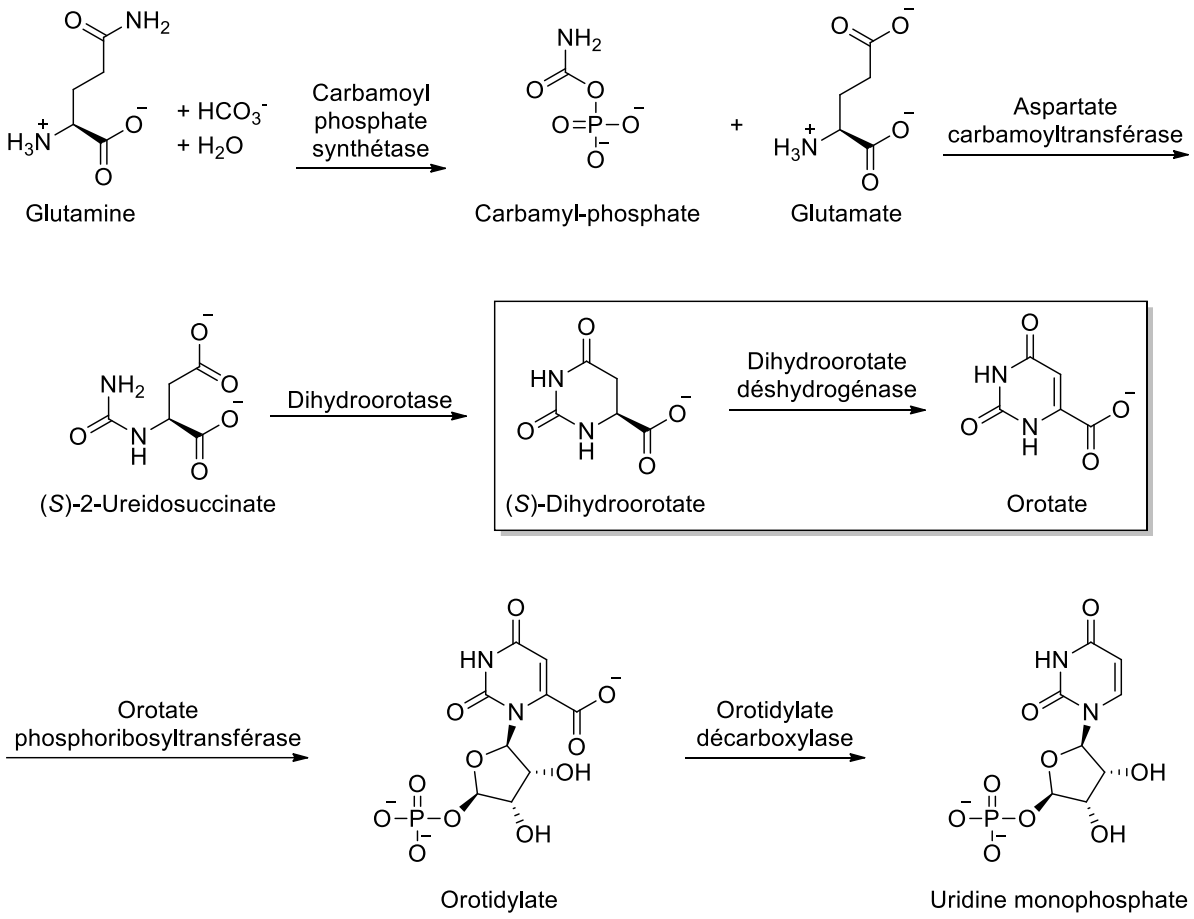

Figure 1.5. Voie de biosynthèse de l'uridine monophosphate (UMP) à partir de la glutamine [60].

La pertinence de la *h*DHODH dans le domaine du cancer a été reconnue il y a environ 60 ans lorsque Smith et ses collaborateurs ont détecté une augmentation de l'activité de la *h*DHODH dans des cellules leucémiques [61]. Ces travaux ont été le point de départ pour la découverte et l'évaluation clinique du bréquinar, un puissant inhibiteur de la *h*DHODH (Figure 1.6A) [62]. Toutefois, le bréquinar n'a pas produit de résultats concluants jusqu'à

présent [63]. Malgré tout, d'autres inhibiteurs de la *h*DHODH ont été développés et sont présentement utilisés en clinique pour le traitement de différentes maladies. Le léflunomide (Figure 1.6B) est un médicament approuvé par la *Food and Drug Administration* (FDA) pour le traitement de l'arthrite rhumatoïde et l'arthrite psoriasique. Il est présentement en étude clinique de phases I/II pour le traitement du myélome multiple [64]. Le tériflunomide (Figure 1.6C), le métabolite actif du léflunomide, est approuvé par la FDA pour le traitement de plusieurs scléroses [64]. Le IMU-838 (Figure 1.6D) est actuellement étudié en phase clinique II pour le traitement de la rectocolite hémorragique [65]. D'autres inhibiteurs comme le BAY2402234 (Figure 1.6E) et l'ASLAN003 (Figure 1.6F) sont étudiés respectivement en phases cliniques I et II pour le traitement de la leucémie myéloïde aiguë (LMA) [66, 67].

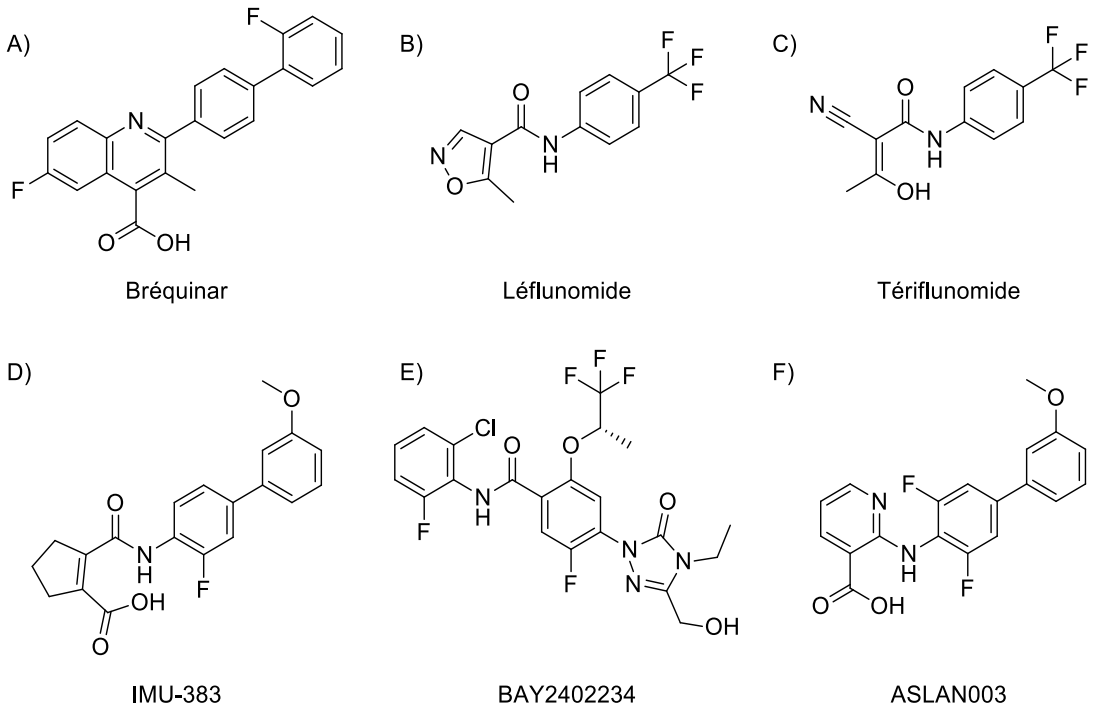

Figure 1.6. Structures moléculaires du A) bréquinar, B) léflunomide, C) tériflunomide, D) IMU-383, E) BAY2402234 et F) ASLAN003.

1.8. Les *N*-phényl uréidobenzènesulfonates (PUB-SOs) et les phényl 4-(2-oxoimidazolidin-1-yl)benzènesulfonates (PIB-SOs)

Les *N*-phényl uréidobenzènesulfonates (PUB-SOs) sont une nouvelle classe d'agents anticancéreux développés par le groupe de recherche du Dr Sébastien Fortin. Ces composés ont été mis au point à partir du gabarit moléculaire des *N*-phényl-*N*'-(2-chloroéthyl)urées (CEUs). Les CEUs ont été élaborés par la combinaison du groupement auxophore des moutardes à l'azote et du groupement pharmacophore de la famille des nitrosourées (Figure 1.7). Plus précisément, la fusion du cycle aromatique du chlorambucil (CBL) avec le groupement chloroéthyle nitrosourée de la lomustine (CCNU) a créé un premier composé de la famille phénylchloroéthylnitrosourée (CENU). Le CBL est un agent anticancéreux moins puissant que la CCNU, mais il génère des effets secondaires moins délétères. La fusion de ces groupements chimiques avait initialement pour but de diminuer la toxicité associée à la classe des nitrosourées en greffant un auxophore pour être plus sélectif aux cellules cancéreuses. Toutefois, le nouveau composé CENU possédait une faible activité antiprolifération. En effet, la concentration nécessaire pour inhiber 50% de sa croissance cellulaire (IC_{50}) était supérieure à 160 µM. Une seconde série de modifications incluant le retrait du groupement nitroso et la transformation de l'acide butyrique en butyrate de méthyle a généré le premier composé de la famille des CEUs avec une IC_{50} de 27 µM [68].

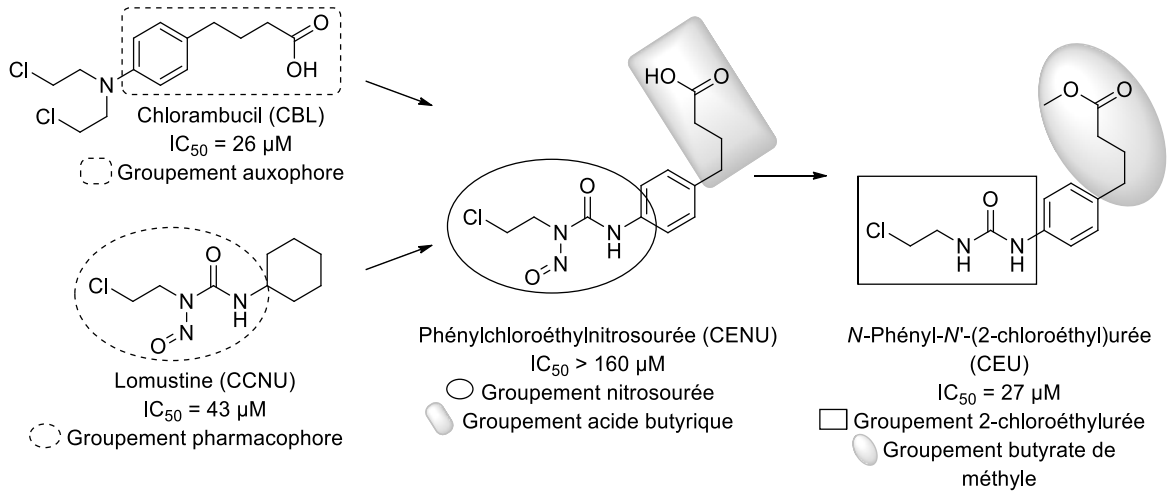

Figure 1.7. Schéma simplifié des structures moléculaires du chlorambucil (CBL) et de la lomustine (CCNU) menant à la conception de la famille phénylchloroéthylnitrosourée (CENU) et de la famille *N*-phényl-*N*'-(2-chloroéthyl)urée (CEU).

Les CEUs sont des agents antimicrotubules possédant un mécanisme d'action similaire à celui de la colchicine et de la combrétastatine A-4 (CA-4, Figure 1.8A). Ils interagissent avec le site de liaison de la colchicine (C-BS) à l'interface de l'α, β-tubuline. Ils inhibent la polymérisation des microtubules et arrêtent la progression du cycle cellulaire en phase G2/M. Par contre, la nature de leurs interactions est différente comparativement à la majorité des autres inhibiteurs de ce site où les interactions avec le C-BS sont exclusivement de nature électrostatiques. En effet, en plus d'interagir électrostatiquement avec le C-BS, les CEUs forment un lien covalent en acylant l'acide glutamique en position 198 de la β-tubuline. Ils sont qualifiés d'agents alkylants « doux », car ils ne ciblent pas l'ADN ni la glutathion réductase. Ils possèdent une activité plus puissante que le CBL et la carmustine sur au moins 30 lignées cellulaires cancéreuses et le test d'Ames démontre qu'ils ne sont pas mutagènes [69-71]. Plusieurs modifications ont été réalisées sur la structure moléculaire des CEUs au cours des dernières années. Le groupement 2-chloroéthylurée a été cyclisé pour former des dérivés 4,5-dihydro-*N*-phényloxazol-2-amines (OXAs, Figure 1.8B). Cette famille possède une activité biologique similaire à leurs analogues CEUs. Par la suite, la longueur de chaîne entre le cycle aromatique A et le groupement urée a été allongée, en plus de substituer le groupement urée par des groupements 3-chloropropyle, acétamide et éthyle menant à la conception des 1-(3-chloropropyl)-3-phénylurées (CPUs), 2-chloro-*N*-

(phénylcarbamoyl)acétamides (CAUs) et des 1-éthyl-3-phénylurées (EUs, Figure 1.8C) [73]. Des bioisostères amides ont été développés en parallèle aux dérivés urées ayant les substituants chlorométhyle, 2-chloroéthyle, 3-chloropropyle et éthènyle sur la portion amide conduisant à des dérivés *N*-benzyl-2-chloroacétamides (CAs), *N*-benzyl-3-chloropropanamides (CPAs), *N*-benzyl-4-chlorobutanamides (CBAs) et *N*-benzylacrylamides (Acrs, Figure 1.8D) [72, 73].

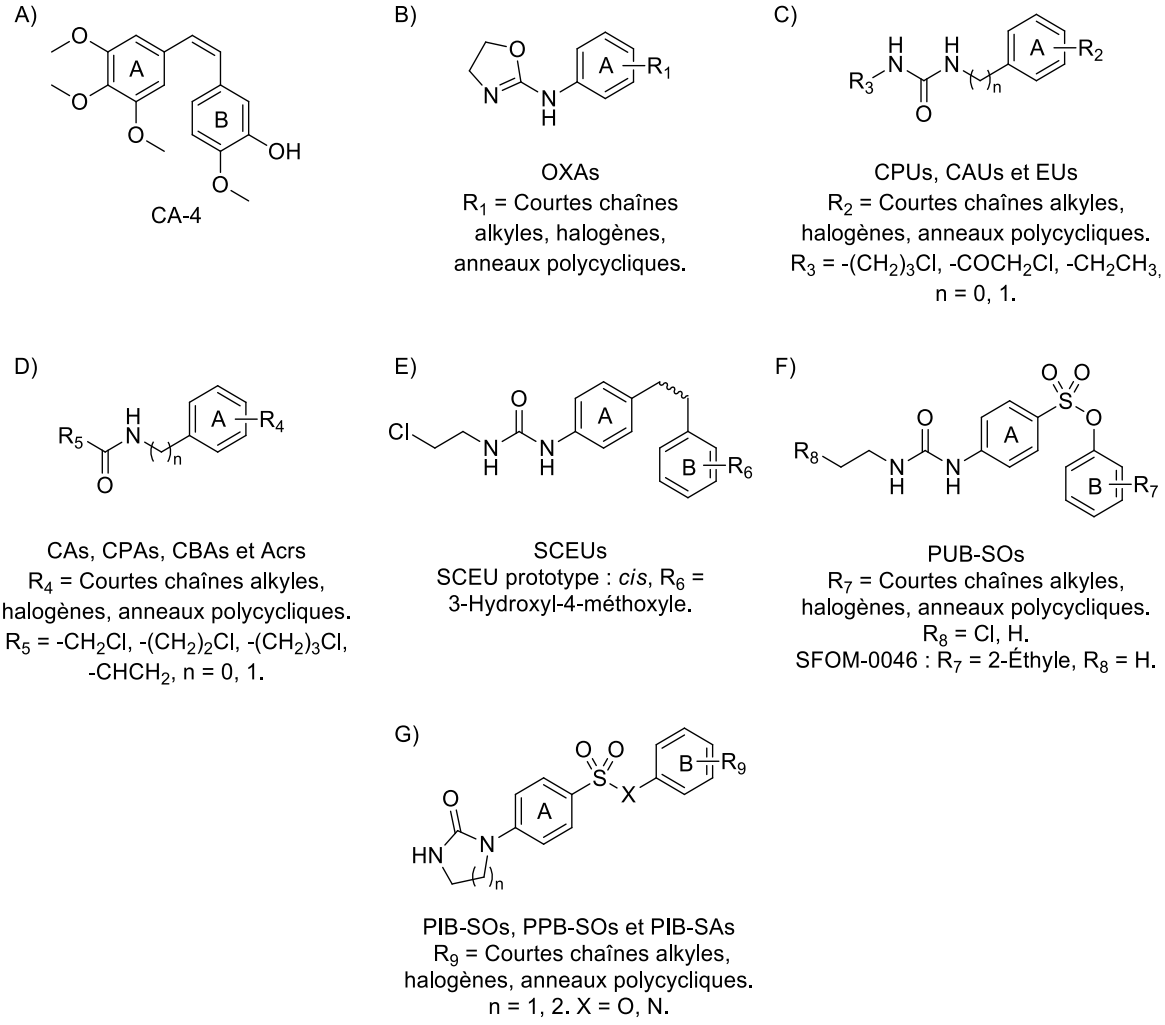

Figure 1.8. Structures moléculaires : A) de la combrétastatine A-4 (CA-4) , B) des 4,5-dihydro-*N*-phényloxazol-2-amines (OXAs), C) des 1-(3-chloropropyl)-3-phénylurées (CPUs), des 2-chloro-*N*-(phénylcarbamoyl)acétamides (CAUs) et des 1-éthyl-3-phénylurées (EUs), D) des *N*-benzyl-2-chloroacétamides (CAs), des *N*-benzyl-3-chloropropanamides (CPAs), des *N*-benzyl-4-chlorobutanamides (CBAs) et des *N*-benzylacrylamides (Acrs), E) des 1-(2-chloroéthyl)-3-(4-phénéthylphényl)urées (SCEUs), F) des *N*-phényl

uréidobenzènesulfonates (PUB-SOs), G) des phényl 4-(2-oxoimidazolidin-1-yl)benzènesulfonates (PIB-SOs), des phényl 4-(2-oxotétrahydropyrimidin-1(2H)-yl)benzènesulfonates (PPB-SOs) et des phényl 4-(2-oxoimidazolidin-1-yl)benzènesulfonamides (PIB-SAs).

Une progression importante du développement de ces composés est survenue lorsqu'un second cycle aromatique a été ajouté à la structure des CEUs pour obtenir les 1-(2-chloroéthyl)-3-(4-phénéthylphényl)urées (SCEUs, Figure 1.8E). La molécule prototype de cette série a été conçue sur la structure de la CA-4. En effet, des travaux en modélisation moléculaire ont montré que le cycle aromatique des CEUs se positionnait approximativement au même endroit dans le C-BS que le cycle aromatique A de la CA-4. Nous avons donc proposé à ce moment que le groupement *N*-phényl-*N'*-(2-chloroéthyl)urée pourrait mimer le groupement triméthoxyphényle de la CA-4. C'est dans ce contexte que les travaux publiés dans le *Eur. J. Med Chem.* et dont je suis premier auteur ont débuté [74]. Ces travaux ont montré que la substitution du groupement triméthoxyphényle de la CA-4 par le groupement *N*-phényl-*N'*-(2-chloroéthyl)urée donne des IC_{50} de l'ordre de la centaine de nanomolaire jusqu'au bas micromolaire, permet l'arrêt du cycle cellulaire en phase G2/M et l'acylation de l'acide glutamique en position 198 dans le C-BS [75, 76]. Toutefois, la conception de ces composés n'est pas optimale. En effet, il est bien connu que l'isomérisation *in vivo* du pont éthènyle *cis* de la CA-4 en isomère *trans* contribue à une perte significative de son activité biologique [77]. Puisque les SCEUs possèdent aussi un pont éthènyle, ils sont potentiellement sujets à cette isomérisation *in vivo* et une baisse d'activité similaire. Afin de contourner cet obstacle, le pont éthènyle des SCEUs a été remplacé par un groupement sulfonate, plus stable et davantage polaire, pour concevoir les premiers PUB-SOs (Figure 1.8F). Les PUB-SOs ont une activité antiprolifération de l'ordre du bas micromolaire sur toutes les lignées cellulaires cancéreuses étudiées. Selon leur structure moléculaire, les PUB-SOs produisent deux mécanismes d'action distincts. D'une part, les PUB-SOs substitués aux positions 3, 4 et/ou 5 sur le cycle aromatique B arrêtent la progression du cycle cellulaire en phase G2/M, ciblent le C-BS et perturbent les microtubules. D'autre part, ils arrêtent le cycle cellulaire en phase S et ciblent les mécanismes de réparation et de réplication de l'ADN lorsque leur cycle aromatique B est substitué en position 2 par des halogènes ou de courtes chaînes alkyles. Ce nouveau mécanisme d'action n'était pas attendu et a été découvert par

observation lors des études de relation structure-activité (RSA) des PUB-SOs. Le mécanisme d'action de cette famille n'agit pas via une alkylation directe, notamment parce que certains dérivés dont le SFOM-0046 (Figure 1.8F), la molécule prototype de cette famille, ne possédent pas de groupement électrophile tel qu'un atome de chlore sur la chaîne alkyle de l'urée. Les études du nouveau mécanisme d'action des PUB-SOs en biologie en utilisant le SFOM-0046 ont montré qu'ils induisent la phosphorylation de l'histone 2AX (H2AX) en γH2AX, un marqueur de stress réplicatifs à l'ADN. De plus, le SFOM-0046 active préférentiellement le sentier signalétique ATR-Chk1 qui est associé à des bris simple-brins et ces lésions sont réparées par recombinaison homologue, un mécanisme de réparation de l'ADN favorisé en phase S [78]. Plusieurs études en biologie ont été conduites pour identifier la cible moléculaire de cette nouvelle famille de composés dont des études sur la topoisomérase I et la thiorédoxine réductase. Néanmoins, ces études n'ont pas été concluantes et la cible moléculaire restait à être identifiée. C'est dans ce contexte que le SFOM-0046, une molécule prototype de cette famille de composé a été envoyée au NCI-60 Human Tumor Cell Lines Screen, un important service pour la recherche dans le domaine du cancer. Ce service effectue rapidement, et ce de façon gratuite des essais antiprolifératifs sur 60 lignées cellulaires cancéreuses. Par la suite, l'algorithme d'analyse COMPARE exploitant les différentes sensibilités des lignées cancéreuses au SFOM-0046 a été utilisé et a permis d'identifier la *h*DHODH comme cibles pharmacologiques potentielles. De récents travaux ont montré que le SFOM-0046 inhibe l'activité de la *h*DHODH d'une manière dépendante de sa concentration. D'autres travaux sont en cours au laboratoire afin de confirmer que la *h*DHODH est à la fois la cible pharmacologique du SFOM-0046 et des autres PUB-SOs arrêtant le cycle cellulaire en phase S et induisant le γH2AX [79].

Par ailleurs, les études de RSA sur ces molécules ont permis de mettre en évidence que la cyclisation du groupement *N*-phényl-*N'*-(2-chloroéthyl)urée des PUB-SOs en phénylimidazolidin-2-one a permis d'obtenir les phényl 4-(2-oxoimidazolidin-1-yl)benzènesulfonates (PIB-SOs) et les tétrahydro-2-oxopyrimidin-1(2*H*)-yl (PPB-SOs, Figure 1.8G) [75, 80]. Les PIB-SOs possèdent une activité antiproliférative sur 16 lignées cellulaires cancéreuses de l'ordre du nanomolaire en plus de ne pas être affectés par les lignées résistantes à la colchicine, au paclitaxel, à la vinblastine et à la surexpression de la glycoprotéine P. Néanmoins, les PPB-SOs sont moins actifs que leurs analogues PIB-SOs.

Les PIB-SOs bloquent le cycle cellulaire en phase G2/M et se lient au C-BS menant à la perturbation du cytosquelette et à la mort cellulaire. Ils sont aussi efficaces pour bloquer l'angiogenèse et la croissance tumorale des cellules HT-1080 greffées dans le modèle de la membrane chorioallantoïque (CAM) d'embryons de poulet. Ils présentent également une faible toxicité sur ce modèle [80].

L'importance du pont sulfonate reliant les deux cycles aromatiques des PIB-SOs a aussi été étudiée par son remplacement avec un groupement sulfonamide. Cette modification a mené à la création des phényl 4-(2-oxoimidazolidin-1-yl)benzènesulfonamides (PIB-SAs, Figure 1.8G). Ces dérivés possèdent également une activité antiprolifération de l'ordre du nanomolaire sur 16 lignées cellulaires cancéreuses. Ils stoppent le cycle cellulaire en phase G2/M menant à la perturbation du cytosquelette et à l'apoptose. Par ailleurs, les PIB-SAs possèdent une faible toxicité sur les embryons de poulet et un puissant effet antitumoral et antiangiogénique sur les cellules HT-1080 greffées sur la CAM. Ces travaux ont démontré que le groupement sulfonate et sulfonamide sont des bioisostères [81].

1.9. Problématique et hypothèse

À ce jour, le cancer est encore un des problèmes de santé les plus importants au monde [82]. Au Canada, une personne sur deux sera atteinte du cancer et une sur quatre va en mourir [83]. Malgré les progrès majeurs réalisés depuis la découverte des premiers traitements anticancéreux, de nombreux cancers ont encore de mauvais pronostics et des taux de mortalité élevés [84]. De plus, certains agents anticancéreux utilisés en clinique possèdent des effets délétères importants en plus d'avoir une efficacité limitée et d'être affectés par les phénomènes de chimiorésistance [85]. Pour ces raisons, le développement de nouveaux médicaments visant à améliorer à la fois l'espérance et la qualité de vie des patients atteints d'un cancer est une priorité. À cet effet, l'équipe de recherche du Dr Sébastien Fortin a découvert et a entamé l'étude et l'optimisation des PIB-SOs et des PUB-SOs. Bien que l'activité et les propriétés de plusieurs de ces composés soient prometteuses, l'optimisation de leurs propriétés physicochimiques, pharmacologiques et pharmacocinétiques peut encore être maximisée afin de contourner des problèmes potentiels pouvant survenir lors de leur développement. Dans ce contexte, nous émettons l'hypothèse qu'il soit possible d'optimiser

la structure moléculaire des PIB-SOs et des PUB-SOs en regard de leurs propriétés physicochimiques, pharmacologiques et pharmacocinétiques.

1.10. Objectifs

Mon objectif de recherche général au doctorat était d'étudier les RSAs des PIB-SOs et des PUB-SOs associées à la modification des groupements chimiques sur les cycles aromatiques A et B et du pont sulfonate. Cet objectif général peut se décliner en quatre objectifs plus spécifiques. **Objectif 1.** Concevoir les modifications à réaliser sur la structure moléculaire des PIB-SOs et des PUB-SOs. **Objectif 2.** Préparer, purifier et caractériser les nouvelles molécules à l'aide des outils de la chimie organique classique. **Objectif 3.** Évaluer leur activité antiprolifératives sur les lignées cellulaires cancéreuses modèles du laboratoire. **Objectif 4.** Étudier le(s) mécanisme(s) d'action des composés les plus prometteurs avec l'aide d'essais biofonctionnels notamment : 1) l'arrêt de la progression du cycle cellulaire, 2) l'intégrité des microtubules par immunofluorescence, 3) l'induction de γH2AX, 4) l'inhibition de la polymérisation des microtubules, 5) l'affinité avec le C-BS, 6) leur chimiorésistance sur des cellules résistantes aux agents antimicrotubules et multirésistantes, 7) leur toxicité chez les embryons de poulet et 8) plusieurs propriétés physicochimiques et pharmacocinétiques théoriques importantes dans la conception de médicaments.

De plus, chaque chapitre de ma thèse correspondant à l'insertion d'un article et possède donc un objectif général qui lui est propre.

Le chapitre 2 intitulé : « *Phenyl 4-(2-oxopyrrolidin-1-yl)benzenesulfonates and phenyl 4-(2-oxopyrrolidin-1-yl)benzenesulfonamides as new antimicrotubule agents targeting the colchicine-binding site* » avait pour objectif d'évaluer l'effet de remplacer le groupement imidazolidin-2-one (IMZ) des PIB-SOs et des PIB-SAs par un groupement pyrrolidin-2-one. Cette modification a permis d'évaluer le rôle du groupement NH du fragment IMZ des PIB-SOs et PIB-SAs sur l'activité antiproliférative, la progression du cycle cellulaire, l'intégrité structurelle du cytosquelette et la dynamique des microtubules. L'évaluation de sa capacité à se lier au C-BS *in vitro* et avec un logiciel de modélisation moléculaire était également un objectif de ce chapitre. Finalement, nous souhaitions étudier leur toxicité avec un modèle

d'embryons de poulet et déterminer leurs propriétés pharmacocinétiques et physicochimiques théoriques.

Le chapitre 3 intitulé : « *Preparation, biological evaluation and structure-activity relationships of new phenyl 4-(dioxoimidazolidin-1-yl)benzenesulfonate and ethyl 2-(3-(4-(phenoxysulfonyl)phenyl)ureido)acetate analogs to phenyl 4-(2-oxoimidazolidin-1-yl)benzenesulfonate: study of the imidazolidin-2-one moiety* » avait pour objectif de réaliser une étude de RSA en modifiant le groupement IMZ des PIB-SOs par les groupements dioxoimidazolidin-1-yle et éthyl 2-uréidoacétate. Par la suite, les objectifs étaient d'évaluer les nouveaux analogues pour leur activité antiproliférative, leur effet sur la progression du cycle cellulaire et sur leur capacité à interférer avec le cytosquelette. Nous voulions également évaluer l'effet de ces modifications sur la dynamique des microtubules et sur leur capacité à se lier au C-BS. La détermination de leur effet sur des lignées cellulaires résistantes au paclitaxel, à la vinblastine et sur une lignée cellulaire surexprimant la glycoprotéine P était aussi planifiée. Finalement, nous voulions étudier en modélisation moléculaire les interactions de ces nouveaux composés avec le C-BS et déterminer leurs propriétés pharmacocinétiques et physicochimiques théoriques.

Le chapitre 4 intitulé : « *Rationale, synthesis and biological evaluation of substituted 1-(4-(phenylthio)phenyl)imidazolidin-2-one, urea, thiourea and amide analogs and derivatives designed to target the colchicine-binding site* » avait pour objectif d'étudier l'importance du pont sulfonate des PIB-SOs en combinaison avec le groupement IMZ. L'objectif de ces travaux était donc de réaliser une étude de RSA en remplaçant le pont sulfonate des PIB-SOs par un atome de soufre et dans un deuxième temps en remplaçant le groupement IMZ des PIB-SOs par des groupements butyramide, éthylthiourée, éthylurée, 2-chloroéthylurée et phénylurée. Nous avions l'intention d'étudier l'effet de ces modifications sur l'activité antiproliférative, la progression du cycle cellulaire, l'intégrité structurelle du cytosquelette et leur capacité de se lier au C-BS. Nous voulions également évaluer si l'activité antiproliférative de ces nouveaux composés serait affectée par des lignées cellulaires résistantes au paclitaxel, à la vinblastine et sur une lignée cellulaire surexprimant la glycoprotéine P. Par ailleurs, la détermination de leur toxicité sur les embryons de poulet et

l'évaluation de leurs propriétés pharmacocinétiques et physicochimiques théoriques était planifiée.

Le chapitre 5 intitulé : « *Synthesis and biological evaluation of novel N-phenyl ureidobenzenesulfonate derivatives as potential anticancer agents. Part 2. Modulation of the ring B* » avait pour objectif d'évaluer l'importance de la nature et de la position des différents groupements présents sur le cycle aromatique B des PUB-SOs. Par conséquent, nous avions comme objectif de préparer plusieurs analogues des PUB-SOs en modifiant les groupements présents sur le cycle aromatique B tout en conservant le fragment 2-chloroéthylurée en position 4 sur le cycle A. Nous voulions par la suite les évaluer pour leur activité antiproliférative, leur effet sur la progression du cycle cellulaire et sur leur capacité à induire la phosphorylation de H2AX.

Finalement, le chapitre 6 intitulé : « *Preparation, characterisation and biological evaluation of new phenyl amidobenzenesulfonates and N-phenyl ureidobenzenesulfonates inducing DNA double-strand breaks. Part 3. Modulation of ring A* » avait pour objectif d'étudier l'importance du groupement 2-chloroéthylurée des PUB-SOs. Nous désirions donc moduler la composante 2-chloroéthylurée de PUB-SOs en préparant différents analogues possédant une variété de groupements urées et amides et les évaluer selon leur activité antiproliférative, leur effet sur la progression du cycle cellulaire et sur leur capacité à induire la phosphorylation de H2AX. Finalement, l'évaluation du potentiel alkylant de ces nouveaux dérivés en plus de la détermination de leurs propriétés pharmacocinétiques et physicochimiques théoriques étaient aussi planifiées.

Chapitre 2. Phenyl 4-(2-oxopyrrolidin-1-yl)benzenesulfonates and phenyl 4-(2-oxopyrrolidin-1-yl)benzenesulfonamides as new antimicrotubule agents targeting the colchicine-binding site

Mathieu Gagné-Boulet[a,b], Chahrazed Bouzriba[a,b], Atziri Corin Chavez Alvarez[a,b], Sébastien Fortin[a,b,*]

[a]Centre de recherche du CHU de Québec - Université Laval, Axe oncologie, Hôpital Saint-François d'Assise, 10 rue de l'Espinay, Québec, QC, G1L 3L5, Canada.

[b]Faculté de pharmacie, Université Laval, Québec, QC, G1V 0A6, Canada.

***Corresponding author:** Faculté de pharmacie, Université Laval, Québec, QC, G1V 0A6, Canada; Phone: 418-525-4444 ext. 52364, Fax: 418-525-4372, e-mail: sebastien.fortin@pha.ulaval.ca.

Publié le 6 janvier 2021 dans le European Journal of Medicinal Chemistry, 213, 113136, doi : 10.1016/j.ejmech.2020.113136.

2.1. Résumé

Nous avons récemment conçu et préparé de nouvelles familles d'agents antimicrotubules puissants désignés sous le nom de *N*-phényl 4-(2-oxoimidazolidin-1-yl)benzènesulfonates (PIB-SOs) et de phényl 4-(2-oxoimidazolidin-1-yl)benzènesulfonamides (PIB-SAs). Le but de la présente étude était d'évaluer l'effet de remplacer le groupement imidazolidin-2-one (IMZ) des PIB-SOs et des PIB-SAs par un groupement pyrrolidin-2-one. À cette fin, 15 nouveaux dérivés phényl 4-(2-oxopyrrolidin-1-yl)benzènesulfonate (PYB-SOs) et 15 dérivés phényl 4- (2-oxopyrrolidin-1-yl)benzènesulfonamides (PYB-SAs) ont été conçus, préparés, caractérisés chimiquement et évalués biologiquement. Les PYB-SOs et les PYB-SAs montrent une activité antiprolifération s'échelonnant du bas nanomolaire jusqu'au bas micromolaire. Ils arrêtent la progression du cycle cellulaire en phase G2/M et ils inhibent la polymérisation des microtubules en ciblant le C-BS. Ils présentent également peu ou pas de toxicité envers les embryons de poulet. Enfin, les propriétés physicochimiques et pharmacocinétiques théoriques calculées avec l'algorithme SwissADME montrent que les PYB-SOs et les PYB-SAs sont de nouvelles familles prometteuses d'agents antimicrotubules.

2.2. Abstract

We recently designed and prepared new families of potent antimicrotubule agents designated as phenyl 4-(2-oxoimidazolidin-1-yl)benzenesulfonates (PIB-SOs) and phenyl 4-(2-oxoimidazolidin-1-yl)benzenesulfonamides (PIB-SAs). Our previous structure-activity relationship studies (SAR) focused on the aromatic ring B of PIB-SOs and PIB-SAs leaving the impact of the phenylimidazolidin-2-one moiety (ring A) on the binding to the colchicine-binding site (C-BS) poorly studied. Therefore, the aim of the present study was to evaluate the effect of replacing the imidazolidin-2-one (IMZ) group by a pyrrolidin-2-one moiety. To that end, 15 new phenyl 4-(2-oxopyrrolidin-1-yl)benzenesulfonate (PYB-SO) and 15 phenyl 4-(2-oxopyrrolidin-1-yl)benzenesulfonamide (PYB-SA) derivatives were designed, prepared, chemically characterised and biologically evaluated. PYB-SOs and PYB-SAs exhibit antiproliferative activity in the low nanomolar to low micromolar range (0.0087-8.6 μM and 0.056-21 μM, respectively) on human HT-1080, HT-29, M21 and MCF7 cancer cell lines. Moreover, they block the cell cycle progression in G2/M phase. Immunofluorescence, tubulin affinity and tubulin polymerisation assays show that they inhibit microtubule polymerisation by docking the C-BS. In addition, docking assays with the most potent derivatives show binding affinity toward the C-BS and they also exhibit weak or no toxicity toward chick embryos. Finally, physicochemical properties calculated using the SwissADME algorithm show that PYB-SOs and PYB-SAs are promising new families of antimicrotubule agents.

2.3. Graphical abstract

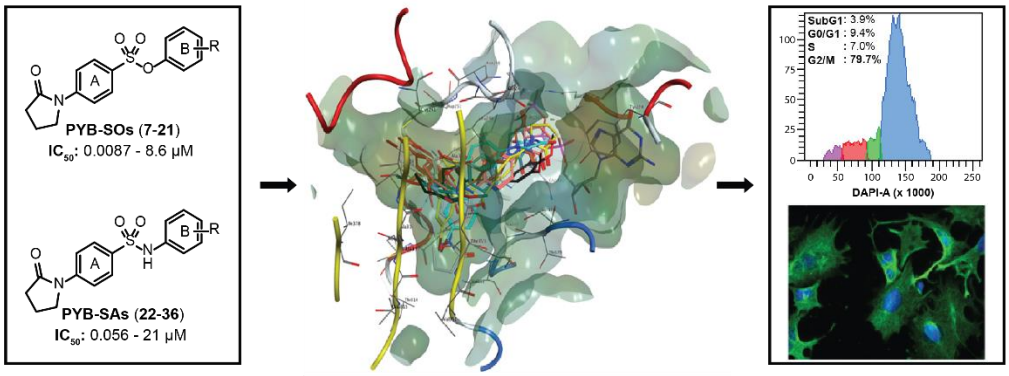

2.4. Introduction

Cancer is a large class of diseases characterised by an uncontrolled and abnormal cellular growth causing serious health issues and ultimately leading to death if untreated. To this day, it is still one of the most important health problems in the world [1]. Indeed, cancer was responsible for approximately 9.6 million deaths worldwide in 2018 [2]. Despite major progress achieved in the past decades, many cancers are still having poor prognoses and high mortality rates [3]. In addition, some anticancer agents currently used in clinical trials still have significant deleterious effects, limited effectiveness and prone to induce chemoresistance. In this context, the development of new antimitotic drugs that aim to improve both the life expectancy and the quality of life of cancer patients is of uttermost importance [4].

Microtubules are the main constituents of the cytoskeleton in eukaryotic cells. They are composed of α, β-tubulin heterodimers, which are in constant dynamic equilibrium between their polymerisation and depolymerisation states [5]. They participate in diverse cellular functions such as cell replication, maintenance of cell shape, mitosis, motility and cellular transport [6]. Therefore, microtubules are an important target in cancer chemotherapy. Antimicrotubule agents are divided into two main classes based on their effect on microtubules: microtubule-stabilising agents and microtubule-destabilising agents. Microtubule-stabilising agents bind to microtubules and stabilise the polymer while microtubule-destabilising agents bind to the tubulin heterodimers and destabilise microtubules. Antimicrotubule agents such as paclitaxel (**1**, Figure 2.1A) have been part of the armamentarium of physicians for treating cancer patients since the 1990s [7, 8]. New antimicrotubule agents are still of interest for several reasons, notably to reduce their toxicity, to improve their effectiveness, to improve their selectivity for given tumours and to reduce their production costs. To that end, new antimicrotubule agents are in preclinical development and are currently undergoing clinical trials [9-11]. Some well-known previously studied compounds include combretastatin A-4 disodium phosphate (CA-4DP, **2**, Figure 2.1B) [12] and T138067 sodium (**3**, Figure 2.1C) [13].

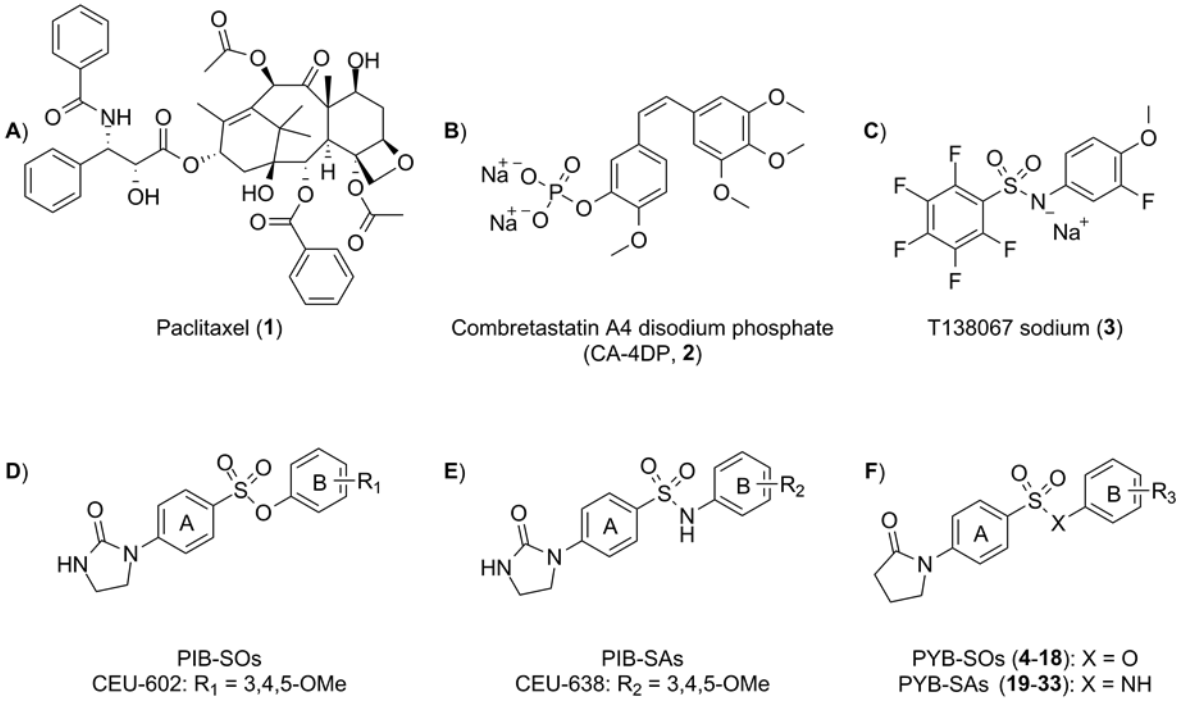

Figure 2.1. Molecular structures of antimicrotubule agents A) paclitaxel (**1**), B) combretastatin A-4 disodium phosphate (CA-4DP, **2**), C) T138067 sodium (**3**), D) phenyl 4-(2-oxoimidazolidin-1-yl)benzenesulfonates (PIB-SOs), E) phenyl 4-(2-oxoimidazolidin-1-yl)benzenesulfonamides (PIB-SAs) F) phenyl 4-(2-oxopyrrolidin-1-yl)benzenesulfonates (PYB-SOs, **4**-**18**) and phenyl 4-(2-oxopyrrolidin-1-yl)-*N*-phenylbenzenesulfonamides (PYB-SAs, **19**-**33**).

To circumvent these impediments, our research group previously designed and developed two new families of antimicrotubule agents designated as phenyl 4-(2-oxoimidazolidin-1-yl)-benzenesulfonates (PIB-SOs, Figure 2.1D) [14] and phenyl 4-(2-oxoimidazolidin-1-yl)-benzenesulfonamides (PIB-SAs, Figure 2.1E) [15]. The molecular structures of PIB-SOs and PIB-SAs comprise two aromatic rings (A and B) linked either by a sulfonate or a sulfonamide bridge. The aromatic ring A is substituted by an imidazolidin-2-one (IMZ) moiety at position 4 while the aromatic ring B bears either a methoxyl group, short alkyl chain or halogen groups in position 3, 4 and/or 5. PIB-SO and PIB-SA derivatives exhibit antiproliferative activity in the nanomolar to low micromolar range on numerous human cancer cell lines, notably HT-1080 fibrosarcoma, HT-29 colon adenocarcinoma, M21

skin melanoma and MCF7 oestrogen-dependent breast adenocarcinoma. Moreover, they induce arrest of the cell cycle progression in G2/M phase and they inhibit microtubule polymerisation and cytoskeleton disruption by targeting the colchicine-binding site (C-BS) located at the interface of the α, β-tubulin heterodimer [14, 15].

Previous structure-activity relationship (SAR) studies were focusing almost exclusively on the aromatic ring B and showed that the substitution in positions 3, 3,5 or 3,4,5 are required to maintain both the antiproliferative activity in the nanomolar range and the high-binding affinity for the C-BS. SAR studies on the aromatic ring A evidenced that the IMZ moiety cannot be modified easily without losing the biological activity [14-17]. In addition, our molecular modeling experiments using PIB-SOs and PIB-SAs suggested that the substituent shape is more important than hydrogen bonds and electrostatic forces since the binding pocket is clearly hydrophobic and mostly driven by van der Waals forces [16]. Consequently, the importance of the NH group of the IMZ moiety for the interaction of PIB-SOs and PIB-SAs with the C-BS remains to be studied.

In this study, we investigate the impact of the NH group of the IMZ moiety of PIB-SOs and PIB-SAs on the biological activity by replacing the NH group by a CH_2 group. Therefore, a new series of phenyl 4-(2-oxopyrrolidin-1-yl)benzenesulfonates (PYB-SOs, Figure 2.1E) as well as a new series of 4-(2-oxopyrrolidin-1-yl)-*N*-phenylbenzenesulfonamides (PYB-SAs, Figure 2.1F) were prepared. PYB-SOs and PYB-SAs were first assessed for their antiproliferative activity on HT-1080, HT-29, M21 and MCF7 human cancer cell lines. The most potent compounds were assessed for their potential to arrest M21 cell cycle progression. Afterwards, they were evaluated for their potency to disrupt the cytoskeleton and inhibit microtubule polymerisation. Furthermore, we assessed our most potent derivatives for their binding affinity for the C-BS and their toxicity on chick embryos. Finally, their biopharmaceutical properties were assessed using SwissADME free web tool [18].

2.5. Chemistry

The preparation of PYB-SOs (**4-18**) and PYB-SAs (**19-33**) is depicted in Scheme 2.1 and was achieved within four steps. Briefly, the general synthesis started with the

nucleophilic addition of aniline on 4-chlorobutanoyl chloride in presence of triethylamine in methylene chloride followed by the intramolecular cyclization of 4-chloro-*N*-phenylbutanamide (**34**) into 1-phenylpyrrolidin-2-one (**35**) by addition of sodium hydride in tetrahydrofuran. Chlorosulfonation of **35** with chlorosulfonic acid gave the 4-(2-oxopyrrolidin-1-yl)benzenesulfonyl chloride (**36**). Finally, PYB-SOs (**4**-**18**) and PYB-SAs (**19**-**33**) were prepared by the nucleophilic addition of a relevant phenol in presence of triethylamine or a relevant aniline in presence of 4-dimethylaminopyridine to **36** in acetonitrile under microwaves.

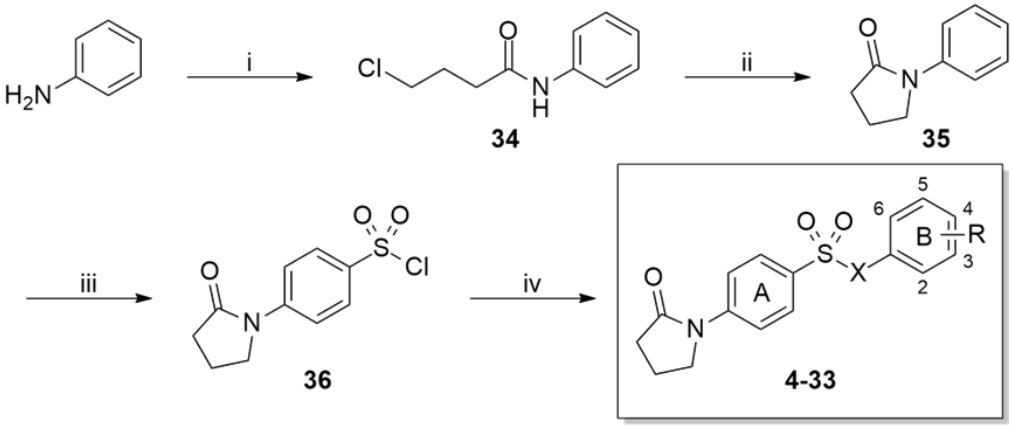

4: X = O, R = H
5: X = O, R = 2-*i*prop
6: X = O, R = 2-Ph
7: X = O, R = 2-OMe
8: X = O, R = 3-OMe
9: X = O, R = 3-F
10: X = O, R = 3-Cl
11: X = O, R = 3-Br
12: X = O, R = 3-I
13: X = O, R = 3,4-OMe
14: X = O, R = 3,5-OMe
15: X = O, R = 3,5-Br
16: X = O, R = 3,4,5-OMe
17: X = O, R = 4-OMe
18: X = O, R = 4-Ph
19: X = NH, R = H
20: X = NH, R = 2-*i*prop
21: X = NH, R = 2-Ph
22: X = NH, R = 2-OMe
23: X = NH, R = 3-OMe
24: X = NH, R = 3-F
25: X = NH, R = 3-Cl
26: X = NH, R = 3-Br
27: X = NH, R = 3-I
28: X = NH, R = 3,4-OMe
29: X = NH, R = 3,5-OMe
30: X = NH, R = 3,5-Br
31: X = NH, R = 3,4,5-OMe
32: X = NH, R = 4-OMe
33: X = NH, R = 4-Ph

Scheme 2.1. Reagents and conditions: (i) 4-chlorobutanoyl chloride, CH_2Cl_2, rt, 24 h, 78%; (ii) NaH, THF, 0 °C to rt, 24 h, 86%; (iii) $ClSO_3H$, 0 °C to rt, overnight, 72%; (iv) relevant phenol, TEA, CH_3CN, 120 °C under microwaves, 8 h, 31 to 97% or relevant aniline, DMAP, CH_3CN, 120 °C under microwaves, 8 h, 18 to 67%.

2.6. Results/discussion

2.6.1. PYB-SOs and PYB-SAs exhibit antiproliferative activity on human cancer cells

The antiproliferative activity of PYB-SOs (**4-18**) and PYB-SAs (**19-33**) was assessed on the HT-1080 fibrosarcoma, HT-29 colon adenocarcinoma, M21 skin melanoma and MCF7 oestrogen-dependent breast adenocarcinoma using the sulforhodamine B colorimetric assay and the results are listed in Table 2.1 and correspond to the concentration of drug needed to inhibit 50% of cell growth (IC_{50}). Combretastatin A-4 (CA-4), PIB-SO (CEU-602) and PIB-SA (CEU-634) bearing a 3,4,5 trimethoxyl group on ring B that were the most potent PIB-SO and PIB-SA prepared so far were used as positive controls [14, 15]. PYB-SOs and PYB-SAs exhibit antiproliferative activity ranging from the low nanomolar to the low micromolar levels on all cancer cell lines tested (0.0087-8.6 μM for PYB-SOs and 0.056-21 μM for PYB-SAs, respectively). Globally, PYB-SOs are more potent than their PYB-SA counterparts. The sensitivity of cell lines to PYB-SOs and PYB-SAs usually decreases according to the following order: MCF7 > HT-29 ≈ M21 > HT-1080. The disubstitution of the aromatic ring B in positions 3 and 5 by methoxyl and bromo groups and trisubstitution in positions 3, 4 and 5 by methoxyl groups are the most favourable substitutions leading to maximal antiproliferative activities. PYB-SOs **15** and PYB-SAs **31** are the most potent derivatives with IC_{50} ranging from 8.7 to 11 nM and 56 to 130 nM, respectively. Furthermore, the most active PYB-SOs, bearing either a 3,5-dimethoxyl (**14**), a 3,5-dibromo (**15**) or a 3,4,5-trimethoxyl (**16**) groups exhibited antiproliferative activities (8.7 to 39 nM) similar to CA-4 (1.9 to 5.1 nM), CEU-602 (4.0 to 5.9 nM) and CEU-638 (13 to 21 nM) used as positive controls. Finally, these results confirm that the NH group of IMZ moiety of PIB-SOs is not essential to the antiproliferative activity.

Table 2.1. Antiproliferative activity (IC_{50}) of PYB-SOs (**4-18**) and PYB-SAs (**19-33**) on HT-1080, HT-29, M21 and MCF7 human cancer cell lines.

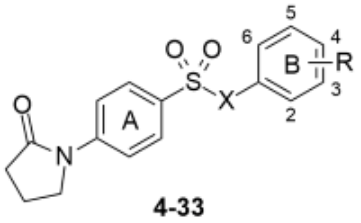

4-33

#	X	R	IC_{50} (nM)[1]			
			HT-1080	**HT-29**	**M21**	**MCF7**
4	O	H	920	480	460	650
5	O	2-*i*prop	840	780	910	500
6	O	2-Ph	370	350	190	210
7	O	2-OMe	1300	1200	1300	890
8	O	3-OMe	190	120	120	100
9	O	3-F	810	310	300	370
10	O	3-Cl	180	120	110	140
11	O	3-Br	80	60	40	60
12	O	3-I	40	59	88	22
13	O	3,4-OMe	590	690	650	290
14	O	3,5-OMe	26	39	12	21
15	O	3,5-Br	11	10	8.7	11
16	O	3,4,5-OMe	11	16	13	17
17	O	4-OMe	8500	4800	7500	4600
18	O	4-Ph	2600	2900	2300	1700
19	NH	H	4900	3400	5600	2800
20	NH	2-*i*prop	21000	12000	9900	16000
21	NH	2-Ph	1200	730	430	960
22	NH	2-OMe	3200	2400	3000	1800
23	NH	3-OMe	1300	860	940	1100
24	NH	3-F	840	5400	2300	680
25	NH	3-Cl	680	680	770	560
26	NH	3-Br	1300	590	950	830
27	NH	3-I	860	390	330	600
28	NH	3,4-OMe	2250	890	5100	2600
29	NH	3,5-OMe	990	1300	390	690
30	NH	3,5-Br	590	390	280	520
31	NH	3,4,5-OMe	130	80	56	88

32	NH	4-OMe	8500	4800	7500	4600
33	NH	4-Ph	8800	5400	4700	7000
CEU-602	O	3,4,5-OMe	5.9	4.0	4.0	5.0
CEU-638	NH	3,4,5-OMe	17	21	13	18
CA-4[2]	N/A	N/A	2.2	5.1	2.2	1.9

[1]IC_{50}: concentration of drug inhibiting cell growth by 50%. [2]CA-4: Combretastatin A-4.

2.6.2. PYB-SO and PYB-SA derivatives arrest the cell cycle progression in G2/M phase

Antimicrotubule agents are known to arrest the cell cycle progression during the G2/M phase. To verify if the mechanism of action underlying the antiproliferative activity of PYB-SOs and PYB-SAs with PIB-SOs and PIB-SAs that were used as molecular scaffolds, we first assessed their effect on the cell cycle progression of M21 cells [14, 15]. To that end, PYB-SOs **11**, **12** and **14**-**16**, and PYB-SAs **21**, **25**, **27** and **29**-**31** were incubated with M21 cells at 2 and 5-times their respective IC_{50} for 24 h. The results depicted in Figure 2.2 show the optimal concentration (either 2- or 5-times the IC_{50}) for a maximal arrest of the cell cycle progression in the G2/M phase. As shown in Figure 2.2, cells treated with 0.5% DMSO (negative control) were at 5.0, 65.5, 16.1 and 13.4% in subG1, G0/G1, S and G2/M phases, respectively. CA-4 was used as positive control and showed a population increase in G2/M phase by 66.1%. Except PYB-SA **21** bearing a phenyl substituent in position 2, all PYB-SOs and PYB-SAs assessed increased the cell population in G2/M phase by 28.8 to 68.4%. Furthermore, PYB-SOs and PYB-SAs bearing the same substituent have a similar effect on the cell cycle progression, which indicates that the modification of the sulfonate bridge by a sulfonamide moiety does not affect their ability to arrest the cell cycle progression in the G2/M phase. In general, PYB-SOs and PYB-SAs bearing multiple substitutions have higher potential to arrest the cell cycle in G2/M phase than those bearing only one substitution. Finally, PYB-SO **16** exhibits the most potent cell cycle arrest in G2/M phase showing a population increase in G2/M phase by 68.4%, which is similar to CA-4.

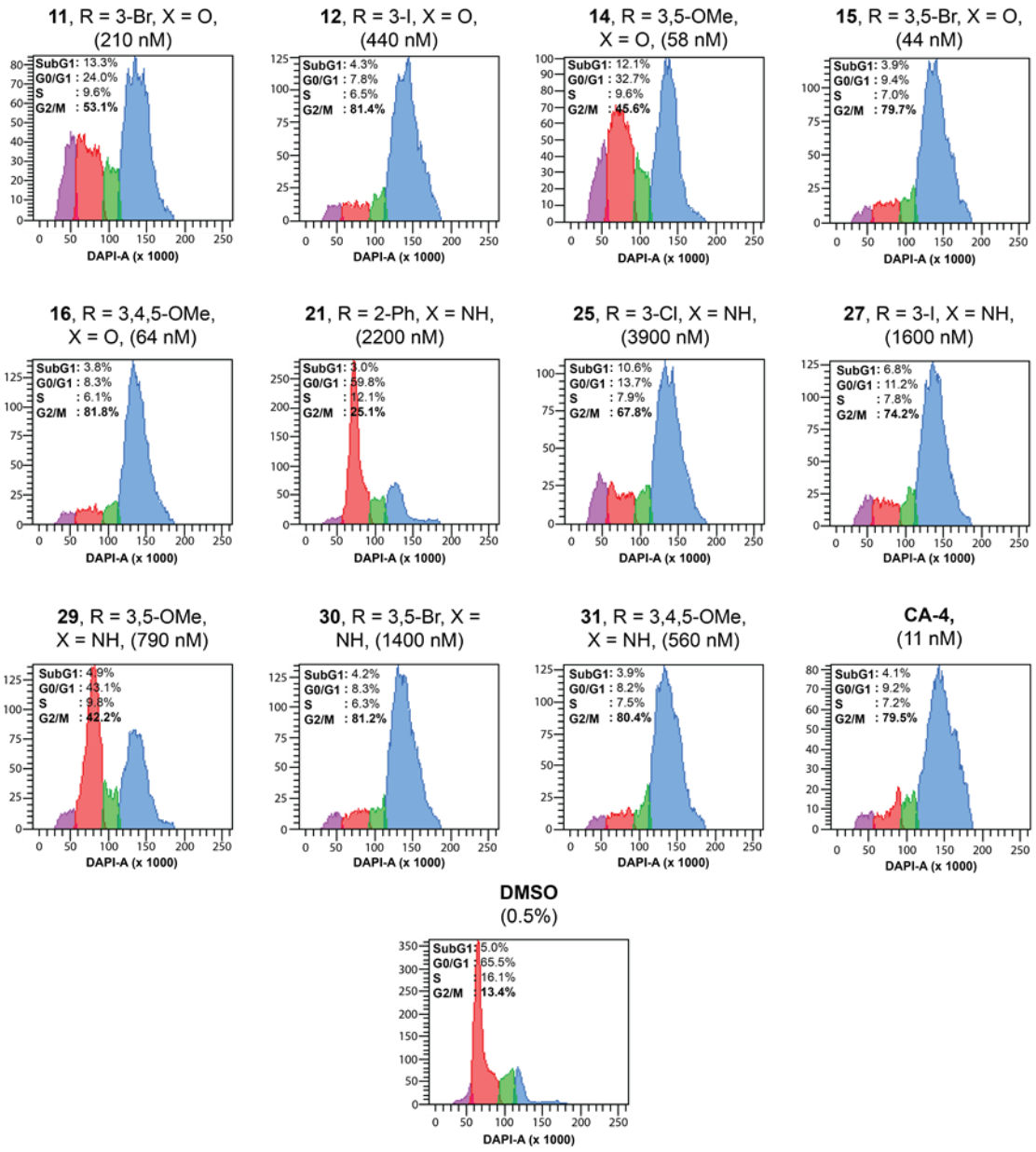

Figure 2.2. Effect of PYB-SOs **11**, **12**, **14-16** and PYB-SAs **21**, **25**, **27**, **29-31** on the cell cycle progression of M21 cells after 24 h of treatment. CA-4 and DMSO were used as controls.

2.6.3. PYB-SOs and PYB-SAs induce cytoskeleton disruption

Since PYB-SOs and PYB-SAs arrest the cell cycle progression in the G2/M phase, we evaluated their ability to induce cytoskeleton disruption by interfering with microtubules. To

that end, we selected our three most potent PYB-SOs (**14-16**) and PYB-SAs (**27**, **30** and **31**) for their effect on microtubules and cytoskeleton integrity of M21 cells when they are incubated at 5-times their respective IC_{50} for 24 h. Cellular microtubule structures were visualised with indirect immunofluorescence using an anti-β-tubulin monoclonal antibody. CA-4 and paclitaxel were used as positive controls while DMSO (0.5%) was used as negative control. As depicted in Figure 2.3, PYB-SOs and PYB-SAs disrupt microtubules and induce mitotic abnormalities similarly to CA-4. Therefore, PYB-SOs and PYB-SAs are antimicrotubule agents inducing cytoskeleton disruption similarly as reported for CA-4, CEU-602 and CEU-638 [14, 15].

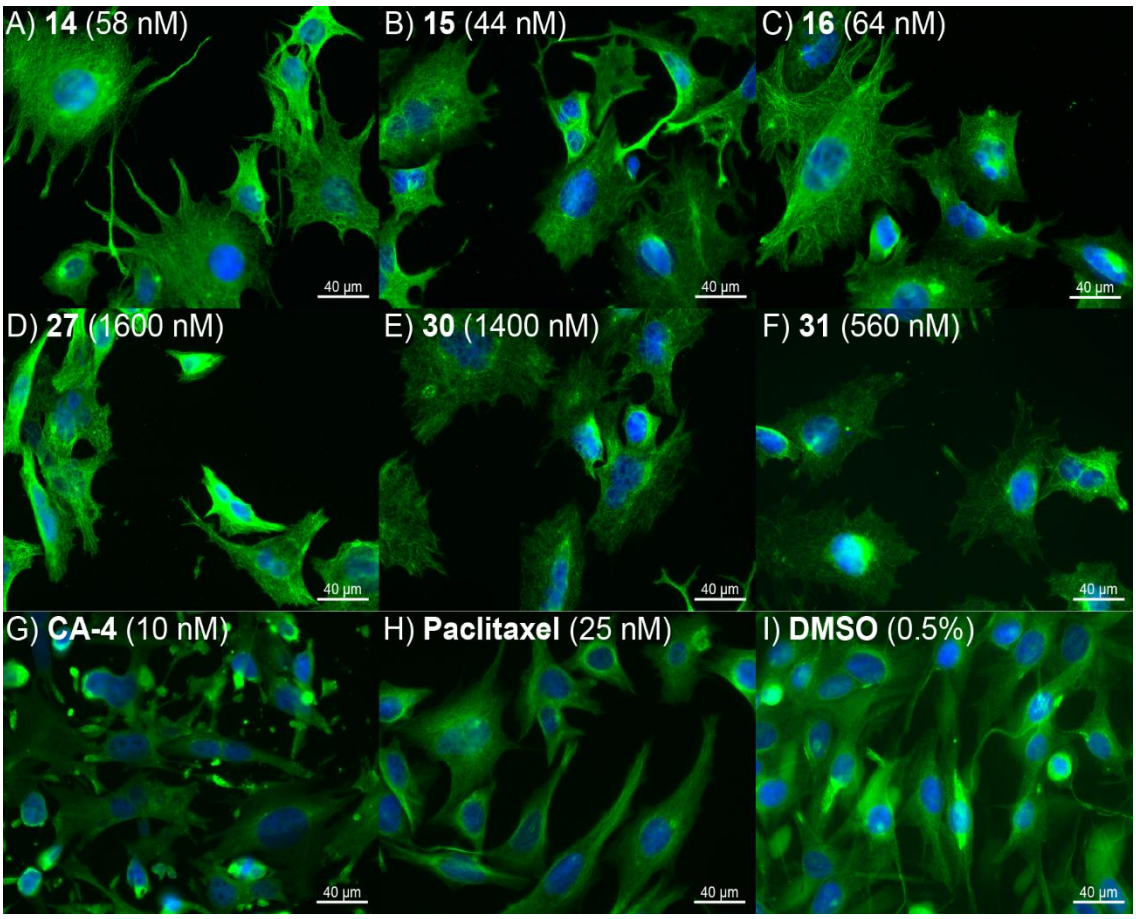

Figure 2.3. Effect of PYB-SOs **14-16** and PYB-SAs **27**, **30** and **31** on cytoskeleton integrity of M21 cells after 24 h of treatment (400-times total magnification). CA-4 and paclitaxel were used as positive controls while DMSO was used as negative control.

2.6.4. PYB-SOs and PYB-SAs inhibit microtubule polymerisation

To confirm the effect of PYB-SOs and PYB-SAs on microtubules, we assessed the effect of PYB-SOs **14** and **15** and PYB-SAs **30** and **31** on dynamic polymerisation of tubulin to microtubules [19]. The curves shown in Figure 2.4 are representative of two separated experiments. As shown in Figure 2.4, microtubule formation rates are displayed over a period of 60 min at 37 °C. 15 µM of a microtubule-destabilising agent (CA-4) and 3.0 µM of a microtubule-stabilising agent (paclitaxel) were used as positive controls while DMSO (0.5%) was used as negative control. The concentrations of PYB-SOs **14** (30 µM) and **15** (3.0 µM) as well as PYB-SAs **30** (3.0 µM) and **31** (15 µM) were determined by maximal solubility in the buffer solution. Our results show that CA-4 inhibits tubulin polymerisation while paclitaxel stabilises tubulin polymerisation. PYB-SOs **14** and **15** and PYB-SA **31** strongly inhibit tubulin polymerisation similarly to CA-4 while the inhibition of tubulin polymerisation by PYB-SA **30** is slightly lower. PYB-SA **31** show the most potent inhibition of tubulin polymerisation. These results strongly indicate that the mechanism of action of PYB-SOs and PYB-SAs is the inhibition of polymerisation of tubulin to microtubules.

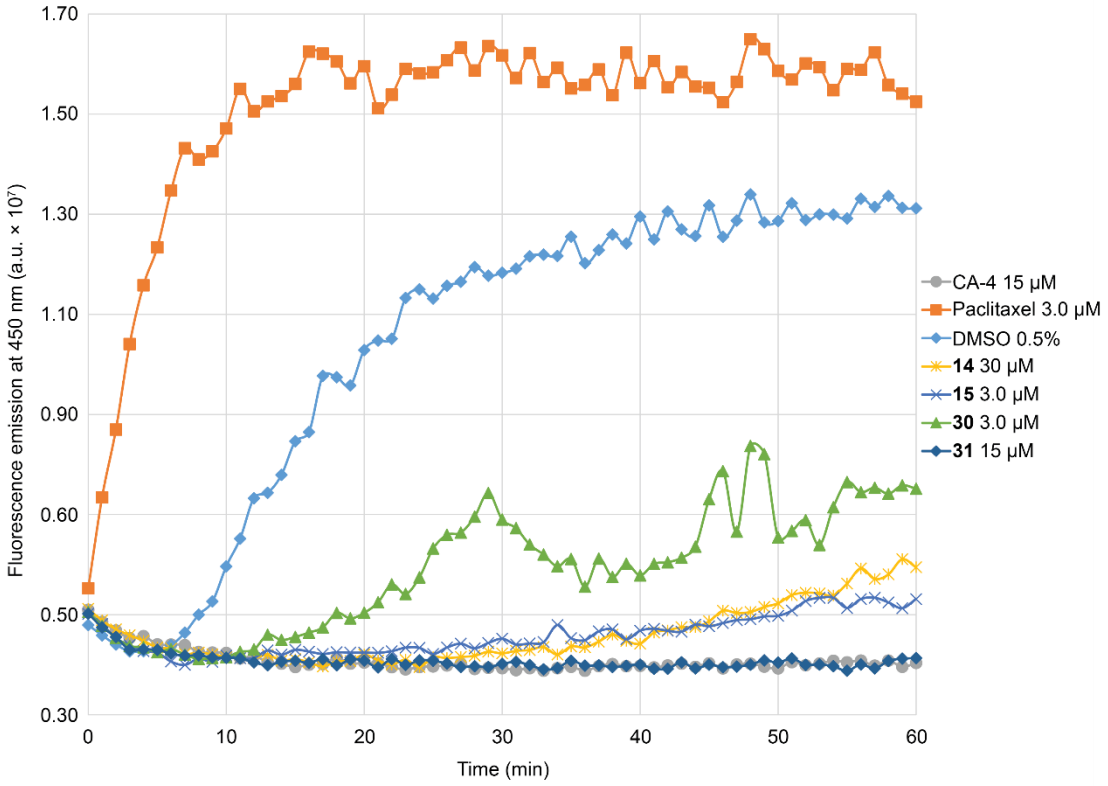

Figure 2.4. Effect of PYB-SOs **14** and **15** and PYB-SAs **30** and **31** on tubulin assembly. CA-4 and paclitaxel were used as positive controls while DMSO was used as negative control.

2.6.5. PYB-SOs and PYB-SAs bind to the colchicine-binding site

It is known that antimicrotubule agents can interact with microtubules or tubulin heterodimers through different binding sites [20]. Moreover, PIB-SOs, PIB-SAs and CA-4 are known to dock into the C-BS [14, 15]. In this context, we used a detection technique developed by our laboratory to study the binding of PYB-SOs and PYB-SAs with the C-BS [21]. This assay is based on the *N*,*N*'-ethylene-bis(iodoacetamide) (EBI) which crosslinks cysteines in positions 239 and 354 located in the C-BS. This adduct is conveniently detectable by Western blot as a second immunoreacting band of β-tubulin. Antimicrotubule compounds that bind to the C-BS inhibit the formation of the β-tubulin adduct with EBI. To that end, we also used PYB-SOs **14-16**, and PYB-SAs **27**, **30**, and **31** at 100- and 1000-times their respective IC_{50}. The maximum concentration used in this experiment was 100 µM. As displayed in Figure 2.5, all PYB-SOs and PYB-SAs tested inhibit the formation of the EBI: β-tubulin adduct similarly to CA-4 and illustrated by the loss of the second immunoreacting

band of β-tubulin and the presence of the native β-tubulin band [21]. These results show that both PYB-SO and PYB-SA derivatives bind efficiently to the C-BS leading to the inhibition of the polymerisation of microtubules, disruption of the cytoskeleton and also the arrest of the cell cycle progression in G2/M phase. This evidences the bioisosterism between 2-oxopyrrolidin-1-yl and the IMZ moieties of PIB-SOs and PIB-SAs and that the nitrogen atom of the IMZ moiety is not involved in indispensable interactions in the C-BS.

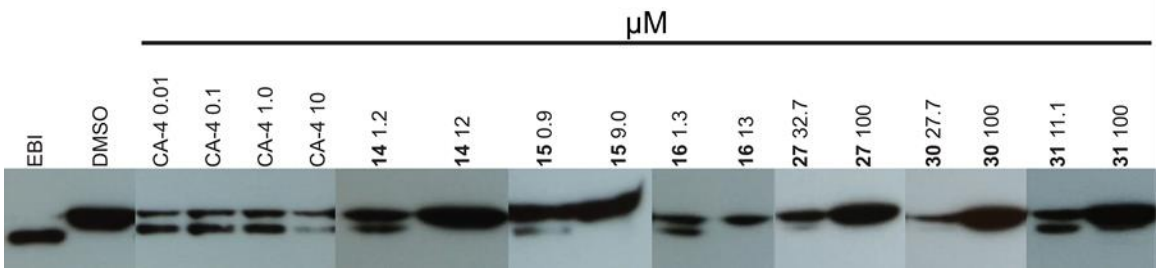

Figure 2.5. Effect of PYB-SOs **14-16** and PYB-SAs **27**, **30** and **31** on the binding of EBI to the colchicine-binding site at 100 and 1000-times their respective IC_{50}. CA-4 was used as positive control while DMSO and EBI were used as negative and positive controls, respectively.

2.6.6. PYB-SOs 14 and 15 and PYB-SAs 30 and 31 dock into the C-BS

In the aim to predict the active conformation of PYB-SOs and PYB-SAs and to identify the key amino acids involved in their interactions with the C-BS, molecular docking studies were performed to prepare a binding model derived from tubulin (protein data bank (PDB): 1SA0) [22] using the docking tool in the Molecular Operating Environment (MOE) software. The C-BS used to build our computational model is constituted of GTP and 32 amino acids distributed in the vicinity of the colchicine and GTP. The energy docking results of the 5 most favourable poses of PYB-SOs **14** and **15** and PYB-SAs **30** and **31** in the C-BS are shown in Table 2.2. Firstly, the most favourable docking poses of PYB-SOs **14** and **15** and PYB-SAs **30** and **31** showing the lowest S-score (-7.49, -7.29, -7.08 and -7.90 kcal/mol, respectively) are depicted in Figure 2.6. In addition, the superposition of these most favourable docking poses is illustrated in Figure 2.7. Our results indicate that the molecular structure of selected PYB-SOs and PYB-SAs has the ability to dock into the C-BS. PYB-SO **14** and PYB-SA **30** are positioned into the C-BS similarly while PYB-SO **15** and PYB-SA

31 adopt different poses. Figure 2.8 illustrates 2D interaction diagrams of the most favourable PYB-SO and PYB-SA poses and Table 2.3 summarises their key interactions with amino acids present into the C-BS. The aromatic ring B of compound **14** perform a pi-H interaction with Leu248, while compound **15** is generating two distinct H-donor interactions with Ala317 and Val238, respectively through its bromine atoms and it also forms an H-acceptor interaction with Lys352 via its ketone moiety. In our model, the most favourable poses for PYB-SAs **30** and **31** are not driven by pi-H, hydrogen bonds or halogen bonds but driven by Van der Waals interaction with the C-BS. These results indicate that both amino acids (Leu248, Ala317, Val238 and Lys352) and conformation poses are important for the interactions of PYB-SOs and PYB-SAs with the C-BS.

Table 2.2. Docking energy scores of the five most favorable poses of PYB-SOs **14** and **15** and PYB-SAs **30** and **31** in the colchicine-binding site.

	14		**15**		**30**		**31**	
Pose	S (kcal/mol)	RMSD refine (Å)	S (kcal/mol)	RMSD refine (Å)	S (kcal/mol)	RMSD refine (Å)	S (kcal/mol)	RMSD refine (Å)
1	-7.49	1.13	-7.29	1.49	-7.08	1.19	-7.90	1.90
2	-7.30	1.79	-7.12	2.67	-7.05	0.91	-7.84	1.96
3	-7.25	2.02	-7.02	2.75	-6.86	2.08	-7.79	1.13
4	-7.23	1.03	-6.91	1.19	-6.79	1.77	-7.76	2.82
5	-7.04	1.85	-6.89	1.99	-6.78	1.56	-7.73	1.61

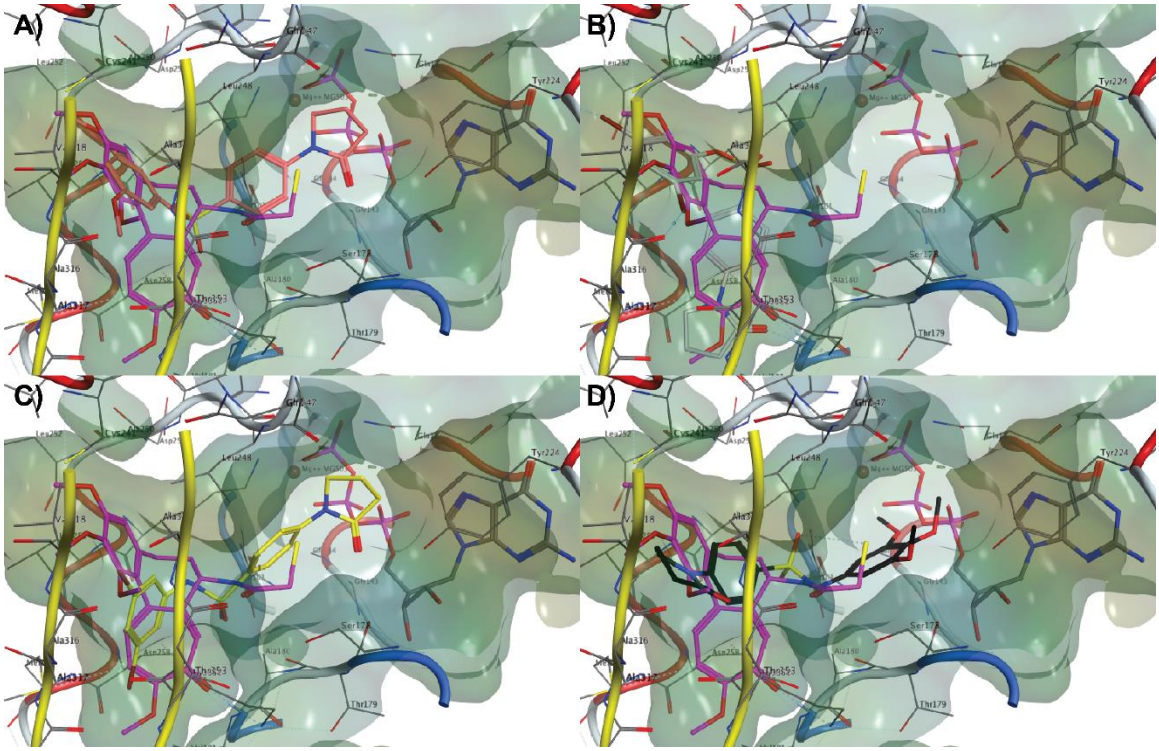

Figure 2.6. Docking of the most stable poses of PYB-SOs and PYB-SAs superposed with colchicine (purple). A) **14** (red), B) **15** (white), C) **30** (yellow) and D) **31** (black) into the colchicine-binding site.

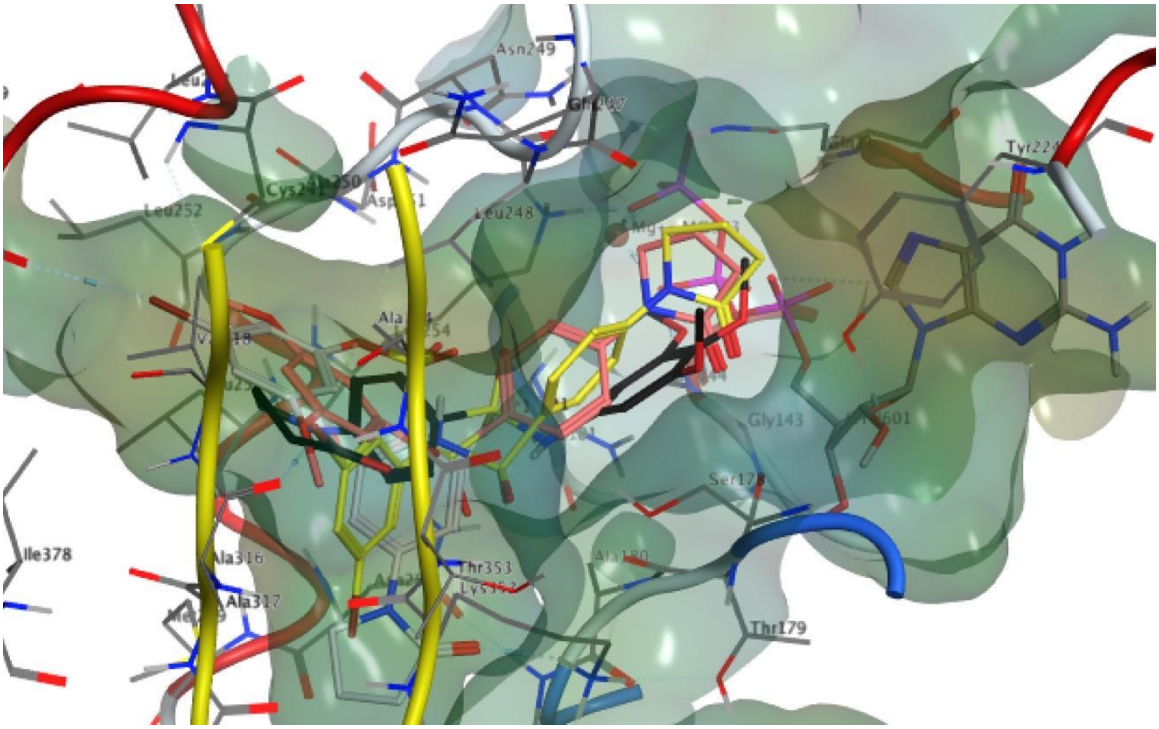

Figure 2.7. Superposition of the docking of the most stable poses of PYB-SOs and PYB-SAs into the colchicine-binding site. Color coding: **14** (red), **15** (white), **30** (yellow) and **31** (black).

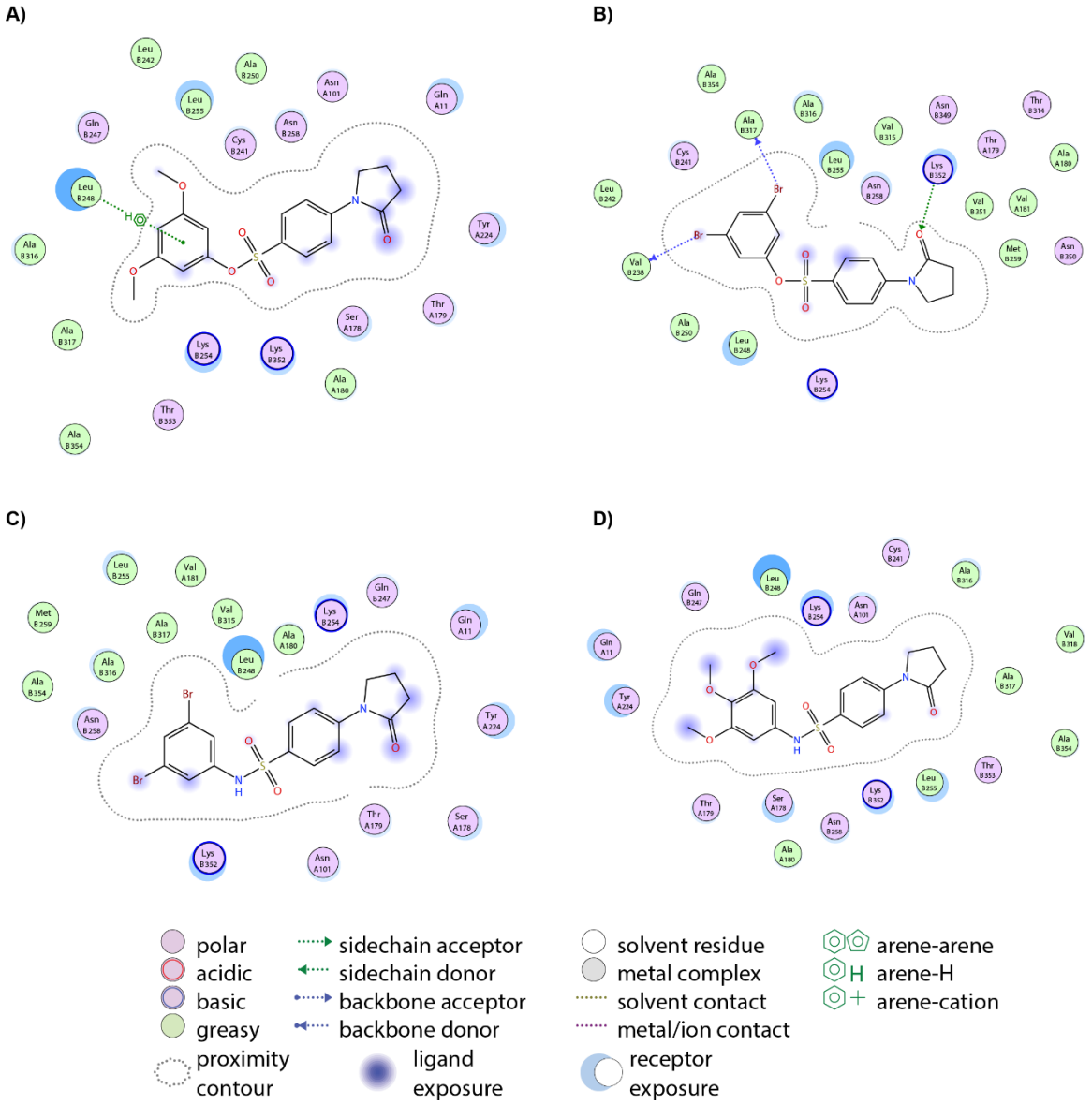

Figure 2.8. 2D interaction diagrams of the most stable poses of PYB-SOs and PYB-SAs into the colchicine-binding site A) **14**, B) **15**, C) **30** and D) **31**.

Table 2.3. Interactions summary of PYB-SOs **14**, **15** and PYB-SAs **30** and **31** with the amino acids of the colchicine-binding site.

	Ligand Atom	Receptor Atom	Interaction		Distance (Å)	Energy (Kcal/mol)
			Amino Acid	Type		
14	6-ring	CD1	Leu248	pi-H	3.53	-0.5
15	Br	O	Ala317	H-donor	3.50	-0.6
	Br	O	Val238	H-donor	3.39	-1.5
	O	NZ	Lys352	H-acceptor	3.20	-6.2
30	-	-	-	-	-	-
31	-	-	-	-	-	-

2.6.7. PYB-SOs and PYB-SAs have low to no toxicity toward chick embryos

The toxicity of the most potent PYB-SOs **14** and **15** and PYB-SAs **30** and **31** was assessed on chick embryos. A mixture of 1.0% DMSO, 6.2% cremophor EL™, 6.2% ethanol (99%) and 86.6% PBS was used as excipient to administrate PYB-SOs **14** (20 μg/egg) and **15** (10 μg/egg) and PYB-SAs **30** (10 μg/egg) and **31** (1 μg/egg). A group of untreated chick embryos as well as another group of chick embryos that were exclusively treated with the excipients were used as negative controls. Drugs were injected at their maximum solubility in the formulation. The percentages of weight of different groups relative to the weight of untreated embryos are depicted in Figure 2.9. First, the formulation is not toxic since there is no statistically significant difference between the untreated and the excipient groups (100% vs 95%, F value of 0.58 compared to a critical F value of 4.11). Second, the percentage of weight of embryos treated by PYB-SOs **14** and **15** and PYB-SAs **30** and **31** relative to the weight of embryos untreated are 95, 93, 83 and 93%, respectively. Third, the percentage of death embryos of untreated, excipient, PYB-SOs **14** and **15** and PYB-SAs **30** and **31** are 17, 18, 18, 18, 25 and 8%, respectively. Although PYB-SA **30** has a lower percentage of embryos weight and a higher death rate, these percentage differences are not statistically significant with the excipient. Our results show that PYB-SOs and PYB-SAs have very low to no toxicity toward chick embryos and present important feature for the future development of this new family of antimicrotubule agents.

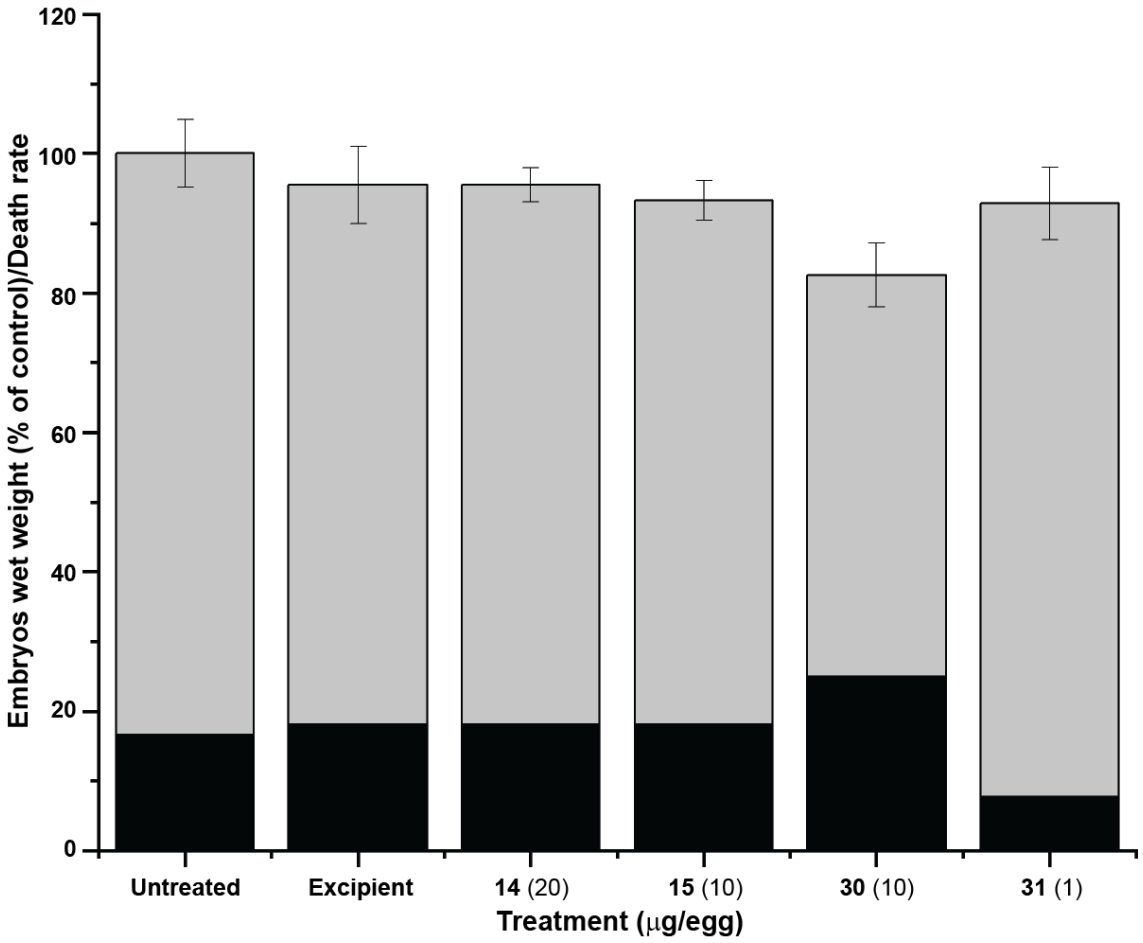

Figure 2.9. Effect of PYB-SOs **14** and **15** and PYB-SAs **30** and **31** on the weight and the mortality of chick embryos. Grey bars represent the percentage of wet weight embryos relative to untreated wet weight embryos. Black bars represent the percentage of chick embryo mortality.

2.6.8. PYB-SOs and PYB-SAs have drug-like properties

Pharmacokinetics, physicochemical and drug-likeness properties are important in the development of new medicinal entities. To that end, we used the SwissADME free online tool to estimate the effect of structural modifications of our new PYB-SOs and PYB-SAs on their theoretical pharmacokinetics, physicochemical and druglikeness properties [18]. PYB-SOs **11**, **12** and **14**-**16** and PYB-SAs **21**, **25**, **27** and **29**-**31** were selected for analysis and the results are summarised in Table 2.4. First, PYB-SOs and PYB-SAs have molecular weights ranging from 377.41 to 475.15 and 350.82 to 474.17 g/mol, respectively. The number of

rotatable bonds varies from 4 to 7 for both classes of compounds. PYB-SO derivatives have 4 to 7 H-bond acceptors and 0 H-bond donor while PYB-SA derivatives have 3 to 6 H-bond acceptors and 1 H-bond donor. The topological polar surface area (TPSA) ranges from 72.06 to 99.75 and 74.86 to 102.55 $Å^2$ for PYB-SOs and PYB-SAs, respectively. The CLogP varies from 2.54 to 3.78 and 1.98 to 3.37 for PYB-SOs and PYB-SAs, respectively while LogS varies from -5.04 to -3.93 and -4.76 to -3.39. In general, compounds bearing a 3,5-dimethoxyl of a 3,4,5-trimethoxyl group are more soluble than their halogenated counterparts regardless of the presence of a sulfonate or a sulfonamide bridge. Globally, all compounds exhibit roughly similar ClogP and LogS and are either in the moderately soluble or soluble class. Moreover, all PYB-SOs and PYB-SAs evaluated so far have a high probability of gastrointestinal absorption (GIA). Beside compounds **11**, **12**, **25** and **27**, all PYB-SOs and PYB-SAs are predicted to be able to diffuse through the blood-brain barrier (BBB). PYB-SOs and PYB-SAs at the exception of compounds **29** and **31** should not be substrate of the P-glycoprotein, an efflux protein that is responsible for multidrug resistance. Of interest, PYB-SOs and PYB-SAs do not exhibit violation of either the Lipinski, Veber, Egan or Muegge filters, which means that these compounds have the potential to be absorbed through the gastrointestinal tract. Therefore, PYB-SOs and PYB-SAs display high theoretical druglikeness properties and bioavailability scores despite chemical and structural modulations showing that PYB-SOs and PYB-SAs are promising for *in vivo* experiments.

Table 2.4. Physicochemical properties, pharmacokinetic properties and druglikeness of PYB-SOs **11**, **12**, **14**-**16**, and PYB-SAs **21**, **25**, **27**, **29**-**31** calculated using the web-based SwissADME application.

#	Rb[1]	H-Ba[2]	H-BD[3]	TPSA[4] (Å^2)	CLogP[5]	LogS[6]	Sclass[7]	GIA[8]	BBBP[9]	Pgp[10]	Drug-like (#viol.)[11]
11	4	4	0	72.06	3.15	-4.32	MS	H	Yes	No	Yes (0)
12	4	4	0	72.06	3.20	-4.27	MS	H	Yes	No	Yes (0)
14	6	6	0	90.52	2.56	-3.93	S	H	No	No	Yes (0)
15	4	4	0	72.06	3.78	-5.04	MS	H	No	No	Yes (0)
16	7	7	0	99.75	2.54	-4.09	MS	H	No	No	Yes (0)
21	5	3	1	74.86	3.37	-4.76	MS	H	No	No	Yes (0)
25	4	3	1	74.86	2.60	-3.72	S	H	Yes	No	Yes (0)
27	4	3	1	74.86	2.75	-3.74	S	H	Yes	No	Yes (0)
29	6	5	1	93.32	2.10	-3.39	S	H	No	Yes	Yes (0)
30	4	3	1	74.86	3.31	-4.50	MS	H	No	No	Yes (0)
31	7	6	1	102.55	1.98	-3.55	S	H	No	Yes	Yes (0)

[1]Rb: number of rotatable bonds. [2]H-Ba: number of H-bond acceptors. [3]H-BD: number of H-bond donors. [4]TPSA: topological polar surface area. [5]CLogP: consensus Log P (average of iLOGP, XLOGP3, WLOGP, MLOGP and Silicos-IT Log P). [6]LogS: Ali topological method Log S. [7]SClass: Ali solubility class (insoluble (IS) < -10 < poorly soluble (PS) < -6 < moderately soluble (MS) < -4< soluble (S) < -2 < very soluble (VS) < 0 < highly soluble (HS)). [8]GIA: gastrointestinal absorption (H means high). [9]BBBP: blood-brain barrier permeability. [10]Pgp: P-glycoprotein substrates. [11]Drug-like: drug-likeness indices (bioavailability) from Lipinski, Ghose, Veber, Egan and Muegge filters. # viol: number of violations of the 5 filters.

2.7. Conclusion

In conclusion, we reported here the synthesis and the biological activity of 30 new PYB-SO and PYB-SA derivatives. They are active in the low nanomolar to the low micromolar levels on the four human cancer cell lines assessed. They arrest the cell cycle progression in G2/M phase, inhibit polymerisation of tubulin to microtubules, bind to the C-BS and exhibit low to no toxicity toward chick embryos. In addition, as determined by the SwissADME algorithm they possess druglikeness properties and bioavailability scores suitable for *in vivo* experiments. Therefore, PYB-SOs and PYB-SAs are a new family of promising antimicrotubule agents.

2.8. Experimental protocols

2.8.1. Biological methods

2.8.1.1. Cell lines culture

HT-1080 human fibrosarcoma, HT-29 human colon carcinoma, and MCF7 human breast carcinoma were purchased from the American Type Culture Collection (Manassa, VA, USA). M21 human skin melanoma cells were provided by Dr. David Cheresh (University of California, San Diego School of Medicine, CA). Cells were cultured in DMEM medium containing sodium bicarbonate, high glucose concentration, glutamine and sodium pyruvate (Hyclone, Logan, UT, USA) supplemented with either 5 or 10% of fetal bovine serum (FBS, Invitrogen, Burlington, ON, Canada) and were maintained at 37 °C in a moisture-saturated atmosphere containing 5% CO_2.

2.8.1.2. Antiproliferative activity assay

The antiproliferative activity of PYB-SOs **4-18** and PYB-SAs **19-33** was assessed using the procedure described by the National Cancer Institute (NCI) Developmental Therapeutics Program for its drug screening program with slight modifications [23]. Briefly, ninety-six-well Costar microtiter clear plates were seeded with 75 µL of a suspension of either HT-1080 (2.5×10^3), HT-29 (4.0×10^3), M21 (3.0×10^3) or MCF7 (2.5×10^3) cells per well in DMEM supplemented with 5 or 10% FBS. Freshly solubilised drugs in DMSO (40

mM) were diluted in fresh supplemented DMEM and 75 µL aliquots containing serially diluted concentrations of the drug were added. Final drug concentrations ranged from 100 µM to 0.39 nM. DMSO concentration was kept constant at 0.5% (V/V) to prevent any related toxicity. Plates were incubated for 48 h, after which growth was stopped by the addition of cold trichloroacetic acid to the wells (10% w/v, final concentration). Afterwards, plates were incubated at 4 °C for 1 h. Then, plates were washed 5-times with distilled water and a sulforhodamine B solution (0.1% w/v) in 1% acetic acid was added to each well. After 15 min at room temperature, the exceeding dye was removed and the plates were washed 5-times with a solution of 1% acetic acid. Bound dye was solubilised in 20 mM Tris base and the absorbance was read using an optimal wavelength (520-580 nm) with a SpectraMax® i3x (Molecular Devices, San Jose, CA, USA). Data obtained from treated cells were compared to the control cell plates fixed on the treatment day and the percentage of cell growth was thus calculated for each drug. The experiments were done at least twice in triplicate. The assays were considered valid when the coefficient of variation was <10% for a given set of conditions within the same experiment.

2.8.1.3. Cell cycle progression analysis

After incubation of 2.5 x 10^5 M21 cells with selected PYB-SOs and PYB-SAs at 2- and 5-times their respective IC_{50} for 24 h, the cells were trypsinised, washed with 750 µL of phosphate buffered saline (PBS) and resuspended in 250 µL of PBS. Cells were fixed by the addition of 750 µL of ice-cold ethanol under agitation and stored at -10 °C until analysis. Prior analysis, cells were washed with 750 µL of PBS and resuspended in 300 µL of PBS containing 2 µg/mL DAPI. Cell cycle distribution of fixed cell suspensions was analysed using an LSR II flow cytometer (BD Biosciences, Franklin Lakes, NJ, USA).

2.8.1.4. Immunofluorescence of microtubules

MCF7 cells were seeded at 2.5 x 10^5 cells per well in 6-well plates (Costar®) containing glass cover slides (22 mm × 22 mm) coated with fibronectin (10 µg/mL) and incubated for 24 h. Tumour cells were treated either with PYB-SOs **14** (58 nM) and **15** (44 nM), PYB-SAs **30** (1400 nM) and **31** (560 nM), paclitaxel (25 nM) or CA-4 (10 nM) for 24 h. DMSO (0.5%) was used as negative control while paclitaxel and CA-4 were used as

positive controls. The cells were then washed thrice with 2 mL of PBS and fixed with 3.7% formaldehyde in PBS for 10 min. After two washes with PBS, the cells were permeabilised with saponin (0.1% in PBS) and blocked with 3% (w/v) BSA in PBS for 45 min at 37 °C. The cells were then incubated for 2 h at room temperature with an anti-β-tubulin monoclonal antibody (clone TUB 2.1, 1:300) in a solution containing 0.1% saponin and 3% BSA in PBS. The cells were washed thrice with PBS containing 0.05% Tween 20 and stained using antimouse IgG Alexa Fluor 488 (Molecular Probes, Eugene, OR, USA; 1:1000) and DAPI (1.25 ng/mL final concentration) in blocking buffer for 1 h at 37 °C. The cover slides were mounted using 25 µL of Fluoromount-G® (SouthernBiotech, Birmingham, AL, USA) before analysis under an Olympus BX51 fluorescence microscope (Olympus BX51, Center Valley, PA, USA). Images were acquired as 8 bit-tagged image format files with a Q imaging RETIGA EXI digital camera (Qimaging, Surrey, BC, Canada) using the Image Pro Express software at a total magnification of 400x.

2.8.1.5. Microtubule polymerisation assay

The effect of PYB-SOs **14** (30 µM) and **15** (3 µM) and PYB-SAs **30** (3 µM) and **31** (15 µM) on dynamic polymerisation of tubulin to microtubules was analysed with the fluorescence based tubulin polymerisation assay using > 99% pure tubulin (Cytoskeleton, Inc., Denver, CO, USA). Drugs were solubilised at the required concentration in DMSO, then 5 µL of drug solutions were diluted in 325 µL of nanopure water to reach 10x of their final concentration. The assay was performed according to the manufacturer guidelines [24]. Briefly, tubulin > 99% (2.0 mg/mL) was dissolved in general tubulin buffer (80 mM PIPES, pH 6.9, 0.5 mM EGTA, 2.0 mM $MgCl_2$) and incubated with drugs at 37 °C. The polymerisation was measured over 60 min with fluorescent excitation at 360 nM and emission at 450 nM in kinetic mode with a SpectraMax® i3x (Molecular Devices, San Jose, CA, USA). The curves shown in Figure 2.4 are representative of two separated experiments.

2.8.1.6. In vitro competition binding assay of EBI to the C-BS

M21 cells were seeded at a concentration of 7.5 x 10^5 M21 cells/well and were incubated overnight in 6-well plates. Then, cells were treated with either PYB-SOs **14** and **15** or PYB-SAs **30** and **31** for 1.5 h at 100- and 1000-times their respective IC_{50} for 2 h. The

maximum concentration of PYB-SOs and PYB-SAs used for the experiments was set at 100 μM. Next, 100 μL of EBI (100 μM, final concentration, Toronto Research Chemicals, North York, ON, Canada) in PBS were added to each well for 1.5 h. After the incubation, the supernatant was withdrawn and the cells in the plates were trypsinised (trypsin-EDTA 0.5%), harvested and centrifuged for 5 min at 1200 rpm. The pellets were washed with 500 μL by cold PBS and stored at -80 °C until analysis.

2.8.1.7. Gel electrophoresis and immunoblot

The cell pellets were resuspended in a buffer containing 0.32 M sucrose, 1 mM EDTA at pH 8, 10 mM Tris at pH 7.4 and protease inhibitor. The protein concentration was assessed using the Bio-Rad protein assay (Bio-Rad laboratories, Mississauga, ON, Canada). Samples were prepared and diluted to obtain proteins at 4 mg/mL in Laemmli sample buffer [25] (60 mM Tris-Cl at pH 6.8, 2% SDS, 10%, glycerol, 5% β-mercaptoethanol, 0.01% bromophenol blue) and boiled for 5 min. Then, 40 μg of proteins from the protein extracts were used for the electrophoresis using 10% polyacrylamide gels. The proteins were transferred onto nitrocellulose membranes that were incubated with TBSTM (Tris-Buffered Saline + 0.1% (V/V) Tween-20 with 5% fat-free dry milk) for 2 h at room temperature. Next, the anti-β-tubulin (clone TUB 2.1, Sigma-Aldrich, St. Louis, MO, USA) primary antibody was incubated in TBSTM (1:500) for 2 h at room temperature. Membranes were washed with TBST (Tris-Buffered Saline with 0.1% (V/V) Tween 20) and incubated with peroxidase conjugated anti-mouse immunoglobulin (Amersham Canada, Oakville, ON, Canada) in TBSMT (1:5000) for 1 h at room temperature. After washing the membranes with TBST, detection of the immunoblot was carried out using Clarity Western enhanced chemiluminescence reagents (Bio-Rad laboratories, Mississauga, ON, Canada). Detection of bands was performed with Super Rx medical X-Ray film (Fujifilm, Tokyo, Japan).

2.8.1.8. Toxicity toward chick embryos

Fertilised eggs were purchased from Couvoir La Coop (Victoriaville, QC, Canada). They were incubated for a 10-day period in a Pro-FI egg incubator (Lyon Electric, Chula Vista, CA, USA) with an automatic turning system. Compounds were solubilised in a formulation containing 1.0% DMSO, 6.2% cremophor EL™, 6.2% ethanol (99%) and 86.6%

PBS. After the incubation period, the veins of the chorioallantoic membrane were identified on the sides of the egg shells. The eggs were opened using a hobby drill (Dremel, Racine, WI) to obtain a 1.5 x 1.5 cm opening directly over the location of the veins. Groups of 10-12 eggs were formed by randomisation and the drugs were intravenously administered at their maximum solubility in our excipient (100 µL/egg). The openings were closed using adhesive tape and the eggs were then incubated in a static incubator (Lyon Electric, Chula Vista, CA, USA) for a 7-day period at 37 °C. The embryos were euthanised at 4 °C for at least 2 h. The wet weight of each embryo and the number of dead embryos were registered. A group of untreated embryos and a group of embryos that were treated only with the excipient were used as negative controls. A one-way ANOVA analysis was used to determine the statistical significance of the results.

2.8.2. Chemical methods

2.8.2.1. General

Proton NMR spectra were recorded on a Bruker AM-300 spectrometer (Bruker, Germany). Chemical shifts (δ) are reported in parts per million (ppm). Reactions requiring microwave heating were performed at 200 watts with an initiator system (Biotage, Charlottesville, VA, USA). Uncorrected melting points were obtained on a MPA100 automated melting point system (SRS Standford Research Systems, Sunnyvale, CA, USA). UHPLC analyses were performed using an ACQUITY Arc system (Waters, Mississauga, ON, Canada) equipped with a 2998 PDA detector. The samples were obtained by solubilisation of the compounds in DMSO and a subsequent solution was produced by diluting the compounds at 1% DMSO in a mixture of MeOH/H_2O 50:50. These samples were then eluted using a mixture of MeOH/H_2O with a linear mobile phase gradient (1.0 mL/min) on a CORTECS C18+ reversed-phase column 3.0 × 50 mm × 2.7 µm. Wavelength was selected at 280 nm and the percentage of all the present compounds was determined. Purity was confirmed by UHPLC and was equal or greater than 95%. All chemicals were supplied by Aldrich Chemicals (Milwaukee, WI, USA), VWR International (Mont-Royal, QC, Canada), Fisher Scientific (Montreal, QC, Canada). Liquid flash chromatography was performed on silica gel F60, 60 Å, 40-63 µm supplied by Silicycle (Quebec, QC, Canada)

using an FPX flash purification system (Biotage, Charlottesville, VA, USA), and using solvent mixtures expressed as V/V ratios. Solvents and reagents were used without purification unless specified otherwise. The progress of all reactions was monitored by TLC on precoated silica gel 60 Å F254 TLC plates provided by VWR International (Mont-Royal, QC, Canada). The chromatograms were viewed under UV light at 254 and/or 275 nm. HRMS were recorded by direct injection in a TOF system 6210 series mass spectrometer (Agilent technologies, Santa Clara, CA, USA).

2.8.2.2. Preparation of compound 34

4-Chlorobutanoyl chloride (6.1 mL, 1.0 Eq.) was added to a solution of aniline (5.0 mL, 1.0 Eq.) in methylene chloride (100 mL) in presence of triethylamine (9.2 mL, 1.2 Eq.). The reaction mixture was stirred at room temperature for 24 h. After completion of the reaction, the mixture was washed twice with HCl 1M (100 mL) and brine (100 mL). The resulting organic solution was dried over anhydrous sodium sulfate, filtered and evaporated to dryness under reduced pressure. The product 4-chloro-*N*-phenylbutanamide (**34**) was used without further purification with a yield of 86%. The ^{1}H and ^{13}C NMR are equivalent to the NMR characterisation published previously [26].

2.8.2.3. Preparation of compound 35

Compound **35** was prepared as published previously with slight modifications [27]. Briefly, sodium hydride (in oil [60%], 2.2 g, 1.2 Eq.) was dissolved in an ice-cold solution of 4-chloro-*N*-phenylbutanamide (**34**, 9.0 g, 1.0 Eq.) in dry THF (250 mL) under argon atmosphere. The ice bath was removed after 10 min. The reaction was stirred at room temperature for 24 h. The reaction was quenched at 0 °C with water (50 mL) and the organic solvent was evaporated. The aqueous solution was extracted with AcOEt (250 mL). The organic solution washed twice with brine (250 mL), dried over anhydrous sodium sulfate, filtered and evaporated to dryness under reduced pressure. The residue was purified by flash chromatography on silica gel (hexanes/AcOEt (75:25) to hexanes/AcOEt (66:33) to obtain 1-phenylpyrrolidin-2-one (**35**) with a yield of 78%. The ^{1}H and ^{13}C NMR are equivalent to the NMR characterisation published previously [28].

2.8.2.4. Preparation of compound 36

Compound **36** was prepared as published previously with slight modifications [29]. Briefly, 1-phenylpyrrolidin-2-one (**35**) (5.0 g, 1.0 Eq.) was dissolved in ice cold chlorosulfonic acid (2.1 mL, 7.7 Eq.) under a dry argon atmosphere. The ice bath was removed after 15 min. The reaction mixture was stirred at room temperature for 16 h. After completion of the reaction, the solution was poured on iced water dropwise. The solid was filtered, rinsed with water (100 mL) and dried for one hour under vacuum. The resulting white 4-(2-oxopyrrolidin-1-yl)benzenesulfonyl chloride (**36**) was used without further purification with a yield of 72%.

2.8.2.5. General preparation of compounds 4-18

The relevant phenol (1.5 Eq.) was added to a solution of the 4-(2-oxopyrrolidin-1-yl)benzenesulfonyl chloride (**36**, 0.10 g) in acetonitrile (3.0 mL) in presence of triethylamine (0.16 mL, 3.0 Eq.). The reaction mixture was stirred at 120 °C under microwave radiation for 8 h. After completion of the reaction, the mixture was cooled at room temperature and the solvent was evaporated under reduced pressure. The residue was diluted with AcOEt (10 mL) and was washed twice with HCl 1M (10 mL), NaOH 1M (10 mL) and brine (10 mL). The resulting solution was dried over anhydrous sodium sulfate, filtered and evaporated to dryness under reduced pressure. The residue was purified by flash chromatography on silica gel.

2.8.2.6. Characterization of compounds 4-18

*2.8.2.6.1. Phenyl 4-(2-oxopyrrolidin-1-yl)benzenesulfonate (**4**).* Flash chromatography (methylene chloride to methylene chloride/ethyl acetate (95:5)). Purity: 100.0%; yield: 83%; white solid; mp: 133-135 °C; ^{1}H NMR ($CDCl_3$): δ 7.82-7.72 (m, 4H, Ar), 7.28-7.21 (m, 3H, Ar), 6.96-6.93 (m, 2H, Ar), 3.86 (t, 2H, J = 7.0 Hz, CH_2), 2.63 (t, 2H, J = 8.0 Hz, CH_2), 2.23-2.13 (m, 2H, CH_2); ^{13}C NMR ($CDCl_3$): δ 175.0, 149.6, 144.5, 129.7, 129.5, 129.4, 127.2, 122.3, 118.7, 48.3, 32.9, 17.7; HRMS (ESI) *m/z* found, 318.0802; $C_{16}H_{16}NO_4S$ (M^+ + H) expected, 318.0801.

*2.8.2.6.2. 2-Isopropylphenyl 4-(2-oxopyrrolidin-1-yl)benzenesulfonate (**5**)*. Flash chromatography (hexanes/methylene chloride (50:50) to methylene chloride). Purity: 99.7%; yield: 61%; white solid; mp: 127-129 °C; ^{1}H NMR ($CDCl_3$): δ 7.84 (brs, 4H, Ar), 7.27-7.18 (m, 2H, Ar), 7.12-7.07 (m, 1H, Ar), 7.01-6.98 (m, 1H, Ar), 3.89 (t, 2H, *J* = 7.0 Hz, CH_2), 3.16-3.10 (m, 1H, CH), 2.66 (t, 2H, *J* = 8.0 Hz, CH_2), 2.26-2.16 (m, 2H, CH_2), 1.07 (d, 6H, *J* = 6.9 Hz, CH_3); ^{13}C NMR ($CDCl_3$): δ 174.9, 147.0, 144.4, 141.8, 130.5, 129.4, 127.3, 127.2, 126.7, 121.9, 118.8, 48.4, 32.8, 26.7, 23.1, 17.7; HRMS (ESI) *m/z* found, 360.1269; $C_{19}H_{22}NO_4S$ (M^+ + H) expected, 360.1269.

*2.8.2.6.3. [1,1'-Biphenyl]-2-yl 4-(2-oxopyrrolidin-1-yl)benzenesulfonate (**6**)*. Flash chromatography (methylene chloride). Purity: 96.5%; yield: 97%; white solid; mp: 157-159 °C; ^{1}H NMR (acetone-d_6): δ 7.66-7.64 (m, 2H, Ar), 7.47-7.13 (m, 11H, Ar), 3.94 (t, 2H, *J* = 6.9 Hz, CH_2), 2.59 (t, 2H, *J* = 7.9 Hz, CH_2), 2.26-2.16 (m, 2H, CH_2); ^{13}C NMR (acetone-d_6): δ 179.9, 151.7, 150.1, 141.8, 140.6, 136.4, 134.3, 134.3, 133.9, 133.9, 133.3, 132.8, 132.6, 129.0, 123.5, 53.2, 37.6, 22.7; HRMS (ESI) *m/z* found, 394.1110; $C_{22}H_{20}NO_4S$ (M^+ + H) expected, 394.1109.

*2.8.2.6.4. 2-Methoxyphenyl 4-(2-oxopyrrolidin-1-yl)benzenesulfonate (**7**)*. Flash chromatography (methylene chloride to methylene chloride/ethyl acetate (97:3)). Purity: 96.5%; yield: 70%; white solid; mp: 157-158 °C; ^{1}H NMR ($CDCl_3$): δ 7.83-7.76 (m, 4H, Ar), 7.20-7.11 (m, 2H, Ar), 6.89-6.81 (m, 2H, Ar), 3.88 (t, 2H, *J* = 7.0 Hz, CH_2), 3.55 (s, 3H, CH_3), 2.64 (t, 2H, *J* = 8.1 Hz, CH_2), 2.24-2.14 (m, 2H, CH_2); ^{13}C NMR ($CDCl_3$): δ 174.9, 151.8, 144.3, 138.3, 130.5, 129.6, 128.1, 123.9, 120.6, 118.5, 112.7, 55.6, 48.4, 32.8, 17.7; HRMS (ESI) *m/z* found, 348.0902; $C_{17}H_{18}NO_5S$ (M^+ + H) expected, 348.0906.

*2.8.2.6.5. 3-Methoxyphenyl 4-(2-oxopyrrolidin-1-yl)benzenesulfonate (**8**)*. Flash chromatography (methylene chloride/ethyl acetate (97:3)). Purity: 99.6%; yield: 71%; pale solid; mp: 122-124 °C; ^{1}H NMR ($CDCl_3$): δ 7.83-7.76 (m, 4H, Ar), 7.16-7.11 (m, 1H, Ar), 6.77-6.74 (m, 1H, Ar), 6.56-6.50 (m, 2H, Ar), 3.87 (t, 2H, *J* = 7.0 Hz, CH_2), 3.70 (s, 3H, CH_3), 2.64 (t, 2H, *J* = 8.0 Hz, CH_2), 2.24-2.14 (m, 2H, CH_2); ^{13}C NMR ($CDCl_3$): δ 175.0, 160.4, 150.4, 144.5, 129.9, 129.5, 129.5, 118.7, 114.2, 113.0, 108.3, 55.5, 48.4, 32.8, 17.7; HRMS (ESI) *m/z* found, 348.0899; $C_{17}H_{18}NO_5S$ (M^+ + H) expected, 348.0906.

*2.8.2.6.6. 3-Fluorophenyl 4-(2-oxopyrrolidin-1-yl)benzenesulfonate (**9**).* Flash chromatography (methylene chloride). Purity: 99.8%; yield: 60%; white solid; mp: 120-122 °C; ^{1}H NMR ($CDCl_3$): δ 7.86-7.77 (m, 4H, Ar), 7.28-7.20 (m, 1H, Ar), 6.99-6.93 (m, 1H, Ar), 6.80-6.74 (m, 2H, Ar), 3.89 (t, 2H, *J* = 7.0 Hz, CH_2), 2.66 (t, 2H, *J* = 8.0 Hz CH_2), 2.26-2.16 (m, 2H, CH_2); ^{13}C NMR ($CDCl_3$): δ 175.0, 164.3, 161.0, 150.2, 150.1, 144.7, 130.5, 130.4, 129.5, 129.2, 118.8, 118.2, 118.1, 114.5, 114.2, 110.6, 110.3, 48.3, 32.8, 17.7; HRMS (ESI) *m/z* found, 336.0696; $C_{16}H_{15}FNO_4S$ (M^+ + H) expected, 336.0707.

*2.8.2.6.7. 3-Chlorophenyl 4-(2-oxopyrrolidin-1-yl)benzenesulfonate (**10**).* Flash chromatography (methylene chloride/ethyl acetate (99:1) to (95:5)). Purity: 100.0%; yield: 79%; white solid; mp: 102-104 °C; ^{1}H NMR ($CDCl_3$): δ 7.85-7.76 (m, 4H, Ar), 7.26-7.16 (m, 2H, Ar), 7.04 (brs, 1H, Ar), 6.87-6.84 (m, 1H, Ar), 3.88 (t, 2H, *J* = 7.0 Hz, CH_2), 2.65 (t, 2H, *J* = 8.0 Hz, CH_2), 2.25-2.15 (m, 2H, CH_2); ^{13}C NMR ($CDCl_3$): δ 175.0, 149.9, 144.8, 134.9, 130.4, 129.5, 129.1, 127.5, 123.0, 120.6, 118.8, 48.3, 32.8, 17.7; HRMS (ESI) *m/z* found, 352.0393; $C_{16}H_{15}ClNO_4S$ (M^+ + H) expected, 352.0411.

*2.8.2.6.8. 3-Bromophenyl 4-(2-oxopyrrolidin-1-yl)benzenesulfonate (**11**).* Flash chromatography (methylene chloride/ethyl acetate (99:1) to (95:5)). Purity: 99.5%; yield: 74%; white solid; mp: 89-92 °C; ^{1}H NMR ($CDCl_3$): δ 7.85-7.76 (m, 4H, Ar), 7.38-7.35 (m, 1H, Ar), 7.20-7.11 (m, 2H, Ar), 6.91-6.88 (m, 1H, Ar), 3.88 (t, 2H, *J* = 7.0 Hz, CH_2), 2.65 (t, 2H, *J* = 8.0 Hz, CH_2), 2.25-2.15 (m, 2H, CH_2); ^{13}C NMR ($CDCl_3$): δ 175.0, 149.9, 144.8, 130.7, 130.4, 129.5, 129.1 125.8, 122.5, 121.1, 118.8, 48.3, 32.8, 17.7; HRMS (ESI) *m/z* found, 395.9898; $C_{16}H_{15}BrNO_4S$ (M^+ + H) expected, 395.9906.

*2.8.2.6.9. 3-Iodophenyl 4-(2-oxopyrrolidin-1-yl)benzenesulfonate (**12**).* Flash chromatography (methylene chloride to methylene chloride/ethyl acetate (95:5)). Purity: 97.6%; yield: 31%; white solid; mp: 103-105 °C; ^{1}H NMR ($CDCl_3$): δ 7.86-7.77 (m, 4H, Ar), 7.59-7.56 (m, 1H, Ar), 7.38 (s, 1H, Ar), 7.03-6.92 (m, 2H, Ar), 3.90 (t, 2H, *J* = 7.0 Hz, CH_2), 2.66 (t, 2H, *J* = 8.0 Hz, CH_2), 2.26-2.16 (m, 2H, CH_2); ^{13}C NMR ($CDCl_3$): δ 175.0, 149.6, 144.7, 136.3, 131.5, 130.9, 129.6, 129.2, 121.7, 118.8, 93.5, 48.4, 32.8, 17.7; HRMS (ESI) *m/z* found, 443.9757; $C_{16}H_{15}INO_4S$ (M^+ + H) expected, 443.9767.

*2.8.2.6.10. 3,4-Dimethoxyphenyl 4-(2-oxopyrrolidin-1-yl)benzenesulfonate (**13**)*. Flash chromatography (methylene chloride/ethyl acetate (97:3) to (95:5)). Purity: 97.6%; yield: 55%; white solid; mp: 152-153 °C; ^{1}H NMR ($CDCl_3$): δ 7.85-7.78 (m, 4H, Ar), 6.71-6.44 (m, 3H, Ar), 3,90 (t, 2H, *J* = 7.0 Hz, Ar), 3.84 (s, 3H, CH_3), 3.77 (s, 3H, CH_3), 2.67 (t, 2H, *J* = 8.0 Hz, CH_2), 2.27-2.17 (m, 2H, CH_2); ^{13}C NMR ($CDCl_3$): δ 175.0, 149.3, 147.9, 144.5, 143.1, 129.7, 129.5, 118.7, 113.8, 110.7, 106.5, 56.1, 56,1, 48.4, 32.9, 17.8; HRMS (ESI) *m/z* found, 378.0991; $C_{18}H_{20}NO_6S$ (M^+ + H) expected, 378.1012.

*2.8.2.6.11. 3,5-Dimethoxyphenyl 4-(2-oxopyrrolidin-1-yl)benzenesulfonate (**14**)*. Flash chromatography (methylene chloride to methylene chloride/ethyl acetate (97:3)). Purity: 99.4%; yield: 39%; white solid; mp: 119-121 °C; ^{1}H NMR ($CDCl_3$): δ 7.82 (brs, 4H, Ar), 6.31 (brs, 1H, Ar), 6.16-6.15 (m, 2H, Ar), 3.88 (t, 2H, *J* = 7.0 Hz, CH_2), 3.68 (s, 6H, CH_3), 2.65 (t, 2H, *J* = 7.4 Hz, CH_2), 2.25-2.15 (m, 2H, CH_2); ^{13}C NMR ($CDCl_3$): δ 174.9, 161.0, 151.0, 144.5, 129.7, 129.5, 118.7, 100.8, 99.3, 55.5, 48.4, 32.8, 17.7; HRMS (ESI) *m/z* found, 378.0998; $C_{18}H_{20}NO_6S$ (M^+ + H) expected, 378.1012.

*2.8.2.6.12. 3,5-Dibromophenyl 4-(2-oxopyrrolidin-1-yl)benzenesulfonate (**15**)*. Flash chromatography (hexanes/ethyl acetate (80:20) to (60:40)). Purity: 99.5%; yield: 54%; white solid; mp: 138-139 °C; ^{1}H NMR ($CDCl_3$): δ 7.86-7.75 (m, 4H, Ar), 7.51 (s, 1H, Ar), 7.11 (s, 2H, Ar), 3.87 (t, 2H, *J* = 7.0 Hz, CH_2), 2.63 (t, 2H, *J* = 8.0 Hz, CH_2), 2.24-2.16 (m, 2H, CH_2); ^{13}C NMR ($CDCl_3$): δ 175.1, 149.9, 145.0, 133.0, 129.5, 128.6, 124.6, 122.9, 118.9, 48.3, 32.8, 17.7; HRMS (ESI) *m/z* found, 473.9003; $C_{16}H_{14}Br_2NO_4S$ (M^+ + H) expected, 473.9009.

*2.8.2.6.13. 3,4,5-Trimethoxyphenyl 4-(2-oxopyrrolidin-1-yl)benzenesulfonate (**16**)*. Flash chromatography (hexanes/ethyl acetate (80:20) to (60:40)). Purity: 96.5%; yield: 67%; pale solid; mp: 129-131 °C; ^{1}H NMR ($CDCl_3$): δ 7.77 (brs, 4H, Ar), 6.17 (s, 2H, Ar), 3.84 (t, 2H, *J* = 7.0 Hz, CH_2), 3.73 (s, 3H, CH_3), 3.65 (s, 6H, CH_3), 2.60 (t, 2H, *J* = 8.0 Hz, CH_2), 2.18-2.13 (m, 2H, CH_2); ^{13}C NMR ($CDCl_3$): δ 175.0, 153.3, 145.4, 144.5, 136.7, 129.6, 129.3, 118.8, 99.8, 60.9, 56.2, 48.3, 32.8, 17.7; HRMS (ESI) *m/z* found, 408.1115; $C_{19}H_{22}NO_7S$ (M^+ + H) expected, 408.1119.

*2.8.2.6.14. 4-Methoxyphenyl 4-(2-oxopyrrolidin-1-yl)benzenesulfonate (**17**)*. Flash chromatography (methylene chloride/ethyl acetate (98:2)). Purity: 100.0%; yield: 42%; white

solid; mp: 120-121 °C; ^{1}H NMR ($CDCl_3$): δ 7.83-7.74 (m, 4H, Ar), 6.88-6.85 (m, 2H, Ar), 6.76-6.73 (m, 2H, Ar), 3.89 (t, 2H, *J* = 7.0 Hz, CH_2), 3.75 (s, 3H, CH_3), 2.65 (t, 2H, *J* = 8.0 Hz, CH_2), 2.25-2.15 (m, 2H, CH_2); ^{13}C NMR ($CDCl_3$): δ 175.0, 158.2, 144.4, 143.0, 129.6, 129.5, 123.3, 118.7, 114.5, 55.6, 48.4, 32.8, 17.7; HRMS (ESI) *m/z* found, 348.0898; $C_{17}H_{18}NO_5S$ (M^+ + H) expected, 348.0906.

*2.8.2.6.15. [1,1'-Biphenyl]-4-yl 4-(2-oxopyrrolidin-1-yl)benzenesulfonate (**18**)*. Flash chromatography (methylene chloride/ethyl acetate (90:10)). Purity: 99.9%; yield: 36%; white solid; mp: 145-147 °C; ^{1}H NMR ($CDCl_3$): δ 7.85-7.79 (m, 4H, Ar), 7.52-7.31 (m, 7H, Ar), 7.05-7.02 (m, 2H, Ar), 3.88 (t, 2H, *J* = 7.0 Hz, CH_2), 2.65 (t, 2H, *J* = 8.0 Hz, CH_2), 2.24-2.17 (m, 2H, CH_2); ^{13}C NMR ($CDCl_3$): δ 175.0, 148.9, 144.6, 140.2, 139.7, 129.6, 129.5, 128.9, 128.3, 127.7, 127.1, 122.6, 118.8, 48.4, 32.9, 17.7; HRMS (ESI) *m/z* found, 394.1103; $C_{22}H_{20}NO_4S$ (M^+ + H) expected, 394.1109.

2.8.2.7. General preparation of compounds 19-33

The relevant aniline (1.5 Eq.) was added to a solution of the 4-(2-oxopyrrolidin-1-yl)benzenesulfonyl chloride (**36**, 0.10 g) in acetonitrile (3.0 mL) in presence of 4-dimethylaminopyridine (0.14 g, 3.0 Eq.). The reaction mixture was stirred at 120 °C under microwave radiations for 8 h. The mixture was cooled at room temperature and the solvent was evaporated under reduced pressure. The residue was diluted with AcOEt (10 mL) and washed twice with HCl 1M (10 mL) and brine (10 mL). The resulting solution was dried over anhydrous sodium sulfate, filtered and evaporated to dryness under reduced pressure. The residue was purified by flash chromatography on silica gel.

2.8.2.8. Characterization of Compounds 19-33

*2.8.2.8.1 4-(2-Oxopyrrolidin-1-yl)-N-phenylbenzenesulfonamide (**19**)*. Flash chromatography (methylene chloride to methylene chloride/ethyl acetate (90:10)). Purity: 100.0%; yield: 38%; white solid; mp: 184-186 °C; ^{1}H NMR (DMSO-d_6): δ 10.20 (s, 1H, NH), 7.81-7.70 (m, 4H, Ar), 7.22-7.17 (m, 2H, Ar), 7.08-6.96 (m, 3H, Ar), 3.79 (t, 2H, *J* = 6.9 Hz, CH_2), 2.48 (t, 2H, *J* = 7.8 Hz, CH_2), 2.06-1.96 (m, 2H, CH_2); ^{13}C NMR (DMSO-d_6):

δ 175.2, 143.5, 138.2, 134.0, 129.6, 128.1, 124.4, 120.4, 119.1, 48.3, 32.9, 17.7; HRMS (ESI) *m/z* found, 317.0957; $C_{16}H_{17}N_2O_3S$ (M^+ + H) expected, 317.0961.

*2.8.2.8.2. N-(2-Isopropylphenyl)-4-(2-oxopyrrolidin-1-yl)benzenesulfonamide (**20**).* Flash chromatography (methylene chloride/ethyl acetate (95:5)). Purity: 96.8%; yield: 39%; white solid; mp: 179-181 °C; ^{1}H NMR (DMSO-d_6): δ 9.60 (s, 1H, NH), 7.89-7.86 (m, 2H, Ar), 7.71-7.69 (m, 2H, Ar), 7.31-7.18 (m, 2H, Ar), 7.09-7.05 (m, 1H, Ar), 6.90-6.87 (m, 1H, Ar), 3.86 (t, 2H, *J* = 6.9 Hz, CH_2), 3.30-3.25 (m, 1H, CH), 2.56 (t, 2H, *J* = 8.0 Hz, CH_2), 2.11-2.06 (m, 2H, CH_2), 1.00 (d, 6H, *J* = 6.7 Hz, CH_3); ^{13}C NMR (DMSO-d_6): δ 175.1, 146.3, 143.4, 135.3, 133.6, 128.1, 127.8, 127.7, 126.8, 126.3, 119.1 48.5, 32.9, 27.2, 24.0, 17.7; HRMS (ESI) *m/z* found, 359.1423; $C_{19}H_{23}N_2O_3S$ (M^+ + H) expected, 359.1429.

*2.8.2.8.3. N-([1,1'-Biphenyl]-2-yl)-4-(2-oxopyrrolidin-1-yl)benzenesulfonamide (**21**).* Flash chromatography (methylene chloride to methylene chloride/ethyl acetate (95:5)). Purity: 98.0%; yield: 52%; pale yellow solid; mp: 104-106 °C; ^{1}H NMR (DMSO-d_6): δ 9.42 (s, 1H, NH), 7.77-7.74 (m, 2H, Ar), 7.57-7.54 (m, 2H, Ar), 7.34-7.21 (m, 8H, Ar), 7.08-7.05 (m, 1H, Ar), 3.83 (t, 2H, *J* = 6.9 Hz, CH_2), 2.55-2.50 (m, 2H, CH_2), 2.10-2.02 (m, 2H, CH_2); ^{13}C NMR (DMSO-d_6): δ 175.1, 143.3, 139.0, 139.0, 135.5, 133.8, 131.4, 129.7, 128.5, 128.4, 127.8, 127.5, 127.1, 126.9, 119.1, 48.4, 32.9, 17.7; HRMS (ESI) *m/z* found, 393.1266; $C_{22}H_{21}N_2O_3S$ (M^+ + H) expected, 393.1269.

*2.8.2.8.4. N-(2-Methoxyphenyl)-4-(2-oxopyrrolidin-1-yl)benzenesulfonamide (**22**).* Flash chromatography (methylene chloride to methylene chloride/ethyl acetate (95:5)). Purity: 100.0%; yield: 39%; pale solid; mp: 190-192 °C; ^{1}H NMR ($CDCl_3$): δ 7.74-7.65 (m, 4H, Ar), 7.51-7.49 (m, 1H, Ar), 7.05-6.98 (m, 2H, Ar and NH), 6.89-6.84 (m, 1H, Ar), 6.73-6.70 (m, 1H, Ar), 3.81 (t, 2H, *J* = 7.0 Hz, CH_2), 3.64 (s, 3H, CH_3), 2.60 (t, 2H, *J* = 8.0 Hz, CH_2), 2.19-2.09 (m, 2H, CH_2); ^{13}C NMR ($CDCl_3$): δ 174.8, 149.4, 143.3, 133.8, 128.2, 125.8, 125.3, 121.1, 120.9, 118.7, 110.6, 55.7, 48.4, 32.8, 17.7; HRMS (ESI) *m/z* found, 347.1058; $C_{17}H_{18}N_2O_4S$ (M^+ + H) expected, 347.1066.

*2.8.2.8.5. N-(3-Methoxyphenyl)-4-(2-oxopyrrolidin-1-yl)benzenesulfonamide (**23**).* Flash chromatography (methylene chloride/ethyl acetate (95:5)). Purity: 99.8%; yield: 62%; brown solid; mp: 173-175 °C; ^{1}H NMR (DMSO-d_6): δ 10.24 (s, 1H, NH), 7.82-7.73 (m, 4H,

Ar), 7.12-7.06 (m, 1H, Ar), 6.67-6.54 (m, 3H, Ar), 3.77 (t, 2H, J = 6.9 Hz, CH_2), 3.63 (s, 3H, CH_3), 2.47 (t, 2H, J = 7.8 Hz, CH_2), 2.02-1.97 (m, 2H, CH_2); ^{13}C NMR (DMSO-d_6): δ 175.2, 160.1, 143.6, 139.5, 134.0, 130.4, 128.1, 119.1, 112.2, 109.3, 106.0, 55.4, 48.3, 32.8, 17.7; HRMS (ESI) *m/z* found, 347.1057; $C_{17}H_{19}N_2O_4S$ (M^+ + H) expected, 347.1066.

2.8.2.8.6. N-(3-Fluorophenyl)-4-(2-oxopyrrolidin-1-yl)benzenesulfonamide ***(24)***. Flash chromatography (hexanes/ethyl acetate (63:37)). Purity: 99.6%; yield: 39%; white solid; mp: 206-208 °C; ^{1}H NMR (DMSO-d_6): δ 10.53 (s, 1H, NH), 7.84-7.75 (m, 4H, Ar), 7.27-7.20 (m, 1H, Ar), 6.91-6.78 (m, 3H, Ar), 3.79 (t, 2H, J = 6.9 Hz, CH_2), 2.48 (t, 2H, J = 7.9 Hz CH_2), 2.05-1.95 (m, 2H, CH_2); ^{13}C NMR (DMSO-d_6): δ 175.2, 164.3, 161.1, 143.8, 140.2, 140.1, 133.6, 131.5, 131.3, 128.1, 119.2, 115.7, 115.6, 110.9, 110.7, 106.7, 106.4, 48.3, 32.9, 17.7; HRMS (ESI) *m/z* found, 335.0859; $C_{16}H_{16}FN_2O_3S$ (M^+ + H) expected, 335.0866.

2.8.2.8.7. N-(3-Chlorophenyl)-4-(2-oxopyrrolidin-1-yl)benzenesulfonamide ***(25)***. Flash chromatography (methylene chloride/ethyl acetate (95:5)). Purity: 99.7%; yield: 43%; white solid; mp: 187-189 °C; ^{1}H NMR (DMSO-d_6): δ 10.52 (s, 1H, NH), 7.84-7.74 (m, 4H, Ar), 7.26-7.20 (m, 1H, Ar), 7.10-7.03 (m, 3H, Ar), 3.81 (t, 2H, J = 6.9 Hz, CH_2), 2.48 (t, 2H, J = 7.9 Hz, CH_2), 2.06-1.98 (m, 2H, CH_2); ^{13}C NMR (DMSO-d_6): δ 175.2, 143.8, 139.9, 133.8, 133.5, 131.4, 128.1, 124.1, 119.3, 119.2, 118.3, 48.3, 32.9, 17.7; HRMS (ESI) *m/z* found, 351.0561; $C_{16}H_{16}ClN_2O_3S$ (M^+ + H) expected, 351.0571.

2.8.2.8.8. N-(3-Bromophenyl)-4-(2-oxopyrrolidin-1-yl)benzenesulfonamide ***(26)***. Flash chromatography (methylene chloride/ethyl acetate (95:5)). Purity: 100.0%; yield: 56%; pale solid; mp: 195-198 °C; ^{1}H NMR (DMSO-d_6): δ 10.50 (s, 1H, NH), 7.84-7.74 (m, 4H, Ar), 7.24-7.09 (m, 4H, Ar), 3.79 (t, 2H, J = 6.9 Hz, CH_2), 2.48 (t, 2H, J = 7.9 Hz, CH_2), 2.06-1.98 (m, 2H, CH_2); ^{13}C NMR (DMSO-d_6): δ 175.2, 143.8, 140.0, 133.5, 131.7, 128.1, 127.0, 122.2, 122.2, 119.2, 118.6, 48.3, 32.9, 17.7; HRMS (ESI) *m/z* found, 395.0049; $C_{16}H_{16}BrN_2O_3S$ (M^+ + H) expected, 395.0066.

2.8.2.8.9. N-(3-Iodophenyl)-4-(2-oxopyrrolidin-1-yl)benzenesulfonamide ***(27)***. Flash chromatography (methylene chloride/ethyl acetate (95:5)). Purity: 99.4%; yield: 54%; pale solid; mp: 188-190 °C; ^{1}H NMR (DMSO-d_6): δ 10.41 (s, 1H, NH), 7.84-7.73 (m, 4H, Ar),

7.42-7.32 (m, 2H, Ar), 7.13-6.97 (m, 2H, Ar), 3.79 (t, 2H, J = 6.9 Hz, CH_2), 2.48 (t, 2H, J = 7.9 Hz, CH_2), 2.05-1.96 (m, 2H, CH_2); ^{13}C NMR (DMSO-d_6): δ 175.2, 143.8, 139.7, 133.6, 132.9, 131.6, 128.1, 128.1, 119.2, 119.0, 95.3, 48.3, 32.9, 17.7; HRMS (ESI) *m/z* found, 442.9908; $C_{16}H_{16}IN_2O_3S$ (M^+ + H) expected, 442.9927.

2.8.2.8.10. N-(3,4-Dimethoxyphenyl)-4-(2-oxopyrrolidin-1-yl)benzenesulfonamide ***(28)***. Flash chromatography (methylene chloride/ethyl acetate (95:5)). Purity: 97.2%; yield: 67%; pale solid; mp: 184-187 °C; ^{1}H NMR (DMSO-d_6): δ 9.84 (s, 1H, NH), 7.80-7.77 (m, 2H, Ar), 7.69-7.66 (m, 2H, Ar), 6.77-6.69 (m, 2H, Ar), 6.54-6.51 (m, 1H, Ar), 3.79 (t, 2H, J = 6.8 Hz, CH_2), 3.63-3.62 (m, 6H, CH_3), 2.49 (t, 2H, J = 8.0 Hz, CH_2), 2.06-1.97 (m, 2H, CH_2); ^{13}C NMR (DMSO-d_6): δ 175.1, 149.2, 146.4, 143.4, 134.0, 131.1, 128.1, 119.0, 113.7, 112.4, 106.7, 56.0, 55.8, 48.3, 32.9, 17.7; HRMS (ESI) *m/z* found, 377.1158; $C_{18}H_{21}N_2O_5S$ (M^+ + H) expected, 377.1172.

2.8.2.8.11. N-(3,5-Dimethoxyphenyl)-4-(2-oxopyrrolidin-1-yl)benzenesulfonamide ***(29)***. Flash chromatography (methylene chloride/ethyl acetate (95:5)). Purity: 96.6%; yield: 60%; white solid; mp: 177-179 °C; ^{1}H NMR DMSO-d_6): δ 10.23 (s, 1H, NH), 7.82-7.75 (m, 4H, Ar), 6.28-6.13 (m, 3H, Ar), 3.76 (t, 2H, J = 6.8 Hz, CH_2), 3.62 (s, 6H, CH_3), 2.47 (t, 2H, J = 7.8 Hz, CH_2), 2.02-1.97 (m, 2H, CH_2); ^{13}C NMR (DMSO-d_6): δ 175.2, 161.2, 143.6, 140.1, 133.9, 128.2, 119.1, 98.1, 95.5, 55.5, 48.3, 32.8, 17.7; HRMS (ESI) *m/z* found, 377.1154; $C_{18}H_{21}N_2O_5S$ (M^+ + H) expected, 377.1172.

2.8.2.8.12. N-(3,5-Dibromophenyl)-4-(2-oxoimidazolidin-1-yl)benzenesulfonamide ***(30)***. Flash chromatography (methylene chloride/ethyl acetate (95:5)). Purity: 96.9%; yield: 18%; white solid; mp: 244-246 °C; ^{1}H NMR (DMSO-d_6): δ 10.77 (s, 1H, NH), 7.88-7.85 (m, 2H, Ar), 7.79-7.76 (m, 2H, Ar), 7.44 (s, 1H, Ar), 7.25 (s, 2H, Ar), 3.82 (t, 2H, J = 6.9 Hz, CH_2), 2.50-2.48 (m, 2H, CH_2), 2.07-1.98 (m, 2H, CH_2); ^{13}C NMR (DMSO-d_6): δ 175.3, 144.0, 141.2, 133.1, 128.8, 128.1, 123.2, 120.8, 119.3, 48.3, 32.9, 17.7; HRMS (ESI) *m/z* found, 472.9156; $C_{16}H_{15}Br_2N_2O_3S$ (M^+ + H) expected, 472.9169.

2.8.2.8.13. 4-(2-Oxopyrrolidin-1-yl)-N-(3,4,5-trimethoxyphenyl)benzenesulfonamide ***(31)***. Flash chromatography (methylene chloride/ethyl acetate (95:5)). Purity: 97.1%; yield: 47%; pale solid; mp: 199-201 °C; ^{1}H NMR (DMSO-d_6): δ 10.07 (s, 1H, NH), 7.83-7.75 (m,

4H, Ar), 6.39 (s, 2H, Ar), 3.78 (t, 2H, *J* = 6.7 Hz, CH_2), 3.64 (s, 6H, CH_3), 3.53 (s, 3H, CH_3), 2.48 (t, 2H, *J* = 7.8 Hz, CH_2), 2.03-1.98 (m, 2H, CH_2); ^{13}C NMR (DMSO-d_6): δ 175.2, 153.4, 143.6, 134.4, 134.2, 133.9, 128.3, 119.1, 98.0, 60.5, 56.2, 48.3, 32.8, 17.7; HRMS (ESI) *m/z* found, 407.1269; $C_{19}H_{23}N_2O_6S$ (M^+ + H) expected, 407.1278.

*2.8.2.8.14. N-(4-Methoxyphenyl)-4-(2-oxopyrrolidin-1-yl)benzenesulfonamide (**32**)*. Flash chromatography (methylene chloride/ethyl acetate (95:5)). Purity: 97.1%; yield: 18%; pale brown solid; mp: 206-209 °C; ^{1}H NMR (DMSO-d_6): δ 9.83 (s, 1H, NH), 7.80-7.62 (m, 4H, Ar), 6.97-6.76 (m, 4H, Ar), 3.80 (t, 2H, *J* = 6.9 Hz, CH_2), 3.64 (s, 3H, CH_3), 2.52-2.47 (m, 2H, CH_2), 2.07-2.00 (m, 2H, CH_2); ^{13}C NMR (DMSO-d_6): δ 175.2, 156.9, 143.4, 134.0, 130.7, 128.1, 123.8, 119.0, 114.7, 55.6, 48.4, 32.9, 17.7; HRMS (ESI) *m/z* found, 347.1061; $C_{17}H_{19}N_2O_4S$ (M^+ + H) expected, 347.1066.

*2.8.2.8.15. N-([1,1'-Biphenyl]-4-yl)-4-(2-oxopyrrolidin-1-yl)benzenesulfonamide (**33**)*. Flash chromatography (methylene chloride/ethyl acetate (95:5) to (85:15)). Purity: 98.2%; yield: 54%; white solid; mp: 177-179 °C; ^{1}H NMR (DMSO-d_6): δ 10.35, (s, 1H, NH), 7.83-7.76 (m, 4H, Ar), 7.56-7.51 (m, 4H, Ar), 7.41-7.26 (m, 3H, Ar), 7.19-7.16 (m, 2H, Ar), 3.78 (t, 2H, *J* = 6.9 Hz, CH_2), 2.50-2.47 (m, 2H, CH_2), 2.05-1.95 (m, 2H, CH_2); ^{13}C NMR (DMSO-d_6): δ 175.2, 143.6, 139.7, 137.7, 136.0, 134.1, 129.3, 128.1, 127.8, 127.6, 126.7, 120.5, 119.2, 48.3, 32.9, 17.7; HRMS (ESI) *m/z* found, 393.1256; $C_{22}H_{21}N_2O_3S$ (M^+ + H) expected, 393.1269.

2.8.3. *In silico* methods

2.8.3.1. Docking studies

Molecular modelling calculations and docking studies were performed using Molecular Operating Environment (MOE) version 2019.01". PYB-SOs **14** and **15**, PYB-SAs **30** and **31** and CA-4 were drawn with ChemBioDraw 13.0 software and imported to MOE as SDF file for docking experiments. The X-ray crystallographic structure of the α, β-tubulin heterodimer was obtained from the RCSB protein data bank (PDB: 1SA0) and loaded to MOE software. The protein was prepared using the QuickPrep tool with default settings to add hydrogens and partial charges, correct Asn/Gln/His orientations, optimise the H-bond network

(protonate 3D), delete water molecules farther than 4.5 Å from the ligand and the receptor, and perform an energy minimisation (RMS gradient of 0.1 kcal/mol/Å). Then, a second energy minimisation was performed prior to the docking of α, β-tubulin heterodimer inhibitors. The default settings were applied to all atoms and included the absence of restriction, a force field Amber10 (ETH; R-Field 1:80; Cutoff [8, 10]), system appearing reasonable for the charges, the rigidity of the water molecules and a gradient of 0.1 RMS kcal/mol/$Å^2$. The surface hydrophobicity (green) and hydrophilicity (brown) of the C-BS was mapped using the Surface and Map Surface and Map tool with default settings. The ligand was isolated and the binding site was created with the amino acids in the vicinity of colchicine and GTP. The binding site was constituted of GTP and 32 amino acids: Gln11, Asn101, Ser178, Thr179, Ala180, Val181, Val215, Tyr224, Val238, Cys241, Leu242, Gln247, Leu248, Asn249, Ala250, Asp251, Lys254, Leu255, Asn258, Met259, Thr314, Val315, Ala316, Ala317, Val318, Asn349, Asn350, Val351, Lys352, Thr353, Ala354 and Ile378. Selected PYB-SOs and PYB-SAs were docked into the C-BS using the selected atoms from the receptor and the selected residues from the binding site. The different conformations, the interactions with the amino acids of the active site and the energies of the complexes were analysed and recorded. Pictures of the most stable conformers in the C-BS site were taken in 3D and 2D models.

2.9. Acknowledgments

This work was supported by grants from Natural Sciences and Engineering Research Council of Canada (NSERC, RGPIN-2016-05069), Fonds de Recherche du Québec - Santé (starting grant for new investigators) and CHU de Quebec-Université Laval Research Center. S. Fortin holds a Junior 1 research scholar award from Fonds de Recherche du Québec - Santé (FRQS). M. Gagné-Boulet and C. Bouzriba are recipients of studentships from the Fonds d'enseignement et de recherche of the Faculty of pharmacy of Université Laval and FRQS, respectively. A.C. Chavez Alvarez is recipient of studentships from Fonds d'enseignement et de recherche of the Faculty of pharmacy of Université Laval.

2.10. Appendix A. Supplementary data

Physicochemical, pharmacokinetics and drug-likeness properties calculated by SwissADME tool together with ^{1}H NMR and ^{13}C NMR spectra, UHPLC chromatograms as well as high resolution mass spectra of the most promising PYB-SOs (**11**, **12**, **14**-**16**) and PYB-SAs (**21**, **25**, **27**, **29**-**31**) are provided in the Supplementary data and can be found online at https://www.sciencedirect.com/science/article/abs/pii/S0223523420311089?via%3Dihub or in the appendix A.

2.11. References

[1] R.L. Siegel, K.D. Miller, A. Jemal, Cancer statistics, 2019, CA Cancer J Clin 69 (2019) 7-34.

[2] Cancer, World Health Organization. https://www.who.int/en/news-room/fact-sheets/detail/cancer, (accessed december 20th, 2019).

[3] E. Mazzotti, G.C.A. Cappellini, S. Buconovo, R. Morese, A. Scoppola, C. Sebastiani, P. Marchetti, Treatment-related side effects and quality of life in cancer patients, Support. Care Cancer 20 (2012) 2553-2557.

[4] J. Ferlay, M. Colombet, I. Soerjomataram, C. Mathers, D.M. Parkin, M. Pineros, A. Znaor, F. Bray, Estimating the global cancer incidence and mortality in 2018: GLOBOCAN sources and methods, Int. J. Cancer 144 (2019) 1941-1953.

[5] J. Lowe, H. Li, K.H. Downing, E. Nogales, Refined structure of αβ-tubulin at 3.5 Å resolution, J. Mol. Biol. 313 (2001) 1045-1057.

[6] D.A. Fletcher, R.D. Mullins, Cell mechanics and the cytoskeleton, Nature 463 (2010) 485-492.

[7] E.K. Rowinsky, R.C. Donehower, Paclitaxel (Taxol), New Engl. J. Med. 332 (1995) 1004-1014.

[8] M.A. Jordan, L. Wilson, Microtubules as a target for anticancer drugs, Nat. Rev. Cancer 4 (2004) 253-265.

[9] S.R. Nasrin, A.M. Rashedul Kabir, A. Konagaya, T. Ishihara, K. Sada, A. Kakugo, Stabilization of microtubules by cevipabulin, Biochem. bioph. res. Co. 516 (2019) 760-764.

[10] A Study of E7130 in Participants With Solid Tumors. https://clinicaltrials.gov/ct2/show/NCT03444701, (accessed November 23th, 2020).

[11] A.M. Olziersky, S.I. Labidi-Galy, Clinical development of anti-mitotic drugs in cancer, Adv. Exp. Med. Biol. 1002 (2017) 125-152.

[12] G.C. Tron, T. Pirali, G. Sorba, F. Pagliai, S. Busacca, A.A. Genazzani, Medicinal chemistry of combretastatin A4: Present and future directions, J. Med. Chem. 49 (2006) 3033-3044.

[13] B. Shan, J.C. Medina, E. Santha, W.P. Frankmoelle, T.C. Chou, R.M. Learned, M.R. Narbut, D. Stott, P.G. Wu, J.C. Jaen, T. Rosen, P. Timmermans, H. Beckmann, Selective, covalent modification of β-tubulin residue Cys-239 by T138067, an antitumor agent with *in vivo* efficacy against multidrug-resistant tumors, Proc. Natl. Acad. Sci. U. S. A. 96 (1999) 5686-5691.

[14] S. Fortin, L. H. Wei, E. Moreau, J. Lacroix, M.-F. Côté, É. Petitclerc, L.P. Kotra, R. C.-Gaudreault, Design, synthesis, biological evaluation, and structure-activity relationships of substituted phenyl 4-(2-oxoimidazolidin-1-yl)-benzenesulfonates as new tubulin inhibitors mimicking combretastatin A-4, J. Med. Chem. 54 (2011) 4559-4580.

[15] S. Fortin, L. Wei, E. Moreau, J. Lacroix, M.-F. Côté, É. Petitclerc, L.P. Kotra, R. C.-Gaudreault, Substituted phenyl 4-(2-oxoimidazolidin-1-yl)benzenesulfonamides as antimitotics. Antiproliferative, antiangiogenic and antitumoral activity, and quantitative structure-activity relationships, Eur. J. Med. Chem. 46 (2011) 5327-5342.

[16] S. Fortin, L. Wei, L.P. Kotra, R. C.-Gaudreault, Novel cytocidal substituted phenyl 4-(2-oxoimidazolidin-1-yl) benzenesulfonates and benzenesulfonamides with affinity to the colchicine-binding site: is the phenyl 2-imidazolidinone moiety a new haptophore for the design of new antimitotics?, Open J. Med. Chem. 5 (2015) 14.

[17] M. Zarifi Khosroshahi, A. C. Chavez Alvarez, M. Gagné-Boulet, R. C.-Gaudreault, S. Gobeil, S. Fortin, Evaluation of the time-dependent antiproliferative activity and liver microsome stability of 3 phenyl 4-(2-oxo-3-alkylimidazolidin-1-yl)benzenesulfonates as promising CYP1A1-dependent antimicrotubule prodrugs, 72 (2020) 249-258.

[18] A. Daina, O. Michielin, V. Zoete, SwissADME: a free web tool to evaluate pharmacokinetics, drug-likeness and medicinal chemistry friendliness of small molecules, Sci. Rep. 7 (2017) 42717.

[19] Tubulin polymerization assay using >99% pure tubulin, fluorescence based. https://www.cytoskeleton.com/kits/tubulin-assays/bk011p, (accessed April 15th, 2020).

[20] A.L. Risinger, F.J. Giles, S. L. Mooberry, Microtubule dynamics as a target in oncology, Cancer. Treat. Rev. 35 (2009) 255-261.

[21] S. Fortin, J. Lacroix, M.-F. Côté, E. Moreau, É. Petitclerc, R. C.-Gaudreault, Quick and simple detection technique to assess the binding of antimicrotubule agents to the colchicine-binding site, Biol. Proced. Online 12 (2010) 113-117.

[22] R.B. Ravelli, B. Gigant, P.A. Curmi, I. Jourdain, S. Lachkar, A. Sobel, M. Knossow, Insight into tubulin regulation from a complex with colchicine and a stathmin-like domain, Nature 428 (2004) 198-202.

[23] National Cancer Institute, NCI 60 cell five-dose screen. https://dtp.cancer.gov/discovery_development/nci-60/default.htm, (accessed April 29th, 2019).

[24] Tubulin polymerization assay kit manual. https://www.cytoskeleton.com/pdf-storage/datasheets/bk011p.pdf, (accessed June 16th, 2020).

[25] U.K. Laemmli, Cleavage of structural proteins during the assembly of the head of bacteriophage T4, Nature 227 (1970) 680-685.

[26] E. Massolo, M. Pirola, A. Puglisi, S. Rossi, M. Benaglia, A one pot protocol to convert nitro-arenes into *N*-aryl amides, RSC Adv. 10 (2020) 4040-4044.

[27] U. Ladziata, A.Y. Koposov, K.Y. Lo, J. Willging, V.N. Nemykin, V.V. Zhdankin, Synthesis, structure, and chemoselective reactivity of *N*-(2-iodylphenyl)acylamides: Hypervalent iodine reagents bearing a pseudo-six-membered ring scaffold, Angew. Chem. Int. Ed. 44 (2005) 7127-7131.

[28] Y.-H. Yang, M. Shi, Ring-expanding reaction of cyclopropyl amides with triphenylphosphine and carbon tetrahalide, J. Org. Chem. 70 (2005) 8645-8648.

[29] S.-Y. Lin, T.-K. Yeh, C.-C. Kuo, J.-S. Song, M.-F. Cheng, F.-Y. Liao, M.-W. Chao, H.-L. Huang, Y.-L. Chen, C.-Y. Yang, M.-H. Wu, C.-L. Hsieh, W. Hsiao, Y.-H. Peng, J.-S. Wu, L.-M. Lin, M. Sun, Y.-S. Chao, C. Shih, S.-Y. Wu, S.-L. Pan, M.-S. Hung, S.-H. Ueng, Phenyl benzenesulfonylhydrazides exhibit selective indoleamine 2,3-dioxygenase inhibition with potent *in vivo* pharmacodynamic activity and antitumor efficacy, J. Med. Chem. 59 (2016) 419-430.

Chapitre 3. Preparation, biological evaluation and structure-activity relationships of new phenyl 4-(dioxoimidazolidin-1-yl)benzenesulfonate and ethyl 2-(3-(4-(phenoxysulfonyl)phenyl)ureido)acetate analogs to phenyl 4-(2-oxoimidazolidin-1-yl)benzenesulfonate: study of the imidazolidin-2-one moiety

Mathieu Gagné-Boulet [a, b], Chahrazed Bouzriba [a, b], Atziri Corin Chavez Alvarez [a, b, c], Sébastien Fortin [a, b, *]

[a]Centre de recherche du CHU de Québec-Université Laval, Axe oncologie, Hôpital Saint-François d'Assise, 10 rue de l'Espinay, Québec, QC, G1L 3L5, Canada.

[b]Faculté de pharmacie, Université Laval, Pavillon Ferdinand-Vandry, 1050 avenue de la Médecine, Québec, QC, G1V 0A6, Canada.

[c]Centre de recherche de l'Institut universitaire de cardiologie et de pneumologie de Québec-Université Laval, 2725 Ch Ste-Foy, Québec, QC, G1V 4G5, Canada.

***Corresponding author:** Sébastien Fortin; Phone: 418-525-4444 ext. 52364, Fax: 418-525-4372, e-mail: sebastien.fortin@pha.ulaval.ca

Soumis le 14 mai 2021 à l'Éditeur du journal Chemical Biology & Drug Design.

3.1. Résumé

Nous avons préparé et évalué l'activité biologique de 32 nouveaux agents antimicrotubules appelés phényl 4-(dioxoimidazolidin-1-yl)benzènesulfonates (PID-SOs) et éthyl 2-(3-(4-(phénoxysulfonyl)phényl)uréido)acétates (EPA-SOs). Les PID-SOs les plus puissants portant un groupement imidazolidin-2,4-dione possèdent une activité antiproliférative de l'ordre du nanomolaire au bas micromolaire (0,092 - 5,0 µM) tandis que les EPA-SOs et PID-SOs ayant un groupement imidazolidin-2,5-dione possèdent généralement une activité antiproliférative supérieure à 100 µM. Les PID-SOs les plus puissants arrêtent la progression du cycle cellulaire en phase G2/M et interagissent avec le site de liaison de la colchicine menant à la perturbation des microtubules et du cytosquelette. De plus, leur activité antiproliférative n'est pas altérée par des lignées cellulaires résistantes aux agents antimicrotubules et multirésistantes. Ils possèdent également des propriétés pharmacocinétiques et physicochimiques théoriques nécessaires pour la poursuite de leur développement. Enfin, notre étude confirme que les PID-SOs portant le groupement imidazolidin-2,4-dione constituent une nouvelle famille d'antimitotiques prometteurs.

3.2. Abstract

We prepared and biologically evaluated 32 novel antimicrotubule agents named phenyl 4-(dioxoimidazolidin-1-yl)benzenesulfonates (PID-SOs) and ethyl 2-(3-(4-(phenoxysulfonyl)phenyl)ureido)acetates (EPA-SOs). The antiproliferative activity of PID-SOs and EPA-SOs were assessed on four cancer cell lines (HT-1080, HT-29, M21 and MCF7). The most potent PID-SOs bearing an imidazolidin-2,4-dione group show antiproliferative activity in the nanomolar to low micromolar range (0.092 - 5.0 μM) while EPA-SOs and PID-SOs bearing an imidazolidin-2,5-dione moiety generally exhibit antiproliferative activity over 100 μM. The most potent PID-SOs arrest the cell cycle progression in G2/M phase and interact with the colchicine-binding site leading to the microtubule and cytoskeleton disruption. Moreover, their antiproliferative activity is not impaired by antimicrotubule- and multidrug-resistant cell lines. In addition, they exhibit theoretical pharmacokinetic and physicochemical properties required for further developments. Finally, our study confirms that PID-SOs bearing the imidazolidin-2,4-dione moiety are a new family of promising antimitotics.

3.3. Graphical abstract

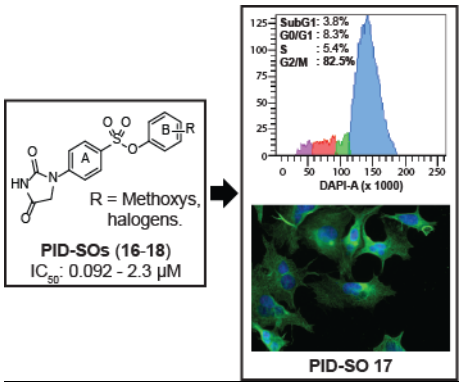

3.4. Introduction

Microtubules are an essential component of the cytoskeleton (Prosser et al., 2017). They have a crucial role in multiple cellular mechanisms such as intracellular vesicle transport, mitochondria function, positioning of membranous organelles, cell motility and signaling (Jordan et al., 2004). Moreover, they play a key role during cell division by forming an important part of the mitotic spindle during mitosis with chromosomes and other proteins leading to the separation of sister chromatids between daughter cells (Asbury, 2017). Since microtubules are of uttermost importance during mitosis, several drugs used in clinics to treat various cancer types are based on the inhibition of this target, for example paclitaxel (**1**) and vinblastine (**2**) (Dumontet et al., 2010). The success of this class of anticancer agents prompted the development of new antimicrotubule agents such as combretastatin A-4 disodium phosphate (CA-4DP, **3**), phenstatin (**4**) and T138067 sodium (**5**) which are known to interfere with microtubule dynamics and disrupt the cytoskeleton which leads to the initiation of apoptosis (Chen et al., 2018; Grosios et al., 1999; Shan et al., 1999).

Although antimicrotubule agents used in clinics are of the highest importance to treat cancer patients, their clinical efficacy is notably restrained by toxicity, limited by suboptimal biopharmaceutical properties and by the induction of chemoresistance (Ferlay et al., 2019; Jordan, et al., 2004). Hence, the development of new antimicrotubule agents is required to circumvent these clinical limitations. To that end, we recently developed a new family of anticancer agents designated as phenyl 4-(2-oxoimidazolidin-1-yl)benzenesulfonates (PIB-SOs, Fig. 3.1A). The molecular structure of PIB-SOs is composed of two aromatic rings (ring

A and B) linked together by a sulfonate bridge and has a relatively small molecular weight (Fortin et al., 2011a; Fortin et al., 2011b). They exhibit antiproliferative activity in the nanomolar range on several human cancer cell lines. They also arrest the cell cycle progression in G2/M phase and disrupt microtubules by binding to the colchicine-binding site (C-BS) (Fortin, et al., 2011b). Our previous structure-activity relationships (SAR) on PIB-SOs are depicted in Fig. 3.1. The first SAR study showed that PIB-SOs must have an imidazolidin-2-one (IMZ) at position four on the ring A and either halogens, methoxys or short alkyl chains on ring B to exhibit potent antimitotic profiles (Fortin, et al., 2011a; Fortin, et al., 2011b). Then, the IMZ moiety was enlarged into a ring of six atoms to form a tetrahydropyrimidin-2(1H)-one group which led to the design of phenyl 4-(2-oxotetrahydropyrimidin-1(2*H*)-yl)benzenesulfonates (PPB-SOs, Fig. 3.1B). The modification of IMZ into tetrahydropyrimidin-2(1H)-one decreases the activity of PIB-SOs (Fortin, et al., 2011b). Moreover, the sulfonate bridge of PIB-SOs was modified by a sulfonamide group to give phenyl 4-(2-oxoimidazolidin-1-yl)benzenesulfonamides (PIB-SAs, Fig. 3.1C). PIB-SAs exhibit slightly weaker antiproliferative activity than their PIB-SO counterparts (Fortin, et al., 2011a). Furthermore, the sulfonate bridge of PIB-SOs was also modified by *cis* or *trans* ethenyl group to mimic the molecular template of CA-4DP (**3**) and lead to styrylphenylimidazolidin-2-ones (*Z*- and *E*-SIMZs, Fig. 3.1D and E). The *Z*-SIMZs were active in the low nanomolar range and were much more potent than their *trans* counterparts (Gagné-Boulet et al., 2015a). Finally, the IMZ moiety was modified into a lactam group which led to the design of phenyl 4-(2-oxopyrrolidin-1-yl)benzenesulfonates (PYB-SOs) and phenyl 4-(2-oxopyrrolidin-1-yl)benzenesulfonamides (PYB-SAs, Fig. 3.1F) bearing a sulfonate and sulfonamide bridge, respectively. PYB-SOs tend to exhibit more potent antiproliferative activity than their PYB-SA analogues (Gagné-Boulet et al., 2021).

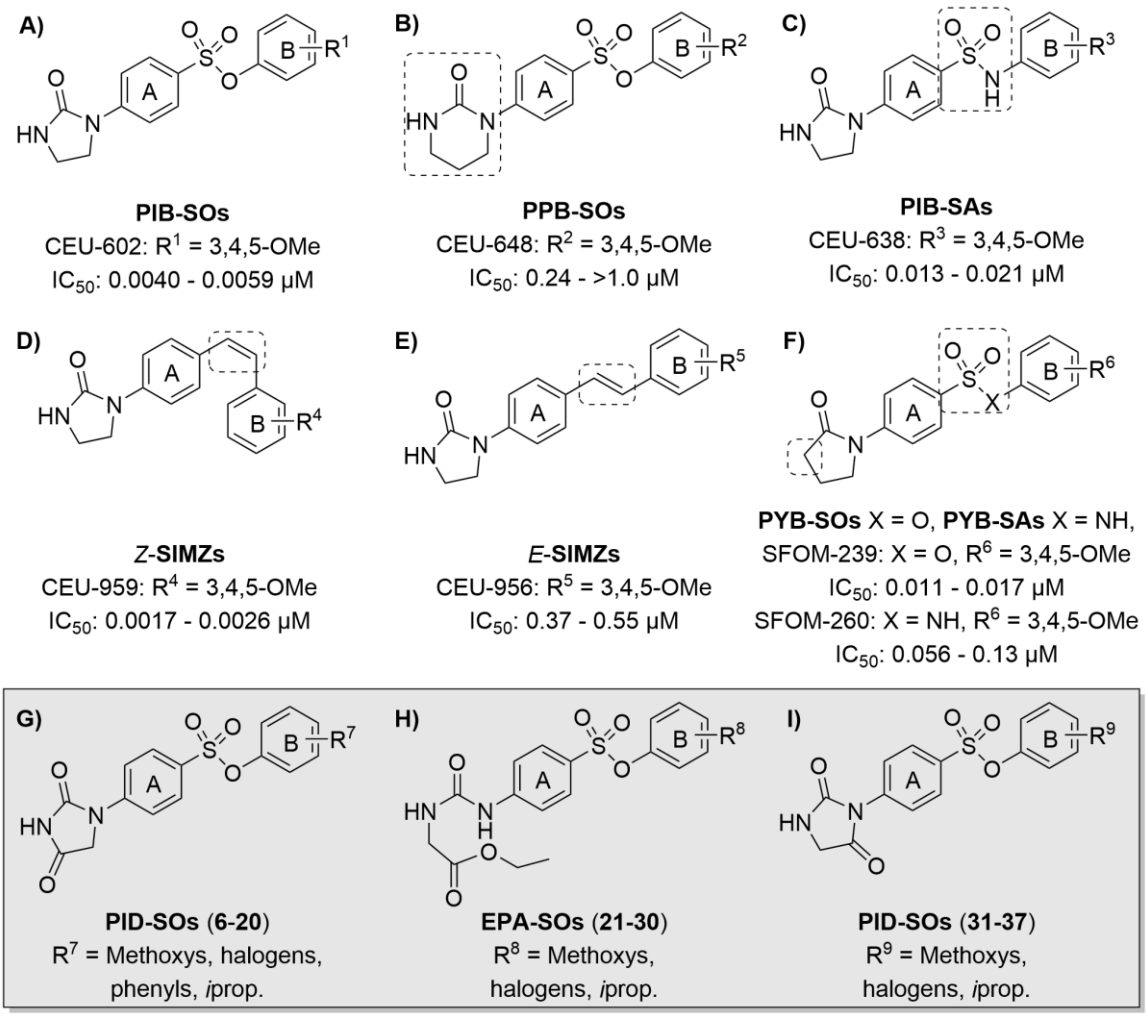

Figure 3.1. Molecular structures and antiproliferative activity of derivatives bearing a 3,4,5-trimethoxy group on the ring B on human cancer cell lines of A) phenyl 4-(2-oxoimidazolidin-1-yl)benzenesulfonates (PIB-SOs), B) phenyl 4-(2-oxotetrahydropyrimidin-1(2*H*)-yl)benzenesulfonates (PPB-SOs), C) phenyl 4-(2-oxoimidazolidin-1-yl)benzenesulfonamides (PIB-SAs), D) *cis*-styrylphenylimidazolidin-2-ones (*Z*-SIMZs), E) *trans*-styrylphenylimidazolidin-2-ones (*E*-SIMZs), F) phenyl 4-(2-oxopyrrolidin-1-yl)benzenesulfonates (PYB-SOs) and phenyl 4-(2-oxopyrrolidin-1-yl)benzenesulfonamides (PYB-SAs), G) phenyl 4-(2,4-dioxoimidazolidin-1-yl)benzenesulfonates (PID-SOs, **6-20**), H) ethyl 2-(3-(4-(phenoxysulfonyl)phenyl)ureido)acetates (EPA-SOs, **21-30**) and I) phenyl 4-(2,5-dioxoimidazolidin-1-yl)benzenesulfonates (PID-SOs, **31-37**). Molecular modifications of

PIB-SOs are framed in dotted rectangles to facilitate their distinction between other families of compounds.

In this study, we assessed the effect of modifying the IMZ moiety of PIB-SOs by an imidazolidin-2,4-dione, an ethyl 2-ureidoacetate or an imidazolidin-2,5-dione group which led to the synthesis of new phenyl 4-(2,4-dioxoimidazolidin-1-yl)benzenesulfonates (PID-SOs **6**-**20**, Fig. 1G), ethyl 2-(3-(4-(phenoxysulfonyl)phenyl)ureido)acetates (EPA-SOs **21**-**30**, Fig. 1H) and phenyl 4-(2,5-dioxoimidazolidin-1-yl)benzenesulfonates (PID-SOs **31**-**37**, Fig. 1I). Foremost, all new compounds were assessed for their antiproliferative activity on HT-1080 fibrosarcoma, HT-29 colon adenocarcinoma, M21 melanoma and MCF7 oestrogen-dependent breast adenocarcinoma. Secondly, the selected derivatives were assessed for their ability to arrest the cell cycle progression, to disrupt the cytoskeleton, to inhibit microtubules polymerisation and to bind to the C-BS. Thirdly, the antiproliferative activity of most potent derivatives were assessed on wild-type (CHO-10001), colchicine- and vinblastine- (CHO-VV 3-2) and paclitaxel-resistant (CHO-TAX 5-6) Chinese hamster ovary cells as well as T lymphoblastoid leukemia CEM and multidrug-resistant CEM-VLB cell lines. Fourthly, docking experiments were performed to study the docking poses of the most potent derivatives. Finally, SwissADME web tool was used to predict their theoretical biopharmaceutical properties.

3.5. Chemistry/methods

The preparation of PID-SOs **6-20** is depicted in Fig. 3.2 and is completed within four steps. Shortly, the synthesis begins with the nucleophilic addition of *N*-phenylurea on 2-chloroacetyl chloride in tetrahydrofuran. Then, the 2-chloro-*N*-(phenylcarbamoyl)acetamide is intramolecularly cyclised with potassium hydroxide in a mixture of water and ethanol to give phenylimidazolidin-2,4-dione as previously described (Hirota et al., 1985). Then, the introduction of the sulfonyl chloride group was performed by the addition of 1-phenylimidazolidin-2,4-dione in chlorosulfonic acid to give 4-(2,4-dioxoimidazolidin-1-yl)benzene-1-sulfonyl chloride. Finally, PID-SOs **6-20** were obtained by the nucleophilic addition of the relevant phenol into 4-(2,4-dioxoimidazolidin-1-yl)benzene-1-sulfonyl chloride in presence of triethylamine in acetonitrile under microwaves.

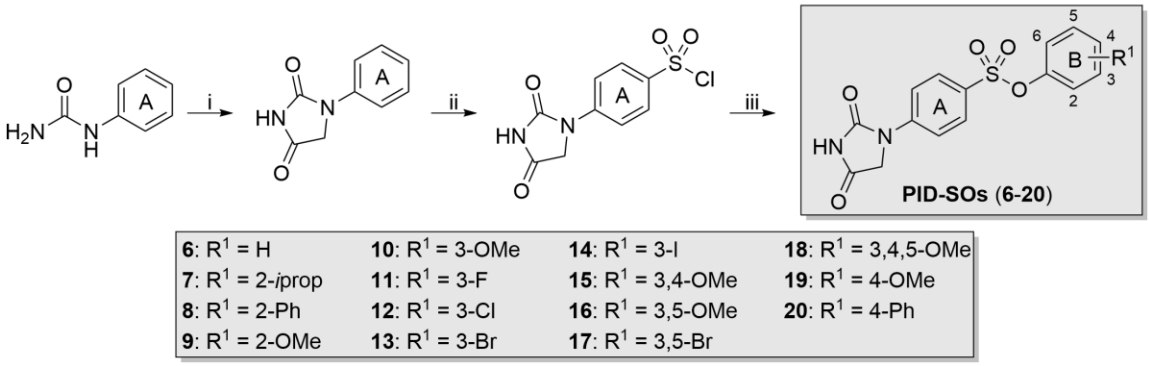

Figure 3.2. Reagents and conditions: (i) 2-chloroacetyl chloride, THF, rt, 2 h, 83%; KOH, H_2O/EtOH, 80 °C, 30 min, 30%; (ii) $HOSO_2Cl$, 0 °C to rt, 16 h, quantitative; (iii) relevant phenol, TEA, CH_3CN, 120 °C under microwaves, 8 h, 4-53%.

The preparation of EPA-SOs **21**-**30** and PID-SOs **31**-**37** is shown in Fig. 3.3 and is completed within three and four steps, respectively. The preparation of new EPA-SOs and PID-SOs is based on the publication described by Gagné-Boulet *et al.* and Turcotte *et al.* with slight modifications (Gagné-Boulet et al., 2018; Gagné-Boulet et al., 2015b; Turcotte et al., 2012). Briefly, 4-aminobenzenesulfonates were prepared by nucleophilic addition of relevant phenol on 4-nitrobenzene-1-sulfonyl chloride in presence of triethylamine in acetonitrile under microwaves followed by a reduction of resulting phenyl nitrobenzenesulfonate with iron powder in presence of HCl in a mixture of ethanol and water (10:1). Then, a nucleophilic addition of appropriate 4-aminobenzenesulfonates on ethyl isocyanatoacetate in diethyl ether yielded the EPA-SOs **21**-**30**. Finally, the preparation of PID-SOs **31**-**37** was performed by intramolecular cyclisation of relevant EPA-SOs in presence of HCl (6 M) in ethanol.

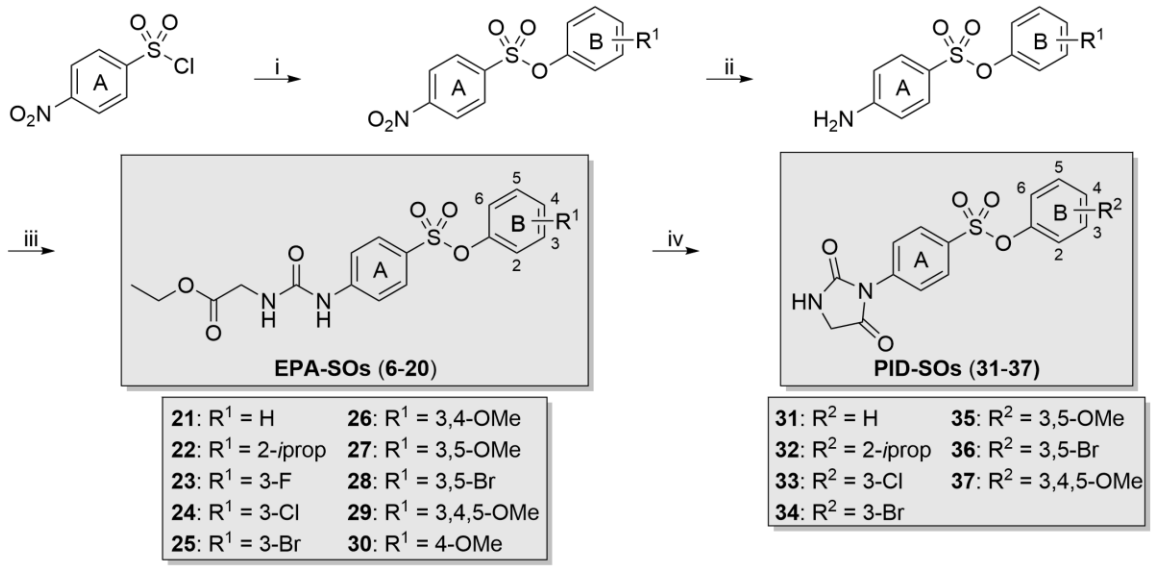

Figure 3.3. Reagents and conditions: (i) relevant phenol, TEA, CH_3CN, 120 °C under microwaves, 8 h, 39-99%; (ii) iron powder, HCl, H_2O/EtOH, 70 °C, 16 h, 13-80%; (iii) ethyl 2-isocyanatoacetate, Et_2O, rt, 24 h, 22-92%; (iv) HCl, EtOH, 80 °C, 16 h, 20-57%.

3.6. Results/discussion

3.6.1. Antiproliferative activity of PID-SOs and EPA-SOs on cancer cell lines

The antiproliferative activity of PID-SOs (**6**-**20**), EPA-SOs (**21**-**30**) and PID-SOs (**31**-**37**) was assessed on four human cancer cell lines namely HT-1080, HT-29, M21 and MCF7 using the sulforhodamine B colorimetric assay (NCI-60, 2020). The results are summarised in Table 3.1 and they are expressed as the concentration of a drug required to inhibit cell growth by 50% (IC_{50}). Combretastatin A-4 (CA-4) was used as positive control. First of all, at the exception of compounds **28** and **29**, all EPA-SOs (**21**-**30**) and PID-SOs bearing an imidazolidin-2,5-dione moiety (**31**-**37**) have minor or no activity (IC_{50}: 4.7 - >100 µM). These results prompt us to stop further investigation on both EPA-SOs and PID-SOs bearing the imidazolidin-2,5-dione moiety. Second, PID-SOs **6**-**20** exhibit nanomolar to mid micromolar antiproliferative activity (0.092 - 70 µM). In general, the most sensitive cancer cell line to PID-SOs follow this decreasing order: M21 > MCF7 > HT-29 > HT-1080. PID-SOs substituted at positions 3, 3,5 or 3,4,5 on ring B by methoxy or halogen groups (PID-SOs **10**-**14**, **16**-**18**) are the most potent derivatives (0.092 - 5.0 µM). PID-SO **18** bearing a

3,4,5-trimethoxy group on ring B is the most potent derivative exhibiting IC_{50} of 0.11, 0.16, 0.092 and 0.17 µM against HT-1080, HT-29, M21 and MCF7, respectively. These results indicate that the ethyl 2-ureidoacetate and imidazolidin-2,5-dione groups are not suited to interact properly with the C-BS, conceivably caused by unfavourable dipolar interactions, hydrogen bonding or steric hindrance. Our study confirms that only few modifications are tolerated on the IMZ moiety to maintain antiproliferative activity in the nanomolar range.

Table 3.1. Antiproliferative activity (IC_{50}) of PID-SOs (**6**-**20**), EPA-SOs (**21**-**30**) and PID-SOs (**31**-**37**) on human HT-1080, HT-29, M21 and MCF7 cancer cell lines.

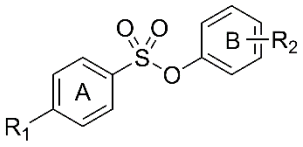

#	R^1	R^2	IC_{50} (µM)[1]			
			HT-1080	**HT-29**	**M21**	**MCF7**
6		H	20	17	2.9	15
7		2-*i*prop	>13	>13	9.1	>13
8		2-Ph	14	17	5.5	10
9		2-OMe	70	55	38	58
10		3-OMe	3.1	2.3	2.4	2.0
11		3-F	4.5	4.7	5.0	3.1
12	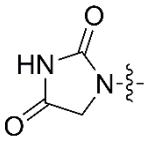	3-Cl	2.1	1.6	2.1	1.1
13		3-Br	1.4	1.1	1.4	1.0
14		3-I	0.61	0.69	0.46	0.64
15		3,4-OMe	7.6	8.3	5.0	8.8
16		3,5-OMe	2.3	0.38	0.27	0.48
17		3,5-Br	0.36	0.30	0.22	0.27
18		3,4,5-OMe	0.11	0.16	0.092	0.17
19		4-OMe	13	8.3	14	5.8
20		4-Ph	8.5	24	13	7.1
21		H	>100	>100	>100	>100
22		2-*i*prop	>100	>100	>100	>100
23		3-F	>100	>100	>100	>100
24	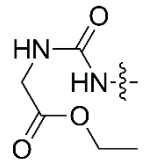	3-Cl	73	>100	>100	>100
25		3-Br	47	55	80	73
26		3,4-OMe	>100	>100	>100	>100
27		3,5-OMe	99	>100	94	>100
28		3,5-Br	31	31	35	0.88
29		3,4,5-OMe	7.6	4.7	5.4	11
30		4-OMe	>100	>100	>100	>100

31	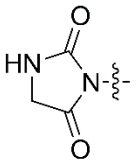	H	>100	>100	>100	>100
32		2-*i*prop	>100	>100	>100	>100
33		3-Cl	>100	>100	>100	>100
34		3-Br	>100	>100	>100	>100
35		3,5-OMe	>100	>100	>100	>100
36		3,5-Br	>100	>100	>100	>100
37		3,4,5-OMe	95	76	57	83
CA-4[2]	N/A	N/A	0.0022	0.0051	0.0019	0.011

[1]IC_{50} represents the concentration of drug inhibiting cell growth by 50% in micromolar. [2]CA-4, combretastatin A-4.

3.6.2. PID-SOs block the cell cycle progression in G2/M phase

PIB-SOs that were used as molecular scaffolds to design PID-SOs are known to arrest the cell cycle progression in G2/M phase (Fortin, et al., 2011b). Therefore, in the aim to study the mechanism of action of PID-SOs, we evaluated their ability to block the cell cycle progression in the G2/M phase. To that end, the most potent PID-SOs **12**-**14** and **16**-**18** were incubated with M21 cells at 2- and 5-times their respective IC_{50} for 24 h. The results are depicted in Fig. 3.4 and illustrated the optimal concentrations that block the cell cycle progression in G2/M phase. CA-4 was used as positive control and 0.5% DMSO was used as negative control. DMSO shows a cell population of 1.8, 58.3, 14.5 and 25.4% for subG1, G0/G1, S and G2/M phases, respectively, while CA-4 shows a cell population of 4.0, 11.0, 13.1 and 71.9% for subG1, G0/G1, S and G2/M phases, respectively. All PID-SOs assessed arrest the cell cycle progression in G2/M phase with a population range varying from 57.9 to 88.9% which is similar to that of CA-4. PID-SO **14** bearing a 3-iodo group exhibits the most effective arrest in G2/M phase with a cell population in G2/M phase of 88.9%.

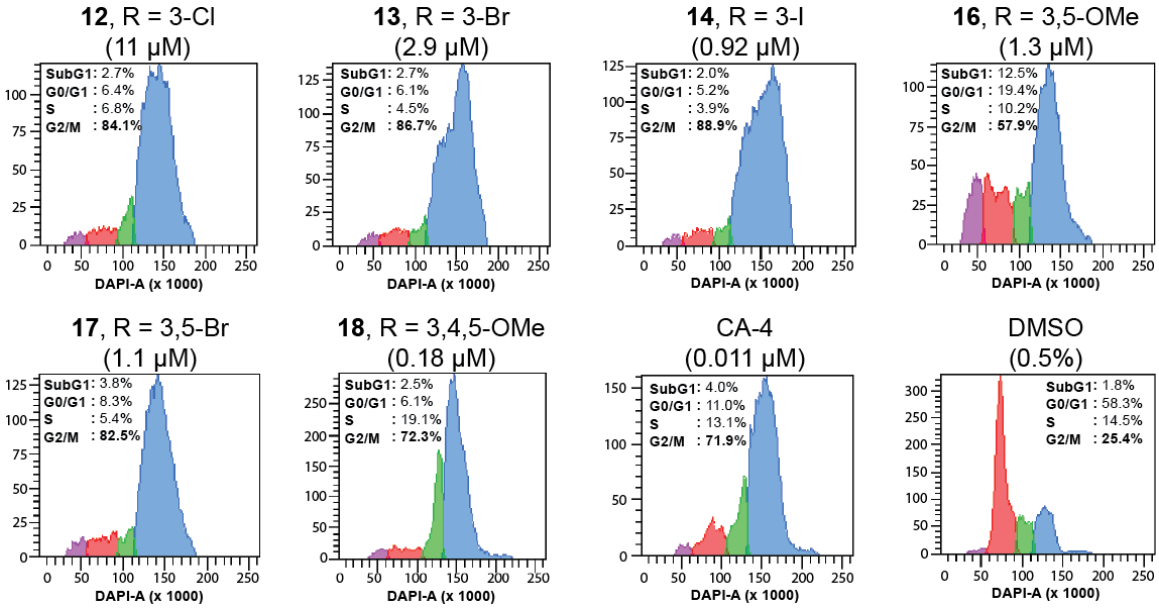

Figure 3.4. Effect of PID-SOs **12-14** and **16-18** on the cell cycle progression on M21 cells after 24 h of treatment. CA-4 and 0.5% DMSO were used as positive and negative controls, respectively.

3.6.3. PID-SOs generate cytoskeleton disruption

Since our previous results suggest that PID-SOs target microtubules, we investigated their capacity to interfere with microtubules and disrupt the cytoskeleton. Therefore, we assessed our three most potent PID-SOs (**16-18**) for their ability to target microtubules and disrupt the cytoskeleton integrity. M21 cells were treated at 5-times their respective IC_{50} for 24 h and cellular microtubule structures were visualised by indirect immunofluorescence using an anti-β-tubulin monoclonal antibody. CA-4 was used as positive control and 0.5% DMSO as negative control. As shown in Fig. 3.5, All PID-SOs assessed lead to cytoskeleton disruption compared to our negative control. Therefore, PID-SOs are a new family of anticancer agents targeting microtubules and inducing cytoskeleton disruption.

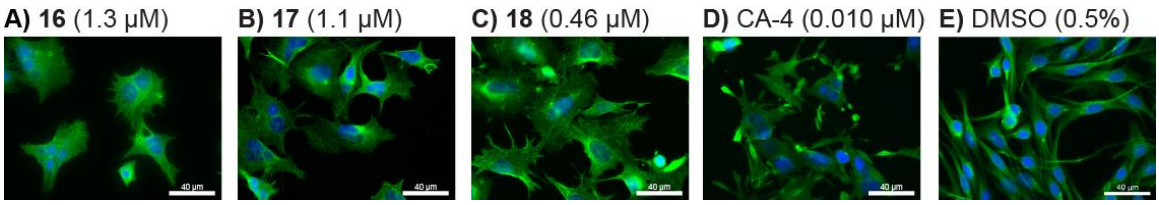

Figure 3.5. Effect of PID-SOs A) **16**, B) **17**, C) **18**, D) CA-4 and E) 0.5% DMSO on the microtubules integrity of M21 cells after 24 h of treatment. CA-4 and 0.5% DMSO were used as positive and negative controls, respectively.

3.6.4. PID-SOs inhibit microtubule polymerisation

To validate the effect of PID-SOs on microtubule polymerisation, we assessed PID-SOs **16-18** for their effect on microtubule dynamics with a polymerisation assay kit (Cytoskeleton Inc, 2020). As illustrated in Fig. 3.6, microtubule formation rates are shown over a period of 60 min at 37 °C. Curves are representative of two separated experiments. CA-4 (15 µM) and paclitaxel (3.0 µM) were used as microtubule polymerisation inhibitor and microtubule-stabilising agent, respectively. DMSO at 1.5% was used as negative control. PID-SOs **16** (3.0 µM), **17** (3.0 µM) and **18** (30 µM) were used at their maximal solubility in the buffer solution. Our results indicate that CA-4 inhibits tubulin polymerisation while paclitaxel enhance tubulin polymerisation. PID-SOs **16** and **18** show a slow tubulin polymerisation rate, though not as strongly as CA-4. However, PID-SO **17** has no marked effect on the tubulin polymerisation rate and shows a similar effect that 1.5% DMSO. We hypothesise that the concentration of PID-SO **17**, the least potent compound of this series, is too low to generate an effect similar to PID-SOs **16** and **18**. Nonetheless, these results confirm that PID-SOs **16** and **18** inhibit the polymerisation of tubulin into microtubules.

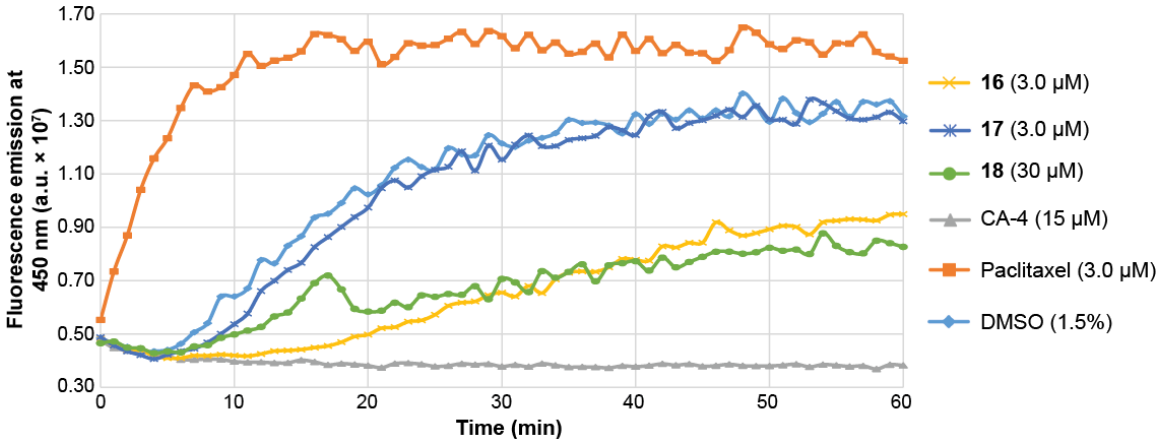

Figure 3.6. Effect of PID-SOs **16**-**18** on tubulin assembly. CA-4 and paclitaxel were used as positive controls while DMSO was used as negative control.

3.6.5. PID-SOs target the colchicine-binding site

There are several binding sites on microtubules and tubulin heterodimers where antimicrotubule agents interact (Field et al., 2013; McLoughlin et al., 2020). However, PID-SOs structures are inspired originally from CA-4 which is known to interact with the C-BS (Fortin, et al., 2011b; Nam, 2003). Therefore, to study the binding site of PID-SOs, we used a quick and efficient detection technique based on the *N*,*N*'-ethylene-bis(iodoacetamide) (EBI) assay (Fortin et al., 2010). EBI is a bis-alkylating agent that cross link cysteines 239 and 354 in the C-BS. The adduct created is detected conveniently by western blot as a second immunoreacting band of β-tubulin. Antimicrotubules that bind to the C-BS prevent the formation of the EBI: β-tubulin adduct. Hence, M21 cells were treated with the three most potent PID-SOs (**16**-**18**) at 100- and 1000-times their respective IC_{50}. As shown in Fig. 3.7, all PID-SOs tested inhibit the formation of the EBI: β-tubulin adduct equivalently to CA-4 (Gagné-Boulet, et al., 2015a). This is illustrated by the loss of the second immunoreacting band of β-tubulin and the presence of the native β-tubulin band. These results demonstrate that PID-SOs inhibit microtubule polymerisation by interacting with the C-BS.

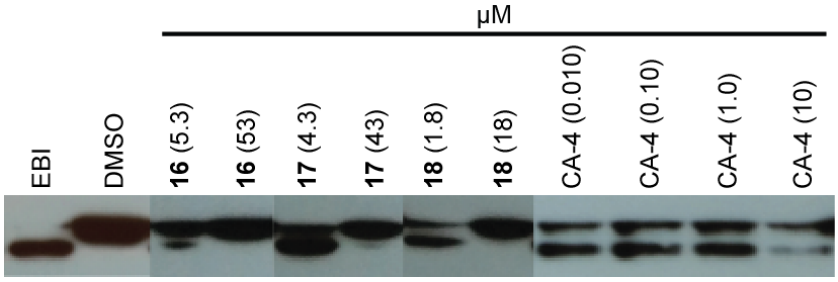

Figure 3.7. Effect of PID-SOs **16-18** on the binding of EBI to the C-BS at 100- and 1000-times their respective IC_{50}. CA-4 was used as a positive control while 0.5% DMSO and EBI were used as negative and reference controls, respectively.

3.6.6. PID-SOs are not affected by alterations in α- and β-tubulin and overexpression of P-glycoprotein

The most potent PID-SOs (**16-18**) were assessed on wild-type (CHO-10001), colchicine- and vinblastine- (CHO-VV 3-2) and paclitaxel-resistant (CHO-TAX 5-6) Chinese hamster ovary cells using the sulforhodamine B colorimetric assay. These cell lines originate from parental CHO-10001 with alterations in α- and β-tubulin. The CHO-VV 3-2 cell line is resistant to vinblastine and colchicine and hypersensitive to paclitaxel, whereas the CHO-TAX 5-6 cell line is resistant to paclitaxel and hypersensitive to vinblastine (Cabral et al., 1980; Schibler et al., 1989; Schibler et al., 1986). Paclitaxel and vinblastine were used as positive controls. As depicted in Table 3.2, PID-SOs **16-18** exhibit the most potent antiproliferative activities on the CHO-TAX 5-6 cell line (0.054 - 1.2 μM) and the weakest on the CHO-VV 3-2 cell line (0.11 - 1.8 μM). Furthermore, the CHO-TAX 5-6/CHO-10001 ratio of PID-SOs **16-18** is under 1.0, meaning they are not affected by the resistant mechanisms of CHO-TAX 5-6 cell line. However, a small resistance effect is observed with the CHO-VV 3-2 cell line albeit weaker than that observed with vinblastine. These results strongly suggest that the cytotoxicity of PID-SOs is not or only slightly affected by alterations in α- and β-tubulin.

Table 3.2. Antiproliferative activity and ratio of resistance of PID-SOs **16-18**, paclitaxel and vinblastine on wild-type (CHO-10001), colchicine- and vinblastine- (CHO-VV 3-2) and paclitaxel-resistant (CHO-TAX 5-6) Chinese hamster ovary cells.

#	IC_{50} (μM)[1]				
				Ratio resistant/wild-type	
	CHO-10001	**CHO-TAX 5-6**	**CHO-VV 3-2**	**CHO-TAX 5-6 /CHO-10001**	**CHO-VV 3-2 /CHO-10001**
16	1.4	1.2	1.8	0.87	1.3
17	1.3	0.72	1.4	0.55	1.1
18	0.059	0.054	0.11	0.92	1.9
Pac[2]	0.65	0.96	0.44	1.5	0.67
Vbl[3]	0.027	0.017	0.067	0.64	2.5

[1]IC_{50} represents the concentration of drug inhibiting cell growth by 50%. [2]Pac, paclitaxel. [3]Vbl, vinblastine.

PID-SOs **16-18** were also evaluated using the MTT cell proliferation assay on T lymphoblastoid leukemia CEM and CEM-VLB cells. CEM-VLB cells overexpress the P-glycoprotein which is responsible for the cellular efflux of several anticancer drugs such as paclitaxel and vinblastine (Struski et al., 2002). Furthermore, the P-glycoprotein is part of an important mechanism of resistance encountered in clinical settings (Beck et al., 1979; Hu et al., 1990; Ueda et al., 1987). As shown in Table 3.3, PID-SOs **16-18** have IC_{50} in the low to high nanomolar ranges. Their resistance ratios are varying from 1.8 to 2.3, while paclitaxel and vinblastine have ratios of 83 and 42, respectively. These results indicate that PID-SOs are poorly affected by the overexpression of P-glycoprotein.

Table 3.3. Cell viability and ratio of resistance of PID-SOs **16-18** on wild-type T lymphoblastoid leukemia CEM and resistant CEM-VLB cells.

#	IC_{50} (µM)[1]		
	CEM	**CEM-VLB**	**Ratio resistant/wild-type CEM-VLB/CEM**
16	0.39	0.83	2.2
17	0.34	0.59	1.8
18	0.014	0.032	2.3
Pac[2]	0.0020	0.16	83
Vbl[3]	0.00088	0.037	42

[1]IC_{50} represents the concentration of drug inhibiting cell growth by 50% in micromolar. [2]Pac, paclitaxel. [3]Vbl, vinblastine.

3.6.7. Molecular docking of PID-SOs in the C-BS

In the aim to identify the most active conformations of PID-SOs and their key interactions with amino acids of the C-BS, PID-SOs **16**-**18** were docked using Molecular Operating Environment (MOE) and X-ray crystallographic structure of the α, β-tubulin heterodimer (RCSB protein data bank: 1SA0), (Ravelli et *al*., 2004). The C-BS model is composed of 32 amino acids distributed in the vicinity of the colchicine and GTP. First of all, our molecular modeling results show that PID-SOs **16** and **17** bearing a 3,5-OMe and a 3,5-Br group, respectively docked into the C-BS while PID-SO **18** bearing 3,4,5-OMe is unable to dock with the C-BS due to the steric hindrance. This result indicates that the C-BS should actually be very flexible which is not the case in our model. The energy score of the five most favourable docking poses in the C-BS of PID-SOs **16** and **17** are shown in Table 3.4. The most favourable poses of PID-SOs **16** and **17** have S scores of -7.42 and -7.18 kcal/mol, respectively and are depicted in Fig. 3.8A and B. Our results showed that PID-SOs **16** and **17** are positioned in a similar way and are able to dock into the C-BS. Fig. 3.8C and D show the 2D interaction diagrams of PID-SOs **16** and **17** with the amino acids of the C-BS. The interactions are summarised in Table 3.5. PID-SOs **16** and **17** have one and two interactions, respectively. The carbonyl at position two of PID-SO **16** achieves a hydrogen bond acceptor interaction with Asn101 while the carbonyl at position four of PID-SO **17**

performs a hydrogen bond acceptor interaction with Gln11. Moreover, the bromine atom of PID-SO **17** harbour an additional hydrogen donor interaction with Ala317. These results show that PID-SOs **16** and **17** can dock into the C-BS and interact with its amino acids.

Table 3.4. Docking energy scores of the five most favourable poses of PID-SOs **16** and **17** in the C-BS.

Poses	**16**		**17**	
	S (kcal/mol)	RMSD refine (Å)	S (kcal/mol)	RMSD refine (Å)
1	-7.42	0.98	-7.18	2.07
2	-7.38	1.86	-7.13	2.79
3	-7.22	1.54	-7.00	1.68
4	-7.20	1.21	-6.96	1.96
5	-7.14	1.90	-6.81	1.29

Table 3.5. Interactions summary of the most favourable poses of PID-SOs **16** and **17** with the amino acids of the C-BS.

	Ligand Atom	Receptor Atom	Interaction		Distance (Å)	Energy (Kcal/mol)
			Amino Acid	Type		
16	O34	ND2	Asn101	H-acceptor	3.17	-1.5
17	Br25	O	Ala317	H-donor	3.28	-0.6
	O35	NE2	Gln11	H-acceptor	2.87	-0.7

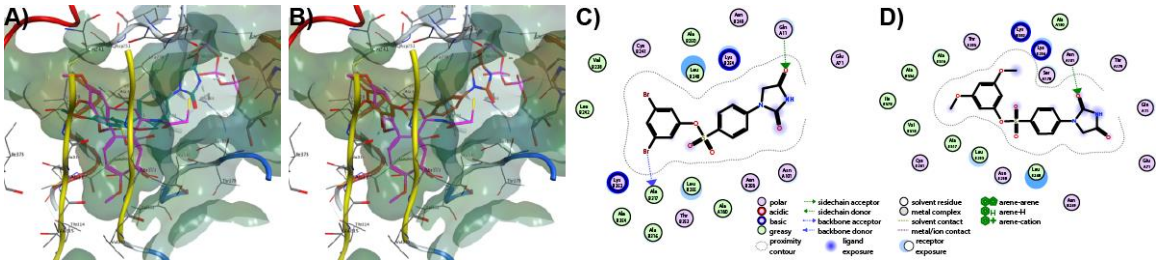

Figure 3.8. Docking of PID-SOs A) **16** (cyan) and B) **17** (red) showing the most stable poses in the C-BS with colchicine (purple). C-BS surface color coding: hydrophobicity (blue) and hydrophilicity (brown). 2D interaction diagrams of the most favourable poses of PID-SOs C) **16** and D) **17** in the C-BS.

3.6.8. PID-SOs exhibit drug-likeness properties

Pharmacokinetic, physicochemical and drug-likeness properties are of the uttermost importance when designing and developing new drugs notably for oral administration and appropriate systemic biological effects. Hence, we used the free online tool SwissADME in an effort to evaluate the effect of chemical modulations on theoretical pharmacokinetic, physicochemical and drug-likeness properties of our new PID-SO derivatives (Cheng et al., 2012; Daina et al., 2017). To that end, the most potent PID-SOs (**12**-**14**, **16**-**18**) were selected for this analysis and the results are shown in Table 3.6. First of all, selected PID-SOs have molecular weights ranging from 366.78 to 490.12 g/mol. The number of rotatable bonds ranges from four to seven. They have five to eight H-bond acceptors and they have one H-bond donor. The topological polar surface area (TPSA) varies from 101.16 to 128.85 $Å^2$. The CLogP fluctuates from 1.50 to 2.73 while LogS varies from -5.11 to -4.00. They are moderately soluble, have a high probability of gastrointestinal absorption (GIA) and cannot cross the blood-brain barrier (BBB). They should not be a substrate of the P-glycoprotein, an important protein involved in multidrug resistance, as confirmed by our previous experiments. Lastly, except for compound **17**, all the selected derivatives have no violation of Lipinski, Veber, Egan and Muegge filters. Compound **17** violation of Ghose drug-likeness properties is due to its molecular weight of 490.12 g/mol higher than 480.00 g/mol. All the parameters of the other filters are respected. Therefore, PID-SOs exhibit high theoretical drug-likeness properties and bioavailability scores making them a new family of promising antimicrotubule agents.

Table 3.6. Physicochemical, pharmacokinetic and drug-likeness properties of PID-SOs **12-14** and **16-18** from SwissADME tool.

#	Rb[1]	H-Ba[2]	H-BD[3]	TPSA[4] (Å^2)	CLogP[5]	LogS[6]	Sclass[7]	GIA[8]	BBBP[9]	P-gp[10]	Drug-like (#viol.)[11]
12	4	5	1	101.16	2.09	-4.33	MS	H	No	No	Yes (0)
13	4	5	1	101.16	2.13	-4.39	MS	H	No	No	Yes (0)
14	4	5	1	101.16	2.12	-4.21	MS	H	No	No	Yes (0)
16	6	7	1	119.62	1.50	-4.00	MS	H	No	No	Yes (0)
17	4	5	1	101.16	2.73	-5.11	MS	H	No	No	Yes (1 Ghose) MW>480
18	7	8	1	128.85	1.54	-4.03	MS	H	No	Yes	Yes (0)

[1]Rb: number of rotatable bonds. [2]H-Ba: number of H-bond acceptors. [3]H-BD: number of H-bond donors. [4]TPSA: topological polar surface area. [5]CLogP: consensus Log P (average of iLOGP, XLOGP3, WLOGP, MLOGP and Silicos-IT Log P). [6]LogS: Ali topological method Log S. [7]SClass: Ali solubility class (insoluble (IS) < -10<poorly soluble (PS) < - 6< moderately soluble (MS) < -4 < soluble (S) < -2 < very soluble (VS) < 0 < highly soluble (HS)). [8]GIA: gastrointestinal absorption (H means high). [9]BBBP: blood-brain barrier permeability. [10]P-gp: P-glycoprotein substrates. [11]Drug-like: drug-likeness indices (bioavailability) from Lipinski, Ghose, Veber, Egan and Muegge filters. # viol: number of violations of the five filters.

3.7. Conclusion

In conclusion, we prepared and biologically evaluated 32 new PID-SO and EPA-SO derivatives. Our SAR studies show that the modification of IMZ moiety of PIB-SOs by an ethyl 2-ureidoacetate or an imidazolidin-2,5-dione moiety is detrimental for the activity while its modification by an imidazolidin-2,4-dione moiety allows an antiproliferative activity in the nanomolar to low micromolar ranges on four human cancer cell lines tested. They arrest the cell cycle progression in G2/M phase, bind to the C-BS leading to the inhibition of microtubules polymerisation and disruption of cytoskeleton. Their antiproliferative activities are not impaired on paclitaxel-resistant cell line and on multidrug-resistant CEM-VBL cell line. Finally, PID-SOs exhibit appropriate theoretical pharmacokinetic and physicochemical properties making them a new family of promising anticancer agents targeting the C-BS.

3.8. Acknowledgments

This work was supported by grants from Natural Sciences and Engineering Research Council of Canada (NSERC, RGPIN-2016-05069), Fonds de Recherche du Québec-Santé (FRQS, starting grant for new investigators) and CHU de Quebec-Université Laval Research Center. S. Fortin holds a Junior 1 research scholar award from FRQS. M. Gagné-Boulet and C. Bouzriba are recipients of studentships from FRQS. A.C. Chavez Alvarez and C. Bouzriba are recipients of studentships from Fonds d'enseignement et de recherche of the Faculty of pharmacy of Université Laval.

3.9. References

Asbury, C. L. (2017). Anaphase A: disassembling microtubules move chromosomes toward spindle poles. *Biology-Basel, 6*, 32. doi: 10.3390/biology6010015

Beck, W. T., Mueller, T. J., & Tanzer, L. R. (1979). Altered surface membrane glycoproteins in *Vinca* alkaloid-resistant human leukemic lymphoblasts. *Cancer Research, 39*, 2070-2076.

Cabral, F., Sobel, M. E., & Gottesman, M. M. (1980). CHO mutants resistant to colchicine, colcemid or griseofulvin have an altered β-tubulin. *Cell, 20*, 29-36. doi: 10.1016/0092-8674(80)90231-7

Chen, X., Wang, S. M., Kumar, G. B., Bare, G. A. L., Leng, J., Bukhari, S. N. A., & Qin, H. L. (2018). Recent developments on phenstatins as potent antimitotic agents. *Current Medicinal Chemistry, 25*, 2329-2352. doi: 10.2174/0929867324666171106162048

Cheng, F. X., Li, W. H., Zhou, Y. D., Shen, J., Wu, Z. R., Liu, G. X., Lee, P. W., & Tang, Y. (2012). AdmetSAR: A comprehensive source and free tool for assessment of chemical ADMET properties. *Journal of Chemical Information and Modeling, 52*, 3099-3105. doi: 10.1021/ci300367a

Cytoskeleton Inc, Tubulin polymerization assay using >99% pure tubulin, fluorescence based. Retrieved from https://www.cytoskeleton.com/kits/tubulin-assays/bk011p

Daina, A., Michielin, O., & Zoete, V. (2017). SwissADME: a free web tool to evaluate pharmacokinetics, drug-likeness and medicinal chemistry friendliness of small molecules. *Scientific Reports, 7*, 42717. doi: 10.1038/srep42717

Dumontet, C., & Jordan, M. A. (2010). Microtubule-binding agents: a dynamic field of cancer therapeutics. *Nature Reviews Drug Discovery, 9*, 790-803. doi: 10.1038/nrd3253

Ferlay, J., Colombet, M., Soerjomataram, I., Mathers, C., Parkin, D. M., Pineros, M., Znaor, A., & Bray, F. (2019). Estimating the global cancer incidence and mortality in 2018: GLOBOCAN sources and methods. *International Journal of Cancer, 144*, 1941-1953. doi: 10.1002/ijc.31937

Field, Jessica J., Díaz, José F., & Miller, John H. (2013). The binding sites of microtubule-stabilizing agents. *Chemistry & Biology, 20*, 301-315. doi: 10.1016/j.chembiol.2013.01.014

Fortin, S., Lacroix, J., Côté, M.-F., Moreau, E., Petitclerc, É., & C.-Gaudreault, R. (2010). Quick and simple detection technique to assess the binding of antimicrotubule agents to the colchicine-binding site. *Biological Procedures Online, 12*, 113-117. doi: 10.1007/s12575-010-9029-5

Fortin, S., Wei, L., Moreau, E., Lacroix, J., Côté, M.-F., Petitclerc, É., Kotra, L. P., & C.-Gaudreault, R. (2011a). Substituted phenyl 4-(2-oxoimidazolidin-1-yl)benzenesulfonamides as antimitotics. Antiproliferative, antiangiogenic and antitumoral activity, and quantitative structure-activity relationships. *European Journal of Medicinal Chemistry, 46*, 5327-5342. doi: 10.1016/j.ejmech.2011.08.034

Fortin, S., Wei, L. H., Moreau, E., Lacroix, J., Côté, M.-F., Petitclerc, É., Kotra, L. P., & C.-Gaudreault, R. (2011b). Design, synthesis, biological evaluation, and structure-activity relationships of substituted phenyl 4-(2-oxoimidazolidin-1-yl)-benzenesulfonates as new tubulin inhibitors mimicking combretastatin A-4. *Journal of Medicinal Chemistry, 54*, 4559-4580. doi: 10.1021/jm200488a

Gagné-Boulet, M., Bouzriba, C., Chavez Alvarez, A. C., & Fortin, S. (2021). Phenyl 4-(2-oxopyrrolidin-1-yl)benzenesulfonates and phenyl 4-(2-oxopyrrolidin-1-

yl)benzenesulfonamides as new antimicrotubule agents targeting the colchicine-binding site. *European Journal of Medicinal Chemistry, 213*, 113136. doi: 10.1016/j.ejmech.2020.113136

Gagné-Boulet, M., Bouzriba, C., Godard, M., & Fortin, S. (2018). Preparation, characterisation and biological evaluation of new *N*-phenyl amidobenzenesulfonates and *N*-phenyl ureidobenzenesulfonates inducing DNA double-strand breaks. Part 3. Modulation of ring A. *European Journal of Medicinal Chemistry, 155*, 681-694. doi: 10.1016/j.ejmech.2018.06.030

Gagné-Boulet, M., Fortin, S., Lacroix, J., Lefebvre, C. A., Côté, M.-F., & C.-Gaudreault, R. (2015a). Styryl-*N*-phenyl-*N*'-(2-chloroethyl)ureas and styrylphenylimidazolidin-2-ones as new potent microtubule-disrupting agents using combretastatin A-4 as model. *European Journal of Medicinal Chemistry, 100*, 34-43. doi: 10.1016/j.ejmech.2015.05.034

Gagné-Boulet, M., Moussa, H., Lacroix, J., Côté, M.-F., Masson, J.-Y., & Fortin, S. (2015b). Synthesis and biological evaluation of novel *N*-phenyl ureidobenzenesulfonate derivatives as potential anticancer agents. Part 2. Modulation of the ring B. *European Journal of Medicinal Chemistry, 103*, 563-573. doi: 10.1016/j.ejmech.2015.09.012

Grosios, K., Holwell, S. E., McGown, A. T., Pettit, G. R., & Bibby, M. C. (1999). *In vivo* and *in vitro* evaluation of combretastatin A-4 and its sodium phosphate prodrug. *British Journal of Cancer, 81*, 1318-1327. doi: 10.1038/sj.bjc.6692174

Hirota, K., Banno, K., Yamada, Y., & Senda, S. (1985). Pyrimidines. Part 53. Novel ring transformation induced by the substituent effect of the phenyl group. Reaction of 5-bromo-6-methyl-1-phenyluracil derivatives with amines and hydrazine to give hydantoins and pyrazolones. *Journal of the Chemical Society, Perkin Transactions 1*, 1137-1142. doi: 10.1039/P19850001137

Hu, X. F., Martin, T. J., Bell, D. R., de Luise, M., & Zalcberg, J. R. (1990). Combined use of cyclosporin A and verapamil in modulating multidrug resistance in human leukemia cell lines. *Cancer Research, 50*, 2953-2957.

Jordan, M. A., & Wilson, L. (2004). Microtubules as a target for anticancer drugs. *Nature Reviews Cancer, 4*, 253-265. doi: 10.1038/nrc1317

McLoughlin, E. C., & O'Boyle, N. M. (2020). Colchicine-binding site inhibitors from chemistry to clinic: a review. *Pharmaceuticals (Basel, Switzerland), 13*, 8. doi: 10.3390/ph13010008

Nam, N. H. (2003). Combretastatin A-4 analogues as antimitotic antitumor agents. *Current Medicinal Chemistry, 10*, 1697-1722. doi: 10.2174/0929867033457151

National Cancer Institute (NCI/NIH), Developmental therapeutics program human tumor cell line screen. Retrieved from http://dtp.nci.nih.gov/branches/btb/ivclsp.html

Prosser, S. L., & Pelletier, L. (2017). Mitotic spindle assembly in animal cells: a fine balancing act. *Nature Reviews Molecular Cell Biology, 18*, 187-201. doi: 10.1038/nrm.2016.162

Ravelli, R. B., Gigant, B., Curmi, P. A., Jourdain, I., Lachkar, S., Sobel, A., Knossow, M. (2004). Tubulin-colchicine: stathmin-like domain complex. *RCSB Protein Data Bank*. doi: 10.2210/pdb1sa0/pdb

Schibler, M. J., Barlow, S. B., & Cabral, F. (1989). Elimination of permeability mutants from selections for drug resistance in mammalian cells. *The FASEB Journal, 3*, 163-168. doi: 10.1096/fasebj.3.2.2563346

Schibler, M. J., & Cabral, F. (1986). Taxol-dependent mutants of Chinese hamster ovary cells with alterations in α- and β-tubulin. *Journal of Cell Biology, 102*, 1522-1531. doi: 10.1083/jcb.102.4.1522

Shan, B., Medina, J. C., Santha, E., Frankmoelle, W. P., Chou, T. C., Learned, R. M., Narbut, M. R., Stott, D., Wu, P. G., Jaen, J. C., Rosen, T., Timmermans, P., & Beckmann, H. (1999). Selective, covalent modification of β-tubulin residue Cys-239 by T138067, an antitumor agent with *in vivo* efficacy against multidrug-resistant tumors. *Proceedings of the National Academy of Sciences of the United States of America, 96*, 5686-5691. doi: 10.1073/pnas.96.10.5686

Struski, S., Cornillet-Lefebvre, P., Doco-Fenzy, M., Dufer, J., Ulrich, E., Masson, L., Michel, N., Gruson, N., & Potron, G. (2002). Cytogenetic characterization of chromosomal rearrangement in a human vinblastine-resistant CEM cell line: use of comparative genomic hybridization and fluorescence in situ hybridization. *Cancer Genetics and Cytogenetics, 132*, 51-54. doi: 10.1016/S0165-4608(01)00519-2

Turcotte, V., Fortin, S., Vevey, F., Coulombe, Y., Lacroix, J., Côté, M.-F., Masson, J.-Y., & C.-Gaudreault, R. (2012). Synthesis, biological evaluation, and structure-activity relationships of novel substituted *N*-phenyl ureidobenzenesulfonate derivatives blocking cell cycle progression in S-phase and inducing DNA double-strand breaks. *Journal of Medicinal Chemistry, 55*, 6194-6208. doi: 10.1021/jm3006492

Ueda, K., Cardarelli, C., Gottesman, M. M., & Pastan, I. (1987). Expression of a full-length cDNA for the human "MDR1" gene confers resistance to colchicine, doxorubicin, and vinblastine. *Proceedings of the National Academy of Sciences of the United States of America, 84*, 3004-3008. doi: 10.1073/pnas.84.9.3004

3.10. Appendix B. Supplementary data

Experimental section, proton and carbon NMR spectra as well as calculated physicochemical, pharmacokinetic and drug-likeness properties by SwissADME tool of the most promising PID-SOs (**12**-**14** and **16**-1**8**) assessed using our biofunctional assays can be found in the appendix B.

Chapitre 4. Rationale, synthesis and biological evaluation of substituted 1-(4-(phenylthio)phenyl)imidazolidin-2-one, urea, thiourea and amide analogs and derivatives designed to target the colchicine-binding site

Mathieu Gagné-Boulet [a, b, *], Chahrazed Bouzriba [a, b], Atziri Corin Chavez Alvarez [a, b, c], Sébastien Fortin [a, b, *]

[a]Centre de recherche du CHU de Québec-Université Laval, Axe oncologie, Hôpital Saint-François d'Assise, 10 rue de l'Espinay, Québec, QC, G1L 3L5, Canada.

[b]Faculté de pharmacie, Université Laval, Pavillon Ferdinand-Vandry, 1050 avenue de la Médecine, Québec, QC, G1V 0A6, Canada.

[c]Centre de recherche de l'Institut universitaire de cardiologie et de pneumologie de Québec-Université Laval, 2725 Ch Ste-Foy, Québec, QC, G1V 4G5, Canada.

***Corresponding authors:** Mathieu Gagné-Boulet; Phone: 418-525-4444 ext. 52425, e-mail: mathieu.gagne-boulet.1@ulaval.ca and Sébastien Fortin; Phone: 418-525-4444 ext. 52364, e-mail: sebastien.fortin@pha.ulaval.ca.

Soumis le 26 mai 2021 à l'Éditeur du journal Bioorganic and Medicinal Chemistry.

4.1. Résumé

Nous avons conçu, préparé et évalué l'activité biologique de 42 nouveaux analogues et dérivés de phényl 4-(2-oxoimidazolidin-1-yl)benzènesulfonates (PIB-SOs) nommés 1-(4-(phénylthio)phényl)imidazolidin-2-ones (TPIs), 1-éthyl-3-(4-(phénylthio)phényl)thiourées (TPTs), 1-(4-(phénylthio)phényl)urées (TPUs), et *N*-(4-(phénylthio)phényl)butyramides (TPAs). L'activité antiproliférative des TPAs, TPTs et des TPUs portant un groupement éthyle ou phényle est généralement de l'ordre du micromolaire alors que les TPUs portant un groupement 2-chloroéthyle et les TPIs possèdent une activité antiproliférative dans le nanomolaire au bas micromolaire. Les TPUs et les TPIs les plus puissants arrêtent le cycle cellulaire en phase G2/M et causent la perturbation du cytosquelette. Les TPIs se lient au site de liaison de la colchicine et les TPUs et TPIs ne sont généralement pas, ou faiblement affectés par des lignées cellulaires résistantes aux agents antimicrotubules et multirésistantes. Leurs propriétés physicochimiques, pharmacocinétiques théoriques sont bien adaptées pour une évaluation préclinique plus poussée. Enfin, les TPIs **40** et **43** présentent une faible toxicité chez les embryons de poulet.

4.2. Abstract

Microtubules are an important biological target in cancer chemotherapy since they are essential to form the mitotic spindle during cell division and in cell morphogenesis. Hence, we previously designed and developed a family of potent antimicrotubule agents designated as phenyl 4-(2-oxoimidazolidin-1-yl)benzenesulfonates (PIB-SOs) that are active at the nanomolar level both *in vitro* and *in vivo*. The aim of this study was to evaluate the effect of replacing 1) the sulfonate bridge of PIB-SOs by a thioether bridge and 2) the imidazolidin-2-one group by either various substituted urea moieties, an ethylthiourea or a butyramide group. To that end, we designed, prepared and biologically evaluated 42 new analogs and derivatives of PIB-SOs namely 1-(4-(phenylthio)phenyl)imidazolidin-2-ones (TPIs), 1-(4-(phenylthio)phenyl)ureas (TPUs), 1-ethyl-3-(4-(phenylthio)phenyl)thioureas (TPTs) and *N*-(4-(phenylthio)phenyl)butyramides (TPAs). The antiproliferative activity of TPAs, TPTs and TPUs bearing an ethyl or a phenyl group tested on HT-1080, HT-29, M21 and MCF7 human cancer cell lines are generally within the micromolar ranges (7.0 - >100, 4.1 - 49, 8.1 - >100 and 1.5 - >100 μM, respectively) while TPUs bearing a 2-chloroethyl group and TPIs exhibit antiproliferative activity in the nanomolar to the low micromolar ranges (0.71 - 16 and 0.13 - >10 μM, respectively). The most potent TPUs and TPIs arrest the cell cycle progression in G2/M phase and cause cytoskeleton disruption. TPIs bind to the colchicine-binding site and the antiproliferative activity of TPU and TPI derivatives is generally not or only weakly hampered in antimicrotubule- and multidrug-resistant cell lines. They also possess suitable theoretical physicochemical, pharmacokinetics and drug-likeness properties supporting further preclinical evaluation. Lastly, TPIs **40** and **43** show low toxicity in chick embryos suggesting that they are a new promising family of antimitotics.

4.3. Graphical abstract

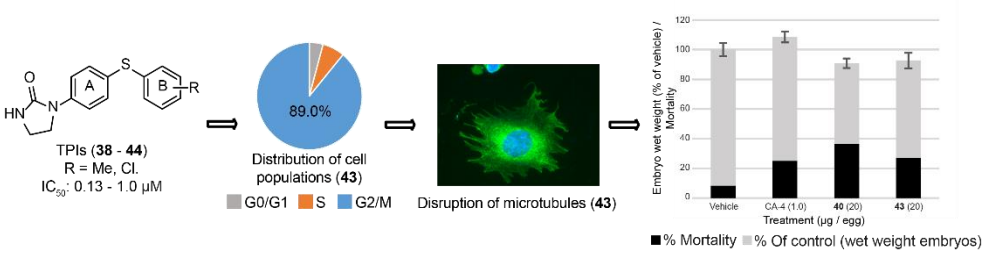

4.4. Introduction

Despite recent advances in medicine, the global burden of cancer is still of outmost concern. In the United States alone, over 600 000 cancer deaths are projected to occur in 2021.[1] Therefore, the development of new treatments is of highest importance. Treatment of cancer patients involves notably surgery, radiotherapy and systemic therapy. Chemotherapy is one of the main approaches for the systemic therapies used to alleviate cancer patients. However, members of the anticancer armamentarium are of limited usage due particularly to chemoresistance, high toxicities and lack of selectivity.[2, 3] Therefore, there are pressing needs to develop new anticancer agents overcoming the aforementioned limitations.

Microtubules are long hollow cylinders composed of α, β-tubulin heterodimers. They are in a constant dynamic equilibrium between polymerization and depolymerization states.[4] They play a crucial role in several eukaryotic cell processes such as cell division and morphogenesis, growth, intracellular signaling, motility, vesicle transport and mitochondrial functions.[5] Especially, they form the mitotic spindle with chromosomes and other proteins during mitosis leading to the separation of the sister chromatids between daughter cells.[6] Therefore, the disruption of microtubules prevents tumor growth and ultimately leads to cancer cell death which makes microtubules a target of choice for the development of new antineoplastic agents.[7]

Antimicrotubule agents or antimitotics are remarkably useful at inhibiting the proliferation of most cancer cells.[8] Indeed, they are commonly administered as first-line treatments against several types of cancer such as lung, breast, prostate, ovarian and leukemia cancers.[9] Antimicrotubule agents can act by to two general mechanisms of action. First, their activity can be based either on the inhibition of the polymerization of microtubules such as for combretastatin A-4 phosphate disodium (CA-4PD, **1**, Fig. 4.1A) or second on the hyperstabilization of microtubules triggered by drugs such as for paclitaxel (**2**, Fig. 4.1B). Both mechanisms induce to the arrest of the cell cycle progression in G2/M phase and ultimately to cell apoptosis.[10, 11]

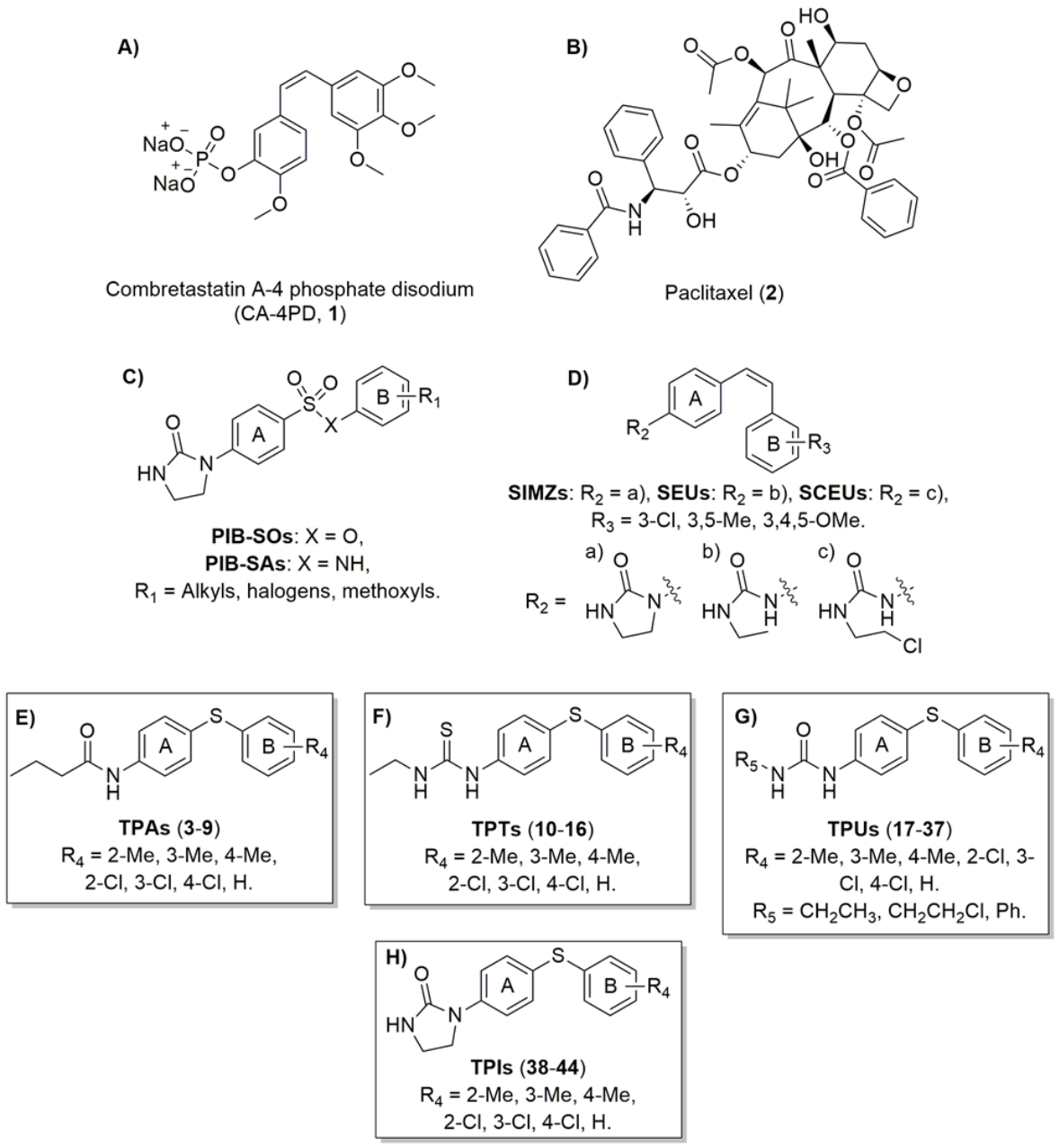

Figure 4.1. Molecular structures of A) combretastatin A-4 phosphate disodium (CA-4PD, **1**), B) paclitaxel (**2**), C) phenyl 4-(2-oxoimidazolidin-1-yl)benzenesulfonates (PIB-SOs), phenyl 4-(2-oxoimidazolidin-1-yl)benzenesulfonamides (PIB-SAs), D) styrylphenylimidazolidin-2-ones (SIMZs), styryl-*N*-phenyl-*N*'-ethylureas (SEUs), styryl-*N*-phenyl-*N*'-(2-chloroethyl)ureas (SCEUs), E) *N*-(4-(phenylthio)phenyl)butyramides (TPAs), F) 1-ethyl-3-(4-(phenylthio)phenyl)thioureas (TPTs), G) 1-(4-(phenylthio)phenyl)ureas (TPUs) and H) 1-(4-(phenylthio)phenyl)imidazolidin-2-ones (TPIs).

Our research group previously developed a family of anticancer agents referred to as phenyl 4-(2-oxoimidazolidin-1-yl)benzenesulfonates (PIB-SOs).[12-14] PIB-SOs have low molecular weights (<500 g/mol) and their molecular scaffold is based upon two aromatic rings (A and B) linked together by a sulfonate bridge (Fig. 4.1C).[15] They bear also an imidazolidin-2-one moiety (IMZ) at position 4 on ring A and either short alkyl chain, methoxyl or halogen groups at positions 2, 3, 4, 3,5 or 3,4,5 on ring B. The antiproliferative activity of the most potent PIB-SOs is in the nanomolar range on numerous human cancer cell lines. They arrest the cell cycle progression in G2/M phase and disrupt the cytoskeleton by binding to the colchicine-binding site (C-BS).[15, 16] Our previous structure-activity relationship studies were focusing on the nature and the position of substituents located on both rings but only two modifications have been studied on the sulfonate bridge so far.[13, 15] The sulfonate group was replaced by a sulfonamide or by an ethenyl group leading to the generation of new phenyl 4-(2-oxoimidazolidin-1-yl)-benzenesulfonamides (PIB-SAs, Fig. 4.1C) and styrylphenylimidazolidin-2-ones (SIMZs, Fig. 4.1D).[13] Moreover, the imidazolidin-2-one moiety of SIMZs was previously substituted by an ethylurea (SEUs, Fig. 4.1D) or a 2-chloroethylurea group (SCEUs, Fig. 4.1D). In this study, we replaced 1) the sulfonate bridge of PIB-SOs by a thioether bridge, and 2) the imidazolidin-2-one moiety by either a butyramide, an ethylthiourea or urea encompassing either ethyl, 2-chloroethyl or phenyl groups leading to four new families of compounds designated as substituted *N*-(4-(phenylthio)phenyl)butyramides (TPAs, **3**-**9**, Fig. 4.1E), 1-ethyl-3-(4-(phenylthio)phenyl)thioureas (TPTs, **10**-**16**, Fig. 4.1F), 1-(4-(phenylthio)phenyl)ureas (TPUs, **17**-**37**, Fig. 4.1G) and 1-(4-(phenylthio)phenyl)imidazolidin-2-one (TPIs, **38**-**44**, Fig. 4.1H).

First, the substitution of the sulfonate bridge of PIB-SOs by a thioether bridge aims to study the importance of the oxygen atoms, the length and the electronegativity of the bridge as well as the importance of the number of vibrational degrees of freedom of both aromatic rings on the antiproliferative activity. In addition, butyramide, ethylthiourea, ethylurea, 2-chloroethylurea and phenylurea groups were studied as a way to find new potent bioisosteres of the IMZ moiety in case that unexpected biopharmaceutical obstacles arise during the development of PIB-SOs. Finally, the nature and the position of substituents on aromatic ring B were selected based on our previous research programs on PIB-SOs, SIMZ

and on the commercial availability of the precursors. All final compounds were assessed for their antiproliferative activity on human HT-1080 fibrosarcoma, HT-29 colon adenocarcinoma, M21 melanoma and MCF7 estrogen-dependent breast adenocarcinoma. The most potent compounds were assessed also for their effect on the cell cycle progression, cytoskeleton disruption and their affinity to the C-BS. Furthermore, the antiproliferative activity of the latter molecules was evaluated on wild-type Chinese hamster ovary (CHO-10001), vinblastine- (CHO-VV 3-2) and paclitaxel-resistant (CHO-TAX 5-6) cells as well as T lymphoblastoid leukemia (CEM) and multidrug-resistant (CEM-VLB) cell lines to determine if they are affected by vinblastine-, paclitaxel- and multidrug-resistant mechanisms. Finally, their theoretical physicochemical and pharmacokinetic properties were calculated using SwissADME, an online web tool and their toxicity was studied on developing chick embryos.

4.5. Chemistry

The preparations of TPAs **3**-**9**, TPTs **10**-**16**, TPUs **17**-**37** and TPIs **38**-**44** are depicted in Scheme 4.1 and were achieved in two steps for TPAs, TPTs and TPUs and in three steps for TPIs. The general synthesis is initiated by the preparation of substituted phenylthioanilines based on slight modifications of the method described by Huang *et al*. with slight modifications.[17] Briefly, 4-iodoaniline is reacted with the corresponding thiophenol using copper oxide and cesium carbonate in toluene under microwaves to give the corresponding phenylthioaniline in fair to excellent yields. Then, the resulting phenylthioaniline was dissolved in acetonitrile with butyryl chloride and triethylamine under microwaves to yield TPAs **3**-**9**. TPTs **10**-**16** and TPUs **17**-**37** were obtained by a nucleophilic addition of the appropriate aniline on ethyl isothiocyanate or the selected isocyanate in ethanol. Finally, intramolecular cyclization of TPUs **24**-**30** with sodium hydride in dry tetrahydrofuran yielded TPIs **38**-**44**.

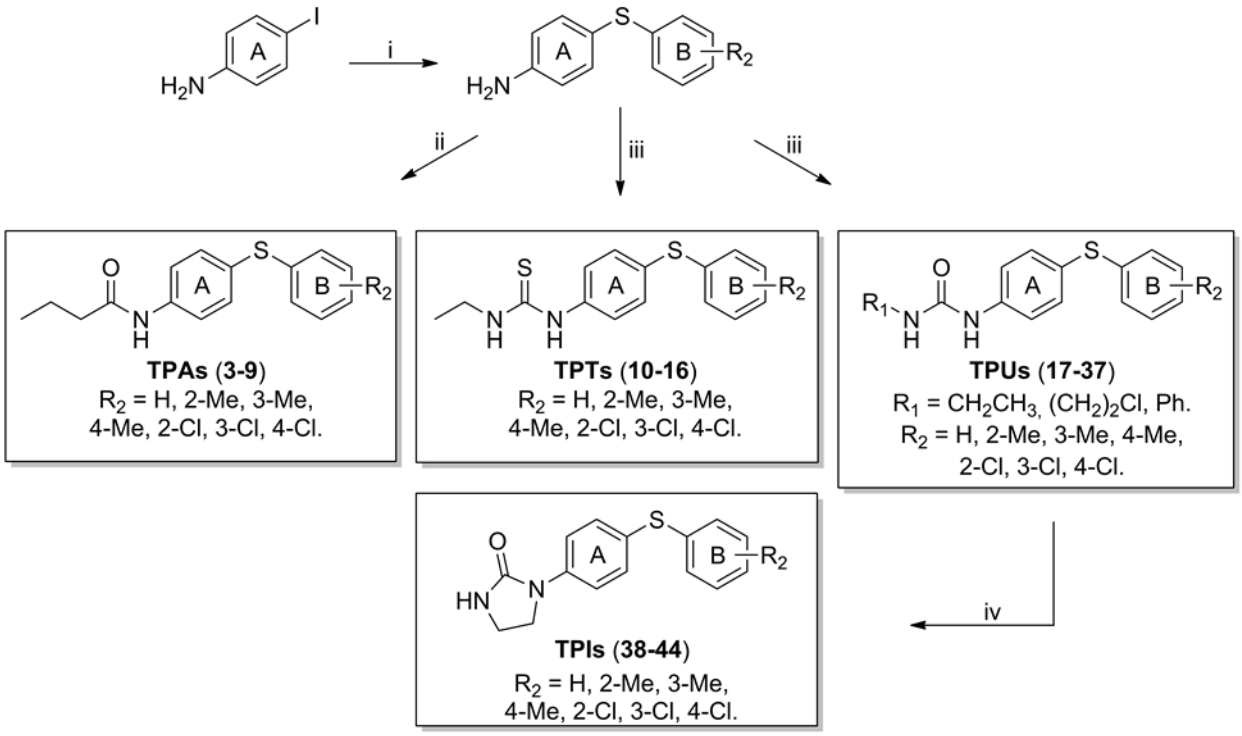

Scheme 4.1. Reagents and conditions: (i) appropriate thiophenol, CuO, Cs_2CO_3, PhMe, 110 °C under microwaves, 24 h, 32% to quantitative; (ii) butyryl chloride, TEA, CH_3CN, 80 °C under microwaves, 8 h, 44 to 99%; (iii) ethyl isothiocyanate or the required isocyanate, EtOH, rt, 24 h, 32% to quantitative; (iv) NaH, THF, 0 °C to rt, 24 h, 36 to 67%.

4.6. Results and discussion

4.6.1. Antiproliferative activity on human cancer cells

The antiproliferative activity of TPAs **3-9**, TPTs **10-16**, TPUs **17-37** and TPIs **38-44** was assessed on human HT-1080, HT-29, M21 and MCF7 tumour cells using the sulforhodamine B colorimetric assay.[18] Results are collated in Table 4.1 and expressed as the concentration of drug inhibiting cell growth by 50% (IC_{50}). Combretastatin A-4 (CA-4) was used as positive control. In general, the sensitivity of cancer cell lines is similar between TPA, TPT, TPU and TPI derivatives. Moreover, the antiproliferative activity of TPAs, TPTs, TPUs and TPIs is only weakly hampered by the nature of the substituent on ring B showing that the position of that substituent on ring B is a factor significantly impacting the antiproliferative activity. The antiproliferative activity of TPAs, TPTs and TPUs bearing an

ethylurea or a phenylurea group is in general in the mid to high micromolar range (1.5 - >100 µM). Therefore, the development of the latter family of PIB-SO analogs was discontinued. TPUs bearing a 2-chloroethylurea moiety show antiproliferative activity in high nanomolar to low micromolar range (0.71 - 16 µM). Except for TPIs **42** and **44**, TPIs exhibit antiproliferative activity in the mid nanomolar to low micromolar ranges (0.13 - 3.0 µM). Moreover, the substitution on the aromatic ring B at position 3 by a methyl group or a chlorine atom yields the most potent TPUs (**26** and **29**) and TPIs (**40** and **43**) exhibiting IC_{50} on the tumor cells ranging from 0.13 to 1.8 µM. Lastly, these results confirm that the sulfonate bridge of PIB-SOs can be replaced by a thioether bridge when the aromatic ring A is substituted either by an imidazolidin-2-one or a 2-chloroethylurea moiety for the inhibition of tumor cells proliferation in nanomolar to low micromolar range.

Table 4.1. Antiproliferative activity (IC_{50}) of TPAs (**3-9**), TPTs (**10-16**), TPUs (**17-37**) and TPIs (**38-44**) on human HT-1080, HT-29, M21 and MCF7 cancer cell lines.

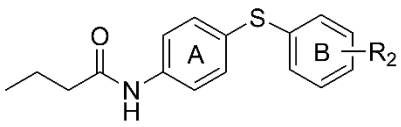

TPAs (3-9)

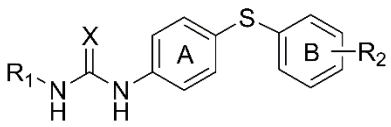

TPTs (10-16)
TPUs (17-37)

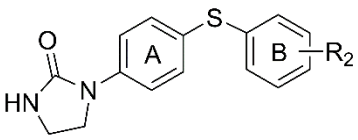

TPIs (38-44)

#	X^2	$R_1{}^2$	R_2	IC_{50} (µM)[1]			
				HT-1080	**HT-29**	**M21**	**MCF7**
3	N/A	N/A	H	25	29	38	7.0
4	N/A	N/A	2-Me	19	12	12	30
5	N/A	N/A	3-Me	29	22	20	37
6	N/A	N/A	4-Me	>100	>100	>100	>100
7	N/A	N/A	2-Cl	17	11	8.0	15
8	N/A	N/A	3-Cl	24	19	15	20
9	N/A	N/A	4-Cl	>100	>100	>100	>100
10	S	Ethyl	H	39	40	49	4.1
11	S	Ethyl	2-Me	37	39	37	41
12	S	Ethyl	3-Me	30	31	32	34
13	S	Ethyl	4-Me	34	36	37	36
14	S	Ethyl	2-Cl	>13	>13	>13	>13
15	S	Ethyl	3-Cl	19	23	22	22
16	S	Ethyl	4-Cl	>25	>25	>25	>25
17	O	Ethyl	H	12	41	50	8.1
18	O	Ethyl	2-Me	42	41	35	40

19	O	Ethyl	3-Me	27	>100	>100	>100
20	O	Ethyl	4-Me	>25	>25	>25	>25
21	O	Ethyl	2-Cl	33	63	44	>100
22	O	Ethyl	3-Cl	35	39	36	31
23	O	Ethyl	4-Cl	>25	>25	>25	>25
24	O	2-chloroethyl	H	3.5	1.0	2.2	2.7
25	O	2-chloroethyl	2-Me	10	6.3	8.8	16
26	O	2-chloroethyl	3-Me	1.8	1.4	1.4	1.4
27	O	2-chloroethyl	4-Me	1.6	1.4	1.7	1.5
28	O	2-chloroethyl	2-Cl	7.6	4.1	5.8	7.5
29	O	2-chloroethyl	3-Cl	1.6	1.3	1.6	0.71
30	O	2-chloroethyl	4-Cl	2.1	1.5	1.3	1.5
31	O	Phenyl	H	15	46	21	2.0
32	O	Phenyl	2-Me	7.5	9.1	10	10
33	O	Phenyl	3-Me	1.5	1.5	1.8	1.7
34	O	Phenyl	4-Me	>100	>100	>100	>100
35	O	Phenyl	2-Cl	17	11	8.0	15
36	O	Phenyl	3-Cl	8.6	9.1	9.4	9.3
37	O	Phenyl	4-Cl	>100	>100	>100	>100
38	N/A	N/A	H	2.6	1.3	1.9	2.7
39	N/A	N/A	2-Me	1.2	0.69	0.63	3.0
40	N/A	N/A	3-Me	0.30	0.15	0.18	1.0
41	N/A	N/A	4-Me	2.2	1.2	1.4	0.15
42	N/A	N/A	2-Cl	2.5	37	1.4	9.5
43	N/A	N/A	3-Cl	0.24	0.18	0.13	0.29
44	N/A	N/A	4-Cl	2.6	1.6	1.3	>10
CA-4[3]	N/A	N/A	N/A	0.0019	0.0051	0.0013	0.018

[1]IC_{50}: concentration of drug inhibiting cell growth by 50%. [2]N/A: Not applicable. [3]CA-4: Combretastatin A-4. The maximum concentration used was set at 100 µM or by solubility limitations.

4.6.2. Arrest of the cell cycle progression

Antimicrotubule agents such as CA-4 and PIB-SOs are known to block the cell cycle progression in G2/M phase.[15, 19] Therefore, the effect of the most potent TPUs (**24**-**30**) and TPIs (**38**-**44**) was assessed on the cell cycle progression. To that end, selected TPUs and TPIs were incubated with M21 cells at 5-times their respective IC_{50} for 24 h. CA-4 and 0.5% DMSO were used as positive and negative controls, respectively. As shown in Table 4.2, cells treated with culture media containing 0.5% DMSO yielded 53.0%, 22.5% and 24.5% in G0/G1, S and G2/M phases, respectively. All TPUs and TPIs assessed inhibited the cell cycle

progression in G2/M phase with a cell distribution in G2/M phase ranging from 59.3% to 85.6% for TPUs and 51.1% to 89.0% for TPIs. TPU **30** bearing a 4-chloro group and TPI **43** bearing a 3-chloro group exhibited the most efficient arrest in G2/M phase with a cell population in G2/M phase of 85.6% and 89.0%, respectively, which is higher than the CA-4 used as positive control (cell distribution in G2/M phase of 74.9%).

Table 4.2. Effect of TPUs **24-30**, TPIs **38-44** and CA-4 on the cell cycle progression on M21 cells after 24 h of treatment.

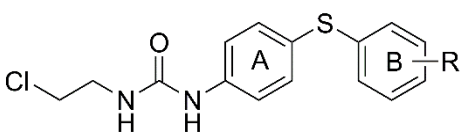

TPUs (24-30)

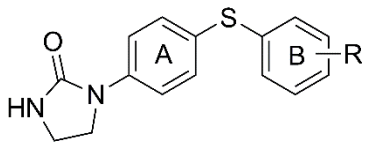

TPIs (38-44)

#	Families	R	Conc. (µM)	Cell cycle progression (%)		
				G0/G1	S	G2/M
24	TPUs	H-	11	14.5	13.6	71.9
25		2-Me	44	28.1	12.6	59.3
26		3-Me	7.0	8.5	6.7	84.8
27		4-Me	8.5	12.5	17.6	69.9
28		2-Cl	29	11.8	7.3	80.9
29		3-Cl	8.0	14.4	15.8	69.8
30		4-Cl	6.5	7.9	6.5	85.6
38	TPIs	H-	9.5	20.0	20.8	59.2
39		2-Me	3.2	13.8	18.2	68.0
40		3-Me	0.90	4.0	8.0	88.0
41		4-Me	7.0	21.5	24.5	54.0
42		2-Cl	7.0	20.6	22.5	56.9
43		3-Cl	0.65	4.2	6.8	89.0
44		4-Cl	6.5	27.0	21.9	51.1
CA-4[1]	N/A	N/A	0.0065	12.0	13.1	74.9
DMSO	N/A	N/A	N/A	53.0	22.5	24.5

[1]CA-4 and 0.5% DMSO were used as positive and negative controls, respectively.

4.6.3. Cytoskeleton disruption

The significant cell cycle progression arrest in G2/M by our most potent TPUs and TPIs prompted us to evaluate their ability to target microtubules and to disrupt the

cytoskeleton integrity. To that end, M21 cells were treated at 5-times their respective IC_{50} for 24 h with TPUs (**26**, **29** and **30**) and TPIs (**39**, **40** and **43**). Cellular microtubule structures were visualized by indirect immunofluorescence using an anti-β-tubulin monoclonal antibody. CA-4 and 0.5% DMSO were used as a positive and negative controls, respectively. As illustrated in Fig. 4.2, all TPUs and TPIs assessed as well as CA-4 induce microtubules disruption and mitotic abnormalities compared to the negative DMSO control. Hence, TPUs and TPIs are antimitotics disrupting microtubules and cytoskeleton integrity.

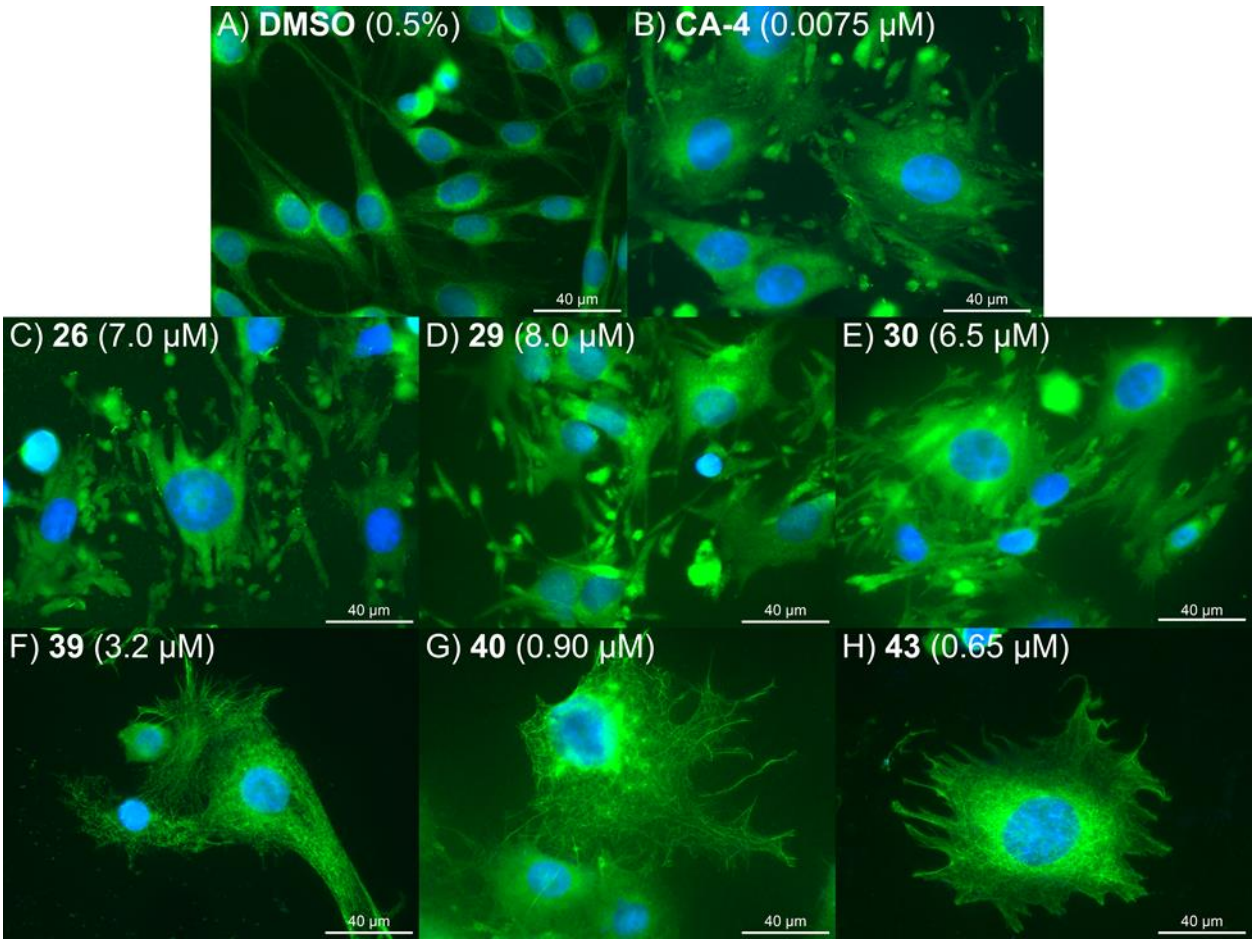

Figure 4.2. Effect of A) 0.5% DMSO, B) CA-4, C) **26**, D) **29**, E) **30,** F) **39**, G) **40** and H) **43** at 5-times their respective IC_{50} for 24 h on the cytoskeleton integrity of M21 cells.

4.6.4. Binding to the colchicine-binding site

Antimicrotubule agents can target the α, β-tubulin heterodimer at various binding sites.[20] However, it was previously reported that PIB-SOs and CA-4 interact in the C-BS.[13, 15, 21] Consequently, the binding of TPUs and TPIs with the C-BS was studied using a detection technique developed in our laboratory.[22] This assay is based on the *N*,*N*'-ethylene-bis(iodoacetamide) (EBI) which crosslinks cysteines at positions 239 and 354 located in the C-BS. The resulting adduct is usefully detectable by Western blot as a second immunoreacting band of β-tubulin. Antimicrotubule compounds that bind to the C-BS prevent the formation of the β-tubulin adduct with EBI. Therefore, M21 cells were treated with TPUs **26**, **29** and **30** and TPIs **39**, **40** and **43** at 100- and 1000-times their respective IC_{50} with a maximum concentration of 100 µM. EBI (100 µM) and 0.5% DMSO were used as reference and negative controls while CA-4 was used as a positive control at 10-, 100- and 1 000-times its IC_{50}. As depicted in Fig. 4.3, TPU **26** tested at 100 µM only barely affect the formation of the β-tubulin adduct with EBI while TPUs **29** and **30** do not affect the formation of this adduct. Moreover, TPIs **39**, **40** and **43** at either 100-times their IC_{50} or at 100 µM inhibit the formation of the EBI: β-tubulin adduct similarly to CA-4. At first glance, these results suggest that the affinity of TPUs for the C-BS is poor while the affinity is high for the TPI derivatives. However, it should be noted that the maximum concentration reacheable by TPUs **26**, **29** and **30** corresponds to 71-, 63- and 77-times their respective IC_{50} which could partly explain the apparent weak affinity observed with TPUs. Nonetheless, these results clearly show that TPIs strongly bind to the C-BS.

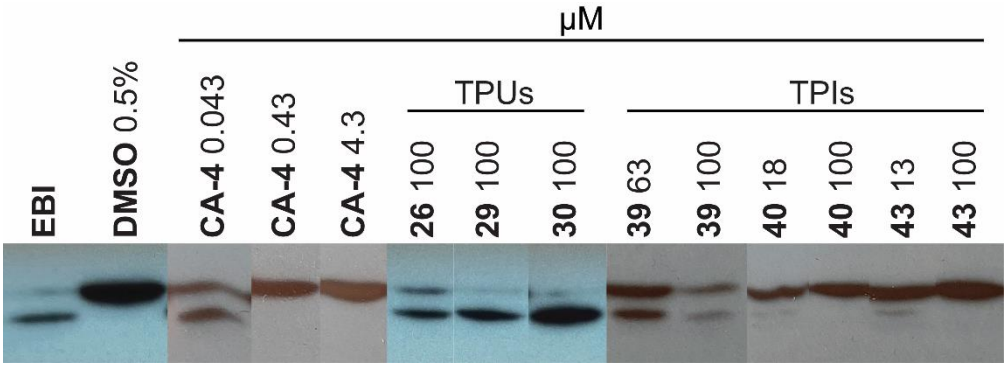

Figure 4.3. Effect of TPUs **26**, **29** and **30** and TPIs **39**, **40** and **43** on the binding of EBI to the C-BS at 100- and 1000-times their respective IC_{50} (maximum concentration at 100 µM).

CA-4 was used as a positive control while 0.5% DMSO and EBI were used as negative and reference controls, respectively.

4.6.5. Antiproliferative activity on cells bearing α, β-tubulin alterations leading to chemoresistance to antimitotics

The antiproliferative activity of the most potent TPUs (**26**, **29** and **30**) and TPIs (**39**, **40** and **43**) was assessed on colchicine- and vinblastine- (CHO-VV 3-2), paclitaxel-resistant (CHO-TAX 5-6) and wild-type Chinese hamster ovary cells (CHO-10001) using the sulforhodamine B colorimetric assay. CHO-VV 3-2 and CHO-TAX 5-6 cell lines originate from parental CHO-10001 with alterations of α, β-tubulin structure. The CHO-VV 3-2 cell line is resistant to vinblastine and colchicine and hypersensitive to paclitaxel, whereas the CHO-TAX 5-6 cell line is resistant to paclitaxel and hypersensitive to vinblastine.[23-25] Consequently, paclitaxel and vinblastine were used as positive controls. As shown in Table 4.3, all TPUs and TPIs assessed exhibit potent antiproliferative activity on CHO-TAX 5-6 cells (0.25 - 1.2 µM) while they exhibit similar antiproliferative activity on both CHO-10001 (0.43 - 6.8 µM) and CHO-VV 3-2 (0.44 - 9.0 µM) cells. Furthermore, the CHO-TAX 5-6/CHO-10001 ratios of tested TPUs and TPIs are ≤ 1, meaning that their antiproliferative activity is not impeded by the chemoresistant mechanisms of CHO-TAX 5-6 cells. Moreover, for TPU **29** and TPI **39**, **40** and **43** the antiproliferative activity is not hampered by the chemoresistance mechanisms of CHO-VV 3-2 cell line while only weakly for TPUs **26** and **30** (resistant/wild-type ratio of 1.3 and 1.4, respectively), which is albeit significantly weaker than that observed with vinblastine used as positive control. These results strongly suggest that the antiproliferative activity of TPUs and TPIs is not or only slightly weakened by α, β-tubulin alterations.

Table 4.3. Antiproliferative activity and ratio of chemoresistance of TPUs **26**, **29** and **30** and TPIs **39**, **40** and **43**, paclitaxel and vinblastine on wild-type, vinblastine- (CHO-VV 3-2) and paclitaxel-resistant (CHO-TAX 5-6) Chinese hamster ovary (CHO-10001) cells.

	IC_{50} (μM)[1]				
				Ratio resistant/wild-type[2]	
#	CHO-10001	CHO-TAX 5-6	CHO-VV 3-2	CHO-TAX 5-6/ CHO-10001	CHO-VV 3-2/ CHO-10001
26	5.2	3.5	7.1	0.68	1.4
29	3.2	1.4	3.0	0.44	0.93
30	6.8	2.4	9.0	0.36	1.3
39	2.6	1.3	2.3	0.51	0.90
40	1.2	0.29	0.83	0.25	0.71
43	0.43	0.25	0.44	0.57	1.0
Pac[3]	0.65	0.96	0.44	1.5	0.67
Vbl[4]	0.027	0.017	0.067	0.64	2.5

[1]IC_{50} represents the concentration of drug inhibiting cell growth by 50%. [2]Ratio > 1: chemoresistance. Ratio < 1: no chemoresistance. [3]Pac: paclitaxel. [4]Vbl: vinblastine.

4.6.6. Antiproliferative activity on cells overexpressing P-glycoprotein

Additionally, the antiproliferative activity of TPUs (**26**, **29** and **30**) and TPIs (**39**, **40** and **43**) was also assessed using the 3-(4,5-dimethylthiazol-2-yl)-2,5-diphenyltetrazolium bromide (MTT) cell proliferation assay on wild-type T lymphoblastoid leukemia CEM and chemoresistant CEM-VLB cells. CEM-VLB cells overexpress the P-glycoprotein which is responsible for the potent cellular efflux of several anticancer drugs such as paclitaxel and vinblastine.[26] Of note, the P-glycoprotein is part of a significant mechanism of chemoresistance encountered in clinical settings.[27-29] As displayed in Table 4.4, TPUs **26**, **29** and **30** and TPIs **39**, **40** and **43** have IC_{50} ranging from 0.12 to 3.5 μM and 0.15 to 0.48 μM, respectively on CEM cells whereas TPUs and TPIs exhibited IC_{50} on CEM-VLB in the mid nanomolar to low micromolar ranges (0.23 - 6.3 μM). First, the antiproliferative activity of TPUs **29** and **30** and TPI **40** is not modified by the overexpression of P-glycoprotein with CEM-VLB (chemoresistant)/CEM (wild-type) ratios ranging from 0.47 - 2.0. Second, the biological activity of TPIs **40** and **43** is weakly hampered by the overexpression of P-glycoprotein with chemoresistance ratios of 12 and 9.0, respectively while the antiproliferative activity of TPU **26** is strongly inhibited by P-glycoprotein with a

chemoresistance ratio of 51, similar to the chemoresistance ratios observed with paclitaxel and vinblastine (83 and 42, respectively). Our results suggest that the chemoresistance tumor cells based on the overexpression of P-glycoprotein is structure-dependent and that the nature and the position of the substituent on ring B are important parameters. Finally and at the exception for TPU **26**, these results confirm that the antiproliferative activity of TPUs and TPIs is not or only weakly affected by the overexpression of P-glycoprotein.

Table 4.4. Cell viability and ratio of chemoresistance of TPUs **26**, **29** and **30** and TPIs **39**, **40** and **43** on wild-type T lymphoblastoid leukemia CEM and resistant CEM-VLB cells.

#	IC_{50} (μM)[1]		
	CEM	**CEM-VLB**	**Ratio resistant/wild-type[2] CEM-VLB/CEM**
26	0.12	6.3	51
29	1.2	2.3	2.0
30	3.5	5.8	1.7
39	0.48	0.23	0.47
40	0.24	2.9	12
43	0.15	1.4	9.0
Pac[3]	0.0020	0.16	83
Vbl[4]	0.00088	0.037	42

[1]IC_{50} represents the concentration of drug inhibiting cell growth by 50%. [2]Ratio > 1: chemoresistance. Ratio < 1: no chemoresistance. [3]Pac: paclitaxel. [4]Vbl: vinblastine.

4.6.7. *In silico* pharmacokinetic, physicochemical and drug-likeness properties of TPUs and TPIs

Poor biopharmaceutical properties (pharmacokinetics, physicochemical and drug-likeness) are often the reason for the termination of the development of hit and lead compounds into drug candidates. Poor evaluation of these parameters usually results in waste of time, higher costs and failure of the drug research programs.[30] Consequently, we used the free online tool SwissADME to calculate the effect of modulation of the chemical structure of our new TPUs and TPIs on their theoretical pharmacokinetic, physicochemical and drug-likeness properties to evaluate the potential of our drugs for further development.[31] All TPUs and TPIs were evaluated and the results are collated in Table 4.5. Foremost, TPUs and TPIs have molecular weights ranging from 306.81 to 341.26 and 270.35 to 304.79 g/mol,

respectively. They exhibit seven and three rotatable bonds and both families have one H-bond acceptor. TPUs are bearing two H-bond donors while TPIs only one. The topological polar surface area (TPSA) is 66.43 $Å^2$ and 57.64 $Å^2$ for TPUs and TPIs, respectively. The ClogP values ranges from 3.56 to 4.03 and 2.84 to 3.39 for TPUs and TPIs, respectively while LogS ranges from -5.31 to -5.02 and -4.48 to -3.82 for TPUs and TPIs, respectively. Except for TPI **38** that is considered soluble, every TPUs and TPIs are considered as moderately soluble. Both families of compounds share a high probability of gastrointestinal absorption (GIA) and are permeable to the blood-brain barrier (BBB). Furthermore, all TPUs and TPIs **43** and **44** should not theoretically be a substrate of the P-glycoprotein while TPIs **38**-**42** should be. At the exception of TPU **26** and TPI **43**, these theoretical results agree with our experimental results described in the section 4.3.6. Finally, TPU **24** and all TPIs do not violate any of the Lipinski, Veber, Egan and Muegge filters. However, although that TPUs **25**-**30** respect all filters, they nevertheless exhibit one violation of the Lipinski filter (MlogP > 4.15). Hence, TPUs and TPIs have similar theoretical drug-likeness properties and bioavailability scores. Lastly, TPUs and TPIs show promising theoretical drug-likeness properties and bioavailability scores supporting their future evaluation in *in vivo* settings.

Table 4.5. Physicochemical, pharmacokinetic and drug-likeness properties of TPUs (**24**-**30**) and TPIs (**38**-**44**) calculated from the web-based SwissADME application.

#	Rb[1]	H-Ba[2]	H-Bd[3]	TPSA[4] (Å^2)	CLogP[5]	LogS[6]	Sclass[7]	GIA[8]	BBBP[9]	P-gp[10]	Drug-like (#viol.)[11]
24	7	1	2	66.43	3.56	-5.02	MS	H	Yes	No	Yes (0)
25	7	1	2	66.43	3.75	-5.05	MS	H	Yes	No	Yes (1) MlogP>4.15
26	7	1	2	66.43	3.83	-5.05	MS	H	Yes	No	Yes (1) MlogP>4.15
27	7	1	2	66.43	3.78	-5.05	MS	H	Yes	No	Yes (1) MlogP>4.15
28	7	1	2	66.43	4.01	-5.31	MS	H	Yes	No	Yes (1) MlogP>4.15
29	7	1	2	66.43	4.03	-5.31	MS	H	Yes	No	Yes (1) MlogP>4.15
30	7	1	2	66.43	4.03	-5.31	MS	H	Yes	No	Yes (1) MlogP>4.15
38	3	1	1	57.64	2.84	-3.82	S	H	Yes	Yes	Yes (0)
39	3	1	1	57.64	3.15	-4.21	MS	H	Yes	Yes	Yes (0)
40	3	1	1	57.64	3.16	-4.21	MS	H	Yes	Yes	Yes (0)
41	3	1	1	57.64	3.16	-4.21	MS	H	Yes	Yes	Yes (0)
42	3	1	1	57.64	3.33	-4.48	MS	H	Yes	Yes	Yes (0)
43	3	1	1	57.64	3.39	-4.48	MS	H	Yes	No	Yes (0)
44	3	1	1	57.64	3.35	-4.48	MS	H	Yes	No	Yes (0)

[1]Rb: number of rotatable bonds. [2]H-Ba: number of H-bond acceptors. [3]H-Bd: number of H-bond donors. [4]TPSA: topological polar surface area. [5]CLogP: consensus Log P (average of iLOGP, XLOGP3, WLOGP, MLOGP and Silicos-IT Log P). [6]LogS: Ali topological method Log S. [7]SClass: Ali solubility class (insoluble (IS) < -10 < poorly soluble (PS) < -6 < moderately soluble (MS) < -4 < soluble (S) < -2 < very soluble (VS) <0 < highly soluble (HS)). [8]GIA: gastrointestinal absorption (H means high). [9]BBBP: blood-brain barrier permeability. [10]P-gp: P-glycoprotein substrates. [11]Drug-like: drug-likeness indices (bioavailability) from Lipinski, Ghose, Veber, Egan and Muegge filters. # viol: number of violations of the 5 filters.

4.6.8. Toxicity toward developing chick embryos

Compounds **40** and **43** were selected as TPIs model for their potent antiproliferative activity on tumor cells and were tested *in ovo* on developing chick embryos to assess their potential toxicity. A mixture of 0.5% DMSO, 5.0% cremophor EL™, 6.3% ethanol 99% and 88.2% PBS 1X was used as excipient (vehicle) to administrate TPIs **40** (20 µg/egg) and **43** (20 µg/egg), which is at their maximum solubility in 100 µL of vehicle. CA-4 was used as a positive control (1.0 µg/egg). A group of chick embryos that were exclusively treated with the vehicle was used as negative controls. The wet weight of treated embryos is represented in percentage relative to the wet weight of the vehicle in Fig. 4.4. Foremost, the weight of the embryos treated by the drugs is expressed in percentage relative to the weight of the embryos treated with the excipient. Accordingly, TPI **40** and **43** exhibit 91 and 93% respectively while it is of 109% for the control drug CA-4. Moreover, the percentage of dead embryos for the group treated with the excipient, CA-4, TPIs **40** and **43** is 8.0, 25, 36 and 27%, respectively. Although TPIs **40** and **43** display a lower impact on the embryos weight, these differences are not statistically significant (one-way ANOVA analysis and t-test) with the weight of the embryos treated with the vehicle. Nonetheless, mortality of embryos in TPIs treated embryos is higher compared to the vehicle and similar to CA-4 treated embryos used as positive controls. Of note, TPIs were assessed at 20-times the dose of CA-4 and this could explain, at least in part the slightly higher toxicity observed. Finally, these results show that TPIs **40** and **43** have low toxicity toward chick embryos.

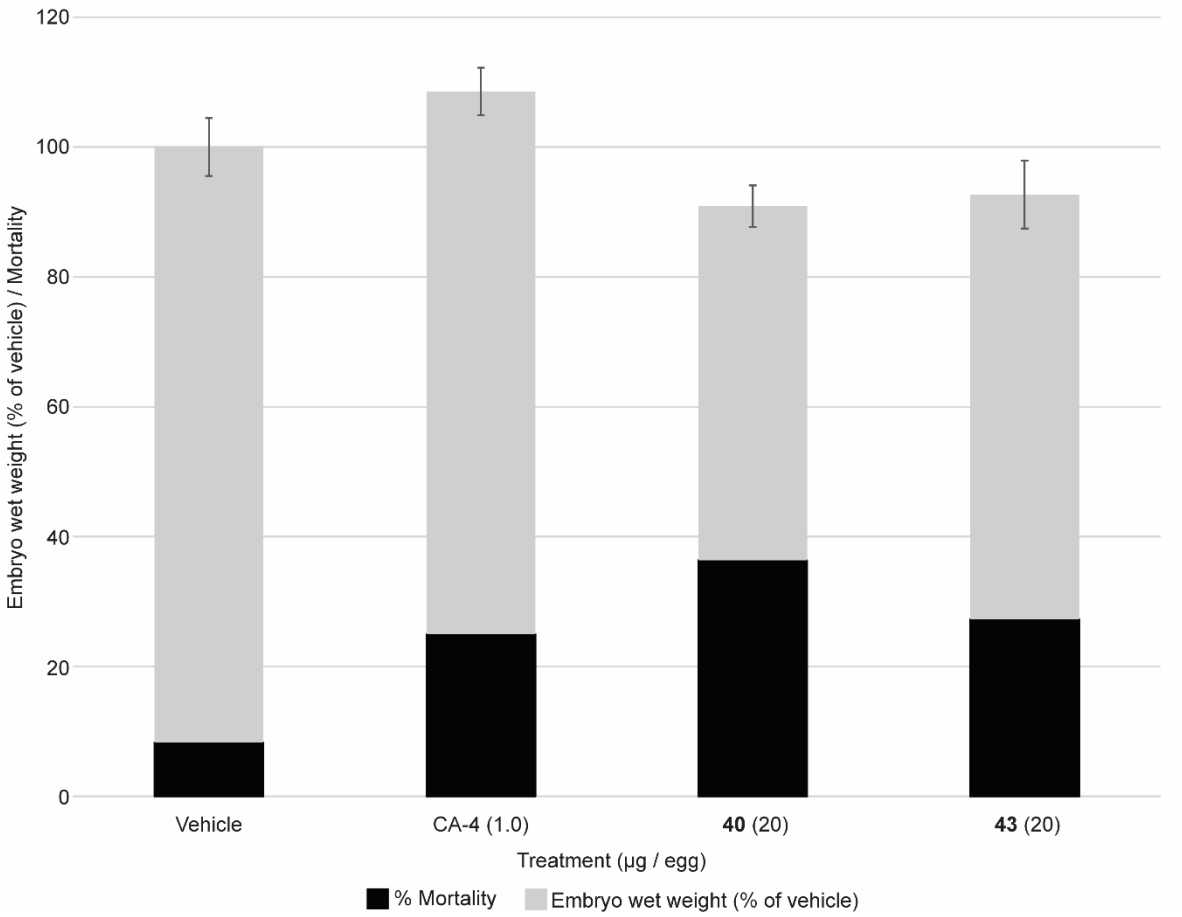

Figure 4.4. Effect of TPIs **40** and **43** on the weight and the mortality of chick embryos.

4.7. Conclusion

In summary, this study reports the synthesis, characterization and biological evaluation of 42 new PIB-SOs derivatives and analogs designated as TPAs, TPTs, TPUs and TPIs that are active in the mid to high micromolar range (8.0 - >100 µM), low to mid micromolar range (4.1 - 49 µM), low to high micromolar range (0.71 - >100 µM) and in the mid nanomolar to mid micromolar range (0.13 - 37 µM), respectively. The most potent TPUs (**26**, **29** and **30**) and TPIs (**39**, **40** and **43**) arrest the cell cycle progression in G2/M phase and induce cytoskeleton disruption. Moreover, TPIs interfere with the colchicine-binding site on microtubules as confirmed by the EBI detection assay. The cytotoxicity of TPIs and TPUs is generally not or only weakly hampered by alterations of α, β-tubulin and overexpression of P-glycoprotein and their theoretical biopharmaceutical properties (physicochemical, pharmacokinetics and drug-likeness) support their further evaluation in preclinical studies.

Finally, TPIs **40** and **43** exhibited a low level of toxicity on chick embryos suggesting that they are a new family of promising antimicrotubule agents.

4.8. Experimental protocols

4.8.1. Biological methods

4.8.1.1. Cell lines culture

HT-1080 human fibrosarcoma, HT-29 human colon carcinoma and MCF7 human breast carcinoma were purchased from the American Type Culture Collection (Manassa, VA, USA). M21 human melanoma cells were provided by Dr. David Cheresh (University of California, San Diego School of Medicine, CA, USA). Wild-type Chinese hamster ovary cells (CHO-10001),[23] colchicine- and vinblastine- resistant cells (CHO-VV 3-2)[24] and paclitaxel-resistant cells (CHO-TAX 5-6)[25] were generously provided by Dr. Fernando Cabral (University of Texas Medical School, Houston, Texas). T cell leukemia CEM and multidrug-resistant leukemia CEM-VLB were generously provided by Dr. William T. Beck (University of Illinois at Chicago, College of Pharmacy, IL).[27] HT-1080, HT-29, M21 and MCF7 cells were cultured in DMEM medium containing sodium bicarbonate, high glucose concentration, glutamine and sodium pyruvate (Hyclone, Logan, UT, USA) supplemented with either 5 or 10% of fetal bovine serum (FBS, Invitrogen, Burlington, ON, Canada). CHO-10001, CHO-VV 3-2, CHO-TAX 5-6, CEM and CEM-VLB were cultured in RPMI 1640 (Hyclone, Logan, UT) supplemented with 10% of fetal bovine serum. The cells were maintained at 37 °C in a moisture saturated atmosphere containing 5% CO_2

4.8.1.2. Antiproliferative activity assay

The antiproliferative activity of TPAs **3-9**, TPTs **10-16**, TPUs **17-37** and TPIs **38-44** was assessed using the procedure described by the National Cancer Institute (NCI) Developmental Therapeutics Program for its drug screening program with slight modifications.[18] Briefly, ninety-six-well Costar microtiter clear plates from Fisher Scientific (Montreal, QC, Canada) were seeded with 75 μL of a suspension of either HT-1080 (3.0×10^3), HT-29 (4.0×10^3), M21 (3.0×10^3) or MCF7 (3.5×10^3) cells per well in DMEM supplemented with either 5 or 10% fetal bovine serum or with CHO-10001 (3.0×10^3), CHO-

VV 3-2 (3.0 x 10^3) or CHO-TAX 5-6 (3.0 x 10^3) cells per well in RPMI 1640 containing 10% fetal bovine serum for 24 h. Freshly solubilized drugs in DMSO (40 mM) were diluted in fresh supplemented DMEM or RPMI 1640 and 75 µL aliquots containing serially diluted concentrations of the drug were added. Final drug concentrations were ranged from 100 µM to 0.78 nM. DMSO concentration was kept constant at 0.5% (V/V) to prevent any related toxicity. Plates were incubated for 48 h and cell growth was stopped by the addition of cold trichloroacetic acid to the wells (10% w/v, final concentration). Afterward, plates were incubated at 4 °C for 30 min. Then, plates were washed 5-times with nanopure water and 75 µL of a sulforhodamine B solution (0.1% w/v) in 1% acetic acid was added to each well. After 15 min at room temperature, the exceeding dye was removed and plates were washed 5-times with an acetic acid solution (1%). Bound dye was solubilized in 20 mM Tris base and the absorbance was read using an optimal wavelength (520-580 nm) with a SpectraMax® i3x (Molecular Devices, San Jose, CA, USA). Data obtained from treated cells were compared to the control cell plates fixed on the treatment day and the percentage of cell growth was thus calculated for each drug. The experiments were done at least twice in triplicate. Assays were considered valid when the coefficient of variation was <10% for a given set of conditions within the same experiment.

4.8.1.3. MTT assay

Cell survival was evaluated using the 3-(4,5-dimethylthiazol-2-yl)-2,5-diphenyltetrazolium bromide (MTT) colorimetric assay and cell viability in the absence of drug corresponds to 100% of cell viability.[32, 33] Briefly, the 96-well microtiter plates were seeded with 75 µL of a cells in suspension of either CEM (1.0 x 10^4) or CEM-VLB (1.0 x 10^4) cells per well in RPMI 1640 containing 10% fetal bovine serum. Plates were incubated at 37 °C with 5% CO_2 for 24 h. Freshly solubilized drugs in DMSO were diluted in fresh medium and 50 µL aliquots containing escalating concentrations of drug were added and the plates were incubated for 48 h. The final concentration of DMSO in the culture media was 0.5% and was kept constant in all experiments. After 48 h, 10 µL of MTT (5 mg/mL in PBS) were added to the wells. Four hours later, 100 µL of the solubilization solution (10% sodium dodecyl sulfate [SDS] in 0.01 M HCl) was added and the plates were incubated in the dark at 37 °C with 5% CO_2 for 16 h. The optical density was read at 565 nm using a SpectraMax®

i3x (Molecular Devices, San Jose, CA, USA). Data obtained from treated cells were compared to the control cell plate fixed on the treatment day and the percentage of cell viability was thus calculated for each drug. The experiments were done at least twice in triplicate. Assays were considered valid when the coefficient of variation was <10% for a given set of conditions within the same experiment.

4.8.1.4. Cell cycle progression analysis

After incubation of 2.5 x 10^5 M21 cells with selected TPUs and TPIs at 2- and 5-times their respective IC_{50} for 24 h, the cells were trypsinized (trypsin EDTA 0.5%), washed with phosphate buffered saline (PBS) and resuspended in 250 µL of PBS. The cells were fixed by addition of 750 µL of ice-cold ethanol under agitation and stored at -20 °C until analysis. Prior to flow cytometry analysis, cells were washed with PBS and resuspended in 300 µL of PBS containing 2 µg/mL DAPI. Cell cycle distribution was analyzed using an LSR II flow cytometer (BD Biosciences, Franklin Lakes, NJ, USA).

4.8.1.5. Immunofluorescence of microtubules

M21 cells were seeded at 2.5 x 10^5 cells per well in 6-well plates (Costar®, Fisher Scientific, Montreal, QC, Canada) containing glass cover slides (22 mm × 22 mm) coated with fibronectin (10 µg/mL) and incubated for 24 h. Tumor cells were incubated either with CA-4 (0.0075 µM), TPUs **26** (7.0 µM), **29** (6.5 µM) and **30** (8.0 µM) as well as TPIs **39** (3.2 µM), **40** (0.9 µM) and **43** (0.65 µM) for 24 h. CA-4 and 0.5% DMSO were used as positive and negative controls, respectively. The cells were then washed thrice with 2.0 mL of PBS and fixed with 3.7% formaldehyde in PBS for 10 min. After two washes with PBS, the cells were permeabilized with saponin (0.1% in PBS) and blocked with 3% (w/v) BSA in PBS for 45 min at 37 °C. The cells were then incubated for 2 h at room temperature with an anti-β-tubulin monoclonal antibody (clone TUB 2.1, Sigma-Aldrich, St. Louis, MO, USA; 1:300) in a solution containing 0.1% saponin and 3% BSA in PBS. The cells were washed twice with PBS containing 0.05% Tween 20 and stained using antimouse IgG Alexa Fluor 488 (Molecular Probes, Eugene, OR, USA; 1:1000) and DAPI (2 µg/mL final concentration) in blocking buffer for 1 h at 37 °C. The cover slides were mounted using 25 µL of Fluoromount-G® (SouthernBiotech, Birmingham, Al, USA) before analysis under an Olympus BX51

fluorescence microscope (Olympus BX51, Center Valley, PA, USA). Images were acquired as 8 bit-tagged image format files with a Q imaging RETIGA EXI digital camera (Qimaging, Surrey, BC, Canada) using the Image Pro Express software at a total magnification of 400x.

4.8.1.6. In vitro competition binding assay of EBI to the C-BS

M21 cells were seeded in 6-well plates (7.5 x 10^5 cells/well) and were incubated overnight. Then, cells were treated with either TPUs **26**, **29**, **30** or TPIs **39**, **40**, **43** for 1.5 h at 100- or 1000-times their respective IC_{50}. CA-4 was used at 10-, 100- and 1 000-time its respective IC_{50}. The maximum concentration of drugs used in this assay was set at 100 µM. Afterward, EBI (100 µM, final concentration, Toronto Research Chemicals, North York, ON, Canada) in PBS was added to each well for 1.5 h. After the incubation, the supernatant was withdrawn and cells were trypsinized, harvested and centrifuged for 5 min at 1 200 rpm. The pellets were washed with 500 µL of cold PBS and stored at -80 °C until analysis.[22]

4.8.1.7. Gel electrophoresis and immunoblot

The dried cell pellets were resuspended in a buffer containing 0.32 M sucrose, 1 mM EDTA at pH 8, 10 mM Tris at pH 7.4 and a protease inhibitor. The protein concentration was assessed with the Bio-Rad Protein assay (Bio-Rad laboratories, Mississauga, ON, Canada). Samples were prepared to obtain proteins at 4 mg/mL in Laemmli sample buffer (60 mM Tris-Cl at pH 6.8, 2% SDS, 10%, glycerol, 5% β-mercaptoethanol, 0.01% bromophenol blue) and boiled for 5 min.[34] Then, 40 µg of proteins were used for the electrophoresis using 10% polyacrylamide gels. The proteins were transferred onto nitrocellulose membranes that were incubated with TBSTM (Tris Buffered Saline + 0.1% (V/V) Tween-20 with 5% fat-free dry milk) for 2 h at room temperature. Subsequently, the anti-β-tubulin (clone TUB 2.1) primary antibody was incubated in TBSTM (1:500) for 2 h at room temperature. Membranes were washed with TBST (Tris-Buffered Saline supplemented with 0.1% (V/V) Tween 20) and incubated with peroxidase conjugated anti-mouse immunoglobulin (Amersham Canada, Oakville, ON, Canada) in TBSMT (1:5000) for 1 h at room temperature. After washing the membranes with TBST, detection of the immunoblot was carried out using Clarity Western enhanced chemiluminescence reagents (Bio-Rad laboratories, Mississauga, ON, Canada).

Detection of bands was performed with Super Rx medical X-Ray film (Fujifilm, Tokyo, Japan).

4.8.1.8. In ovo toxicity toward chick embryos

Fertilized eggs were purchased from Couvoir La Coop (Victoriaville, QC, Canada). They were incubated for a 10-day period in a Pro-FI egg incubator (Lyon Electric, Chula Vista, CA, USA) with an automatic turning system. TPIs **40** and **43** and CA-4 were solubilized in a formulation containing a mixture of 0.5% DMSO, 5.0% cremophor EL^{TM}, 6.3% ethanol (99%) and 88.2% PBS 1X. After the incubation period, the veins of the chorioallantoic membrane were identified on the sides of the egg shells. The eggs were opened using a hobby drill (Dremel, Racine, WI) to obtain a 1.5 x 1.5 cm opening directly over the location of the veins. Groups of 25-29 eggs were formed by randomization and the drugs were administered intravenously (100 µL/egg). After administration, the openings were closed using adhesive tape and the eggs were then incubated in a static incubator (Lyon Electric, Chula Vista, CA, USA) for a 7-day period at 37 °C. Three days after administrations, the embryos that do not support the procedure or that do not grow were withdrawn from the experience. After the 7-days incubation period, the embryos were euthanized at 4 °C for at least 2 h. Then, the wet weight of each embryo and the number of dead embryos were recorded. A group of embryos that were treated only with the excipient was used as a negative control. A one-way ANOVA analysis and t-test were used to determine the statistical significance of the results.

4.8.2. Chemical methods

4.8.2.1. General

Proton NMR spectra were recorded on a Bruker AM-300 spectrometer (Bruker, Germany). Chemical shifts (δ) are reported in parts per million (ppm). Reactions requiring microwave heating were performed at 200 watts with a Discover SP Explorer Hybrid microwave synthesiser (CEM, Matthews, NC, USA). Uncorrected melting points were obtained on a MPA100 automated melting point system (Standford Research Systems, Sunnyvale, CA, USA). UHPLC analyses were performed using an ACQUITY Arc system

(Waters, Mississauga, ON, Canada) equipped with a 2998 PDA detector. The samples were obtained by solubilization of the compounds in DMSO and a subsequent solution was produced by diluting the compounds at 1.0 to 20% DMSO depending on solubility, in a mixture of MeOH/H_2O. The samples were then eluted using a mixture of MeOH/H_2O with a linear mobile phase gradient (1.0 mL/min) on a CORTECS C18+ reversed-phase column 3.0 × 50 mm × 2.7 μm. Wavelength was selected at 280 nm and the purity of all compounds was confirmed by UHPLC and was equal or over 95%. All chemicals were supplied by Aldrich Chemicals (Milwaukee, WI, USA), VWR International (Mont-Royal, QC, Canada) or Fisher Scientific (Montreal, QC, Canada). Liquid flash chromatography was performed on silica gel F60, 60 Å, 40-63 μm supplied by Silicycle (Quebec City, QC, Canada) using an FPX flash purification system (Biotage, Charlottesville, VA, USA) and using solvent mixtures expressed as V/V ratios. Solvents and reagents were used without purification unless specified otherwise. The progress of all reactions was monitored by TLC on precoated silica gel 60 Å F254 TLC plates provided by VWR International (Mont-Royal, QC, Canada). The chromatograms were viewed under UV light at 254 and 275 nm. HRMS were recorded by direct injection in a TOF system 6210 series mass spectrometer (Agilent technologies, Santa Clara, CA, USA).

4.8.2.2. General preparation of TPAs 3-9

Butyryl chloride (0.1 mL, 1.1 Eq.) was added to a solution of the relevant phenythioaniline (1.0 Eq.) in presence of triethylamine (0.19 mL, 3.0 Eq.) in acetonitrile (4 mL). The reaction mixture was stirred under pressure with microwaves at 80 °C for 8 h. The mixture was evaporated and then dissolved in methylene chloride (10 mL). The organic layer was washed successively with solutions of HCl (1 M, 10 mL), NaOH (1 M, 10 mL) and brine (10 mL), dried over anhydrous sodium sulfate, filtered and evaporated to dryness under reduced pressure. The residue was purified by flash chromatography on silica gel.

4.8.2.3. Characterization of TPAs 3-9

*4.8.2.3.1. N-(4-(Phenylthio)phenyl)butyramide (**3**).* Flash chromatography (hexanes/ethyl acetate (90:10 to 60:40)). Yield: 44%; yellow solid; mp: 87-89 °C; ^{1}H NMR ($CDCl_3$): δ 7.93 (s, 1H, NH), 7.55-7.53 (m, 2H, Ar), 7.36-7.33 (m, 2H, Ar), 7.27-7.20 (m,

5H, Ar), 2.35 (t, 2H, *J* = 7.3 Hz, CH_2), 1.82-1.70 (m, 2H, CH_2), 1.00 (t, 3H, *J* = 7.3 Hz, CH_3); ^{13}C NMR ($CDCl_3$): δ 171.9, 137.8, 136.9, 133.1, 129.7, 129.6, 129.2, 126.6, 120.8, 39.6, 19.1, 13.8; HRMS (ESI) *m/z* found, 272.1110; $C_{16}H_{18}NOS$ (M^+ + H) expected 272.1110.

*4.8.2.3.2. N-(4-(o-Tolylthio)phenyl)butyramide (**4**).* Flash chromatography (methylene chloride). Yield: 63%; colorless oil; ^1H NMR ($CDCl_3$): δ 7.49-7.46 (m, 3H, Ar and NH), 7.23-7.09 (m, 6H, Ar), 2.37-2.30 (m, 5H, CH_2 and CH_3), 1.78-1.71 (m, 2H, CH_2), 0.99 (t, 3H, *J* = 7.3 Hz, CH_3); ^{13}C NMR ($CDCl_3$): δ 171.6, 138.7, 137.2, 135.0, 131.8, 131.3, 130.5, 130.0, 127.2, 126.6, 120.7, 39.6, 20.5, 19.1, 13.8; HRMS (ESI) *m/z* found, 286.1270; $C_{17}H_{20}NOS$ (M^+ + H) expected 286.1269.

*4.8.2.3.3. N-(4-(m-Tolylthio)phenyl)butyramide (**5**).* Flash chromatography (methylene chloride). Yield: 62%; pale beige solid; mp: 49-51 °C; ^1H NMR ($CDCl_3$): δ 7.54-7.49 (m, 3H, NH and Ar), 7.35-7.32 (m, 2H, Ar), 7.19-7.00 (m, 4H, Ar), 2.36-2.29 (m, 5H, CH_2 and CH_3), 1.81-1.69 (m, 2H, CH_2), 0.99 (t, 3H, *J* = 7.3 Hz, CH_3); ^{13}C NMR ($CDCl_3$): δ 171.6, 139.0, 137.5, 136.4, 132.9, 130.5, 130.0, 129.0, 127.5, 127.0, 120.6, 39.6, 21.3, 19.1, 13.8; HRMS (ESI) *m/z* found, 286.1268; $C_{17}H_{20}NOS$ (M^+ + H) expected 286.1269.

*4.8.2.3.4. N-(4-(p-Tolylthio)phenyl)butyramide (**6**).* Flash chromatography (hexanes/methylene chloride (50:50) to methylene chloride). Yield: 71%; white solid; mp: 114-116 °C; ^1H NMR ($CDCl_3$): δ 8.00 (s, 1H, NH), 7.50-7.47 (m, 2H, Ar), 7.27-7.09 (m, 6H, Ar), 2.35-2.30 (m, 5H, CH_2 and CH_3), 1.79-1.67 (m, 2H, CH_2), 0.97 (t, 3H, *J* = 7.3 Hz, CH_3); ^{13}C NMR ($CDCl_3$): δ 172.0, 137.2, 137.1, 132.4, 131.8, 131.1, 131.0, 130.0, 120.8, 39.5, 21.1, 19.1, 13.8; HRMS (ESI) *m/z* found, 286.1270; $C_{17}H_{20}NOS$ (M^+ + H) expected 286.1269.

*4.8.2.3.5. N-(4-((2-Chlorophenyl)thio)phenyl)butyramide (**7**).* Flash chromatography (hexanes/ethyl acetate (80:20)). Yield: 67%; white solid; mp: 86-188 °C; ^1H NMR ($CDCl_3$): δ 7.91 (s, 1H, NH), 7.60-7.68 (m, 2H, Ar), 7.41-7.32 (m, 3H, Ar), 7.07-7.03 (m, 2H, Ar), 6.86-6.83 (m, 1H, Ar), 2.36 (t, 2H, *J* = 7.3 Hz, CH_2), 1.81-1.69 (m, 2H, CH_2), 0.98 (t, 3H, *J* = 7.3 Hz, CH_3); ^{13}C NMR ($CDCl_3$): δ 172.0, 138.7, 137.4, 135.0, 132.2, 129.7, 129.0, 127.2, 126.8, 126.7, 121.0, 39.6, 19.1, 13.8; HRMS (ESI) *m/z* found, 306.0717; $C_{16}H_{17}ClNOS$ (M^+ + H) expected 306.0719.

*4.8.2.3.6. N-(4-((3-Chlorophenyl)thio)phenyl)butyramide (**8**).* Flash chromatography (hexanes/ethyl acetate (90:10 to 80:20)). Yield: 100%; white solid; mp: 105-107 °C; ^{1}H NMR ($CDCl_3$): δ 7.87 (s, 1H, NH), 7.57-7.55 (m, 2H, Ar), 7.38-7.36 (m, 2H, Ar), 7.18-7.04 (m, 4H, Ar), 2.35 (t, 2H, *J* = 7.3 Hz, CH_2), 1.84-1.68 (m, 2H, CH_2), 0.98 (t, 3H, *J* = 7.3 Hz, CH_3); ^{13}C NMR ($CDCl_3$): δ 171.9, 139.9, 138.5, 134.9, 134.2, 130.1, 128.3, 127.8, 126.7, 126.3, 120.8, 39.6, 19.1, 13.8; HRMS (ESI) *m/z* found, 306.0720; $C_{16}H_{17}ClNOS$ (M^+ + H) expected 306.0719.

*4.8.2.3.7. N-(4-((4-Chlorophenyl)thio)phenyl)butyramide (**9**).* Flash chromatography (hexanes/ethyl acetate (85:15)). Yield: 66%; white solid; mp: 139-141 °C; ^{1}H NMR (DMSO-d_6): δ 10.06 (s, 1H, NH), 7.71-7.68 (m, 2H, Ar), 7.40-7.32 (m, 4H, Ar), 7.16-7.13 (m, 2H, Ar), 2.30 (t, 2H, *J* = 7.2 Hz, CH_2), 1.65-1.58 (m, 2H, CH_2), 0.91 (t, 3H, *J* = 7.3 Hz, CH_3); ^{13}C NMR (DMSO-d_6): δ 171.9, 140.5, 137.1, 134.5, 131.4, 130.2, 129.7, 125.9, 120.6, 38.9, 19.1, 14.1; HRMS (ESI) *m/z* found, 306.0714; $C_{16}H_{17}ClNOS$ (M^+ + H) expected 306.0719.

4.8.3.1. General preparation of TPTs 10-16 and TPUs 17-37

The relevant isocyanate or ethyl isothiocyanate (1.2 Eq.) was added to a solution of the appropriate aniline (0.1g, 1.0 Eq.) in ethanol (3 mL). The reaction mixture was stirred at room temperature for 24 h. After the completion of the reaction, the mixture was purified by flash chromatography on silica gel.

4.8.3.2. Characterization of TPTs 10-16 and TPUs 17-37

*4.8.3.2.1. 1-Ethyl-3-(4-(phenylthio)phenyl)thiourea (**10**).* Flash chromatography (hexanes/ethyl acetate (90:10 to 75:25)). Yield: 71%; colorless oil; ^{1}H NMR (DMSO-d_6): δ 9.57 (s, 1H, NH), 7.86 (s, 1H, NH), 7.50-7.47 (m, 2H, Ar), 7.37-7.25 (m, 7H, Ar), 3.50-3.46 (m, 2H, CH_2), 1.12 (t, 3H, *J* = 7.1 Hz, CH_3); ^{13}C NMR (DMSO-d_6): δ 180.4, 139.9, 136.6, 132.9, 129.9, 129.9, 128.4, 127.2, 123.9, 14.6; HRMS (ESI) *m/z* found, 289.0829; $C_{15}H_{17}N_2S_2$ (M^+ + H) expected 289.0834.

*4.8.3.2.2. 1-Ethyl-3-(4-(o-tolylthio)phenyl)thiourea (**11**).* Flash chromatography (methylene chloride/ethyl acetate (60:40 to 2:98)). Yield: 52%; colorless oil; ^{1}H NMR (DMSO-d_6): δ 9.51 (s, 1H, NH), 7.82 (s, 1H, NH), 7.46-7.43 (m, 2H, Ar), 7.31-7.29 (m, 1H,

Ar), 7.22-7.11 (m, 5H, Ar), 3.49-3.45 (m, 2H, CH_2), 2.32 (s, 3H, CH_3), 1.11 (t, 3H, *J* = 7.1 Hz, CH_3); ^{13}C NMR (DMSO-d_6): δ 180.4, 139.3, 138.4, 134.8, 131.7, 131.3, 131.0, 128.8, 127.9, 127.4, 124.1, 20.5, 14.6; HRMS (ESI) *m/z* found, 303.0984; $C_{16}H_{19}N_2S_2$ (M^+ + H) expected 303.0989.

4.8.3.2.3. 1-Ethyl-3-(4-(m-tolylthio)phenyl)thiourea ***(12)***. Flash chromatography (methylene chloride to methylene chloride/ethyl acetate (80:20)). Yield: 42%; purple oil; ^{1}H NMR (DMSO-d_6): δ 9.56 (s, 1H, NH), 7.85 (s, 1H, NH), 7.49-7.46 (m, 2H, Ar), 7.32-7.20 (m, 3H, Ar), 7.12-7.04 (m, 3H, Ar), 3.50-3.46 (m, 2H, CH_2), 2.26 (s, 3H, CH_3), 1.12 (t, 3H, *J* = 7.1 Hz, CH_3); ^{13}C NMR (DMSO-d_6): δ 180.4, 139.7, 139.3, 136.1, 132.6, 130.6, 129.7, 128.8, 128.2, 127.3, 123.9, 39.2, 21.3, 14.6; HRMS (ESI) *m/z* found, 303.0993; $C_{16}H_{19}N_2S_2$ (M^+ + H) expected 303.0989.

4.8.3.2.4. 1-Ethyl-3-(4-(p-tolylthio)phenyl)thiourea ***(13)***. Flash chromatography (hexanes/ethyl acetate (85:15)). Yield: 61%; pale yellow solid; mp: 121-123 °C; ^{1}H NMR ($CDCl_3$): δ 8.30 (s, 1H, NH), 7.34-7.32 (m, 2H, Ar), 7.21-7.15 (m, 4H, Ar), 7.10-7.07 (m, 2H, Ar), 6.00 (brs, 1H, NH), 3.67-3.60 (m, 2H, CH_2), 2.35 (s, 3H, CH_3), 1.16 (t, 3H, *J* = 7.2 Hz, CH_3); ^{13}C NMR ($CDCl_3$): δ 180.1, 138.6, 137.1, 134.1, 133.3, 130.4, 130.1, 129.6, 125.7, 40.3, 21.2, 14.3; HRMS (ESI) *m/z* found, 303.0992; $C_{16}H_{19}N_2S_2$ (M^+ + H) expected 303.0989.

4.8.3.2.5. 1-(4-((2-Chlorophenyl)thio)phenyl)-3-ethylthiourea ***(14)***. Flash chromatography (hexanes/ethyl acetate (85:15 to 70:30)). Yield: 85%; orange solid; mp: 133-134 °C; ^{1}H NMR (DMSO-d_6): δ 9.65 (s, 1H, NH), 7.94 (s, 1H, NH), 7.61-7.59 (m, 2H, Ar), 7.51-7.41 (m, 3H, Ar), 7.25-7.20 (m, 2H, Ar), 6.89-6.86 (m, 1H, Ar), 3.52-3.49 (m, 2H, CH_2), 1.13 (t, 3H, *J* = 7.1 Hz, CH_3); ^{13}C NMR (DMSO-d_6): δ 180.4, 141.1, 137.2, 135.0, 131.4, 130.2, 129.1, 128.4, 127.9, 124.8, 123.9, 39.2, 14.6; HRMS (ESI) *m/z* found, 323.0436; $C_{15}H_{16}ClN_2S_2$ (M^+ + H) expected 323.0449.

4.8.3.2.6. 1-(4-((3-Chlorophenyl)thio)phenyl)-3-ethylthiourea ***(15)***. Flash chromatography (hexanes/ethyl acetate (80:20)). Yield: 100%; pale grey sticky solid; ^{1}H NMR (DMSO-d_6): δ 9.62 (s, 1H, NH), 7.92 (s, 1H, NH), 7.58-7.56 (m, 2H, Ar), 7.43-7.25 (m, 4H, Ar), 7.16-7.13 (m, 2H, Ar), 3.51-3.47 (m, 2H, CH_2), 1.13 (t, 3H, *J* = 7.1 Hz, CH_3);

^{13}C NMR (DMSO-d_6): δ 180.4, 140.9, 140.3, 134.4, 134.0, 131.4, 127.7, 127.2, 126.7, 126.1, 123.9, 39.2, 14.6; HRMS (ESI) *m/z* found, 323.0441; $C_{15}H_{16}ClN_2S_2$ (M^+ + H) expected 323.0449.

4.8.3.2.7. 1-(4-((4-Chlorophenyl)thio)phenyl)-3-ethylthiourea ***(16)***. Flash chromatography (hexanes/ethyl acetate (80:20)). Yield: 70%; white solid; mp: 105-107 °C; ^{1}H NMR (DMSO-d_6): δ 9.59 (s, 1H, NH), 7.88 (s, 1H, NH),7.55-7.52 (m, 2H, Ar), 7.40-7.34 (m, 4H, Ar), 7.24-7.21 (m, 2H, Ar), 3.51-3.47 (m, 2H, CH_2), 1.12 (t, 3H, *J* = 7.1 Hz, CH_3); ^{13}C NMR (DMSO-d_6): δ 180.5, 140.4, 136.2, 133.5, 131.9, 131.1, 129.8, 127.4, 123.9, 39.2, 14.6; HRMS (ESI) *m/z* found, 323.0440; $C_{15}H_{16}ClN_2S_2$ (M^+ + H) expected 323.0449.

4.8.3.2.8. 1-Ethyl-3-(4-(phenylthio)phenyl)urea ***(17)***. Flash chromatography (hexanes/ethyl acetate (75:25)). Yield: 75%; pale beige solid; mp: 144-146 °C; ^{1}H NMR (DMSO-d_6): δ 8.65 (s, 1H, NH), 7.49-7.46 (m, 2H, Ar), 7.35-7.26 (m, 4H, Ar), 7.19-7.11 (m, 3H, Ar), 6.19-6.16 (m, 1H, NH), 3.13-3.06 (m, 2H, CH_2), 1.05 (t, 3H, *J* = 7.1 Hz, CH_3); ^{13}C NMR (DMSO-d_6): δ 155.4, 141.8, 138.5, 135.0, 129.7, 128.2, 126.4, 123.4, 119.1, 34.5, 15.9; HRMS (ESI) *m/z* found, 273.1061; $C_{15}H_{17}N_2OS$ (M^+ + H) expected 273.1062.

4.8.3.2.9. 1-Ethyl-3-(4-(o-tolylthio)phenyl)urea ***(18)***. Flash chromatography (hexanes/ethyl acetate (80:20 to 60:40)). Yield: 32%; pale yellow solid; mp: 154-156 °C; ^{1}H NMR (DMSO-d_6): δ 8.62 (s, 1H, NH), 7.48-7.45 (m, 2H, Ar), 7.26-7.21 (m, 3H, Ar), 7.11-7.09 (m, 2H, Ar), 6.91-6.88 (m, 1H, Ar), 6.18-6.15 (m, 1H, NH), 3.15-3.06 (m, 2H, CH_2), 2.30 (s, 3H, CH_3), 1.05 (t, 3H, *J* = 7.0 Hz, CH_3); ^{13}C NMR (DMSO-d_6): δ 155.4, 141.4, 137.0, 136.6, 134.2, 130.7, 128.8, 127.1, 126.7, 123.5, 119.1, 34.4, 20.2, 15.9; HRMS (ESI) *m/z* found, 287.1219; $C_{16}H_{19}N_2OS$ (M^+ + H) expected 287.1219.

4.8.3.2.10. 1-Ethyl-3-(4-(m-tolylthio)phenyl)urea ***(19)***. Flash chromatography (methylene chloride to methylene chloride/ethyl acetate (50:50)). Yield: 84%; gray solid; mp: 144-146 °C; 1H NMR (DMSO-d_6): δ 8.64 (s, 1H, NH), 7.48-7.45 (m, 2H, Ar), 7.33-7.30 (m, 2H, Ar), 7.19-7.14 (m, 1H, Ar), 6.99-6.90 (m, 3H, Ar), 6.19-6.16 (m, 1H, NH), 3.15-3.06 (m, 2H, CH_2), 2.22 (s, 3H, CH_3), 1.05 (t, 3H, *J* = 7.1 Hz, CH_3); ^{13}C NMR (DMSO-d_6): δ 155.4, 141.6, 139.0, 138.1, 134.8, 129.5, 128.7, 127.2, 125.5, 123.6, 119.0, 34.4, 21.3, 15.9; HRMS (ESI) m/z found, 287.1224; $C_{16}H_{19}N_2OS$ (M+ + H) expected 287.1219.

*4.8.3.2.11. 1-Ethyl-3-(4-(p-tolylthio)phenyl)urea (**20**).* Flash chromatography (hexanes/ethyl acetate (70:30)). Yield: 71%; white solid; mp: 146-147 °C; ^{1}H NMR (DMSO-d_6): δ 8.60 (s, 1H, NH), 7.44-7.42 (m, 2H, Ar), 7.28-7.25 (m, 2H, Ar), 7.13-7.06 (m, 4H, Ar), 6.17-6.13 (m, 1H, NH), 3.14-3.06 (m, 2H, CH_2), 2.25 (s, 3H, CH_3), 1.04 (t, 3H, *J* = 7.1 Hz, CH_3); ^{13}C NMR (DMSO-d_6): δ 155.4, 141.3, 136.3, 134.2, 133.9, 130.4, 129.3, 124.8, 119.0, 34.4, 21.0, 15.9; HRMS (ESI) *m/z* found, 287.1220; $C_{16}H_{19}N_2OS$ (M+ + H) expected 287.1219.

*4.8.3.2.12. 1-(4-((2-Chlorophenyl)thio)phenyl)-3-ethylurea (**21**).* Flash chromatography (hexanes/ethyl acetate (75:25 to 50:50)). Yield: 80%; light red solid; mp: 76-78 °C; ^{1}H NMR (DMSO-d_6): δ 8.73 (s, 1H, NH), 7.57-7.54 (m, 2H, Ar), 7.45-7.38 (m, 3H, Ar), 7.21-7.11 (m, 2H, Ar), 6.70-6.68 (m, 1H, Ar), 6.24-6.20 (m, 1H, NH), 3.17-3.08 (m, 2H, CH_2), 1.06 (t, 3H, *J* = 7.1 Hz, CH_3); ^{13}C NMR (DMSO-d_6): δ 155.4, 142.7, 138.6, 136.4, 130.2, 130.0, 128.2, 127.6, 127.1, 120.5, 119.3, 34.5, 15.9; HRMS (ESI) *m/z* found, 307.0670; $C_{15}H_{16}ClN_2OS$ (M^+ + H) expected 307.0669.

*4.8.3.2.13. 1-(4-((3-Chlorophenyl)thio)phenyl)-3-ethylurea (**22**).* Flash chromatography (hexanes/ethyl acetate (60:40)). Yield: 100%; pale beige sticky solid; ^{1}H NMR (DMSO-d_6): δ 8.71 (s, 1H, NH), 7.54-7.51 (m, 2H, Ar), 7.40-7.38 (m, 2H, Ar), 7.31-7.26 (m, 1H, Ar), 7.20-7.18 (m, 1H, Ar), 7.05-7.02 (m, 2H, Ar), 6.21 (brs, 1H, NH), 3.16-3.08 (m, 2H, CH_2), 1.05 (t, 3H, *J* = 7.1 Hz, CH_3); ^{13}C NMR (DMSO-d_6): δ 155.4, 142.5, 141.8, 135.9, 134.3, 131.3, 126.3, 126.0, 125.8, 121.6, 119.2, 34.5, 15.9; HRMS (ESI) *m/z* found, 307.0670; $C_{15}H_{16}ClN_2OS$ (M^+ + H) expected 307.0669.

*4.8.3.2.14. 1-(4-((4-Chlorophenyl)thio)phenyl)-3-ethylurea (**23**).* Flash chromatography (hexanes/ethyl acetate (80:20)). Yield: 50%; pale beige solid; mp: 181-183 °C; ^{1}H NMR (DMSO-d_6): δ 8.67 (s, 1H, NH), 7.51-7.48 (m, 2H, Ar), 7.36-7.31 (m, 4H, Ar), 7.11-7.08 (m, 2H, Ar), 6.18 (brs, 1H, NH), 3.13-3.09 (m, 2H, CH_2), 1.05 (t, 3H, *J* = 7.1 Hz, CH_3); ^{13}C NMR (DMSO-d_6): δ 155.4, 142.2, 137.9, 135.3, 130.9, 129.6, 129.5, 122.7, 119.2, 34.5, 15.9; HRMS (ESI) *m/z* found, 307.0669; $C_{15}H_{16}ClN_2OS$ (M^+ + H) expected 307.0669.

4.8.3.2.15. 1-(2-Chloroethyl)-3-(4-(phenylthio)phenyl)urea ***(24)***. Flash chromatography (hexanes/ethyl acetate (75:25)). Yield: 44%; pale pink solid; mp: 146-148 °C; ^{1}H NMR (DMSO-d_6): δ 8.89, (s, 1H, NH), 7.50-7.47 (m, 2H, Ar), 7.36-7.26 (m, 4H, Ar), 7.19-7.12 (m, 3H, Ar), 6.51-6.47 (m, 1H, NH), 3.66 (t, 2H, J = 6.0 Hz, CH_2), 3.46-3.40 (m, 2H, CH_2); ^{13}C NMR (DMSO-d_6): δ 155.4, 141.4, 138.4, 134.9, 129.7, 128.3, 126.5, 124.0, 119.2, 44.9, 41.7; HRMS (ESI) *m/z* found, 307.0674; $C_{15}H_{16}ClN_2OS$ (M^+ + H) expected 307.0673.

4.8.3.2.16. 1-(2-Chloroethyl)-3-(4-(o-tolylthio)phenyl)urea ***(25)***. Flash chromatography (methylene chloride/ethyl acetate (95:5)). Yield: 78%; pale brown solid; mp: 134-136 °C; ^{1}H NMR (DMSO-d_6): δ 8.87, (s, 1H, NH), 7.49-7.46 (m, 2H, Ar), 7.26-7.24 (m, 3H, Ar), 7.21-7.09 (m, 2H, Ar), 6.93-6.90 (m, 1H, Ar), 6.50-6.47 (m, 1H, NH), 3.66 (t, 2H, J = 5.9 Hz, CH_2), 3.46-3.40 (m, 2H, CH_2), 2.30 (s, 3H, CH_3); ^{13}C NMR (DMSO-d_6): δ 155.3, 141.0, 136.8, 134.0, 130.7, 129.1, 127.2, 126.8, 124.1, 119.2, 44.8, 41.7, 20.3; HRMS (ESI) *m/z* found, 321.0832; $C_{16}H_{18}ClN_2OS$ (M^+ + H) expected 321.0829.

4.8.3.2.17. 1-(2-Chloroethyl)-3-(4-(m-tolylthio)phenyl)urea ***(26)***. Flash chromatography (methylene chloride to methylene chloride/ethyl acetate (85:15)). Yield: 85%; pink solid; mp: 69-71 °C; ^{1}H NMR (DMSO-d_6): δ 8.90 (s, 1H, NH), 7.49-7.46 (m, 2H, Ar), 7.34-7.31 (m, 2H, Ar), 7.19-7.14 (m, 1H, Ar), 6.99-6.91 (m, 3H, Ar), 6.52-6.48 (m, 1H, NH), 3.66 (t, 2H, J = 6.0 Hz, CH_2), 3.46-3.41 (m, 2H, CH_2), 2.22 (s, 3H, CH_3); ^{13}C NMR (DMSO-d_6): δ 155.3, 141.3, 139.0, 137.9, 134.7, 129.5, 128.9, 127.3, 125.6, 124.2, 119.1, 44.8, 41.7, 21.3; HRMS (ESI) *m/z* found, 321.0834; $C_{16}H_{18}ClN_2OS$ (M^+ + H) expected 321.0829.

4.8.3.2.18. 1-(2-Chloroethyl)-3-(4-(p-tolylthio)phenyl)urea ***(27)***. Flash chromatography (hexanes/ethyl acetate (80:20 to 60:40)). Yield: 99%; white solid; mp: 161-163 °C; ^{1}H NMR (DMSO-d_6): δ 8.88 (s, 1H, NH), 7.49-7.46 (m, 2H, Ar), 7.29-7.27 (m, 2H, Ar), 7.09 (brs, 4H, Ar), 6.52-6.49 (m, 1H, NH), 3.66 (t, 2H, J = 6.0 Hz, CH_2), 3.47-3.41 (m, 2H, CH_2), 2.23 (s, 3H, CH_3); ^{13}C NMR (DMSO-d_6): δ 155.4, 140.9, 136.4, 134.0, 133.7, 130.3, 129.5, 125.5, 119.1, 44.8, 41.7, 21.0; HRMS (ESI) *m/z* found, 321.0833; $C_{16}H_{18}ClN_2OS$ (M^+ + H) expected 321.0829.

*4.8.3.2.19. 1-(2-Chloroethyl)-3-(4-((2-chlorophenyl)thio)phenyl)urea (**28**).* Flash chromatography (methylene chloride to methylene chloride/ethyl acetate (95:5)). Yield: 98%; light red sticky solid; ^{1}H NMR (DMSO-d_6): δ 8.99 (s, 1H, NH), 7.59-7.56 (m, 2H, Ar), 7.43-7.39 (m, 3H, Ar), 7.19-7.10 (m, 2H, Ar), 6.72-6.69 (m, 1H, Ar), 6.57-6.53 (m, 1H, NH), 3.67 (t, 2H, J = 6.0 Hz, CH_2), 3.48-3.43 (m, 2H, CH_2); ^{13}C NMR (DMSO-d_6): δ 155.4, 142.4, 138.5, 136.4, 130.4, 130.0, 128.2, 127.8, 127.1, 121.1, 119.5, 44.8, 41.7; HRMS (ESI) *m/z* found, 341.0285; $C_{15}H_{15}Cl_2N_2OS$ (M^+ + H) expected 341.0279.

*4.8.3.2.20. 1-(2-Chloroethyl)-3-(4-((3-chlorophenyl)thio)phenyl)urea (**29**).* Flash chromatography (hexanes/ethyl acetate (80:20)). Yield: 100%; light green sticky solid; ^{1}H NMR (DMSO-d_6): δ 8.96 (s, 1H, NH), 7.54-7.52 (m, 2H, Ar), 7.41-7.39 (m, 2H, Ar), 7.31-7.18 (m, 2H, Ar), 7.05-7.03 (m, 2H, Ar), 6.52-6.51 (m, 1H, NH), 3.66 (t, 2H, J = 5.7 Hz, CH_2), 3.47-3.40 (m, 2H, CH_2); ^{13}C NMR (DMSO-d_6): δ 155.4, 142.2, 141.7, 135.9, 134.3, 131.3, 126.5, 126.0, 126.0, 122.1, 119.4, 44.8, 41.7; HRMS (ESI) *m/z* found, 341.0280; $C_{15}H_{15}Cl_2N_2OS$ (M^+ + H) expected 341.0279.

*4.8.3.2.21. 1-(2-Chloroethyl)-3-(4-((4-chlorophenyl)thio)phenyl)urea (**30**).* Flash chromatography (hexanes/ethyl acetate (80:20 to 60:40)). Yield: 79%; white solid; mp: 162-164 °C; ^{1}H NMR (DMSO-d_6): δ 8.92 (s, 1H, NH), 7.54-7.51 (m, 2H, Ar), 7.37-7.28 (m, 4H, Ar), 7.11-7.08 (m, 2H, Ar), 6.52 (s, 1H, NH), 3.67 (t, 2H, J = 5.5 Hz, CH_2), 3.46-3.45 (m, 2H, CH_2); ^{13}C NMR (DMSO-d_6): δ 155.4, 141.8, 137.8, 135.2, 131.1, 129.6, 129.6, 123.3, 119.3, 44.9, 41.8; HRMS (ESI) *m/z* found, 341.0283; $C_{15}H_{15}Cl_2N_2OS$ (M^+ + H) expected 341.0279.

*4.8.3.2.22. 1-Phenyl-3-(4-(phenylthio)phenyl)urea (**31**).* Flash chromatography (hexanes/ethyl acetate (85:15)). Yield: 44%; white solid; mp: 183-185 °C; ^{1}H NMR (DMSO-d_6): δ 8.89, (s, 1H, NH), 8.74 (s, 1H, NH), 7.57-7.54 (m, 2H, Ar), 7.50-7.47 (m, 2H, Ar), 7.41-7.38 (m, 2H, Ar), 7.30-7.26 (m, 4H, Ar), 7.21-7.16 (m, 3H, Ar), 7.00-6.95 (m, 1H, Ar); ^{13}C NMR (DMSO-d_6): δ 152.9, 140.8, 140.0, 138.1, 134.7, 129.8, 129.3, 128.6, 126.6, 125.0, 122.5, 119.7, 118.8; HRMS (ESI) *m/z* found, 321.1062; $C_{19}H_{17}N_2OS$ (M^+ + H) expected 321.1062.

*4.8.3.2.23. 1-Phenyl-3-(4-(o-tolylthio)phenyl)urea (**32**).* Flash chromatography (methylene chloride to methylene chloride/ethyl acetate (95:5)). Yield: 67%; pale beige solid; mp: 162-164 °C; ^{1}H NMR (DMSO-d_6): δ 8.85, (s, 1H, NH), 8.72 (s, 1H, NH), 7.55-7.46 (m, 4H, Ar), 7.30-7.23 (m, 5H, Ar), 7.14-7.12 (m, 2H, Ar), 7.00-6.95 (m, 2H, Ar), 2.32 (s, 3H, CH_3); ^{13}C NMR (DMSO-d_6): δ 152.9, 140.3, 140.0, 137.1, 136.4, 133.7, 130.8, 129.5, 129.3, 127.2, 127.0, 125.1, 122.4, 119.7, 118.7, 20.3; HRMS (ESI) *m/z* found, 335.1224; $C_{20}H_{19}N_2OS$ (M^+ + H) expected 335.1219.

*4.8.3.2.24. 1-Phenyl-3-(4-(m-tolylthio)phenyl)urea (**33**).* Flash chromatography (methylene chloride to methylene chloride/ethyl acetate (85:15)). Yield: 84%; white solid; mp: 176-177 °C; ^{1}H NMR (DMSO-d_6): δ 8.89 (s, 1H, NH), 8.75 (s, 1H, NH), 7.57-7.48 (m, 4H, Ar), 7.39-7.36 (m, 2H, Ar), 7.31-7.26 (m, 2H, Ar), 7.20-7.15 (m, 1H, Ar), 7.03-6.95 (m, 4H, Ar), 2.23 (s, 3H, CH_3); ^{13}C NMR (DMSO-d_6): δ 152.9, 140.6, 140.0, 139.1, 137.6, 134.4, 129.6, 129.3, 127.5, 126.0, 125.3, 122.5, 119.6, 118.8, 21.3; HRMS (ESI) *m/z* found, 335.1223; $C_{20}H_{19}N_2OS$ (M^+ + H) expected 335.1219.

*4.8.3.2.25. 1-Phenyl-3-(4-(p-tolylthio)phenyl)urea (**34**).* Flash chromatography (hexanes/ethyl acetate (90:10) to ethyl acetate). Yield: 100%; pale solid; mp: 137-139 °C; ^{1}H NMR (DMSO-d_6): δ 8.84 (s, 1H, NH), 8.72 (s, 1H, NH), 7.53-7.46 (m, 4H, Ar), 7.33-7.25 (m, 4H, Ar), 7.13 (brs, 4H, Ar), 6.99-6.95 (m, 1H, Ar), 2.25 (s, 3H, CH_3); ^{13}C NMR (DMSO-d_6): δ 152.9, 140.2, 140.0, 136.6, 133.7, 133.5, 130.4, 129.9, 129.3, 126.4, 122.4, 119.6, 118.7, 21.0; HRMS (ESI) *m/z* found, 335.1220; $C_{20}H_{19}N_2OS$ (M^+ + H) expected 335.1219.

*4.8.3.2.26. 1-(4-((2-Chlorophenyl)thio)phenyl)-3-phenylurea (**35**).* Flash chromatography (hexanes/ethyl acetate (90:10)). Yield: 43%; pale purple solid; mp: 189-191 °C; ^{1}H NMR (DMSO-d_6): δ 8.95 (s, 1H, NH), 8.76 (s, 1H, NH), 7.62-7.59 (m, 2H, Ar), 7.48-7.44 (m, 5H, Ar), 7.32-7.15 (m, 4H, Ar), 7.01-6.96 (m, 1H, Ar), 6.77-6.74 (m, 1H, Ar); ^{13}C NMR (DMSO-d_6): δ 152.8, 141.7, 139.9, 138.1, 136.3, 130.4, 130.0, 129.3, 128.3, 128.0, 127.3, 122.5, 121.8, 119.9, 118.8; HRMS (ESI) *m/z* found, 355.0669; $C_{19}H_{16}ClN_2OS$ (M^+ + H) expected 355.0669.

*4.8.3.2.27. 1-(4-((3-Chlorophenyl)thio)phenyl)-3-phenylurea (**36**).* Flash chromatography (hexanes/ethyl acetate (80:20)). Yield: 32%; white solid; mp: 129-131 °C;

^{1}H NMR (DMSO-d_6): δ 8.93 (s, 1H, NH), 8.74 (s, 1H, NH), 7.60-7.57 (m, 2H, Ar), 7.48-7.44 (m, 4H, Ar), 7.35-7.22 (m, 4H, Ar), 7.10-7.08 (m, 2H, Ar), 7.01-6.96 (m, 1H, Ar); ^{13}C NMR (DMSO-d_6): δ 152.8, 141.4, 141.3, 139.9, 135.7, 134.3, 131.3, 129.3, 126.6, 126.2, 123.0, 122.5, 119.7, 118.8, 118.6; HRMS (ESI) *m/z* found, 355.0671; $C_{19}H_{16}ClN_2OS$ (M^+ + H) expected 355.0669.

*4.8.3.2.28. 1-(4-((4-Chlorophenyl)thio)phenyl)-3-phenylurea (**37**).* Flash chromatography (hexanes/ethyl acetate (90:10)). Yield: 67%; white solid; mp: 215-217 °C; ^{1}H NMR (DMSO-d_6): δ 8.91 (s, 1H, NH), 8.74 (s, 1H, NH), 7.59-7.26 (m, 10H, Ar), 7.16-7.13 (m, 2H, Ar), 7.00-6.95 (m, 1H, Ar); ^{13}C NMR (DMSO-d_6): δ 152.9, 141.2, 140.0, 137.5, 135.1, 131.2, 129.9, 129.7, 129.3, 124.2, 122.6, 119.8, 118.9; HRMS (ESI) *m/z* found, 355.0669; $C_{19}H_{16}ClN_2OS$ (M^+ + H) expected 355.0669.

4.8.3.3. General preparation of TPIs 38-44

Sodium hydride (1.0 Eq.) was dissolved in an ice-cold solution of the appropriate 2-chloroethylurea derivative (TPUs **24**-**30**, 0.1g, 1.0 Eq.) in dry THF (10 mL) under argon atmosphere. The ice bath was removed after 5 min. The reaction was stirred at room temperature for 24 h. The reaction was quenched at 0 °C with water (10 mL) and the organic solvent was evaporated. The aqueous solution was extracted thrice with AcOEt (15 mL). Then, the combined organic solution was washed twice with brine (15 mL), dried over anhydrous sodium sulfate, filtered and evaporated to dryness under reduced pressure. The residue was purified by flash chromatography on silica gel.

4.8.3.4. Characterization of TPIs 38-44

*4.8.3.4.1. 1-(4-(Phenylthio)phenyl)imidazolidin-2-one (**38**).* Flash chromatography (hexanes/ethyl acetate (50:50 to 25:75)). Yield: 63%; white solid; mp: 172-174 °C; ^{1}H NMR (DMSO-d_6): δ 7.64-7.61 (m, 2H, Ar), 7.41-7.38 (m, 2H, Ar), 7.31-7.26 (m, 2H, Ar), 7.20-7.10 (m, 4H, NH and Ar), 3.84 (t, 2H, J = 7.4 Hz, CH_2), 3.43-3.39 (m, 2H, CH_2); ^{13}C NMR (DMSO-d_6): δ 159.3, 141.6, 138.2, 134.5, 129.8, 128.5, 126.6, 124.5, 118.3, 44.8, 37.0; HRMS (ESI) *m/z* found, 271.0907; $C_{15}H_{15}N_2OS$ (M^+ + H) expected 271.0906.

*4.8.3.4.2. 1-(4-(o-Tolylthio)phenyl)imidazolidin-2-one (**39**).* Flash chromatography (hexanes/ethyl acetate (50:50 to 25:75)). Yield: 64%; white solid; mp: 170-172 °C; ^{1}H NMR ($CDCl_3$): δ 7.52-7.49 (m, 2H, Ar), 7.32-7.29 (m, 2H, Ar), 7.21-7.09 (m, 4H, Ar), 5.27 (brs, 1H, NH), 3.91 (t, 2H, *J* = 7.2 Hz, CH_2), 3.60-3.55 (m, 2H, CH_2), 2.38 (s, 3H, CH_3); ^{13}C NMR ($CDCl_3$): δ 159.8, 139.5, 138.0, 135.9, 132.6, 130.5, 130.4, 127.6, 126.8, 126.6, 118.6, 45.2, 37.5, 20.4; HRMS (ESI) *m/z* found, 285.1059; $C_{16}H_{17}N_2OS$ (M^+ + H) expected 285.1062.

*4.8.3.4.3. 1-(4-(m-Tolylthio)phenyl)imidazolidin-2-one (**40**).* Flash chromatography (hexanes/ethyl acetate (50:50 to 25:75)). Yield: 41%; white solid; mp: 154-155 °C; ^{1}H NMR ($CDCl_3$): δ 7.53-7.51 (m, 2H, Ar), 7.42-7.39 (m, 2H, Ar), 7.17-6.97 (m, 4H, Ar), 5.50 (brs, 1H, NH), 3.91 (t, 2H, *J* = 7.3 Hz, CH_2), 3.60-3.55 (m, 2H, CH_2), 2.28 (s, 3H, CH_3); ^{13}C NMR ($CDCl_3$): δ 159.9, 139.9, 138.9, 137.2, 133.5, 129.8, 128.9, 127.5, 127.2, 126.4, 118.5, 45.2, 37.5, 21.4; HRMS (ESI) *m/z* found, 285.1054; $C_{16}H_{17}N_2OS$ (M^+ + H) expected 285.1062.

*4.8.3.4.4. 1-(4-(p-Tolylthio)phenyl)imidazolidin-2-one (**41**).* Flash chromatography (hexanes/ethyl acetate (50:50 to 25:75)). Yield: 65%; white solid; mp: 186-188 °C; ^{1}H NMR (DMSO-d_6): δ 7.60-7.57 (m, 2H, Ar), 7.34-7.31 (m, 2H, Ar), 7.15-7.06 (m, 5H, Ar and NH), 3.83 (m, 2H, *J* = 7.4 Hz, CH_2), 3.42-3.35 (m, 2H, CH_2), 2.25 (s, 3H, CH_3); ^{13}C NMR (DMSO-d_6): δ 159.3, 141.2, 136.6, 133.9, 133.5, 130.5, 129.7, 125.9, 118.3, 44.8, 37.0, 21.1; HRMS (ESI) *m/z* found, 285.1055; $C_{16}H_{17}N_2OS$ (M^+ + H) expected 285.1062.

*4.8.3.4.5. 1-(4-((2-Chlorophenyl)thio)phenyl)imidazolidin-2-one (**42**).* Flash chromatography (hexanes/ethyl acetate (50:50 to 25:75)). Yield: 57%; white solid; mp: 202-203 °C; ^{1}H NMR (DMSO-d_6): δ 7.71-7.69 (m, 2H, Ar), 7.48-7.45 (m, 3H, Ar), 7.22-7.16 (m, 3H, Ar and NH), 6.73-6.70 (m, 1H, Ar), 3.88 (t, 2H, *J* = 7.4 Hz, CH_2), 3.45-3.40 (m, 2H, CH_2); ^{13}C NMR (DMSO-d_6): δ 159.2, 142.5, 138.2, 136.0, 130.4, 130.1, 128.3, 127.9, 127.3, 121.4, 118.6, 44.8, 37.0; HRMS (ESI) *m/z* found, 305.0508; $C_{15}H_{14}ClN_2OS$ (M^+ + H) expected 305.0516.

*4.8.3.4.6. 1-(4-((3-Chlorophenyl)thio)phenyl)imidazolidin-2-one (**43**).* Flash chromatography (hexanes/ethyl acetate (50:50 to 25:75)). Yield: 36%; white solid; mp: 148-149 °C; ^{1}H NMR ($CDCl_3$): δ 7.59-7.56 (m, 2H, Ar), 7.46-7.43 (m, 2H, Ar), 7.17-7.02 (m, 4H, Ar), 5.45 (brs, 1H, NH), 3.94 (t, 2H, *J* = 7.3 Hz, CH_2), 3.62-3.57 (m, 2H, CH_2); ^{13}C NMR

($CDCl_3$): δ 159.7, 140.7, 140.6, 134.8, 134.7, 129.9, 127.7, 126.2, 125.9, 125.3, 118.5, 45.1, 37.4; HRMS (ESI) *m/z* found, 305.0510; $C_{15}H_{14}ClN_2OS$ (M^+ + H) expected 305.0516.

*4.8.3.4.7. 1-(4-((4-Chlorophenyl)thio)phenyl)imidazolidin-2-one (**44**).* Flash chromatography (hexanes/ethyl acetate (50:50 to 5:95)). Yield: 67%; white solid; mp: 146-147 °C; ^{1}H NMR (DMSO-d_6): δ 7.66-7.63 (m, 2H, Ar), 7.44-7.34 (m, 4H, Ar), 7.13-7.11 (m, 3H, Ar and NH), 3.86 (m, 2H, J = 7.3 Hz, CH_2), 3.44-3.39 (m, 2H, CH_2); ^{13}C NMR (DMSO-d_6): δ 159.1, 141.9, 137.6, 134.9, 131.0, 129.6, 123.5, 118.4, 44.7, 36.9; HRMS (ESI) *m/z* found, 305.0515; $C_{15}H_{14}ClN_2OS$ (M^+ + H) expected 305.0516.

4.8.3.5. Preparation of phenylthioanilines

The relevant thiophenol (1.2 Eq.) was added to a solution of 4-iodoaniline (3.0g, 1.0 Eq.), copper(II) oxide (0.11g, 0.1 Eq.) and cesium carbonate (6.7g, 1.5 Eq.) in toluene (5 mL). The reaction mixture was stirred in a dry argon atmosphere under pressure with microwaves at 110 °C for 24 h. After completion of the reaction, the mixture was diluted with ethyl acetate (100 mL) and filtered through celite. The resulting solution was washed twice with NaOH (1 M, 10 mL) and brine (10 mL), dried over anhydrous sodium sulfate, filtered and evaporated to dryness under reduced pressure. The residue was purified by flash chromatography on silica gel. The ^{1}H and ^{13}C NMR correspond to the NMR characterization reported by Fang *et al*. and Lui *et al.*[35, 36]

4.9. Acknowledgments

This work was supported by grants from Natural Sciences and Engineering Research Council of Canada (NSERC, RGPIN-2016-05069), Fonds de Recherche du Québec-Santé (FRQS, starting grant for new investigators) and CHU de Quebec-Université Laval Research Center. S. Fortin holds a Junior 1 research scholar award from FRQS. M. Gagné-Boulet and C. Bouzriba are recipients of studentships from the Fonds d'enseignement et de recherche of the Faculty of pharmacy at Université Laval and FRQS. A.C. Chavez Alvarez is recipient of studentships from Fonds d'enseignement et de recherche of the Faculty of pharmacy at Université Laval.

4.10. Appendix C. Supplementary data

Proton and carbon NMR spectra and calculated physicochemical, pharmacokinetic and drug-likeness properties by SwissADME tool of TPUs **24**-**30** and TPIs **38**-**44** can be found in the appendix C.

4.11. References

1. Siegel, R. L.; Miller, K. D.; Fuchs, H. E.; Jemal, A., Cancer Statistics, 2021. *CA Cncer J. Clin.* **2021**, *71*, 7-33.

2. Jones, R.; Ocen, J., Cytotoxic chemotherapy: clinical aspects. *Medicine* **2020**, *48*, 97-102.

3. Hirsch, F. R.; Scagliotti, G. V.; Mulshine, J. L.; Kwon, R.; Curran, W. J.; Wu, Y.-L.; Paz-Ares, L., Lung cancer: current therapies and new targeted treatments. *Lancet* **2017**, *389*, 299-311.

4. Calligaris, D.; Verdier-Pinard, P.; Devred, F.; Villard, C.; Braguer, D.; Lafitte, D., Microtubule targeting agents: from biophysics to proteomics. *Cell. Mol. Life Sci.* **2010**, *67*, 1089-1104.

5. Jordan, M. A.; Wilson, L., Microtubules as a target for anticancer drugs. *Nat. Rev. Cancer* **2004**, *4*, 253-265.

6. Asbury, C. L., Anaphase A: disassembling microtubules move chromosomes toward spindle poles. *Biology-Basel* **2017**, *6*, 32.

7. Ilan, Y., Microtubules: from understanding their dynamics to using them as potential therapeutic targets. *J. Cell. Physiol.* **2019**, *234*, 7923-7937.

8. Mukhtar, E.; Adhami, V. M.; Mukhtar, H., Targeting microtubules by natural agents for cancer therapy. *Mol. Cancer Ther.* **2014**, *13*, 275-284.

9. Cheng, B.; Crasta, K., Consequences of mitotic slippage for antimicrotubule drug therapy. *Endocr.-Relat. Cancer* **2017**, *24*, 97-106.

10. Grosios, K.; Holwell, S. E.; McGown, A. T.; Pettit, G. R.; Bibby, M. C., *In vivo* and *in vitro* evaluation of combretastatin A-4 and its sodium phosphate prodrug. *Brit. J. Cancer.* **1999**, *81*, 1318-1327.

11. Thirumaran, R.; Prendergast, G. C.; Gilman, P. B., Chapter 7 - Cytotoxic chemotherapy in clinical treatment of cancer. In *Cancer Immunotherapy*, Prendergast, G. C.; Jaffee, E. M., Eds. Academic Press: Burlington, 2007; pp 101-116.

12. Turcotte, V.; Fortin, S.; Vevey, F.; Coulombe, Y.; Lacroix, J.; Côté, M.-F.; Masson, J.-Y.; C.-Gaudreault, R., Synthesis, biological evaluation, and structure-activity relationships of novel substituted *N*-phenyl ureidobenzenesulfonate derivatives blocking cell cycle progression in S-phase and inducing DNA double-strand breaks. *J. Med. Chem.* **2012**, *55*, 6194-6208.

13. Gagné-Boulet, M.; Fortin, S.; Lacroix, J.; Lefebvre, C. A.; Côté, M.-F.; C.-Gaudreault, R., Styryl-*N*-phenyl-*N*'-(2-chloroethyl)ureas and styrylphenylimidazolidin-2-ones as new potent microtubule-disrupting agents using combretastatin A-4 as model. *Eur. J. Med. Chem.* **2015**, *100*, 34-43.

14. Gagné-Boulet, M.; Moussa, H.; Lacroix, J.; Côté, M.-F.; Masson, J.-Y.; Fortin, S., Synthesis and biological evaluation of novel *N*-phenyl ureidobenzenesulfonate derivatives as potential anticancer agents. Part 2. Modulation of the ring B. *Eur. J. Med. Chem.* **2015**, *103*, 563-573.

15. Fortin, S.; Wei, L. H.; Moreau, E.; Lacroix, J.; Côté, M.-F.; Petitclerc, É.; Kotra, L. P.; C.-Gaudreault, R., Design, synthesis, biological evaluation, and structure-activity relationships of substituted phenyl 4-(2-oxoimidazolidin-1-yl)-benzenesulfonates as new tubulin inhibitors mimicking combretastatin A-4. *J. Med. Chem.* **2011**, *54*, 4559-4580.

16. Gagné-Boulet, M.; Bouzriba, C.; Godard, M.; Fortin, S., Preparation, characterisation and biological evaluation of new *N*-phenyl amidobenzenesulfonates and *N*-phenyl ureidobenzenesulfonates inducing DNA double-strand breaks. Part 3. Modulation of ring A. *Eur. J. Med. Chem.* **2018**, *155*, 681-694.

17. Huang, Y.-T.; Tsai, W.-T.; Badsara, S. S.; Chan, C.-C.; Lee, C.-F., Copper-catalyzed cross-coupling ligand-free conditions reaction of thiols with aryl iodides under ligand-free conditions. *J. Chin. Chem. Soc-taip.* **2014**, *61*, 967-974.

18. National Cancer Institute (NCI/NIH), Developmental therapeutics program human tumor cell line screen. http://dtp.nci.nih.gov/branches/btb/ivclsp.html (accessed 20 December 2019).

19. Shan, Y.; Zhang, J.; Liu, Z.; Wang, M.; Dong, Y., Developments of combretastatin A-4 derivatives as anticancer agents. *Curr. Med. Chem.* **2011**, *18*, 523-538.

20. Steinmetz, M. O.; Prota, A. E., Microtubule-targeting agents: strategies to hijack the cytoskeleton. *Trends Cell Biol.* **2018**, *28*, 776-792.

21. Fortin, S.; Wei, L.; Moreau, E.; Lacroix, J.; Côté, M.-F.; Petitclerc, É.; Kotra, L. P.; C.-Gaudreault, R., Substituted phenyl 4-(2-oxoimidazolidin-1-yl)benzenesulfonamides as antimitotics. Antiproliferative, antiangiogenic and antitumoral activity, and quantitative structure-activity relationships. *Eur. J. Med. Chem.* **2011**, *46*, 5327-5342.

22. Fortin, S.; Lacroix, J.; Côté, M.-F.; Moreau, E.; Petitclerc, É.; C.-Gaudreault, R., Quick and simple detection technique to assess the binding of antimicrotubule agents to the colchicine-binding site. *Biol. Proced. Online* **2010**, *12*, 113-117.

23. Cabral, F.; Sobel, M. E.; Gottesman, M. M., CHO mutants resistant to colchicine, colcemid or griseofulvin have an altered b-tubulin. *Cell* **1980**, *20*, 29-36.

24. Schibler, M. J.; Barlow, S. B.; Cabral, F., Elimination of permeability mutants from selections for drug resistance in mammalian cells. *FASEB J.* **1989**, *3*, 163-168.

25. Schibler, M. J.; Cabral, F., Taxol-dependent mutants of Chinese hamster ovary cells with alterations in a- and b-tubulin. *J. Cell. Biol.* **1986**, *102*, 1522-1531.

26. Struski, S.; Cornillet-Lefebvre, P.; Doco-Fenzy, M.; Dufer, J.; Ulrich, E.; Masson, L.; Michel, N.; Gruson, N.; Potron, G., Cytogenetic characterization of chromosomal rearrangement in a human vinblastine-resistant CEM cell line: use of comparative genomic hybridization and fluorescence in situ hybridization. *Cancer Genet. Cytogen.* **2002**, *132*, 51-54.

27. Beck, W. T.; Mueller, T. J.; Tanzer, L. R., Altered surface membrane glycoproteins in *Vinca* alkaloid-resistant human leukemic lymphoblasts. *Cancer Res.* **1979**, *39*, 2070-2076.

28. Hu, X. F.; Martin, T. J.; Bell, D. R.; de Luise, M.; Zalcberg, J. R., Combined use of cyclosporin A and verapamil in modulating multidrug resistance in human leukemia cell lines. *Cancer Res.* **1990**, *50*, 2953-7.

29. Ueda, K.; Cardarelli, C.; Gottesman, M. M.; Pastan, I., Expression of a full-length cDNA for the human "MDR1" gene confers resistance to colchicine, doxorubicin, and vinblastine. *Proc. Natl. Acad. Sci. U S A* **1987**, *84*, 3004-8.

30. Panchagnula, R.; Thomas, N. S., Biopharmaceutics and pharmacokinetics in drug research. *Int. J. Pharm.* **2000**, *201*, 131-150.

31. Daina, A.; Michielin, O.; Zoete, V., SwissADME: a free web tool to evaluate pharmacokinetics, drug-likeness and medicinal chemistry friendliness of small molecules. *Sci. Rep.* **2017**, *7*, 42717.

32. Carmichael, J.; DeGraff, W. G.; Gazdar, A. F.; Minna, J. D.; Mitchell, J. B., Evaluation of a tetrazolium-based semiautomated colorimetric assay: assessment of chemosensitivity testing. *Cancer Res* **1987**, *47*, 936-42.

33. Ford, C. H.; Richardson, V. J.; Tsaltas, G., Comparison of tetrazolium colorimetric and [3H]-uridine assays for *in vitro* chemosensitivity testing. *Cancer Chemoth. Pharm.* **1989**, *24*, 295-301.

34. Laemmli, U. K., Cleavage of structural proteins during the assembly of the head of bacteriophage T4. *Nature* **1970**, *227*, 680-685.

35. Fang, X.-L.; Tang, R.-Y.; Zhang, X.-G.; Li, J.-H., FeF3/I2-catalyzed synthesis of 4-chalcogen-substituted arylamines by direct thiolation of an arene C-H bond. *Synthesis* **2011**, *2011*, 1099-1105.

36. Liu, Y.; Kim, J.; Seo, H.; Park, S.; Chae, J., Copper(II)-catalyzed single-step synthesis of aryl thiols from aryl halides and 1,2-ethanedithiol. *Adv. Synth. Catal.* **2015**, *357*, 2205-2212.

Chapitre 5. Synthesis and biological evaluation of novel *N*-phenyl ureidobenzenesulfonate derivatives as potential anticancer agents. Part 2. Modulation of the Ring B

Mathieu Gagné-Boulet [a,b,1], Hanane Moussa [a,b,1], Jacques Lacroix [a,b], Marie-France Côté [a], Jean-Yves Masson [c,d,e] Sébastien Fortin [a,b,*]

[a]Centre de recherche du CHU de Québec-Université Laval, axe Oncologie, Hôpital Saint-François d'Assise, 10 Rue de l'Espinay, Québec, QC, G1L 3L5, Canada

[b]Faculté de Pharmacie, Université Laval, Québec, QC, G1V 0A6, Canada

[c]Genome Stability Laboratory, CHU de Québec Research Centre, Oncology Division, Hôtel-Dieu-de-Québec, 9 rue McMahon, Quebec City, QC, G1R 2J6, Canada.

[d]Department of Molecular Biology, Medical Biochemistry and Pathology, Faculty of Medicine, Laval University, Quebec City, QC, G1V 0A6, Canada.

[e]FRQS Chercheur National Investigator.

[1]These authors contributed equally.

***Corresponding author:** Sébastien Fortin; Phone: 418-525-4444 ext. 52364, Fax: 418-525-4372, e-mail: sebastien.fortin@pha.ulaval.ca

Publié le 20 octobre 2015 dans le European Journal of Medicinal Chemistry, 103, 563-573, doi : 10.1016/j.ejmech.2015.09.012.

5.1. Résumé

Nous avons récemment découvert une nouvelle famille d'agents anticancéreux appelés *N*-phényl uréidobenzènesulfonates (PUB-SOs) qui bloquent la progression du cycle cellulaire en phase S et induisent des bris double-brins à l'ADN. Cependant, l'effet de la nature et de la position des substituants sur le cycle aromatique B est encore peu étudié. Dans cette étude, nous décrivons la préparation et l'évaluation biologique de 45 nouveaux dérivés de PUB-SOs substitués par des groupements alkyles, alcoxys, halogènes et nitros à différentes positions sur le cycle aromatique B. Tous les PUB-SOs étaient actifs du haut nanomolaire au bas micromolaires (0,24-20 µM). Les PUB-SOs substitués en position 2 stoppent la progression du cycle cellulaire en phase S et induisent la phosphorylation de H2AX (γH2AX). Cette étude montre que les PUB-SOs sont des composés anticancéreux prometteurs qui pourraient être utilisés comme alternative pour contourner les complications probables rencontrées lors de leur développement.

5.2. Abstract

DNA double strand-breaks (DSBs) are the most deleterious lesions that can affect the genome of living beings and are lethal if not quickly and properly repaired. Recently, we discovered a new family of anticancer agents designated as *N*-phenyl ureidobenzenesulfonates (PUB-SOs) that are blocking the cells cycle progression in S-phase and inducing DNA DSBs. Previously, we have studied the effect of several modifications on the molecular scaffold of PUB-SOs on their cytocidal properties. However, the effect of the nature and the position of substituents on the aromatic ring B is still poorly studied. In this study, we report the preparation and the biological evaluation of 45 new PUB-SO derivatives substituted by alkyl, alkoxy, halogen and nitro groups at different positions on the aromatic ring B. All PUB-SOs were active in the submicromolar to low micromolar range (0.24-20 μM). The cell cycle progression analysis showed that PUB-SOs substituted at position 2 by alkyl, halogen or nitro groups or substituted at position 4 by a hydroxyl group arrest the cell cycle progression in S-phase. Interestingly, all others PUB-SOs substituted at positions 3 and 4 arrested the cell cycle in G2/M-phase. PUB-SOs arresting the cell cycle progression in S-phase also induced the phosphorylation of H2AX (γH2AX) which is indicating the generation of DNA DSBs. We evidenced that few modifications on the ring B of PUB-SOs scaffold lead to cytocidal derivatives arresting the cell cycle in S-phase and inducing γH2AX and DSBs. In addition, this study shows that these new anticancer agents are promising and could be used as alternative to circumvent some of the biopharmaceutical complications that might be encountered during the development of PUB-SOs.

5.3. Graphical abstract

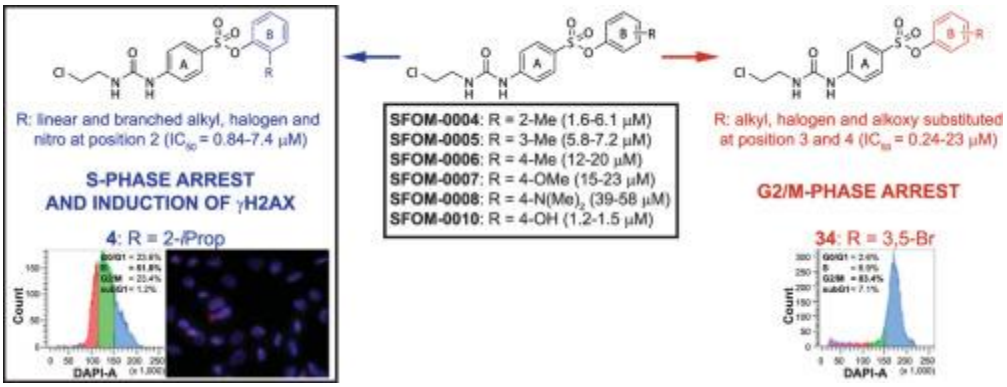

5.4. Introduction

Spontaneous DNA damage occurs frequently in living cells. It is estimated that the number of DNA lesions including base losses, single- and double-strand breaks (DSBs) can be close to 100 000 lesions per cell per day [1]. On one hand, cells exploit a variety of specialized DNA repair mechanisms to restore the integrity of the DNA. These DNA repair mechanisms collectively termed the DNA damage response are responsible to detect DNA damage and arrest the cell cycle to repair DNA lesions [2]. On the other hand, DNA lesions that are left unrepaired or inappropriately repaired induce genomic instability that may cause senescence, cell death or carcinogenesis [3]. Among all identified DNA damage, DSBs are one of the most cytotoxic lesions and the most difficult DNA lesion to repair [4]. Accordingly, as little as one DSB can kill a cell [5]. Several types of DNA lesions (e.g. DNA-DNA crosslinks, DNA-protein crosslinks and DNA alkylation), inhibition of topoisomerase or other mechanisms blocking the DNA replication fork machinery can result in the formation of DSBs [6]. For these reasons, several cancer treatments notably radiation therapy and conventional chemotherapeutic drugs including DNA crosslinkers (e.g. cisplatin (**1**) [7], Fig. 5.1A), topoisomerase inhibitors (e.g. topotecan (**2**) [8]) and antimetabolites (e.g. 5-fluorouracil (**3**) [9]) induce DNA DSBs and contribute to kill cancer cells. Moreover, it is known that various cancer cells, including cells mutated in BRCA1 or BRCA2, are particularly sensitive to the induction of DNA DSBs [10]. In this context, the development of new anticancer agents inducing DNA DSBs is a promising strategy in cancer drug therapy.

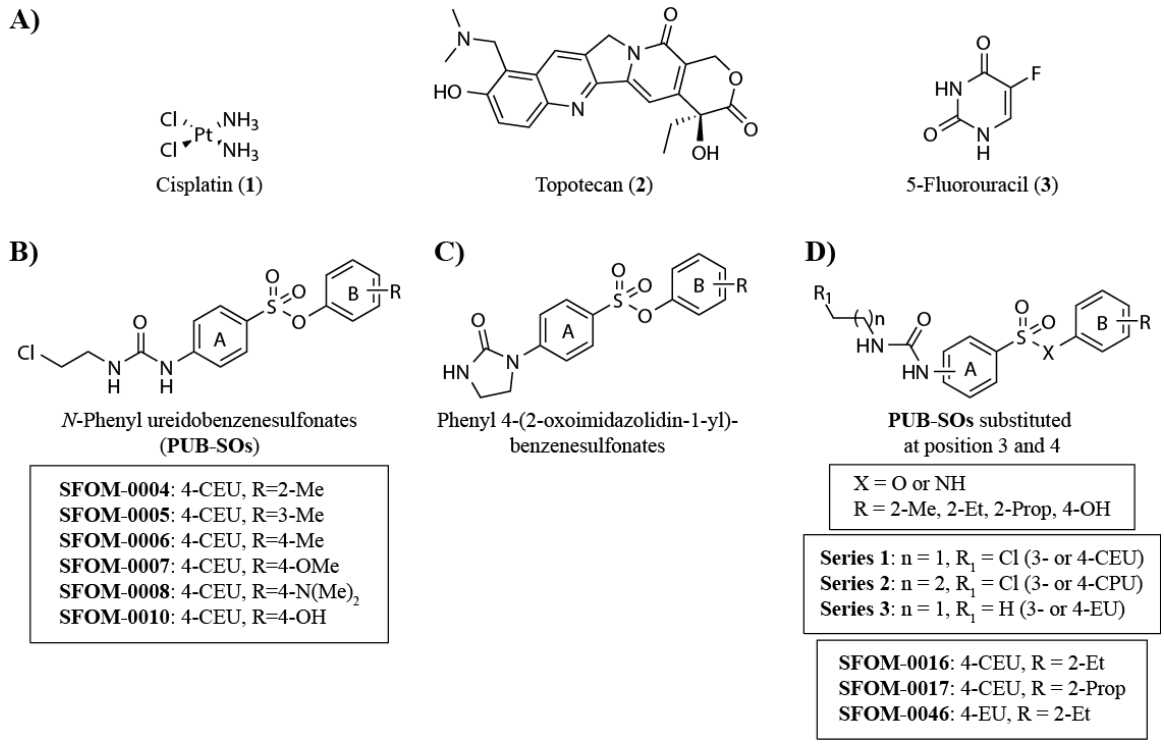

Figure. 5.1. Molecular structures of A) cisplatin (**1**), topotecan (**2**), 5-fluorouracil (**3**), B) *N*-phenyl ureidobenzenesulfonates (PUB-SOs, SFOM-0004 to SFOM-0010), C) phenyl 4-(2-oxoimidazolidin-1-yl)-benzenesulfonates as well as D) the 3 series of PUB-SOs substituted at position 3 and 4 on the ring A by a 2-chloroethylurea (CEU, Series 1), a 3-chloropropylurea (CPU, Series 2) or an ethylurea group (EU, Series 3) previously prepared and studied.

We recently identified and developed a new class of anticancer agents referred to as *N*-phenyl ureidobenzenesulfonate derivatives (PUB-SOs, Fig. 5.1B). PUB-SOs emerged from our structure-activity relationship studies of phenyl 4-(2-oxoimidazolidin-1-yl)-benzenesulfonate derivatives (Fig. 5.1C) which are new microtubule-disrupting agents targeting the colchicine-binding site [11]. Beside apparent structure similarities between PUB-SOs and phenyl 4-(2-oxoimidazolidin-1-yl)-benzenesulfonates, their mechanisms of action are dramatically different. Indeed, we found that PUB-SOs bearing a 2-Me (SFOM-0004, Fig. 5.1) or a 4-OH (SFOM-0010) substituent block the cell cycle progression in S-phase and induce the phosphorylation of histone H2AX (γH2AX), which evidences the induction of DNA DSBs instead of the expected arrest of the cell cycle in the G2/M-phase

and disruption of the cytoskeleton observed with phenyl 4-(2-oxoimidazolidin-1-yl)-benzenesulfonates [11, 12] and *N*-phenyl-*N'*-(2-chloroethyl)ureas studied so far [13-17].

In this context, we performed a concise structure-activity relationship study based on modification (Fig. 5.1D) of: 1) the substitution of the urea group at position 3 or 4 of the aromatic ring A, 2) the urea group by its substitution by either a 2-chloroethylurea (CEU, series 1), a 3-chloropropylurea (CPU, series 2) or an ethylurea group (EU, series 3), 3) the group bridging the two phenyl rings by a sulfonate and a sulfonamide group, 4) the position 2 by addition of a lower alkyl group (Me, Et, Prop) and 5) the position 4 by addition of an hydroxyl group [18]. In this study, we showed that the replacement of the sulfonate linking group by its bioisosteric sulfonamide functionality almost abrogates both the antiproliferative activity and cell cycle arrest in S-phase. In addition, we found that a combination of EU or CEU moieties at position 4 on the ring A and lower alkyl group at position 2 or hydroxyl group at position 4 on the ring B leads to PUB-SO derivatives with optimal antiproliferative activity and cell cycle arrest in S-phase. Moreover, PUB-SOs exhibit antitumor activity on human fibrosarcoma HT-1080 tumours grafted onto chick chorioallantoic membranes with low to very low toxicity on the chick embryos [18]. Interestingly, SFOM-0005, SFOM-0006 and SFOM-007 bearing a 3-Me, 4-Me or a 4-OMe, respectively show a low percentage of cell in S-phase but they exhibit approximately a 0.5 log lower activity than SFOM-004 and SFOM-0010 [18].

Based on these previous structure-activity relationship results, we hypothesized that the antiproliferative activity, the arrest of the cell cycle progression in the S-phase and the induction of the γH2AX could be improved by modifying the position and the nature of the substituents grafted on the aromatic ring B. To this end, we investigated here the substitution effect on the antiproliferative activity by varying both the substituents (lower alkyl chains, halogen, alkoxy and nitro groups) and positions on this aromatic ring using four cancer cell lines. Moreover, PUBSOs exhibiting a significant antiproliferative activity (IC_{50} < 10 µM) were evaluated for their effects on the cells cycle progression. Finally, the most potent inhibitors of the S-phase progression were assessed for their ability to induce H2AX phosphorylation which correlates with the induction of DNA DSBs.

5.5. Chemistry

The preparation of PUB-SOs bearing deactivating groups on aromatic ring B is not easily achieved. The final step of the previously used classical method is troublesome (low yields, long reaction time or no reaction of some aniline derivatives) [18]. To circumvent this problem, we chose an alternate synthetic approach (Scheme 5.1) which is brief and efficient in producing PUB-SO derivatives with a wide variety of substituents at different positions on the aromatic ring B. As shown in Scheme 5.1, the target compounds **4**-**48** were derived from 1-(2-chloroethyl)-3-phenylurea **49**. This compound was prepared in quantitative yield by treating aniline with 2-chloroethyl isocyanate in methylene chloride, as described in our previous publications [11,12]. Chlorosulfonation of **49** using chlorosulfonic acid in carbon tetrachloride gave the sulfonyl chloride **50** in 18% yield. Finally, the desired PUB-SO derivatives **4**-**48** were acquired in moderate to high yields upon reaction of the sulfonyl chloride **50** with appropriate phenol in the presence of triethylamine in methylene chloride.

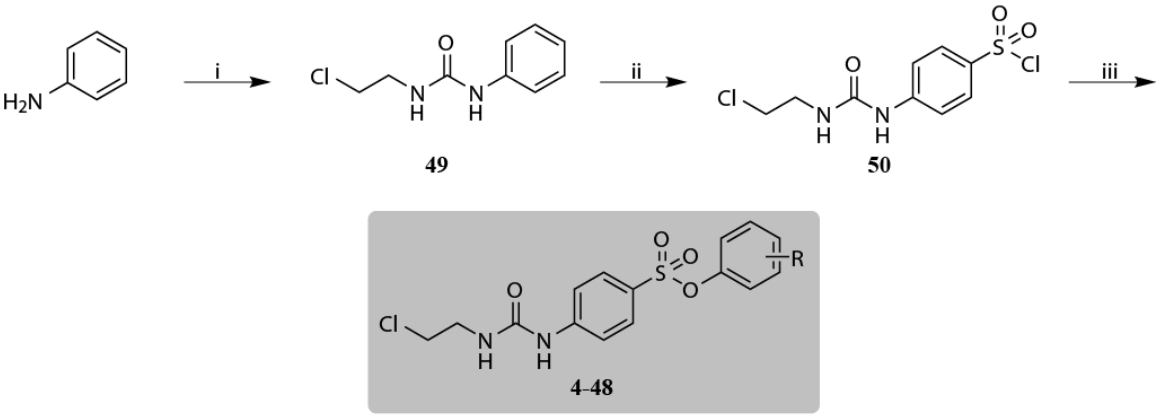

4: 2-*i*Prop	**13**: 2,6-Me	**22**: 3-OEt	**31**: 3,4-F	**40**: 4-*tert*But
5: 2-OMe	**14**: 2,4-F	**23**: 3-F	**32**: 3,5-F	**41**: 4-OEt
6: 2-OEt	**15**: 2,6-F	**24**: 3-Cl	**33**: 3,5-Cl	**42**: 4-OBut
7: 2-F	**16**: 2,4,5-Me	**25**: 3-Br	**34**: 3,5-Br	**43**: 4-F
8: 2-Cl	**17**: 2,4,5-Cl	**26**: 3-I	**35**: 3,4,5-Me	**44**: 4-Cl
9: 2-I	**18**: 2,4,6-Cl	**27**: 3-NO_2	**36**: 3,4,5-OMe	**45**: 4-Br
10: 2-NO_2	**19**: 3-Et	**28**: 3,5-Me	**37**: 3,4,5-F	**46**: 4-I
11: 2,4-Me	**20**: 3-Prop	**29**: 3,4-OMe	**38**: 4-Et	**47**: 4-CN
12: 2,5-Me	**21**: 3-OMe	**30**: 3,5-OMe	**39**: 4-Prop	**48**: H

Scheme 5.1. Synthesis of PUB-SOs **4**-**48**. Reagents and conditions: (i) 2-chloroethyl isocyanate, DCM, rt, 24 h quant.; (ii) $ClSO_3H$, CCl_4, 0 °C 4 h, 18%; (iii) relevant phenol, triethylamine, DCM, rt, 24 h, 28% to quant. yield.

5.6. Results/Discussion

5.6.1. PUB-SOs exhibit antiproliferative activity on human tumor cell lines

Using the sulforhodamine B method and according to the NCI/NIH Developmental Therapeutics Program [19], the antiproliferative activity of PUB-SOs (**4**-**48**) was assessed on four human tumor cell lines namely HT-1080 fibrosarcoma, HT-29 colon adenocarcinoma, M21 skin melanoma and estrogen-dependent MCF7 breast adenocarcinoma. The results are summarized in Table 5.1 and expressed as the concentration of drug inhibiting cell growth by 50% (IC_{50}). Beside compounds **5**, **27**, **29**, **37**, **38**, **39**, **40**, **43**, **46**, **47** and **48**, all PUB-SOs exhibited antiproliferative activity at concentrations lower than 10 μM on all cancer cell lines studied; activity that is higher than cisplatin (9.6 to 19 μM) used as positive control. The effect of the position and the nature of the substituent affected within a one log range the antiproliferative activity of PUB-SOs and it was therefore difficult to determine absolute structure-activity relationships. However, a number of interesting observations were made. First, the sensitivity of cancer cell lines toward PUB-SOs generally follows this order: HT-1080 > M21 > HT-29 > MCF7. Second, PUB-SOs substituted at position 2 of ring B are more active than PUB-SOs substituted at position 3, and PUB-SOs substituted at position 3 are more active than those substituted at position 4. Third, the cytocidal activity of PUB-SOs generally increases with the size of groups in a series of PUB-SO derivatives at a given position (e.g. 8-I (**26**) > 8-Br (**25**) > 8-Cl (**24**) > 8-F (**23**)). Fourth, PUB-SOs **4**, **16**, **34** and **36** bearing on the aromatic ring B a 2-*i*Prop, 2,4,5-Me, 3,5-Br and 3,4,5-OMe substituents have an antiproliferative activity in the nanomolar range (0.24-2.96 μM) which is at least equivalent to topotecan used as control on HT-1080, HT-29 and MCF7 (0.18, 0.23 and 1.4 μM, respectively). Finally, we found that the PUB-SO **34** is the most potent compound exhibiting an antiproliferative activity between 240 and 400 nM.

Table 5.1. Antiproliferative activity (IC_{50}) of PUB-SOs on human HT-1080 fibrosarcoma, HT-29 colon adenocarcinoma, M21 skin melanoma and estrogen-dependent MCF7 breast adenocarcinoma cell lines.

Compd	R	IC_{50} (μM)[1]			
		HT-1080	HT-29	M21	MCF7

SFOM-0004	2-Me	1.6	4.9	4.5	6.1
SFOM-0016	2-Et	1.2	3.3	2.1	4.1
SFOM-0017	2-Prop	1.9	1.9	1.3	2.1
4	2-*i*Prop	0.84	1.5	1.5	1.8
5	2-OMe	8.3	13	15	19
6	2-OEt	2.2	1.4	1.1	1.7
7	2-F	3.2	5.4	4.0	6.0
8	2-Cl	1.1	3.5	2.1	4.2
9	2-I	1.2	1.5	1.9	1.51
10	2-NO_2	2.4	5.7	3.9	7.4
11	2,4-Me	1.3	3.6	2.1	3.9
12	2,5-Me	1.7	1.5	1.5	1.9
13	2,6-Me	1.1	2.8	2.0	3.7
14	2,4-F	9.4	9.6	9.6	9.3
15	2,6-F	3.2	4.1	3.2	4.8
16	2,4,5-Me	1.0	2.3	1.7	3.0
17	2,4,5-Cl	1.4	1.2	1.0	1.2
18	2,4,6-Cl	1.5	1.5	1.3	1.7
SFOM-0005	3-Me	5.8	6.0	6.2	7.2
19	3-Et	3.8	5.6	6.0	7.1
20	3-Prop	2.6	3.4	3.3	3.9
21	3-OMe	3.1	3.8	3.6	4.2
22	3-OEt	3.3	3.2	2.4	3.3
23	3-F	4.5	5.5	5.3	7.8
24	3-Cl	2.6	2.8	2.6	3.7
25	3-Br	2.0	2.1	2.2	2.6
26	3-I	1.4	1.3	1.2	1.8
27	3-NO_2	10	17	17	18
28	3,5-Me	2.4	1.8	1.7	2.9
29	3,4-OMe	11	13	12	15
30	3,5-OMe	1.5	1.1	1.1	2.0
31	3,4-F	8.1	7.0	7.3	8.9
32	3,5-F	5.7	4.8	5.0	5.7
33	3,5-Cl	1.1	0.55	0.51	1.0
34	3,5-Br	0.40	0.30	0.24	0.40
35	3,4,5-Me	9.0	6.6	6.5	9.4
36	3,4,5-OMe	0.64	0.50	0.47	0.66
37	3,4,5-F	9.8	9.9	11.3	11.3
SFOM-0006	4-Me	12	20	17	19
38	4-Et	9.8	15	16	16
39	4-Prop	5.2	11	12	13
40	4-*tert*But	6.8	15	18	17
SFOM-0007	4-OMe	15	22	17	23
41	4-OEt	8.3	7.8	8.3	9.5
42	4-OBut	3.4	6.5	7.7	7.1
43	4-F	11	12	12	14
44	4-Cl	5.9	6.3	6.0	7.3

45	4-Br	9.6	8.3	8.1	9.4
46	4-I	8.7	9.5	11	11
47	4-CN	14	18	19	19
SFOM-0008	4-$N(Me)_2$	N.E.[2]	39	43	58
SFOM-0010	4-OH	N.E.	1.5	1.2	1.3
48	H	8.8	17	16	19
SFOM-0046	-	0.36	12	2.5	3.4
Cisplatin	-	19	17	23	9.6
Topotecan	-	0.18	0.23	1.4	0.024

[1]IC_{50} is expressed as the concentration of drug inhibiting cell growth by 50% after two days of treatment. [2]N.E.: Not evaluated.

5.6.2. PUB-SOs arrest the cell cycle progression in S- and G2/M-phase

Based on their significant antiproliferative activity (< 10 μM) and the limited data on the structure-activity relationships related to aromatic ring B, most PUB-SOs were assessed for their effect on the cell cycle progression. Figure 5.2 and Table 5.2 show the percentage of M21 cells in G0/G1, S, G2/M and subG1 phases, respectively, after treatment for 24 h with PUB-SOs, cisplatin and topotecan at 2 or 5-times their respective IC_{50}. The results show the concentrations required to obtain optimal arrest of cell cycle progression in S- or G2/M-phase. Control cells treated with 0.5% DMSO were in G0/G1, S, G2/M and subG1 phases at 65.1%, 17.4%, 16.0% and 1.5%, respectively. At the exception of compounds **6**, **12**, **17** and **18** bearing a 2-OEt, 2,5-Me, 2,4,5-Cl or a 2,4,6-Cl group on ring B, respectively all PUB-SOs substituted at position 2 exhibited a significant arrest of the cell cycle in S-phase. Compounds **4**, **7**, **8**, **9**, **10**, **11**, **13**, **16**, SFOM-0004, SFOM-0016 and SFOM-0017 increase the percentage of cells in S-phase by 19.6% to 29.7% (Fig. 5.2). These results are higher to those observed with topotecan and equivalent to those obtained with cisplatin where the percentage of cells in S-phase was increased by 14.4% and 27%, respectively. In contrast, all other PUB-SOs substituted at position 3 and 4, including compounds **6**, **12**, **17** and **18** arrested the cell cycle progression in the G2/M-phase; the percentage of cells in G2/M-phase increasing by 26.9% to 76.4% (Table 5.2). This subset of PUB-SOs is probably acting as microtubule-disrupting agents binding to the colchicine-binding site similarly as the phenyl

4-(2-oxoimidazolidin-1-yl)-benzenesulfonates [11] and other *N*-phenyl-*N'*-(2-chloroethyl)ureas studied so far in our laboratory [13-17].

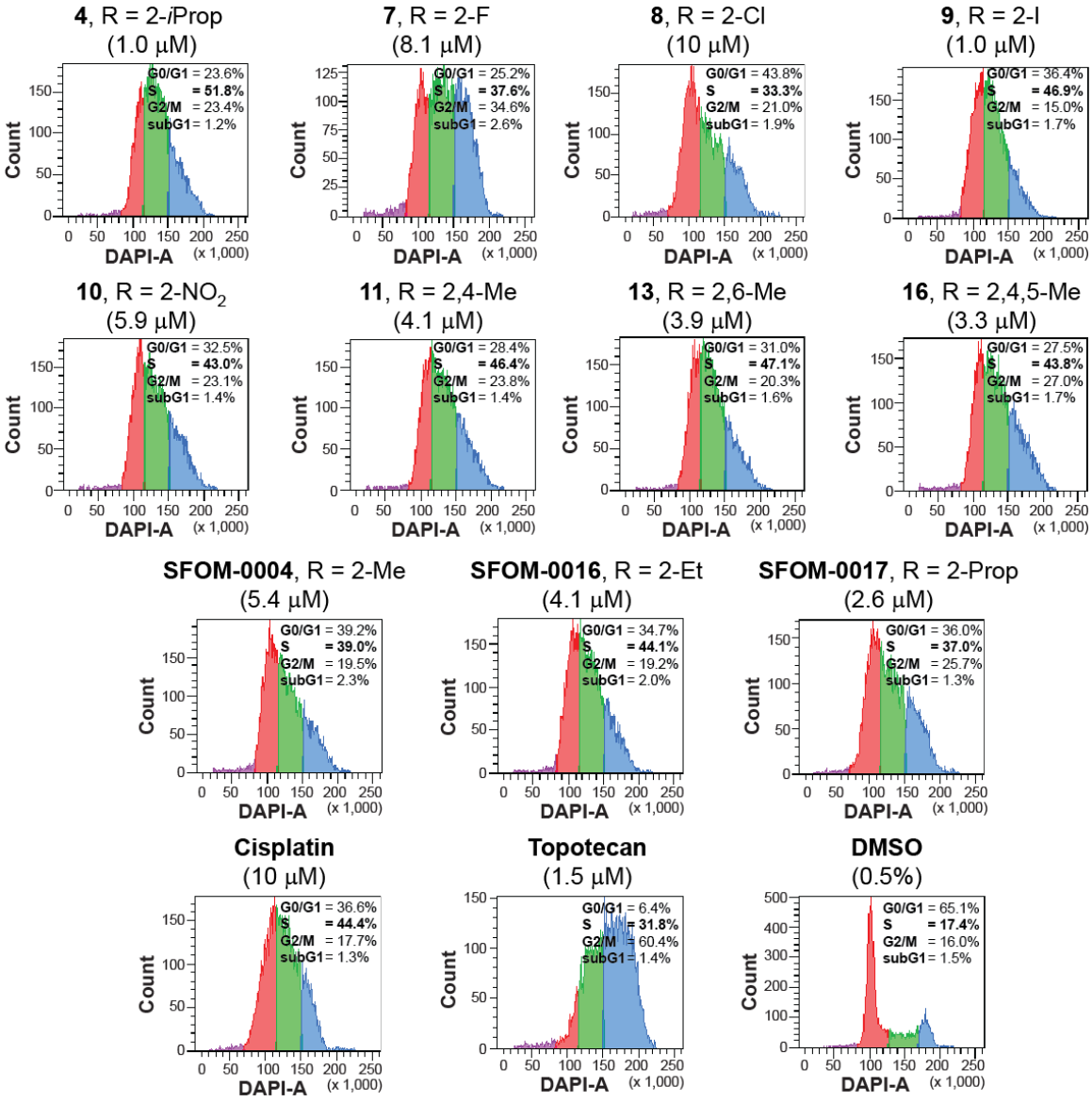

Figure. 5.2. PUB-SO derivatives substituted at position 2, cisplatin and topotecan arresting the cell cycle progression of M21 cells in S-phase after 24 h of treatment.

Table 5.2. PUB-SO derivatives arresting the cell cycle progression of M21 cells in G2/M-phase after 24 h of treatment.

Compd	R	Conc. (μM)	Cell cycle progression (%)			
			Sub-G_1	G0/G1	S	G2/M
6	2-OEt	2.2	6.7	28.8	11.8	52.7
12	2,5-Me	7.6	5.5	7.2	11.9	75.4
14	2,4-F	48	5.2	13.4	10.0	71.4
15	2,6-F	16	8.7	29.4	15.1	46.8
17	2,4,5-Cl	5.1	5.5	3.3	8.6	82.6
18	2,4,6-Cl	6.5	8.5	11.6	7.3	72.6
19	3-Et	39	5.0	15.2	11.3	68.5
20	3-Prop	22	6.0	9.9	5.8	78.3
21	3-OMe	25	3.5	2.5	6.3	87.7
22	3-OEt	11	8.4	22.2	13.5	55.9
23	3-F	34	6.2	2.5	4.4	86.9
24	3-Cl	13	5.2	7.2	7.0	80.6
25	3-Br	13	4.4	1.6	1.6	92.4
26	3-I	7.6	3.6	2.0	4.9	89.5
30	3,5-OMe	7.5	11.4	9.3	5.2	74.1
31	3,4-F	42	7.6	11.6	18.3	62.5
32	3,5-F	32	6.7	7.4	10.2	75.7
33	3,5-Cl	3.8	7.2	2.5	6.0	84.3
34	3,5-Br	1.2	7.1	2.6	6.9	83.4
35	3,4,5-Me	39	8.7	11.4	14.8	65.1
36	3,4,5-OMe	1.7	9.3	15.6	9.0	66.1
41	4-OEt	49	3.5	13.4	8.2	74.9
42	4-OBut	43	8.3	39.7	9.1	42.9
44	4-Cl	34	8.6	19.0	6.6	65.8
45	4-Br	40	7.5	12.0	4.4	76.1

5.6.3. PUB-SOs substituted at position 2 induce the phosphorylation of H2AX into γH2AX

Our previous studies showed that the arrest of the cell cycle progression in S-phase by PUB-SOs was associated with an induction DNA DSBs. To confirm that the arrest of the cells in the S-phase by the new PUB-SO derivatives is still associated with an induction of DNA DSBs, we assessed their effect on the induction of phosphorylation of H2AX into γH2AX by immunocytochemistry. In this assay, the number of γH2AX foci correlates with the number of DNA DSBs [9, 20]. Figure 5.3 shows γH2AX foci (nuclear red spot) and nuclei (stained in blue using 4′,6-diamidino-2-phenylindole (DAPI)) of M21 cells after treatment

with PUB-SO derivatives, cisplatin and topotecan for 24 h at 2- or 5-times their respective IC_{50}. The results show the concentration required to obtain optimal induction of γH2AX. As illustrated in Figure 5.3, compounds **4**, **7**, **8**, **9**, **10**, **11**, **13**, **16** and SFOM-0004 that are arresting the cell cycle progression in S-phase induced DNA DSBs as shown by the induction of γH2AX foci in treated cells when compared to control cells that are exhibiting low to very low levels of γH2AX. Interestingly, cisplatin and topotecan used as controls induced a high number of γH2AX foci that are drastically different from PUB-SOs. This confirms previous results suggesting that the mechanism of action of PUB-SOs is different of cisplatin (inter, intra and DNA-protein crosslinker [21]) and topotecan (intercalation and topoisomerase I poisoning [22]). Although the determination of the exact molecular target of PUB-SOs is not confirmed yet, our results strongly suggest that PUB-SOs inhibit proteins or enzymes involved in critical DNA repair/replication mechanisms, particularly those involving in the replication forks [18].

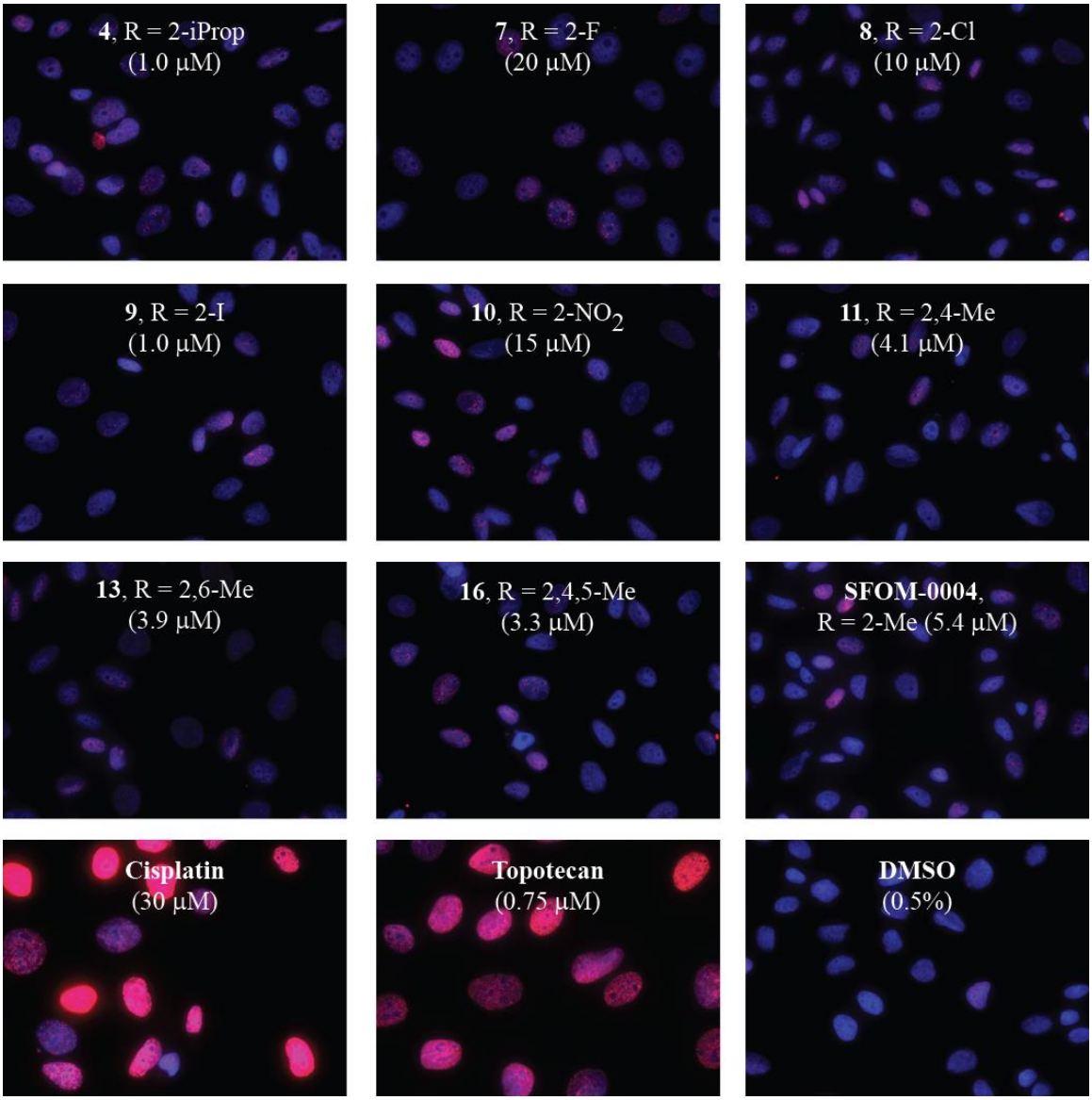

Figure. 5.3. Effect of PUB-SOs **4**, **7**, **8**, **9**, **10**, **11**, **13**, **16**, SFOM-0004, cisplatin and topotecan on the phosphorylation of H2AX into γH2AX after 24 h of treatment.

5.7. Conclusions

In summary, we report here the preparation and the structure-activity relationships of new PUB-SO derivatives where the nature and the position of the substituents were modified on the aromatic ring B. First, we designed a new synthetic approach to access quickly and efficiently to the desired PUB-SO derivatives. We found that the antiproliferative activity of most PUB-SO derivatives is in the low micromolar range and four of them (**4**, **16**, **34** and **36**)

are in the submicromolar range. This indicates that several modifications on the aromatic ring B such as linear and branched alkyl, halogen and nitro group can be performed to optimize the antiproliferative activity. However, at the exception of hydroxyl substituted at position 4 on the aromatic ring B of PUB-SOs, the substituents have to be grafted at position 2 to maintain both a significant arrest of the cell cycle progression in S-phase and the induction of γH2AX and DNA DSBs. All others PUB-SOs substituted at position 3 or 4 arrest the cell cycle progression in G2/M-phase leading probably to new subsets of antimicrotubule agents targeting the colchicine-binding site. Finally, this study provides new promising anticancer agents that will be further optimized in our research program.

5.8. Experimental protocols

5.8.1. Cell lines culture

HT-1080 human fibrosarcoma, HT-29 human colon carcinoma and MCF7 human breast carcinoma were purchased from the American Type Culture Collection (Manassas, VA). M21 human skin melanoma cells were kindly provided by Dr. David Cheresh (University of California, San Diego School of Medicine, USA). Cells were cultured in DMEM medium containing sodium bicarbonate, high glucose concentration, glutamine and sodium pyruvate (Hyclone, Logan, UT) supplemented with 5% of fetal bovine serum (FBS, Invitrogen, Burlington, ON) and were maintained at 37 ºC in a moisture-saturated atmosphere containing 5% CO_2.

5.8.2. Antiproliferative activity assay

The antiproliferative activity assay of all compounds was assessed using the procedure recommended by the National Cancer Institute for its drug screening program with minor modifications [19]. Briefly, 96-well microtiter plates were seeded with 75 μL of a suspension of either HT-1080 (2.5×10^3), HT-29 (4.0×10^3), M21 (3.0×10^3) or MCF7 (2.5×10^3) cells per well in DMEM and incubated for 24 h. Drugs freshly solubilized in DMSO were diluted in fresh DMEM, and 75 μL aliquots containing serially diluted concentrations of the drug were added. Final drug concentrations ranged from 50 μM to 98 nM. DMSO was maintained at a concentration of < 0.5% (v/v) to avoid any related cytotoxicity. Plates were

incubated for 48 h. Afterward, cell growth was stopped by addition of cold trichloroacetic acid to the wells (10% w/v, final concentration), followed by a 1 h incubation at 4 °C. Plates were washed 5-times with water. Then, 75 μL of a sulforhodamine B solution (0.1% w/v) in 1% acetic acid was added to each well, and the plates were incubated for 15 min at room temperature. After staining, unbound dye was removed by washing 5-times with 1% acetic acid. Bound dye was solubilized in 20 mM Tris base, and the absorbance was read using an optimal wavelength (530−568 nm) with a μQuant Universal microplate spectrophotometer (Biotek, Winooski, VT). Readings obtained from treated cells were compared with measurements from control cell plates fixed on treatment day, and the percentage of cell growth inhibition was calculated for each drug. The experiments were performed at least twice in triplicate. The assays were considered valid when the coefficient of variation for a given set of conditions and within the same experiment was < 10%.

5.8.3. Cell Cycle Progression Analysis

After incubating 2.5 x 10^5 M21 cells with the drugs at 2- and 5-times their respective IC_{50} for 24 h, cells were trypsinized, washed with Phosphate Buffered Saline (PBS), resuspended in 250 μL of PBS, fixed by the addition of 750 μL of ice-cold EtOH under agitation, and stored at -20 °C until analysis. Prior to fluorescence-activated cell sorting analysis, cells were washed with PBS and resuspended in 500 μL of PBS containing 2 μg/mL 4′,6-diamidino-2-phenylindole (DAPI). Cell cycle distribution of fixed cell suspensions was analyzed using an LSR II flow cytometer (BD Biosciences, Franklin Lakes, NJ).

5.8.4. Immunocytochemistry

Cover slides (22 mm × 22 mm) sterilized with 70% (v/v) EtOH were placed in six-well plates. To promote cell adhesion, cover slides were treated with 1.5 mL of a fibronectin solution in PBS (5 μg/mL) for 1 h at 37 °C. Slides were then rinsed twice with PBS. M21 cells (1 x 10^5) were seeded onto the plates and incubated for 24 h. Cells were then incubated with the compound to be tested at 2- and 5-times their respective IC_{50} for 24 h. The control solution was DMSO diluted in the culture medium at 0.2%, (v/v). Cells were fixed using 1 mL of formaldehyde at 3.7% and permeabilized by addition of a saponin solution (0.1% in PBS) containing 3% (w/v) BSA (saponin-BSA). Cells were incubated with mouse anti-

H2AX pS139 antibody (1/4000 in saponin-BSA, Millipore, Billerica, MA). Cover slides were next incubated for 2 h at room temperature and then washed twice with PBS supplemented with 0.05% (v/v) Tween 20 (PBST). Saponin-BSA containing goat anti-mouse IgG conjugated to AlexaFluor 594 (1/1000, Invitrogen, Burlington, Ontario, Canada), and DAPI (0.3 μg/mL, Sigma, Oakville, Ontario, Canada) was then added. The cover slides were incubated for 1 h at room temperature and then washed 4-times with PBST. The cover slides were mounted with Fluorescence Mounting Medium (Dako, Burlington, Ontario, Canada). Cells were visualized using an epifluorescence microscope (Olympus BX51, Center Valley, PA) with a Qimaging RETIGA EXi camera (Qimaging, Surrey, British Columbia, Canada).

5.9. Chemical methods

5.9.1. General

Proton NMR spectra were recorded on a Bruker AM-300 spectrometer (Bruker, Germany). Chemical shifts (δ) are reported in parts per million. Uncorrected melting points were determined on an electrothermal melting point apparatus. HPLC analyses were performed using a Prominence LCMS-2020 system with binary solvent equipped with an UV/vis photodiode array and an APCI probe (Shimadzu, Columbia, MD). Compounds were eluted within 23 min on an Alltech Alltima C18 reversed-phase column (5 μm, 250 mm × 4.6 mm) equipped with an Alltech Alltima C18 precolumn (5 μm, 7.5 mm × 4.6 mm) with a MeOH/H_2O linear gradient at 1.0 mL/min. The purities of the final compounds were > 95%. All reactions were performed under dry argon. All chemicals were supplied by Sigma-Aldrich Canada (Oakville, Ontario, Canada) or VWR International (Mont-Royal, Québec, Canada) and used as received unless specified otherwise. Liquid flash chromatography was performed on silica gel F60, 60 Å, 40−63 μm supplied by Silicycle (Quebec city, Québec, Canada) using a FPX flash purification system (Biotage, Charlottesville, VA) and using solvent mixtures expressed as v/v ratios. Solvents and reagents were used without purification unless specified otherwise. The progress of the chemical reaction was monitored by TLC using precoated silica gel 60 F254 TLC plates (VWR International, Mont-Royal, Québec, Canada). The chromatograms and spots were visualized under UV light at 254 and/or 265 nm.

5.9.2. General preparation of compounds 4-48

Typically, 4-(3-(2-chloroethyl)ureido)benzenesulfonyl chloride (**50**, 0.336 mmol, 1.0 Eq.) was suspended in dry methylene chloride (10 mL) under a dry Ar atmosphere. The relevant phenol (0.504 mmol, 1.5 Eq.) and trietylamine (0.504 mmol, 1.5 Eq.) were then added dropwise to the solution. The reaction mixture was stirred for 24 h at room temperature and then acidified with 1 N HCl (10 mL) and extracted thrice with methylene chloride (10 mL). The combined organic extracts were washed successively with 1 N NaOH (20 mL) and brine (20 mL), dried over sodium sulfate, filtered, and evaporated to dryness under reduced pressure. The residue was purified by flash chromatography on silica gel.

5.9.3. Characterization of compounds 4-48

5.9.3.1. 2-Isopropylphenyl 4-(3-(2-chloroethyl)ureido)benzenesulfonate (**4**). Flash chromatography (methylene chloride to methylene chloride/ethyl acetate (90:10)). Yield: 79%; white solid; mp: 93-95 °C; ^{1}H NMR ($CDCl_3$): δ 7.76 (s, 1H, NH), 7.72 (d, 2H, J = 8.8 Hz, Ar), 7.53 (d, 2H, J = 8.8 Hz, Ar), 7.25-7.18 (m, 2H, Ar), 7.11-7.06 (m, 1H, Ar), 6.99 (d, 1H, J = 8.0 Hz, Ar), 5.85 (t, 1H, J = 5.2 Hz, NH), 3.63-3.58 (m, 4H, 2x CH_2), 3.13 (q, 1H, J = 6.9 Hz, CH), 1.05 (d, 6H, J = 6.9 Hz, 2x CH_3); ^{13}C NMR ($CDCl_3$): δ 154.7, 146.9, 145.0, 141.8, 129.9, 128.1, 127.6, 127.3, 126.8, 121.9, 118.1, 44.3, 42.0, 26.8, 23.1. MS (ES+) found 397.10; $C_{18}H_{22}ClN_2O_4S$ (M^+ + H) requires 397.10.

5.9.3.2. 2-Methoxyphenyl 4-(3-(2-chloroethyl)ureido)benzenesulfonate (**5**). Flash chromatography (methylene chloride to methylene chloride/ethyl acetate (90:10)). Yield: 54%; white solid; mp: 101-102 °C; ^{1}H NMR ($CDCl_3$ and MeOD): δ 7.66 (d, 2H, J = 8.8 Hz, Ar), 7.48 (d, 2H, J = 8.8 Hz, Ar), 7.17-7.05 (m, 2H, Ar), 6.86-6.79 (m, 2H, Ar), 3.62-3.53 (m, 7H, 2x CH_2 and OCH_3); ^{13}C NMR ($CDCl_3$ and MeOD): δ 155.0, 151.8, 145.3, 138.3, 130.0, 128.1, 127.7, 123.9, 120.6, 117.2, 112.7, 55.6, 44.4, 41.6. MS (ES+) found 385.10; $C_{16}H_{18}ClN_2O_5S$ (M^+ + H) requires 385.06.

5.9.3.3. 2-Ethoxyphenyl 4-(3-(2-chloroethyl)ureido)benzenesulfonate (**6**). Flash chromatography (methylene chloride to methylene chloride/ethyl acetate (90:10)). Yield: 83%; white solid; mp: 128-129 °C; ^{1}H NMR ($CDCl_3$ and MeOD): δ 7.62 (d, 2H, J = 8.6 Hz,

Ar), 7.43 (d, 2H, J = 8.6 Hz, Ar), 7.11-7.04 (m, 2H, Ar), 6.80-6.74 (m, 2H, Ar), 3.78-3.67 (m, 2H, CH_2), 3.57-3.46 (m, 4H, 2x CH_2), 1.16 (t, 3H, J = 6.9 Hz, CH_3); ^{13}C NMR ($CDCl_3$ and MeOD): δ 155.2, 151.1, 145.3, 138.3, 129.9, 128.0, 127.7, 123.9, 120.4, 117.1, 113.6, 64.1, 44.2, 41.5, 14.3. MS (ES+) found 399.10; $C_{17}H_{20}ClN_2O_5S$ (M^+ + H) requires 399.08.

5.9.3.4. 2-Fluorophenyl 4-(3-(2-chloroethyl)ureido)benzenesulfonate (**7**). Flash chromatography (methylene chloride to methylene chloride/ethyl acetate (90:10)). Yield: quantitative; white sticky solid; ^1H NMR ($CDCl_3$): δ 7.82 (s, 1H, NH), 7.70 (d, 2H, J = 8.7 Hz, Ar), 7.52 (d, 2H, J = 8.7 Hz, Ar), 7.21-7.00 (m, 4H, Ar), 5.89 (t, 1H, J = 4.8 Hz, NH), 3.61 (brs, 4H, 2x CH_2); ^{13}C NMR ($CDCl_3$): δ 156.2, 154.8, 152.8, 145.3, 136.7, 136.5, 130.1, 128.7, 128.6, 127.1, 124.7, 124.7, 118.1, 117.3, 117.1, 44.3, 42.0. MS (ES+) found 373.05; $C_{15}H_{15}ClFN_2O_4S$ (M^+ + H) requires 373.04.

5.9.3.5. 2-Chlorophenyl 4-(3-(2-chloroethyl)ureido)benzenesulfonate (**8**). Flash chromatography (methylene chloride to methylene chloride/ethyl acetate (90:10)). Yield: 58%; white solid; mp: 93-95 °C; ^1H NMR ($CDCl_3$): δ 7.77 (s, 1H, NH), 7.72 (d, 2H, J = 8.9 Hz, Ar), 7.52 (d, 2H, J = 8.9 Hz, Ar), 7.33-7.14 (m, 4H, Ar), 5.85 (t, 1H, J = 5.2 Hz, NH), 3.64-3.57 (m, 4H, 2x CH_2); ^{13}C NMR ($CDCl_3$): δ 154.7, 145.4, 145.3, 130.9, 130.2, 128.2, 128.0, 127.6, 127.5, 124.1, 118.0, 44.4, 42.0. MS (ES+) found 389.00; $C_{15}H_{15}Cl_2N_2O_4S$ (M^+ + H) requires 389.01.

5.9.3.6. 2-Iodophenyl 4-(3-(2-chloroethyl)ureido)benzenesulfonate (**9**). Flash chromatography (methylene chloride to methylene chloride/ethyl acetate (90:10)). Yield: 79%; white solid; mp: 116-117 °C; ^1H NMR ($CDCl_3$): δ 7.94 (s, 1H, NH), 7.77-7.71 (m, 3H, Ar), 7.53 (d, 2H, J = 8.6 Hz, Ar), 7.33-7.24 (m, 2H, Ar), 6.96 (t, 1H, J = 6.9 Hz, Ar), 5.96 (brs, 1H, NH), 3.61 (brs, 4H, 2x CH_2); ^{13}C NMR ($CDCl_3$): δ 154.9, 149.8, 145.4, 140.2, 130.4, 129.7, 128.7, 127.5, 122.9, 118.1, 90.4, 44.4, 42.0. MS (ES+) found 480.95; $C_{15}H_{15}ClIN_2O_4S$ (M^+ + H) requires 480.95.

5.9.3.7. 2-Nitrophenyl 4-(3-(2-chloroethyl)ureido)benzenesulfonate (**10**). Flash chromatography (methylene chloride to methylene chloride/ethyl acetate (90:10)). Yield: 69%; brown oil; ^1H NMR ($CDCl_3$): δ 7.91-7.83 (m, 2H, Ar and NH), 7.70-7.52 (m, 5H, Ar), 7.46-7.38 (m, 1H, Ar), 7.31-7.28 (m, 1H, Ar), 5.95 (t, 1H, J = 5.0 Hz, NH), 3.63-3.59 (m,

4H, 2x CH_2); ^{13}C NMR ($CDCl_3$): δ 154.8, 145.7, 142.9, 141.4, 134.6, 130.2, 127.9, 126.3, 126.0, 125.3, 118.3, 44.3, 42.0. MS (ES+) found 400.05; $C_{15}H_{15}ClN_3O_6S$ (M^+ + H) requires 400.04.

5.9.3.8. 2,4-Dimethylphenyl 4-(3-(2-chloroethyl)ureido)benzenesulfonate (**11**). Flash chromatography (methylene chloride to methylene chloride/ethyl acetate (95:5)). Yield: quantitative; yellowish solid; mp: 125-127 °C; ^1H NMR ($CDCl_3$): δ 7.96 (s, 1H, NH), 7.68 (d, 2H, J = 8.6 Hz, Ar), 7.51 (d, 2H, J = 8.6 Hz, Ar), 6.92 (s, 1H, Ar), 6.89-6.81 (m, 2H, Ar), 5.98 (s, 1H, NH), 3.63-3.56 (m, 4H, 2x CH_2), 2.24 (s, 3H, CH_3), 2.01 (s, 3H, CH_3); ^{13}C NMR ($CDCl_3$): δ 154.9, 146.0, 145.1, 137.1, 132.3, 131.0, 129.8, 128.0, 127.6, 121.9, 118.0, 44.2, 42.0, 20.8, 16.2. MS (ES+) found 383.10; $C_{17}H_{20}ClN_2O_4S$ (M^+ + H) requires 383.08.

5.9.3.9. 2,5-Dimethylphenyl 4-(3-(2-chloroethyl)ureido)benzenesulfonate (**12**). Flash chromatography (methylene chloride to methylene chloride/ethyl acetate (90:10)). Yield: 90%; white solid; mp: 119-121 °C; ^1H NMR ($CDCl_3$): δ 7.80 (s, 1H, NH). 7.70 (d, 2H, J = 8.8 Hz, Ar), 7.52 (d, 2H, J = 8.8 Hz, Ar), 7.01-6.92 (m, 2H, Ar), 6.87 (s, 1H, Ar), 5.88 (t, 1H, J = 5.2 Hz, NH), 3.58-3.63 (m, 4H, 2x CH_2), 2.23 (s, 3H, CH_3), 1.97 (s, 3H, CH_3); ^{13}C NMR ($CDCl_3$): δ 154.8, 147.9, 145.1, 137.2, 131.3, 129.8, 128.1, 128.0, 122.8, 118.0, 44.3, 41.9, 20.9, 15.9. MS (ES+) found 383.10; $C_{17}H_{20}ClN_2O_4S$ (M^+ + H) requires 383.08.

5.9.3.10. 2,6-Dimethylphenyl 4-(3-(2-chloroethyl)ureido)benzenesulfonate (**13**). Flash chromatography (methylene chloride to methylene chloride/ethyl acetate (90:10)). Yield: 61%; white solid; mp: 145-147 °C; ^1H NMR ($CDCl_3$): δ 7.82 (d, 2H, J = 8.8 Hz, Ar), 7.55-7.52 (m, 3H, Ar and NH), 7.05-6.99 (m, 3H, Ar), 5.68 (t, 1H, J = 6.2 Hz, NH), 3.64-3.59 (m, 4H, 2x CH_2), 2.12 (s, 6H, 2x CH_3); ^{13}C NMR ($CDCl_3$): δ 154.6, 147.4, 144.8, 132.2, 129.5, 129.4, 126.9, 118.2, 44.4, 42.0, 17.4. MS (ES+) found 383.10; $C_{17}H_{20}ClN_2O_4S$ (M^+ + H) requires 383.08.

5.9.3.11. 2,4-Difluorophenyl 4-(3-(2-chloroethyl)ureido)benzenesulfonate (**14**). Flash chromatography (methylene chloride to methylene chloride/ethyl acetate (95:5)). Yield: 87%; white solid; mp: 125-126 °C; ^1H NMR ($CDCl_3$ and MeOD): δ 7.64 (d, 2H, J = 8.8 Hz, Ar), 7.50 (d, 2H, J = 8.8 Hz, Ar), 7.12-7.04 (m, 1H, Ar), 6.78-6.73 (m, 2H, Ar), 3.60-3.51 (m, 4H, 2x CH_2); ^{13}C NMR ($CDCl_3$ and MeOD): δ 162.4, 162.3, 159.1, 159.0, 156.5,

156.3, 155.1, 155.0, 153.1, 146.0, 145.9, 129.9, 126.2, 125.6, 125.4, 117.6, 117.5, 111.6, 111.6, 111.3, 111.2, 105.7, 105.4, 105.3, 105.0, 44.3, 41.6. MS (ES+) found 391.00; $C_{15}H_{14}ClF_2N_2O_4S$ (M^+ + H) requires 391.03.

5.9.3.12. 2,6-Difluorophenyl 4-(3-(2-chloroethyl)ureido)benzenesulfonate (**15**). Flash chromatography (methylene chloride to methylene chloride/ethyl acetate (90:10)). Yield: 28%; white solid; mp: 144-145 °C; ^{1}H NMR ($CDCl_3$ and MeOD): δ 7.68 (d, 2H, J = 8.8 Hz, Ar), 7.49 (d, 2H, J = 8.8 Hz, Ar), 7.14-7.05 (m, 1H, Ar), 6.83 (t, 2H, J = 8.2 Hz, Ar), 3.55-3.52 (m, 2H, CH_2), 3.48-3.45 (m, 2H, CH_2); ^{13}C NMR ($CDCl_3$ and MeOD): δ 157.7, 157.6, 155.2, 154.3, 154.3, 146.0, 129.8, 127.8, 127.7, 127.5, 126.6, 117.5, 117.4, 112.5, 112.5, 112.5, 112.3, 112.2, 112.2, 44.1, 41.5. MS (ES+) found 391.05; $C_{15}H_{14}ClF_2N_2O_4S$ (M^+ + H) requires 391.03.

5.9.3.13. 2,4,5-Trimethylphenyl 4-(3-(2-chloroethyl)ureido)benzenesulfonate (**16**). Flash chromatography (methylene chloride to methylene chloride/ethyl acetate (90:10)). Yield: 69%; white solid; mp: 127-128 °C; ^{1}H NMR ($CDCl_3$): δ 7.72-6.69 (m, 3H, Ar and NH), 7.51 (d, 2H, J = 8.8 Hz, Ar), 6.87 (s, 1H, Ar), 6.81 (s, 1H, Ar), 5.82 (t, 1H, J = 5.3 Hz, NH), 3.64-3.58 (m, 4H, 2x CH_2), 2.14 (s, 3H, CH_3), 2.12 (s, 3H, CH_3), 1.94 (s, 3H, CH_3); ^{13}C NMR ($CDCl_3$): δ 154.6, 145.9, 145.0, 135.7, 135.5, 132.6, 129.8, 128.3, 128.0, 123.1, 118.0, 44.3, 42.0, 19.4, 19.1, 15.7. MS (ES+) found 397.05; $C_{18}H_{22}ClN_2O_4S$ (M^+ + H) requires 397.10.

5.9.3.14. 2,4,5-Trichlorophenyl 4-(3-(2-chloroethyl)ureido)benzenesulfonate (**17**). Flash chromatography (methylene chloride to methylene chloride/ethyl acetate (95:5)). Yield: 69%; white solid; mp: 143-145 °C; ^{1}H NMR ($CDCl_3$ and MeOD): δ 7.67 (d, 2H, J = 8.8 Hz, Ar), 7.51 (d, 2H, J = 8.8 Hz, Ar), 7.47-7.40 (m, 2H, Ar), 3.60-3.49 (m, 4H, 2x CH_2); ^{13}C NMR ($CDCl_3$ and MeOD): δ 155.0, 146.2, 144.2, 131.5, 131.5, 130.1, 126.8, 126.2, 125.6, 117.6, 117.5, 44.3, 41.6. MS (ES+) found 456.95; $C_{15}H_{13}Cl_4N_2O_4S$ (M^+ + H) requires 456.94.

5.9.3.15. 2,4,6-Trichlorophenyl 4-(3-(2-chloroethyl)ureido)benzenesulfonate (**18**). Flash chromatography (methylene chloride to methylene chloride/ethyl acetate (95:5)). Yield: 58%; white solid; mp: 157-158 °C; ^{1}H NMR ($CDCl_3$ and MeOD): δ 7.80 (d, 2H, J =

8.8 Hz, Ar), 7.55 (d, 2H, J = 8.8 Hz, Ar), 7.29 (s, 2H, Ar), 3.61-3.51 (m, 4H, 2x CH_2); ^{13}C NMR ($CDCl_3$ and MeOD): δ 155.0, 146.0, 132.7, 130.9, 130.0, 129.1, 128.3, 117.5, 117.4, 44.4, 41.6. MS (ES+) found 456.95; $C_{15}H_{13}Cl_4N_2O_4S$ (M^+ + H) requires 456.94.

5.9.3.16. 3-Ethylphenyl 4-(3-(2-chloroethyl)ureido)benzenesulfonate (**19**). Flash chromatography (hexane/ethyl acetate (70:30)). Yield: 70%; sticky solid; ^1H NMR ($CDCl_3$ and MeOD): δ 8.67 (s, 1H, NH), 7.51 (d, 2H, J = 8.6 Hz, Ar), 7.41 (d, 2H, J = 8.5 Hz, Ar), 7.02 (t, 1H, J = 7.7 Hz, Ar), 6.93-6.90 (m, 1H, Ar), 6.65-6.59 (m, 2H, Ar), 6.24 (s, 1H, NH), 3.49-3.47 (m, 2H, CH_2), 3.43-3.41 (m, 2H, CH_2), 2.42 (q, 2H, J = 7.5 Hz, CH_2), 0.99 (t, 3H, J = 7.4 Hz, CH_3); ^{13}C NMR ($CDCl_3$ and MeOD): δ 155.2, 149.5, 146.2, 145.5, 129.7, 129.2, 126.7, 126.6, 121.6, 119.2, 117.4, 43.9, 41.5, 28.3, 14.9. MS (ES+) found 383.10; $C_{17}H_{20}ClN_2O_4S$ (M^+ + H) requires 383.08.

5.9.3.17. 3-Propylphenyl 4-(3-(2-chloroethyl)ureido)benzenesulfonate (**20**). Flash chromatography (hexane/ethyl acetate (65:35)). Yield: 82%; sticky solid; ^1H NMR ($CDCl_3$ and MeOD): δ 8.31 (s, 1H, NH), 7.62 (d, 2H, J = 8.8 Hz, Ar), 7.49 (d, 2H, J = 8.8 Hz, Ar), 7.12 (t, 1H, J = 7.8 Hz, Ar), 7.00 (d, 1H, J = 7.6 Hz, Ar), 6.77-6.71 (m, 2H, Ar), 6.10 (s, 1H, NH), 3.60-3.54 (m, 4H, 2x CH_2), 2.47 (t, 2H, J = 7.3Hz, CH_2), 1.50 (m, 2H, CH_2), 0.82 (t, 3H, J = 7.3 Hz, CH_3); ^{13}C NMR ($CDCl_3$ and MeOD): δ 154.9, 149.5, 145.4, 144.8, 129.9, 129.3, 127.4, 127.1, 122.3, 119.4, 117.6, 44.3, 41.8, 37.5, 24.1, 13.5. MS (ES+) found 397.10; $C_{18}H_{22}ClN_2O_4S$ (M^+ + H) requires 397.10.

5.9.3.18. 3-Methoxyphenyl 4-(3-(2-chloroethyl)ureido)benzenesulfonate (**21**). Flash chromatography (hexane/ethyl acetate (65:35)). Yield: 64%; sticky solid; ^1H NMR ($CDCl_3$ and MeOD): δ 8.29 (s, 1H, NH), 7.68-7.62 (m, 2H, Ar), 7.54-7.48 (m, 2H, Ar), 7.14-7.08 (m, 1H, Ar), 6.78-6.72 (m, 1H, Ar), 6.53-6.47 (m, 2H, Ar), 6.10 (m, 1H, NH), 3.71-3.56 (m, 7H, OCH_3 and 2x CH_2); ^{13}C NMR ($CDCl_3$ and MeOD): δ 160.4, 154.9, 150.3, 145.3, 130.1, 129.9, 127.0, 117.7, 114.2, 113.0, 108.4, 55.5, 44.4, 41.8. MS (ES+) found 385.05; $C_{16}H_{18}ClN_2O_5S$ (M^+ + H) requires 385.06.

5.9.3.19. 3-Ethoxyphenyl 4-(3-(2-chloroethyl)ureido)benzenesulfonate (**22**). Flash chromatography (methylene chloride/ethyl acetate (97:3)). Yield: 64%; sticky solid; ^1H NMR ($CDCl_3$ and MeOD): δ 8.48 (s, 1H, NH),7.65-7.63 (m, 2H, Ar), 7.51-7.49 (m, 2H, Ar),

7.12-7.07 (m, 1H, Ar), 6.74-6.71 (m, 1H, Ar), 6.54 (s, 1H, Ar), 6.47-6.45 (m, 1H, Ar), 6.17 (s, 1H, NH), 3.90 (q, 2H, J = 6.6 Hz, CH_2) 3.60-3.53 (m, 4H, 2x CH_2), 1.39-1.23 (m, 3H, CH_3); ^{13}C NMR ($CDCl_3$ and MeOD): δ 159.8, 155.0, 150.4, 145.4, 129.9, 126.9, 117.6, 117.5, 114.1, 113.6, 108.8, 63.8, 44.3, 41.7, 14.5. MS (ES+) found 399.10; $C_{17}H_{20}ClN_2O_5S$ (M^+ + H) requires 399.08.

5.9.3.20. 3-Fluorophenyl 4-(3-(2-chloroethyl)ureido)benzenesulfonate (**23**). Flash chromatography (hexane/ethyl acetate (65:35)). Yield: 64%; white solid; mp: 130-132 °C; ^1H NMR ($CDCl_3$ and MeOD): δ 8.61 (s, 1H, NH), 7.62-7.59 (m, 2H, Ar), 7.50-7.47 (m, 2H, Ar), 7.22-7.14 (m, 1H, Ar), 6.93-6.87 (m, 1H, Ar), 6.72-6.68 (m, 2H, Ar), 6.21 (s, 1H, NH), 3.59-3.58 (m, 2H, CH_2), 3.52-3.51 (m, 2H, CH_2); ^{13}C NMR ($CDCl_3$ and MeOD): δ 164.2, 160.9, 155.1, 150.2, 150.1, 145.8, 145.7, 130.5, 130.4, 129.8, 126.4, 118.2, 118.1, 117.6, 117.6, 114.4, 114.1, 110.6, 110.3, 44.3, 41.6. MS (ES+) found 373.05; $C_{15}H_{15}ClFN_2O_4S$ (M^+ + H) requires 373.04.

5.9.3.21. 3-Chlorophenyl 4-(3-(2-chloroethyl)ureido)benzenesulfonate (**24**). Flash chromatography (hexane/ethyl acetate (65:35)). Yield: 58%; sticky solid; ^1H NMR ($CDCl_3$ and MeOD): δ 8.45 (s, 1H, NH), 7.67-7.61 (m, 2H, Ar), 7.55-7.50 (m, 2H, Ar), 7.21-7.13 (m, 2H, Ar), 7.01 (s, 1H, Ar), 6.85-6.80 (m, 1H, Ar), 6.15 (s, 1H, NH), 3.60-3.54 (m, 4H, 2x CH_2); ^{13}C NMR ($CDCl_3$ and MeOD): δ 154.9, 149.8, 145.6, 134.8, 130.4, 129.9, 127.4, 126.5, 123.0, 120.6, 117.6, 44.4, 41.7. MS (ES+) found 389.00; $C_{15}H_{15}Cl_2N_2O_4S$ (M^+ + H) requires 389.01.

5.9.3.22. 3-Bromophenyl 4-(3-(2-chloroethyl)ureido)benzenesulfonate (**25**). Flash chromatography (hexane/ethyl acetate (65:35)). Yield: 49%; white solid; mp: 99-100 °C; ^1H NMR ($CDCl_3$ and MeOD): δ 8.58 (s, 1H, NH), 7.63-7.61 (m, 2H, Ar), 7.52-7.50 (m, 2H, Ar), 7.34-7.32 (m, 1H, Ar), 7.16-7.08 (m, 2H, Ar), 6.86-6.83 (m, 1H, Ar), 6.20 (s, 1H, NH), 3.59-3.54 (m, 4H, 2x CH_2); ^{13}C NMR ($CDCl_3$ and MeOD): δ 155.0, 149.9, 145.7, 130.7, 130.3, 129.9, 126.4, 125.8, 122.4, 121.1, 117.7, 44.3, 41.6. MS (ES+) found 432.95; $C_{15}H_{15}BrClN_2O_4S$ (M^+ + H) requires 432.96.

5.9.3.23. 3-Iodophenyl 4-(3-(2-chloroethyl)ureido)benzenesulfonate (**26**). Flash chromatography (hexane/ethyl acetate (65:35)). Yield: 63%; sticky solid; ^1H NMR ($CDCl_3$

and MeOD): δ 8.54 (s, 1H, NH), 7.64-7.50 (m, 5H, Ar), 7.35 (s, 1H, Ar), 6.98-6.85 (m, 2H, Ar), 6.17 (s, 1H, NH), 3.60 (t, 2H, J = 4.9Hz, CH_2) 3.53 (t, 2H, J = 4.9 Hz, CH_2); ^{13}C NMR ($CDCl_3$ and MeOD): δ 154.9, 149.6, 145.6, 136.3, 131.6, 130.9, 129.9, 126.6, 121.8, 117.7, 93.4, 44.4, 41.7. MS (ES+) found 480.95; $C_{15}H_{15}ClIN_2O_4S$ (M^+ + H) requires 480.95.

5.9.3.24. 3-Nitrophenyl 4-(3-(2-chloroethyl)ureido)benzenesulfonate (**27**). Flash chromatography (hexane/ethyl acetate (65:35)). Yield: 68%; yellow solid; mp: 128-132 °C; ^{1}H NMR ($CDCl_3$ and MeOD): δ 8.69 (s, 1H, NH), 8.07-8.04 (m, 1H, Ar), 7.78-7.72 (m, 1H, Ar), 7.63-7.60 (m, 2H, Ar), 7.52-7.42 (m, 3H, Ar), 7.32-7.29 (m, 1H, Ar), 6.10 (m, 1H, NH), 3.59-3.50 (m, 4H, 2x CH_2); ^{13}C NMR ($CDCl_3$ and MeOD): δ 155.0, 149.7, 148.6, 146.1, 130.4, 129.9, 128.8, 125.8, 121.9, 118.0, 117.6, 44.3, 41.6. MS (ES+) found 400.00; $C_{15}H_{15}ClN_3O_6S$ (M^+ + H) requires 400.04.

5.9.3.25. 3,5-Dimethylphenyl 4-(3-(2-chloroethyl)ureido)benzenesulfonate (**28**). Flash chromatography (methylene chloride/ethyl acetate (96:4)). Yield: 75%; white solid; mp: 110-113 °C; ^{1}H NMR ($CDCl_3$ and MeOD): δ 8.49 (s, 1H, NH), 7.63 (d, 2H, J = 8.6 Hz, Ar), 7.48 (d, 2H, J = 8.6 Hz, Ar), 6.80 (s, 1H, Ar), 6.54 (s, 2H, Ar), 6.16 (s, 1H, NH), 3.58-3.51 (m, 4H, 2x CH_2), 2.17 (s, 6H, 2x CH_3); ^{13}C NMR ($CDCl_3$ and MeOD): δ 155.1, 149.4, 145.3, 139.5, 129.8, 128.8, 127.1, 119.7, 117.4, 44.4, 41.6, 21.1. MS (ES+) found 383.10; $C_{17}H_{20}ClN_2O_4S$ (M^+ + H) requires 383.08.

5.9.3.26. 3,4-Dimethoxyphenyl 4-(3-(2-chloroethyl)ureido)benzenesulfonate (**29**). Flash chromatography (hexane/ethyl acetate (60:40)). Yield: 61%; brown solid; mp: 144-148 °C; ^{1}H NMR ($CDCl_3$ and MeOD): δ 8.40 (s, 1H, NH), 7.62 (d, 2H, J = 8.8 Hz, Ar), 7.49 (d, 2H, J = 8.8 Hz, Ar), 6.65 (d, 1H, J = 8.7 Hz, Ar), 6.52-6.51 (m, 1H, Ar), 6.43-6.39 (m, 1H, Ar), 6.10 (s, 1H, NH), 3.78 (s, 3H, OCH_3), 3.71 (s, 3H, OCH_3), 3.62-3.59 (m, 2H, CH_2), 3.55-3.53 (m, 2H, CH_2); ^{13}C NMR ($CDCl_3$ and MeOD): δ 154.9, 149.2, 147.8, 145.4, 143.1, 130.0, 126.8, 117.4, 113.9, 110.9, 106.6, 56.1, 56.0, 44.5, 41.7. MS (ES+) found 415.10; $C_{17}H_{20}ClN_2O_6S$ (M^+ + H) requires 415.07.

5.9.3.27. 3,5-Dimethoxyphenyl 4-(3-(2-chloroethyl)ureido)benzenesulfonate (**30**). Flash chromatography (hexane/ethyl acetate (50:50)). Yield: 66%; white solid; mp: 120-123 °C; ^{1}H NMR ($CDCl_3$ and MeOD): δ 7.59-7.55 (m, 2H, Ar), 7.44-7.41 (m, 2H, Ar), 6.19-6.18

(m, 1H, Ar), 6.00 (s, 2H, Ar), 3.92 (s, 6H, 2x OCH_3), 3.50-3.42 (m, 4H, 2x CH_2); ^{13}C NMR ($CDCl_3$ and MeOD)): δ 160.9, 155.2, 150.9, 145.6, 129.7, 126.5, 117.4, 100.7, 99.1, 55.3, 44.0, 41.5. MS (ES+) found 415.10; $C_{17}H_{20}ClN_2O_6S$ (M^+ + H) requires 415.07.

5.9.3.28. 3,4-Difluorophenyl 4-(3-(2-chloroethyl)ureido)benzenesulfonate (**31**). Flash chromatography (hexane/ethyl acetate (50:50)). Yield: 72%; white solid; mp: 127-130 °C; ^1H NMR ($CDCl_3$ and MeOD): δ 8.08 (s, 1H, NH), 7.64 (d, 2H, J = 8.7 Hz, Ar), 7.52 (d, 2H, J = 8.7 Hz, Ar), 7.10-7.01 (m, 1H, Ar), 6.90-6.83 (m, 1H, Ar), 6.72-6.69 (m, 1H, Ar), 5.96 (s, 1H, NH), 3.63-3.59 (m, 4H, 2x CH_2); ^{13}C NMR ($CDCl_3$ and MeOD): δ 154.8, 154.7, 151.7, 151.6, 151.0, 150.9, 148.4, 148.2, 147.7, 147.6, 145.6, 145.5, 144.9, 144.9, 144.8, 144.8, 130.0, 126.5, 126.4, 118.8, 118.7, 118.7, 118.6, 117.9, 117.8, 117.7, 117.4, 112.7, 112.4, 44.5, 41.8. MS (ES+) found 391.05; $C_{15}H_{14}ClF_2N_2O_4S$ (M^+ + H) requires 391.03.

5.9.3.29. 3,5-Difluorophenyl 4-(3-(2-chloroethyl)ureido)benzenesulfonate (**32**). Flash chromatography (hexane/ethyl acetate (75:25)). Yield: 81%; white solid; mp: 141-143 °C; ^1H NMR ($CDCl_3$ and MeOD): δ 8.69 (s, 1H, NH), 7.61 (d, 2H, J = 8.8 Hz, Ar), 7.50 (d, 2H, J = 8.8 Hz, Ar), 6.68-6.61 (m, 1H, Ar), 6.54-6.49 (m, 2H, Ar), 6.24 (s, 1H, NH), 3.58-3.50 (m, 4H, 2x CH_2); ^{13}C NMR ($CDCl_3$ and MeOD): δ 164.5, 164.3, 161.1, 161.0, 155.2, 155.1, 150.7, 150.5, 146.1, 146.0, 129.8, 125.9, 117.6, 117.5, 106.8, 106.6, 106.5, 106.4, 103.3, 103.0, 102.6, 44.2, 41.5. MS (ES+) found 391.05; $C_{15}H_{14}ClF_2N_2O_4S$ (M^+ + H) requires 391.03.

5.9.3.30. 3,5-Dichlorophenyl 4-(3-(2-chloroethyl)ureido)benzenesulfonate (**33**). Flash chromatography (methylene chloride/ethyl acetate (97:3)). Yield: 79%; white solid; mp: 136-140 °C; ^1H NMR ($CDCl_3$ and MeOD): δ 8.48 (s, 1H, NH), 7.68-7.65 (m, 2H, Ar), 7.56-7.53 (m, 2H, Ar), 7.22-7.21 (m, 1H, Ar), 6.92-6.91 (m, 2H, Ar), 6.13 (s, 1H, NH), 3.63-3.55 (m, 4H, 2x CH_2); ^{13}C NMR ($CDCl_3$ and MeOD): δ 154.9, 150.0, 145.9, 135.4, 129.9, 127.6, 126.1, 121.5, 117.7, 44.5, 41.6. MS (ES+) found 423.00; $C_{15}H_{14}Cl_3N_2O_4S$ (M^+ + H) requires 422.97.

5.9.3.31. 3,5-Dibromophenyl 4-(3-(2-chloroethyl)ureido)benzenesulfonate (**34**). Flash chromatography (hexane/ethyl acetate (70:30)). Yield: 68%; white solid; mp: 140-142 °C; ^1H NMR ($CDCl_3$ and MeOD): δ 7.60-7.46 (m, 5H, Ar), 7.03 (s, 2H, Ar), 3.54-3.46

(m, 4H, 2x CH_2); ^{13}C NMR ($CDCl_3$ and MeOD): δ 155.1, 150.0, 146.1, 132.9, 129.8, 125.8, 124.6, 122.8, 117.5, 44.1, 41.5. MS (ES+) found 510.90; $C_{15}H_{14}Br_2ClN_2O_4S$ (M^+ + H) requires 510.87.

5.9.3.32. 3,4,5-Trimethylphenyl 4-(3-(2-chloroethyl)ureido)benzenesulfonate (**35**). Flash chromatography (methylene chloride/ethyl acetate (95:5)). Yield: 63%; sticky solid; ^1H NMR ($CDCl_3$ and MeOD): δ 8.08 (s, 1H, NH), 7.68-7.65 (m, 2H, Ar), 7.52-7.49 (m, 2H, Ar), 6.61 (s, 2H, Ar), 6.01 (s, 1H, NH), 3.61-3.58 (m, 4H, 2x CH_2), 2.15 (s, 6H, 2x CH_3), 2.06 (s, 3H, CH_3); ^{13}C NMR ($CDCl_3$ and MeOD): δ 154.9, 146.6, 145.1, 138.1, 134.3, 129.8, 127.4, 120.8, 117.6, 44.4, 41.7, 20.7, 15.0. MS (ES+) found 397.10; $C_{18}H_{22}ClN_2O_4S$ (M^+ + H) requires 397.10.

5.9.3.33. 3,4,5-Trimethoxyphenyl 4-(3-(2-chloroethyl)ureido)benzenesulfonate (**36**). Flash chromatography (methylene chloride to methylene chloride/ethyl acetate (90:10)). Yield: 43%; white solid; mp: 153-154 °C; ^1H NMR ($CDCl_3$): δ 7.70-7.64 (m, 3H, Ar and NH), 7.51 (d, 2H, J = 8.9 Hz, Ar), 6.21 (brs, 2H, Ar), 5.81 (t, 1H, J = 5.5 Hz, NH), 3.82 (s, 3H, OCH_3), 3.73-3.60 (m, 10H, 2x CH_2 and 2x OCH_3); ^{13}C NMR ($CDCl_3$ and MeOD): 154.4, 153.3, 145.8, 145.3, 136.1, 130.1, 127.0, 117.7, 100.1, 61.2, 56.3, 44.5, 42.0. MS (ES+) found 445.05; $C_{18}H_{22}ClN_2O_7S$ (M^+ + H) requires 445.08.

5.9.3.34. 3,4,5-Trifluorophenyl 4-(3-(2-chloroethyl)ureido)benzenesulfonate (**37**). Flash chromatography (methylene chloride to methylene chloride/ethyl acetate (90:10)). Yield: 58%; white solid; mp: 98-99 °C; ^1H NMR ($CDCl_3$ and MeOD): δ 7.63 (d, 2H, J = 8.9 Hz, Ar), 7.53 (d, 2H, J = 8.9 Hz, Ar), 6.66 (t, 2H, J = 6.1 Hz, Ar), 3.61-3.51 (m, 4H, 2x CH_2); ^{13}C NMR ($CDCl_3$ and MeOD): δ 155.1, 152.6, 152.5, 149.3, 149.2, 149.1, 146.7, 146.2, 144.8, 144.0, 129.9, 125.6, 117.7, 117.6, 108.1, 108.0, 107.9, 107.8, 44.4, 41.7. MS (ES+) found 409.00; $C_{15}H_{13}ClF_3N_2O_4S$ (M^+ + H) requires 409.02.

5.9.3.35. 4-Ethylphenyl 4-(3-(2-chloroethyl)ureido)benzenesulfonate (**38**). Flash chromatography (hexane/ethyl acetate (70:30)). Yield: 73%; white solid; mp: 99-101 °C; ^1H NMR ($CDCl_3$ and MeOD): δ 8.50 (s, 1H, NH), 7.62-7.60 (m, 2H, Ar), 7.50-7.48 (m, 2H, Ar), 7.05-7.02 (m, 2H, Ar), 6.83-6.80 (m, 2H, Ar), 6.19 (s, 1H, NH), 3.59-3.54 (m, 4H, 2x CH_2), 2.56-2.54 (m, 2H, CH_2), 1.16-1.11 (m, 3H, CH_3); ^{13}C NMR ($CDCl_3$ and MeOD): δ 155.0,

147.5, 145.5, 143.3, 129.8, 128.9, 127.0, 122.1, 117.5, 44.4, 41.6, 28.2, 15.3. MS (ES+) found 383.10; $C_{17}H_{20}ClN_2O_4S$ (M^+ + H) requires 383.08.

5.9.3.36. 4-Propylphenyl 4-(3-(2-chloroethyl)ureido)benzenesulfonate (**39**). Flash chromatography (methylene chloride/ethyl acetate (97:3)). Yield: 50%; white solid; mp: 114-117 °C; ^{1}H NMR ($CDCl_3$ and MeOD): δ 8.20 (s, 1H, NH), 7.62 (d, 2H, J = 8.8 Hz, Ar), 7.49 (d, 2H, J = 8.8 Hz, Ar), 7.03 (d, 2H, J = 8.3 Hz, Ar), 6.83 (d, 2H, J = 8.4 Hz, Ar), 6.02 (s, 1H, NH), 3.61-3.56 (m, 4H, 2x CH_2), 2.50 (t, 2H, J = 7.4 Hz, CH_2), 1.62-1.50 (m, 2H, CH_2), 0.87 (t, 3H, J = 7.3 Hz, CH_3); ^{13}C NMR ($CDCl_3$ and MeOD): δ 154.8, 147.5, 145.3, 141.9, 129.9, 129.5, 127.2, 122.0, 117.6, 44.4, 41.8, 37.3, 24.3, 13.7. MS (ES+) found 397.10; $C_{18}H_{22}ClN_2O_4S$ (M^+ + H) requires 397.10.

5.9.3.37. 4-(tert-Butyl)phenyl 4-(3-(2-chloroethyl)ureido)benzenesulfonate (**40**). Flash chromatography (methylene chloride/ethyl acetate (97:3)). Yield: 58%; white solid; mp: 144-148 °C; ^{1}H NMR ($CDCl_3$ and MeOD): δ 8.34 (s, 1H, NH), 7.65 (d, 2H, J = 8.8 Hz, Ar), 7.50 (d, J = 8.8 Hz, 2H, Ar), 7.24 (d, 2H, J = 8.8 Hz, Ar), 6.87-6.83 (m, 2H, Ar), 6.08 (s, 1H, NH), 3.63-3.55 (m, 4H, 2x CH_2), 1.24 (s, 9H, 3x CH_3); ^{13}C NMR ($CDCl_3$ and MeOD): δ 154.9, 150.2, 147.2, 145.3, 129.6, 127.3, 126.5, 121.6, 117.5, 44.5, 41.7, 31.3. MS (ES+) found 411.10; $C_{19}H_{24}ClN_2O_4S$ (M^+ + H) requires 411.11.

5.9.3.38. 4-Ethoxyphenyl 4-(3-(2-chloroethyl)ureido)benzenesulfonate (**41**). Flash chromatography (hexane/ethyl acetate (70:30)). Yield: 82%; white solid; mp: 116-117 °C; ^{1}H NMR ($CDCl_3$ and MeOD): δ 8.52 (s, 1H, NH), 7.58 (d, 2H, J = 8.7 Hz, Ar), 7.47 (d, 2H, J = 8.7 Hz, Ar), 6.80-6.78 (m, 2H, Ar), 6.70-6.67 (m, 2H, Ar), 6.19 (s, 1H, NH), 3.90 (q, 2H, J = 7.1 Hz, CH_2), 3.58-3.51 (m, 4H, 2x CH_2), 1.32 (t, 3H, J = 6.8 Hz, CH_3); ^{13}C NMR ($CDCl_3$ and MeOD): δ 157.6, 155.1, 145.5, 142.8, 129.9, 126.7, 123.3, 117.5, 115.0, 63.9, 44.3, 41.6, 14.6. MS (ES+) found 399.05; $C_{17}H_{20}ClN_2O_5S$ (M^+ + H) requires 399.08.

5.9.3.39. 4-Butoxyphenyl 4-(3-(2-chloroethyl)ureido)benzenesulfonate (**42**). Flash chromatography (hexane/ethyl acetate (65:35)). Yield: 73%; sticky solid; ^{1}H NMR ($CDCl_3$ and MeOD): δ 8.27 (s, 1H, NH), 7.61 (d, 2H, J = 8.8 Hz, Ar), 7.49 (d, 2H, J = 8.9 Hz, Ar), 6.83-8.80 (m, 2H, Ar), 6.73-6.69 (m, 2H, Ar), 6.07 (s, 1H, NH), 3.85 (t, 2H, J = 6.4 Hz, CH_2), 3.62-3.55 (m, 4H, 2x CH_2), 1.73-1.65 (m, 2H, CH_2), 1.47-1.37 (m, 2H, CH_2), 0.92 (t, 3H, J

= 7.3 Hz, CH_3); ^{13}C NMR ($CDCl_3$ and MeOD): δ 157.9, 154.9, 145.2, 142.8, 129.9, 126.9, 123.3, 117.6, 115.1, 68.1, 44.4, 41.8, 31.2, 19.2, 13.8. MS (ES+) found 427.10; $C_{19}H_{24}ClN_2O_5S$ (M^+ + H) requires 427.11.

5.9.3.40. 4-Fluorophenyl 4-(3-(2-chloroethyl)ureido)benzenesulfonate (**43**). Flash chromatography (hexane/ethyl acetate (70:30)). Yield: 69%; white solid; mp: 120-123 °C; ^1H NMR ($CDCl_3$ and MeOD): δ 8.38 (s, 1H, NH), 7.61 (d, 2H, J = 8.8 Hz, Ar), 7.51 (d, 2H, J = 8.8 Hz, Ar), 6.95-6.88 (m, 4H, Ar), 6.10 (s, 1H, NH), 3.63-3.56 (m, 4H, 2x CH_2); ^{13}C NMR ($CDCl_3$ and MeOD): δ 162.7, 159.4, 154.9, 154.9, 145.6, 145.5, 145.4, 145.4, 129.9, 126.6, 124.1, 124.0, 117.7, 117.6, 116.5, 116.2, 44.5, 41.7. MS (ES+) found 373.00; $C_{15}H_{15}ClFN_2O_4S$ (M^+ + H) requires 373.04.

5.9.3.41. 4-Chlorophenyl 4-(3-(2-chloroethyl)ureido)benzenesulfonate (**44**). Flash chromatography (hexane/ethyl acetate (65:35)). Yield: 79%; sticky solid; ^1H NMR ($CDCl_3$ and MeOD): δ 8.55 (s, 1H, NH), 7.60 (d, 2H, J = 8.8 Hz, Ar), 7.49 (d, 2H, J = 8.9 Hz, Ar), 7.21-7.16 (m, 2H, Ar), 6.87-6.83 (m, 2H, Ar), 6.17 (s, 1H, NH), 3.59 (t, 2H, J = 4.9 Hz, CH_2), 3.52 (t, 2H, J = 4.9 Hz, CH_2); ^{13}C NMR ($CDCl_3$ and MeOD): δ 150.0, 148.0, 145.7, 132.8, 129.9, 129.7, 126.4, 123.8, 117.6, 44.4, 41.6. MS (ES+) found 389.00; $C_{15}H_{15}Cl_2N_2O_4S$ (M^+ + H) requires 389.01.

5.9.3.42. 4-Bromophenyl 4-(3-(2-chloroethyl)ureido)benzenesulfonate (**45**). Flash chromatography (hexane/ethyl acetate (70:30)). Yield: 81%; white solid; mp: 115-118 °C; ^1H NMR ($CDCl_3$ and MeOD): δ 8.41 (s, 1H, NH), 7.61 (d, 2H, J = 8.7 Hz, Ar), 7.51 (d, 2H, J = 8.8 Hz, Ar), 7.36 (d, 2H, J = 8.7 Hz, Ar), 6.81 (d, 2H, J = 8.7 Hz, Ar), 6.13 (s, 1H, NH), 3.61-3.55 (m, 4H, 2x CH_2); ^{13}C NMR ($CDCl_3$ and MeOD): δ 154.9, 148.5, 145.6, 132.8, 129.9, 126.5, 124.2, 120.7, 117.7, 44.4, 41.7. MS (ES+) found 432.95; $C_{15}H_{15}BrClN_2O_4S$ (M^+ + H) requires 432.96.

5.9.3.43. 4-Iodophenyl 4-(3-(2-chloroethyl)ureido)benzenesulfonate (**46**). Flash chromatography (methylene chloride/ethyl acetate (97:3)). Yield: 70%; white solid; mp: 138-142 °C; ^1H NMR ($CDCl_3$ and MeOD): δ 8.60 (s, 1H, NH), 7.62-7.48 (m, 6H, Ar), 6.69-6.65 (m, 2H, Ar), 6.20 (s, 1H, NH), 3.59 (t, 2H, J = 5.0 Hz, CH_2), 3.52 (t, 2H, J = 5.0 Hz, CH_2);

^{13}C NMR ($CDCl_3$ and MeOD): δ 155.0, 149.4, 145.7, 138.7, 129.9, 126.4, 124.5, 117.6, 91.7, 44.4, 41.6. MS (ES+) found 480.95; $C_{15}H_{15}ClIN_2O_4S$ (M^+ + H) requires 480.95.

5.9.3.44. 4-Cyanophenyl 4-(3-(2-chloroethyl)ureido)benzenesulfonate (**47**). Flash chromatography (hexane/ethyl acetate (65:35)). Yield: 33%; white solid; mp: 87-89 °C; ^1H NMR ($CDCl_3$ and MeOD): δ 8.51 (s, 1H, NH), 7.63-7.50 (m, 6H, Ar), 7.10-7.07 (d, 2H, J = 8.6 Hz, Ar), 6.16 (s, 1H, NH), 362-3.54 (m, 4H, 2x CH_2); ^{13}C NMR ($CDCl_3$ and MeOD): δ 154.9, 152.7, 146.0, 145.9, 134.0, 129.9, 126.2, 123.5, 117.8, 117.7, 110.9, 44.4, 41.7, 41.7. MS (ES+) found 380.05; $C_{16}H_{15}ClN_3O_4S$ (M^+ + H) requires 380.05.

5.9.3.45. Phenyl 4-(3-(2-chloroethyl)ureido)benzenesulfonate (**48**). Flash chromatography (methylene chloride/ethyl acetate (97:3)). Yield: 39%; white solid; mp: 126-127 °C; ^1H NMR ($CDCl_3$ and MeOD): δ 8.33 (s, 1H, NH), 7.62 (d, 2H, J = 8.8 Hz, Ar), 7.49 (d, 2H, J = 8.8 Hz, Ar), 7.27-7.17 (m, 3H, Ar), 6.95-6.93 (m, 2H, Ar), 6.09 (s, 1H, NH), 3.62-3.55 (m, 4H, 2x CH_2); ^{13}C NMR ($CDCl_3$ and MeOD): δ 154.9, 149.6, 145.3, 129.9, 129.7, 127.2, 127.0, 122.4, 117.6, 44.4, 41.7. MS (ES+) found 355.05; $C_{15}H_{16}ClN_2O_4S$ (M^+ + H) requires 355.05.

5.9.4. Preparation and characterization of compound 50

The synthesis 4-(3-(2-chloroethyl)ureido)benzenesulfonyl chloride (**50**) begins by the synthesis of 1-(2-chloroethyl)-3-phenylurea (**49**) which has been previously reported [11, 12]. Then, compound **49** (3.0 mmol. 1.5 Eq.) was added slowly to chlorosulfonic acid (23.1 mmol, 7.7 Eq.) in carbon tetrachloride (5 mL) at 0 °C for 4 h. Thereafter, the reaction mixture was poured slowly into ice water (with sustained agitation) and then filtered to collect the solid. The latter was dried overnight under vacuum. The filtrate was extracted thrice with methylene chloride. The combined organic extracts were washed with brine (20 mL), dried over sodium sulfate, filtered, and evaporated to dryness under reduced pressure.

5.9.4.1. 4-(3-(2-Chloroethyl)ureido)benzenesulfonyl chloride (**50**). Yield: 18%; white solid; mp: 162-164 °C; ^1H NMR (DMSO-d_6): δ 8.94 (s, 1H, NH), 7.48 (d, 2H, J = 8.6 Hz, Ar), 7.37 (d, 2H, J = 8.6 Hz, Ar), 6.58 (brs, 1H, NH), 3.66 (t, 2H, J = 6.1 Hz, CH_2), 3.42 (t, 2H, J = 6.1 Hz, CH_2); ^{13}C NMR (DMSO-d_6): δ 155.0, 140.9, 140.4, 126.3, 116.5, 44.3, 41.2.

5.10. Acknowledgments

We are thankful for the financial support from CHU de Quebec Research Center (SF) and Canadian Institutes of Health Research (JYM).

5.11. References

[1] J.H. Hoeijmakers, DNA damage, aging, and cancer, N. Engl. J. Med. 361 (2009) 1475-1485.

[2] S.P. Jackson, J. Bartek, The DNA-damage response in human biology and disease, Nature 461 (2009) 1071-1078.

[3] K.K. Khanna, S.P. Jackson, DNA double-strand breaks: signaling, repair and the cancer connection, Nat. Genet. 27 (2001) 247-254.

[4] K.A. Biedermann, J.R. Sun, A.J. Giaccia, L.M. Tosto, J.M. Brown, Scid mutation in mice confers hypersensitivity to ionizing radiation and a deficiency in DNA double-strand break repair, Proc. Natl. Acad. Sci. U.S.A. 88 (1991) 1394-1397.

[5] T. Rich, R.L. Allen, A.H. Wyllie, Defying death after DNA damage, Nature 407 (2000) 777-783.

[6] L.H. Swift, R.M. Golsteyn, Genotoxic anti-cancer agents and their relationship to DNA damage, mitosis, and checkpoint adaptation in proliferating cancer cells, Int. J. Mol. Sci. 15 (2014) 3403-3431.

[7] C.R. Sears, J.J. Turchi, Complex cisplatin-double strand break (DSB) lesions directly impair cellular non-homologous end-joining (NHEJ) independent of downstream damage response (DDR) pathways, J. Biol. Chem. 287 (2012) 24263-24272.

[8] M.T. Tomicic, M. Christmann, B. Kaina, Topotecan-triggered degradation of topoisomerase I is p53-dependent and impacts cell survival, Cancer Res. 65 (2005) 8920-8926.

[9] M. Ikeda, A. Kurose, E. Takatori, T. Sugiyama, F. Traganos, Z. Darzynkiewicz, T. Sawai, DNA damage detected with gammaH2AX in endometrioid adenocarcinoma cell lines, Int. J. Oncol. 36 (2010) 1081-1088.

[10] D. Huhn, H.A. Bolck, A.A. Sartori, Targeting DNA double-strand break signalling and repair: recent advances in cancer therapy, Swiss Med. Wkly 143 (2013) w13837.

[11] S. Fortin, L. Wei, E. Moreau, J. Lacroix, M.-F. Côté, E. Petitclerc, L. P. Kotra, R. C.-Gaudreault, Design, synthesis, biological evaluation, and structure-activity relationships of substituted phenyl 4-(2-oxoimidazolidin-1-yl)benzenesulfonates as new tubulin inhibitors mimicking combretastatin A-4, J. Med. Chem. 54 (2011) 4559-4580.

[12] S. Fortin, L. Wei, E. Moreau, J. Lacroix, M.F. Côté, E. Petitclerc, L.P. Kotra, R. C.-Gaudreault, Substituted phenyl 4-(2-oxoimidazolidin-1-yl)benzenesulfonamides as antimitotics. Antiproliferative, antiangiogenic and antitumoral activity, and quantitative structure-activity relationships, Eur. J. Med. Chem. 46 (2011) 5327-5342.

[13] S. Fortin, B. Bouchon, C. Chambon, J. Lacroix, E. Moreau, J.-M. Chezal, F. Degoul, R. C.-Gaudreault, Characterization of the covalent binding of *N*-phenyl-*N'*-(2-chloroethyl)ureas to β-tubulin: importance of glutamic acid 198 in microtubule stability, J. Pharmacol. Exp. Ther. 336 (2011) 460-467.

[14] S. Fortin, E. Moreau, J. Lacroix, J.C. Teulade, A. Patenaude, R. C.-Gaudreault, *N*-Phenyl-*N'*-(2-chloroethyl)urea analogues of combretastatin A-4: Is the *N*-phenyl-*N'*-(2-chloroethyl)urea pharmacophore mimicking the trimethoxy phenyl moiety ?, Bioorg. Med. Chem. Lett. 17 (2007) 2000-2004.

[15] S. Fortin, E. Moreau, A. Patenaude, M. Desjardins, J. Lacroix, J.L. Rousseau, R. C.-Gaudreault, *N*-Phenyl-*N'*-(2-chloroethyl)ureas (CEU) as potential antineoplastic agents. Part 2: Role of omega-hydroxyl group in the covalent binding to beta-tubulin, Bioorg. Med. Chem. 15 (2007) 1430-1438.

[16] E. Moreau, S. Fortin, M. Desjardins, J.L. Rousseau, E. Petitclerc, R. C.-Gaudreault, Optimized *N*-phenyl-*N'*-(2-chloroethyl)ureas as potential antineoplastic agents: synthesis and growth inhibition activity, Bioorg. Med. Chem. 13 (2005) 6703-6712.

[17] E. Moreau, S. Fortin, J. Lacroix, A. Patenaude, J.L. Rousseau, R. C.-Gaudreault, *N*-Phenyl-*N'*-(2-chloroethyl)ureas (CEUs) as potential antineoplastic agents. Part 3: role of carbonyl groups in the covalent binding to the colchicine-binding site, Bioorg. Med. Chem. 16 (2008) 1206-1217.

[18] V. Turcotte, S. Fortin, F. Vevey, Y. Coulombe, J. Lacroix, M.F. Côté, J.Y. Masson, R. C-Gaudreault, Synthesis, biological evaluation, and structure-activity relationships of novel substituted *N*-phenyl ureidobenzenesulfonate derivatives blocking cell cycle progression in S-phase and inducing DNA double-strand breaks, J. Med. Chem. 55 (2012) 6194-6208.

[19] National Cancer Institute (NCI/NIH), Developmental therapeutics program human tumor cell line screen, URL: http://dtp.nci.nih.gov/branches/btb/ivclsp.html [accessed February 17, 2015].

[20] A.N. Ivashkevich, O.A. Martin, A.J. Smith, C.E. Redon, W.M. Bonner, R.F. Martin, P.N. Lobachevsky, γH2AX foci as a measure of DNA damage: a computational approach to automatic analysis, Mutat. Res. 711 (2011) 49-60.

[21] Z.H. Siddik, Cisplatin: mode of cytotoxic action and molecular basis of resistance, Oncogene 22 (2003) 7265-7279.

[22] B.L. Staker, K. Hjerrild, M.D. Feese, C.A. Behnke, A.B. Burgin, Jr., L. Stewart, The mechanism of topoisomerase I poisoning by a camptothecin analog, Proc. Natl. Acad. Sci. U.S.A. 99 (2002) 15387-15392.

5.12. Appendix D. Supplementary data

Representative ^{1}H and ^{13}C NMR spectra blocking the cell cycle progression in the S-phase and inducing DNA DSB (compounds **4**, **7**, **8**, **9**, **10**, **11**, **13**, **16**) as well as the most potent PUB-SOs (compounds **34** and **36**) can be found online at https://www.sciencedirect.com/science/article/abs/pii/S0223523415302567?via%3Dihub or in the appendix D.

Chapitre 6. Preparation, characterisation and biological evaluation of new *N*-phenyl amidobenzenesulfonates and *N*-phenyl ureidobenzenesulfonates inducing DNA double-strand breaks. Part 3. Modulation of ring A

Mathieu Gagné-Boulet [a,b], Chahrazed Bouzriba [a,b], Marvin Godard [a,b], Sébastien Fortin [a,b,*]

[a]Centre de recherche du CHU de Québec-Université Laval, axe Oncologie, Hôpital Saint-François d'Assise, 10 Rue de l'Espinay, Québec, QC, G1L 3L5, Canada

[b]Faculté de Pharmacie, Université Laval, Québec, QC, G1V 0A6, Canada

***Corresponding author:** Sébastien Fortin; Phone: 418-525-4444 ext. 52364, Fax: 418-525-4372, e-mail: sebastien.fortin@pha.ulaval.ca

Publié le 21 juin 2018 dans le European Journal of Medicinal Chemistry, 155, 681-694, doi : 10.1016/j.ejmech.2018.06.030.

6.1. Résumé

Notre étude vise à évaluer l'effet de la modification de la nature et de la position de différents substituants sur le cycle A des *N*-phényl uréidobenzènesulfonates (PUB-SOs) sur leur activité biologique. À cet effet, le groupement urée des PUB-SOs a été modifié par un groupement amide menant à de nouveaux analogues PUB-SOs appelés *N*-phényl amidobenzènesulfonates (PAB-SOs). Le fragment 2-chloroéthyle sur le cycle A a également été substitué par différents groupes alkyles, cycloalkyles et chloroalkyles. Les nouveaux PAB-SOs et PUB-SOs bloquant la progression du cycle cellulaire en phase S possèdent une activité antiprolifération dans la gamme du haut nanomolaire au bas micromolaire. De plus, certains PUB-SOs et PAB-SOs induisent la phosphorylation de H2AX et ne possèdent pas ou très peu d'activité alkylante. Enfin, nos résultats montrent que les modulations structurelles effectuées affectent faiblement leurs propriétés physicochimiques et pharmacocinétiques. Les PAB-SOs et les PUB-SOs sont donc des agents anticancéreux prometteurs.

6.2. Abstract

N-Phenyl ureidobenzenesulfonates (PUB-SOs) are a new class of anticancer agents blocking the cell cycle progression in S-phase, inducing replicative stress and DNA double-strand breaks (DSBs). In this study, we evaluate the effect of modifying the nature and the position of different substituents on ring A of PUB-SOs on the antiproliferative activity, pharmacological activity as well as on calculated physicochemical, pharmacokinetic and drug-likeness properties. Modification of the urea group by an amide group led to new PUB-SO analogs designated as *N*-phenyl amidobenzenesulfonates (PAB-SOs). The 2-chloroethyl moiety on ring A was also substituted by different alkyl, cycloalkyl and chloroalkyl groups. The new PAB-SOs and PUB-SOs blocking the cell cycle progression in S-phase exhibit antiproliferative activity in the submicromolar to low micromolar range (0.14-27 μM) on four human cancer cell lines, namely HT-1080, HT-29, M21 and MCF7. Moreover, selected PUB-SO and PAB-SO derivatives induced the phosphorylation of H2AX in M21 cells and do not exhibit or only slightly alkylating activity as confirmed by the 4-(4-nitrobenzyl)pyridine (NBP) assay. Finally, our results show that structure modifications weakly affect the calculated physicochemical, pharmacokinetic and drug-likeness properties of PAB-SOs and PUB-SOs. Therefore, PAB-SOs and PUB-SOs are promising anticancer agents inducing replicative stress and DNA damage via a mechanism of action unrelated to DNA alkylation.

6.3. Graphical abstract

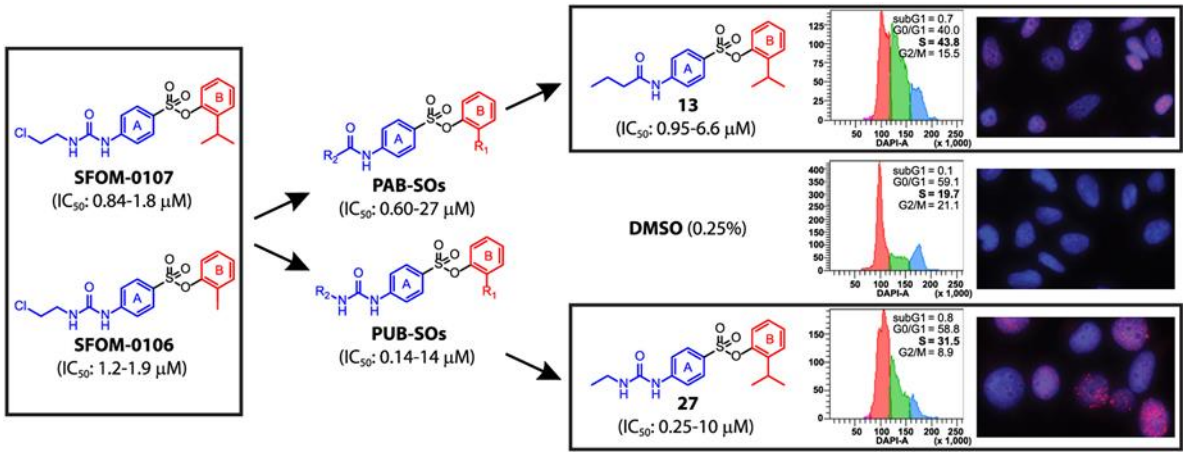

6.4. Introduction

Cancer is a group of diseases which figures among the leading causes of deaths worldwide. The treatments currently available are not completely effective and exhibit deleterious effects that are reducing the quality and the quantity of life of cancer patients [1]. Therefore, the development of new anticancer agents exhibiting better efficiency and selectivity is urgently needed. To that end, we developed a new family of anticancer agents named *N*-phenyl ureidobenzenesulfonates (PUB-SOs, Fig. 6.1A) [2-4]. The molecular structure of PUB-SOs is constituted of 2 aromatic rings (rings A and B) and a sulfonate group bridging the two aromatic rings. They were discovered from the screening of *N*-phenyl-*N'*-(2-chloroethyl)ureas as synthetic intermediates of potent antimicrotubule agents named phenyl 4-(2-oxoimidazolidin-1-yl)-benzenesulfonates and benzenesulfonamides (Fig. 6.1B). In contrast with the expected arrest in G2/M-phase, targeting of the colchicine-binding site and disruption of microtubules, PUB-SOs instead block the cell cycle progression in S-phase and induce the phosphorylation of H2AX into γH2AX. The latter indicates production of DNA damage and replicative stress [5-10]. Hitherto, we found that PUB-SOs bearing 2-alkyls, 2-halogens, 2-nitro or 4-hydroxyl groups substituting ring B and an ethylurea, a 2-chloroethylurea or a 3-chloropropylurea groups substituting position 4 of ring A lead to derivatives exhibiting antiproliferative activity at the micromolar level, blocking the cell cycle progression in S-phase and inducing γH2AX formation [2-4].

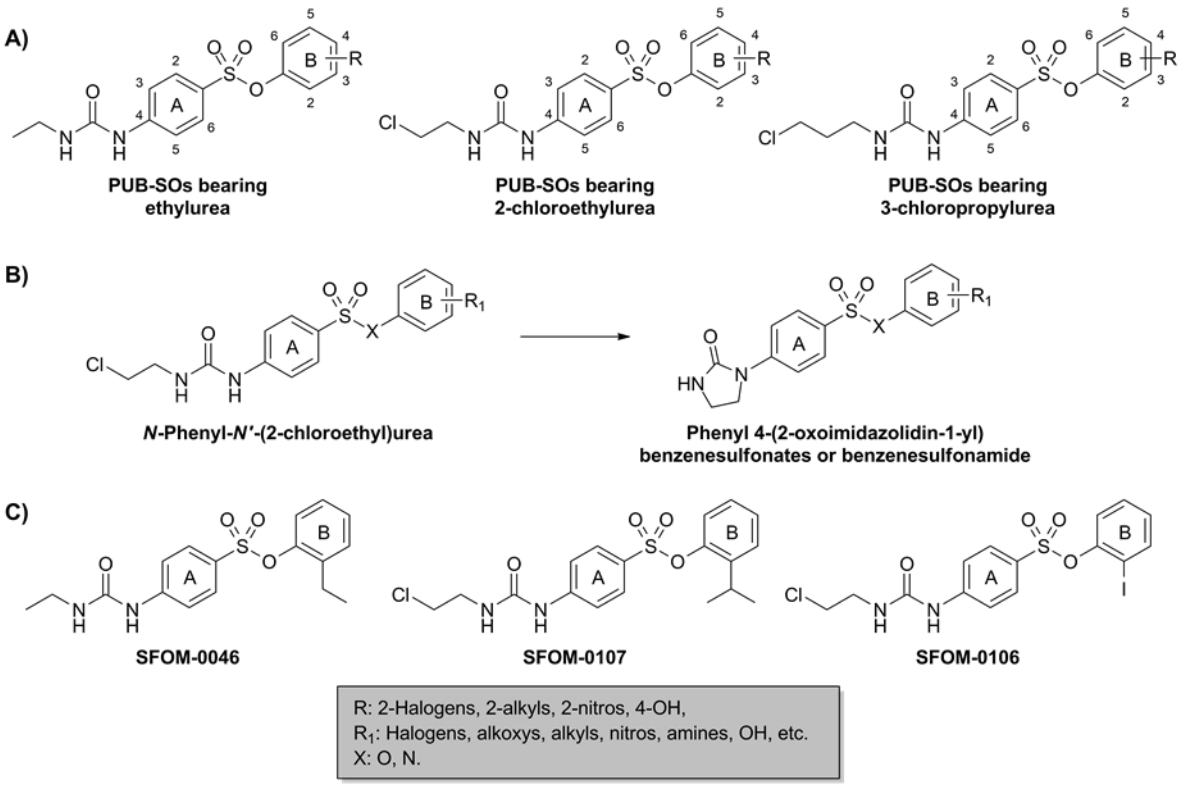

Figure 6.1. Molecular structures of A) *N*-phenyl ureidobenzenesulfonates (PUB-SOs) bearing either an ethylurea, a 2-chloroethylurea or a 3-chloropropylurea group. Molecular structures of B) *N*-phenyl-*N'*-(2-chloroethyl)urea intermediates of phenyl 4-(2-oxoimidazolidin-1-yl)-benzenesulfonates or benzenesulfonamides leading to the discovery of PUB-SOs and C) SFOM-0046, SFOM-0107 and SFOM-0106.

The study of the mechanism of action and DNA damage response of the prototypical PUB-SO named 2-ethylphenyl 4-(3-ethylureido)benzenesulfonate (SFOM-0046, Fig. 6.1C) evidenced that S-phase arrest and the induction of γH2AX is not cell type specific [11]. Moreover, SFOM-0046 induced DNA damage response by the activation of ATR-Chk1 and ATM-Chk2 pathways. It also gave rise to the phosphorylation of RAD52 and not DNA-PKcs that colocalised with γH2AX foci confirming that the DNA DSBs induced are mainly repaired by homologous recombination. Finally, SFOM-0046 and several other PUB-SOs showed potent antitumoral activity on human HT-1080 fibrosarcoma tumors grafted onto the chorioallantoic membrane of chick embryos with low toxicity toward the embryos showing that PUB-SOs are a promising family of anticancer agents [2,11]. So far, structure-activity

relationships (SAR) were mainly based on the modifications of ring B of PUB-SOs because ethylurea and 2-chloroethylurea substituted at position 4 on ring A were considered requisite for significant antiproliferative and pharmacologic activities of PUB-SOs. Of note, the modification of ring A substituted at position 3 or by a 3-chloropropylurea group led to PUB-SOs exhibiting weaker antiproliferative activities or losing the arrest of the cell cycle progression in S-phase [2]. In addition, our previous SAR studies involving ring B modifications using a 2-chloroethylurea moiety at position 4 on ring A showed that PUB-SOs bearing a 2-isopropyl or a 2-iodo groups on ring B referred to as 2-isopropylphenyl 4-(3-(2-chloroethyl)ureido)benzenesulfonate (SFOM-0107) and 2-iodophenyl 4-(3-(2-chloroethyl)ureido)benzenesulfonate (SFOM-0106, Fig. 6.1C), respectively are the most potent antiproliferative PUB-SOs prepared so far and exhibit the highest blocking activity of the cell cycle progression in S-phase [4]. Consequently, the aim of this study is to evaluate the effect of modifying the ring A of PUB-SOs using the aforementioned biofunctional assays. To that end, our study was based on PUB-SOs bearing either a 2-isopropyl or a 2-iodo substituent on ring B (SFOM-0107 and SFOM-0106) that gave rise to our most potent compounds, so far. First, we evaluated the importance of the urea moiety by its substitution by an amide group leading to PUB-SO analogs referred to as *N*-phenyl amidobenzenesulfonates (PAB-SOs). We also studied the importance of the chlorine atom and the effect of lengthening and cyclizing the carbon chain of 2-chloroethylurea moiety by substituting the urea and amide groups by different alkyl, cycloalkyl and chloroalkyl groups. In addition, we assessed the effect to substitute the ring A of PAB-SOs at position 3 to confirm our previous SAR on PUB-SOs showing that the substitution at position 3 lost the arrest of the cell cycle progression in S-phase. Finally, we studied the alkylating potency of PAB-SO and PUB-SO derivatives using the 4-(4-nitrobenzyl)pyridine (NBP) assay [12-14] as well as calculated physicochemical, pharmacokinetic and drug-likeness properties.

6.5. Chemistry

The preparation of PAB-SOs **1-26** and PUB-SOs **27-38** is illustrated in Scheme 6.1 and was achieved within three steps. First, phenyl nitrobenzenesulfonates **39-41** were prepared by nucleophilic addition of relevant phenols either to 3- or 4-nitrobenzenesulfonyl chloride. Resulting phenyl nitrobenzenesulfonates **39-41** were then reduced to the

corresponding phenyl aminobenzenesulfonates **42-44** with iron powder and HCl in a mixture of EtOH and H_2O (10:1). Finally, PAB-SOs **1-26** were prepared by nucleophilic addition of phenyl aminobenzenesulfonates **42-44** to the relevant acyl chloride in a mixture of K_2CO_3 or triethylamine in acetonitrile while PUB-SOs **27-38** were prepared by nucleophilic addition of phenyl aminobenzenesulfonates **43** and **44** to the corresponding isocyanate in acetonitrile in the presence or absence of K_2CO_3. In some cases, the last nucleophilic addition requires heating under pressure in the presence or absence of microwaves.

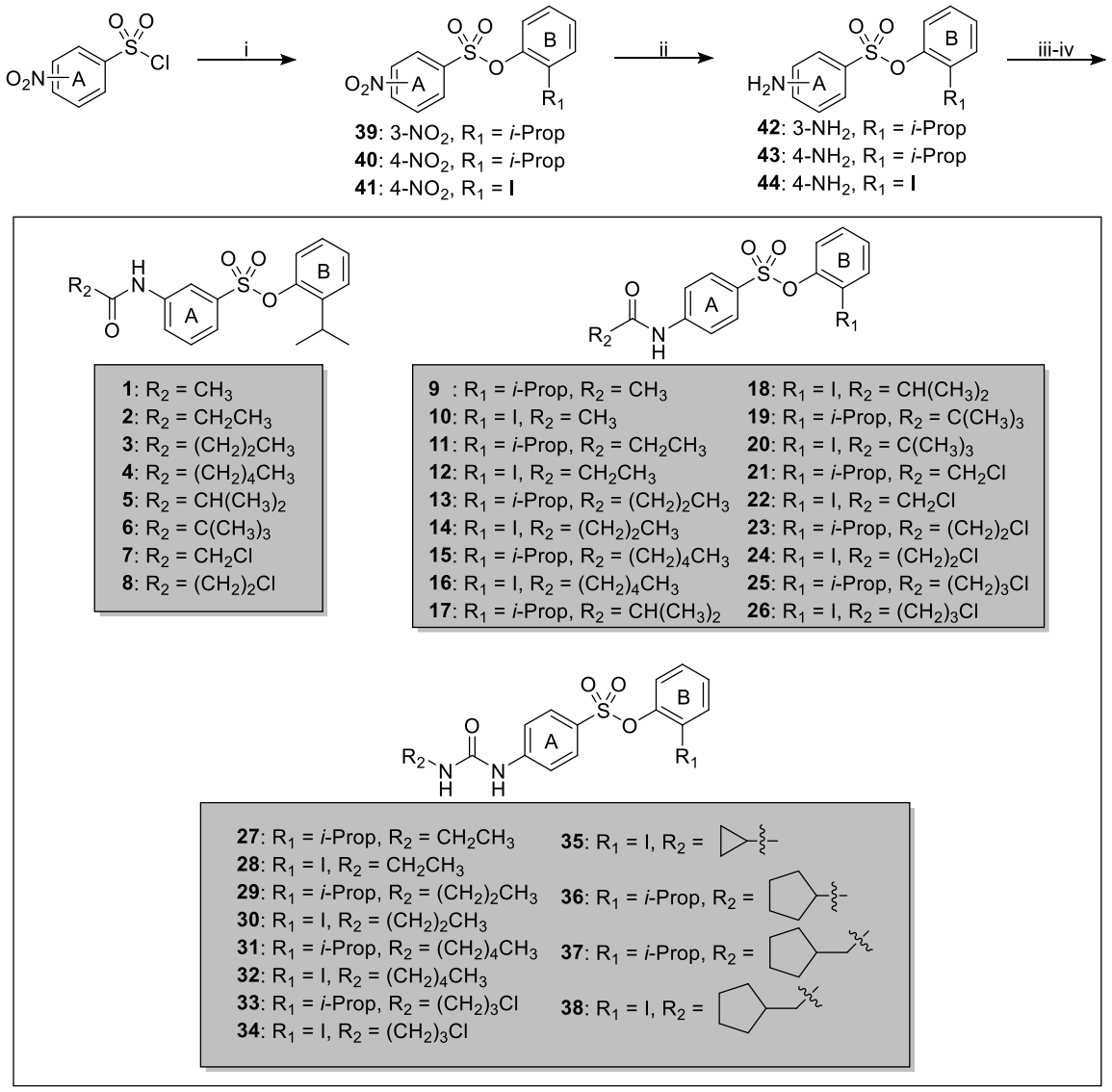

Scheme 6.1. Reagents: (i) relevant phenol, TEA/DCM or TEA/AcOEt; (ii) Fe, HCl, EtOH/H_2O; (iii) relevant acyl chloride, K_2CO_3/ CH_3CN or relevant acyl chloride, TEA/ CH_3CN or relevant acyl chloride, CH_3CN; (iv) relevant isocyanate, K_2CO_3/ CH_3CN.

6.6. Results/discussion

6.6.1. PAB-SO and PUB-SO derivatives exhibit antiproliferative activity on human cancer cells

PAB-SOs **1-26** and PUB-SOs **27-38** were assessed for their antiproliferative activity on four human cancer cell lines namely HT-1080 fibrosarcoma, HT-29 colon adenocarcinoma, M21 skin melanoma and MCF7 estrogen-dependent breast adenocarcinoma. The antiproliferative activity experiments were performed accordingly to the NCI/NIH Developmental Therapeutics Program with slight modifications [15]. Topotecan, SFOM-0106, SFOM-0107 and SFOM-0046 were used as reference controls [2,4]. Antiproliferative activities are shown in Table 6.1 and represent the concentration of the drug inhibiting cell growth by 50% (IC_{50}). In general, HT-1080 is the most sensitive cancer cell line followed by HT-29, M21 and MCF7 cell lines, respectively. Moreover, PAB-SOs (**9-26**) and PUB-SOs (**27-38**) substituted at position 4 on ring A are active in the submicromolar to the low micromolar range on all cancer cell lines assessed, so far (0.60-27 µM and 0.14-14 µM, respectively). In addition, PUB-SO derivatives are usually more potent than their PAB-SO counterparts. This result shows that the urea group of PUB-SOs is beneficial but nonessential for the anticancer activity. In contrast and at the exception of compound **7** bearing a chloroacetamide group, PAB-SOs **1-8** substituted at position 3 on ring A show a weaker activity than derivatives substituted at position 4 exhibiting an antiproliferative activity in the micromolar range (8.2 to >40 µM). The carbon chain length substituting the urea and the amide groups on ring A also impacts the antiproliferative activity of PAB-SOs and PUB-SOs. Indeed, a chain length of 5 atoms is optimal for the antiproliferative activity (ethylurea and propylamide moieties); longer or shorter alkyl, cycloalkyl or substituted alkyl groups lead to weaker antiproliferative activities. In addition, and except for PAB-SOs **7**, **21** and **22** bearing a strong electrophilic chloroacetamide group, the presence of a C-terminal chlorine atom on the alkyl chain of the amide and urea groups

on ring A of PAB-SO and PUB-SO derivatives have a weaker antiproliferative activity than their PAB-SO and PUB-SO counterparts. These results strongly suggest that the binding site is sterically hindered and does not require nucleophilic or strong dipole-dipole interactions for binding. Therefore, PAB-SOs **13** and **14** bearing a propyl group and PUB-SOs **27** and **28** bearing an ethyl group on ring A exhibit the most potent and promising antiproliferative activity. PAB-SOs **7**, **21** and **22** bearing a chloroacetamide group on ring A are too reactive to be considered for further biological evaluation. Finally, PAB-SOs **13** and PUB-SO **28** are the most potent compounds showing antiproliferative activity ranging from 0.14 to 6.6 µM which is almost equipotent to topotecan used as positive control (0.2-1.4 µM).

Table 6.1. Antiproliferative activity (IC_{50}) of PAB-SO (**1**-**26**) and PUB-SO (**27**-**38**) derivatives on human HT-1080 fibrosarcoma, HT-29 colon adenocarcinoma, M21 skin melanoma and MCF7 breast adenocarcinoma cell lines.

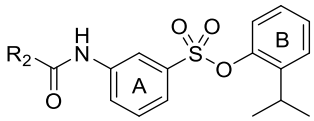

1-8

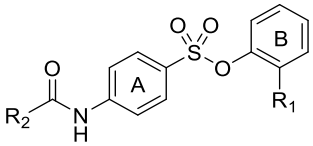

9-26

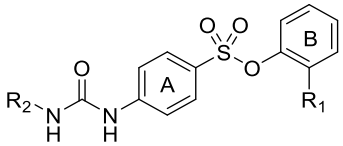

27-38

#	R_1	R_2	IC_{50} (µM)[1]			
			HT-1080	**HT-29**	**M21**	**MCF7**
1	-	CH_3	21	27	31	21
2	-	CH_2CH_3	12	22	25	14
3	-	$(CH_2)_2CH_3$	15	13	20	9.4
4	-	$(CH_2)_4CH_3$	11	19	11	12
5	-	$CH(CH_3)_2$	16	16	17	13
6	-	$C(CH_3)_3$	11	19	13	14
7	-	CH_2Cl	0.78	4.5	3.9	2.2
8	-	$(CH_2)_2Cl$	8.2	11	>40	12
9	*i*-Prop	CH_3	12	23	21	16
10	I	CH_3	17	23	27	27
11	*i*-Prop	CH_2CH_3	2.1	7.4	11	11
12	I	CH_2CH_3	7.2	11	11	8.1
13	*i*-Prop	$(CH_2)_2CH_3$	0.95	4.9	6.1	6.6
14	I	$(CH_2)_2CH_3$	2.0	11	9.0	9.7
15	*i*-Prop	$(CH_2)_4CH_3$	6.3	6.4	6.7	5.3
16	I	$(CH_2)_4CH_3$	9.6	13	11	10

17	*i*-Prop	$CH(CH_3)_2$	4.9	14	11	8.6
18	I	$CH(CH_3)_2$	3.3	13	13	8.1
19	*i*-Prop	$C(CH_3)_3$	11	15	6.2	6.5
20	I	$C(CH_3)_3$	2.6	9.5	8.3	6.6
21	*i*-Prop	CH_2Cl	1.0	5.6	3.9	2.9
22	I	CH_2Cl	0.60	4.1	3.9	2.5
23	*i*-Prop	$(CH_2)_2Cl$	6.5	16	14	9.0
24	I	$(CH_2)_2Cl$	4.2	14.3	12.1	8.9
25	*i*-Prop	$(CH_2)_3Cl$	3.8	6.2	5.1	5.2
26	I	$(CH_2)_3Cl$	12	9.1	7.2	6.3
27	*i*-Prop	CH_2CH_3	0.25	1.1	4.7	10
28	I	CH_2CH_3	0.14	5.3	5.6	1.1
29	*i*-Prop	$(CH_2)_2CH_3$	0.68	6.3	5.1	2.7
30	I	$(CH_2)_2CH_3$	0.70	6.8	5.4	2.9
31	*i*-Prop	$(CH_2)_4CH_3$	4.7	4.9	4.6	4.0
32	I	$(CH_2)_4CH_3$	6.9	6.6	5.9	5.4
SFOM-0107 [4]	*i*-Prop	$(CH_2)_2Cl$	0.84	1.5	1.5	1.8
SFOM-0106 [4]	I	$(CH_2)_2Cl$	1.2	1.5	1.9	1.5
33	*i*-Prop	$(CH_2)_3Cl$	2.7	6.9	9.3	7.4
34	I	$(CH_2)_3Cl$	2.8	9.6	4.6	7.6
35	I	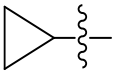	1.3	14	11	7.4
36	*i*-Prop	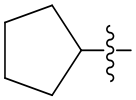	3.9	7.4	6.1	6.2
37	*i*-Prop	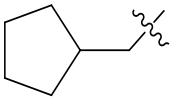	6.0	6.8	6.6	7.1
38	I	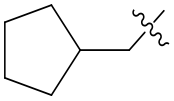	6.1	7.6	7.6	6.6
SFOM-0046 [4]	Ethyl	CH_3CH_2	0.45	13	1.6	6.4
Tpt[2]	-	-	0.50	0.41	1.4	0.20

[1]IC_{50} represents the concentration of drug inhibiting cell growth by 50%. [2]Tpt: Topotecan.

6.6.2. PAB-SO and PUB-SO derivatives arrest the cell cycle progression in S-phase

SFOM-0107 and SFOM-0106 substituted by either a 2-isopropyl or a 2-iodo group on ring B and bearing a 2-chloroethylurea moiety at position 4 on ring A are known to block the cell cycle progression in S-phase [4]. Therefore, to evaluate the impact of modifying the ring A of PUB-SOs, PAB-SOs **3-7** and **11-26** as well as PUB-SOs **27-38** were selected and were assessed on the cell cycle progression of M21 cells. Results are summarized in Table

6.2 and show that the percentage of cells found in sub-G1, G0/G1, S and G2/M-phases after 24 h of treatment at 2-folds their respective IC_{50} that represents the optimal concentration arresting the cell cycle progression in S-phase. SFOM-0046, SFOM-0106 and topotecan were used as positive controls. Control cells were treated with DMSO (0.5%). First, PAB-SO derivatives substituted at position 3 on ring A do not induce arrest of the cell cycle progression in S-phase. Moreover, PAB-SOs **16**, **21**, **22**, **25**, **26** and PUB-SOs **31**, **32** and **36-38** bearing sterically hindered or chloroacetamide groups on ring A also lose their property to arrest the cell cycle progression in S-phase. In general, PAB-SO derivatives induce an S-phase arrest more efficiently than their PUB-SO counterparts. In addition, the S-phase arrest is much more important with PAB-SO and PUB-SO derivatives bearing a 2-isopropyl group on ring B than PAB-SO and PUB-SO counterparts bearing a 2-iodo group. Finally, PAB-SOs **11**, **13** and **19** as well as PUB-SOs **27**, **33** and **34** exhibit the most potent arrest in S-phase of each series of compounds showing a population increase in S-phase by 24.7, 24.3, 27.2, 11.8, 18.9 and 12.3%, respectively.

Table 6.2. Effect of selected PAB-SO and PUB-SO derivatives on the cell cycle progression of M21 cells after 24 h of treatment.

#	Conc. (μM)	Cell cycle progression (%)			
		Sub-G1	G0/G1	S	G2/M
3	39.8	3.0	64.2	14.4	18.4
4	21.9	1.5	69.0	16.0	13.5
5	34.5	0.1	54.5	12.9	32.5
6	24.9	0.7	61.1	20.0	18.2
7	7.8	0.0	64.1	17.1	18.8
11	21.6	0.6	39.6	44.4	15.4
12	22.6	0.2	60.4	28.0	11.4
13	12.2	0.7	40.0	43.8	15.5
14	17.9	0.1	37.0	22.8	40.1
15	13.3	3.7	41.4	28.3	26.6
16	21.5	0.2	42.6	12.9	44.3
17	21.8	0.2	62.0	27.3	10.5
18	26.3	0.2	62.0	23.6	14.2
19	12.3	0.4	36.7	46.9	16.0
20	16.6	0.0	55.0	29.1	15.9
21	7.8	0.1	60.9	18.0	21.0
22	7.7	0.3	71.1	16.5	12.1
23	27.7	0.1	33.7	35.6	30.6
24	24.3	0.2	27.5	34.9	37.4
25	10.2	0.2	55.3	19.3	25.2
26	14.5	0.2	42.0	17.1	40.7
27	9.5	0.8	58.8	31.5	8.9
28	11.1	0.3	67.6	23.4	8.7
29	10.1	0.3	64.6	25.1	10.0
30	10.7	0.1	62.6	26.6	10.7
31	9.3	0.3	60.6	12.2	26.9
32	11.8	0.1	62.2	14.7	23.0
33	18.5	0.8	43.4	38.6	17.2
34	9.3	0.1	54.4	32.0	13.5
35	21.2	0.1	61.5	26.9	11.5
36	12.3	0.1	60.2	12.5	27.2
37	13.3	0.1	63.9	14.3	21.7
38	15.2	0.1	56.2	18.9	24.8
SFOM-0106	8.6	0.1	56.8	30.9	12.2
Topotecan	1.8	0.1	45.2	31.9	22.8
DMSO	0.5%	0.1	59.1	19.7	21.1

6.6.3. PUB-SOs and PAB-SOs induce phosphorylation of H2AX into γH2AX

Our previous SAR studies have shown that PUB-SOs bearing an ethylurea, a 2-chloroethylurea or a 3-chloropropylurea group on ring A are blocking the cell cycle progression in S-phase and induce the phosphorylation of H2AX into γH2AX [2,4,11]; a marker of DNA damage and DNA DSBs [5-10]. Therefore, the phosphorylation of H2AX was used in this study to confirm that the most potent PAB-SOs (**11**, **13**, **19**, **23** and **24**) and PUB-SOs (**27**, **33** and **34**) exhibiting the highest potency to block cell cycle progression in S-phase also induce DNA damage and DNA DSBs. In addition to the later compounds, PAB-SOs **12** and **14** as well as PUB-SO **28** and **30** were also selected to study the impact of the substitution of ring B by a 2-iodo group on the induction of γH2AX. Fig. 6.2 shows the nucleus stained in blue with 4',6-diamidino-2-phenylindole (DAPI) and γH2AX foci in red of cells treated with PAB-SOs and PUB-SOs at 5-times their respective IC_{50} for 24 h. SFOM-0106 and topotecan were used as positive controls while DMSO (0.25%) was used as a negative control. As depicted in Fig. 6.2, all PAB-SOs and PUB-SOs studied blocking the cell cycle progression in S-phase induce the phosphorylation of H2AX into γH2AX. The nature of the groups studied on both aromatic rings therefore does not affect the induction of γH2AX. Thus, the induction of DNA damage and DNA DSBs also characterized the mechanism of action of new PAB-SOs and PUB-SOs.

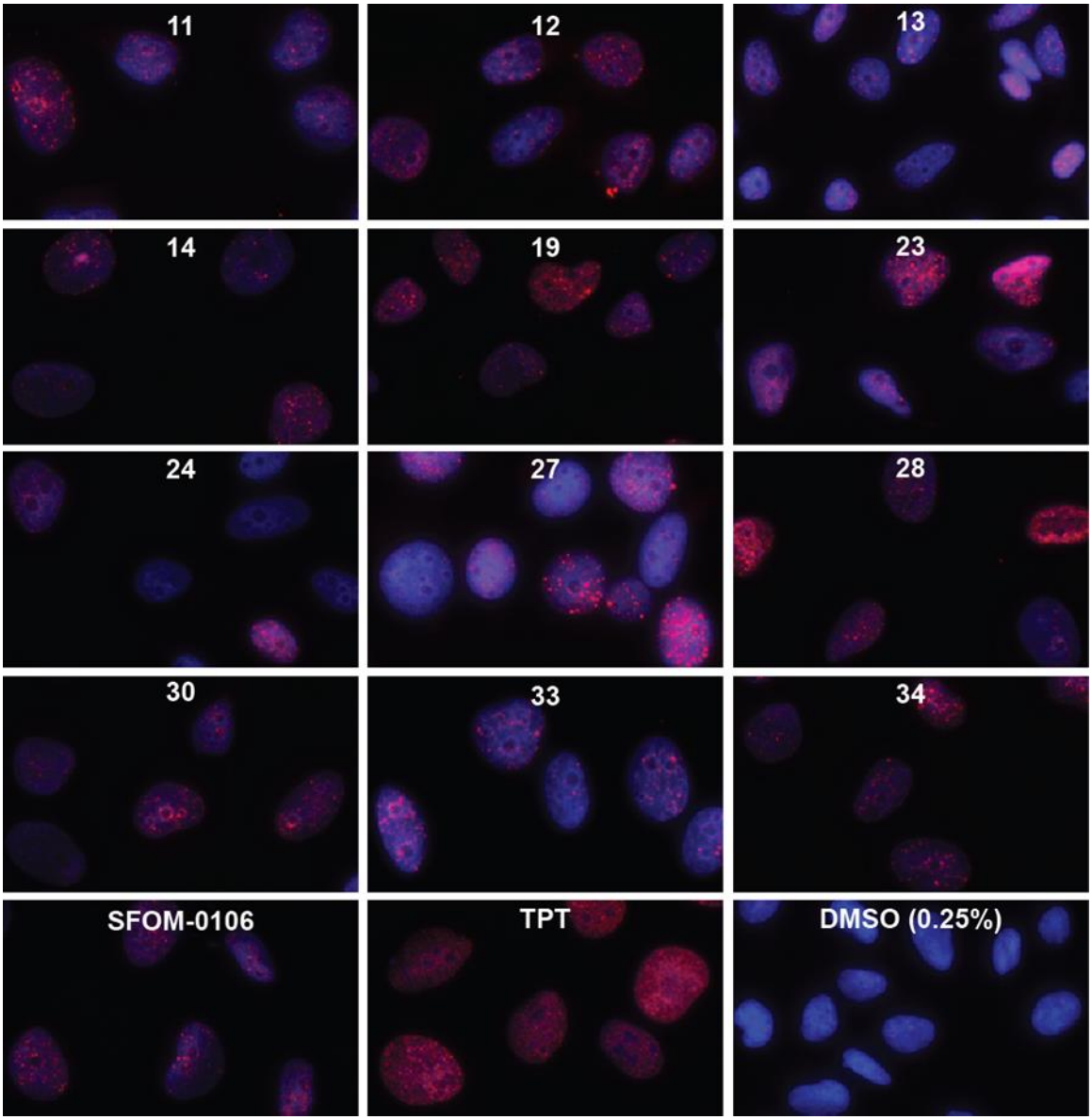

Figure 6.2. Effect of PAB-SOs **11**-**14**, **19**, **23** and **24** as well as PUB-SOs **27**, **28**, **30**, **33** and **34** on the phosphorylation of H2AX into γH2AX after 24 h of treatment of M21 cells. SFOM-0106, topotecan (TPT) and DMSO (0.25%) were used as positive and negative controls, respectively.

6.6.4. PAB-SOs and PUB-SOs have weak or no alkylating activity properties in the NBP assay

Alkyl esters of alkyl or aryl sulfonic acids are considered as potentially genotoxic and alkylating agents in biological systems since the sulfonate group can be displaced by a variety

of nucleophilic groups including DNA bases [16,17]. Moreover, aliphatic organochlorides are also potential alkylating agents because the chloride atom is a leaving group. Since the molecular structure of PAB-SOs and PUB-SOs is constituted of 1) a benzyl ester group of aryl sulfonic acids and 2) a few derivatives bear an aliphatic organochloride group, we evaluated the alkylating potency of PAB-SOs and PUB-SOs using the colorimetric NBP assay [12,18,19]. NBP assay is one of the suitable techniques to assess the alkylating potency of electrophilic compounds. NBP exhibits similar nucleophilic characteristics to those of DNA bases and the assay is based on the formation of a chromophore in an alkaline medium when alkylating agents react with NBP. The alkylating activity of PAB-SOs **9**, **11-14**, **19**, **23** and **24** as well as PUB-SOs **27**-**30**, **33**, **34**, SFOM-0046, SFOM-0106 and SFOM-0107 were assessed using the NBP assay. Chlorambucil was used as positive control. The alkylating potency in the NBP assay is expressed as the alkylation rate constant determined by linear regression of the absorbance curve of each drug. As depicted in Fig. 6.3, the alkylation rate constant of PAB-SOs and PUB-SOs assessed were between 0.49 and 0.0034 × 10^{-3}/s comparatively to 5.3 × 10^{-3}/s for chlorambucil (Fig. 6.3). The NBP experiment evidenced that PAB-SOs and PUB-SOs are much weaker alkylating agents than chlorambucil by 11-1600-folds. PAB-SOs **9**, **11-14** and **24** as well as PUB-SOs **27**, **28**, **30**, **34** and SFOM-0106 are weak alkylating agents (alkylation rate constant of 0.49 to 0.063 × 10^{-3}/s) while PAB-SOs **19** and **23** as well as PUB-SOs **29**, **33**, SFOM-0046 and SFOM-0107 are very weak or not alkylating agents exhibiting rates constant of 0.033 to 0.0034 × 10^{-3}/s. The alkylating activity of PAB-SOs and PUB-SOs does not correlate with the arrest of the cell cycle progression in S-phase nor with the induction of γH2AX and the nature of the group on ring A. Therefore, the alkylating activity experiments show that the alkylating potency is not prerequisite for the biological activity of PAB-SOs and PUB-SOs. This corroborates the study by Glowienke *et al.* using computeraided analysis (multiple computer automated structure evaluation) showing that deactivating fragments such as benzene in the molecular structure of PAB-SOs and PUB-SOs inactivate the alkylating potency of sulfonates [20]. In addition, the weak alkylating potency of PAB-SOs and PUB-SOs confirms also our previous observations using 4-*tert*-butyl-(3-(2-chloroethyl)ureido) benzene (*t*BCEU) that aliphatic chlorine group may lead to weak alkylation activity [21].

A)

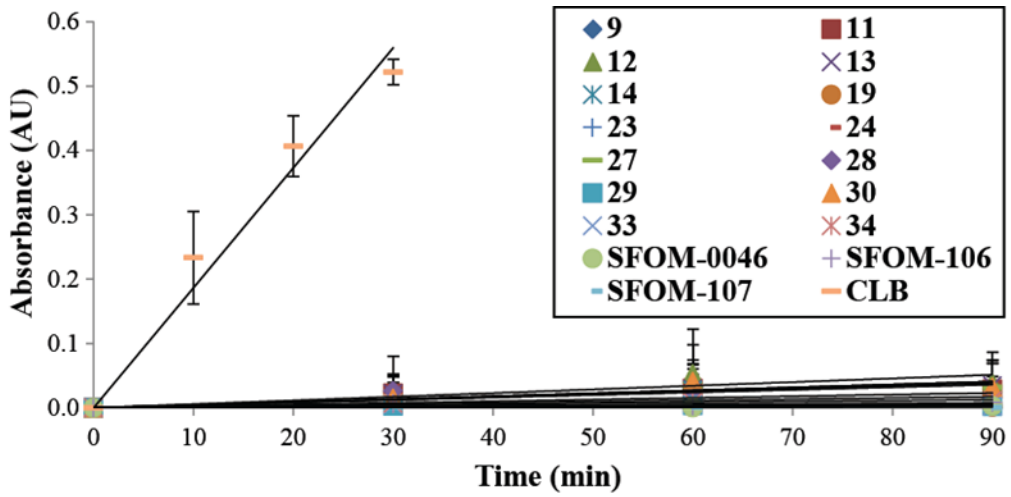

B)

#	Rate constant (10^{-3} s^{-1})	Ratio of CBL[1]	#	Rate constant (10^{-3} s^{-1})	Ratio of CBL[1]
9	0.36	14	**28**	0.12	42
11	0.31	17	**29**	0.027	200
12	0.49	11	**30**	0.40	13
13	0.37	14	**33**	0.033	160
14	0.088	60	**34**	0.12	44
19	0.007	780	**SFOM-0046**	0.032	170
23	0.024	220	**SFOM-0106**	0.071	75
24	0.063	84	**SFOM-0107**	0.0034	1600
27	0.37	14	**CLB[2]**	5.3	N/A

[1]Ratio of CBL: The ratio of CBL is calculated as the ratio of the rate constant of CBL to that measured for each compound. [2]CBL: chlorambucil, N/A: not applicable

Figure 6.3. A) Relative alkylation of PAB-SOs **9**, **11-14**, **19**, **23** and **24** as well as PUB-SOs **28-30**, **33**, **34**, SFOM-0046, SFOM-0106 and SFOM-0107 by 4-(nitrobenzyl)pyridine (NBP). Chlorambucil was used as positive control. B) Rate constant of alkylation determined by linear regression of the absorbance curve and ratio of rate constant of chlorambucil (CBL) comparatively to that of each compound.

6.6.5. Effect of structure modifications on pharmacokinetic, druglikeness and physicochemical properties of PAB-SO and PUB-SO derivatives

Physicochemical properties are important aspects to consider in drug design and drug development. They affect both pharmacokinetic and pharmacological properties leading ultimately to modification of the biological activity. On the one hand, the structure modifications that we made on PUB-SOs were expected to change both their

physicochemical properties and their biological activity. On the other hand, many state-of-the art free web-based computer-aided drug design tools are readily available to predict pharmacokinetic, drug-likeness and physicochemical properties such as pk-CSM [22], admetSAR [23] and SwissADME [24]. In this context, we used SwissADME tool to predict the effect of structure modifications of most promising compounds assessed using our biofunctional assays (compounds **11**, **12**, **13**, **14**, **19**, **23**, **24**, **27**, **28**, **30**, **33** and **34**) on physicochemical, pharmacokinetic and drug-likeness properties. SwissADME was selected because it is freely accessible, fast and produce robust predictive models using different input methods to calculate several ADME properties of small molecules. A summary of these predictions is shown in Table 6.3 and the complete prediction results are available in the supplementary material section. First, the physicochemical properties of PAB-SO and PUB-SO derivatives are similar. The molecular weights of PAB-SO and PUB-SO derivatives vary from 347.4 to 494.7 g/mol. The number of rotatable bonds and H-bond donors vary from 6 to 10 and 1 to 2, respectively while H-bond acceptors remain constant. The molar refractivity and the topological polar surface area (TPSA) vary from 92.6 to 107.2 and 80.85 to 92.88 $Å^2$, respectively. The lipophilicity is expressed as consensus Log P (CLogP) and varies from 2.99 to 4.20. The water solubility is expressed as Log S and varies from -4.66 to -6.15 (9.85-0.27 × 10^{-3} mg/mL). At the exception of compound **19** bearing a pivalamide moiety at position 4 on ring A that falls in the class of poorly soluble molecules, all other selected PAB-SO and PUB-SO derivatives display CLogP and LogS in the same order of magnitude and fall within the class of moderately soluble compounds. Moreover, SwissADME predicts that a probable high gastrointestinal absorption (GIA) of all selected PAB-SO and PUB-SO derivatives. In addition, they are not expected to be permeant to blood-brain barrier nor substrates of the P-glycoprotein. Finally, at the exception of **34** and SFOM-0106 showing only one violation for Ghose filter (molecular weight > 480 g/mol), all other selected PAB-SO and PUB-SO derivatives do not show violation toward Lipinski, Ghose, Veber, Egan and Muegge filters. These results show that our selected PAB-SOs and PUB-SOs exhibit high drug-likeness and bioavailability scores. Altogether, these results show that structure modifications weakly affect the physicochemical properties of PAB-SOs and PUB-SOs. Moreover, their pharmacokinetics and drug-likeness properties calculated using SwissADME are also similar. These predictions confirm that the results obtained from our

biofunctional assays are mainly due to the docking and the affinity of PAB-SOs and PUB-SOs to biological target that has not been identified yet.

Table 6.3. Pharmacokinetics, drug-likeness and biophysical properties of selected PAB-SO and PUB-SO derivatives calculated using the free web-based SwissADME application [24].

#	RB[1]	H-BA[2]	H-BD[3]	MR[4]	TPSA[5](Å^2)	CLogP[6]	LogS[7]	SClass[8]	GIA[9]	BBBP[10]	Pgp[11]	Drug-like (# viol.)[12]
11	7	4	1	94.4	80.85	3.56	-5.18	MS	H	No	No	Yes (0)
12	6	4	1	92.6	80.85	3.29	-4.69	MS	H	No	No	Yes (0)
13	8	4	1	99.3	80.85	3.91	-5.56	MS	H	No	No	Yes (0)
14	7	4	1	97.4	80.85	3.64	-5.06	MS	H	No	No	Yes (0)
19	7	4	1	103.8	80.85	4.20	-6.15	PS	H	No	No	Yes (0)
23	8	4	1	99.2	80.85	3.80	-5.24	MS	H	No	No	Yes (0)
24	7	4	1	97.4	80.85	3.53	-4.75	MS	H	No	No	Yes (0)
27	8	4	2	97.6	92.88	3.27	-5.15	MS	H	No	No	Yes (0)
28	7	4	2	95.8	92.88	3.02	-4.66	MS	H	No	No	Yes (0)
30	8	4	2	100.6	92.88	3.38	-5.21	MS	H	No	No	Yes (0)
33	10	4	2	107.2	92.88	3.84	-5.76	MS	H	No	No	Yes (0)
34	9	4	2	105.4	92.88	3.60	-5.26	MS	H	No	No	Yes (1)
SFOM-0046	8	4	2	92.8	92.88	2.99	-4.81	MS	H	No	No	Yes (0)
SFOM-0106	8	4	2	100.6	92.88	3.26	-4.89	MS	H	No	No	Yes (1)
SFOM-00107	9	4	2	102.4	92.88	3.52	-5.38	MS	H	No	No	Yes (0)
Tpt[13]	3	7	2	114.8	104.89	1.86	-3.02	S	H	No	Yes	Yes (0)

[1]RB: number of rotatable bonds. [2]H-BA: number of H-bond acceptors. [3]H-BD: number of H-bond acceptors. [4]MR: molar refractivity. [5]TPSA: topological polar surface area. [6]CLogP: consensus Log P (average from iLOGP, XLOGP3, WLOGP, MLOGP and Silicos-IT Log P). [7]LogS: Ali topological method Log S. [8]SClass: Ali solubility class (insoluble (IS) < -10 < poorly soluble (PS) < -6 < moderately soluble (MS) < -4 < soluble (S) < -2 < very soluble (VS) < 0 < highly soluble (HS). [9]GIA: gastrointestinal absorption (H means high). [10]BBBP: blood-brain barrier permeability. [11]Pgp: P-glycoprotein substrates. [12]Druglike: drug-likeness indices (bioavailability) from Lipinski, Ghose, Veber, Egan and Muegge filters. # viol: number of violations of the five filters. [13]Tpt: Topotecan.

6.7. Conclusion

In conclusion, we report herein the synthesis and the biological activity of 26 novel PAB-SO and 12 PUB-SO derivatives. They were evaluated for their antiproliferative activity on four human cancer cell lines (HT-1080, HT-29, M21 and MCF7) and for their potency to arrest the cell cycle progression in S-phase. Our SAR study shows that PAB-SOs and PUB-SOs must be substituted at position 4 on the aromatic ring A to maintain a significant antiproliferative activity in the low micromolar to submicromolar range and to arrest the cell cycle progression in S-phase. PAB-SOs and PUB-SOs blocking the cell cycle progression in S-phase induce also DNA DSBs as shown by the induction of γH2AX. Moreover, the NBP assay shows that PUB-SOs and PAB-SOs exhibit no or only weak alkylating potency and confirms that alkylating activity is not essential to their biological activity. In addition, our results show that structure modifications weakly affect the calculated physicochemical, pharmacokinetic and drug-likeness properties of PAB-SOs and PUB-SOs. Finally, our work confirms that urea group is not essential for the activity of this class of compounds and paves the way for further exploration of this moiety for the development and optimization of this promising family of new anticancer agents.

6.8. Experimental protocols

6.8.1. Biological methods

6.8.1.1. Biological methods

HT-1080 human fibrosarcoma, HT-29 human colon carcinoma, M21 human skin melanoma and MCF7 human breast carcinoma were purchased from the American Type Culture Collection (Manassa, VA). Cells were cultured in DMEM medium containing sodium bicarbonate, high glucose concentration, glutamine and sodium pyruvate (Hyclone, Logan, UT) supplemented with 5% of fetal bovine serum (FBS, Invitrogen, Burlington, ON) and were maintained at 37 °C in a moisture-saturated atmosphere containing 5% CO_2.

6.8.1.2. Antiproliferative activity assay

The growth inhibition potency of all compounds was assessed using the procedure recommended by the National Cancer Institute (NCI) Developmental Therapeutics Program for its drug screening program with slight modifications [86]. Briefly, 96-well Costar microtiter clear plates were seeded with 75 µL of a suspension of either HT-1080 (2.5×10^3), HT-29 (4.0×10^3), M21 (3.0×10^3) or MCF7 (2.5×10^3) cells per well in DMEM. Freshly solubilised drugs in DMSO (40 mM) were diluted in fresh DMEM and 75 µL aliquots containing serially diluted concentrations of the drug were added. Final drug concentrations ranged from 100 µM to 78 nM. DMSO concentration was kept constant at <0.5% (V/V) to prevent any related toxicity. Plates were incubated for 48 h, after which growth was stopped by the addition of cold trichloroacetic acid to the wells (10% w/v, final concentration). Afterward, plates were incubated à 4 °C for 1 h. Then, plates were washed 5-times with distilled water and a sulforhodamine B solution (0.1% w/v) in 1% acetic acid was added to each well. After 15 min at room temperature, the exceeding dye was removed and was washed 5-times with a solution of 1% acetic acid. Bound dye was solubilized in 20 mM Tris base and the absorbance was read using an optimal wavelength (530-580 nm) with a SpectraMax® i3x (Molecular Devices). Data obtained from treated cells were compared to the control cell plates fixed on the treatment day and the percentage of cell growth was thus calculated for each drug. The experiments were done at least twice in triplicate. The assays were considered valid when the coefficient of variation was <10% for a given set of conditions within the same experiment.

6.8.1.3. Cell cycle progression analysis

M21 cells (2.5×10^5) were seeded onto the six-well plates and incubated for 24 h. Then, after incubation of M21 cells with selected PAB-SOs and PUB-SOs at 2- and 5-times their respective IC_{50} for 24 h, the cells were trypsinized, washed with phosphate buffered saline (PBS) and resuspended in 250 mL of PBS. Cells were fixed by the addition of 750 mL of ice-cold EtOH under agitation and stored at -4 °C until analysis. Prior to fluorescence-activated cell sorting analysis, cells were washed with PBS and resuspended in 500 mL of PBS containing 2 mg/mL DAPI. Cell cycle distribution of fixed cell suspensions was analyzed using an LSR II flow cytometer (BD Biosciences, Franklin Lakes, NJ).

6.8.1.4. Immunofluorescence of H2AX

Cover slides (22 mm × 22 mm) sterilized with 70% (V/V) EtOH were placed in six-well plates. To promote cell adhesion, cover slides were treated with 1.5 mL of a fibronectin solution in PBS (5 μg/mL) for 1 h at 37 °C. Slides were then rinsed thrice with PBS. M21 cells (1 x 10^5) were seeded onto the plates and incubated for 24 h. Cells were then incubated with selected PAB-SOs and PUB-SOs at 2- and 5-times their respective IC_{50} for 24 h at 37 °C. The control solution consisted of DMSO dissolved in culture medium (0.25%, V/V). Cells were fixed using 1.5 mL of formaldehyde at 3.7% and permeabilized by addition of a saponin and bovine serum albumin (BSA) solution (0.1% and 3% w/v in PBS, respectively). Cells were incubated with mouse anti-H2AX pS139 antibody (Millipore, Billerica, MA) (1:8000). Cover slides were next incubated for 3 h at room temperature and then washed thrice with PBS supplemented with 0.05% (V/V) Tween 20 (PBS-T). Saponin−BSA solution containing goat anti-mouse IgG conjugated to AlexaFluor 594 (Invitrogen, Burlington, Ontario, Canada) (1:1000, 2 mg/mL), and DAPI (Sigma, Oakville, Ontario, Canada) (1:3000, 1 mg/mL) was then added. The cover slides were incubated for 2 h at room temperature and then washed 5-times with PBS-T. The cover slides were mounted with Fluoromount-G (Southern Biotech no: 0100-01). Cells were visualized using an epifluorescence microscope (Olympus BX51, Center Valley, PA) with a Qimaging RETIGA EXi camera (Qimaging, Surrey, British Columbia, Canada).

6.8.1.5. Kinetics of alkylation of 4-(4-nitrobenzyl)pyridine by PUB-SOs and PAB-SOs

The kinetics of alkylation of PAB-SOs and PUB-SOs was assessed by a colorimetric assay developed by Bardos *et al.* [14]. Chlorambucil was used as positive control. Briefly, 1 mL of ethanol containing 400 nmol of the selected drug, 1 mL of a solution of NBP (10% (V/V) in ethanol 95%), 1 mL of acetate buffer solution (50 mM at pH 4.3) and 1 mL of ethanol were mixed together and kept on ice prior to the initiation of the reaction. The reaction was initiated by heating the solutions at 80 °C in a shaking water bath. The reaction was stopped by cooling down the mixtures on ice for 5 min after periods of incubation of 0, 30, 60 and 90 min. Then, 1.5 mL of a solution of 0.1 M KOH:ethanol (1:2 (V/V)) was added to the reaction mixture. Thereafter, the mixtures were vortexed for 12 s and 2.5 min later the absorbance was read at 570 nm. The values were compared with those obtained using a blank

where the drug solutions were replaced by ethanol. The rate constant of alkylation was determined by linear regression of the absorbance curve generated for each drug.

6.8.2. Chemical methods

6.8.2.1. General

Proton NMR spectra were recorded on a Bruker AM-300 spectrometer (Bruker, Germany) or an NMR Varian Inova 400 MHz. Chemical shifts (δ) are reported in parts per million (ppm). Reactions requiring microwave heating were performed with an Initiator system (Biotage, Charlottesville, VA). Uncorrected melting points were determined on an electrothermal melting point apparatus. HPLC analyses were performed using a Prominence LCMS-2020 system with binary solvent equipped with an UV/vis photodiode array and an APCI probe (Shimadzu, Columbia, MD). Compounds were eluted within 25 min on an Alltech Alltima C18 reversed-phase column (5 mm, 250 mm x 4.6 mm) equipped with an Alltech Alltima C18 precolumn (5 mm, 7.5 mm x 4.6 mm) with a MeOH/H_2O linear gradient at 1.0 mL/min. Some HPLC analyses were also performed using an ACQUITY Arc system (Waters, Mississauga, Ontario). The purity of all final compounds was >95%. HRMS were recorded by direct injection in a TOF system 6210 series mass spectrometer (Agilent technologies, Santa Clara, CA). All chemicals were supplied by Aldrich Chemicals (Milwaukee, WI), VWR International (Mont-Royal, QC, Canada) or Enamine LLC (Cincinnati, USA) and used as received unless specified otherwise. Liquid flash chromatography was performed on silica gel F60, 60 Å, 40-63 μm supplied by Silicycle (Québec, QC, Canada) using an FPX flash purification system (Biotage, Charlottesville, VA), and using solvent mixtures expressed as V/V ratios. Solvents and reagents were used without purification unless specified otherwise. The progress of all reactions was monitored by TLC on precoated silica gel 60 F254 TLC plates (VWR). The chromatograms were viewed under UV light at 254 and/or 265 nm.

6.8.2.2. General preparation of compounds 1-26

Method A. The relevant acid chloride was added to a solution of the appropriate aniline (**42-44**) in acetonitrile (2 mL) with triethylamine (1.2 Eq.). The reaction mixture was

stirred at 80 °C under pressure for 1-7 days. The mixture was cooled at room temperature and the solvent was evaporated under reduced pressure. The residue was diluted with in AcOEt (10 mL) and was washed successively with water (10 mL) and brine (10 mL), dried over sodium sulfate, filtered and evaporate to dryness under reduced pressure. The residue was purified by flash chromatography on silica gel.

Method B. The relevant acid chloride was added to a solution of the appropriate aniline (**42-44**) in acetonitrile (2 mL) and with or without triethylamine (1.2 Eq.) and potassium carbonate (1.2 Eq.). The reaction mixture was stirred at room temperature for 1-5 days. After completion of the reaction, the solvent was evaporated under reduced pressure, the mixture was diluted in AcOEt (10 mL) and was washed successively with water (10 mL) and brine (10 mL), dried over sodium sulfate, filtered and evaporate to dryness under reduced pressure. The residue was purified by flash chromatography on silica gel.

6.8.2.3. Characterization of compounds 1-26

6.8.2.3.1. 2-Isopropylphenyl 3-acetamidobenzenesulfonate (**1**). Method A, 7 days, flash chromatography (hexanes/methylene chloride (50:50)). Yield: 61%; pale yellow solid; mp: 98-99 °C; ^{1}H NMR ($CDCl_3$): δ 8.38 (brs, 1H, NH), 8.10-7.97 (m, 2H, Ar), 7.55-7.43 (m, 2H, Ar), 7.26-7.18 (m, 2H, Ar), 7.09-6.98 (m, 2H, Ar), 3.16-3.06 (m, 1H, CH), 2.17 (s, 3H, CH_3), 1.04 (d, 6H, J = 6.8 Hz, 2x CH_3); ^{13}C NMR ($CDCl_3$): δ 169.3, 146.9, 141.7, 139.4, 136.3, 130.0, 127.6, 127.3, 126.7, 125.3, 123.4, 121.8, 118.8, 26.8, 24.4, 23.1; MS (APSI+) *m/z* found 334.10; $C_{17}H_{20}NO_4S$ (M^+ + H) expected, 334.11.

6.8.2.3.2. 2-Isopropylphenyl 3-propionamidobenzenesulfonate (**2**). Method A, 7 days, flash chromatography (hexanes/methylene chloride (75:25) to methylene chloride). Yield: 47%; colorless oil; ^{1}H NMR ($CDCl_3$): δ 8.48 (brs, 1H, NH), 8.27-7.85 (m, 2H, Ar), 7.53-7.51 (m, 1H, Ar), 7.45-7.41 (m, 1H, Ar), 7.25-7.17 (m, 2H, Ar), 7.08-6.97 (m, 2H, Ar), 3.15-3.09 (m, 1H, CH), 2.40 (q, 2H, J = 7.5 Hz, CH_2), 1.19 (t, 3H, J = 7.5 Hz, CH_3), 1.04 (d, 6H, J = 6.9 Hz, 2x CH_3); ^{13}C NMR ($CDCl_3$): δ 173.3, 146.9, 141.7, 139.6, 136.3, 130.0, 127.6, 127.3, 126.7, 125.3, 123.2, 121.8, 118.8, 30.5, 26.8, 23.1, 9.5; MS (APSI+) *m/z* found 348.05; $C_{18}H_{22}NO_4S$ (M^+ + H) expected, 348.13.

6.8.2.3.3. 2-Isopropylphenyl 3-butyramidobenzenesulfonate (**3**). Method A, 7 days, flash chromatography (hexanes/methylene chloride (50:50)). Yield: 33%; white solid; mp: 78-79 °C;^{1}H NMR ($CDCl_3$): δ 8.49 (brs, 1H, NH), 8.11-8.05 (m, 2H, Ar), 7.53-7.51 (m, 1H, Ar), 7.45-7.41 (m, 1H, Ar), 7.26-7.17 (m, 2H, Ar), 7.08-7.05 (m, 1H, Ar), 7.00-6.98 (m, 1H, Ar), 3.17-3.07 (m, 1H, CH), 2.35 (t, 2H, *J* = 7.3 Hz, CH_2), 1.76-1.67 (m, 2H, CH_2), 1.04 (d, 6H, *J* = 6.8 Hz, 2x CH_3), 0.94 (t, 3H, *J* = 7.3 Hz, CH_3); ^{13}C NMR ($CDCl_3$): δ 172.9, 146.9, 141.7, 139.7, 136.3, 129.9, 127.6, 127.3, 126.8, 125.4, 123.2, 121.8, 119.1, 39.2, 26.7, 23.1, 19.0, 13.6; MS (APSI+) *m/z* found 362.10; $C_{19}H_{24}NO_4S$ (M^+ + H) expected, 362.14.

6.8.2.3.4. 2-Isopropylphenyl 3-hexanamidobenzenesulfonate (**4**). Method A, 7 days, flash chromatography (hexanes/ethyl acetate (90:10)). Yield: 60%; colorless oil; ^{1}H NMR ($CDCl_3$): δ 8.46 (brs, 1H, NH), 8.13-8.11 (m, 1H, Ar), 8.04 (s, 1H, Ar), 7.52-7.50 (m, 1H, Ar), 7.45-7.41 (m, 1H, Ar), 7.26-7.17 (m, 2H, Ar), 7.08-7.05 (m, 1H, Ar), 7.01-6.99 (m, 1H, Ar), 3.17-3.07 (m, 1H, CH), 2.37 (t, 2H, *J* = 7.4 Hz, CH_2), 1.71-1.67 (m, 2H, CH_2), 1.30-1.29 (m, 4H, 2x CH_2), 1.04 (d, 6H, *J* = 6.9 Hz, 2x CH_3), 0.86 (t, 3H, *J* = 4.9 Hz, CH_3); ^{13}C NMR ($CDCl_3$): δ 172.6, 146.8, 141.7, 139.6, 136.2, 129.9, 127.5, 127.3, 126.7, 125.3, 123.2, 121.8, 118.8, 37.5, 31.3, 26.7, 25.2, 23.1, 22.4, 13.9; MS (APSI+) *m/z* found 390.15; $C_{21}H_{28}NO_4S$ (M^+ + H) expected, 390.17.

6.8.2.3.5. 2-Isopropylphenyl 3-isobutyramidobenzenesulfonate (**5**). Method B without base, 1 day, flash chromatography (hexanes/ethyl acetate (90:10)). Yield: 56%; orange solid; mp: 95-96 °C; ^{1}H NMR ($CDCl_3$): δ 8.20-8.18 (m, 1H, Ar), 7.98-7.95 (m, 2H, Ar and NH), 7.54-7.51 (m, 1H, Ar), 7.47-7.43 (m, 1H, Ar), 7.27-7.19 (m, 2H, Ar), 7.10-7.06 (m, 1H, Ar), 7.00-6.98 (m, 1H, Ar), 3.17-3.10 (m, 1H, CH), 2.58-2.52 (m, 1H, CH), 1.23 (d, 6H, *J* = 6.8 Hz, 2x CH_3), 1.05 (d, 6H, *J* = 6.9 Hz, 2x CH_3); ^{13}C NMR ($CDCl_3$): δ 176.0, 146.9, 141.7, 139.5, 136.3, 130.0, 127.5, 127.3, 126.7, 125.3, 123.3, 121.9, 118.8, 36.6, 26.7, 23.1, 19.5; MS (APSI+) *m/z* found 362.05; $C_{19}H_{24}NO_4S$ (M^+ + H) expected, 362.14.

6.8.2.3.6. 2-Isopropylphenyl 3-pivalamidobenzenesulfonate (**6**). Method A, 7 days, flash chromatography (hexanes/ethyl acetate (80:20)). Yield: 25%; yellow oil; ^{1}H NMR ($CDCl_3$): δ 8.16-8.14 (m, 1H, Ar), 8.02-8.01 (m, 1H, Ar), 7.95 (brs, 1H, NH), 7.51-7.49 (m, 1H, Ar), 7.44-7.40 (m, 1H, Ar), 7.26-7.24 (m, 1H, Ar), 7.21-7.17 (m, 1H, Ar), 7.07-7.04 (m, 1H, Ar), 6.96-6.94 (m, 1H, Ar), 3.20-3.09 (m, 1H, CH), 1.30 (s, 9H, 3x CH_3), 1.05 (d, 6H, *J*

= 6.9 Hz 2x CH_3); ^{13}C NMR ($CDCl_3$): δ 177.4, 146.9, 141.7, 139.6, 136.3, 129.8, 127.5, 127.2, 126.7, 125.8, 123.4, 121.9, 119.3, 39.8, 27.4, 26.7, 23.1; MS (APSI+) *m/z* found 376.10; $C_{20}H_{26}NO_4S$ (M^+ + H) expected, 376.16.

6.8.2.3.7. 2-Isopropylphenyl 3-(2-chloroacetamido)benzenesulfonate (**7**). Method B with potassium carbonate, 4 days, flash chromatography (hexanes/methylene chloride (80:20)). Yield: 73%; colorless oil; ^1H NMR ($CDCl_3$): δ 8.79 (brs, 1H, NH), 8.15 (m, 1H, Ar), 7.98-7.96 (m, 1H, Ar), 7.61-7.59 (m, 1H, Ar), 7.49-7.45 (m, 1H, Ar), 7.26-7.17 (m, 2H, Ar), 7.09-7.05 (m, 1H, Ar), 7.00-6.99 (m, 1H, Ar), 4.15 (s, 2H, CH_2), 3.15-3.08 (m, 1H, CH), 1.04 (d, 6H, *J* = 6.9 Hz, 2x CH_3); ^{13}C NMR ($CDCl_3$): δ 165.0, 146.8, 141.7, 138.2, 136.7, 130.1, 127.6, 127.3, 126.8, 125.7, 124.4, 121.9, 119.5, 43.0, 26.8, 23.1; MS (APSI+) *m/z* found 368.00; $C_{17}H_{19}ClNO_4S$ (M^+ + H) expected, 368.07.

6.8.2.3.8. 2-Isopropylphenyl 3-(3-chloropropanamido)benzenesulfonate (**8**). Method B with potassium carbonate, 3 days, flash chromatography (hexanes/ethyl acetate (75:25)). Yield: 84%; colorless oil; ^1H NMR ($CDCl_3$): δ 8.63 (brs, 1H, NH), 8.16-8.13 (m, 1H, Ar), 8.02-7.98 (m, 1H, Ar), 7.56-7.54 (m, 1H, Ar), 7.47-7.43 (m, 1H, Ar), 7.26-7.18 (m, 2H, Ar), 7.09-7.06 (m, 1H, Ar), 7.01-6.99 (m, 1H, Ar), 3.82 (t, 2H, J = 6.1 Hz, CH_2), 3.15-3.08 (m, 1H, CH), 2.85 (t, 2H, *J* = 6.1 Hz, CH_2), 1.05 (d, 6H, *J* = 6.9 Hz, 2x CH_3); ^{13}C NMR ($CDCl_3$): δ 169.0, 146.8, 141.7, 139.0, 136.4, 130.1, 127.7, 127.3, 126.8, 125.6, 123.7, 121.8, 119.1, 40.0, 39.6, 26.8, 23.1; MS (APSI+) *m/z* found 382.00; $C_{18}H_{21}ClNO_4S$ (M^+ + H) expected, 382.09.

6.8.2.3.9. 2-Isopropylphenyl 4-acetamidobenzenesulfonate (**9**). Method A, 7 days, flash chromatography (methylene chloride/methanol (97:3)). Yield: 59%; yellow oil; ^1H NMR ($CDCl_3$): δ 8.85-8.69 (brs, 1H, NH), 7.97-7.53 (m, 4H, Ar), 7.25-7.17 (m, 2H, Ar), 7.07 (t, 1H, *J* = 7.7 Hz, Ar), 7.00-6.98 (m, 1H, Ar), 3.14-3.04 (m, 1H, CH), 2.18 (s, 3H, CH_3), 1.03 (d, 6H, *J* = 6.9 Hz, 2x CH_3); ^{13}C NMR ($CDCl_3$): δ 169.7, 146.8, 143.9, 141.7, 129.8, 129.6, 127.6, 127.3, 126.7, 121.8, 119.3, 26.7, 24.6, 23.1, MS (APSI+) *m/z* found 334.05; $C_{17}H_{20}NO_4S$ (M^+ + H) expected, 334.11.

6.8.2.3.10. 2-Iodophenyl 4-acetamidobenzenesulfonate (**10**). Method B with triethylamine, 5 days, flash chromatography (methylene chloride to methylene chloride/ethyl

acetate (90:10)). Yield: 58%; white solid; mp: 113-115 °C; ^{1}H NMR ($CDCl_3$): δ 8.20 (s, 1H, NH), 7.82-7.80 (m, 2H Ar), 7.74-7.72 (m, 3H, Ar), 7.33-7.26 (m, 2H, Ar), 6.98-6.94 (m, 1H, Ar), 2.21 (s, 3H, CH_3); ^{13}C NMR ($CDCl_3$): δ 169.3, 149.8, 144.0, 140.2, 130.2, 129.6, 129.5, 128.6, 122.9, 119.1, 90.3, 24.8; MS (APSI+) *m/z* found 417.90; $C_{14}H_{13}INO_4S$ (M^+ + H) expected, 417.96.

6.8.2.3.11. 2-Isopropylphenyl 4-propionamidobenzenesulfonate (**11**). Method A, 7 days, flash chromatography (hexanes/methylene chloride (50:50)). Yield: 24%; colorless oil; ^{1}H NMR ($CDCl_3$): δ 7.89-7.71 (m, 5H, Ar and NH), 7-26-7.19 (m, 2H, Ar), 7.09 (t, 1H, *J* = 7.9 Hz, Ar), 7.00-6.98 (m, 1H, Ar), 3.17-3.07 (m, 1H, CH), 2.43 (q, 2H, *J* = 7.4 Hz, CH_2), 1.23 (t, 3H, *J* = 7.4 Hz, CH_3), 1.05 (d, 6H, *J* = 6.8 Hz, 2x CH_3); ^{13}C NMR ($CDCl_3$): δ 172.7, 146.9, 143.6, 141.7, 130.0, 129.7, 127.4, 127.2, 126.7, 121.9, 119.1, 30.8, 26.7, 23.1, 9.3; MS (APSI+) *m/z* found 348.05; HRMS (ESI) *m/z* found 348.1262; $C_{18}H_{22}NO_4S$ (M^+ + H) expected, 348.1270.

6.8.2.3.12. 2-Iodophenyl 4-propionamidobenzenesulfonate (**12**). Method A, 5 days, flash chromatography (methylene chloride/ethyl acetate (90:10)). Yield: 70%; yellowish oil; ^{1}H NMR ($CDCl_3$): δ 8.28 (s, 1H, NH), 7.81-7.70 (m, 5H, Ar), 7.21-7.25 (m, 2H, Ar), 6.97-6.93 (m, 1H, Ar), 2.43 (q, 2H, *J* = 7.5 Hz, CH_2), 1.19 (t, 3H, *J* = 7.5 Hz, CH_3); ^{13}C NMR ($CDCl_3$): δ 173.2, 149.8, 144.2, 140.2, 130.2, 129.7, 129.2, 128.7, 122.9, 119.2, 90.3, 30.8, 9.4; MS (APSI+) *m/z* found 431.95; HRMS (ESI) *m/z* found 431.9763; $C_{15}H_{15}INO_4S$ (M^+ + H) expected, 431.9767.

6.8.2.3.13. 2-Isopropylphenyl 4-butyramidobenzenesulfonate (**13**). Method A, 7 days, flash chromatography (hexanes/methylene chloride (75:25)). Yield: 37%; colorless oil; ^{1}H NMR ($CDCl_3$): δ 8.37 (brs, 1H, NH), 7.98-7.53 (m, 4H, Ar), 7.26-7.18 (m, 2H, Ar), 7.10-7.06 (m, 1H, Ar), 7.00-6.98 (m, 1H, Ar), 3.12-3.09 (m, 1H, CH), 2.37 (t, 2H, *J* = 7.4 Hz, CH_2), 1.76-1.67 (m, 2H, CH_2), 1.04 (d, 6H, *J* = 6.9 Hz, 2x CH_3), 0.95 (t, 3H, *J* = 7.4 Hz, CH_3); ^{13}C NMR ($CDCl_3$): δ 172.1, 146.9, 143.6, 141.7, 130.0, 129.7, 127.5, 127.2, 126.7, 121.9, 119.1, 39.6, 26.7, 23.1, 18.8, 13.7; MS (APSI+) *m/z* found 362.10; HRMS (ESI) *m/z* found 362.1418; $C_{19}H_{24}NO_4S$ (M^+ + H) expected, 362.1427.

6.8.2.3.14. 2-Iodophenyl 4-butyramidobenzenesulfonate (**14**). Method B with triethylamine, 5 days, flash chromatography (methylene chloride/hexanes (90:10) to methylene chloride). Yield: 58%; white solid; mp: 105-106 °C; ^{1}H NMR ($CDCl_3$): δ 8.03 (s, 1H, NH), 7.82-7.80 (m, 2H, Ar), 7.76-7.72 (m, 3H, Ar), 7.33-7.26 (m, 2H, Ar), 6.98-6.94 (m, 1H, Ar), 2.38 (t, 2H, *J* = 7.4 Hz, CH_2), 1.78-1.69 (m, 2H, CH_2), 0.97 (t, 3H, *J* = 7.4 Hz, CH_3); ^{13}C NMR ($CDCl_3$): δ 172.2, 149.8, 144.0, 140.2, 130.2, 129.6, 129.4, 128.6, 122.9, 119.1, 90.3, 39.6, 18.8, 13.7; MS (APSI+) *m/z* found 445.95; HRMS (ESI) *m/z* found 445.9916; $C_{16}H_{17}INO_4S$ (M^+ + H) expected, 445.9924.

6.8.2.3.15. 2-Isopropylphenyl 4-hexanamidobenzenesulfonate (**15**). Method A, 7 days, flash chromatography (hexanes/ethyl acetate (80:20)). Yield: 86%; colorless oil; ^{1}H NMR ($CDCl_3$): δ 8.47 (brs, 1H, NH), 7.76 (s, 4H, Ar), 7.26-7.18 (m, 2H, Ar), 7.08 (t, 1H, *J* = 7.5 Hz, Ar), 7.00-6.98 (m, 1H, Ar), 3.16-3.06 (m, 1H, CH), 2.38 (t, 2H, *J* = 7.5 Hz, CH_2), 1.70-1.67 (m, 2H, CH_2), 1.29-1.28 (m, 4H, 2x CH_2), 1.40 (d, 6H, *J* = 6.8 Hz, 2x CH_3), 0.86-0.83 (m, 3H, CH_3); ^{13}C NMR ($CDCl_3$): δ 172.8, 146.8, 144.0, 141.7, 129.7, 129.6, 127.5, 127.3, 126.7, 121.8, 119.2, 37.6, 31.3, 26.7, 25.1, 23.1, 22.4, 13.9; MS (APSI+) *m/z* found 390.10; $C_{21}H_{28}NO_4S$ (M^+ + H) expected, 390.17.

6.8.2.3.16. 2-Iodophenyl 4-hexanamidobenzenesulfonate (**16**). Method B with triethylamine, 5 days, flash chromatography (methylene chloride/hexanes (75:25)). Yield: 63%; colorless oil; ^{1}H NMR ($CDCl_3$): δ 8.21 (s, 1H, NH), 7.82-7.71 (m, 5H, Ar), 7.32-7.26 (m, 2H, Ar), 6.97-6.94 (m, 1H, Ar), 2.39 (t, 2H, *J* = 7.6 Hz, CH_2), 1.71-1.67 (m, 2H, CH_2), 1.30-1.28 (m, 4H, 2x CH_2), 0.87-0.84 (m, 3H, CH_3); ^{13}C NMR ($CDCl_3$): δ 172.6, 149.8, 144.2, 140.2, 130.2, 129.6, 129.3, 128.6, 122.9, 119.1, 90.3, 37.7, 31.3, 25.1, 22.4, 13.9; MS (APSI+) *m/z* found 473.95; $C_{18}H_{21}INO_4S$ (M^+ + H) expected, 474.02.

6.8.2.3.17. 2-Isopropylphenyl 4-isobutyramidobenzenesulfonate (**17**). Method B with triethylamine, 1 day, flash chromatography (hexanes/ethyl acetate (90:10)). Yield: 62%; whitish solid; mp: 125-127 °C; ^{1}H NMR ($CDCl_3$): δ 7.87-7.84 (m, 2H, Ar), 7.79-7.76 (m, 2H, Ar), 7.54 (brs, 1H, NH), 7.33-7.23 (m, 2H, Ar), 7.18-7.12 (m, 1H, Ar), 7.05-7.03 (m, 1H, Ar), 3.24-3.15 (m, 1H, CH), 2.64-2.55 (m, 1H, CH), 1.32 (d, 6H, *J* = 9.2 Hz, 2xCH_3), 1.12 (d, 6H, *J* = 9.2 Hz, 2x CH_3); ^{13}C NMR ($CDCl_3$): δ 175.9, 147.0, 143.5, 141.8, 130.2,

129.8, 127.4, 127.2, 126.7, 121.9, 119.1, 36.8, 26.7, 23.1, 19.4; MS (APSI+) *m/z* found 362.10; $C_{19}H_{24}NO_4S$ (M^+ + H) expected, 362.14.

6.8.2.3.18. 2-Iodophenyl 4-isobutyramidobenzenesulfonate (**18**). Method B with triethylamine, 5 days, flash chromatography (methylene chloride/hexanes (75:25)). Yield: 84%; orange solid; mp: 106-107 °C; ^{1}H NMR ($CDCl_3$): δ 8.10 (s, 1H, NH), 7.82-7.71 (m, 5H, Ar), 7.32-7.26 (m, 2H, Ar), 6.97-6.94 (m, 1H, Ar), 2.61-2.54 (m, 1H, CH), 1.22 (d, 6H, *J* = 6.7 Hz, 2x CH_3); ^{13}C NMR ($CDCl_3$): δ 176.4, 149.8, 144.2, 140.2, 130.2, 129.6, 129.4, 128.6, 122.9, 119.3, 90.3, 36.7, 19.5; MS (APSI+) *m/z* found 445.90; $C_{16}H_{17}INO_4S$ (M^+ + H) expected, 445.99.

6.8.2.3.19. 2-Isopropylphenyl 4-pivalamidobenzenesulfonate (**19**). Method B with triethylamine, 2 days, flash chromatography (hexanes/ethyl acetate (80:20)). Yield: 54%; orange oil; ^{1}H NMR ($CDCl_3$): δ 7.75-7.71 (m, 5H, 4x Ar and NH), 7.26-7.17 (m, 2H, Ar), 7.10-7.04 (m, 1H, Ar), 6.96-6.94 (m, 1H, Ar), 3.15-3.11 (m, 1H, CH), 1.30 (s, 9H, 3x CH_3), 1.05 (d, 6H, *J* = 6.9 Hz, 2x CH_3); ^{13}C NMR ($CDCl_3$): δ 177.2, 147.0, 143.5, 141.8, 130.3, 129.7, 127.4, 127.2, 126.7, 121.8, 119.4, 40.0, 27.5, 26.7, 23.1; MS (APSI+) *m/z* found 376.05; HRMS (ESI) *m/z* found 376.1576; $C_{20}H_{26}NO_4S$ (M^+ + H) expected, 376.1583.

6.8.2.3.20. 2-Iodophenyl 4-pivalamidobenzenesulfonate (**20**). Method B without base, 2 days, flash chromatography (methylene chloride to methylene chloride/ethyl acetate (95:5)). Yield: 74%; yellowish solid; mp: 174-175 °C; ^{1}H NMR ($CDCl_3$): δ 7.84-7.82 (m, 2H, Ar), 7.75-7.72 (m, 3H, Ar), 7.64 (s, 1H, NH), 7.34-7.29 (m, 2H, Ar), 6.99-6.95 (m, 1H, Ar), 1.32 (s, 9H, 3x CH_3); ^{13}C NMR ($CDCl_3$): δ 177.1, 149.9, 143.8, 140.1, 130.2, 129.9, 129.6, 128.5, 123.0, 119.3, 90.3, 40.0, 27.5; MS (APSI+) *m/z* found 459.95; $C_{17}H_{19}INO_4S$ (M^+ + H) expected, 460.01.

6.8.2.3.21. 2-Isopropylphenyl 4-(2-chloroacetamido)benzenesulfonate (**21**). Method B with potassium carbonate, 1 day, flash chromatography (methylene chloride/methanol (95:5)). Yield: 96%; white solid; mp: 151-153 °C; ^{1}H NMR ($CDCl_3$): δ 8.46 (brs, 1H, NH), 7.88-7.85 (m, 2H, Ar), 7.77-7.75 (m, 2H, Ar), 7.28-7.21 (m, 2H, Ar), 7.13-7.09 (m, 1H, Ar), 7.02-7.00 (m, 1H, Ar), 4.23 (s, 2H, CH_2), 3.17-3.07 (m, 1H, CH), 1.07 (d, 6H, *J* = 6.9 Hz, 2x CH_3); ^{13}C NMR ($CDCl_3$): δ 164.2, 146.9, 141.9, 141.7, 131.8, 129.9, 127.4, 127.2, 126.7,

121.9, 119.5, 42.8, 26.7, 23.1; MS (APSI+) *m/z* found 368.05; $C_{17}H_{19}ClNO_4S$ (M^+ + H) expected, 368.07.

6.8.2.3.22. 2-Iodophenyl 4-(2-chloroacetamido)benzenesulfonate (**22**). Method B with potassium carbonate, 5 days, flash chromatography (methylene chloride/hexanes (50/50) to methylene chloride/hexane (75:25)). Yield: 73%; white solid; mp: 110-111 °C; ^{1}H NMR ($CDCl_3$): δ 8.56 (s, 1H, NH), 7.87-7.85 (m, 2H, Ar), 7.77-7.71 (m, 3H, Ar), 7.34-7.26 (m, 2H, Ar), 6.98-6.95 (m, 1H, Ar), 4.20 (s, 2H, CH_2); ^{13}C NMR ($CDCl_3$): δ 164.5, 149.8, 142.5, 140.2, 131.0, 130.3, 129.7, 128.6, 123.0, 119.6, 90.2, 42.9; MS (APSI+) *m/z* found 451.90; $C_{14}H_{12}ClINO_4S$ (M^+ + H) expected, 451.92.

6.8.2.3.23. 2-Isopropylphenyl 4-(3-chloropropanamido)benzenesulfonate (**23**). Method B with potassium carbonate, 3 days, flash chromatography (hexanes/methylene chloride (50:50) to (20:80)). Yield: 52%; white solid; mp: 119-120 °C; ^{1}H NMR ($CDCl_3$): δ 7.84-7.82 (m, 2H, Ar), 7.73-7.71 (m, 2H, Ar), 7.60 (brs, 1H, NH), 7.28-7.20 (m, 2H, Ar), 7.13-7.09 (m, 1H, Ar), 7.02-7.00 (m, 1H, Ar), 3.88 (t, 2H, *J* = 6.3 Hz, CH_2), 3.15-3.08 (m, 1H, CH), 2.87 (t, 2H, *J* = 6.3 Hz, CH_2), 1.07 (d, 6H, *J* = 6.9 Hz, 2x CH_3); ^{13}C NMR ($CDCl_3$): δ 168.3, 146.9, 142.8, 141.8, 130.9, 129.8, 127.5, 127.3, 126.7, 121.9, 119.4, 40.5, 39.4, 26.8, 23.1; MS (APSI+) *m/z* found 382.05; HRMS (ESI) *m/z* found 382.0874; $C_{18}H_{21}ClNO_4S$ (M^+ + H) expected, 382.0881.

6.8.2.3.24. 2-Iodophenyl 4-(3-chloropropanamido)benzenesulfonate (**24**). Method B with potassium carbonate, 5 days, flash chromatography (methylene chloride/hexanes (75:25) to methylene chloride). Yield: 38%; whitish solid; mp: 143-144 °C; ^{1}H NMR ($CDCl_3$): δ 7.89-7.86 (m, 2H, Ar), 7.76-7.71 (m, 3H, Ar), 7.55 (s, 1H, NH), 7.34-7.25 (m, 2H, Ar), 7.01-6.95 (m, 1H, Ar), 3.89 (t, 2H, *J* = 6.3 Hz, CH_2), 2.87 (t, 2H, *J* = 6.3 Hz, CH_2); ^{13}C NMR ($CDCl_3$): δ 168.2, 150.0, 143.1, 140.2, 130.6, 130.4, 129.6, 128.5, 123.1, 119.3, 90.2, 40.7, 39.4; MS (APSI+) *m/z* found 465.90; HRMS (ESI) *m/z* found 465.9354; $C_{15}H_{14}ClINO_4S$ (M^+ + H) expected, 465.9377.

6.8.2.3.25. 2-Isopropylphenyl 4-(4-chlorobutanamido)benzenesulfonate (**25**). Method B with potassium carbonate, 3 days, flash chromatography (hexanes/methylene chloride (50:50). Yield: 70%; brown oil; ^{1}H NMR ($CDCl_3$): δ 8.65-8.56 (brs, 1H, NH), 7.78-

7.74 (m, 4H, Ar), 7.26-7.18 (m, 2H, Ar), 7.10-7.06 (m, 1H, Ar), 7.01-6.99 (m, 1H, Ar), 3.60-3.57 (m, 2H, CH_2), 3.13-3.07 (m, 1H, CH), 2.59 (t, 2H, J = 7.0 Hz, CH_2), 2.16-2.12 (m, 2H, CH_2), 1.03 (d, 6H, J = 6.8 Hz, 2x CH_3); ^{13}C NMR ($CDCl_3$): δ 171.4, 146.8, 143.8, 143.8, 141.7, 129.7, 127.6, 127.3, 126.8, 121.8, 119.3, 44.3, 34.2, 27.7, 26.8, 23.1; MS (APSI+) *m/z* found 396.00 $C_{19}H_{23}ClNO_4S$ (M^+ + H) expected, 396.10.

6.8.2.3.26. 2-Iodophenyl 4-(4-chlorobutanamido)benzenesulfonate (**26**). Method B with potassium carbonate, 5 days, flash chromatography (methylene chloride). Yield: 79%; orange oil; ^{1}H NMR ($CDCl_3$): δ 8.16 (s, 1H, NH), 7.83-7.71 (m, 5H, Ar), 7.34-7.25 (m, 2H, Ar), 6.99-6.93 (m, 1H, Ar), 3.63 (t, 2H, J = 8.0 Hz, CH_2), 2.63-2.58 (m, 2H, CH_2), 2.21-2.12 (m, 2H, CH_2); ^{13}C NMR ($CDCl_3$): δ 171.0, 149.8, 143.9, 140.2, 130.3, 129.7, 129.5, 128.7, 122.9, 119.2, 90.3, 44.4, 34.2, 27.6; MS (APSI+) *m/z* found 479.90; $C_{16}H_{16}ClINO_4S$ (M^+ + H) expected, 479.95.

6.8.2.4. General preparation of compounds 27-38

Method C. The relevant isocyanate was added to a solution of the appropriate aniline (**43** or **44**) in acetonitrile (3 mL) with potassium carbonate (1.0 Eq.). The reaction mixture was stirred at room temperature for 1-2 days. After completion of the reaction, the solvent was evaporated under reduced pressure, the mixture was diluted with in AcOEt (10 mL) and was washed successively with water (10 mL) and brine (10 mL), dried over sodium sulfate, filtered and evaporated to dryness under reduced pressure. The residue was purified by flash chromatography on silica gel or by recrystallization.

Method D. The relevant isocyanate was added to a solution of the appropriate aniline (**43** or **44**) in acetonitrile (3 mL) with potassium carbonate (1.0 Eq.). The reaction mixture was stirred at 100 °C for 4-5 days under pressure. After completion of the reaction, the solvent was evaporated under reduced pressure, the mixture was diluted with in AcOEt (10 mL) and was washed successively with water (10 mL) and brine (10 mL), dried over sodium sulfate, filtered and evaporated to dryness under reduced pressure. The residue was purified by flash chromatography on silica gel.

Method E. The relevant isocyanate was added to a solution of the appropriate aniline (**43** or **44**) in acetonitrile (3 mL) with potassium carbonate (1.0 Eq.). The reaction mixture was stirred at 110 °C for 2 h under microwaves. After completion of the reaction, the solvent was evaporated under reduced pressure, the mixture was diluted with in AcOEt (10 mL) and was washed successively with water (10 mL) and brine (10 mL), dried over sodium sulfate, filtered and evaporated to dryness under reduced pressure. The residue was purified by flash chromatography on silica gel or by recrystallization.

6.8.2.5. Characterization of Compounds 27-38

6.8.2.5.1. 2-Isopropylphenyl 4-(3-ethylureido)benzenesulfonate (**27**). Method C, 2 days, flash chromatography (hexanes/ethyl acetate (90:10)). Yield: 39%; white solid; mp: 141-142 °C; ^{1}H NMR ($CDCl_3$): δ 8.06-8.01 (m, 1H, NH), 7.71-7.69 (m, 2H, Ar), 7.53-7.51 (m, 2H, Ar), 7.26-7.18 (m, 2H, Ar), 7.09-7.05 (m, 1H, Ar), 6.99-6.97 (m, 1H, Ar), 5.69 (brs, 1H, NH), 3.29-3.21 (m, 2H, CH_2), 3.15-3.08 (m, 1H, CH), 1.09 (t, 3H, J = 7.2 Hz, CH_3), 1.04 (d, 6H, J = 6.8 Hz, 2x CH_3); ^{13}C NMR ($CDCl_3$): δ 155.2, 146.8, 145.5, 141.7, 129.8, 127.6, 127.5, 127.3, 126.7, 121.8, 117.8, 35.0, 26.7, 23.1, 15.1; MS (APSI+) *m/z* found 363.10; HRMS (ESI) *m/z* found 363.1374; $C_{18}H_{23}N_2O_4S$ (M^+ + H) expected, 363.1379.

6.8.2.5.2. 2-Iodophenyl 4-(3-ethylureido)benzenesulfonate (**28**). Method C, 1 day, multi-solvent recrystallization (ethyl acetate/hexanes until precipitation). Yield: 18%; white solid; mp: 130-131 °C; ^{1}H NMR ($CDCl_3$/CD_3OD): δ 7.60-7.54 (m, 3H, Ar), 7.41-7.37 (m, 2H, Ar), 7.18-7.08 (m, 2H, Ar), 6.83-6.78 (m, 1H, Ar), 3.07 (q, 2H, J = 7.2 Hz, CH_2), 0.98 (t, 3H, J = 7.2 Hz, CH_3); ^{13}C NMR ($CDCl_3$/CD_3OD): δ 155.4, 149.9, 146.1, 139.9, 130.1, 129.3, 128.2, 126.5, 122.7, 117.1, 90.1, 34.4, 14.7; MS (APSI+) *m/z* found 446.90; HRMS (ESI) *m/z* found 446.9864; $C_{15}H_{16}IN_2O_4S$ (M^+ + H) expected, 446.9876.

6.8.2.5.3. 2-Isopropylphenyl 4-(3-propylureido)benzenesulfonate (**29**). Method C, 1 day, flash chromatography (hexanes to hexanes/ethyl acetate (80:20)). Yield: 30%; colorless oil; ^{1}H NMR ($CDCl_3$): δ 7.83 (s, 1H, NH), 7.71-7.69 (m, 2H, Ar), 7.53-7.51(m, 2H, Ar), 7.26-7.18 (m, 2H, Ar), 7.09-7.05 (m, 1H, Ar), 6.99-6.97 (m, 1H, Ar), 5.60 (brs, 1H, NH), 3.19-3.09 (m, 3H, CH and CH_2), 1.53-1.44 (m, 2H, CH_2), 1.05 (d, 6H, J = 6.9 Hz, 2x CH_3), 0.88 (t, 3H, J = 7.4 Hz, CH_3); ^{13}C NMR ($CDCl_3$): δ 155.2, 146.8, 145.4, 141.7, 129.8, 127.7,

127.5, 127.3, 126.7, 121.8, 117.8, 42.0, 26.7, 23.1, 23.1, 11.3; MS (APSI+) *m/z* found 377.10; HRMS (ESI) *m/z* found 377.1532; $C_{19}H_{25}N_2O_4S$ (M^+ + H) expected, 377.1536.

6.8.2.5.4. 2-Iodophenyl 4-(3-propylureido)benzenesulfonate (**30**). Method C, 1 day, flash chromatography (hexanes to hexanes/ethyl acetate (80:20)). Yield: 12%; white solid; mp: 101-102 °C; ^{1}H NMR ($CDCl_3$): δ 7.97 (s, 1H, NH), 7.77-7.72 (m, 3H, Ar), 7.55-7.52 (m, 2H, Ar), 7.34-7.25 (m, 2H, Ar), 7.00-6.94 (m, 1H, Ar), 5.83-5.60 (brs, 1H, NH), 3.20 (t, 2H, CH_2), 1.57-1.45 (m, 2H, CH_2), 0.89 (t, 3H, *J* = 9.7 Hz, CH_3); ^{13}C NMR ($CDCl_3$): δ 155.3, 149.8, 145.8, 140.2, 130.4, 129.7, 128.7, 127.2, 122.9, 117.9, 90.4, 42.0, 23.2, 11.4; MS (APSI+) *m/z* found 460.90; $C_{16}H_{18}IN_2O_4S$ (M^+ + H) expected, 461.00.

6.8.2.5.5. 2-Isopropylphenyl 4-(3-pentylureido)benzenesulfonate (**31**). Method D, 5 days, flash chromatography (hexanes to hexanes/ethyl acetate (80:20)). Yield: 35%; white sticky solid; ^{1}H NMR ($CDCl_3$): δ 7.98 (brs, 1H, NH), 7.71-7.69 (m, 2H, Ar), 7.54-7.52 (m, 2H, Ar), 7.26-7.18 (m, 2H, Ar), 7.09-7.05 (m, 1H, Ar), 6.99-6.97 (m, 1H, Ar), 5.69 (brs, 1H, NH), 3.22-3.09 (m, 3H, CH and CH_2), 1.48-1.45 (m, 2H, CH_2), 1.31-1.19 (m, 4H, 2x CH_2), 1.05 (d, 6H, *J* = 6.8 Hz, 2x CH_3), 0.84-0.81 (m, 3H, CH_3); ^{13}C NMR ($CDCl_3$): δ 155.3, 146.8, 145.5, 141.7, 129.8, 127.6, 127.5, 127.3, 126.7, 121.8, 117.8, 40.3, 29.6, 29.0, 26.7, 23.1, 22.3, 14.0; MS (APSI+) *m/z* found 405.10; $C_{21}H_{29}N_2O_4S$ (M^+ + H) expected, 405.18.

6.8.2.5.6. 2-Iodophenyl 4-(3-pentylureido)benzenesulfonate (**32**). Method D, 5 days, flash chromatography (hexanes to hexanes/ethyl acetate (80:20)). Yield: 56%; white sticky solid; ^{1}H NMR ($CDCl_3$): δ 7.92 (s, 1H, NH), 7.78-7.72 (m, 3H, Ar), 7.56-7.53 (m, 2H, Ar), 7.34-7.25 (m, 2H, Ar), 7.00-6.94 (m, 1H, Ar), 5.66 (brs, 1H, NH), 3.23 (t, 2H, *J* = 7.1 Hz, CH_2), 1.53-1.44 (m, 2H, CH_2), 1.31-1.24 (m, 4H, 2x CH_2), 0.87-0.82 (m, 3H, CH_3); ^{13}C NMR ($CDCl_3$): δ 155.2, 149.8, 145.8, 140.2, 130.4, 129.7, 128.7, 127.2, 122.9, 117.8, 90.4, 40.3, 29.6, 29.0, 22.4, 14.0; MS (APSI+) *m/z* found 489.00; $C_{18}H_{22}IN_2O_4S$ (M^+ + H) expected, 489.03.

6.8.2.5.7. 2-Isopropylphenyl 4-(3-(3-chloropropyl)ureido)benzenesulfonate (**33**). Method D, 4 days, flash chromatography (hexanes/ethyl acetate (75:25). Yield: 75%; whitish solid; mp: 115-117 °C; ^{1}H NMR ($CDCl_3$): δ 7.73-7.71 (m, 2H, Ar), 7.52-7.50 (m, 2H, Ar), 7.41 (brs, 1H, NH), 7.26-7.19 (m, 2H, Ar), 7.11-7.07 (m, 1H, Ar), 7.00-6.98 (m, 1H, Ar),

5.43-5.41 (m, 1H, NH), 3.59 (t, 2H, *J* = 6.0 Hz, CH_2), 3.44-3.39 (m, 2H, CH_2), 3.17-3.10 (m, 1H, CH), 2.02-1.96 (m, 2H, CH_2), 1.06 (d, 6H, *J* = 6.8 Hz, 2x CH_3); ^{13}C NMR ($CDCl_3$): δ 154.8, 146.9, 145.1, 141.7, 129.8, 128.0, 127.5, 127.3, 126.7, 121.8, 117.9, 42.4, 37.6, 32.3, 26.7, 23.1; MS (APSI+) *m/z* found 411.10; HRMS (ESI) *m/z* found 411.1144; $C_{19}H_{24}ClN_2O_4S$ (M^+ + H) expected, 411.1146.

6.8.2.5.8. 2-Iodophenyl 4-(3-(3-chloropropyl)ureido)benzenesulfonate (**34**). Method C, 2 days, flash chromatography (hexanes/ethyl acetate (80:20)). Yield: 22%; colorless oil; ^1H NMR ($CDCl_3$): δ 8.03 (s, 1H, NH), 7.74-7.70 (m, 3H, Ar), 7.53-7.50 (m, 2H, Ar), 7.32-7.21 (m, 2H, Ar), 6.98-6.92 (m, 1H, Ar), 3.56 (t, 2H, *J* = 6.2 Hz, CH_2), 3.39 (t, 2H, *J* = 6.5 Hz, CH_2), 2.00-1.92 (m, 2H, CH_2); ^{13}C NMR ($CDCl_3$): δ 155.3, 149.7, 145.6, 140.2, 130.3, 129.7, 128.7, 127.3, 122.8, 118.0, 90.4, 42.4, 37.5, 32.3; MS (APSI+) *m/z* found 494.95; HRMS (ESI) *m/z* found 494.9624; $C_{16}H_{17}ClIN_2O_4S$ (M^+ + H) expected, 494.9643.

6.8.2.5.9. 2-Iodophenyl 4-(3-cyclopropylureido)benzenesulfonate (**35**). Method D, 4 days, flash chromatography (methylene chloride). Yield: 27%; colorless oil; ^1H NMR ($CDCl_3$): δ 7.82-7.74 (m, 3H, Ar), 7.63-7.56 (m, 3H, Ar and NH), 7.37-7.30 (m, 2H, Ar), 7.01-6.95 (m, 1H, Ar), 2.66-2.60 (m, 1H, CH), 0.90-0.83 (m, 2H, CH_2), 0.69-0.63 (m, 2H, CH_2); ^{13}C NMR ($CDCl_3$): δ 156.6, 149.9, 145.8, 140.0, 130.2, 129.5, 128.4, 127.0, 122.8, 117.5, 90.2, 22.2, 6.6; MS (APSI+) *m/z* found 458.95; $C_{16}H_{16}IN_2O_4S$ (M^+ + H) expected, 458.99.

6.8.2.5.10. 2-Isopropylphenyl 4-(3-cyclopentylureido)benzenesulfonate (**36**). Method E, 2 hours, flash chromatography (hexanes/ethyl acetate (90:10)). Yield: 9%; colorless oil; ^1H NMR ($CDCl_3$): δ 7.72-7.69 (m, 2H, Ar), 7.53-7.50 (m, 2H, Ar), 7.46 (brs, 1H, NH), 7.28-7.18 (m, 2H, Ar), 7.11-7.05 (m, 1H, Ar), 6.99-6.96 (m, 1H, Ar), 4.13-4.04 (m, 1H, CH), 3.18-3.09 (m, 1H, CH), 2.01-1.89 (m, 2H, CH_2), 1.66-1.54 (m, 4H, 2x CH_2), 1.44-1.35 (m, 2H, CH_2), 1.05 (d, 6H, *J* = 6.9 Hz, 2x CH_3); ^{13}C NMR ($CDCl_3$): δ 154.4, 146.9, 145.3, 141.8, 129.8, 127.8, 127.5, 127.3, 126.7, 121.9, 117.8, 52.1, 33.3, 26.7, 23.5, 23.1; MS (APSI+) *m/z* found 403.10; $C_{21}H_{27}N_2O_4S$ (M^+ + H) expected, 403.17.

6.8.2.5.11. 2-Isopropylphenyl 4-(3-(cyclopentylmethyl)ureido)benzenesulfonate (**37**). Method E, 2 hours, flash chromatography (hexanes/ethyl acetate (85:15)). Yield: 16%;

colorless oil; ^{1}H NMR ($CDCl_3$): δ 7.73-7.70 (m, 2H, Ar), 7.53-7.50 (m, 2H, Ar), 7.28-7.18 (m, 3H, Ar and NH), 7.12-7.06 (m, 1H, Ar), 7.00-6.97 (m, 1H, Ar), 3.19-3.09 (m, 3H, CH and CH_2), 2.07-1.97 (m, 1H, CH), 1.78-1.68 (m, 2H, CH_2), 1.63-1.50 (m, 4H, 2x CH_2), 1.25-1.11 (m, 2H, CH_2), 1.06 (d, 6H, *J* = 6.9 Hz, 2x CH_3); ^{13}C NMR ($CDCl_3$): δ 154.7, 146.9, 145.1, 141.8, 129.8, 128.0, 127.4, 127.2, 126.7, 121.9, 117.9, 45.3, 39.9, 30.3, 26.7, 25.2, 23.1; MS (APSI+) *m/z* found 417.10; $C_{22}H_{29}N_2O_4S$ (M^+ + H) expected, 417.18.

6.8.2.5.12. 2-Iodophenyl 4-(3-(cyclopentylmethyl)ureido)benzenesulfonate (**38**). Method E, 2 hours, multi-solvent recrystallization (methylene chloride/hexanes until precipitation). Yield: 7%; colorless oil; ^{1}H NMR (CD_3OD): δ 7.81-7.71 (m, 3H, Ar), 7.59-7.55 (m, 2H, Ar), 7.41-7.29 (m, 2H, Ar), 7.04-6.99 (m, 1H, Ar), 3.14 (d, 2H, *J* = 7.2 Hz, CH_2), 2.13-2.03 (m, 1H, CH), 1.84-1.73 (m, 2H, CH_2), 1.70-1.55 (m, 4H, 2x CH_2), 1.31-1.22 (m, 2H, CH_2); ^{13}C NMR (CD_3OD): δ 155.8, 150.2, 146.3, 140.0, 130.0, 129.3, 128.1, 126.9, 122.6, 117.1, 89.8, 44.3, 39.9, 29.8, 24.8; MS (APSI+) *m/z* found 500.95; $C_{19}H_{22}IN_2O_4S$ (M^+ + H) expected, 501.03.

6.8.2.6. General preparation of compounds 39-41

The relevant 2-iodophenol or 2-isopropylphenol was added to a solution of a 3- or 4-nitrobenzenesulfonyl chloride in ethyl acetate or methylene chloride (50 mL) in presence of triethylamine (1.5 Eq.). The reaction mixture was stirred at room temperature for 1-2 days. After completion of the reaction, the solvent was evaporated under reduced pressure, the mixture was diluted in AcOEt (50 mL) and was washed successively with water (50 mL) and brine (50 mL), dried over sodium sulfate, filtered and evaporated to dryness under reduced pressure. The residue was purified by recrystallization or by flash chromatography on silica gel.

6.8.2.7. Characterization of Compounds 39-41

6.8.2.7.1. 2-Isopropylphenyl 3-nitrobenzenesulfonate (**39**). Methylene chloride, 1 day, flash chromatography (hexanes/ethyl acetate (90:10)). Yield: 66%; pale yellow oil; ^{1}H NMR ($CDCl_3$): δ 8.75-8.74 (m, 1H, Ar), 8.56-8.52 (m, 1H, Ar), 8.24-8.20 (m, 1H, Ar), 7.82-7.77 (m, 1H, Ar), 7.32-7.24 (m, 2H, Ar), 7.18-7.13 (m, 1H, Ar), 7.04-7.02 (m, 1H, Ar), 3.16-

3.02 (m, 1H, CH), 1.08 (d, 6H, J = 6.9 Hz, 2x CH_3); ^{13}C NMR ($CDCl_3$): δ 148.2, 146.6, 141.5, 138.1, 133.8, 130.8, 128.6, 128.0, 127.6, 127.0, 123.6, 121.7, 26.9, 23.1.

6.8.2.7.2. 2-Isopropylphenyl 4-nitrobenzenesulfonate (**40**). Ethyl acetate, 2 days, recrystallization in ethanol. Yield: 85%; white solid; mp: 101-103 °C; ^1H NMR ($CDCl_3$): δ 8.42-8.37 (m, 2H, Ar), 8.12-8.08 (m, 2H, Ar), 7.32-7.23 (m, 2H, Ar), 7.17-7.11 (m, 1H, Ar), 7.01-6.97 (m, 1H, Ar), 3.15-3.01 (m, 1H, CH), 1.08 (d, 6H, J = 6.9 Hz, 2x CH_3); ^{13}C NMR ($CDCl_3$): δ 150.9, 146.7, 141.7, 141.6, 129.8, 127.9, 127.6, 127.0, 124.4, 121.7, 26.9, 23.1.

6.8.2.7.3. 2-Iodophenyl 4-nitrobenzenesulfonate (**41**). Methylene chloride, 1 day, flash chromatography (hexanes/ethyl acetate (95:5)). Yield: 68%; white solid; mp: 108-110 °C; ^1H NMR ($CDCl_3$): δ 8.40-8.38 (m, 2H, Ar), 8.14-8.12 (m, 2H, Ar), 7.78-7.76 (m, 1H, Ar), 7.41-7.40 (m, 2H, Ar), 7.05-7.02 (m, 1H, Ar); ^{13}C NMR ($CDCl_3$): δ 151.2 149.5, 141.3, 140.3, 130.3, 129.9, 129.1, 124.4, 123.2, 89.6.

6.8.2.8. General preparation of compounds 42-44

The relevant phenyl nitrobenzenesulfonate **39-41** was added to a solution of iron powder (6 Eq.) and concentrated hydrochloric acid (1 mL) in a mixture of ethanol 95% and water (10:1, 150 mL). The reaction mixture was reflux one day. After completion of the reaction, the solvent was evaporated under reduced pressure, the mixture was diluted in AcOEt (75 mL) and was washed successively with a saturated solution of sodium bicarbonate (75 mL) and brine (75 mL), dried over sodium sulfate, filtered and evaporated to dryness under reduced pressure. The residue was purified by flash chromatography on silica gel or by recrystallization in methylene chloride.

6.8.2.9. Characterization of Compounds 42-44

6.8.2.9.1. 2-Isopropylphenyl 3-aminobenzenesulfonate (**42**). Method A, 1 day, flash chromatography (hexanes/ethyl acetate (95:5)). Yield: 68%; pale solid; mp: 87-89 °C; ^1H NMR ($CDCl_3$): δ 7.30-7.19 (m, 4H, Ar), 7.14-7.02 (m, 3H, Ar), 6.92-6.88 (m, 1H, Ar), 3.93 (brs, 2H, NH_2), 3.21-3.07 (m, 1H, CH), 1.07 (d, 6H, J = 6.9 Hz, 2x CH_3); ^{13}C NMR ($CDCl_3$): δ 147.2, 147.1, 141.8, 136.9, 130.0, 127.2, 127.1, 126.6, 122.0, 120.0, 117.8, 113.7, 26.6, 23.1.

6.8.2.9.2. 2-Isopropylphenyl 4-aminobenzenesulfonate (**43**). Method A, 1 day, flash chromatography (hexanes/methylene chloride (70:30)). Yield: 96%; pale orange solid; mp: 108-112 °C; ^{1}H NMR ($CDCl_3$): δ 7.60-7.57 (m, 2H, Ar), 7.27-7.12 (m, 2H, Ar), 7.13-7.03 (m, 2H, Ar), 6.66-6.63 (m, 2H, Ar), 4.31 (brs, 2H, NH_2), 3.20-3.11 (m, 1H, CH), 1.06 (d, 6H, J = 6.9 Hz, 2x CH_3); ^{13}C NMR ($CDCl_3$): δ 151.8, 147.1, 141.9, 130.6, 127.1, 127.0, 126.5, 123.4, 122.2, 114.0, 26.6, 23.1.

6.8.2.9.3. 2-Iodophenyl 4-aminobenzenesulfonate (**44**). Method A, 1 day, recrystallization in methylene chloride. Yield: 51%; white solid; mp: 109-111 °C; ^{1}H NMR (d_6-DMSO): δ 7.80-7.78 (m, 1H, Ar), 7.42-7.34 (m, 3H, Ar), 7.13-7.11 (m, 1H, Ar), 7.02-6.98 (m, 1H, Ar), 6.58-6.56 (m, 2H, Ar), 6.38 (brs, 2H, NH_2); ^{13}C NMR ($CDCl_3$): δ 155.3, 150.2, 140.3, 131.1, 130.1, 129.0, 122.8, 118.4, 113.1, 92.2.

6.8.3. SwissADME web tool

The free web-based SwissADME tool [24] was used to calculate and predict the physicochemical, pharmacokinetic, drug-likeness and medicinal chemistry properties of PAB-SOs and PUB-SOs **11**, **12**, **13**, **14**, **19**, **23**, **24**, **27**, **28**, **30**, **33** and **34**. The chemical structures of PAB-SO and PUB-SO derivatives were drawn, translated to simplify molecular input line entry specification (SMILES) and analyzed by the SwissADME tool. Briefly, TPSA is calculated from Ertl *et al.* [25]. The CLogP is the average of five predictions (iLOGP [26], XLOGP3 [27], WLOGP [28], MLOGP [29-31] and Silicos-IT Log P [32]). The topological Ali Log S was calculated from Ali *et al.* method [33]. GIA and blood-brain barrier permeability (BBBP) were calculated according to BOILED-Egg model while P-glycoprotein substrate was predicted using support vector machines model (SVM). Drug-likeness predictions were implemented from Lipinski (Pfizer) [31], Ghose [34], Veber (GSK) [35], Egan (Pharmacia) [36] and Muegge (Bayer) [37] filters.

6.9. Acknowledgments

This work was supported by grants from CHU de Quebec Research Center and Natural Sciences and Engineering Research Council of Canada (NSERC, RGPIN-2016-05069). M. Gagné-Boulet is the recipient of studentships from the Fonds de recherche du

Québec-Santé (FRQS) and from Fonds d'enseignement et de recherche of the Faculty of pharmacy of Laval University.

6.10. Appendix E. Supplementary data

Supplementary data related to this article can be found online at https://www.sciencedirect.com/science/article/abs/pii/S022352341830521X?via%3Dihub or in the appendix E.

6.11. References

[1] E. Mazzotti, G.C. Antonini Cappellini, S. Buconovo, R. Morese, A. Scoppola, C. Sebastiani, P. Marchetti, Treatment-related side effects and quality of life in cancer patients, Support. Care Canc. 20 (2012) 2553-2557.

[2] V. Turcotte, S. Fortin, F. Vevey, Y. Coulombe, J. Lacroix, M.F. Côté, J.Y. Masson, R. C.-Gaudreault, Synthesis, biological evaluation, and structure-activity relationships of novel substituted N-phenyl ureidobenzenesulfonate derivatives blocking cell cycle progression in S-phase and inducing DNA double-strand breaks, J. Med. Chem. 55 (2012) 6194-6208.

[3] M. Gagne-Boulet, S. Fortin, J. Lacroix, C.A. Lefebvre, M.F. Côté, R. C.-Gaudreault, Styryl-*N*-phenyl-*N*'-(2-chloroethyl)ureas and styrylphenylimidazolidin-2-ones as new potent microtubule-disrupting agents using combretastatin A-4 as model, Eur. J. Med. Chem. 100 (2015) 34-43.

[4] M. Gagne-Boulet, H. Moussa, J. Lacroix, M.F. Côté, J.Y. Masson, S. Fortin, Synthesis and biological evaluation of novel N-phenyl ureidobenzenesulfonate derivatives as potential anticancer agents. Part 2. Modulation of the ring B, Eur. J. Med. Chem. 103 (2015) 563-573.

[5] W.M. Bonner, C.E. Redon, J.S. Dickey, A.J. Nakamura, O.A. Sedelnikova, S. Solier, Y. Pommier, γH2AX and cancer, Nat. Rev. Canc. 8 (2008) 957-967.

[6] O. Fernandez-Capetillo, A. Lee, M. Nussenzweig, A. Nussenzweig, H2AX: the histone guardian of the genome, DNA Repair 3 (2004) 959-967.

[7] M. Ikeda, A. Kurose, E. Takatori, T. Sugiyama, F. Traganos, Z. Darzynkiewicz, T. Sawai, DNA damage detected with γH2AX in endometrioid adenocarcinoma cell lines, Int. J. Oncol. 36 (2010) 1081-1088.

[8] A.N. Ivashkevich, O.A. Martin, A.J. Smith, C.E. Redon, W.M. Bonner, R.F. Martin, P.N. Lobachevsky, γH2AX foci as a measure of DNA damage: a computational approach to automatic analysis, Mutat. Res. 711 (2011) 49-60.

[9] C.E. Redon, J.S. Dickey, W.M. Bonner, O.A. Sedelnikova, γH2AX as a biomarker of DNA damage induced by ionizing radiation in human peripheral blood lymphocytes and artificial skin, Adv. Space Res. 43 (2009) 1171-1178.

[10] T.T. Paull, E.P. Rogakou, V. Yamazaki, C.U. Kirchgessner, M. Gellert, W.M. Bonner, A critical role for histone H2AX in recruitment of repair factors to nuclear foci after DNA damage, Curr. Biol. 10 (2000) 886-895.

[11] J. Pauty, M.-F. Côté, A. Rodrigue, D. Velic, J.-Y. Masson, S. Fortin, Investigation of the DNA damage response to SFOM-0046, a new small-molecule drug inducing DNA double-strand breaks, Sci. Rep. 6 (2016), 23302.

[12] R. Gomez-Bombarelli, M. Gonzalez-Perez, E. Calle, J. Casado, Potential of the NBP method for the study of alkylation mechanisms: NBP as a DNA-model, Chem. Res. Toxicol. 25 (2012) 1176-1191.

[13] D. Thaens, D. Heinzelmann, A. Bohme, A. Paschke, G. Schuurmann, Chemoassay screening of DNA-reactive mutagenicity with 4-(4-nitrobenzyl)pyridine application to epoxides, oxetanes, and sulfur heterocycles, Chem. Res. Toxicol. 25 (2012) 2092-2102.

[14] T.J. Bardos, N. Datta-Gupta, P. Hebborn, D.J. Triggle, A study of comparative chemical and biological activities of alkylating agents, J. Med. Chem. 8 (1965) 167-174.

[15] National Cancer Institute (NCI/NIH), Developmental therapeutics program human tumor cell line screen. https://dtp.cancer.gov/discovery_development/nci-60/default.htm [accessed May 23, 2017].

[16] D.P. Elder, A. Teasdale, A.M. Lipczynski, Control and analysis of alkyl esters of alkyl and aryl sulfonic acids in novel active pharmaceutical ingredients (APIs), J. Pharmaceut. Biomed. Anal. 46 (2008) 1-8.

[17] D.P. Elder, D.J. Snodin, Drug substances presented as sulfonic acid salts: overview of utility, safety and regulation, J. Pharm. Pharmacol. 61 (2009) 269-278.

[18] R. Gomez-Bombarelli, M. Gonzalez-Perez, J. Arenas-Valganon, I.F. Cespedes-Camacho, E. Calle, J. Casado, DNA-damaging disinfection by products: alkylation mechanism of mutagenic mucohalic acids, Environ. Sci. Technol. 45 (2011) 9009-9016.

[19] M.T. Perez-Prior, J.A. Manso, P. Garcia-Santos Mdel, E. Calle, J. Casado, Alkylating potential of potassium sorbate, J. Agric. Food Chem. 53 (2005) 10244-10247.

[20] S. Glowienke, W. Frieauff, T. Allmendinger, H.J. Martus, W. Suter, L. Mueller, Structure-activity considerations and *in vitro* approaches to assess the genotoxicity of 19 methane-, benzene- and toluenesulfonic acid esters, Mutat. Res. 581 (2005) 23-34.

[21] R. C.-Gaudreault, M.A. Alaui-Jamali, G. Batist, P. Bechard, J. Lacroix, P. Poyet, Lack of cross-resistance to a new cytotoxic arylchloroethyl urea in various drug-resistant tumor cells, Canc. Chemother. Pharmacol. 33 (1994) 489-492.

[22] D.E. Pires, T.L. Blundell, D.B. Ascher, pkCSM: predicting small-molecule pharmacokinetic and toxicity properties using graph-based signatures, J. Med. Chem. 58 (2015) 4066-4072.

[23] F. Cheng, W. Li, Y. Zhou, J. Shen, Z. Wu, G. Liu, P.W. Lee, Y. Tang, admetSAR: a comprehensive source and free tool for assessment of chemical ADMET properties, J. Chem. Inf. Model. 52 (2012) 3099-3105.

[24] A. Daina, O. Michielin, V. Zoete, SwissADME: a free web tool to evaluate pharmacokinetics, drug-likeness and medicinal chemistry friendliness of small molecules, Sci. Rep. 7 (2017) 42717.

[25] P. Ertl, B. Rohde, P. Selzer, Fast calculation of molecular polar surface area as a sum of fragment-based contributions and its application to the prediction of drug transport properties, J. Med. Chem. 43 (2000) 3714-3717.

[26] A. Daina, O. Michielin, V. Zoete, iLOGP: a simple, robust, and efficient description of n-octanol/water partition coefficient for drug design using the GB/SA approach, J. Chem. Inf. Model. 54 (2014) 3284-3301.

[27] XLOGP program, version 3.2.2, Shanghai Institute of Organic Chemistry, Chinese Academy of Sciences.

[28] S.A. Wildman, M.M. Crippen, Prediction of physicochemical parameters by atomic contributions, J. Chem. Inf. Comput. Sci. 39 (1999) 868-873.

[29] I. Moriguchi, H. Shuichi, Q. Liu, I. Nakagome, Y. Matsushita, Simple method of calculating octanol/water partition coefficient, Chem. Pharm. Bull. 40 (1992) 127-130.

[30] I. Moriguchi, H. Shuichi, I. Nakagome, H. Hirano, Comparison of reliability of log P values for drugs calculated by several methods, Chem. Pharm. Bull. 42 (1994) 976-978.

[31] C.A. Lipinski, F. Lombardo, B.W. Dominy, P.J. Feeney, Experimental and computational approaches to estimate solubility and permeability in drug discovery and development settings, Adv. Drug Deliv. Rev. 46 (2001) 3-26.

[32] FILTER-IT program, version 1.0.2, Silicos-it, Wervehof 5B/7, 2110 Wijnegem, Belgium.

[33] J. Ali, P. Camilleri, M.B. Brown, A.J. Hutt, S.B. Kirton, Revisiting the general solubility equation: *in silico* prediction of aqueous solubility incorporating the effect of topographical polar surface area, J. Chem. Inf. Model. 52 (2012) 420-428.

[34] A.K. Ghose, V.N. Viswanadhan, J.J. Wendoloski, A knowledge-based approach in designing combinatorial or medicinal chemistry libraries for drug discovery. 1. A qualitative and quantitative characterization of known drug databases, J. Comb. Chem. 1 (1999) 55-68.

[35] D.F. Veber, S.R. Johnson, H.Y. Cheng, B.R. Smith, K.W. Ward, K.D. Kopple, Molecular properties that influence the oral bioavailability of drug candidates, J. Med. Chem. 45 (2002) 2615-2623.

[36] W.J. Egan, K.M. Merz Jr., J.J. Baldwin, Prediction of drug absorption using multivariate statistics, J. Med. Chem. 43 (2000) 3867-3877.

[37] I. Muegge, S.L. Heald, D. Brittelli, Simple selection criteria for drug-like chemical matter, J. Med. Chem. 44 (2001) 1841-1846.

Chapitre 7. Discussion et perspectives

7.1. Discussion

Le Dr Fortin et son équipe développent depuis plusieurs années de nouvelles familles d'agents anticancéreux, notamment les PIB-SOs et les PUB-SOs [78, 80]. Ils sont formés de deux cycles aromatiques identifiés A et B qui sont reliés entre eux par un groupement sulfonate. D'un côté, les PIB-SOs sont constitués d'un groupement IMZ en position 4 sur le cycle aromatique A ainsi que des groupements halogènes, méthoxyles et de courtes chaînes alkyles sur le cycle aromatique B. D'un autre côté, les PUB-SOs possèdent des groupements alkylurées en position 4 sur le cycle aromatique A et de courtes chaînes alkyles en position 2 sur le cycle aromatique B. Les précédents travaux sur les PUB-SOs ont démontré qu'ils agissaient comme agents antimicrotubules arrêtant la progression du cycle cellulaire en phase G2/M s'ils étaient substitués aux positions 3, 4 et/ou 5 sur le cycle B. [69]. Toutefois, des RSAs plus approfondies sur le cycle aromatique B des PUB-SOs ont mis en évidence qu'une substitution en position 2 sur le cycle aromatique B par de courtes chaînes alkyles modifie leurs propriétés pharmacologiques [87]. Ces résultats indiquent que cette nouvelle famille de PUB-SOs possède potentiellement un nouveau mécanisme d'action et une cible pharmacologique différente.

L'objectif général de mon projet de doctorat était d'étudier les RSAs des PIB-SOs et des PUB-SOs associées à la modification des groupements chimiques sur les cycles aromatiques A et B et du pont sulfonate. C'est dans ce contexte que j'ai amorcé mes travaux de doctorat sur les PIB-SOs et les PUB-SOs. Ces derniers sont respectivement de puissants agents antimicrotubules et des inhibiteurs des mécanismes de réparation et de réplication de l'ADN qui ont été développés avant mon arrivée dans l'équipe de recherche du Dr Fortin. La majorité des modifications apportées à la structure de ces molécules avaient été réalisées sur leur cycle aromatique B. En effet, peu d'études avaient été réalisées sur la section de l'anneau aromatique A et sur le pont sulfonate. Dans ce contexte, j'ai proposé que ces sections moléculaires des PIB-SOs et des PUB-SOs puissent être modifiées par différents groupements bioisostères en conservant à la fois leurs propriétés antiprolifératives et

pharmacologiques. Ces modifications ont été réalisées dans le but d'améliorer les propriétés physicochimiques, pharmacocinétiques et pharmacologiques des PIB-SOs et des PUB-SOs.

7.1.1. Conception des nouveaux dérivés et analogues des PIB-SOs et PUB-SOs

Dans un premier temps, j'ai proposé que le groupement IMZ des PIB-SOs puisse être remplacé par les groupements pyrrolidin-2-one, imidazolidine-2,4-dione, imidazolidine-2,5-dione et éthyle 2-uréidoacétate (chapitres 2 et 3). J'ai sélectionné le groupement pyrolidin-2-one afin de déterminer si le site du C-BS pouvait accommoder des groupements similaires à l'IMZ. Les études en modélisation moléculaire sur les PIB-SOs et les PIB-SAs ont suggéré que la forme des molécules est potentiellement plus importante que les interactions électrostatiques avec le site de liaison. En effet, les travaux réalisés au niveau du C-BS montrent qu'il est particulièrement hydrophobique et qu'il est principalement influencé par les forces de Van der Waals [88]. De plus, je voulais également évaluer si le groupement NH de l'IMZ est essentiel à l'activité biologique des PIB-SOs. Dans un deuxième temps, j'ai substitué le groupement IMZ des PIB-SOs par des groupements imidazolidine-2,4-dione et imidazolidine-2,5-dione afin d'évaluer la possibilité qu'un second groupement carbonyle puisse effectuer des ponts-H additionnels avec le C-BS. Ce design avait pour but d'améliorer l'affinité avec le C-BS tout en maintenant une similitude structurelle avec le groupement IMZ. Le groupement éthyle 2-uréidoacétate a quant à lui été étudié principalement, car j'avais préparé cet intermédiaire de synthèse pour accéder au PID-SOs ayant un groupement imidazolidin-2,5-dione. Bien que ce groupement était peu comparable au groupement IMZ, je voulais évaluer 1) l'espace disponible dans le C-BS pour accommoder ce type de groupement et 2) déterminer si des effets stériques dans le C-BS pouvait être favorables. Finalement, j'ai modifié le groupement sulfonate de certains analogues des PIB-SOs par un groupement sulfonamide afin de valider nos RSA antérieures.

Par la suite, j'ai travaillé à la fois sur le design des PIB-SOs et des PUB-SOs en modifiant le pont sulfonate par un groupement thioéther. De plus, j'ai modifié la section IMZ ainsi que les groupements 2-chloroéthylurée ou éthylurée de l'anneau aromatique A respectivement des PIB-SOs et des PUB-SOs par des groupements butyramide, éthylthiourée et phénylurée (chapitre 4). Tel que mentionné précédemment, le pont sulfonate des PIB-SOs et des PUB-SOs avait été peu étudié auparavant. Il avait été initialement remplacé par un

pont éthènyle *cis* et par un pont sulfonamide. D'un côté, la modification du groupement sulfonate par un pont éthènyle *cis* avait été inspirée par la structure de la CA-4 et de ses analogues [80]. D'un autre côté, la modification du groupement sulfonate des PIB-SOs par un pont sulfonamide a mené à plusieurs dérivés antimicrotubules PIB-SAs qui conservaient à la fois leur activité antiproliférative et leur cible moléculaire, illustrant le bioisostérisme de ces groupements pour cette famille de composés [81]. Néanmoins, le remplacement du pont sulfonate des PUB-SOs par un pont sulfonamide avait découlé en une perte significative à la fois de l'activité antiproliférative et de l'arrêt de la progression du cycle cellulaire en phase S [78]. Ces différents résultats montrent donc l'importance de cette section moléculaire pour l'activité des nouvelles familles de composés. C'est dans ce contexte que j'ai remplacé le groupement sulfonate des PIB-SOs et des PUB-SOs par un groupement thioéther. Cette modification a permis d'évaluer le rôle des atomes d'oxygène du groupement sulfonate dans l'activité biologique des PIB-SOs et des PUB-SOs. En outre, cette modification diminue le nombre de degrés de liberté de la molécule, sa longueur et sa polarité en plus de modifier son électrophilicité et l'angle entre les deux cycles aromatiques. Les groupements butyramide, éthylthiourée et phénylurée modifiant la section de l'aromatique A des PUB-SOs possédant un pont thioéther ont été sélectionnés pour plusieurs raisons. Premièrement, le groupement butyramide a été sélectionné pour évaluer le rôle de l'atome d'azote dans le groupement éthylurée pour l'interaction avec le récepteur. Deuxièmement, j'ai étudié le rôle de l'atome d'oxygène du groupement urée avec sa cible pharmacologique en modifiant le groupement éthylurée par un groupement éthylthiourée afin d'évaluer le bioisostérisme de l'atome de soufre dans ce groupement. Troisièmement, le groupement phénylurée a été utilisé pour déterminer si des interactions aromatique-aromatique sont possibles et envisageables pour améliorer l'activité biologique des nouveaux dérivés et analogues.

La modification des groupements présents sur les PUB-SOs s'est faite en deux temps. Dans un premier temps, les groupements présents sur le cycle B des PUB-SOs ont été remplacés par différents groupements halogènes, alkoxys, alkyles, nitros et cyanos aux positions 2, 3 et/ou 4 (chapitre 5). Ce grand éventail de groupements a été utilisé pour déterminer quelles positions et quelles caractéristiques stériques/électroniques de ces groupements contribuent à l'augmentation de la puissance de l'activité antiproliférative.

Dans un deuxième temps, la modification des substituants du cycle aromatique A des PUB-SOs a été étudiée par une variété de groupements amides aux positions 3 et 4 et par différents groupements urées en position 4 (chapitre 6). Les groupements amides ont été sélectionnés pour évaluer le rôle de l'atome d'azote du groupement urée des PUB-SOs pour l'affinité avec le récepteur. En outre, la position du groupement amide sur le cycle aromatique a été modifiée pour vérifier les RSAs des familles antérieures. Les groupements urées et amides en position 4 ont été substitués par des chaînes alkyles ramifiées, linéaires et par des groupements cycloalkyles pour évaluer la dimension de la poche lipophile du site actif du récepteur [88].

Finalement, plusieurs modifications ont été réalisées sur le cycle aromatique B afin de générer une variété de composés possédant des propriétés différentes dans nos chimiothèques et améliorer leur affinité avec leur cible pharmacologique. Pour les familles de dérivés et analogues aux PIB-SOs, l'anneau aromatique B a été substitué en position 2, 3 et/ou 4 avec plusieurs groupements dont les principaux sont de courtes chaînes alkyles, des méthoxyles et des halogènes. Pour les familles de dérivés et analogues aux PUB-SOs, j'ai utilisé de courts groupements alkyles linéaires et ramifiés, des méthoxyles et des groupements halogènes principalement en position 2 puisque cette position est responsable de l'arrêt de la progression du cycle cellulaire en phase S. Néanmoins, nous avons aussi vérifié les positions 3 et 4 dans plusieurs familles de PUB-SOs afin de valider nos RSAs précédentes.

7.1.2. Préparation et caractérisation chimique des nouveaux dérivés et analogues des PIB-SOs et PUB-SOs

Au cours de mes travaux au doctorat, j'ai synthétisé, purifié et caractérisé plus de 40 intermédiaires de synthèse menant à la préparation de 104 dérivés et analogues de PIB-SOs ainsi que 83 dérivés et analogues de PUB-SOs. Plus spécifiquement, j'ai préparé avec un haut degré de pureté 15 PYB-SOs, 15 PYB-SAs, 22 PID-SOs, 10 EPA-SOs, 7 TPAs, 7 TPTs 21 TPUs, 7 TPIs, 26 PAB-SOs et 57 PUB-SOs. Toutes les nouvelles molécules ont été synthétisées avec les méthodes de la chimie organique classique et purifiées à l'aide de méthodes couramment employées dans le laboratoire du Dr Fortin (p. ex. extraction liquide-liquide et chromatographie éclair). Tous les produits ont été caractérisés par résonance magnétique nucléaire (RMN) du proton (^{1}H) et du carbone 13 (^{13}C). De plus, la masse des

produits finaux a été confirmée par spectrométrie de masse à haute résolution et le point de fusion des solides a été déterminé par un appareil à point de fusion automatique. Finalement, la pureté des composés finaux a été évaluée par UHPLC-UV et était au-dessus de 95%.

7.1.3. Évaluation de l'activité antiproliférative des nouveaux dérivés et analogues des PIB-SOs et PUB-SOs

L'évaluation de l'activité antiproliférative des nouveaux dérivés et analogues des PIB-SOs et des PUB-SOs a été réalisée avec la méthode à la sulforhodamine B du NCI/NIH sur les lignées cellulaires cancéreuses humaines HT-1080 (fibrosarcome), HT-29 (adénocarcinome colorectal), M21 (mélanome) et MCF7 (cancer du sein). Les essais antiprolifératifs ont pour but de réaliser un premier criblage des molécules afin de déterminer la puissance et les RSAs de chaque nouvelle famille de composés. Les premières familles étudiées ont été les PYB-SOs et PYB-SAs analogues et dérivés des PIB-SOs. Les PYB-SOs et les PYB-SAs possèdent une activité antiproliférative s'échelonnant respectivement de 0,0087 à 8,6 μM et 0,056 à 21 μM. Comme dans le cas des PIB-SOs, la substitution du cycle aromatique B en position 3, 3,5 et 3,4,5 est généralement très favorable à l'activité antiproliférative. La substitution du cycle aromatique B par des groupements méthoxyles et halogènes donne les meilleures activités antiprolifératives.

Les secondes familles étudiées étaient les PID-SOs et les EPA-SOs, également des analogues et dérivés des PIB-SOs. Les PID-SOs substitués par le groupement 2,5-dioxoimidazolidin-1-yl et les EPA-SOs montrent généralement des activités antiprolifératives supérieures à 100 μM et ont rapidement été mis de côté. Ces résultats montrent que les groupements éthyle 2-uréidoacétate et imidazolidine-2,5-dione sont possiblement mal adaptés pour interagir adéquatement avec le C-BS. Ces résultats ont probablement été engendrés par des interactions défavorables ou de l'encombrement stérique. Les 15 PID-SOs ayant le groupement 2,4-dioxoimidazolidin-1-yle ont des activités antiprolifératives allant de 0,092 à 14 μM. Les dérivés substitués en positions 3, 3,5 et 3,4,5 sur le cycle aromatique B par des halogènes ou des méthoxyles sont ceux ayant les activités antirolifératives les plus puissantes de manière analogue au PIB-SOs.

Le troisième groupe de molécules étudiées était les TPAs, les TPTs, les TPUs et les TPIs. Les TPAs, les TPTs et les TPUs portant un groupement éthylurée ou phénylurée ont des activités antiprolifératives se situant entre 1,5 µM jusqu'à des valeurs supérieures à 100 µM. Par conséquent, le développement de ces molécules a été interrompu. Les TPUs portant un groupement 2-chloroétylurée ont une activité antiproliférative dans le haut nanomolaire au bas micromolaire (0,71 à 16 µM). À l'exception de deux cas, les TPIs possèdent une activité antiproliférative de la centaine de nanomolaire au bas micromolaire (0,13 à 3,0 µM). De plus, la substitution sur le cycle aromatique B en position 3 par un groupement méthyle ou un atome de chlore génère également les TPUs et les TPIs les plus puissants (0,13 à 1,8 µM). Ces résultats confirment que le pont sulfonate des PIB-SOs et des PUB-SOs peut être remplacé par un pont thioéther lorsque le cycle aromatique A est substitué soit par un groupement imidazolidin-2-one ou 2-chloroéthylurée pour l'inhibition de la prolifération cellulaire tumorale de la centaine de nanomolaire au bas micromolaire.

Les derniers groupes de composés évalués étaient les PAB-SOs et les PUB-SOs portant sur le groupement urée des chaînes alkyles ramifiées, linéaires, halogénoalkyles ou cycloalkyles. Les PUB-SOs substitués en position 4 sur le cycle aromatique A avec le groupement 2-chloroéthylurée ont majoritairement des activités antiprolifératives inférieures à 10 µM. Les PUB-SOs les plus puissants sont ceux substitués en position 2 sur le cycle B avec des groupements alkyles ou halogènes. Les PAB-SOs substitués en position 3 sur le cycle aromatique A ont des activités antiprolifératives moins puissantes (8,2 à >40 µM) que ceux substitués en position 4 (0,60 à 27 µM). En général, les dérivés PUB-SOs (0,14 à 14 µM) ont une activité antiproliférative plus puissante que celle des dérivés PAB-SOs indiquant que le groupement urée est favorable, mais non essentiel pour l'activité anticancéreuse. Les groupements montrant l'activité antiproliférative maximale sont ceux avec les groupements éthylurée et propylamide. Les chaînes halogènoalkyles ou alkyles plus longues ont une activité antiproliférative moins puissante. Ces résultats suggèrent fortement que la liaison au site de liaison est stériquement limitante est que la liaison ne requière pas une addition nucléophile ou d'interactions dipôle-dipôles.

7.1.4. Évaluation du mécanisme d'action, de la toxicité et des propriétés biopharmaceutiques théoriques des dérivés et analogues des PIB-SOs et PUB-SOs les plus prometteurs

Les dérivés et analogues des PIB-SOs et PUB-SOs les plus prometteurs ont été évalués avec les outils de la biologie cellulaire et de la biologie moléculaire en utilisant plusieurs essais biofonctionnels. Les essais biofonctionnels pour les analogues des PIB-SOs comprennent notamment l'évaluation 1) de l'arrêt de la progression du cycle cellulaire, 2) de l'intégrité des microtubules par immunofluorescence, 3) de l'inhibition de la polymérisation des microtubules, 4) de l'affinité avec le C-BS, 5) de leur chimiorésistance sur des cellules résistantes aux agents antimicrotubules et multirésistantes, 6) de leur toxicité chez les embryons de poulet et 7) de plusieurs propriétés physicochimiques et pharmacocinétiques théoriques importantes dans la conception de médicaments. Les essais biofonctionnels pour les analogues des PUB-SOs comprennent notamment l'évaluation 1) de l'arrêt de la progression du cycle cellulaire, 2) de l'induction de H2AX en γH2AX, 3) de leur pouvoir alkylant et 4) de plusieurs propriétés physicochimiques et pharmacocinétiques théoriques.

Les deux premières familles d'agents antimicrotubules qui ont été évaluées biologiquement pour leur mécanisme d'action sont les PYB-SOs et les PYB-SAs. Les dérivés PYB-SOs et PYB-SAs les plus puissants bloquent la progression du cycle cellulaire en phase G2/M de manière similaire à la CA-4. Des essais en immunofluorescence, des essais d'affinité avec la tubuline et des essais de polymérisation *in vitro* avec l'α, β-tubuline ont montré que les PYB-SOs et les PYB-SAs inhibent la polymérisation des microtubules en ciblant le C-BS. De plus, des essais en modélisation moléculaire montrent que les dérivés les plus puissants interagissent et ont une affinité pour le C-BS. Les essais de toxicité effectués sur des embryons de poulets ont mis en évidence peu ou pas de toxicité des PYB-SOs et PYB-SAs dans ce modèle. Finalement, les propriétés biopharmaceutiques théoriques calculées à l'aide de l'algorithme SwissADME ont révélé que les PYB-SOs et les PYB-SAs possèdent des propriétés physicochimiques, pharmacocinétiques et « *drug-like* » théoriques adéquates pour des essais précliniques avancés.

Les PID-SOs portant un groupement 2,4-dioxoimidazolidin-1-yle les plus puissants arrêtent également le cycle cellulaire dans la phase G2/M et perturbent les microtubules en agissant au niveau du C-BS. Par ailleurs, des essais de modélisation moléculaire montrent que les PID-SOs les plus puissants interagissent dans le C-BS. Les PID-SOs ne sont pas ou seulement faiblement affectés par des altérations de l'α, β-tubuline présentes dans les lignées cellulaires cancéreuses résistantes au paclitaxel (CHO-TAX 5-6) ou à la vinblastine (CHO-VV 3-2). De plus, ils sont très faiblement affectés par des cellules de leucémie lymphoblastique T (CEM) surexprimant la glycoprotéine P (CEM-VLB) et possèdent des ratios de résistance (CEM-VLB/CEM) nettement inférieurs par rapport à ceux du paclitaxel et de la vinblastine. Finalement, les propriétés physicochimiques, pharmacocinétiques et « *drug-like* » théoriques ont également été calculées à l'aide de l'algorithme SwissADME et montrent que les PID-SOs les plus puissants possèdent des propriétés biopharmaceutiques théoriques appropriées pour des essais précliniques plus avancés.

Les TPUs portant un groupement 2-chloroéthylurée et les TPIs arrêtent le cycle cellulaire en phase G2/M, perturbent les microtubules en interagissant dans le C-BS et inhibent la polymérisation des microtubules. Il est à noter que les TPUs portant un groupement méthyle et chloro en position 2 n'arrêtent pas le cycle cellulaire en phase S. Dans ce contexte, le remplacement du pont sulfonate par un pont thioéther conserve une activité antiproliférative intéressante, mais perd son activité pharmacologique liée à l'arrêt de la progression du cycle cellulaire en phase S. Par ailleurs, l'activité antiproliférative des TPUs et des TPIs les plus puissantes n'est pas ou n'est que légèrement affectée par des altérations de l'α, β-tubuline des lignées cellulaires cancéreuses résistantes au paclitaxel et à la vinblastine. À l'exception du TPU avec un groupement 3-méthyle, les TPUs et les TPIs ne sont pas ou uniquement légèrement affectés par les cellules de leucémie lymphoblastique T surexprimant la glycoprotéine P. Les essais de toxicité sur les embryons de poulet indiquent que les TPIs avec les groupements 3-méthyle ou 3-chloro ont peu de toxicité sur ce modèle. Pour terminer, les TPUs et TPIs ont des propriétés physicochimiques théoriques adéquates calculées à l'aide de l'algorithme SwissADME pour des essais précliniques plus avancés.

Les PAB-SOs et les nouveaux PUB-SOs les plus puissants arrêtent le cycle cellulaire en phase S et induisent la phosphorylation de H2AX en γH2AX. Les composés avec de

courtes chaînes linéaires et ramifiées alkyles, des groupements halogènes et nitro en position 2 et un groupement hydroxyl en position 4 sur le cycle aromatique B stoppent la progression du cycle cellulaire en phase S [87]. Ces résultats indiquent que ces nouvelles familles de PUB-SOs possèdent potentiellement un nouveau mécanisme d'action et une cible pharmacologique différente. Toutefois, les PAB-SOs et PUB-SOs substitués en position 3, 4 ou 5 sur le cycle B stoppent la progression du cycle cellulaire en phase G2/M. Nous avons aussi évalué leur potentiel alkylant à l'aide de l'essai colorimétrique au 4-(p-nitrobenzyl)pyridine (NBP). En effet, les esters d'alkyle sulfoniques sont considérés comme des agents potentiellement génotoxiques et alkylants dans les systèmes biologiques puisque le groupe sulfonate peut être déplacé par une variété de nucléophiles dont l'ADN. Par ailleurs, les groupements aliphatiques organochlorés sont aussi potentiellement des agents alkylants, car l'atome de chlore peut jouer le rôle de groupe partant en présence d'un nucléophile. Puisque les PAB-SOs et les PUB-SOs possèdent ces groupements, nous avons donc évalué leur potentiel alkylant. Les constantes de taux d'alkylation des PAB-SOs et des PUB-SOs (entre 0,49 et 0,0034 $\times 10^{-3}$/s) sont de faible à très faible et toutes inférieures au chlorambucil (5,3 $\times 10^{-3}$/s) ce qui correspond à des ratios de 11 à 1600 fois moins alkylants que le chlorambucil. Par ailleurs, le potentiel alkylant ne corrèle pas avec l'arrêt du cycle cellulaire en phase S, l'induction de γH2AX ou la nature du groupement sur le cycle A. Ces résultats montrent clairement que le potentiel alkylant n'est lié et n'est pas essentiel à l'activité biologique des PAB-SOs et des PUB-SOs. De plus, les PAB-SOs et les PUB-SOs possèdent des propriétés physicochimiques, pharmacocinétiques et « *drug-like* » prometteuses calculées à l'aide de l'algorithme SwissADME pour des essais précliniques plus poussés.

7.1.5. Modélisation moléculaire

Les PYB-SOs, PYB-SAs et PID-SOs les plus prometteurs ont été évalués avec des essais de modélisation moléculaire dans le C-BS. Ces essais ont permis notamment de déterminer les conformations actives les plus stables de ces composés et d'identifier leurs interactions avec les acides aminés du C-BS. À l'exception d'un composé PID-SO, les résultats indiquent que la structure moléculaire des PYB-SOs, des PYB-SAs et des PID-SOs

permet d'entrer et d'interagir dans le C-BS. Les principales interactions comprennent les donneurs de pont-H, les accepteurs de pont-H et les interactions pi-H.

7.2. Perspectives

Les travaux de ma formation doctorale m'ont permis de mieux comprendre les RSAs de deux familles d'agents anticancéreux développées par notre groupe de recherche. Bien que le fruit de ces travaux soit prometteur, ils ne représentent qu'une infime partie de ce qui doit être réalisé pour qu'un composé soit étudié en clinique et ultimement commercialisé. En effet, le développement de nouveaux médicaments est un processus long, complexe et demandant beaucoup de ressources matérielles, financières et humaines. En moyenne, entre 10 000 et 25 000 nouvelles molécules doivent être synthétisées pour en commercialiser qu'une seule. Néanmoins, mes travaux constituent un premier jalon guidant le chemin pour ouvrir plusieurs avenues de recherche. Ces avenues possibles comprennent notamment 1) le développement de dérivés et analogues aux PIB-SOs et aux PUB-SOs plus hydrosolubles, 2) la poursuite des études pharmacocinétiques et pharmacologiques *in vitro* des composés les plus prometteurs et 3) les études pharmacocinétiques et pharmacologiques *in vivo* des dérivés et analogues aux PIB-SOs et aux PUB-SOs les plus prometteurs.

Les nouveaux dérivés et analogues aux PIB-SOs et aux PUB-SOs possèdent des propriétés intéressantes, mais ils sont limités entre autres par leur solubilité. Dans ce contexte, des travaux importants devront être réalisés sur la formulation de ces composés pour les administrer à des doses appropriées chez des modèles animaux et ultimement chez l'homme. Une autre stratégie envisagée au laboratoire est l'insertion de groupements ionisables afin de concevoir des sels qui seront théoriquement plus hydrosolubles. Finalement, l'architecture moléculaire des PIB-SOs et des PUB-SOs peut encore être étudiée pour moduler les propriétés physicochimiques et biopharmaceutiques de ces composés.

Tel que mentionné précédemment, il reste encore beaucoup de travaux à réaliser afin de bien caractériser les dérivés et analogues aux PIB-SOs et aux PUB-SOs les plus prometteurs. À titre d'exemple, des essais *in vitro* permettant de déterminer leur lipophilicité (log P), leur solubilité, leur stabilité ou leur pka pourraient être effectués. Des essais de stabilité métabolique ou plasmatique, de clairance hépatique, d'induction ou d'inhibition de

cytochromes, de perméabilité et de liaisons aux protéines plasmatiques pourraient aussi être envisagés pour répondre davantage au volet de caractérisation des propriétés pharmacocinétiques. Un profil pharmacocinétique chez un modèle de souris ou de rat pourrait être déterminé avec l'étude des paramètres d'absorption, de biodisponibilité, de distribution, de métabolisation, de voies d'excrétion et de toxicité.

Finalement, j'aimerais mentionner que la *h*DHODH vient d'être identifiée par notre laboratoire comme cible moléculaire des PUB-SOs. L'identification de la cible moléculaire des PUB-SOs ouvre la porte pour une conception rationnelle et l'élaboration de nouveaux PUB-SOs basés sur les molécules anti-*h*DHODH déjà connues ainsi que sur le site actif de cette enzyme. Elle ouvre aussi la porte pour appliquer les PUB-SOs à d'autres maladies que le cancer telles que les maladies auto-immunes (p. ex. polyarthrite rhumatoïde, arthrite psoriasique et sclérose en plaques). Des essais sont en cours au laboratoire pour confirmer que la cible moléculaire de tous les PUB-SOs arrêtant le cycle cellulaire en phase S est bel et bien la *h*DHODH et que ces molécules peuvent être appliquées à d'autres traitements.

Conclusion

En guise de conclusion, les traitements utilisés de nos jours pour soigner les patients atteints d'un cancer ne sont pas encore entièrement efficaces et leur utilisation est associée à des effets secondaires délétères significatifs. C'est pourquoi le développement de nouveaux traitements anticancéreux permettant une amélioration de la survie et de la qualité de vie est primordial. Les nouvelles entités moléculaires que nous avons développées au cours de ma formation doctorale possèdent des propriétés anticancéreuses intéressantes et pourraient éventuellement être utilisées ou servir de modèle pour de nouveaux traitements plus efficaces et moins toxiques. Le développement de ces nouvelles familles d'agents thérapeutiques pourrait éventuellement permettre d'ajouter des outils thérapeutiques supplémentaires à l'arsenal des médecins oncologues pour soigner les patients atteints de cancer. Notre combat contre le cancer ne sera pas, à mon avis, remporté par la découverte ou la mise au point d'un médicament, mais bien par la combinaison de plusieurs traitements, technologies et expertises de chercheurs de différents domaines.

Références

[1] Centre Paul Strauss, Histoire et définition. http://www.centre-paul-strauss.fr/comprendre-le-cancer/histoire-et-definition, (consulté le 28 septembre 2020).

[2] M.D. Freeman, J.M. Gopman, C.A. Salzberg, The evolution of mastectomy surgical technique: from mutilation to medicine, Gland Surg. 7 (2018) 308-315.

[3] W.A. Creasey, Cancer, an introduction, Oxford University Press, 1981.

[4] B.M. Rothschild, D.H. Tanke, M. Helbling, 2nd, L.D. Martin, Epidemiologic study of tumors in dinosaurs, Naturwissenschaften 90 (2003) 495-500.

[5] J. Laszlo, Understanding Cancer, HarperCollins, 1987.

[6] The American Cancer Society medical and editorial content team, Early theories about cancer causes. https://www.cancer.org/cancer/cancer-basics/history-of-cancer/cancer-causes-theories-throughout-history.html, (consulté le 15 septembre 2020).

[7] A. Sudhakar, History of cancer, ancient and modern treatment methods, J. Cancer Sci. Ther. 1 (2009) 1-4.

[8] R.L.K. Virchow, La pathologie cellulaire basée sur l'étude physiologique et pathologique des tissus, J.-B. Baillière et Fils, 1861.

[9] P. Pinell, Naissance d'un fléau. Histoire de la lutte contre le cancer en France (1890-1940), Éditions Métailié, 1992.

[10] G.B. Faguet, A brief history of cancer: age-old milestones underlying our current knowledge database, Int. J. Cancer 136 (2015) 2022-2036.

[11] D.S. Fischer, J.C. Marsh, M.E. Morra, Cancer therapy, G.K. Hall Medical Publishers, 1982.

[12] E. Frei, 3rd, J.F. Holland, M.A. Schneiderman, D. Pinkel, G. Selkirk, E.J. Freireich, R.T. Silver, G.L. Gold, W. Regelson, A comparative study of two regimens of combination chemotherapy in acute leukemia, Blood 13 (1958) 1126-1148.

[13] N.E. Davidson, S.A. Armstrong, L.M. Coussens, M.R. Cruz-Correa, R.J. DeBerardinis, J.H. Doroshow, M. Foti, P. Hwu, T.W. Kensler, M. Morrow, C.G. Mulligan, W. Pao, E.A. Platz, T.J. Smith, C.L. Willman, AACR Cancer Progress Report 2016, 22 (2016) S1-S137.

[14] Société canadienne du cancer, Médecine personnalisée. https://www.cancer.ca/fr-ca/cancer-information/cancer-101/cancer-research/personalized-medicine/?region=on, (consulté le 6 septembre 2020).

[15] P. Krzyszczyk, A. Acevedo, E.J. Davidoff, L.M. Timmins, I. Marrero-Berrios, M. Patel, C. White, C. Lowe, J.J. Sherba, C. Hartmanshenn, K.M. O'Neill, M.L. Balter, Z.R. Fritz, I.P. Androulakis, R.S. Schloss, M.L. Yarmush, The growing role of precision and personalized medicine for cancer treatment, Technology (Singap. World Sci.) 6 (2018) 79-100.

[16] World Health Organization, Cancer. https://www.who.int/en/news-room/fact-sheets/detail/cancer, (consulté le 20 décembre 2019).

[17] C. Tomasetti, L. Li, B. Vogelstein, Stem cell divisions, somatic mutations, cancer etiology, and cancer prevention, Science 355 (2017) 1330-1334.

[18] Société canadienne du cancer, Apprenez à connaître votre environnement. https://www.cancer.ca/fr-ca/prevention-and-screening/reduce-cancer-risk/make-informed-decisions/know-your-environment/?region=mb, (consulté le 15 septembre 2020).

[19] H. Li, J. Hu, X. Luo, A.M. Bode, Z. Dong, Y. Cao, Therapies based on targeting Epstein-Barr virus lytic replication for EBV-associated malignancies, Cancer Sci. 109 (2018) 2101-2108.

[20] M.L. Andréola, V. Parissi, S. Litvak, DNA polymerases: reverse transcriptase integrase, and retrovirus replication, Academic Press, 2013.

[21] M.C. Botelho, J.P. Teixeira, P.A. Oliveira, Carcinogenesis, Academic Press, 2014.

[22] World cancer research Fund, Worldwide cancer data. https://www.wcrf.org/dietandcancer/cancer-trends/worldwide-cancer-data, (consulté le 6 septembre 2020).

[23] International agency for research on cancer, Estimated number of deaths in 2018, worldwide, both sexes, all ages. https://gco.iarc.fr/today/online-analysis-pie?v=2018&mode=cancer&mode_population=continents&population=900&populations=900&key=total&sex=0&cancer=39&type=1&statistic=5&prevalence=0&population_group=0&ages_group%5B%5D=0&ages_group%5B%5D=17&nb_items=7&group_cancer=1&include_nmsc=1&include_nmsc_other=1&half_pie=0&donut=0&population_group_globocan_id=, (consulté le 5 septembre 2020).

[24] Société canadienne du cancer, Vue d'ensemble des statistiques sur le cancer. http://www.cancer.ca/fr-ca/cancer-information/cancer-101/cancer-statistics-at-a-glance/?region=qc, (consulté le 12 mars 2020).

[25] Comité consultatif de la Société canadienne du cancer : Statistiques canadiennes sur le cancer 2019. https://www.cancer.ca/~/media/cancer.ca/CW/cancer%20information/cancer%20101/Canadian%20cancer%20statistics/Canadian-Cancer-Statistics-2019-FR.pdf?la=fr-CA, (consulté le 17 septembre 2020).

[26] N.A. Campbell, J.B. Reece, Biologie, Éditions du renouveau pédagogique inc., 2007.

[27] P. Romé, C. Prigent, R. Giet, Le fuseau mitotique, le centrosome et le cancer : trouvez l'intrus !, Med Sci 26 (2010) 377-383.

[28] C.P.C. De Souza, S.A. Osmani, Mitosis, not just open or closed, Eukaryot. cell 6 (2007) 1521.

[29] J.R. McIntosh, Mitosis, Cold Spring Harb. Perspect. Biol. 8 (2016) a023218.

[30] I.G. Motofei, Biology of cancer; from cellular cancerogenesis to supracellular evolution of malignant phenotype, Cancer Invest. 36 (2018) 309-317.

[31] The American Cancer Society medical and editorial content team, Evolution of cancer treatments: Surgery. https://www.cancer.org/cancer/cancer-basics/history-of-cancer/cancer-treatment-surgery.html, (consulté le 14 septembre 2020).

[32] In memoriam: William Sampson Handley, Ann. R. Coll. Surg. Engl. 30 (1962) 344-346.

[33] R.A. Kazi, R.E. Peter, Christian Albert Theodor Billroth: master of surgery, J. Postgrad. Med. 50 (2004) 82-83.

[34] American Cancer Society, Evolution of Cancer Treatments: Surgery. https://www.cancer.org/cancer/cancer-basics/history-of-cancer/cancer-treatment-surgery.html, (consulté le 20 septembre 2020).

[35] G.C. Barnett, C.M.L. West, A.M. Dunning, R.M. Elliott, C.E. Coles, P.D.P. Pharoah, N.G. Burnet, Normal tissue reactions to radiotherapy: towards tailoring treatment dose by genotype, Nat. Rev. Cancer 9 (2009) 134-142.

[36] R. Baskar, J. Dai, N. Wenlong, R. Yeo, K.-W. Yeoh, Biological response of cancer cells to radiation treatment, Front. Mol. Biosci. 1 (2014) 24-24.

[37] S. Brown, P. Kirkbride, E. Marshall, Radiotherapy in the acute medical setting, Clin. Med. (Lond.) 15 (2015) 382-387.

[38] C. Verry, E. Porcel, C. Chargari, C. Rodriguez-Lafrasse, J. Balosso, Utilisation de nanoparticules comme agent radiosensibilisant en radiothérapie : où en est-on ?, Cancer Radiother. 23 (2019) 917-921.

[39] Société canadienne du cancer, Radiothérapie externe. https://www.cancer.ca/fr-ca/cancer-information/diagnosis-and-treatment/radiation-therapy/external-radiation-therapy/?region=qc, (consulté le 23 avril 2021).

[40] National Cancer Institute, Types of radiation therapy. https://training.seer.cancer.gov/treatment/radiation/types.html, (consulté le 5 septembre 2020).

[41] W.N. Hittelman, Y. Liao, L. Wang, L. Milas, Are cancer stem cells radioresistant?, Future Oncol. 6 (2010) 1563-1576.

[42] M. Gray, A.K. Turnbull, C. Ward, J. Meehan, C. Martínez-Pérez, M. Bonello, L.Y. Pang, S.P. Langdon, I.H. Kunkler, A. Murray, D. Argyle, Development and characterisation of acquired radioresistant breast cancer cell lines, Radiat. Oncol. 14 (2019) 64.

[43] National Cancer Institute, Immunotherapy to treat cancer. https://www.cancer.gov/about-cancer/treatment/types/immunotherapy, (consulté le 2 octobre 2020).

[44] Société canadienne du cancer, Immunothérapie. https://www.cancer.ca/fr-ca/cancer-information/diagnosis-and-treatment/chemotherapy-and-other-drug-therapies/immunotherapy/?region=qc, (consulté le 23 avril 2021).

[45] K. Esfahani, L. Roudaia, N. Buhlaiga, S.V. Del Rincon, N. Papneja, W.H. Miller Jr, A review of cancer immunotherapy: from the past, to the present, to the future, Curr. Oncol. 27 (2019).

[46] Collège national de pharmacologie médicale, Hormonothérapies anticancéreuses : les points essentiels https://pharmacomedicale.org/medicaments/par-specialites/item/hormonotherapies-anticancereuses-les-points-essentiels, (consulté le 4 octobre 2020).

[47] Société canadienne du cancer, Hormonothérapie. https://www.cancer.ca/fr-ca/cancer-information/diagnosis-and-treatment/chemotherapy-and-other-drug-therapies/hormonal-therapy/?region=qc, (consulté le 23 avril 2021).

[48] V.T. DeVita, E. Chu, A history of cancer chemotherapy, Cancer Res. 68 (2008) 8643.

[49] K.K. Kwok, E.C. Vincent, J.N. Gibson, 36 - Antineoplastic Drugs, Mosby, 2017.

[50] R.E. de Lima Procópio, I.R. da Silva, M.K. Martins, J.L. de Azevedo, J.M. de Araújo, Antibiotics produced by Streptomyces, Braz. J. Infect. Dis. 16 (2012) 466-471.

[51] G. Minotti, P. Menna, E. Salvatorelli, G. Cairo, L. Gianni, Anthracyclines: molecular advances and pharmacologic developments in antitumor activity and cardiotoxicity, pharmacol. Rev. 56 (2004) 185.

[52] X. Hui, L. Min, T. Xuan, A review on hemisynthesis, biosynthesis, biological activities, mode of action, and structure-activity relationship of podophyllotoxins: 2003-2007, Curr. Med. Chem. 16 (2009) 327-349.

[53] Z. Franco, D. Sabrina, L. Diletta, B. Giovanni, M. Lucio, P. Graziella, Current status and perspectives in the development of camptothecins, Curr. Pharm. design. 8 (2002) 2505-2520.

[54] G. Kuznetsov, M.J. Towle, H. Cheng, T. Kawamura, K. TenDyke, D. Liu, Y. Kishi, M.J. Yu, B.A. Littlefield, Induction of morphological and biochemical apoptosis following prolonged mitotic blockage by Halichondrin B macrocyclic ketone analog E7389, Cancer Res. 64 (2004) 5760.

[55] A.K. Singla, A. Garg, D. Aggarwal, Paclitaxel and its formulations, Int. J. Pharm. 235 (2002) 179-192.

[56] D.A. Fletcher, R.D. Mullins, Cell mechanics and the cytoskeleton, Nature 463 (2010) 485-492.

[57] G. Wiche, Role of plectin in cytoskeleton organization and dynamics, J. Cell. Sci. 111 (Pt 17) (1998) 2477-2486.

[58] A.L. Risinger, F.J. Giles, S.L. Mooberry, Microtubule dynamics as a target in oncology, Cancer. Treat. Rev. 35 (2009) 255-261.

[59] V.K. Vyas, M. Ghate, Recent developments in the medicinal chemistry and therapeutic potential of dihydroorotate dehydrogenase (DHODH) inhibitors, Mini Rev. Med. Chem. 11 (2011) 1039-1055.

[60] H. Munier-Lehmann, P.-O. Vidalain, F. Tangy, Y.L. Janin, On dihydroorotate dehydrogenases and their inhibitors and uses, J. Med. Chem. 56 (2013) 3148-3167.

[61] L.H. Smith, JR., F.A. Baker, M. Sullivan, Pyrimidine metabolism in man. II. Studies of leukemic cells, Blood 15 (1960) 360-369.

[62] D.L. Dexter, D.P. Hesson, R.J. Ardecky, G.V. Rao, D.L. Tippett, B.A. Dusak, K.D. Paull, J. Plowman, B.M. DeLarco, V.L. Narayanan, M. Forbes, Activity of a novel 4-quinolinecarboxylic acid, NSC 368390 [6-fluoro-2-(2′-fluoro-1,1′-biphenyl-4-yl)-3-methyl-4-quinolinecarboxylic acid sodium salt], against experimental tumors, Cancer Res. 45 (1985) 5563-5568.

[63] J.T. Madak, A. Bankhead, C.R. Cuthbertson, H.D. Showalter, N. Neamati, Revisiting the role of dihydroorotate dehydrogenase as a therapeutic target for cancer, Pharmacol. Therapeut. 195 (2019) 111-131.

[64] Y.D. Fragoso, J.B.B. Brooks, Leflunomide and teriflunomide: altering the metabolism of pyrimidines for the treatment of autoimmune diseases, Expert Rev. Clin. Phar. 8 (2015) 315-320.

[65] U.S. National Library of Medicine, Phase 2 dose-finding IMU-838 for ulcerative colitis (CALDOSE-1). https://clinicaltrials.gov/ct2/show/NCT03341962, (consulté le 29 septembre 2020).

[66] U.S. National Library of Medicine, A dose optimisation study of ASLAN003 in acute myeloid leukemia. https://clinicaltrials.gov/ct2/show/NCT03451084, (consulté le 4 octobre 2020).

[67] S.N. Gradl, D. Nguyen, K. Eis, J. Günther, T. Stellfeld, A. Janzer, S. Christian, T. Mueller, S.E. Sheikh, H. Zhou, C. Zhao, D.B. Sykes, S.J. Ferrara, K. Liu, M. Kröber, C. Merz, M. Niehues, M. Schäfer, K. Zimmermann, C.F. Nising, 2,4,5-Trisubstituted 1,2,4-triazolones useful as inhibitors of DHODH, 20200123129, (2020).

[68] J. Lacroix, R. C.-Gaudreault, M. Page, L.P. Joly, *In vitro* and *in vivo* activity of 1-aryl-3-(2-chloroethyl) urea derivatives as new antineoplastic agents, Anticancer Res. 8 (1988) 595-598.

[69] S. Fortin, L. Wei, E. Moreau, P. Labrie, É. Petitclerc, L.P. Kotra, R. C.-Gaudreault, Mechanism of action of *N*-phenyl-*N′*-(2-chloroethyl)ureas in the colchicine-binding site at the interface between α- and β-tubulin, Bioorg. Med. Chem. 17 (2009) 3690-3697.

[70] E. Mounetou, J. Legault, J. Lacroix, R. C.-Gaudreault, Antimitotic antitumor agents: Synthesis, structure-activity relationships, and biological characterization of *N*-aryl-*N*'-(2-chloroethyl)ureas as new selective alkylating agents, J. Med. Chem. 44 (2001) 694-702.

[71] P. Bechard, J. Lacroix, P. Poyet, R. C.-Gaudreault, Synthesis and cytotoxic activity of new alkyl 3-(2-chloroethyl)ureido benzene derivatives, Eur. J. Med. Chem. 29 (1994) 963-966.

[72] J.S. Fortin, M.-F. Côté, J. Lacroix, É. Petitclerc, R. C.-Gaudreault, Aromatic 2-chloroethyl urea derivatives and bioisosteres. Part 2: Cytocidal activity and effects on the nuclear translocation of thioredoxin-1, and the cell cycle progression, Bioorg. Med. Chem. 16 (2008) 7477-7488.

[73] S. Fortin, E. Moreau, J. Lacroix, M.-F. Côté, É. Petitclerc, R. C.-Gaudreault, Synthesis, antiproliferative activity evaluation and structure-activity relationships of novel aromatic urea and amide analogues of *N*-phenyl-*N′*-(2-chloroethyl)ureas, Eur. J. Med. Chem. 45 (2010) 2928-2937.

[74] M. Gagné-Boulet, S. Fortin, J. Lacroix, C.A. Lefebvre, M.-F. Côté, R. C.-Gaudreault, Styryl-*N*-phenyl-*N*'-(2-chloroethyl)ureas and styrylphenylimidazolidin-2-ones as new potent microtubule-disrupting agents using combretastatin A-4 as model, Eur. J. Med. Chem. 100 (2015) 34-43.

[75] S. Fortin, E. Moreau, J. Lacroix, J.-C. Teulade, A. Patenaude, R. C.-Gaudreault, *N*-Phenyl-*N′*-(2-chloroethyl)urea analogues of combretastatin A-4: Is the *N*-phenyl-*N′*-(2-chloroethyl)urea pharmacophore mimicking the trimethoxy phenyl moiety?, Bioorg. Med. Chem. Lett. 17 (2007) 2000-2004.

[76] S. Fortin, B. Bouchon, C. Chambon, J. Lacroix, E. Moreau, J.M. Chezal, F. Degoul, R. C.-Gaudreault, Characterization of the covalent binding of *N*-phenyl-*N*'-(2-chloroethyl)ureas to β-tubulin: Importance of Glu198 in microtubule stability, J. Pharmacol. exp. ther. 336 (2011) 460-467.

[77] R. Gaspari, A.E. Prota, K. Bargsten, A. Cavalli, M.O. Steinmetz, Structural basis of *cis*- and *trans*-combretastatin binding to tubulin, Chem. 2 (2017) 102-113.

[78] V. Turcotte, S. Fortin, F. Vevey, Y. Coulombe, J. Lacroix, M.-F. Côté, J.-Y. Masson, R. C.-Gaudreault, Synthesis, biological evaluation, and structure–activity relationships of novel Substituted *N*-phenyl ureidobenzenesulfonate derivatives blocking cell cycle progression in S-phase and inducing DNA double-strand breaks, J. Med. Chem. 55 (2012) 6194-6208.

[79] C. Bouzriba, L. Larcher, M. Gagné-Boulet, S. Fortin, *N*-phenyl ureidobenzenesulfonates, a novel class of promising human dihydroorotate dehydrogenase inhibitors, Bioorg. Med. Chem. 28 (2020) 115739.

[80] S. Fortin, L.H. Wei, E. Moreau, J. Lacroix, M.-F. Côté, É. Petitclerc, L.P. Kotra, R. C.-Gaudreault, Design, synthesis, biological evaluation, and structure-activity relationships of substituted phenyl 4-(2-oxoimidazolidin-1-yl)-benzenesulfonates as new tubulin inhibitors mimicking combretastatin A-4, J. Med. Chem. 54 (2011) 4559-4580.

[81] S. Fortin, L. Wei, E. Moreau, J. Lacroix, M.-F. Côté, É. Petitclerc, L.P. Kotra, R. C.-Gaudreault, Substituted phenyl 4-(2-oxoimidazolidin-1-yl)benzenesulfonamides as antimitotics. Antiproliferative, antiangiogenic and antitumoral activity, and quantitative structure-activity relationships, Eur. J. Med. Chem. 46 (2011) 5327-5342.

[82] R.L. Siegel, K.D. Miller, A. Jemal, Cancer statistics, 2020, CA-Cancer J. Clin. 70 (2020) 7-30.

[83] D.R. Brenner, H.K. Weir, A.A. Demers, L.F. Ellison, C. Louzado, A. Shaw, D. Turner, R.R. Woods, L.M. Smith, Projected estimates of cancer in Canada in 2020, Can. Med. Assoc. J. 192 (2020) 199-205.

[84] E. Mazzotti, G.C.A. Cappellini, S. Buconovo, R. Morese, A. Scoppola, C. Sebastiani, P. Marchetti, Treatment-related side effects and quality of life in cancer patients, Support. Care Cancer 20 (2012) 2553-2557.

[85] J. Ferlay, M. Colombet, I. Soerjomataram, C. Mathers, D.M. Parkin, M. Pineros, A. Znaor, F. Bray, Estimating the global cancer incidence and mortality in 2018: GLOBOCAN sources and methods, Int. J. Cancer 144 (2019) 1941-1953.

[86] M.J. Kim, W.S. Kim, D.O. Kim, J.E. Byun, H. Huy, S.Y. Lee, H.Y. Song, Y.J. Park, T.D. Kim, S.R. Yoon, E.J. Choi, H. Ha, H. Jung, I. Choi, Macrophage migration inhibitory factor interacts with thioredoxin-interacting protein and induces NF-κB activity, 34 (2017) 110-120.

[87] M. Gagné-Boulet, C. Bouzriba, M. Godard, S. Fortin, Preparation, characterisation and biological evaluation of new *N*-phenyl amidobenzenesulfonates and *N*-phenyl ureidobenzenesulfonates inducing DNA double-strand breaks. Part 3. Modulation of ring A, Eur. J. Med. Chem. 155 (2018) 681-694.

[88] S. Fortin, L. Wei, L.P. Kotra, R. C.-Gaudreault, Novel cytocidal substituted phenyl 4-(2-oxoimidazolidin-1-yl) benzenesulfonates and benzenesulfonamides with affinity to the colchicine-binding site: is the phenyl 2-imidazolidinone moiety a new haptophore for the design of new antimitotics?, Open J. Med. Chem. 5 (2015) 14.

Annexe A : Données supplémentaires du chapitre 2

Compound 11

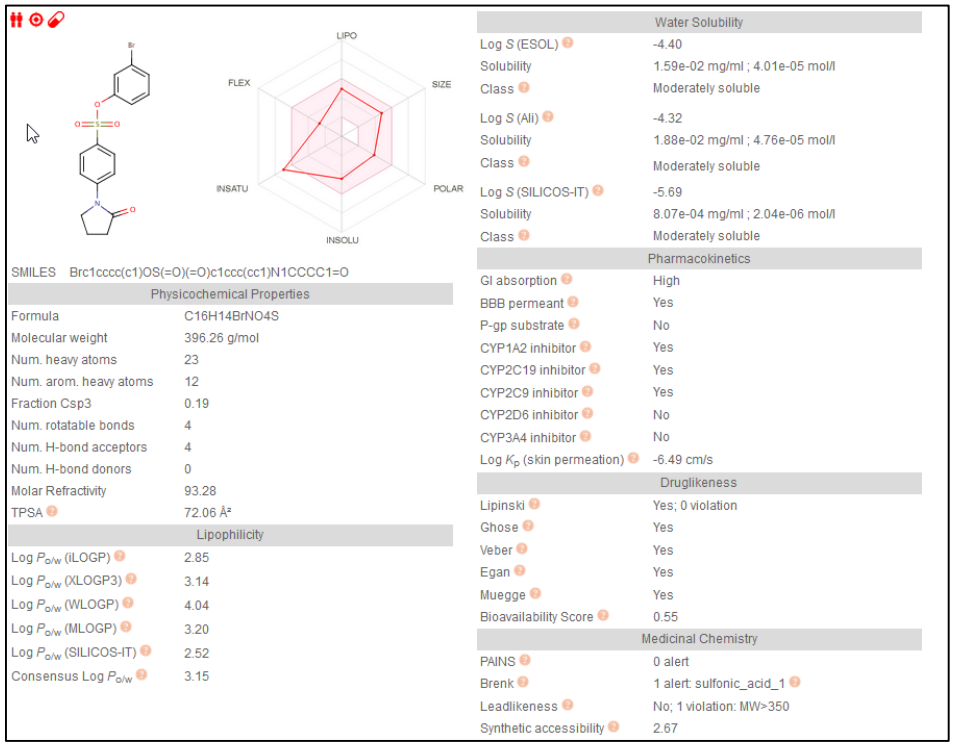

SMILES Brc1cccc(c1)OS(=O)(=O)c1ccc(cc1)N1CCCC1=O

Physicochemical Properties	
Formula	C16H14BrNO4S
Molecular weight	396.26 g/mol
Num. heavy atoms	23
Num. arom. heavy atoms	12
Fraction Csp3	0.19
Num. rotatable bonds	4
Num. H-bond acceptors	4
Num. H-bond donors	0
Molar Refractivity	93.28
TPSA	72.06 Å²

Lipophilicity	
Log $P_{o/w}$ (iLOGP)	2.85
Log $P_{o/w}$ (XLOGP3)	3.14
Log $P_{o/w}$ (WLOGP)	4.04
Log $P_{o/w}$ (MLOGP)	3.20
Log $P_{o/w}$ (SILICOS-IT)	2.52
Consensus Log $P_{o/w}$	3.15

Water Solubility	
Log *S* (ESOL)	-4.40
Solubility	1.59e-02 mg/ml ; 4.01e-05 mol/l
Class	Moderately soluble
Log *S* (Ali)	-4.32
Solubility	1.88e-02 mg/ml ; 4.76e-05 mol/l
Class	Moderately soluble
Log *S* (SILICOS-IT)	-5.69
Solubility	8.07e-04 mg/ml ; 2.04e-06 mol/l
Class	Moderately soluble

Pharmacokinetics	
GI absorption	High
BBB permeant	Yes
P-gp substrate	No
CYP1A2 inhibitor	Yes
CYP2C19 inhibitor	Yes
CYP2C9 inhibitor	Yes
CYP2D6 inhibitor	No
CYP3A4 inhibitor	No
Log K_p (skin permeation)	-6.49 cm/s

Druglikeness	
Lipinski	Yes; 0 violation
Ghose	Yes
Veber	Yes
Egan	Yes
Muegge	Yes
Bioavailability Score	0.55

Medicinal Chemistry	
PAINS	0 alert
Brenk	1 alert: sulfonic_acid_1
Leadlikeness	No; 1 violation: MW>350
Synthetic accessibility	2.67

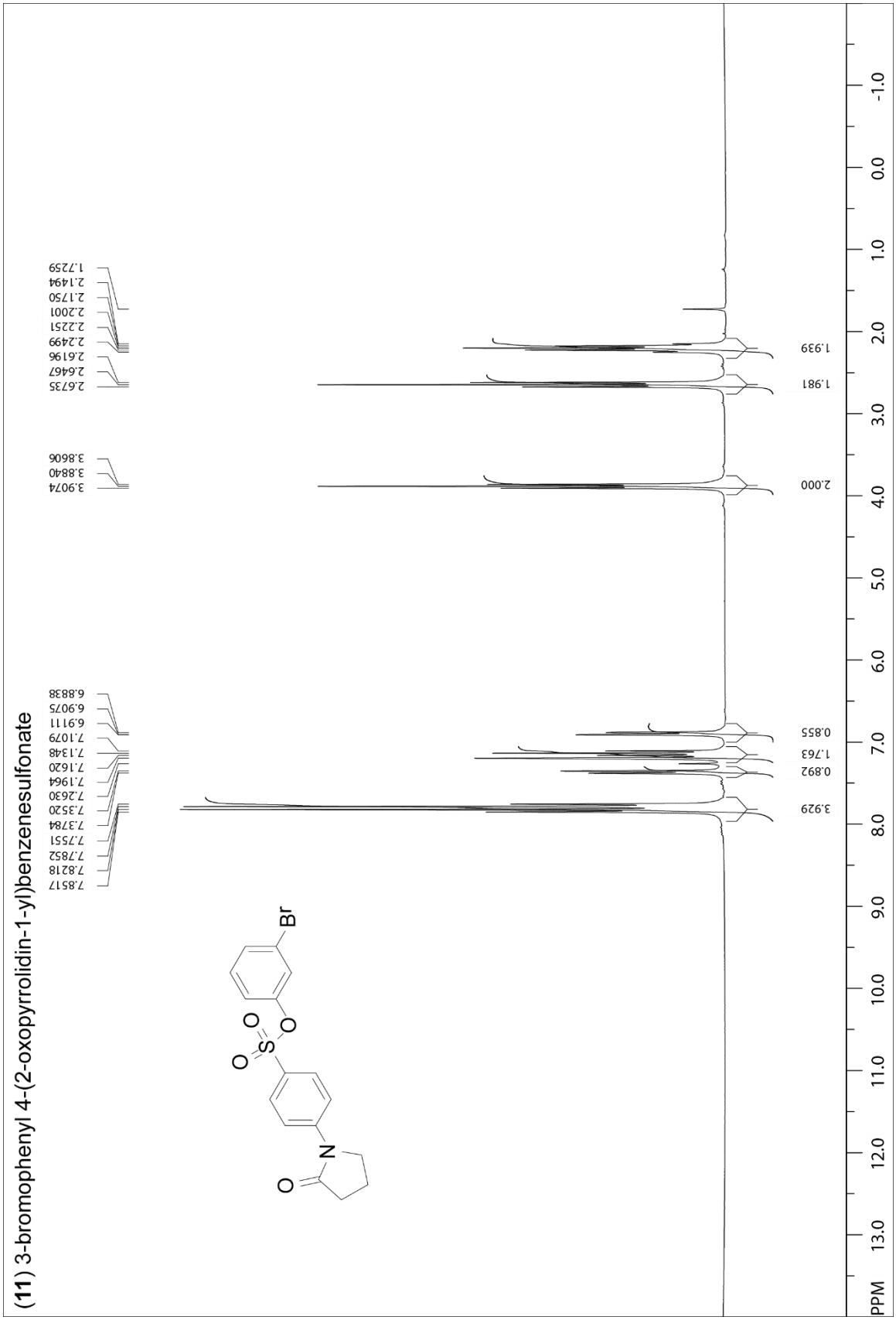
(11) 3-bromophenyl 4-(2-oxopyrrolidin-1-yl)benzenesulfonate
Br
O
S
O
O
N
O
7.8517
7.8218
7.7852
7.7551
7.3784
7.3520
7.2630
7.1964
7.1620
7.1348
7.1079
6.9111
6.9075
6.8838
3.9074
3.8840
3.8606
2.6735
2.6467
2.6196
2.2499
2.2251
2.2001
2.1750
2.1494
1.7259
3.929
0.892
1.763
0.855
2.000
1.981
1.939
PPM
13.0
12.0
11.0
10.0
9.0
8.0
7.0
6.0
5.0
4.0
3.0
2.0
1.0
0.0
-1.0

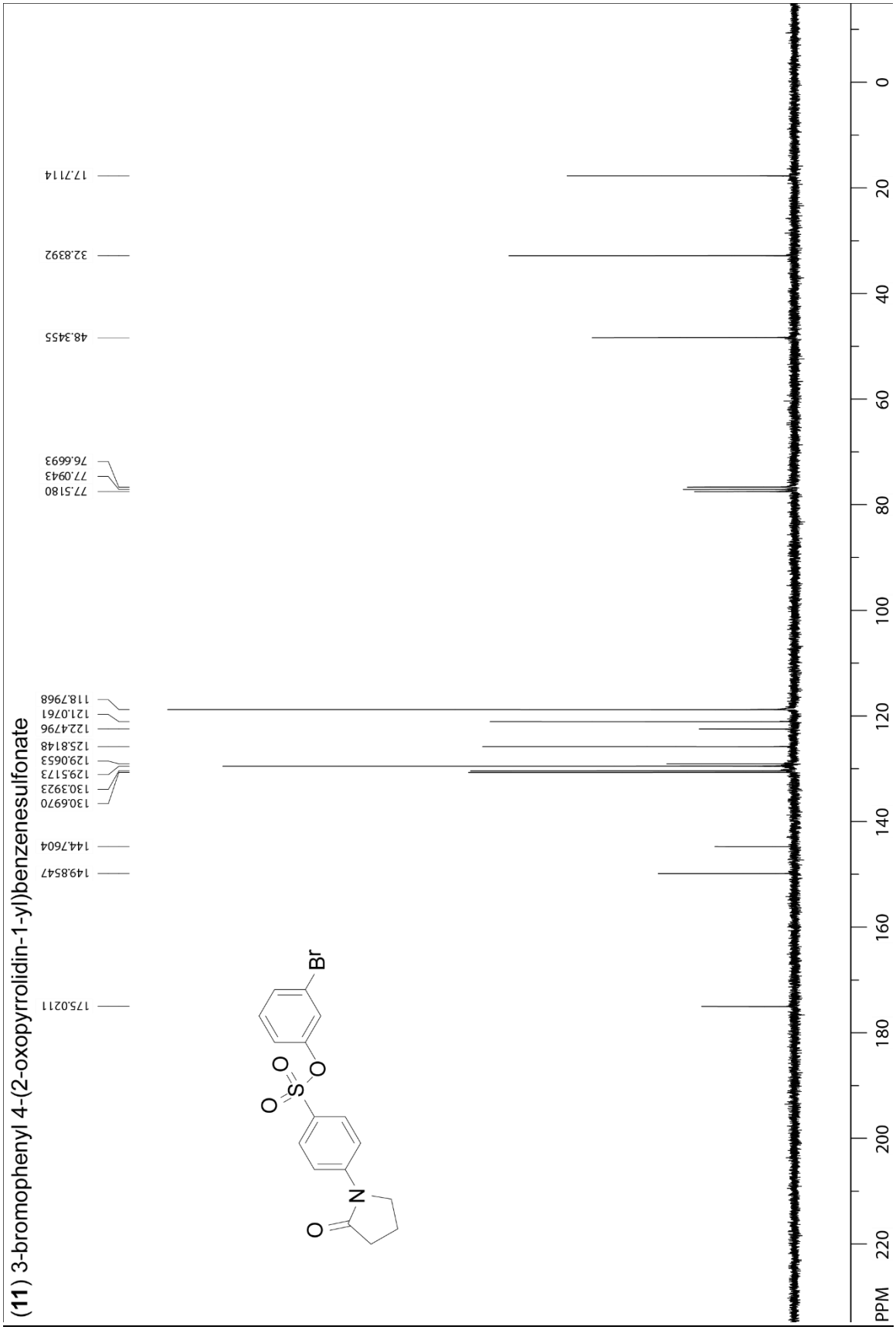
(11) 3-bromophenyl 4-(2-oxopyrrolidin-1-yl)benzenesulfonate
175.0211
149.8547
144.7604
130.6970
130.3923
129.5173
129.0653
125.8148
122.4796
121.0761
118.7968
77.5180
77.0943
76.6693
48.3455
32.8392
17.7114
Br
O
S
O
O
N
O
PPM
0
20
40
60
80
100
120
140
160
180
200
220

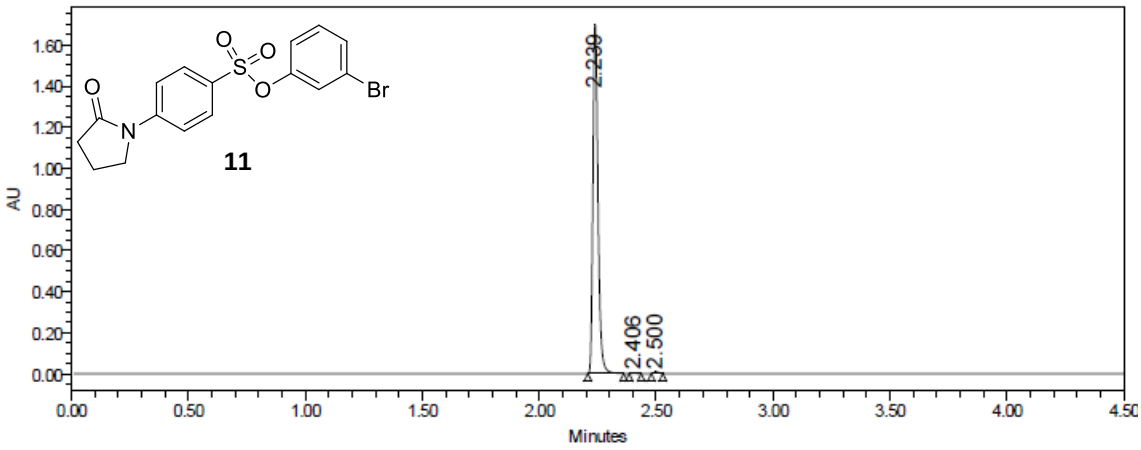

	RT	Area	% Area	Height
1	2.239	2586003	99.45	1702324
2	2.406	2351	0.09	1789
3	2.500	11924	0.46	9203

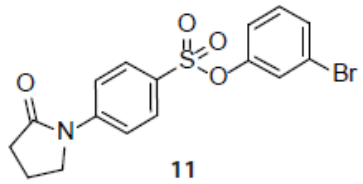

11

m/z	*Calc m/z*	Diff(ppm)	z	Abund	Formula	Ion
395.9898	395.99	-0.48		337817	C16 H15 Br N O4 S	(M+H)+
396.2346				24553		
396.9923	396.9931	-1.84		53551	C16 H15 Br N O4 S	(M+H)+
397.9879	397.988	-0.38		361496	C16 H15 Br N O4 S	(M+H)+
398.237				29459		
398.9904	398.991	-1.5		56522	C16 H15 Br N O4 S	(M+H)+
399.9867	399.9873	-1.38		15341	C16 H15 Br N O4 S	(M+H)+
400.9884	400.9892	-1.86		2022	C16 H15 Br N O4 S	(M+H)+

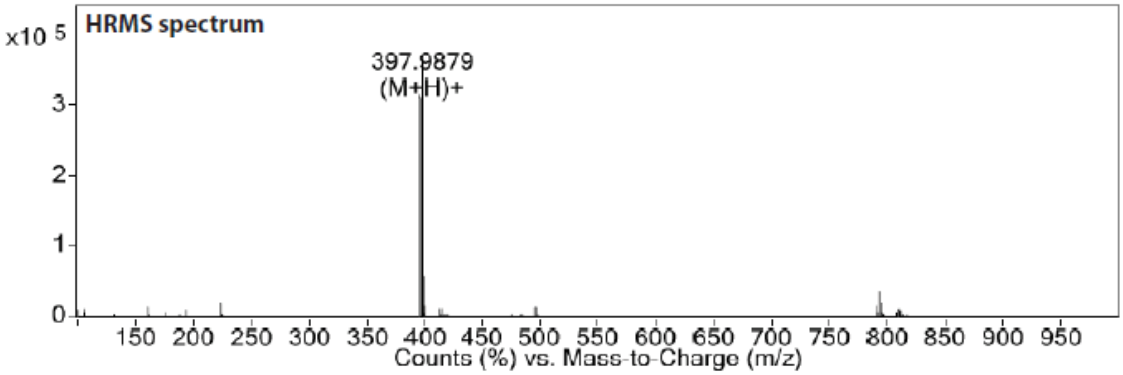

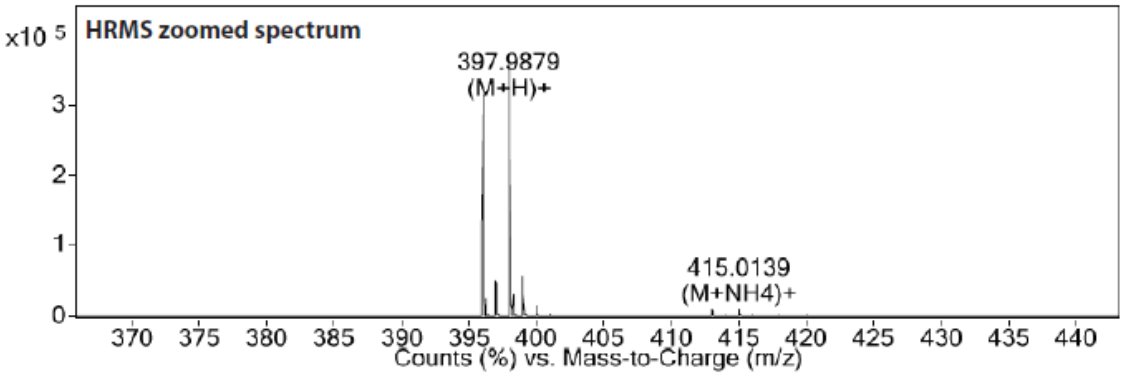

Compound 12

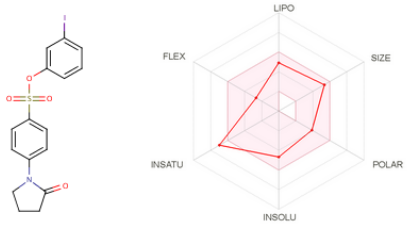

SMILES Ic1cccc(c1)OS(=O)(=O)c1ccc(cc1)N1CCCC1=O

Physicochemical Properties	
Formula	C16H14INO4S
Molecular weight	443.26 g/mol
Num. heavy atoms	23
Num. arom. heavy atoms	12
Fraction Csp3	0.19
Num. rotatable bonds	4
Num. H-bond acceptors	4
Num. H-bond donors	0
Molar Refractivity	98.30
TPSA	72.06 Å²

Lipophilicity	
Log $P_{o/w}$ (iLOGP)	2.89
Log $P_{o/w}$ (XLOGP3)	3.09
Log $P_{o/w}$ (WLOGP)	3.89
Log $P_{o/w}$ (MLOGP)	3.32
Log $P_{o/w}$ (SILICOS-IT)	2.81
Consensus Log $P_{o/w}$	3.20

Water Solubility	
Log *S* (ESOL)	-4.66
Solubility	9.77e-03 mg/ml ; 2.20e-05 mol/l
Class	Moderately soluble
Log *S* (Ali)	-4.27
Solubility	2.38e-02 mg/ml ; 5.36e-05 mol/l
Class	Moderately soluble
Log *S* (SILICOS-IT)	-5.75
Solubility	7.96e-04 mg/ml ; 1.79e-06 mol/l
Class	Moderately soluble

Pharmacokinetics	
GI absorption	High
BBB permeant	Yes
P-gp substrate	No
CYP1A2 inhibitor	Yes
CYP2C19 inhibitor	Yes
CYP2C9 inhibitor	Yes
CYP2D6 inhibitor	No
CYP3A4 inhibitor	No
Log K_p (skin permeation)	-6.81 cm/s

Druglikeness	
Lipinski	Yes; 0 violation
Ghose	Yes
Veber	Yes
Egan	Yes
Muegge	Yes
Bioavailability Score	0.55

Medicinal Chemistry	
PAINS	0 alert
Brenk	2 alerts: iodine, sulfonic_acid_1
Leadlikeness	No; 1 violation: MW>350
Synthetic accessibility	2.77

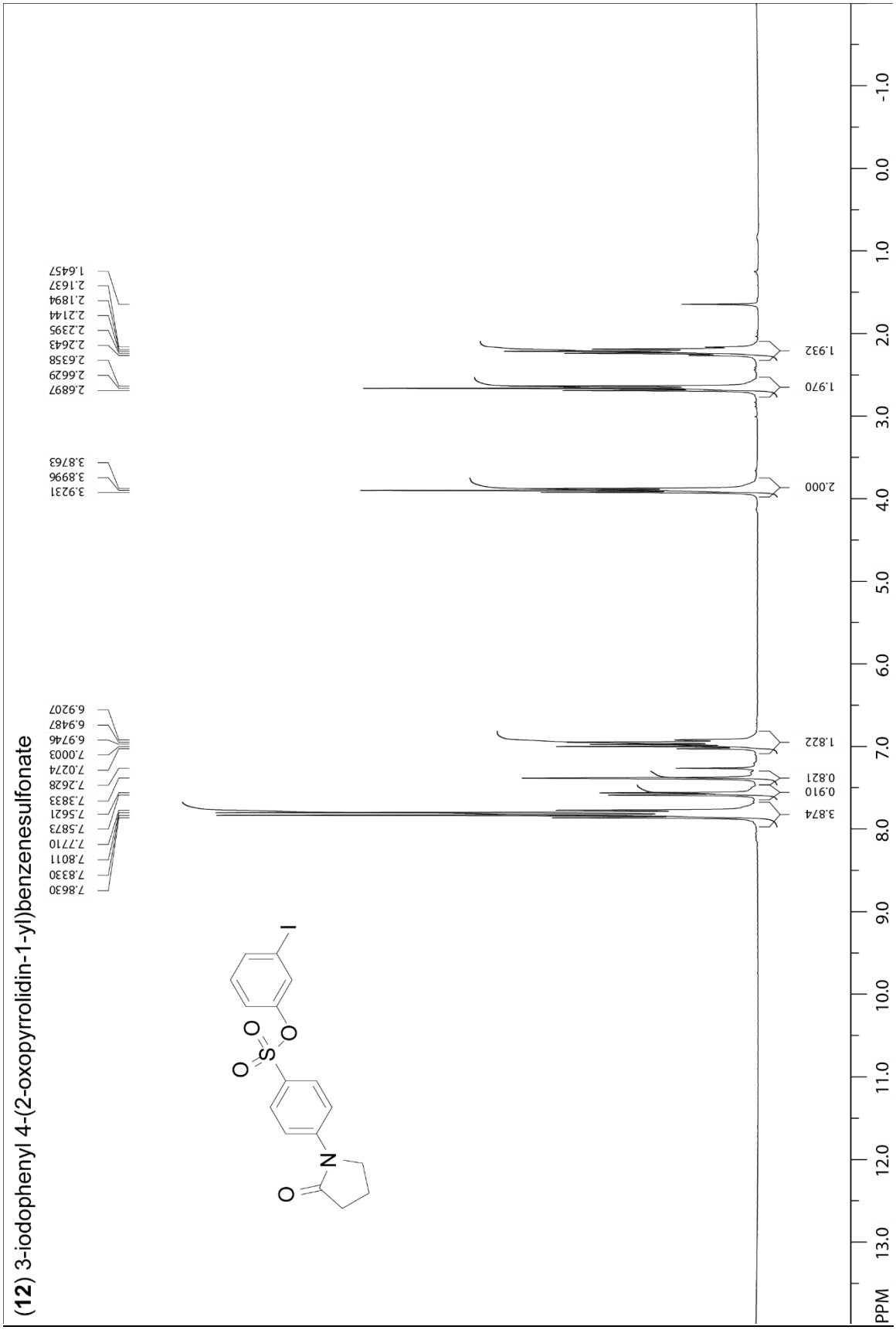
(12) 3-iodophenyl 4-(2-oxopyrrolidin-1-yl)benzenesulfonate
7.8630
7.8330
7.8011
7.7710
7.5873
7.5621
7.3833
7.2628
7.0274
7.0003
6.9746
6.9487
6.9207
3.9231
3.8996
3.8763
2.6897
2.6629
2.6358
2.2643
2.2395
2.2144
2.1894
2.1637
1.6457
3.874
0.910
0.821
1.822
2.000
1.970
1.932
PPM
13.0
12.0
11.0
10.0
9.0
8.0
7.0
6.0
5.0
4.0
3.0
2.0
1.0
0.0
-1.0

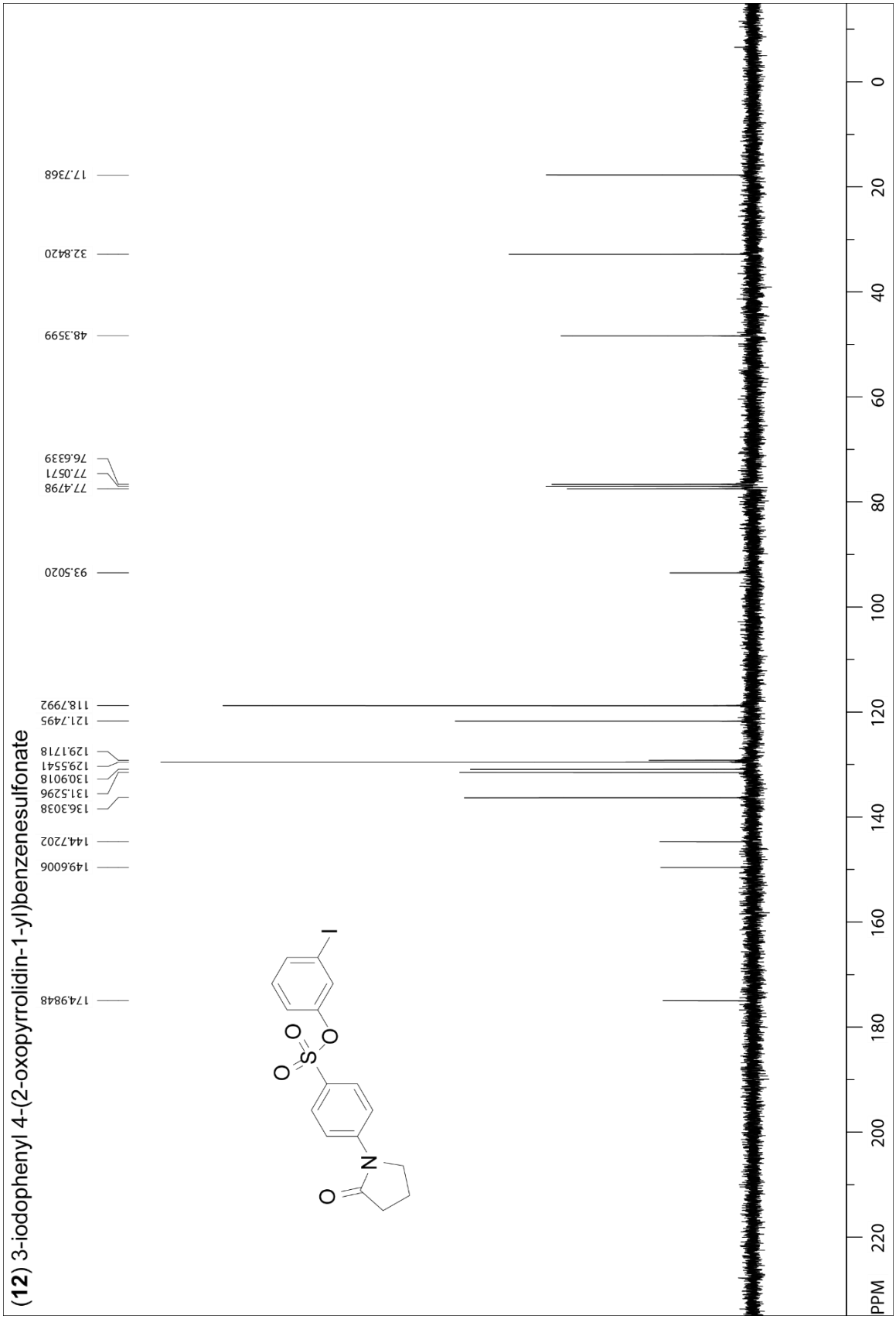
(12) 3-iodophenyl 4-(2-oxopyrrolidin-1-yl)benzenesulfonate
17.7368
32.8420
48.3599
76.6339
77.0571
77.4798
93.5020
118.7992
121.7495
129.1718
129.5541
130.9018
131.5296
136.3038
144.7202
149.6006
174.9848
I
O
S
O
O
N
O
PPM
0
20
40
60
80
100
120
140
160
180
200
220

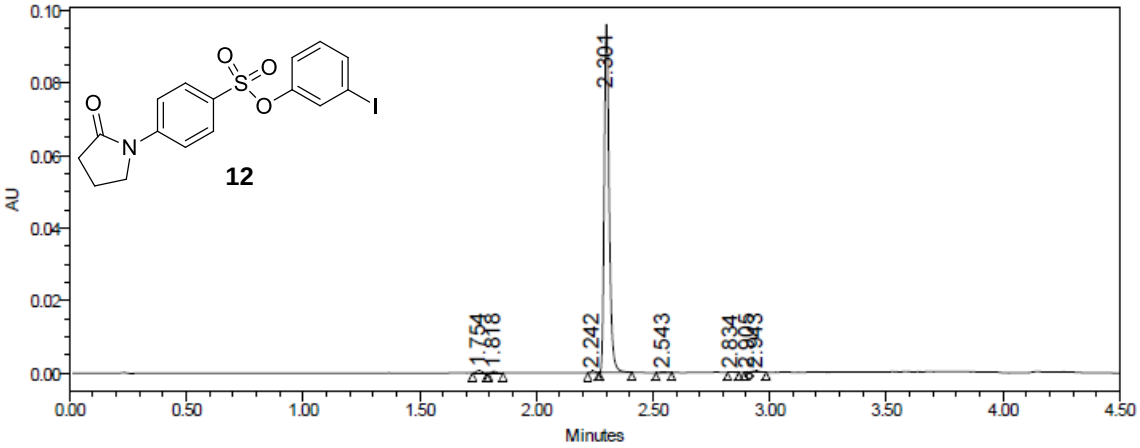

	RT	Area	% Area	Height
1	1.754	1014	0.69	621
2	1.818	623	0.43	409
3	2.242	600	0.41	452
4	2.301	142671	97.58	96277
5	2.543	314	0.21	203
6	2.834	132	0.09	111
7	2.905	115	0.08	121
8	2.943	739	0.51	359

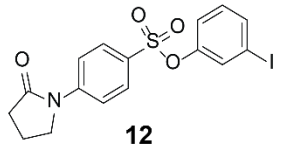

12

m/z	*Calc m/z*	Diff(ppm)	z	Abund	Formula	Ion
443.9757	443.9761	-1		334699	C16 H15 I N O4 S	(M+H)+
444.2359				26433		
444.3603				1080		
444.5004				1418		
444.9782	444.9792	-2.28		51761	C16 H15 I N O4 S	(M+H)+
445.2433				1434		
445.9753	445.9754	-0.23		15377	C16 H15 I N O4 S	(M+H)+
446.9761	446.9773	-2.54		1807	C16 H15 I N O4 S	(M+H)+

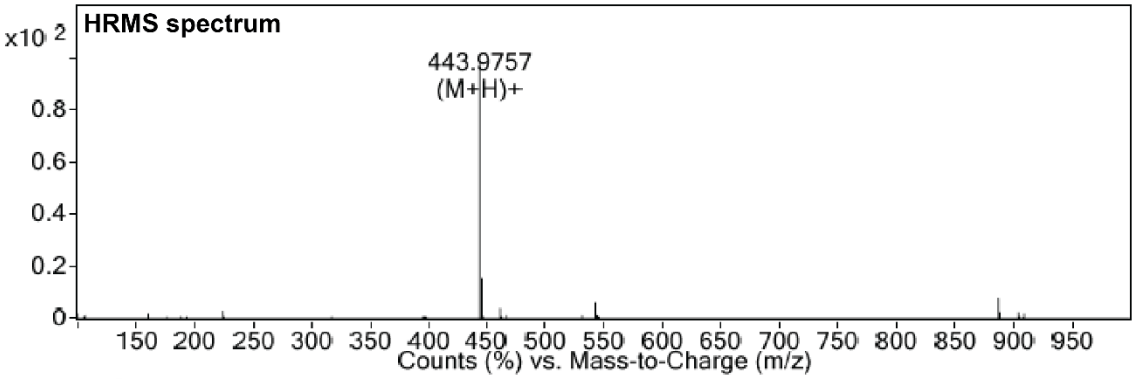

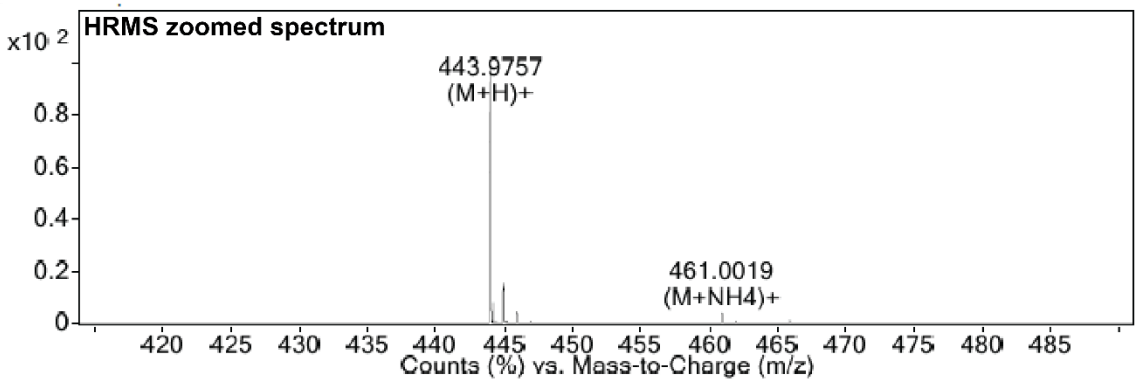

Compound 14

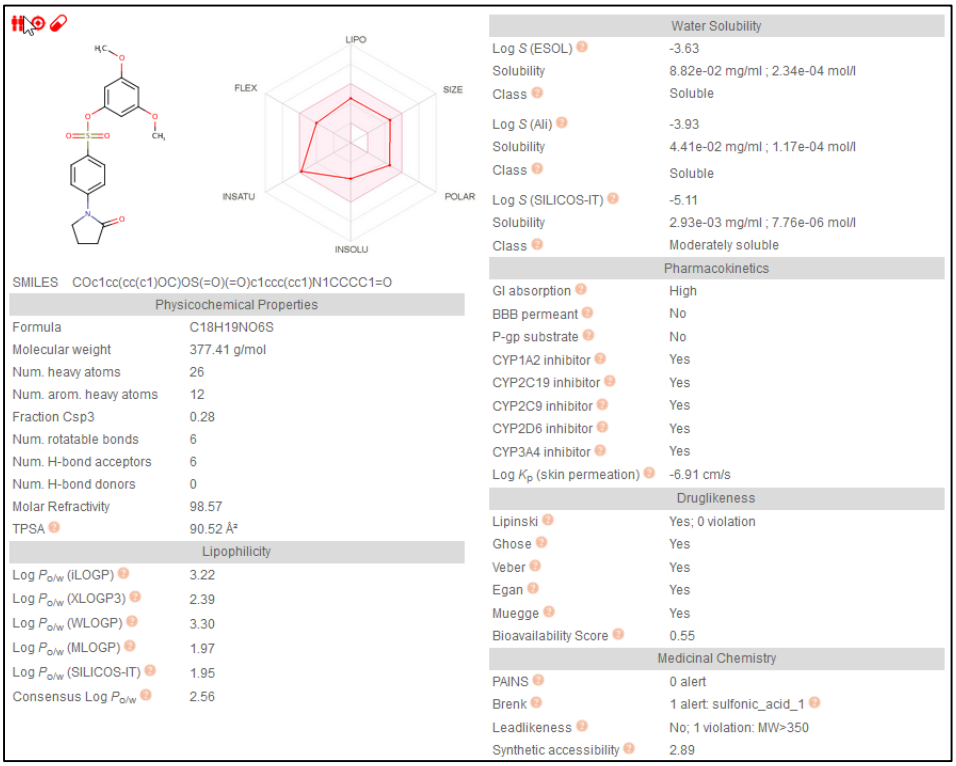

SMILES COc1cc(cc(c1)OC)OS(=O)(=O)c1ccc(cc1)N1CCCC1=O

Physicochemical Properties	
Formula	C18H19NO6S
Molecular weight	377.41 g/mol
Num. heavy atoms	26
Num. arom. heavy atoms	12
Fraction Csp3	0.28
Num. rotatable bonds	6
Num. H-bond acceptors	6
Num. H-bond donors	0
Molar Refractivity	98.57
TPSA	90.52 Å²

Lipophilicity	
Log $P_{o/w}$ (iLOGP)	3.22
Log $P_{o/w}$ (XLOGP3)	2.39
Log $P_{o/w}$ (WLOGP)	3.30
Log $P_{o/w}$ (MLOGP)	1.97
Log $P_{o/w}$ (SILICOS-IT)	1.95
Consensus Log $P_{o/w}$	2.56

Water Solubility	
Log *S* (ESOL)	-3.63
Solubility	8.82e-02 mg/ml ; 2.34e-04 mol/l
Class	Soluble
Log *S* (Ali)	-3.93
Solubility	4.41e-02 mg/ml ; 1.17e-04 mol/l
Class	Soluble
Log *S* (SILICOS-IT)	-5.11
Solubility	2.93e-03 mg/ml ; 7.76e-06 mol/l
Class	Moderately soluble

Pharmacokinetics	
GI absorption	High
BBB permeant	No
P-gp substrate	No
CYP1A2 inhibitor	Yes
CYP2C19 inhibitor	Yes
CYP2C9 inhibitor	Yes
CYP2D6 inhibitor	Yes
CYP3A4 inhibitor	Yes
Log K_p (skin permeation)	-6.91 cm/s

Druglikeness	
Lipinski	Yes; 0 violation
Ghose	Yes
Veber	Yes
Egan	Yes
Muegge	Yes
Bioavailability Score	0.55

Medicinal Chemistry	
PAINS	0 alert
Brenk	1 alert: sulfonic_acid_1
Leadlikeness	No; 1 violation: MW>350
Synthetic accessibility	2.89

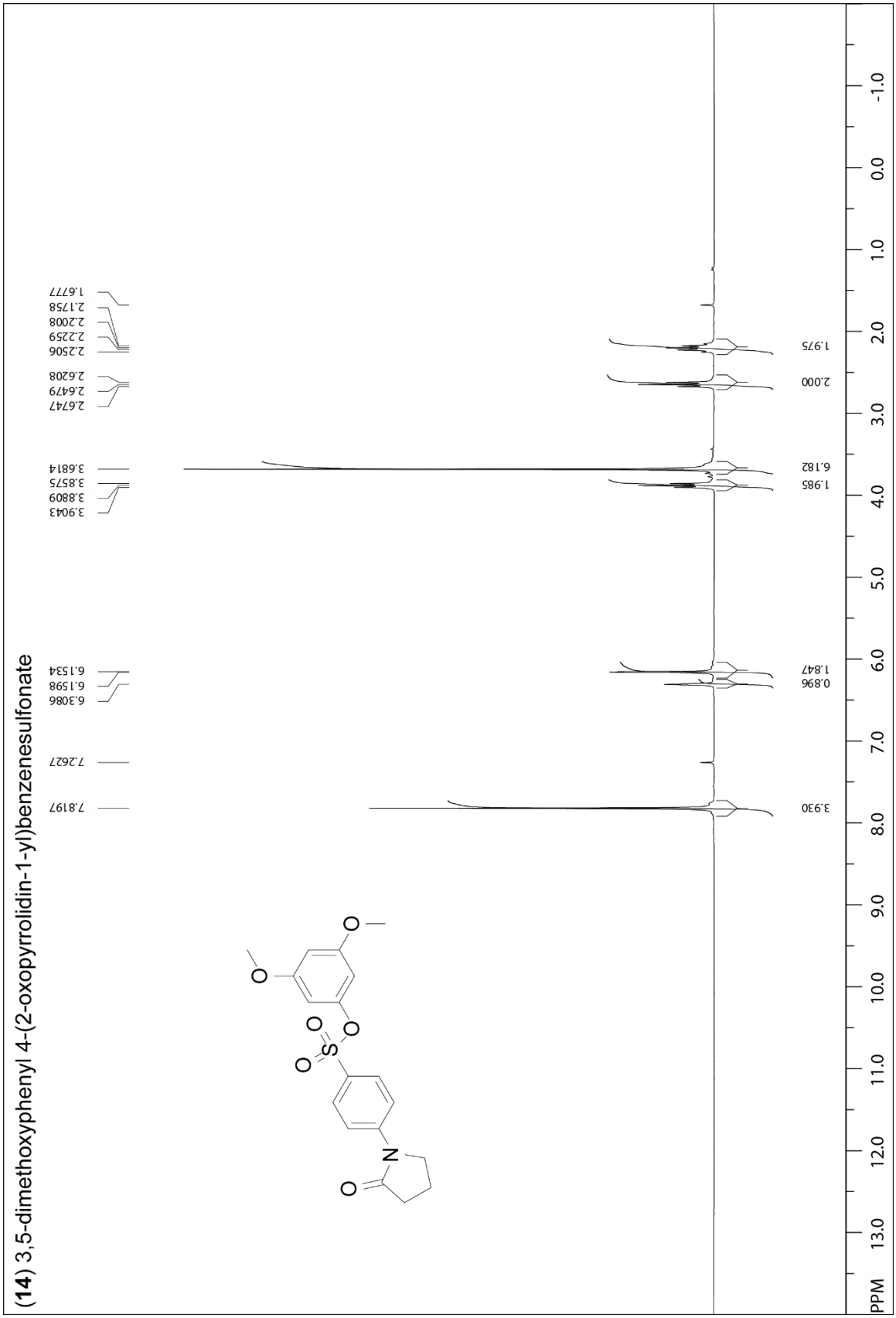
(14) 3,5-dimethoxyphenyl 4-(2-oxopyrrolidin-1-yl)benzenesulfonate
7.8197
7.2627
6.3086
6.1598
6.1534
3.9043
3.8809
3.8575
3.6814
2.6747
2.6479
2.6208
2.2506
2.2259
2.2008
2.1758
1.6777
3.930
0.896
1.847
6.182
1.985
2.000
1.975
PPM
13.0
12.0
11.0
10.0
9.0
8.0
7.0
6.0
5.0
4.0
3.0
2.0
1.0
0.0
-1.0

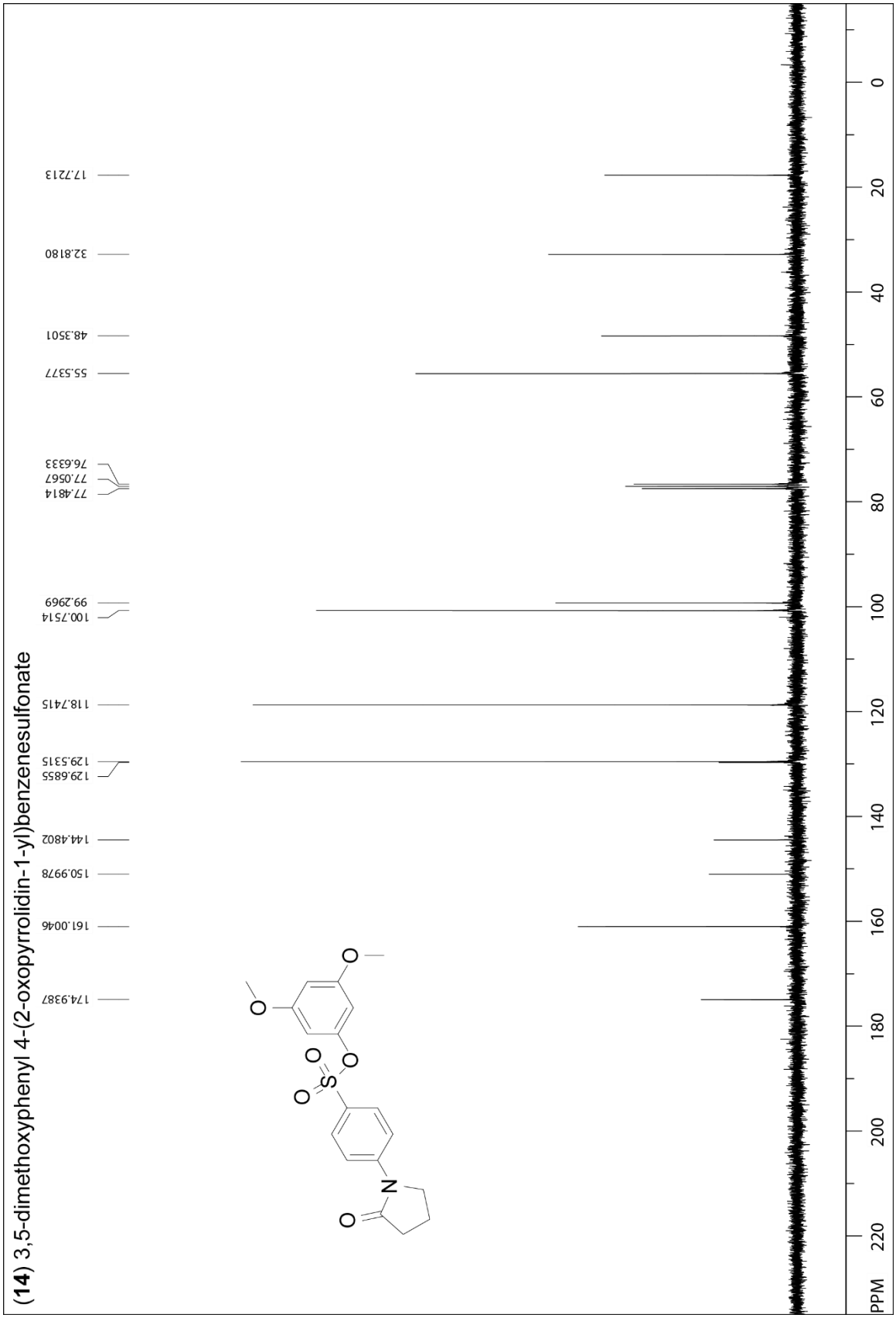
(14) 3,5-dimethoxyphenyl 4-(2-oxopyrrolidin-1-yl)benzenesulfonate
174.9387
161.0046
150.9978
144.4802
129.6855
129.5315
118.7415
100.7514
99.2969
77.4814
77.0567
76.6333
55.5377
48.3501
32.8180
17.7213
PPM
0
20
40
60
80
100
120
140
160
180
200
220

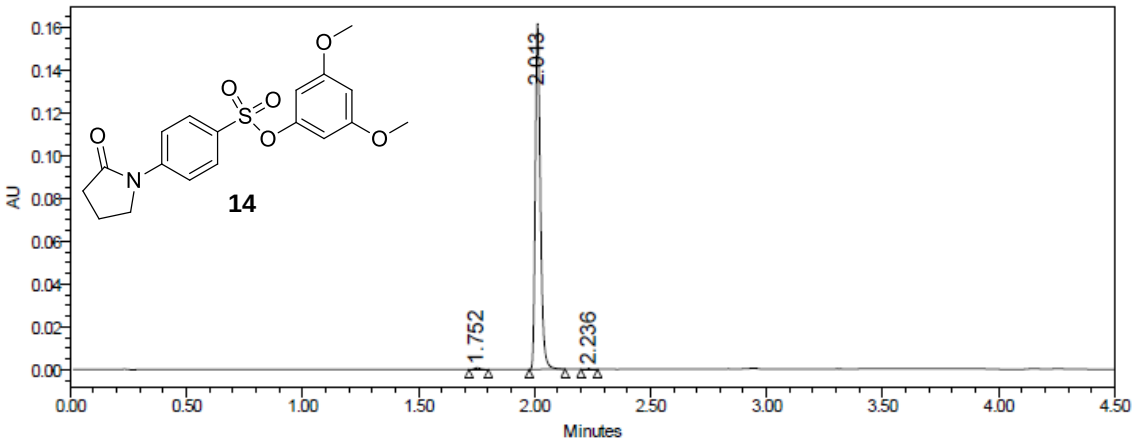

	RT	Area	% Area	Height
1	1.752	1272	0.50	749
2	2.013	251227	99.35	161482
3	2.236	380	0.15	238

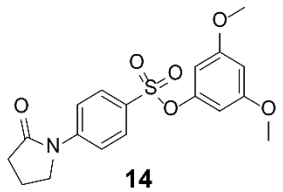

14

m/z	*Calc m/z*	Diff(ppm)	z	Abund	Formula	Ion
378.0998	378.1006	-2.03		354585	C18 H20 N O6 S	(M+H)+
378.3397				28870		
378.4542				1162		
378.5838				1603		
379.1024	379.1037	-3.49		63939	C18 H20 N O6 S	(M+H)+
379.3425				2121		
380.0996	380.1005	-2.53		18738	C18 H20 N O6 S	(M+H)+
381.1021	381.1024	-0.86		2540	C18 H20 N O6 S	(M+H)+

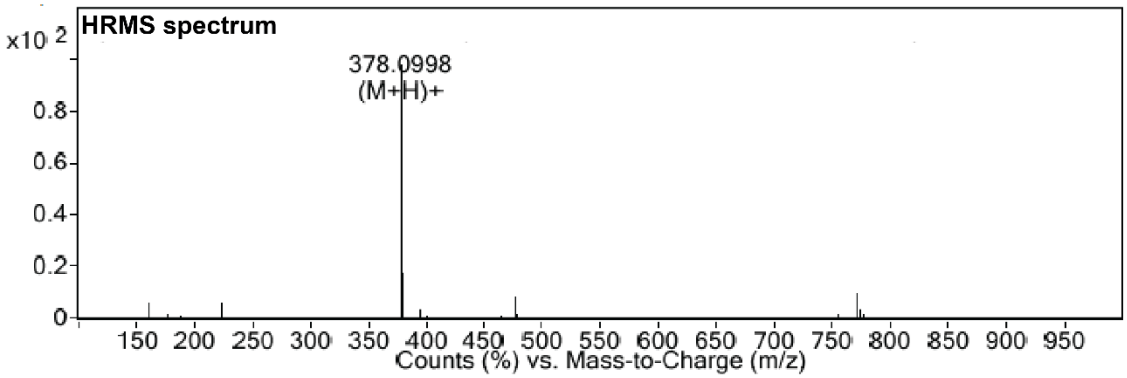

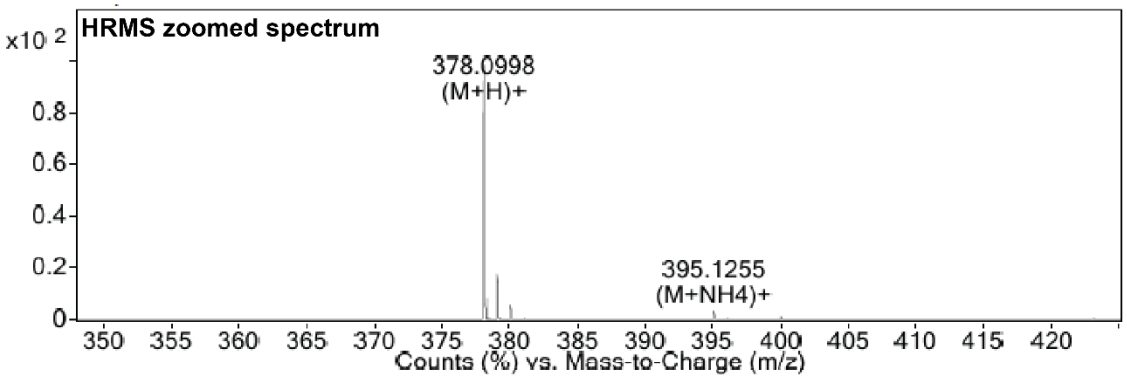

Compound 15

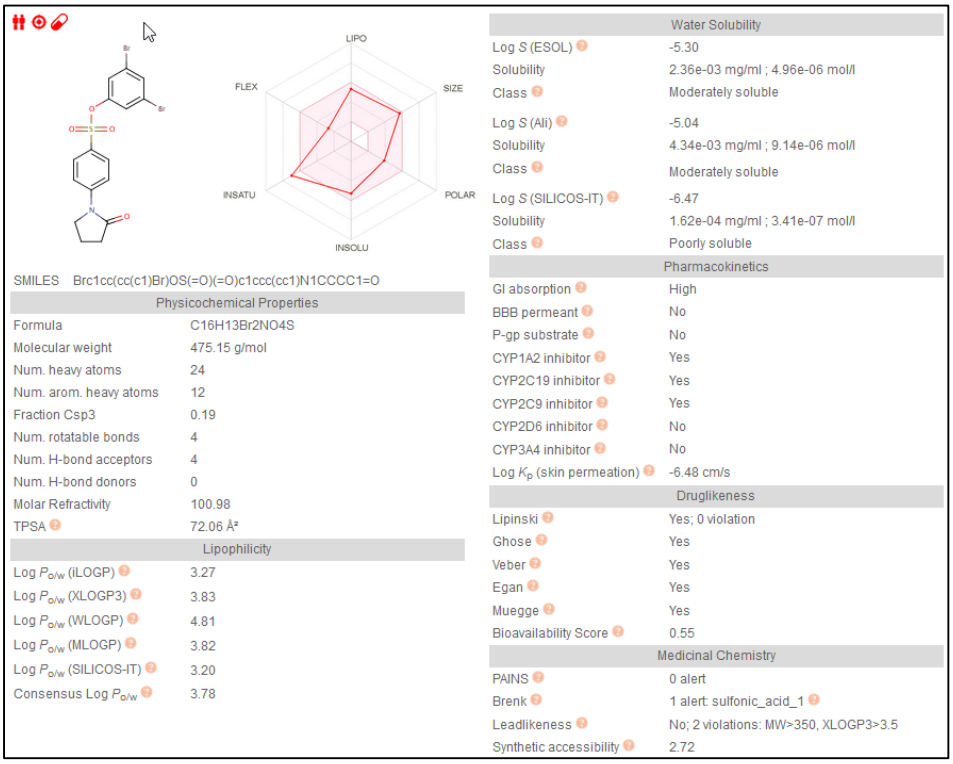

SMILES Brc1cc(cc(c1)Br)OS(=O)(=O)c1ccc(cc1)N1CCCC1=O

Physicochemical Properties	
Formula	C16H13Br2NO4S
Molecular weight	475.15 g/mol
Num. heavy atoms	24
Num. arom. heavy atoms	12
Fraction Csp3	0.19
Num. rotatable bonds	4
Num. H-bond acceptors	4
Num. H-bond donors	0
Molar Refractivity	100.98
TPSA	72.06 Å²

Lipophilicity	
Log $P_{o/w}$ (iLOGP)	3.27
Log $P_{o/w}$ (XLOGP3)	3.83
Log $P_{o/w}$ (WLOGP)	4.81
Log $P_{o/w}$ (MLOGP)	3.82
Log $P_{o/w}$ (SILICOS-IT)	3.20
Consensus Log $P_{o/w}$	3.78

Water Solubility	
Log *S* (ESOL)	-5.30
Solubility	2.36e-03 mg/ml ; 4.96e-06 mol/l
Class	Moderately soluble
Log *S* (Ali)	-5.04
Solubility	4.34e-03 mg/ml ; 9.14e-06 mol/l
Class	Moderately soluble
Log *S* (SILICOS-IT)	-6.47
Solubility	1.62e-04 mg/ml ; 3.41e-07 mol/l
Class	Poorly soluble

Pharmacokinetics	
GI absorption	High
BBB permeant	No
P-gp substrate	No
CYP1A2 inhibitor	Yes
CYP2C19 inhibitor	Yes
CYP2C9 inhibitor	Yes
CYP2D6 inhibitor	No
CYP3A4 inhibitor	No
Log K_p (skin permeation)	-6.48 cm/s

Druglikeness	
Lipinski	Yes; 0 violation
Ghose	Yes
Veber	Yes
Egan	Yes
Muegge	Yes
Bioavailability Score	0.55

Medicinal Chemistry	
PAINS	0 alert
Brenk	1 alert: sulfonic_acid_1
Leadlikeness	No; 2 violations: MW>350, XLOGP3>3.5
Synthetic accessibility	2.72

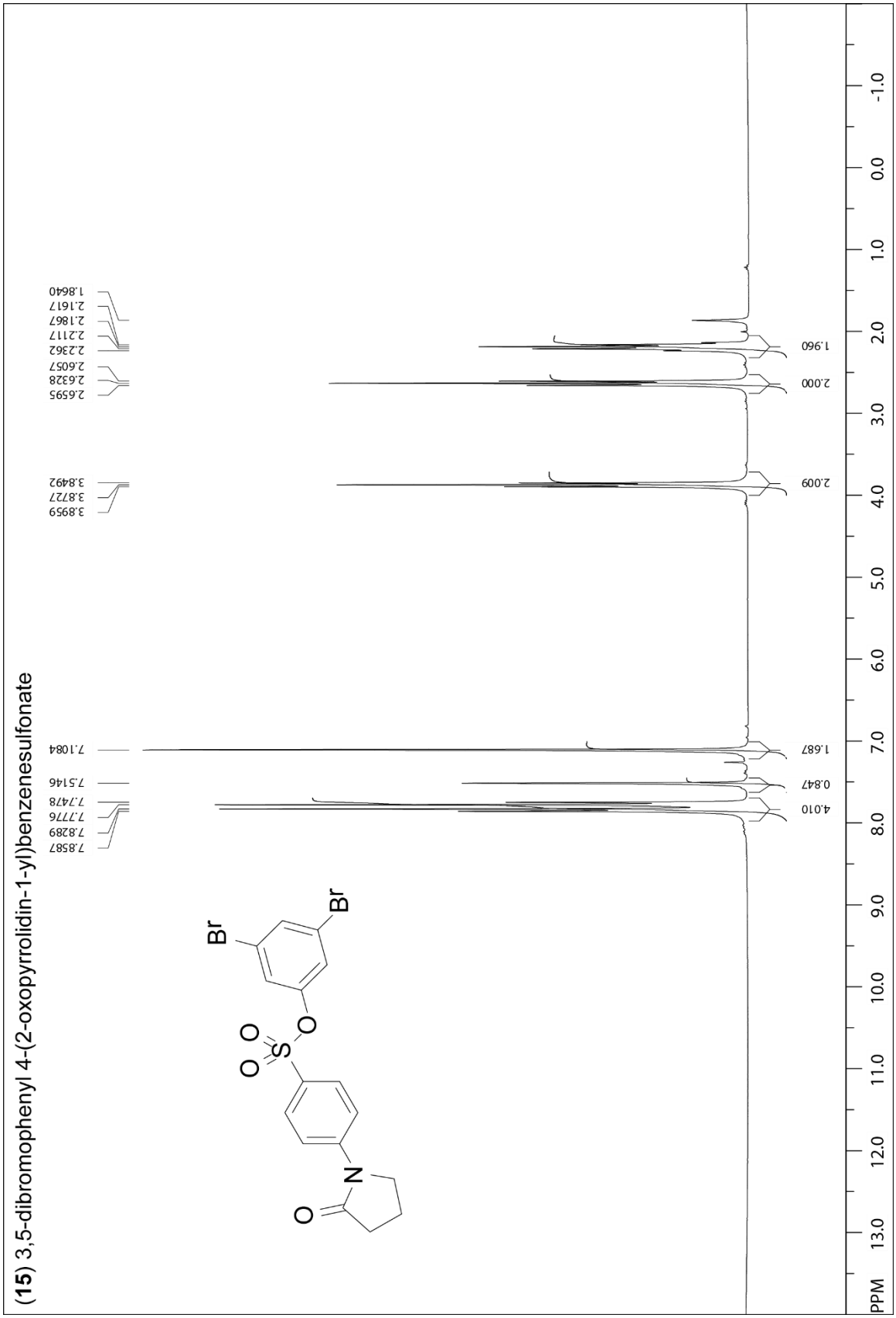
(15) 3,5-dibromophenyl 4-(2-oxopyrrolidin-1-yl)benzenesulfonate
Br
Br
O
O
S
O
N
O
7.8587
7.8289
7.7776
7.7478
7.5146
7.1084
3.8959
3.8727
3.8492
2.6595
2.6328
2.6057
2.2362
2.2117
2.1867
2.1617
1.8640
4.010
0.847
1.687
2.009
2.000
1.960
PPM
13.0
12.0
11.0
10.0
9.0
8.0
7.0
6.0
5.0
4.0
3.0
2.0
1.0
0.0
-1.0

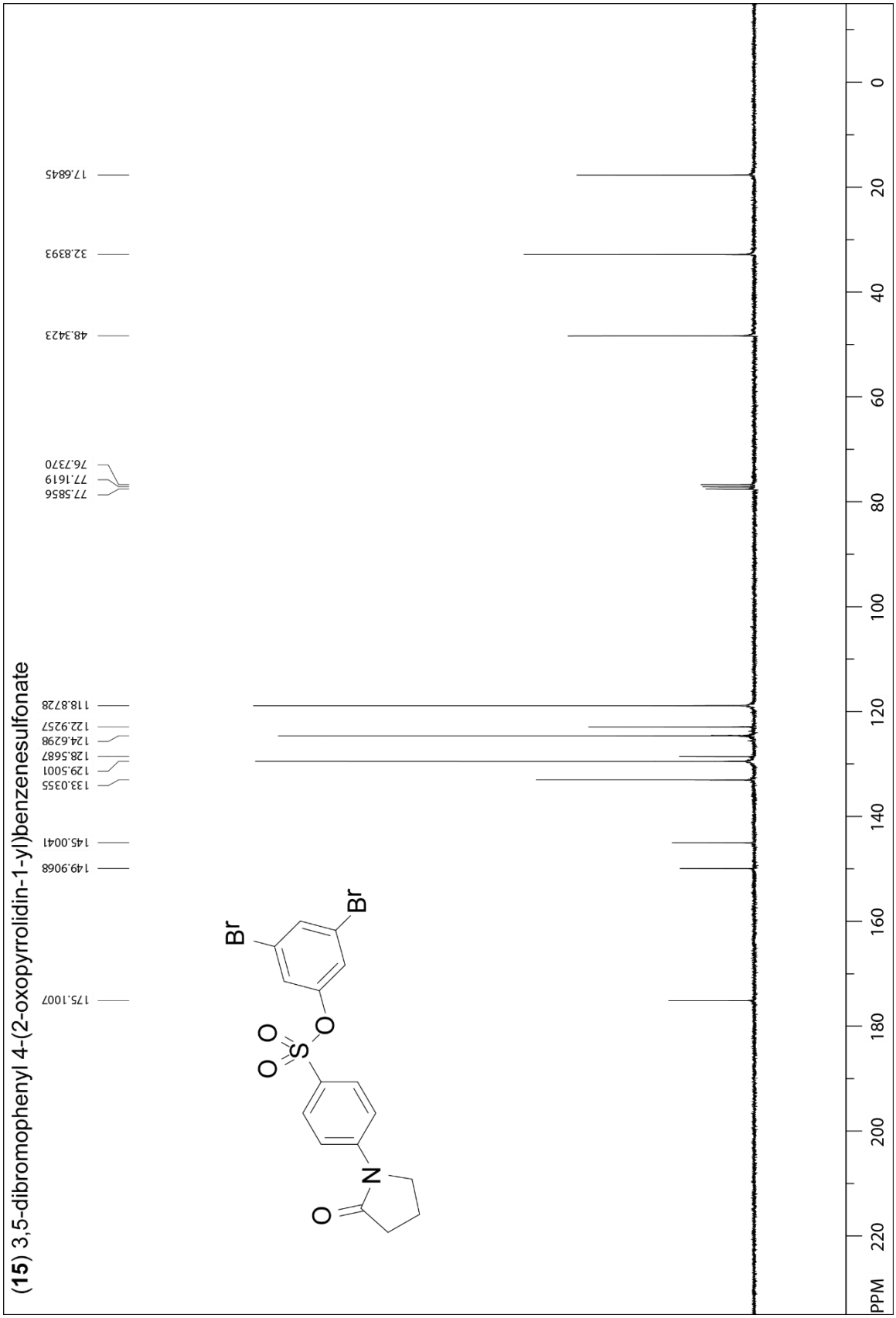
(15) 3,5-dibromophenyl 4-(2-oxopyrrolidin-1-yl)benzenesulfonate
175.1007
149.9068
145.0041
133.0355
129.5001
128.5687
124.6298
122.9257
118.8728
77.5856
77.1619
76.7370
48.3423
32.8393
17.6845
Br
Br
O
O
S
O
N
O
PPM
0
20
40
60
80
100
120
140
160
180
200
220

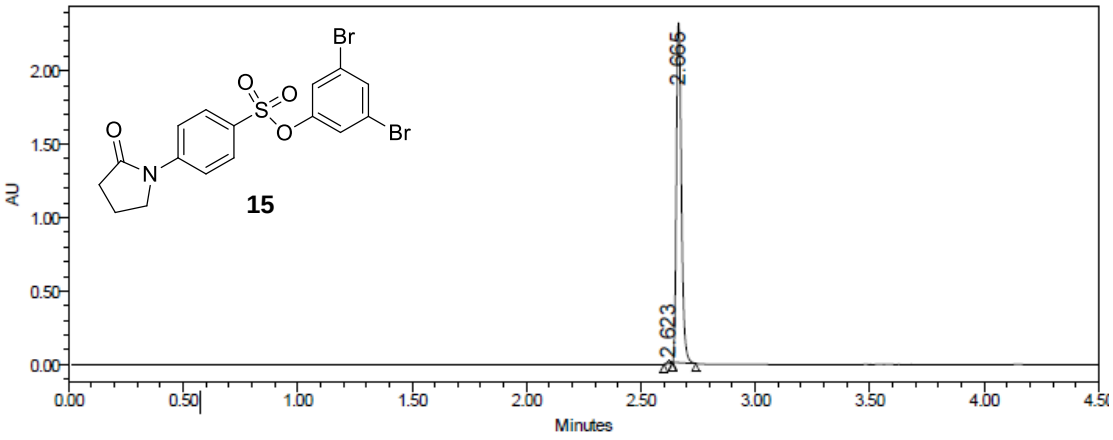

	RT	Area	% Area	Height
1	2.623	18712	0.53	18947
2	2.665	3509783	99.47	2313557

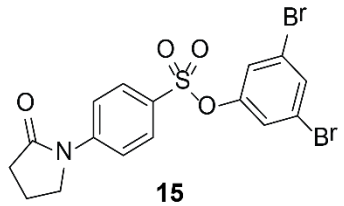

15

m/z	*Calc m/z*	Diff(ppm)	z	Abund	Formula	Ion
473.9003	473.9005	-0.37		79934	C16 H14 Br2 N O4 S	(M+H)+
474.9031	474.9036	-0.91		10795	C16 H14 Br2 N O4 S	(M+H)+
475.8983	475.8985	-0.45		177177	C16 H14 Br2 N O4 S	(M+H)+
476.1692				9282		
476.9013	476.9015	-0.55		25215	C16 H14 Br2 N O4 S	(M+H)+
477.8963	477.8966	-0.51		88253	C16 H14 Br2 N O4 S	(M+H)+
478.8995	478.8995	-0.07		11773	C16 H14 Br2 N O4 S	(M+H)+
490.9266	490.927	-0.9	1	3745	C16 H17 Br2 N2 O4 S	(M+NH4)+

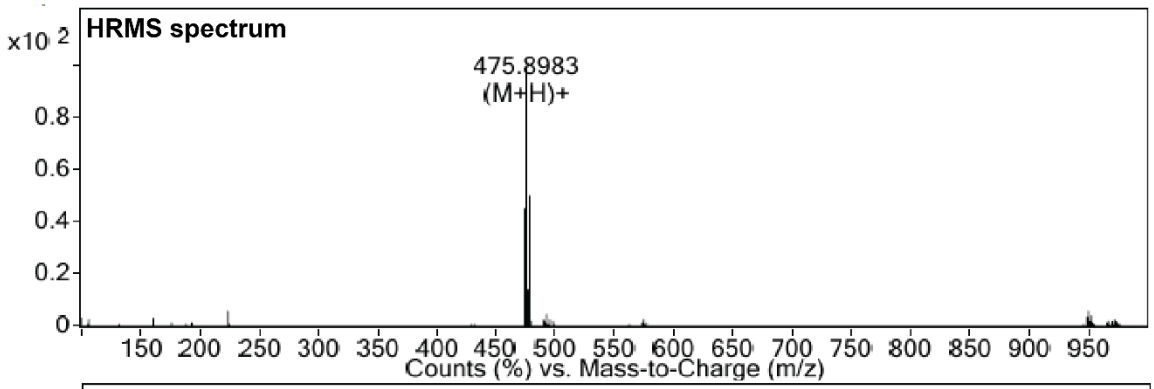

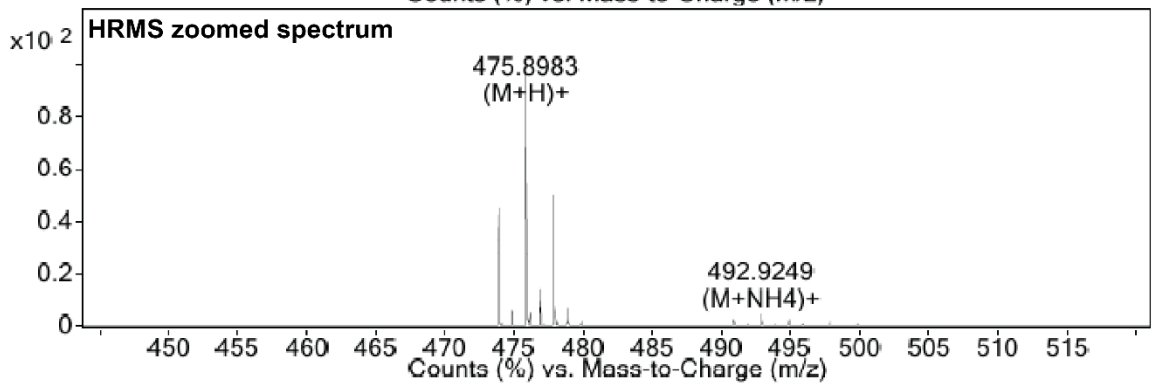

Compound 16

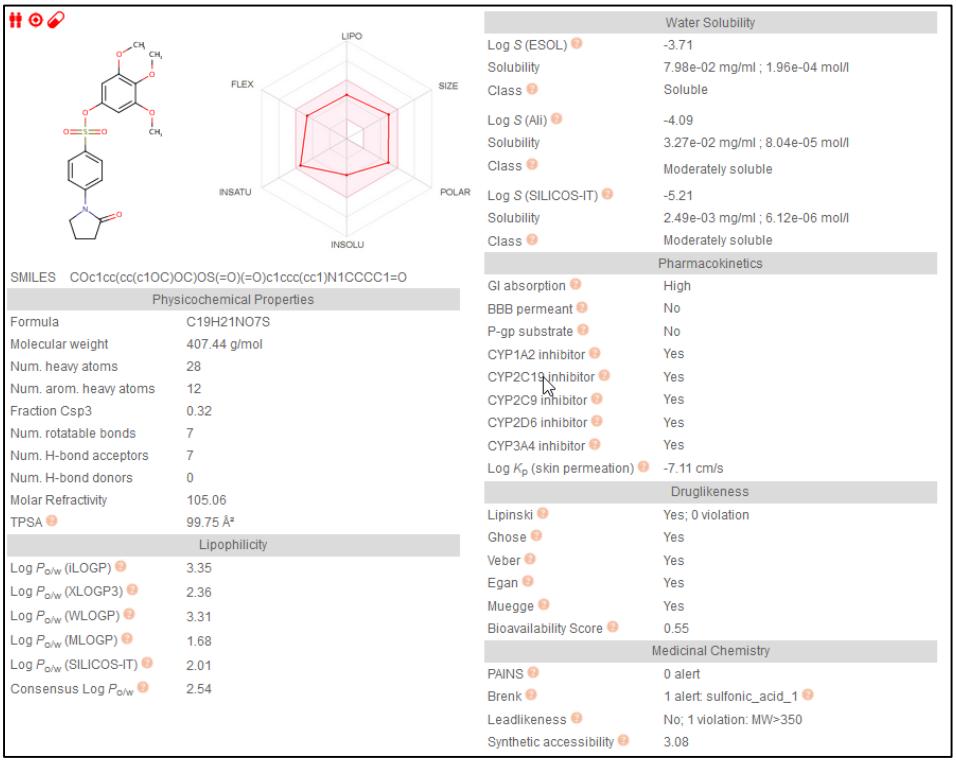

SMILES COc1cc(cc(c1OC)OC)OS(=O)(=O)c1ccc(cc1)N1CCCC1=O

Physicochemical Properties	
Formula	C19H21NO7S
Molecular weight	407.44 g/mol
Num. heavy atoms	28
Num. arom. heavy atoms	12
Fraction Csp3	0.32
Num. rotatable bonds	7
Num. H-bond acceptors	7
Num. H-bond donors	0
Molar Refractivity	105.06
TPSA	99.75 Å²

Lipophilicity	
Log $P_{o/w}$ (iLOGP)	3.35
Log $P_{o/w}$ (XLOGP3)	2.36
Log $P_{o/w}$ (WLOGP)	3.31
Log $P_{o/w}$ (MLOGP)	1.68
Log $P_{o/w}$ (SILICOS-IT)	2.01
Consensus Log $P_{o/w}$	2.54

Water Solubility	
Log *S* (ESOL)	-3.71
Solubility	7.98e-02 mg/ml ; 1.96e-04 mol/l
Class	Soluble
Log *S* (Ali)	-4.09
Solubility	3.27e-02 mg/ml ; 8.04e-05 mol/l
Class	Moderately soluble
Log *S* (SILICOS-IT)	-5.21
Solubility	2.49e-03 mg/ml ; 6.12e-06 mol/l
Class	Moderately soluble

Pharmacokinetics	
GI absorption	High
BBB permeant	No
P-gp substrate	No
CYP1A2 inhibitor	Yes
CYP2C19 inhibitor	Yes
CYP2C9 inhibitor	Yes
CYP2D6 inhibitor	Yes
CYP3A4 inhibitor	Yes
Log K_p (skin permeation)	-7.11 cm/s

Druglikeness	
Lipinski	Yes; 0 violation
Ghose	Yes
Veber	Yes
Egan	Yes
Muegge	Yes
Bioavailability Score	0.55

Medicinal Chemistry	
PAINS	0 alert
Brenk	1 alert: sulfonic_acid_1
Leadlikeness	No; 1 violation: MW>350
Synthetic accessibility	3.08

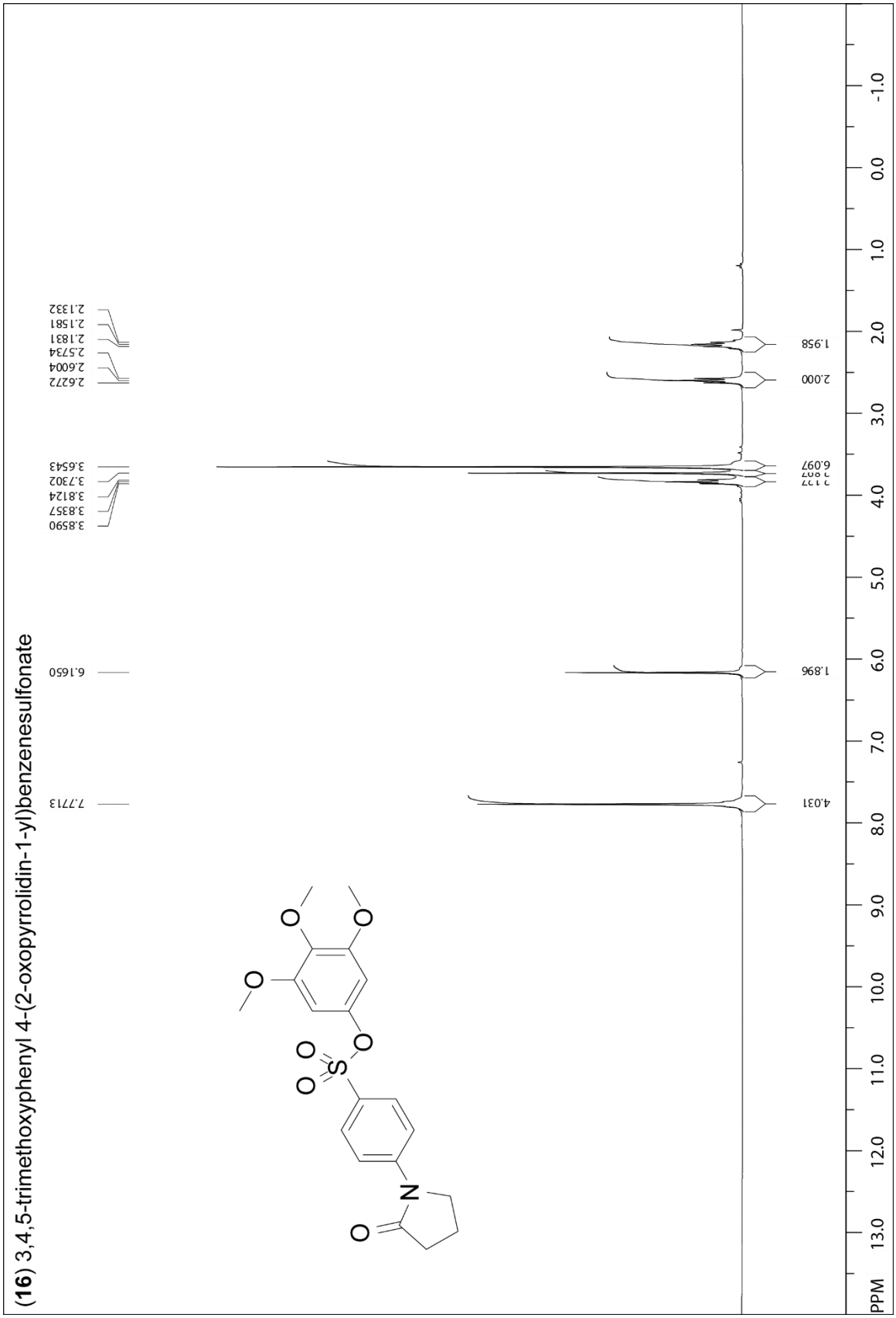
(16) 3,4,5-trimethoxyphenyl 4-(2-oxopyrrolidin-1-yl)benzenesulfonate
7.7713
6.1650
3.8590
3.8357
3.8124
3.7302
3.6543
2.6272
2.6004
2.5734
2.1831
2.1581
2.1332
4.031
1.896
6.097
2.000
1.958
PPM

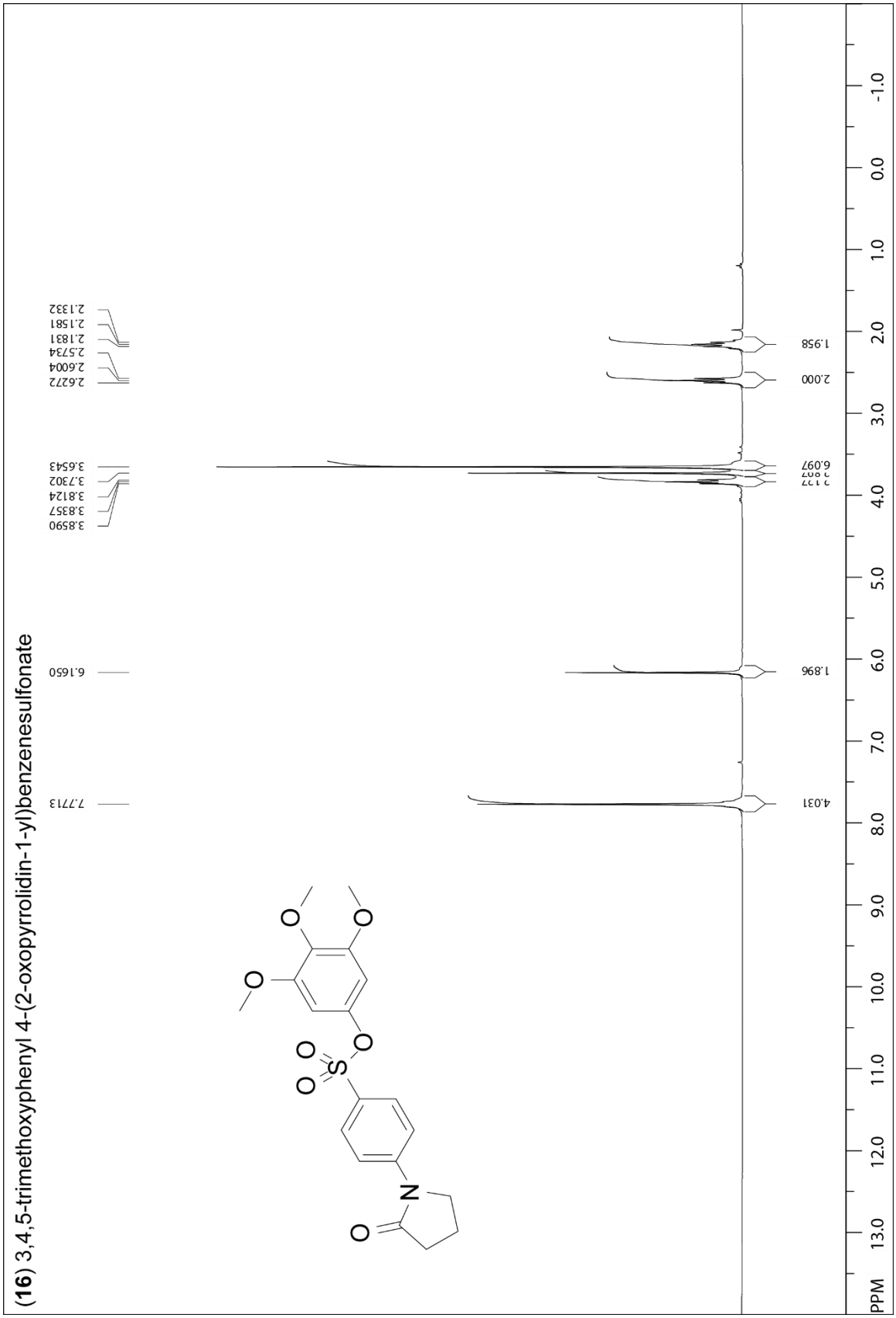
(16) 3,4,5-trimethoxyphenyl 4-(2-oxopyrrolidin-1-yl)benzenesulfonate
7.7713
6.1650
3.8590
3.8357
3.8124
3.7302
3.6543
2.6272
2.6004
2.5734
2.1831
2.1581
2.1332
4.031
1.896
6.097
2.000
1.958
PPM

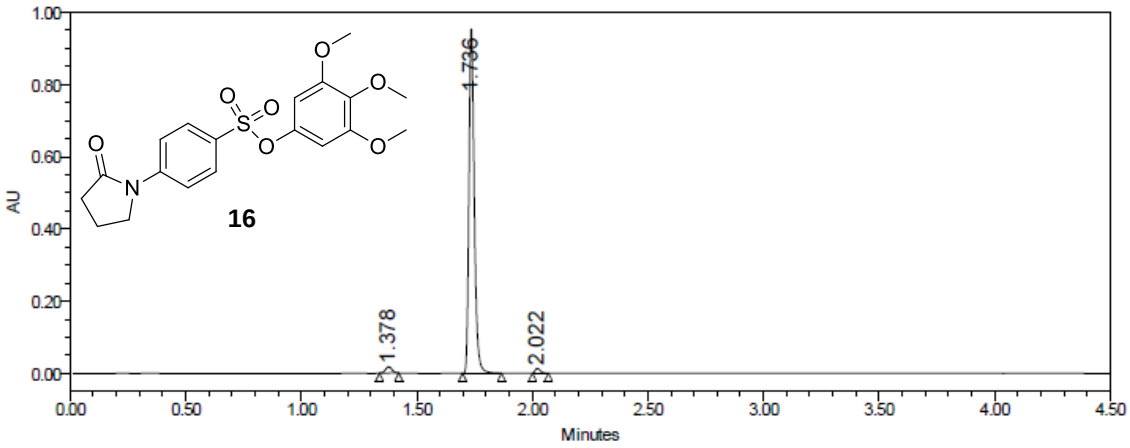

16

	RT	Area	% Area	Height
1	1.378	34498	2.19	17874
2	1.736	1519129	96.51	955568
3	2.022	20361	1.29	13427

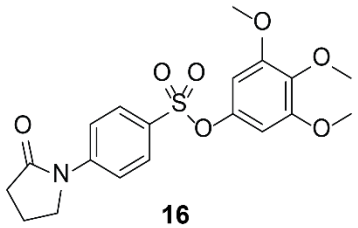

16

m/z	*Calc m/z*	Diff(ppm)	z	Abund	Formula	Ion
408.1115	408.1111	0.94		364725	C19 H22 N O7 S	(M+H)+
408.3615				30460		
408.6154				1780		
409.1141	409.1143	-0.51		68029	C19 H22 N O7 S	(M+H)+
409.3638				2186		
410.1114	410.1114	-0.13		20342	C19 H22 N O7 S	(M+H)+
411.1153	411.1132	5.17		3585	C19 H22 N O7 S	(M+H)+
425.1374	425.1377	-0.61	1	98729	C19 H25 N2 O7 S	(M+NH4)+

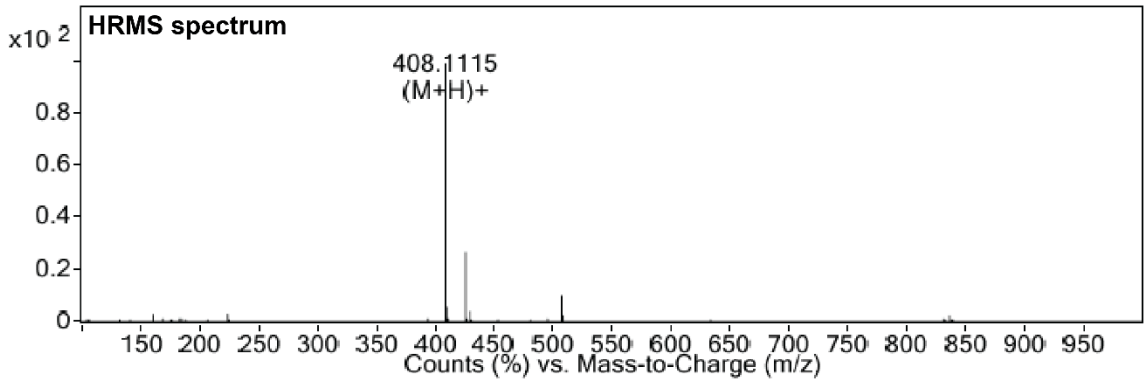

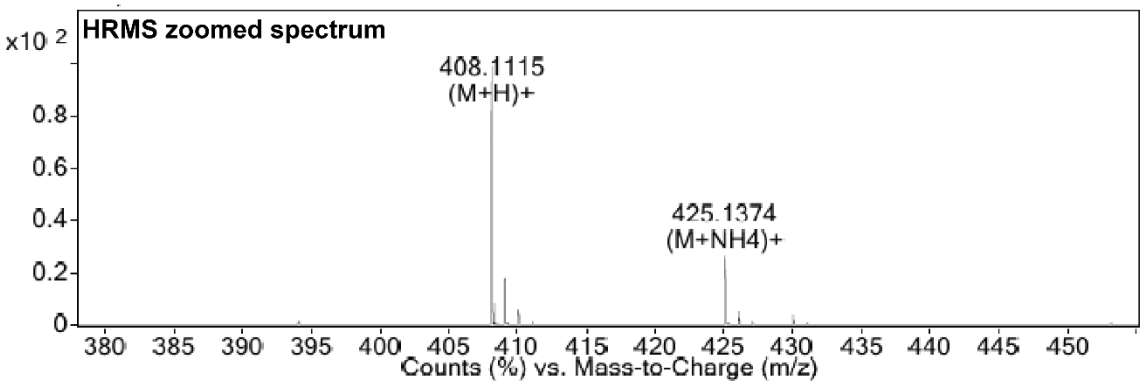

Compound 21

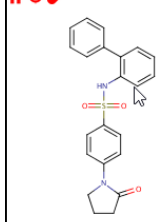

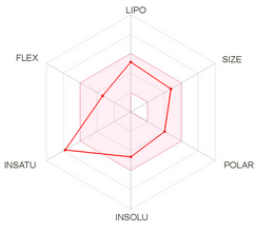

SMILES O=C1CCCN1c1ccc(cc1)S(=O)(=O)Nc1ccccc1c1ccccc1

Physicochemical Properties	
Formula	C22H20N2O3S
Molecular weight	392.47 g/mol
Num. heavy atoms	28
Num. arom. heavy atoms	18
Fraction Csp3	0.14
Num. rotatable bonds	5
Num. H-bond acceptors	3
Num. H-bond donors	1
Molar Refractivity	113.83
TPSA	74.86 Å²

Lipophilicity	
Log $P_{o/w}$ (iLOGP)	2.54
Log $P_{o/w}$ (XLOGP3)	3.50
Log $P_{o/w}$ (WLOGP)	4.79
Log $P_{o/w}$ (MLOGP)	2.92
Log $P_{o/w}$ (SILICOS-IT)	3.08
Consensus Log $P_{o/w}$	3.37

Water Solubility	
Log *S* (ESOL)	-4.62
Solubility	9.33e-03 mg/ml ; 2.38e-05 mol/l
Class	Moderately soluble
Log *S* (Ali)	-4.76
Solubility	6.90e-03 mg/ml ; 1.76e-05 mol/l
Class	Moderately soluble
Log *S* (SILICOS-IT)	-7.67
Solubility	8.39e-06 mg/ml ; 2.14e-08 mol/l
Class	Poorly soluble

Pharmacokinetics	
GI absorption	High
BBB permeant	No
P-gp substrate	No
CYP1A2 inhibitor	Yes
CYP2C19 inhibitor	Yes
CYP2C9 inhibitor	Yes
CYP2D6 inhibitor	Yes
CYP3A4 inhibitor	Yes
Log K_p (skin permeation)	-6.21 cm/s

Druglikeness	
Lipinski	Yes; 0 violation
Ghose	Yes
Veber	Yes
Egan	Yes
Muegge	Yes
Bioavailability Score	0.55

Medicinal Chemistry	
PAINS	0 alert
Brenk	0 alert
Leadlikeness	No; 1 violation: MW>350
Synthetic accessibility	2.78

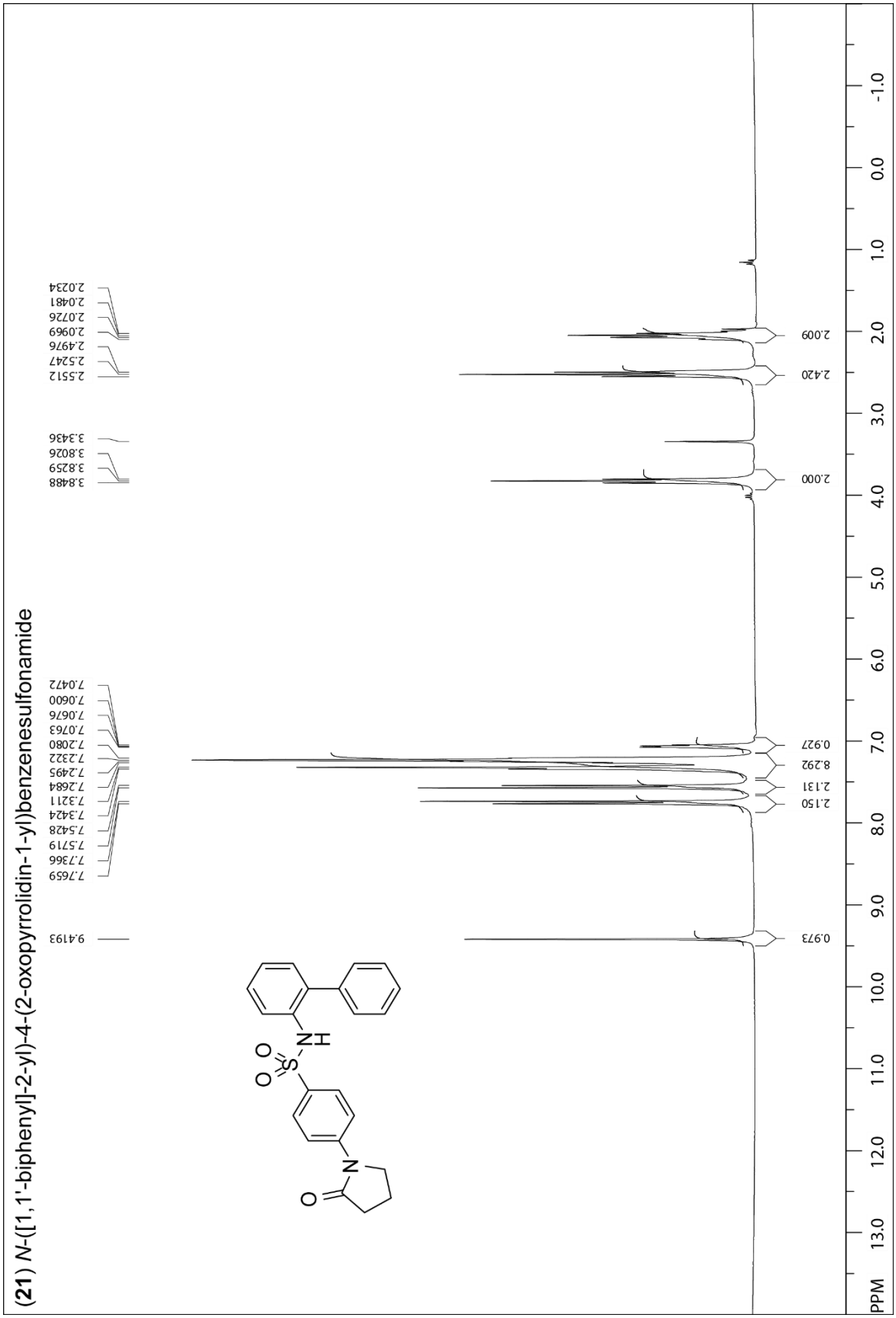
(21) N-([1,1'-biphenyl]-2-yl)-4-(2-oxopyrrolidin-1-yl)benzenesulfonamide
9.4193
7.7659
7.7366
7.5719
7.5428
7.3424
7.3211
7.2684
7.2495
7.2322
7.2080
7.0763
7.0676
7.0600
7.0472
3.8488
3.8259
3.8026
3.3436
2.5512
2.5247
2.4976
2.0969
2.0726
2.0481
2.0234
0.973
2.009
2.420
2.000
0.927
8.292
2.131
2.150
PPM
13.0
12.0
11.0
10.0
9.0
8.0
7.0
6.0
5.0
4.0
3.0
2.0
1.0
0.0
-1.0

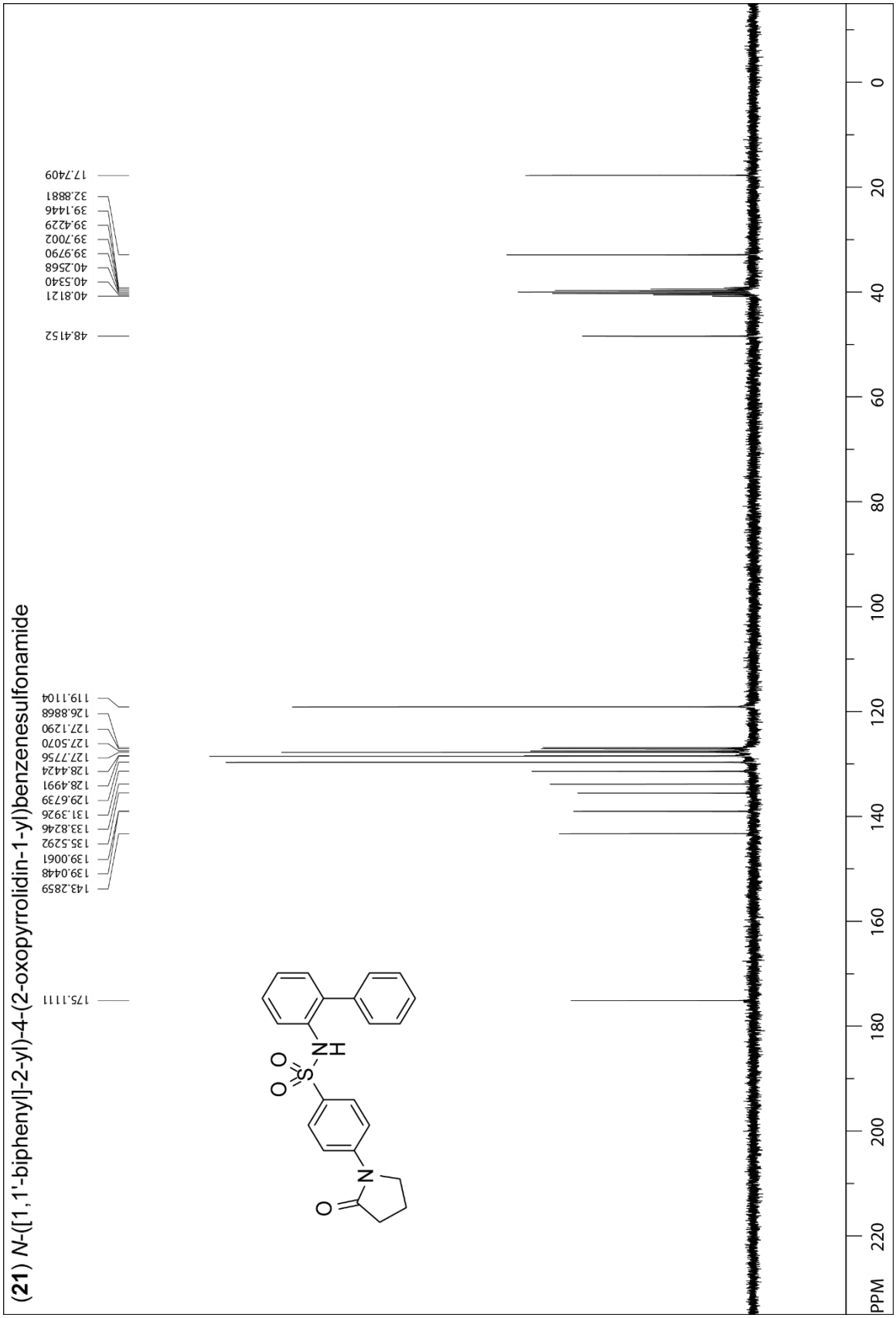
(21) N-([1,1'-biphenyl]-2-yl)-4-(2-oxopyrrolidin-1-yl)benzenesulfonamide
175.1111
143.2859
139.0448
139.0061
135.5292
133.8246
131.3926
129.6739
128.4991
128.4424
127.7756
127.5070
127.1290
126.8868
119.1104
48.4152
40.8121
40.5340
40.2568
39.9790
39.7002
39.4229
39.1446
32.8881
17.7409
PPM
220
200
180
160
140
120
100
80
60
40
20
0

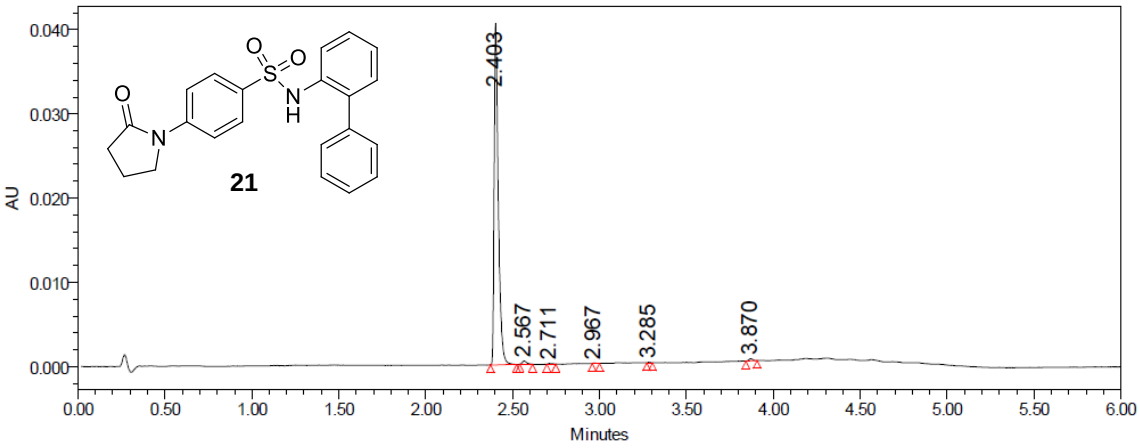

	RT	Area	% Area	Height
1	2.403	66463	98.04	40554
2	2.567	671	0.99	398
3	2.711	123	0.18	71
4	2.967	49	0.07	38
5	3.285	96	0.14	76
6	3.870	393	0.58	249

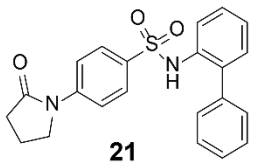

21

m/z	*Calc m/z*	Diff(ppm)	z	Abund	Formula	Ion
393.1266	393.1267	-0.32		221245	C22 H21 N2 O3 S	(M+H)+
393.3701				13342		
393.6197				582		
394.1287	394.1298	-2.77		48776	C22 H21 N2 O3 S	(M+H)+
394.3731				1122		
395.1266	395.1271	-1.32		12236	C22 H21 N2 O3 S	(M+H)+
396.1275	396.1283	-1.89		1929	C22 H21 N2 O3 S	(M+H)+
410.1531	410.1533	-0.51	1	11769	C22 H24 N3 O3 S	(M+NH4)+

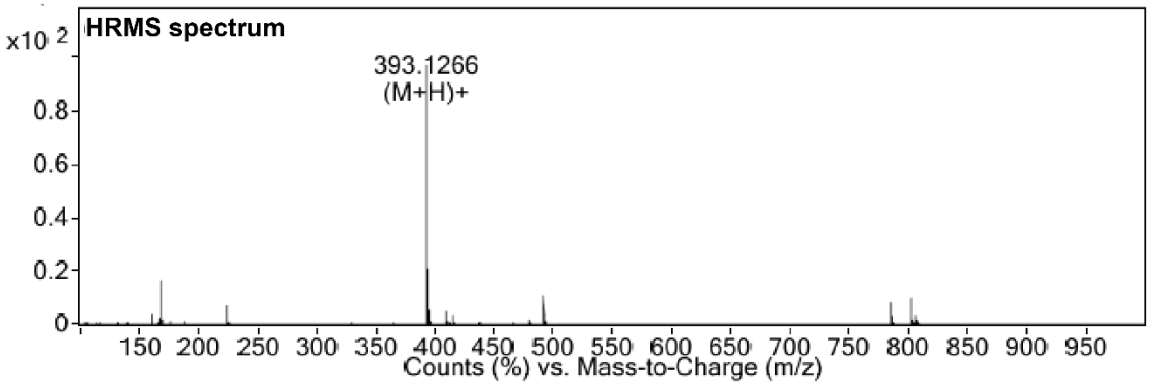

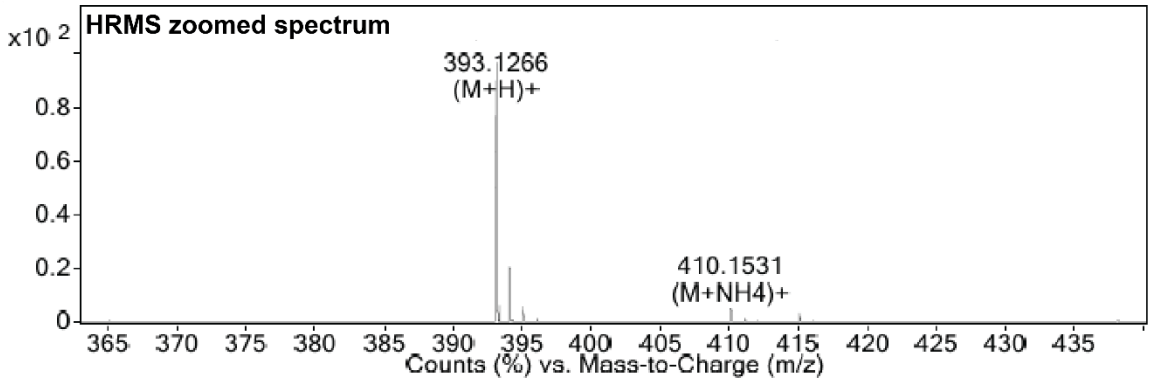

Compound 25

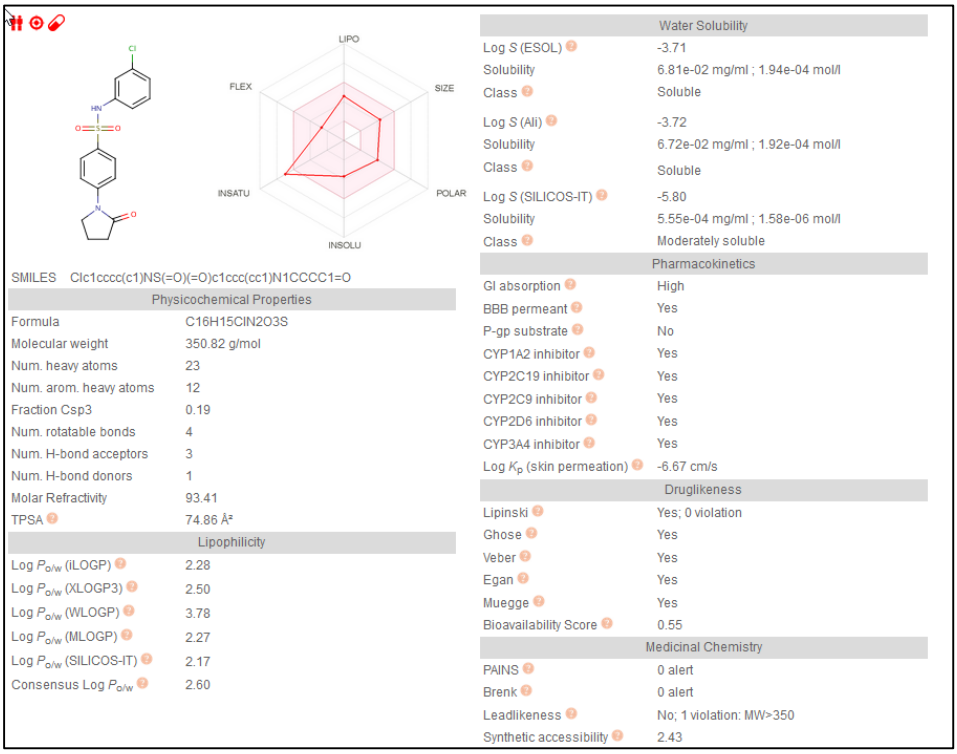

SMILES ClC1cccc(c1)NS(=O)(=O)c1ccc(cc1)N1CCCC1=O

Physicochemical Properties	
Formula	C16H15ClN2O3S
Molecular weight	350.82 g/mol
Num. heavy atoms	23
Num. arom. heavy atoms	12
Fraction Csp3	0.19
Num. rotatable bonds	4
Num. H-bond acceptors	3
Num. H-bond donors	1
Molar Refractivity	93.41
TPSA	74.86 Å²

Lipophilicity	
Log $P_{o/w}$ (iLOGP)	2.28
Log $P_{o/w}$ (XLOGP3)	2.50
Log $P_{o/w}$ (WLOGP)	3.78
Log $P_{o/w}$ (MLOGP)	2.27
Log $P_{o/w}$ (SILICOS-IT)	2.17
Consensus Log $P_{o/w}$	2.60

Water Solubility	
Log *S* (ESOL)	-3.71
Solubility	6.81e-02 mg/ml ; 1.94e-04 mol/l
Class	Soluble
Log *S* (Ali)	-3.72
Solubility	6.72e-02 mg/ml ; 1.92e-04 mol/l
Class	Soluble
Log *S* (SILICOS-IT)	-5.80
Solubility	5.55e-04 mg/ml ; 1.58e-06 mol/l
Class	Moderately soluble

Pharmacokinetics	
GI absorption	High
BBB permeant	Yes
P-gp substrate	No
CYP1A2 inhibitor	Yes
CYP2C19 inhibitor	Yes
CYP2C9 inhibitor	Yes
CYP2D6 inhibitor	Yes
CYP3A4 inhibitor	Yes
Log K_p (skin permeation)	-6.67 cm/s

Druglikeness	
Lipinski	Yes; 0 violation
Ghose	Yes
Veber	Yes
Egan	Yes
Muegge	Yes
Bioavailability Score	0.55

Medicinal Chemistry	
PAINS	0 alert
Brenk	0 alert
Leadlikeness	No; 1 violation: MW>350
Synthetic accessibility	2.43

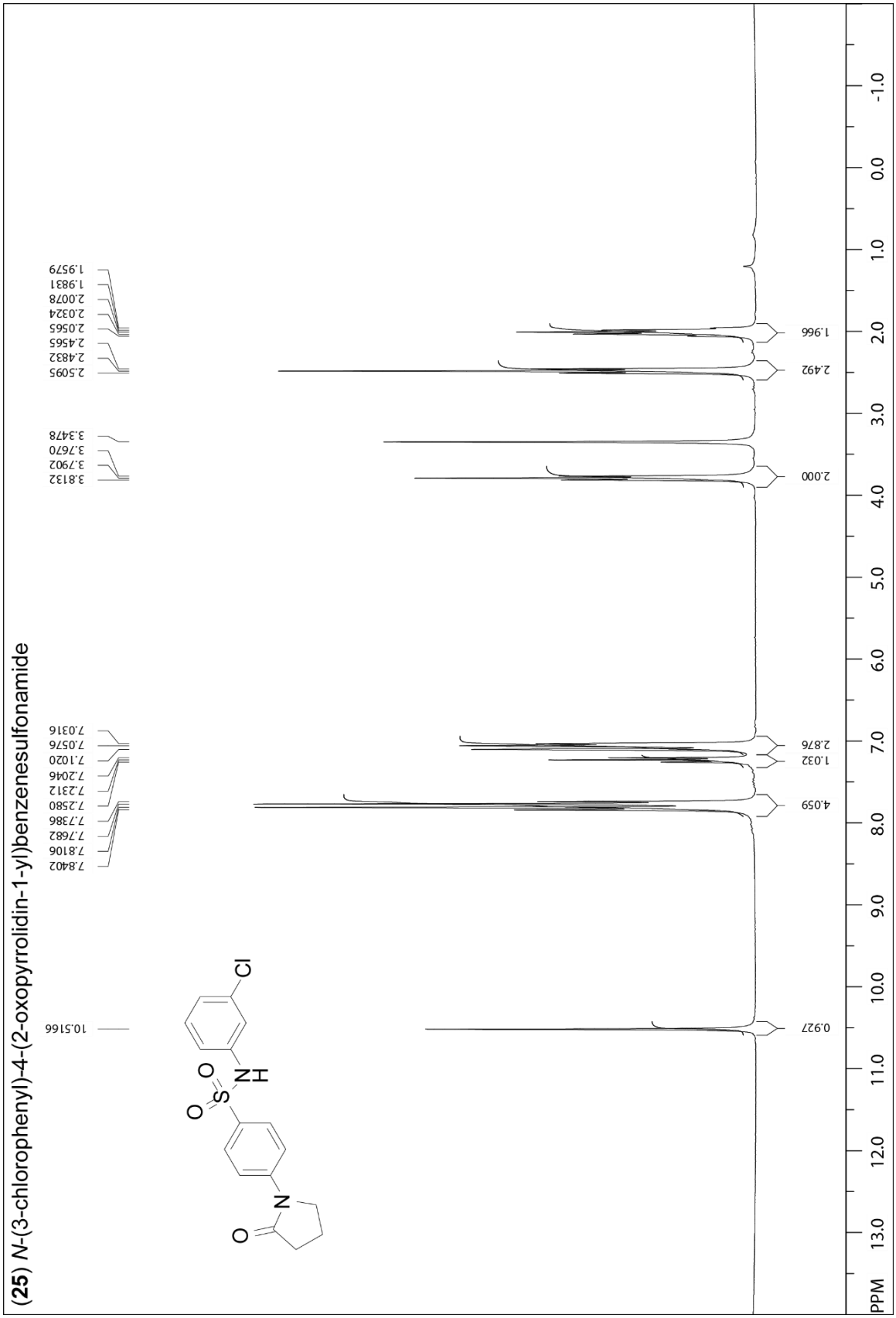
(25) N-(3-chlorophenyl)-4-(2-oxopyrrolidin-1-yl)benzenesulfonamide
10.5166
7.8402
7.8106
7.7682
7.7386
7.2580
7.2312
7.2046
7.1020
7.0576
7.0316
3.8132
3.7902
3.7670
3.3478
2.5095
2.4832
2.4565
2.0565
2.0324
2.0078
1.9831
1.9579
0.927
4.059
1.032
2.876
2.000
2.492
1.966
PPM
13.0
12.0
11.0
10.0
9.0
8.0
7.0
6.0
5.0
4.0
3.0
2.0
1.0
0.0
-1.0

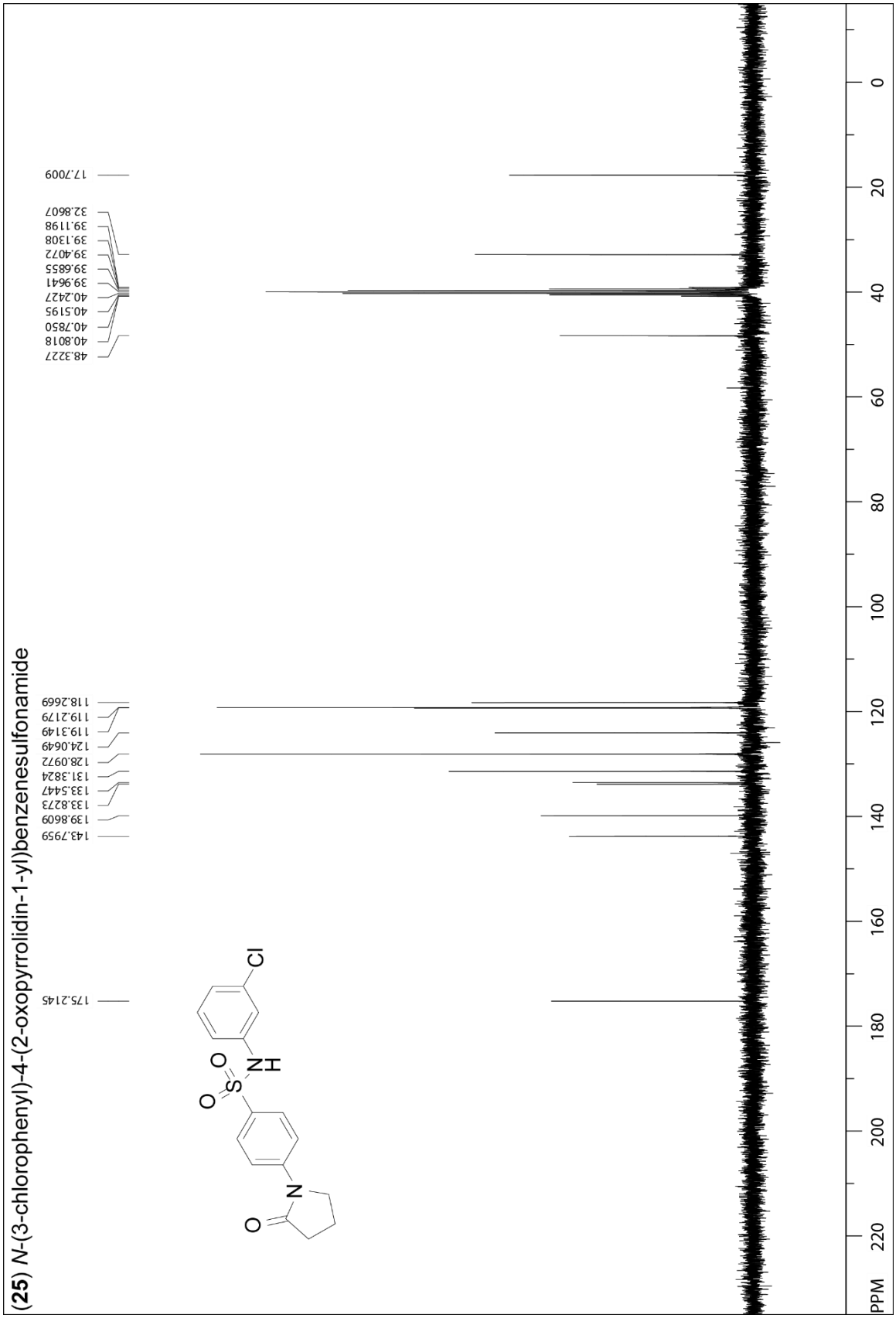
(25) N-(3-chlorophenyl)-4-(2-oxopyrrolidin-1-yl)benzenesulfonamide
175.2145
143.7959
139.8609
133.8273
133.5447
131.3824
128.0972
124.0649
119.3149
119.2179
118.2669
48.3227
40.8018
40.7850
40.5195
40.2427
39.9641
39.6855
39.4072
39.1308
39.1198
32.8607
17.7009
PPM
220
200
180
160
140
120
100
80
60
40
20
0

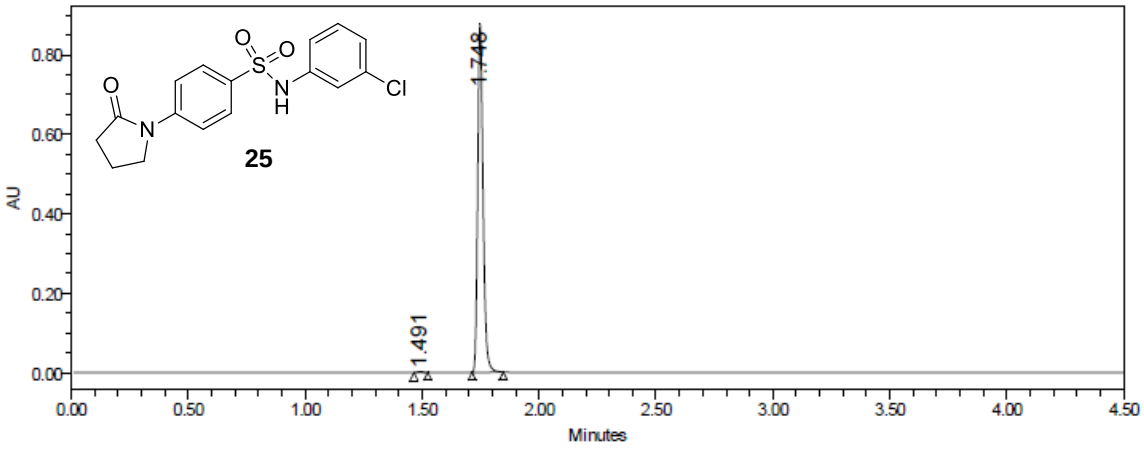

	RT	Area	% Area	Height
1	1.491	4252	0.30	2585
2	1.748	1396223	99.70	877439

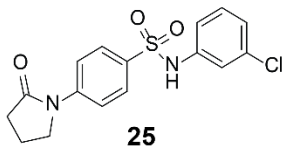

25

m/z	*Calc m/z*	Diff(ppm)	z	Abund	Formula	Ion
351.0561	351.0565	-1		195087	C16 H16 Cl N2 O3 S	(M+H)+
351.293				10014		
352.0589	352.0595	-1.52		28326	C16 H16 Cl N2 O3 S	(M+H)+
352.2908				516		
353.0534	353.0539	-1.26		66145	C16 H16 Cl N2 O3 S	(M+H)+
353.2915				1527		
354.0564	354.0566	-0.56		9078	C16 H16 Cl N2 O3 S	(M+H)+
355.0526	355.053	-1.11		2501	C16 H16 Cl N2 O3 S	(M+H)+

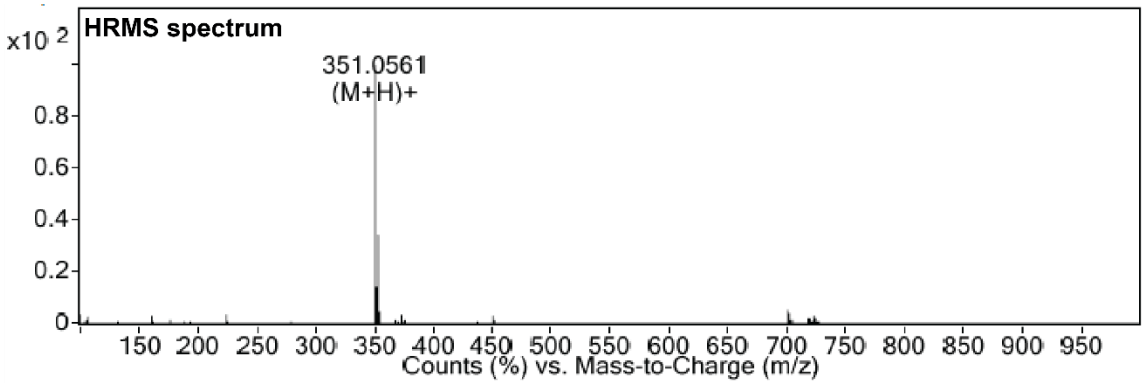

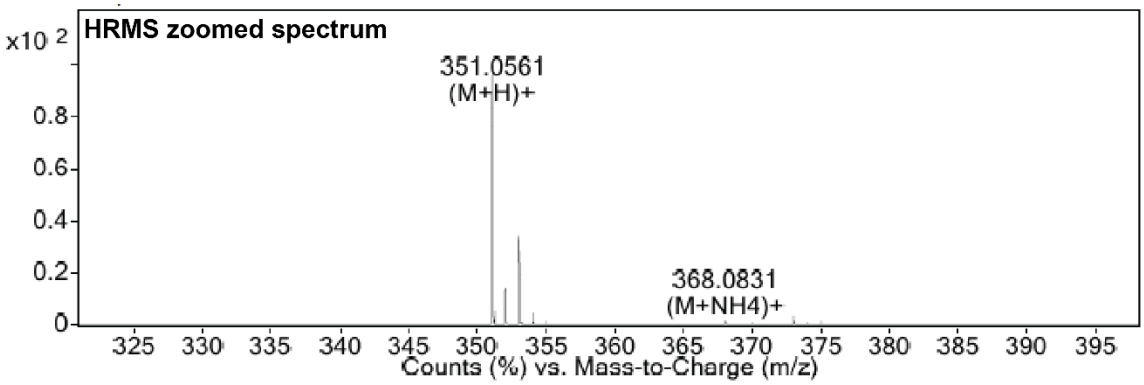

Compound 27

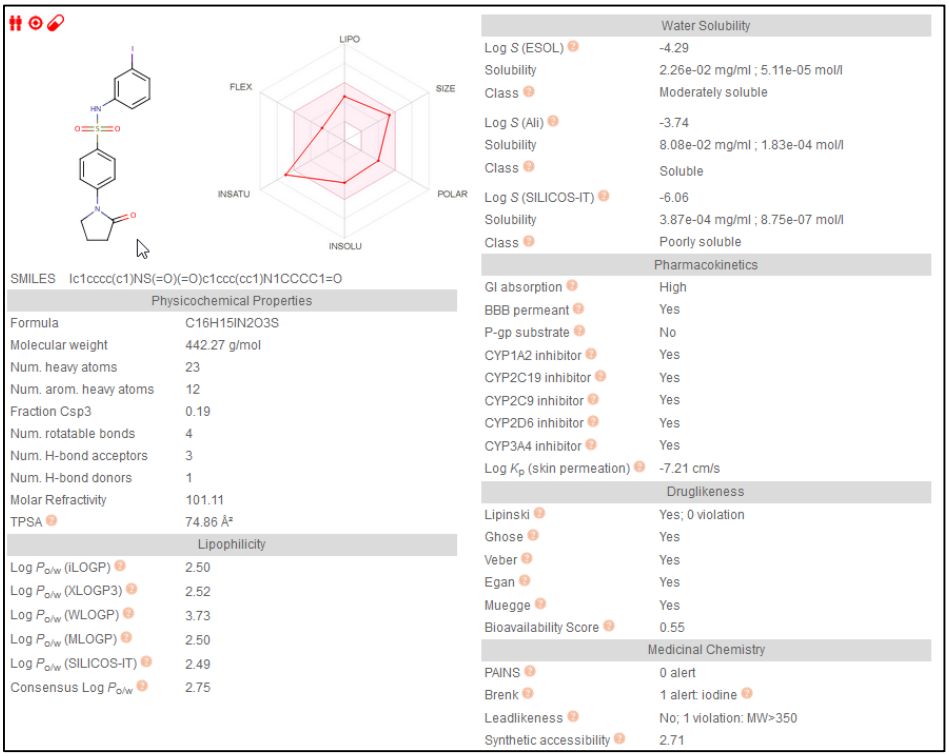

SMILES Ic1cccc(c1)NS(=O)(=O)c1ccc(cc1)N1CCCC1=O

Physicochemical Properties	
Formula	C16H15IN2O3S
Molecular weight	442.27 g/mol
Num. heavy atoms	23
Num. arom. heavy atoms	12
Fraction Csp3	0.19
Num. rotatable bonds	4
Num. H-bond acceptors	3
Num. H-bond donors	1
Molar Refractivity	101.11
TPSA	74.86 Å²

Lipophilicity	
Log $P_{o/w}$ (iLOGP)	2.50
Log $P_{o/w}$ (XLOGP3)	2.52
Log $P_{o/w}$ (WLOGP)	3.73
Log $P_{o/w}$ (MLOGP)	2.50
Log $P_{o/w}$ (SILICOS-IT)	2.49
Consensus Log $P_{o/w}$	2.75

Water Solubility	
Log *S* (ESOL)	-4.29
Solubility	2.26e-02 mg/ml ; 5.11e-05 mol/l
Class	Moderately soluble
Log *S* (Ali)	-3.74
Solubility	8.08e-02 mg/ml ; 1.83e-04 mol/l
Class	Soluble
Log *S* (SILICOS-IT)	-6.06
Solubility	3.87e-04 mg/ml ; 8.75e-07 mol/l
Class	Poorly soluble

Pharmacokinetics	
GI absorption	High
BBB permeant	Yes
P-gp substrate	No
CYP1A2 inhibitor	Yes
CYP2C19 inhibitor	Yes
CYP2C9 inhibitor	Yes
CYP2D6 inhibitor	Yes
CYP3A4 inhibitor	Yes
Log K_p (skin permeation)	-7.21 cm/s

Druglikeness	
Lipinski	Yes; 0 violation
Ghose	Yes
Veber	Yes
Egan	Yes
Muegge	Yes
Bioavailability Score	0.55

Medicinal Chemistry	
PAINS	0 alert
Brenk	1 alert: iodine
Leadlikeness	No; 1 violation: MW>350
Synthetic accessibility	2.71

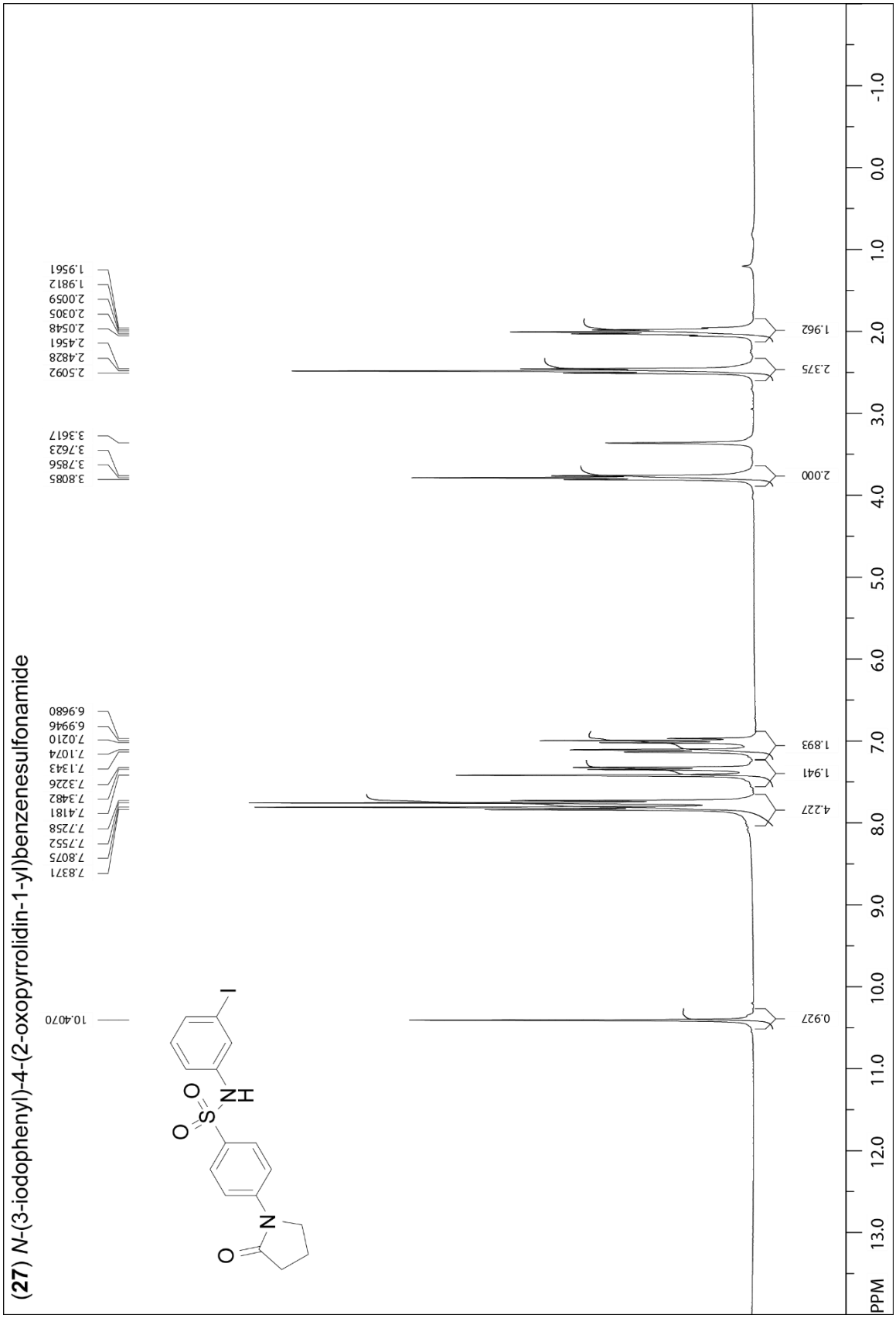
(27) N-(3-iodophenyl)-4-(2-oxopyrrolidin-1-yl)benzenesulfonamide
10.4070
7.8371
7.8075
7.7552
7.7258
7.4181
7.3482
7.3226
7.1343
7.1074
7.0210
6.9946
6.9680
3.8085
3.7856
3.7623
3.3617
2.5092
2.4828
2.4561
2.0548
2.0305
2.0059
1.9812
1.9561
0.927
4.227
1.941
1.893
2.000
2.375
1.962
PPM
13.0
12.0
11.0
10.0
9.0
8.0
7.0
6.0
5.0
4.0
3.0
2.0
1.0
0.0
-1.0

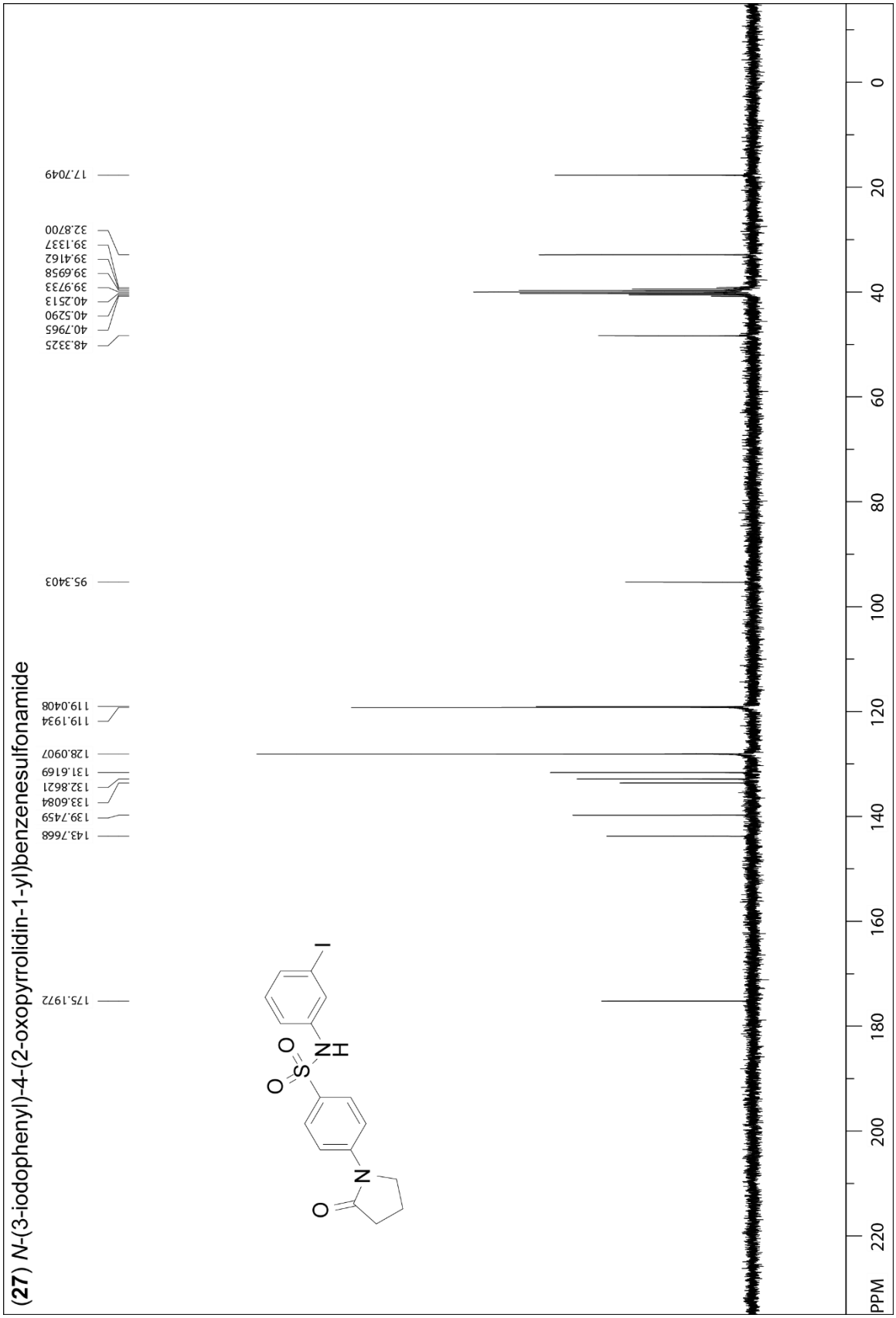
(27) N-(3-iodophenyl)-4-(2-oxopyrrolidin-1-yl)benzenesulfonamide
175.1972
143.7668
139.7459
133.6084
132.8621
131.6169
128.0907
119.1934
119.0408
95.3403
48.3325
40.7965
40.5290
40.2513
39.9733
39.6958
39.4162
39.1337
32.8700
17.7049
PPM
220
200
180
160
140
120
100
80
60
40
20
0

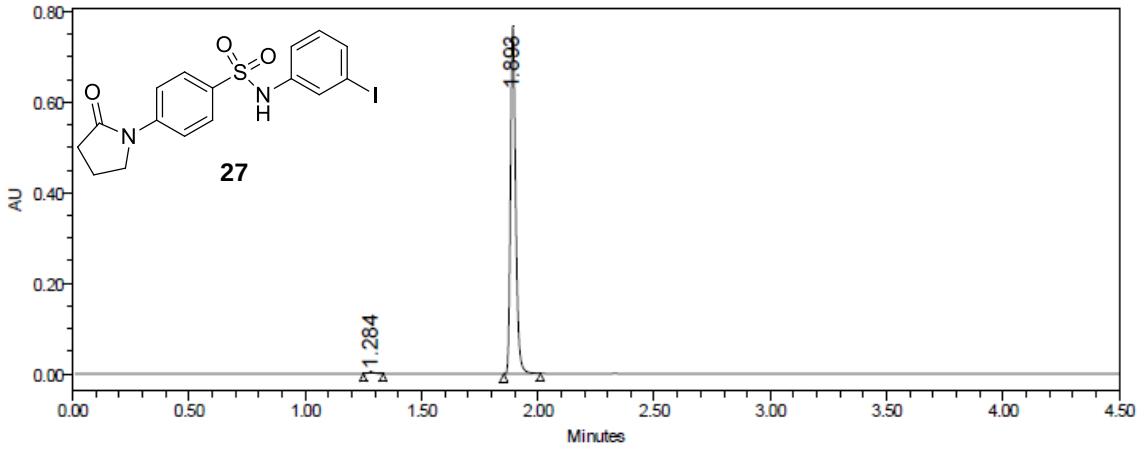

	RT	Area	% Area	Height
1	1.284	7623	0.64	3765
2	1.893	1185401	99.36	768137

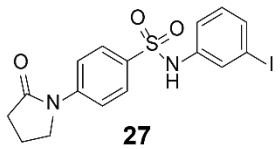

27

m/z	*Calc m/z*	Diff(ppm)	z	Abund	Formula	Ion
442.9908	442.9921	-3.01		155614	C16 H16 I N2 O3 S	(M+H)+
443.2521				6897		
443.3662				296		
443.5169				285		
443.9933	443.9951	-3.87		21685	C16 H16 I N2 O3 S	(M+H)+
444.2585				355		
444.9903	444.9912	-2.07		6238	C16 H16 I N2 O3 S	(M+H)+
445.9915	445.9929	-3.2		835	C16 H16 I N2 O3 S	(M+H)+

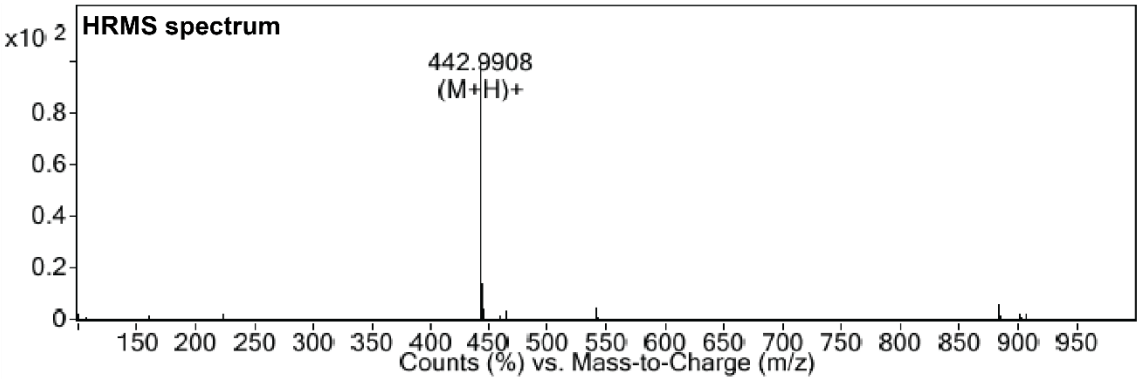

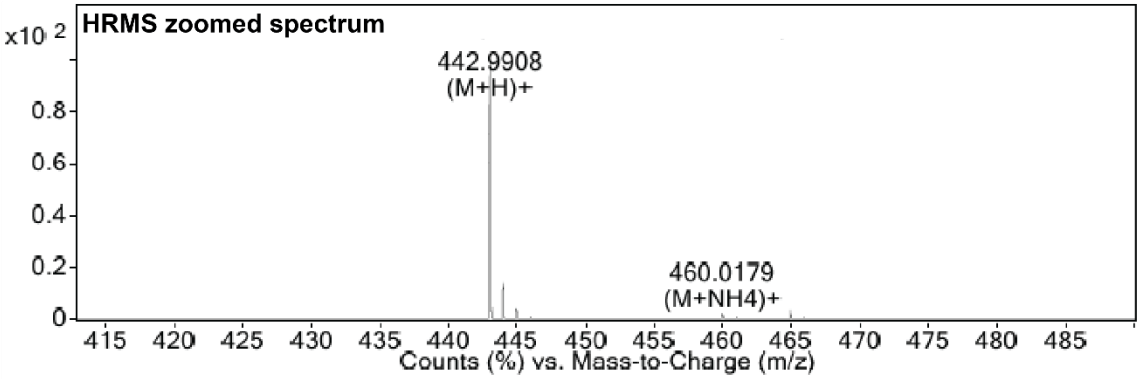

Compound 29

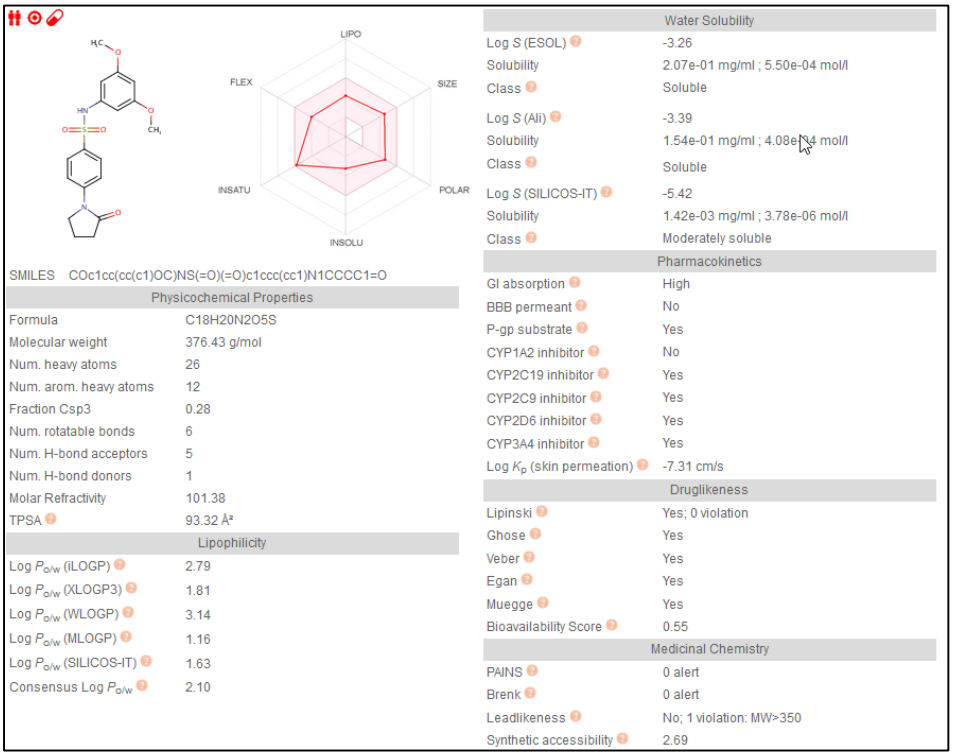

SMILES COc1cc(cc(c1)OC)NS(=O)(=O)c1ccc(cc1)N1CCCC1=O

Physicochemical Properties	
Formula	C18H20N2O5S
Molecular weight	376.43 g/mol
Num. heavy atoms	26
Num. arom. heavy atoms	12
Fraction Csp3	0.28
Num. rotatable bonds	6
Num. H-bond acceptors	5
Num. H-bond donors	1
Molar Refractivity	101.38
TPSA	93.32 Å²

Lipophilicity	
Log $P_{o/w}$ (iLOGP)	2.79
Log $P_{o/w}$ (XLOGP3)	1.81
Log $P_{o/w}$ (WLOGP)	3.14
Log $P_{o/w}$ (MLOGP)	1.16
Log $P_{o/w}$ (SILICOS-IT)	1.63
Consensus Log $P_{o/w}$	2.10

Water Solubility	
Log *S* (ESOL)	-3.26
Solubility	2.07e-01 mg/ml ; 5.50e-04 mol/l
Class	Soluble
Log *S* (Ali)	-3.39
Solubility	1.54e-01 mg/ml ; 4.08e-04 mol/l
Class	Soluble
Log *S* (SILICOS-IT)	-5.42
Solubility	1.42e-03 mg/ml ; 3.78e-06 mol/l
Class	Moderately soluble

Pharmacokinetics	
GI absorption	High
BBB permeant	No
P-gp substrate	Yes
CYP1A2 inhibitor	No
CYP2C19 inhibitor	Yes
CYP2C9 inhibitor	Yes
CYP2D6 inhibitor	Yes
CYP3A4 inhibitor	Yes
Log K_p (skin permeation)	-7.31 cm/s

Druglikeness	
Lipinski	Yes; 0 violation
Ghose	Yes
Veber	Yes
Egan	Yes
Muegge	Yes
Bioavailability Score	0.55

Medicinal Chemistry	
PAINS	0 alert
Brenk	0 alert
Leadlikeness	No; 1 violation: MW>350
Synthetic accessibility	2.69

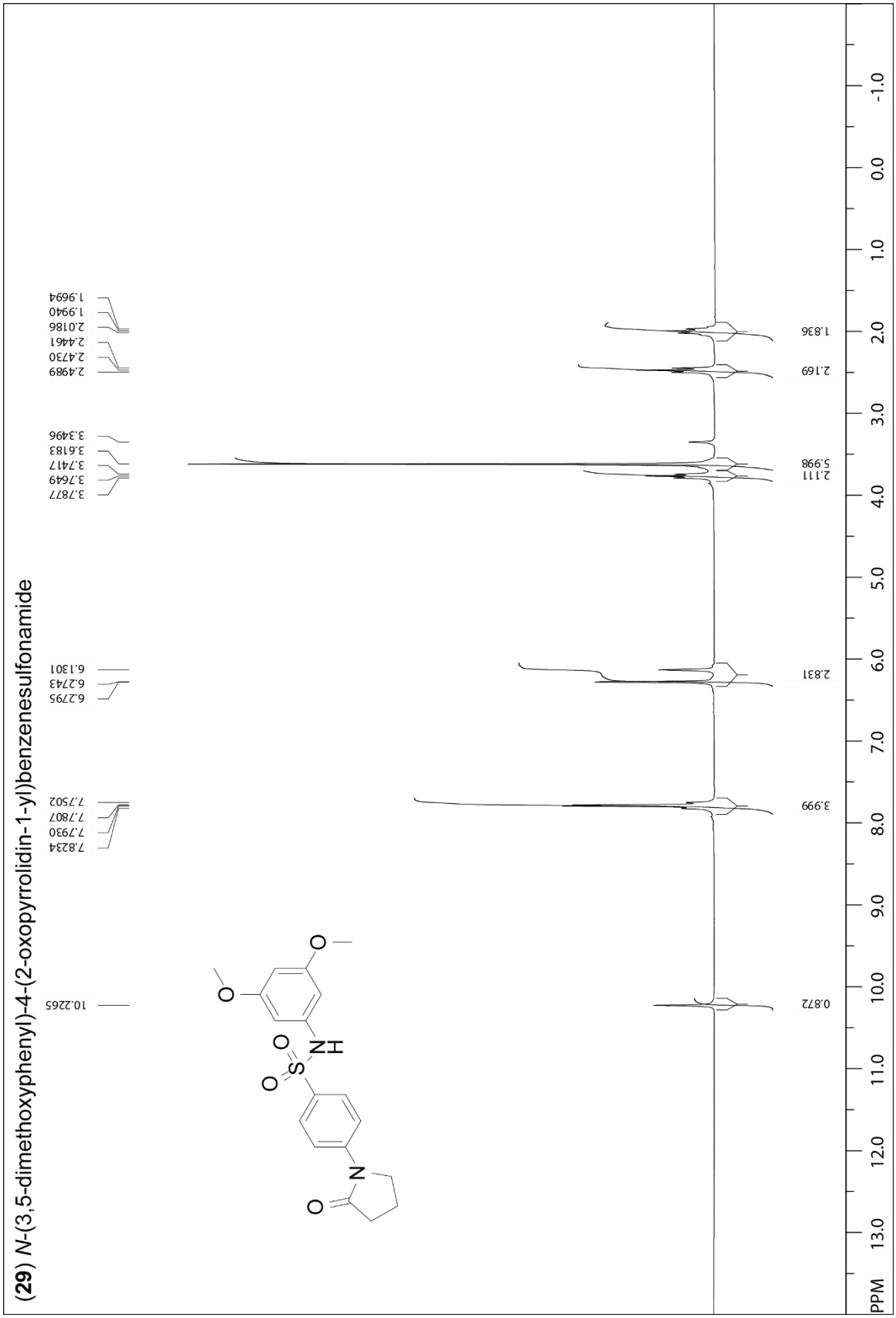
(29) N-(3,5-dimethoxyphenyl)-4-(2-oxopyrrolidin-1-yl)benzenesulfonamide
10.2265
7.8234
7.7930
7.7807
7.7502
6.2795
6.2743
6.1301
3.7877
3.7649
3.7417
3.6183
3.3496
2.4989
2.4730
2.4461
2.0186
1.9940
1.9694
0.872
3.999
2.831
5.998
2.111
2.169
1.836
PPM
13.0
12.0
11.0
10.0
9.0
8.0
7.0
6.0
5.0
4.0
3.0
2.0
1.0
0.0
-1.0

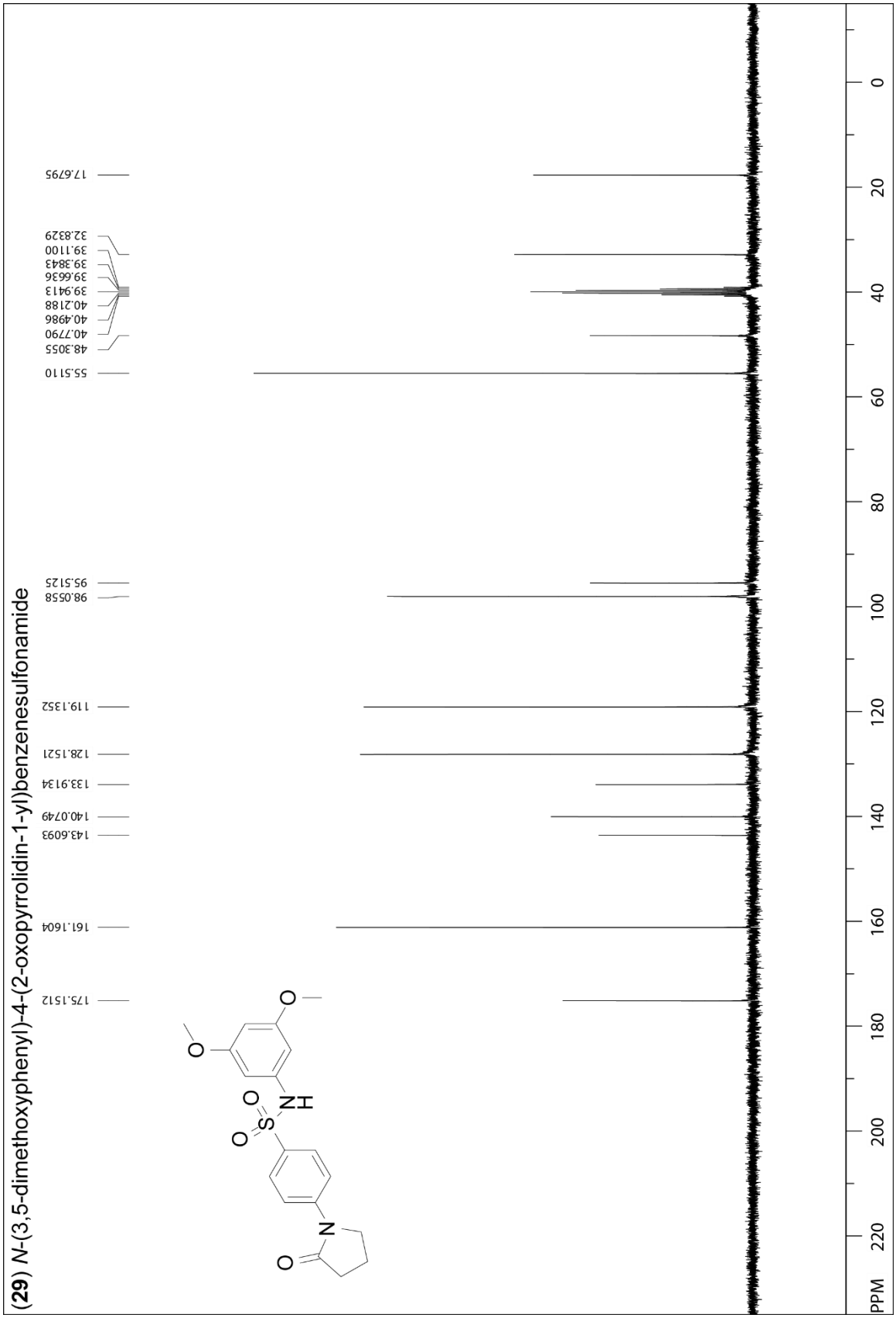
(29) N-(3,5-dimethoxyphenyl)-4-(2-oxopyrrolidin-1-yl)benzenesulfonamide
175.1512
161.1604
143.6093
140.0749
133.9134
128.1521
119.1352
98.0558
95.5125
55.5110
48.3055
40.7790
40.4986
40.2188
39.9413
39.6636
39.3843
39.1100
32.8329
17.6795
PPM
0
20
40
60
80
100
120
140
160
180
200
220

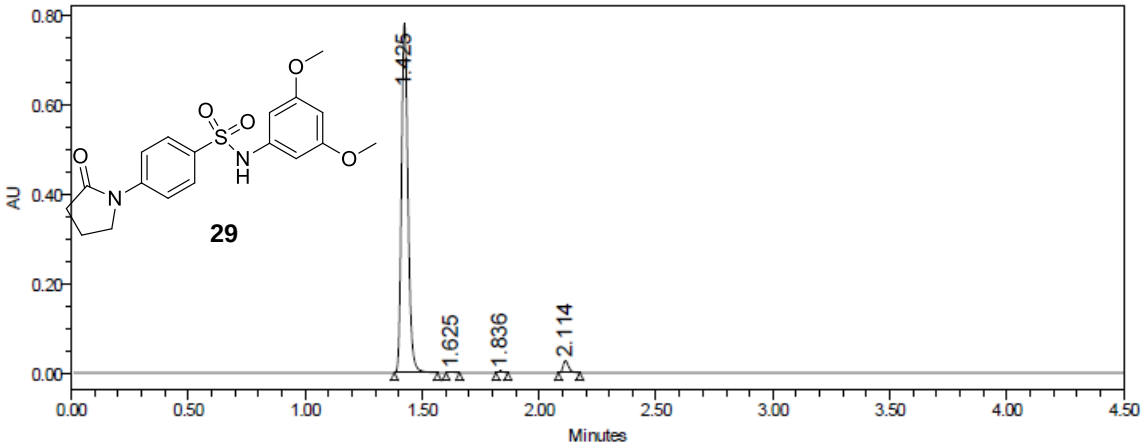

29

	RT	Area	% Area	Height
1	1.425	1503348	96.64	783023
2	1.625	2628	0.17	1627
3	1.836	4749	0.31	3332
4	2.114	44952	2.89	27137

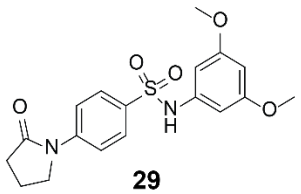

29

m/z	*Calc m/z*	Diff(ppm)	z	Abund	Formula	Ion
377.1154	377.1166	-3		302812	C18 H21 N2 O5 S	(M+H)+
377.36				20561		
377.4714				859		
377.5986				904		
377.7107				394		
378.118	378.1196	-4.15		54909	C18 H21 N2 O5 S	(M+H)+
378.3636				1487		
379.1149	379.1164	-3.98		15017	C18 H21 N2 O5 S	(M+H)+

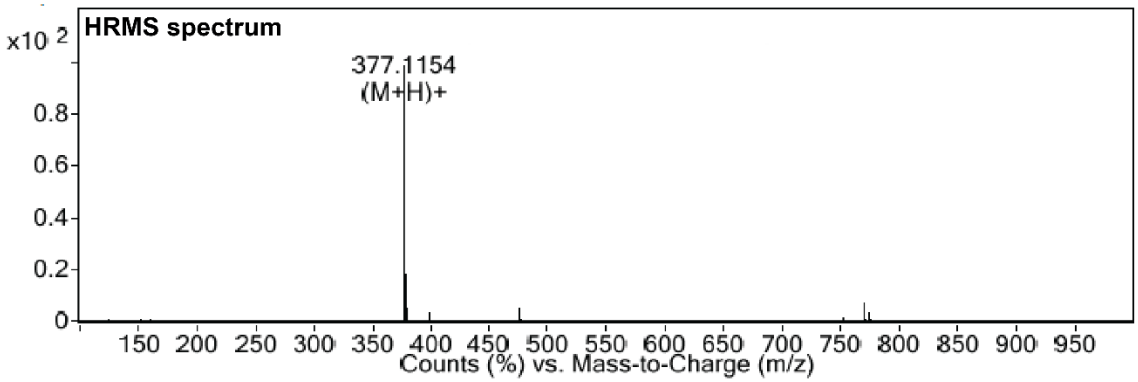

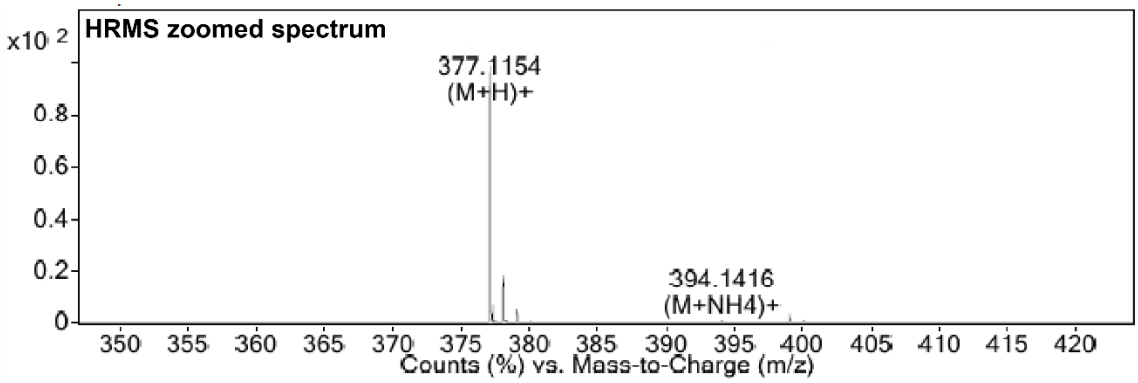

Compound 30

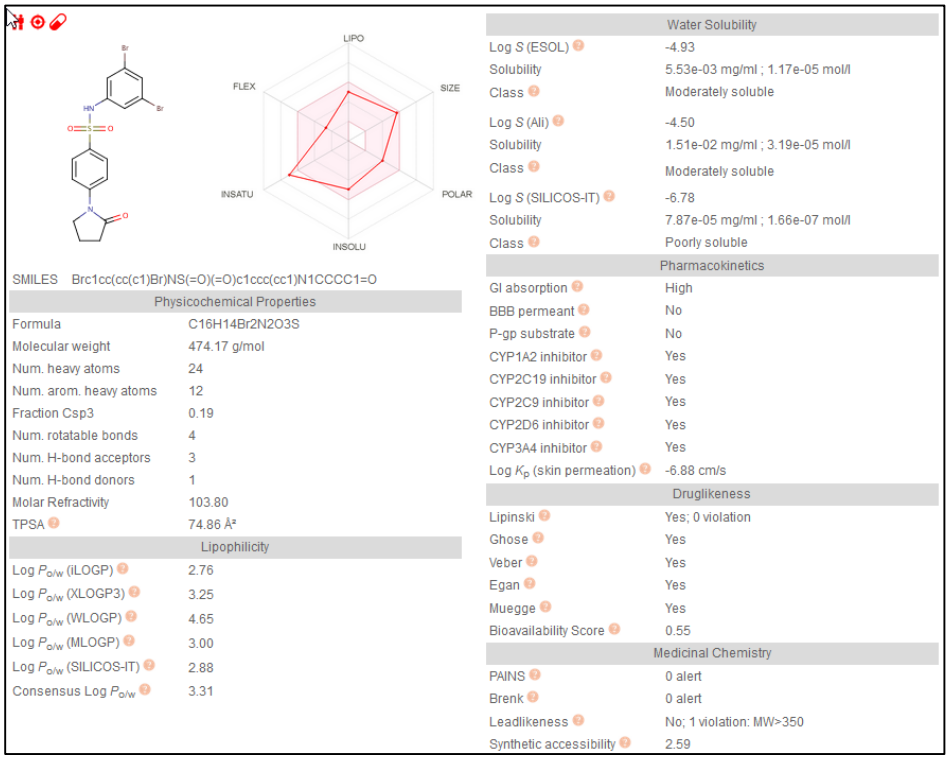

SMILES Brc1cc(cc(c1)Br)NS(=O)(=O)c1ccc(cc1)N1CCCC1=O

Physicochemical Properties	
Formula	C16H14Br2N2O3S
Molecular weight	474.17 g/mol
Num. heavy atoms	24
Num. arom. heavy atoms	12
Fraction Csp3	0.19
Num. rotatable bonds	4
Num. H-bond acceptors	3
Num. H-bond donors	1
Molar Refractivity	103.80
TPSA	74.86 Å²

Lipophilicity	
Log $P_{o/w}$ (iLOGP)	2.76
Log $P_{o/w}$ (XLOGP3)	3.25
Log $P_{o/w}$ (WLOGP)	4.65
Log $P_{o/w}$ (MLOGP)	3.00
Log $P_{o/w}$ (SILICOS-IT)	2.88
Consensus Log $P_{o/w}$	3.31

Water Solubility	
Log *S* (ESOL)	-4.93
Solubility	5.53e-03 mg/ml ; 1.17e-05 mol/l
Class	Moderately soluble
Log *S* (Ali)	-4.50
Solubility	1.51e-02 mg/ml ; 3.19e-05 mol/l
Class	Moderately soluble
Log *S* (SILICOS-IT)	-6.78
Solubility	7.87e-05 mg/ml ; 1.66e-07 mol/l
Class	Poorly soluble

Pharmacokinetics	
GI absorption	High
BBB permeant	No
P-gp substrate	No
CYP1A2 inhibitor	Yes
CYP2C19 inhibitor	Yes
CYP2C9 inhibitor	Yes
CYP2D6 inhibitor	Yes
CYP3A4 inhibitor	Yes
Log K_p (skin permeation)	-6.88 cm/s

Druglikeness	
Lipinski	Yes; 0 violation
Ghose	Yes
Veber	Yes
Egan	Yes
Muegge	Yes
Bioavailability Score	0.55

Medicinal Chemistry	
PAINS	0 alert
Brenk	0 alert
Leadlikeness	No; 1 violation: MW>350
Synthetic accessibility	2.59

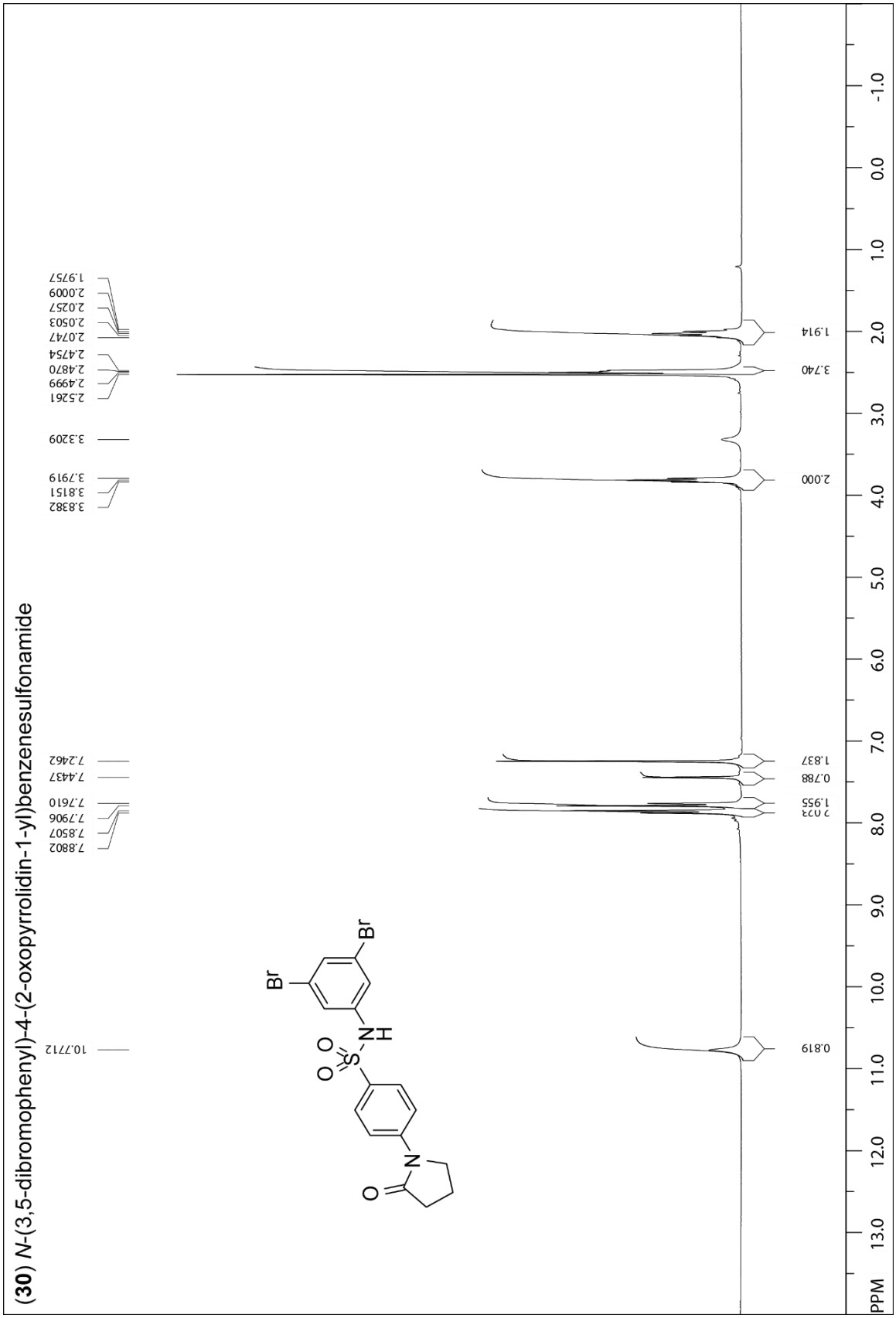
(30) N-(3,5-dibromophenyl)-4-(2-oxopyrrolidin-1-yl)benzenesulfonamide
10.7712
7.8802
7.8507
7.7906
7.7610
7.4437
7.2462
3.8382
3.8151
3.7919
3.3209
2.5261
2.4999
2.4870
2.4754
2.0747
2.0503
2.0257
2.0009
1.9757
0.819
2.000
3.740
1.914
PPM

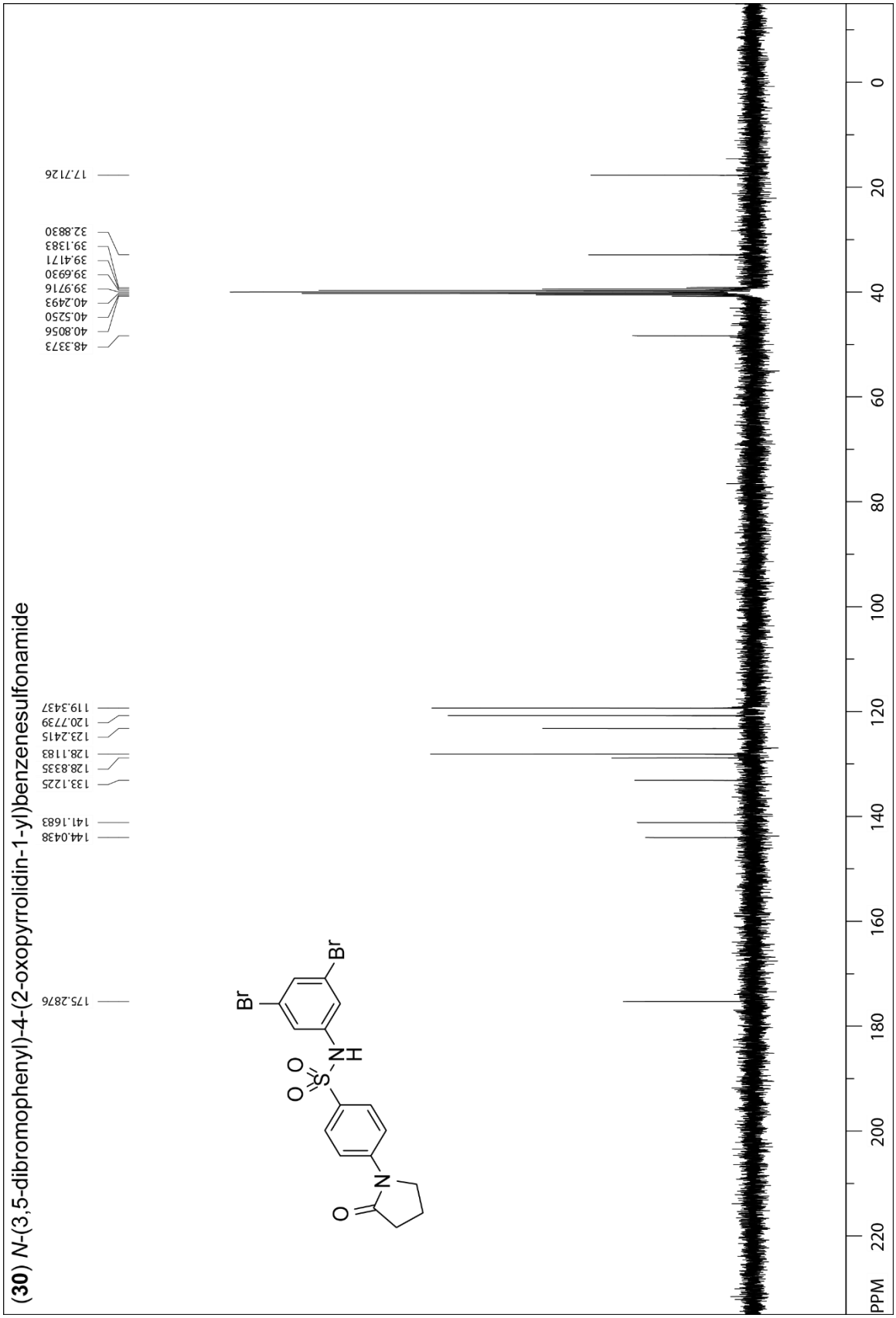
(30) N-(3,5-dibromophenyl)-4-(2-oxopyrrolidin-1-yl)benzenesulfonamide
175.2876
144.0438
141.1683
133.1225
128.8335
128.1183
123.2415
120.7739
119.3437
48.3373
40.8056
40.5250
40.2493
39.9716
39.6930
39.4171
39.1383
32.8830
17.7126
Br
Br
H
N
O
O
S
O
N
O
PPM
220
200
180
160
140
120
100
80
60
40
20
0

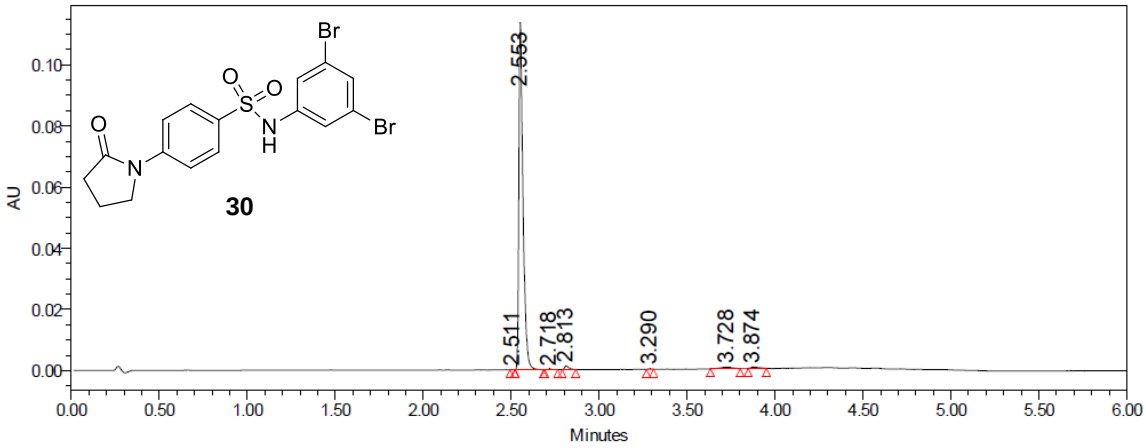

	RT	Area	% Area	Height
1	2.511	65	0.03	84
2	2.553	185435	96.93	113464
3	2.718	354	0.18	213
4	2.813	1983	1.04	1206
5	3.290	108	0.06	103
6	3.728	2140	1.12	442
7	3.874	1233	0.64	394

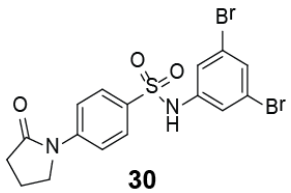

30

m/z	*Calc m/z*	Diff(ppm)	z	Abund	Formula	Ion
472.9156	472.9165	-1.87		13639	C16 H15 Br2 N2 O3 S	(M+H)+
473.9184	473.9194	-2.15		2067	C16 H15 Br2 N2 O3 S	(M+H)+
474.9134	474.9145	-2.23		31205	C16 H15 Br2 N2 O3 S	(M+H)+
475.9165	475.9174	-1.83		4508	C16 H15 Br2 N2 O3 S	(M+H)+
476.9115	476.9125	-2.18		14788	C16 H15 Br2 N2 O3 S	(M+H)+
477.9144	477.9153	-2.06		2215	C16 H15 Br2 N2 O3 S	(M+H)+
478.9113	478.9117	-0.74		684	C16 H15 Br2 N2 O3 S	(M+H)+
489.9423	489.943	-1.4	1	546	C16 H18 Br2 N3 O3 S	(M+NH4)+

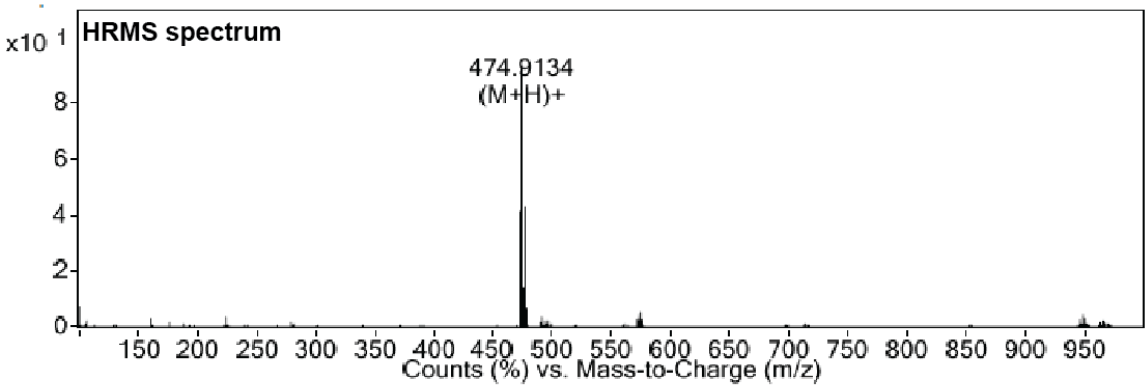

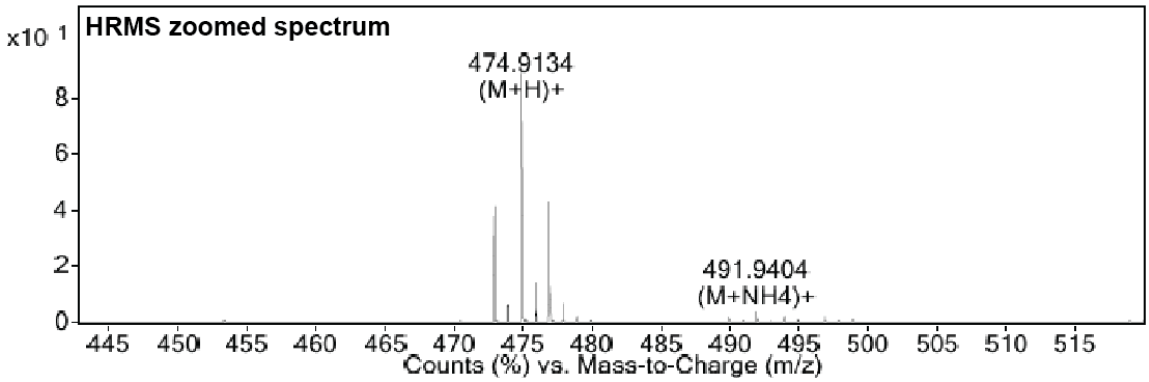

Compound 31

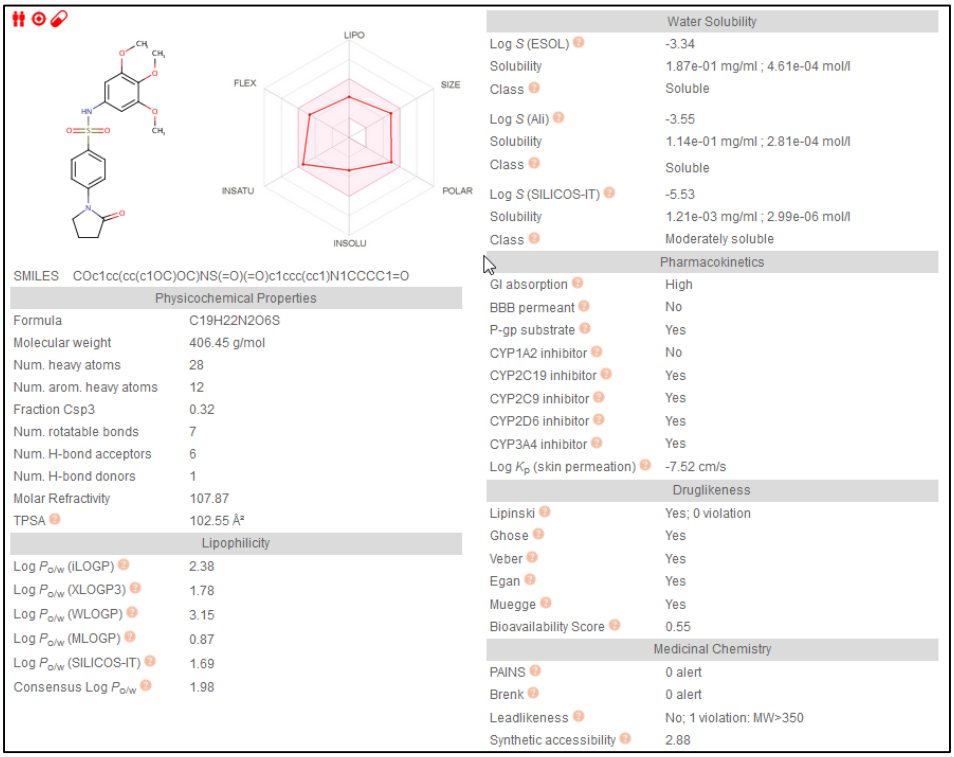

SMILES COc1cc(cc(c1OC)OC)NS(=O)(=O)c1ccc(cc1)N1CCCC1=O

Physicochemical Properties	
Formula	C19H22N2O6S
Molecular weight	406.45 g/mol
Num. heavy atoms	28
Num. arom. heavy atoms	12
Fraction Csp3	0.32
Num. rotatable bonds	7
Num. H-bond acceptors	6
Num. H-bond donors	1
Molar Refractivity	107.87
TPSA	102.55 Å²

Lipophilicity	
Log $P_{o/w}$ (iLOGP)	2.38
Log $P_{o/w}$ (XLOGP3)	1.78
Log $P_{o/w}$ (WLOGP)	3.15
Log $P_{o/w}$ (MLOGP)	0.87
Log $P_{o/w}$ (SILICOS-IT)	1.69
Consensus Log $P_{o/w}$	1.98

Water Solubility	
Log *S* (ESOL)	-3.34
Solubility	1.87e-01 mg/ml ; 4.61e-04 mol/l
Class	Soluble
Log *S* (Ali)	-3.55
Solubility	1.14e-01 mg/ml ; 2.81e-04 mol/l
Class	Soluble
Log *S* (SILICOS-IT)	-5.53
Solubility	1.21e-03 mg/ml ; 2.99e-06 mol/l
Class	Moderately soluble

Pharmacokinetics	
GI absorption	High
BBB permeant	No
P-gp substrate	Yes
CYP1A2 inhibitor	No
CYP2C19 inhibitor	Yes
CYP2C9 inhibitor	Yes
CYP2D6 inhibitor	Yes
CYP3A4 inhibitor	Yes
Log K_p (skin permeation)	-7.52 cm/s

Druglikeness	
Lipinski	Yes; 0 violation
Ghose	Yes
Veber	Yes
Egan	Yes
Muegge	Yes
Bioavailability Score	0.55

Medicinal Chemistry	
PAINS	0 alert
Brenk	0 alert
Leadlikeness	No; 1 violation: MW>350
Synthetic accessibility	2.88

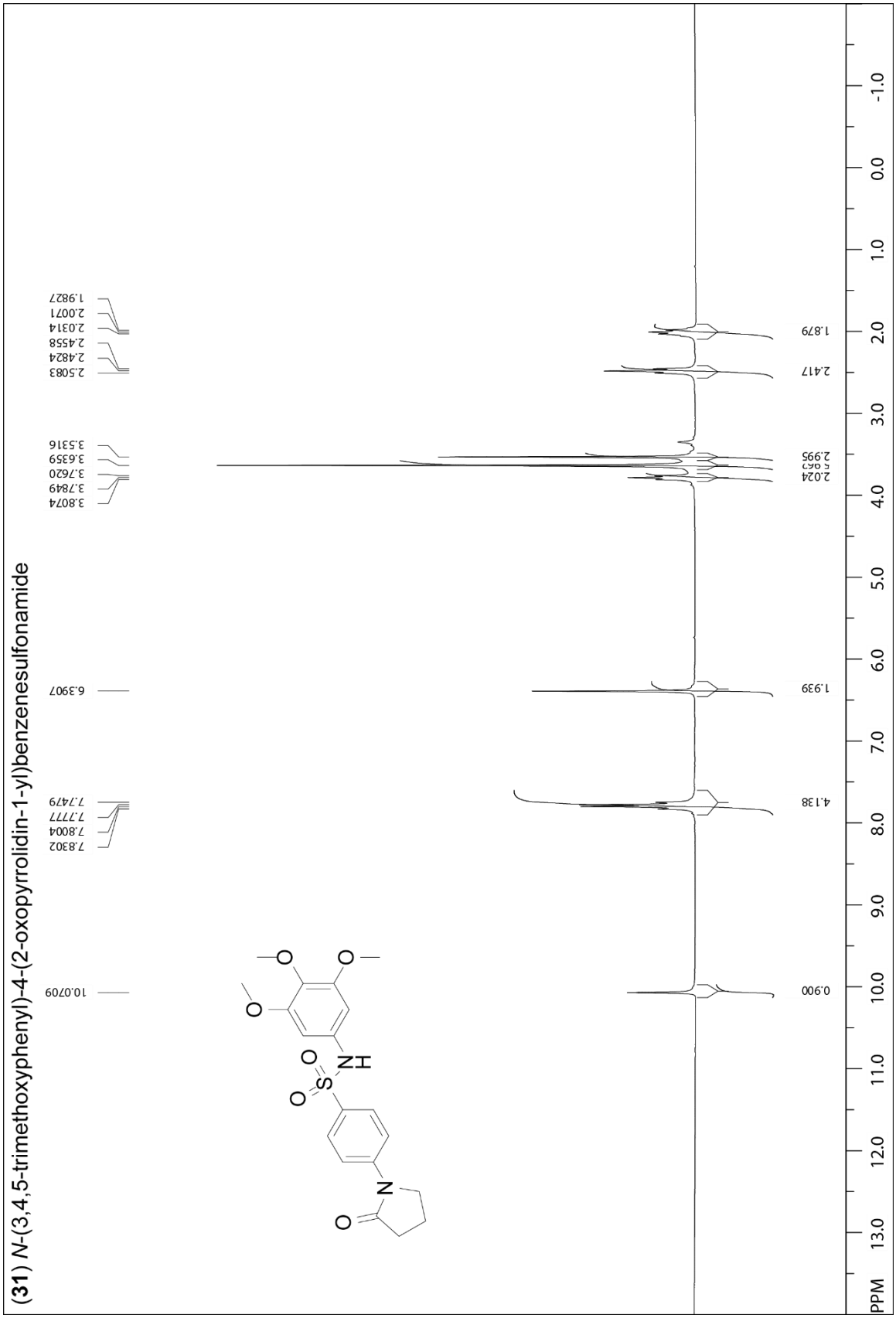
(31) N-(3,4,5-trimethoxyphenyl)-4-(2-oxopyrrolidin-1-yl)benzenesulfonamide
10.0709
7.8302
7.8004
7.7777
7.7479
6.3907
3.8074
3.7849
3.7620
3.6359
3.5316
2.5083
2.4824
2.4558
2.0314
2.0071
1.9827
0.900
4.138
1.939
2.024
5.063
2.995
2.417
1.879
PPM
13.0
12.0
11.0
10.0
9.0
8.0
7.0
6.0
5.0
4.0
3.0
2.0
1.0
0.0
-1.0

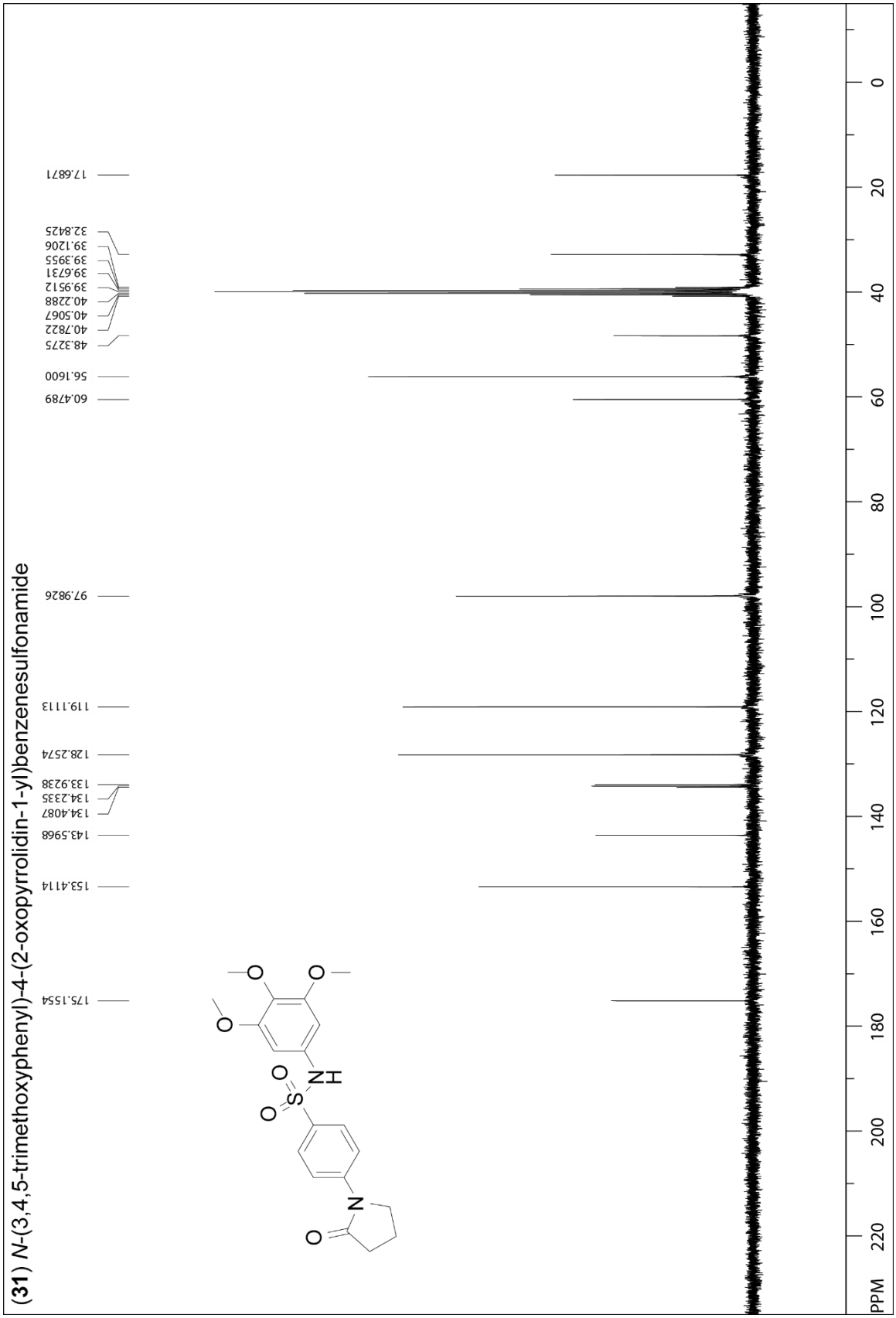
(31) N-(3,4,5-trimethoxyphenyl)-4-(2-oxopyrrolidin-1-yl)benzenesulfonamide
175.1554
153.4114
143.5968
134.4087
134.2335
133.9238
128.2574
119.1113
97.9826
60.4789
56.1600
48.3275
40.7822
40.5067
40.2288
39.9512
39.6731
39.3955
39.1206
32.8425
17.6871
PPM
220
200
180
160
140
120
100
80
60
40
20
0

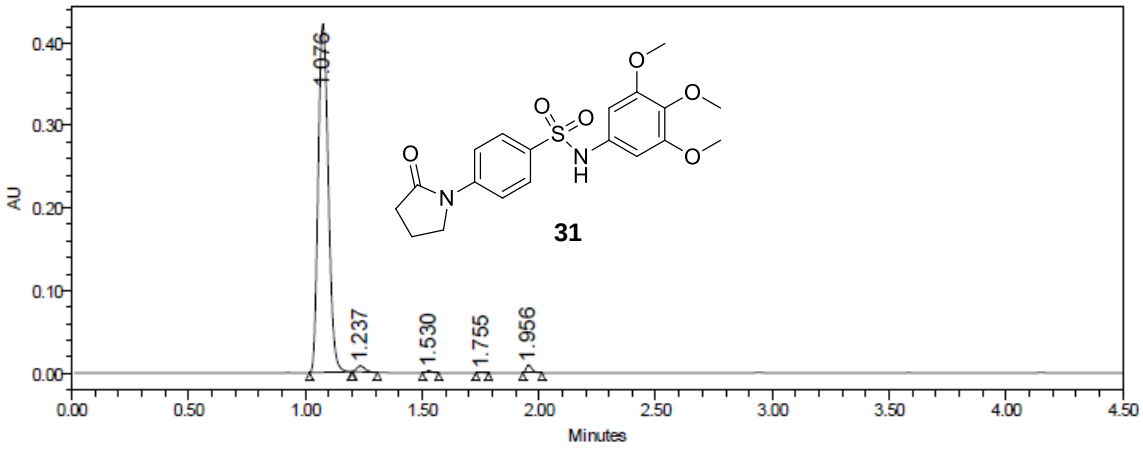

31

	RT	Area	% Area	Height
1	1.076	1277234	97.07	422123
2	1.237	17513	1.33	7175
3	1.530	4350	0.33	2575
4	1.755	730	0.06	480
5	1.956	16000	1.22	9548

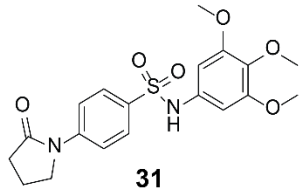

31

m/z	*Calc m/z*	Diff(ppm)	z	Abund	Formula	Ion
402.1476				520		
407.1269	407.1271	-0.49		171922	C19 H23 N2 O6 S	(M+H)+
407.3749				7705		
408.1304	408.1302	0.44		31405	C19 H23 N2 O6 S	(M+H)+
408.3845				538		
409.1276	409.1273	0.7		9084	C19 H23 N2 O6 S	(M+H)+
410.1285	410.1289	-1.06		1379	C19 H23 N2 O6 S	(M+H)+
424.1533	424.1537	-0.91	1	31105	C19 H26 N3 O6 S	(M+NH4)+

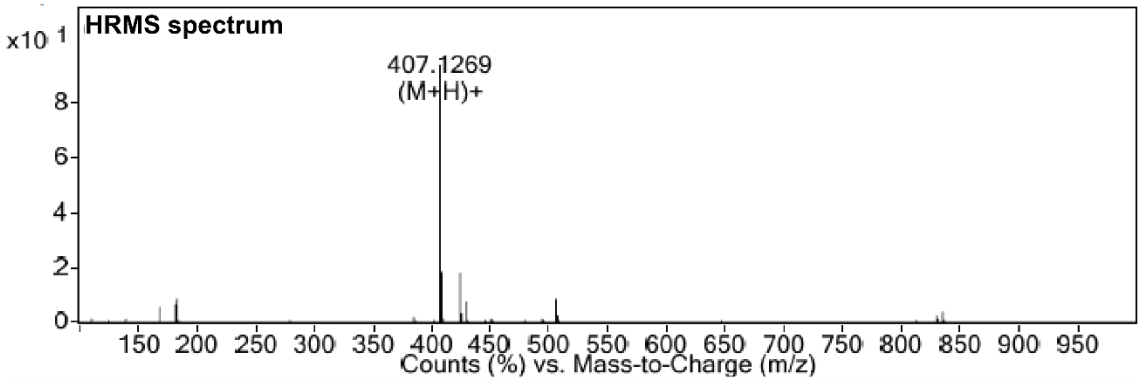

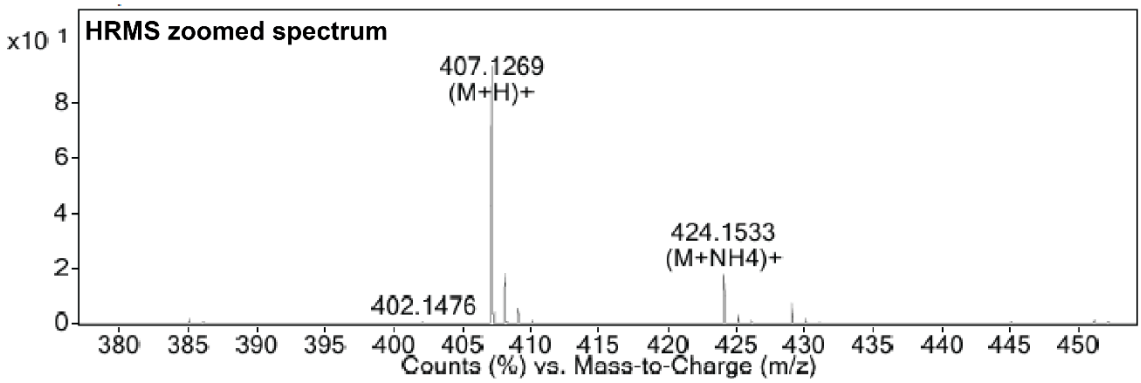

Annexe B : Données supplémentaires du chapitre 3

B.1. Experimental section

B.1.1. Biological methods

B.1.1.1. Cell lines culture

HT-1080 human fibrosarcoma, HT-29 human colon carcinoma and MCF7 human breast carcinoma were purchased from the American Type Culture Collection ATCC® (Manassa, VA, USA). M21 human melanoma cells were provided by Dr. David Cheresh (University of California, San Diego School of Medicine, CA, USA). Wild-type Chinese hamster ovary cells (CHO-10001) (Cabral, et al., 1980), colchicine- and vinblastine- resistant cells (CHO-VV 3-2) (Schibler, et al., 1989) and paclitaxel-resistant cells (CHO-TAX 5-6) (Schibler, et al., 1986) were generously provided by Dr. Fernando Cabral (University of Texas Medical School, Houston, Texas). T cell leukemia CEM and multidrug-resistant leukemia CEM-VLB were generously provided by Dr. William T. Beck (University of Illinois at Chicago, College of Pharmacy, IL) (Beck, et al., 1979). HT-1080, HT-29, M21 and MCF7 cells were cultured in DMEM medium containing sodium bicarbonate, high glucose concentration, glutamine and sodium pyruvate (Hyclone, Logan, UT, USA) supplemented with either 5 or 10% of fetal bovine serum (FBS, Invitrogen, Burlington, ON, Canada). CHO-10001, CHO-VV 3-2, CHO-TAX 5-6, CEM and CEM-VLB were cultured in RPMI 1640 (Hyclone, Logan, UT) supplemented with 10% of fetal bovine serum. The cells were maintained at 37 °C in a moisture saturated atmosphere containing 5% CO_2.

B.1.1.2. Antiproliferative activity assay

The antiproliferative activity of PID-SOs **6**-**20** and **31**-**37** as well as EPA-SOs **21**-**30** was assessed with the procedure described by the National Cancer Institute (NCI) Developmental Therapeutics Program for its drug screening program with slight modifications (NCI-60, 2020). Briefly, ninety-six-well Costar microtiter clear plates from Fisher Scientific (Montreal, QC, Canada) were seeded with 75 μL of a suspension of either HT-1080 (3.0×10^3), HT-29 (4.0×10^3), M21 (3.0×10^3), MCF7 (3.5×10^3) cells per well in DMEM supplemented with either 5 or 10% fetal bovine serum or with CHO-10001 (3.0×10^3), CHO-VV 3-2 (3.0×10^3) or CHO-TAX 5-6 (3.0×10^3) cells per well in RPMI 1640

containing 10% fetal bovine serum for 24 h. Freshly solubilised drugs in DMSO (40 mM) were diluted in fresh supplemented DMEM or RPMI 1640 and 75 µL aliquots containing serially diluted concentrations of the drug were added. Final drug concentrations were ranged from 100 µM to 0.78 nM. DMSO concentration was kept constant at 0.5% (V/V) to prevent any related toxicity. Plates were incubated for 48 h and growth was stopped by the addition of cold trichloroacetic acid to the wells (10% w/v, final concentration). Afterward, plates were incubated at 4 °C for 30 min. Then, plates were washed 5-times with nanopure water and a sulforhodamine B solution (0.1% w/v) in 1% acetic acid was added to each well. After 15 min at room temperature, the exceeding dye was removed and plates were washed 5-times with an acetic acid solution (1%). Bound dye was solubilised in 20 mM Tris base and the absorbance was read using an optimal wavelength (520 - 580 nm) with a SpectraMax® i3x (Molecular Devices, San Jose, CA, USA). Data obtained from treated cells were compared to the control cell plates fixed on the treatment day and the percentage of cell growth was thus calculated for each drug. The experiments were done at least twice in triplicate. Assays were considered valid when the coefficient of variation was <10% for a given set of conditions within the same experiment.

B.1.1.3. MTT assay

Cell survival treated with the most potent PID-SOs (**16-18**) was evaluated using the MTT colorimetric assay, 100% survival representing cell viability in the absence of drug (Carmichael et al., 1987; Ford et al., 1989). Briefly, the 96-well microtiter plates were seeded with 75 µL of a suspension of either CEM (1.0×10^4) or CEM-VLB (1.0×10^4) cells per well in RPMI 1640 containing 10% fetal bovine serum. Plates were incubated at 37 °C with 5% CO_2 for 24 h. Freshly solubilized drugs in DMSO were diluted in fresh medium, and 50 µL aliquots containing escalating concentrations of drug were added and the plates were incubated for 48 h. The final concentration of DMSO in the culture media was 0.5% and was kept constant in all experiments. After 48 h, 10 µL of 3-(4,5-dimethylthiazol-2-yl)-2,5-diphenyltetrazolium bromide (MTT, 5 mg/mL in PBS) were added to the wells. Four hours later, 100 µL of the solubilisation solution (10% sodium dodecyl sulfate [SDS] in 0.01 M HCl) was added and the plate was incubated in the dark at 37 °C with 5% CO_2 for 16 h. The optical density was read at 565 nm using a SpectraMax® i3x (Molecular Devices, San Jose,

CA, USA). Data obtained from treated cells were compared to the control cell plates fixed on the treatment day and the percentage of cell viability was thus calculated for each drug. The experiments were done at least twice in triplicate. Assays were considered valid when the coefficient of variation was <10% for a given set of conditions within the same experiment.

B.1.1.4. Cell cycle progression analysis

After incubation of 2.5 x 10^5 M21 cells with selected PID-SOs at 2- and 5-times their respective IC_{50} for 24 h, cells were trypsinised, washed with phosphate buffered saline (PBS) and resuspended in 250 µL of PBS. Cells were fixed by the addition of 750 µL of ice-cold ethanol under agitation and stored at -20 °C until analysis. Prior analysis, cells were washed with 750 µL of PBS and resuspended in 300 µL of PBS containing 2 µg/mL DAPI. Cell cycle distribution of fixed cell suspensions was analysed using an LSR II flow cytometer (BD Biosciences, Franklin Lakes, NJ, USA).

B.1.1.5. Immunofluorescence of microtubules

M21 cells were seeded at 2.5 x 10^5 cells per well in 6-well plates (Costar®, Fisher Scientific, Montreal, QC, Canada) containing glass cover slides (22 × 22 mm) coated with fibronectin (10 µg/mL) and incubated for 24 h. Tumor cells were incubated either with PID-SOs **16** (1.3 µM), **17** (1.1 µM), **18** (0.46 µM) or CA-4 (0.010 µM) for 24 h. DMSO (0.5%) was used as negative control while CA-4 was used as positive control. The cells were then washed thrice with 2 mL of PBS and fixed with 3.7% formaldehyde in PBS for 10 min. After two washes with PBS, the cells were permeabilised with saponin (0.1% in PBS) and blocked with 3% (w/v) BSA in PBS for 45 min at 37 °C. The cells were then incubated for 2 h at room temperature with an anti-β-tubulin monoclonal antibody (clone TUB 2.1, Sigma-Aldrich, St. Louis, MO, USA; 1:300) in a solution containing 0.1% saponin and 3% BSA in PBS. The cells were washed twice with PBS containing 0.05% Tween 20 and stained using antimouse IgG Alexa Fluor 488 (Molecular Probes, Eugene, OR, USA; 1:1000) and DAPI (2 µg/mL final concentration) in blocking buffer for 1 h. The cover slides were mounted using 25 µL of Fluoromount-G® (SouthernBiotech, Birmingham, Al, USA) before analysis under an Olympus BX51 fluorescence microscope (Olympus BX51, Center Valley, PA,

USA). Images were acquired as 8 bit-tagged image format files with a Q imaging RETIGA EXI digital camera (Qimaging, Surrey, BC, Canada) using the Image Pro Express software at a total magnification of 400x.

B.1.1.6. Microtubule polymerisation assay

The effect of PID-SOs **16** (3.0 µM), **17** (3.0 µM) and **18** (30 µM) on dynamic polymerisation of tubulin into microtubules was analysed using the fluorescence based tubulin polymerisation assay using >99% pure tubulin (Cytoskeleton, Inc., Denver, CO, USA). Drugs were used in DMSO at their maximal soluble concentration in the buffer 1 (80 mM piperazine-*N*,*N*'-bis[2-ethanesulfonic acid] sequisodium salt; 2.0 mM magnesium chloride; 0.5 mM ethylene glycol-bis(β-amino-ethyl ether) *N*,*N*,*N*',*N*'-tetra-acetic acid, pH 6.9, 10 µM fluorescent reporter). First, 5 µL of drug solutions were diluted in 325 µL of nanopure water to reach 10x of their final concentration. The assay was performed accordingly to the manufacturer guidelines (Cytoskeleton Inc, 2020). Briefly, 85 µL of tubulin >99% (10 mg/mL) was dissolved in 205 µL of buffer 1, 150 µL of tubulin glycerol buffer (80 mM piperazine-*N*,*N*'-bis[2-ethanesulfonic acid] sesquisodium salt; 2.0 mM magnesium chloride; 0.5 mM ethylene glycol-bis(β-amino-ethyl ether) *N*,*N*,*N*',*N*'-tetra-acetic acid, 60% V/V glycerol, pH 6.9) and 4.4 µL of GTP stock (100 mM in sterile distilled water). The resulting tubulin mixture was added (50 µL) 96-well plate (Black, flat bottom, Corning Costar Cat. # 3686) with 5 µL of drug solutions at 37 °C. The polymerisation was measured over 60 min by fluorescence (excitation: 360 nM, emission: 450 nM) using a SpectraMax® i3x (Molecular Devices, San Jose, CA, USA) in kinetic mode. The results are representative of two separated experiments.

B.1.1.7. In vitro competition binding assay of EBI to the C-BS

M21 cells were seeded in 6-well plates (7.5 x 10^5 cells/well) and were incubated overnight. Then, cells were treated with either PID-SOs **16**-**18** or CA-4 for 1.5 h at 100- or 1000-times their respective IC_{50}. Thereafter, EBI (100 µM, final concentration, Toronto Research Chemicals, North York, ON, Canada) in PBS was added to each well for 1.5 h. After the incubation, the supernatant was withdrawn and cells were trypsinised (trypsin-

EDTA 0.5%), harvested and centrifuged 5 min at 1 200 rpm. The pellets were washed with 500 µL of cold PBS and stored at -80 °C until analysis (Fortin, et al., 2010).

B.1.1.8. Gel electrophoresis and immunoblot

The cell pellets were resuspended in a buffer containing 0.32 M sucrose, 1 mM EDTA at pH 8, 10 mM Tris at pH 7.4 and protease inhibitor. The protein concentration was assessed with the Bio-Rad Protein assay (Bio-Rad laboratories, Mississauga, ON, Canada). Samples were prepared to obtain proteins at 4 mg/mL in Laemmli sample buffer (60 mM Tris-Cl at pH 6.8, 2% SDS, 10%, glycerol, 5% β-mercaptoethanol, 0.01% bromophenol blue) (Laemmli, 1970) and boiled for 5 min. Then, 40 µg of proteins were used for the electrophoresis using 10% polyacrylamide gels. The proteins were transferred onto nitrocellulose membranes that were incubated with TBSTM (Tris Buffered Saline + 0.1% (V/V) Tween-20 with 5% fat-free dry milk) for 2 h at room temperature. Subsequently, the anti-β-tubulin (clone TUB 2.1) primary antibody was incubated in TBSTM (1:500) for 2 h at room temperature. Membranes were washed with TBST (Tris-Buffered Saline supplemented with 0.1% (V/V) Tween 20) and incubated with peroxidase conjugated anti-mouse immunoglobulin (Amersham Canada, Oakville, ON, Canada) in TBSMT (1:5000) for 1 h at room temperature. After washing the membranes with TBST, detection of the immunoblot was carried out using Clarity Western enhanced chemiluminescence reagents (Bio-Rad laboratories, Mississauga, ON, Canada). Detection of bands was performed with Super Rx medical X-Ray film (Fujifilm, Tokyo, Japan).

B.1.2. Chemical methods

B.1.2.1. General

Proton NMR spectra were recorded on a Bruker AM-300 spectrometer (Bruker, Germany). Chemical shifts (δ) are reported in parts per million (ppm). Reactions requiring microwave heating were performed at 200 watts with a Discover SP Explorer Hybrid microwave synthesiser (CEM, Matthews, NC, USA). Uncorrected melting points were obtained on a MPA100 automated melting point system (Standford Research Systems, Sunnyvale, CA, USA). UHPLC analyses were performed using an ACQUITY Arc system

(Waters, Mississauga, ON, Canada) equipped with a 2998 PDA detector. The samples were dissolved in DMSO and were eluted using a mixture of MeOH/H_2O with a linear mobile phase gradient (1.0 mL/min) on a CORTECS C18+ reversed-phase column 3.0 × 50 mm × 2.7 μm equipped with an Alltech Alltima C18 precolumn (5 mm, 7.5mm × 4.6 mm). Wavelength was selected at 280 nm and the purity of all compounds was confirmed by UHPLC and was equal or over 95% except for compounds **14** (93.9%) and **35** (91.8%). All chemicals were supplied by Aldrich Chemicals (Milwaukee, WI, USA), VWR International (Mont-Royal, QC, Canada) or Fisher Scientific (Montreal, QC, Canada). Liquid flash chromatography was performed on silica gel F60, 60 Å, 40-63 μm supplied by Silicycle (Quebec City, QC, Canada) using an FPX flash purification system (Biotage, Charlottesville, VA, USA) and using solvent mixtures expressed as V/V ratios. Solvents and reagents were used without purification unless specified otherwise. The progress of all reactions was monitored by TLC on precoated silica gel 60 Å F254 TLC plates provided by VWR International (Mont-Royal, QC, Canada). The chromatograms were viewed under UV light at 254 and 275 nm. HRMS were recorded by direct injection in a TOF system 6210 series mass spectrometer (Agilent technologies, Santa Clara, CA, USA).

B.1.2.2. General preparation of PID-SOs 6-20

The relevant phenol (1.5 Eq.) was added to a solution of 4-(2,4-dioxoimidazolidin-1-yl)benzene-1-sulfonyl chloride (0.10 g, 1.0 Eq.) with triethylamine (0.15 mL, 3.0 Eq.) in acetonitrile (3-5 mL). The reaction mixture was stirred under pressure with microwaves at 120 °C for 8 h. The mixture was evaporated and then dissolved in methylene chloride (10 mL). The organic layer was washed successively with solutions of HCl (1 M, 10 mL), NaOH (1 M, 10 mL) and brine (10 mL), dried over sodium sulfate, filtered and evaporate to dryness under reduced pressure. The residue was purified by flash chromatography on silica gel.

B.1.2.3. Characterisation of PID-SOs 6-20

*1.2.3.1. Phenyl 4-(2,4-dioxoimidazolidin-1-yl)benzenesulfonate (**6**).* Flash chromatography (hexanes/ethyl acetate (75:35)). Yield: 13%; white solid; mp: 243-245 °C; ^{1}H NMR (DMSO-d_6): δ 11.54 (brs, 1H, NH), 7.89 (brs, 4H, Ar), 7.46-7.33 (m, 3H, Ar), 7.09-7.06 (m, 2H, Ar), 4.53 (s, 2H, CH_2); ^{13}C NMR (DMSO-d_6): δ 170.5, 155.7, 149.6, 144.1,

130.6, 130.2, 128.0, 122.5, 122.5, 118.2, 51.4; HRMS (ESI) *m/z* found 333.0529; $C_{15}H_{13}N_2O_5S$ (M^+ + H) expected 333.0549.

*1.2.3.2. 2-Isopropylphenyl 4-(2,4-dioxoimidazolidin-1-yl)benzenesulfonate (**7**)*. Flash chromatography (methylene chloride/ethyl acetate (90:10)). Yield: 4%; white solid; mp: 217-219 °C; ^{1}H NMR (DMSO-d_6): δ 11.53 (brs, 1H, NH), 7.98-7.94 (m, 4H, Ar), 7.46-7.23 (m, 3H, Ar), 7.03-7.00 (m, 1H, Ar), 4.55 (s, 2H, CH_2), 3.15-3.10 (m, 1H, CH), 1.09 (d, 6H, *J* = 6.8 Hz, 2x CH_3); ^{13}C NMR (DMSO-d_6): δ 170.5, 155.7, 146.9, 144.1, 141.7, 130.0, 128.8, 128.2, 128.0, 127.6, 122.0, 118.4, 51.4, 26.8, 23.4; HRMS (ESI) *m/z* found 375.1006; $C_{18}H_{19}N_2O_5S$ (M^+ + H) expected 375.1019.

1.2.3.3. [*1,1'-Biphenyl]-2-yl 4-(2,4-dioxoimidazolidin-1-yl)benzenesulfonate (**8**)*. Flash chromatography (hexanes/ethyl acetate (63:37) to (40:60)). Yield: 10%; white solid; mp: 174-177 °C; ^{1}H NMR (DMSO-d_6): δ 11.44 (brs, 1H, NH), 7.55-7.52 (m, 2H, Ar), 7.47-7.26 (m, 9H, Ar), 7.13-7.10 (m, 2H, Ar), 4.43 (s, 2H, CH_2); ^{13}C NMR (DMSO-d_6): δ 170.4, 155.5, 146.3, 143.7, 136.4, 135.4, 131.7, 129.4, 129.4, 129.3, 128.7, 128.3, 128.0, 127.8, 123.8, 117.8, 51.3; HRMS (ESI) *m/z* found 408.0855; $C_{21}H_{16}N_2O_5S$ (M^+ + H) expected 409.0859.

*1.2.3.4. 2-Methoxyphenyl 4-(2,4-dioxoimidazolidin-1-yl)benzenesulfonate (**9**)*. Flash chromatography (hexanes/ethyl acetate (50:50)). Yield: 39%; white solid; mp: 174-177 °C; ^{1}H NMR (DMSO-d_6): δ 11.46 (brs, 1H, NH), 7.84-7.77 (m, 4H, Ar), 7.28-7.23 (m, 1H, Ar), 7.08-7.03 (m, 2H, Ar), 6.94-6.89 (m, 1H, Ar), 4.48 (s, 2H, CH_2), 3.51 (s, 3H, CH_3); ^{13}C NMR (DMSO-d_6): δ 170.5, 155.6, 151.8, 143.9, 138.0, 130.1, 128.9, 128.8, 123.9, 121.0, 117.8, 113.9, 56.0, 51.4; HRMS (ESI) *m/z* found 363.0639; $C_{16}H_{15}N_2O_6S$ (M^+ + H) expected 363.0649.

*1.2.3.5. 3-Methoxyphenyl 4-(2,4-dioxoimidazolidin-1-yl)benzenesulfonate (**10**)*. Flash chromatography (hexanes/ethyl acetate (50:50)). Yield: 11%; pale orange solid; mp: 215-217 °C; ^{1}H NMR (DMSO-d_6): δ 11.46 (brs, 1H, NH), 7.85 (brs, 4H, Ar), 7.30-7.24 (m, 1H, Ar), 6.89-6.86 (m, 1H, Ar), 6.59-6.57 (m, 2H, Ar), 4.47 (s, 2H, CH_2), 3.68 (s, 3H, CH_3); ^{13}C NMR (DMSO-d_6): δ 170.4, 160.6, 155.6, 150.4, 144.0, 130.9, 130.2, 127.9, 118.1, 114.3,

113.5, 108.5, 55.9, 51.3; HRMS (ESI) *m/z* found 363.0643; $C_{16}H_{15}N_2O_6S$ (M^+ + H) expected 363.0649.

*1.2.3.6. 3-Fluorophenyl 4-(2,4-dioxoimidazolidin-1-yl)benzenesulfonate (**11**).* Flash chromatography (hexanes/ethyl acetate (50:50)). Yield: 16%; white solid; mp: 231-235 °C; ^{1}H NMR (DMSO-d_6): δ 11.47 (brs, 1H, NH), 7.86 (brs, 4H, Ar), 7.47-7.39 (m, 1H, Ar), 7.22-7.17 (m, 1H, Ar), 7.02-6.99 (m, 1H, Ar), 6.91-6.88 (m, 1H, Ar), 4.47 (s, 2H, CH_2); ^{13}C NMR (DMSO-d_6): δ 170.4, 164.1, 160.8, 155.6, 150.1, 150.0, 144.2, 131.9, 131.8, 130.2, 127.4, 118.8, 118.7, 118.2, 115.2, 115.0, 110.8, 110.4, 51.3; HRMS (ESI) *m/z* found 351.0451; $C_{15}H_{12}FN_2O_5S$ (M^+ + H) expected 351.0452.

*1.2.3.7. 3-Chlorophenyl 4-(2,4-dioxoimidazolidin-1-yl)benzenesulfonate (**12**).* Flash chromatography (hexanes/ethyl acetate (50:50)). Yield: 15%; white solid; mp: 241-243 °C; ^{1}H NMR (DMSO-d_6): δ 11.47 (brs, 1H, NH), 7.86 (brs, 4H, Ar), 7.42-7.40 (m, 2H, Ar), 7.22 (brs, 1H, Ar), 7.02-6.98 (m, 1H, Ar), 4.48 (s, 2H, CH_2); ^{13}C NMR (DMSO-d_6): δ 170.4, 155.6, 149.9, 144.3, 134.2, 131.9, 130.2, 128.2, 127.4, 122.9, 121.4, 118.2, 51.3; HRMS (ESI) *m/z* found 367.0152; $C_{15}H_{12}ClN_2O_5S$ (M^+ + H) expected 367.0156.

*1.2.3.8. 3-Bromophenyl 4-(2,4-dioxoimidazolidin-1-yl)benzenesulfonate (**13**).* Flash chromatography (hexanes/ethyl acetate (50:50)). Yield: 21%; white solid; mp: 233-236 °C; ^{1}H NMR (DMSO-d_6): δ 11.47 (brs, 1H, NH), 7.87-7.78 (m, 4H, Ar), 7.55-7.53 (m, 1H, Ar), 7.37-7.31 (m, 2H, Ar), 7.05-7.02 (m, 1H, Ar), 4.48 (s, 2H, CH_2); ^{13}C NMR (DMSO-d_6): δ 170.4, 155.6, 149.9, 144.3, 132.2, 131.0, 130.2, 127.4, 125.7, 122.3, 121.7, 118.2, 51.3; HRMS (ESI) *m/z* found 410.9641; $C_{15}H_{12}BrN_2O_5S$ (M^+ + H) expected 410.9651.

*1.2.3.9. 3-Iodophenyl 4-(2,4-dioxoimidazolidin-1-yl)benzenesulfonate (**14**).* Flash chromatography (hexanes/ethyl acetate (75:25) to (50:50)). Yield: 53%; pale solid; mp: 244-246 °C; ^{1}H NMR (DMSO-d_6): δ 11.47 (brs, 1H, NH), 7.86 (brs, 4H, Ar), 7.70-7.68 (m, 1H, Ar), 7.46 (brs, 1H, Ar), 7.19-7.14 (m, 1H, Ar), 7.04-7.01 (m, 1H, Ar), 4.48 (s, 2H, CH_2); ^{13}C NMR (DMSO-d_6): δ 170.4, 155.6, 149.6, 144.2, 136.8, 132.2, 131.2, 130.2, 127.5, 122.0, 118.2, 95.2, 51.4; HRMS (ESI) *m/z* found 458.9510; $C_{15}H_{12}IN_2O_5S$ (M^+ + H) expected 458.9509.

*1.2.3.10. 3,4-Dimethoxyphenyl 4-(2,4-dioxoimidazolidin-1-yl)benzenesulfonate (**15**)*. Flash chromatography (hexanes/ethyl acetate (75:25) to (60:40)). Yield: 49%; orange solid; mp: sticky solid °C; ^{1}H NMR (DMSO-d_6): δ 11.47 (brs, 1H, NH), 7.84 (brs, 4H, Ar), 6.89-6.86 (m, 1H, Ar), 6.59-6.49 (m, 2H, Ar), 4,47 (s, 2H, CH_2), 3.70 (s, 3H, CH_3), 3.61 (s, 3H, CH_3); ^{13}C NMR (DMSO-d_6): δ 170.4, 155.6, 149.4, 148.1, 144.0, 142.8, 130.2, 127.9, 118.1, 113.8, 111.9, 106.9, 56.1, 56.1, 51.3; HRMS (ESI) *m/z* found 393.0755; $C_{17}H_{17}N_2O_7S$ (M^+ + H) expected 393.0759.

*1.2.3.11. 3,5-Dimethoxyphenyl 4-(2,4-dioxoimidazolidin-1-yl)benzenesulfonate (**16**)*. Flash chromatography (methylene chloride/methanol (95:5)). Yield: 25%; pale grey solid; mp: 234-236 °C; ^{1}H NMR (DMSO-d_6): δ 11.52 (brs, 1H, NH), 7.96-7.85 (m, 4H, Ar), 6.50 (brs, 1H, Ar), 6.24-6.23 (m, 2H, Ar), 4.54 (s, 2H, CH_2), 3.72 (s, 6H, 2x CH_3); ^{13}C NMR (DMSO-d_6): δ 170.5, 161.3, 155.7, 151.0, 144.1, 130.3, 128.0, 118.2, 101.0, 99.5, 56.1, 51.4; HRMS (ESI) *m/z* found 393.0750; $C_{17}H_{17}N_2O_7S$ (M^+ + H) expected 393.0759.

*1.2.3.12. 3,5-Dibromophenyl 4-(2,4-dioxoimidazolidin-1-yl)benzenesulfonate (**17**)*. Flash chromatography (hexanes/ethyl acetate (70:30) to (20:80)). Yield: 9%; white solid; mp: 191-193 °C; ^{1}H NMR (DMSO-d_6): δ 11.54 (brs, 1H, NH), 7.99-7.87 (m, 5H, Ar), 7.46-7.43 (m, 2H, Ar), 4.55 (s, 2H, CH_2); ^{13}C NMR (DMSO-d_6): δ 170.4, 155.7, 150.1, 144.5, 133.4, 130.4, 127.1, 125.2, 123.3, 118.3, 51.4; HRMS (ESI) *m/z* found 505.9021; $C_{15}H_{11}Br_2N_2O_5S$ (M^+ + NH_4) expected 505.9015.

*1.2.3.13. 3,4,5-Trimethoxyphenyl 4-(2,4-dioxoimidazolidin-1-yl)benzenesulfonate (**18**)*. Flash chromatography (hexanes/ethyl acetate (50:50) to (10:90)). Yield: 49%; white solid; mp: 233-235 °C; ^{1}H NMR (DMSO-d_6): δ 11.50 (brs, 1H, NH), 7.91 (brs, 4H, Ar), 6.35 (brs, 2H, Ar), 4.52 (s, 2H, CH_2), 3.68 (s, 6H, 2x CH_3), 3.65 (s, 3H, CH_3); ^{13}C NMR (DMSO-d_6): δ 170.4, 155.6, 153.6, 145.5, 144.1, 136.8, 130.4, 127.9, 118.2, 100.4, 60.6, 56.6, 51.4; HRMS (ESI) *m/z* found 423.0867; $C_{18}H_{19}N_2O_8S$ (M^+ + H) expected 423.0859.

*1.2.3.14. 4-Methoxyphenyl 4-(2,4-dioxoimidazolidin-1-yl)benzenesulfonate (**19**)*. Flash chromatography (hexanes/ethyl acetate (50:50)). Yield: 11%; pale grey solid; mp: 229-232 °C; ^{1}H NMR (DMSO-d_6): δ 11.46 (brs, 1H, NH), 7.86-7.78 (m, 4H, Ar), 6.94-6.87 (m, 4H, Ar), 4.47 (s, 2H, CH_2), 3.70 (s, 3H, CH_3); ^{13}C NMR (DMSO-d_6): δ 170.4, 158.4, 155.6,

144.0, 142.8, 130.1, 127.9, 123.6, 118.1, 115.3, 55.9, 51.3; HRMS (ESI) *m/z* found 363.0646; $C_{16}H_{15}N_2O_6S$ (M^+ + H) expected 363.0652.

*1.2.3.15. [1,1'-Biphenyl]-4-yl 4-(2,4-dioxoimidazolidin-1-yl)benzenesulfonate (**20**).* Flash chromatography (hexanes/ethyl acetate (75:25) to (50:50)). Yield: 11%; white solid; mp: 233-235 °C; ^{1}H NMR (DMSO-d_6): δ 11.45 (brs, 1H, NH), 7.87-7.83 (m, 4H, Ar), 7.68-7.60 (m, 4H, Ar), 7.46-7.35 (m, 3H, Ar), 7.12-7.09 (m, 2H, Ar), 4.47 (s, 2H, CH_2); ^{13}C NMR (DMSO-d_6): δ 170.4, 155.6, 149.0, 144.1, 139.7, 139.1, 130.1, 129.5, 128.7, 128.3, 128.0, 127.2, 122.9, 118.2, 51.3; HRMS (ESI) *m/z* found 407.0710; $C_{21}H_{15}N_2O_5S$ (M^+ + H) expected 407.0707.

B.1.2.4. General preparation of EPA-SOs 21-30

The preparation of EPA-SOs **21**-**30** begins with the synthesis of phenyl nitrobenzenesulfonate derivatives prepared accordingly to Gagné-Boulet *et al*. and Turcotte *et al.* with slight modifications (Gagné-Boulet, et al., 2018; Gagné-Boulet, et al., 2015; Turcotte, et al., 2012). Briefly, the relevant phenol (1.2 Eq.) was added to a solution of 4-nitrobenzenesulfonyl chloride (5.0 g, 1 Eq.) in acetonitrile (15 mL) in presence of triethylamine (4.7 mL, 1.5 Eq.). The reaction mixture was stirred under microwaves 8 h at 120 °C. After completion of the reaction, the solvent was evaporated under reduced pressure, the mixture was diluted in AcOEt (100 mL) and was extracted twice in the presence of 1M HCl (100 mL), 1M NaOH (100 mL) and then washed with brine (100 mL), dried over sodium sulfate, filtered and evaporated to dryness under reduced pressure. The residue was purified by flash chromatography on silica gel (hexanes/methylene chloride (90:10) to (50:50)) to give phenyl nitrobenzenesulfonates with yields ranging from 39 to 99%. The next step was prepared accordingly to Gagné-Boulet *et al*. and Turcotte *et al.* with slight modifications (Gagné-Boulet, et al., 2015; Hirota, et al., 1985; Turcotte, et al., 2012). The phenyl nitrobenzenesulfonates (1.0 Eq.) were added to a solution of iron powder (6.0 Eq.) and hydrochloric acid (12 M, 1.0 mL) in a mixture of EtOH (95%) and water (10:1, 150 mL). The reaction mixture was heated at reflux for 16 h. After completion of the reaction, the solvent was evaporated under reduced pressure, the mixture was diluted in AcOEt (75 mL), basified with a saturated solution of $NaHCO_3$ and filtered through celite®. The organic layer was washed successively with a saturated solution of sodium bicarbonate (75 mL) and brine

(75 mL), dried over sodium sulfate, filtered and evaporated to dryness under reduced pressure. The residue was purified by flash chromatography on silica gel (hexanes/ethyl acetate (90:10) to (50:50)) or by recrystallisation in methylene chloride to give phenyl 4-aminobenzenesulfonate derivatives with yields ranging from 13 to 80%. The ^{1}H and ^{13}C NMR were equivalent to the NMR characterisations published previously (Gagné-Boulet, et al., 2018; Gagné-Boulet, et al., 2015; Turcotte, et al., 2012). The relevant phenyl 4-aminobenzenesulfonate (0.2 g, 1.0 Eq.) was added to a solution of diethyl ether and ethyl 2-isocyanatoacetate (3.0 Eq.). The mixture was stirred at room temperature for 24 h. After completion of the reaction, the solvent was evaporated under reduced pressure and the residue was purified by flash chromatography on silica gel.

B.1.2.5. Characterisation of EPA-SOs 21-30

*1.2.5.1. Ethyl 2-(3-(4-(phenoxysulfonyl)phenyl)ureido)acetate (**21**).* Flash chromatography (hexanes/ethyl acetate (90:10) to (50:50)). Yield: 69%; white solid; mp: 156-158 °C; ^{1}H NMR (acetone-d_6): δ 8.87 (brs, 1H, NH), 7.75-7.66 (m, 4H, Ar), 7.39-7.29 (m, 3H, Ar), 7.04-7.01 (m, 2H, Ar), 6.37 (brs, 1H, NH), 4.19-4.12 (m, 4H, 2x CH_2), 1,23 (t, 3H, J = 7.1 Hz, CH_3); ^{13}C NMR (acetone-d_6): δ 170.3, 154.6, 149.9, 146.3, 129.8, 127.1, 126.8, 122.3, 117.4, 117.3, 60.6, 41.5, 13.6; HRMS (ESI) *m/z* found 379.0960; $C_{17}H_{19}N_2O_6S$ (M^+ + H) expected 379.0965.

*1.2.5.2. Ethyl 2-(3-(4-((2-isopropylphenoxy)sulfonyl)phenyl)ureido)acetate (**22**).* Flash chromatography (hexanes/ethyl acetate (90:10) to (50:50)). Yield: 92%; colorless oil; ^{1}H NMR ($CDCl_3$): δ 8.24 (brs, 1H, NH), 7.65-7.63 (m, 2H, Ar), 7.49-7.46 (m, 2H, Ar), 7.23-7.14 (m, 2H, Ar), 7.07-6.94 (m, 2H, Ar), 6.21-6.17 (m, 1H, NH), 4.15 (q, 2H, J = 7.1 Hz, CH_2), 4.01-3.99 (m, 2H, CH_2), 3.13-3.04 (m, 1H, CH), 1.21 (t, 3H, J = 7.1 Hz, CH_3), 1.01 (d, 6H, J = 6.8 Hz, 2x CH_3); ^{13}C NMR ($CDCl_3$): δ 171.5, 155.2, 146.8, 145.1, 141.7, 129.6, 127.9, 127.5, 127.2, 126.7, 121.9, 118.0, 61.8, 42.0, 26.7, 23.1, 14.1; HRMS (ESI) *m/z* found 421.1429; $C_{20}H_{25}N_2O_6S$ (M^+ + H) expected 421.1434.

*1.2.5.3. Ethyl 2-(3-(4-((3-fluorophenoxy)sulfonyl)phenyl)ureido)acetate (**23**).* Flash chromatography (hexanes/ethyl acetate (90:10) to (50:50)). Yield: 65%; white solid; mp: 145-147 °C; ^{1}H NMR (acetone-d_6): δ 8.87 (brs, 1H, NH), 7.76-7.70 (m, 4H, Ar), 7.45-7.37

(m, 1H, Ar), 7.13-7.07 (m, 1H, Ar), 6.89-6.87 (m, 2H, Ar), 6.38 (brs, 1H, NH), 4.16 (q, 2H, J = 7.1 Hz, CH_2), 4.00-3.98 (m, 2H, CH_2), 1.23 (t, 3H, J = 7.1 Hz, CH_3); ^{13}C NMR (acetone-d_6): δ 170.2, 164.2, 160.9, 154.6, 150.4, 146.5, 131.0, 130.9, 129.8, 126.3, 118.5, 118.4, 117.5, 117.4, 114.2, 113.9, 110.4, 110.1, 60.6, 41.5, 13.6; HRMS (ESI) *m/z* found 397.0871; $C_{17}H_{18}FN_2O_6S$ (M^+ + H) expected 397.0870.

*1.2.5.4. Ethyl 2-(3-(4-((3-chlorophenoxy)sulfonyl)phenyl)ureido)acetate (**24**).* Flash chromatography (hexanes/ethyl acetate (90:10) to (50:50)). Yield: 77%; white solid; mp: 131-133 °C; ^{1}H NMR (acetone-d_6): δ 8.88 (brs, 1H, NH), 7.77-7.70 (m, 4H, Ar), 7.41-7.33 (m, 2H, Ar), 7.13 (brs, 1H, Ar), 7.00-6.98 (m, 1H, Ar), 6.39 (brs, 1H, NH), 4.15 (q, 2H, J = 7.1 Hz, CH_2), 4.01-3.99 (m, 2H, CH_2), 1.23 (t, 3H, J = 7.1 Hz, CH_3); ^{13}C NMR (acetone-d_6): δ 170.3, 154.6, 150.2, 146.5, 134.2, 131.0, 129.9, 127.3, 126.2, 122.8, 121.1, 117.5, 60.6, 41.5, 13.6; HRMS (ESI) *m/z* found 413.0572; $C_{17}H_{18}ClN_2O_6S$ (M^+ + H) expected 413.0575.

*1.2.5.5. Ethyl 2-(3-(4-((3-bromophenoxy)sulfonyl)phenyl)ureido)acetate (**25**).* Flash chromatography (hexanes/ethyl acetate (90:10) to (50:50)). Yield: 78%; white solid; mp: 122-124 °C; ^{1}H NMR ($CDCl_3$): δ 8.21 (brs, 1H, NH), 7.58-7.55 (m, 2H, Ar), 7.44-7.41 (m, 2H, Ar), 7.33-7.31 (m, 1H, Ar), 7.18 (brs, 1H, Ar), 7.12-7.06 (m, 1H, Ar), 6.85-6.82 (m, 1H, Ar), 6.18 (brs, 1H, NH), 4.17 (q, 2H, J = 7.1 Hz, CH_2), 4.03-4.02 (m, 2H, CH_2), 1.23 (t, 3H, J = 7.1 Hz, CH_3); ^{13}C NMR ($CDCl_3$): δ 171.8, 155.0, 149.7, 145.3, 130.8, 130.5, 129.7, 126.7, 125.8, 122.5, 121.0, 118.0, 62.0, 42.0, 14.1; HRMS (ESI) *m/z* found 457.0061; $C_{17}H_{18}BrN_2O_6S$ (M^+ + H) expected 457.0070.

*1.2.5.6. Ethyl 2-(3-(4-((3,4-dimethoxyphenoxy)sulfonyl)phenyl)ureido)acetate (**26**).* Flash chromatography (hexanes/ethyl acetate (90:10) to (50:50)). Yield: 41%; dark brown oil; ^{1}H NMR ($CDCl_3$): δ 8.10 (brs, 1H, NH), 7.59-7.56 (m, 2H, Ar), 7.44-7.42 (m, 2H, Ar), 6.67-6.64 (m, 1H, Ar), 6.54-6.53 (m, 1H, Ar), 6.42-6.38 (m, 1H, Ar), 6.07-6.03 (m, 1H, NH), 4.16 (q, 2H, J = 7.1 Hz, CH_2), 4.01-4.00 (m, 2H, CH_2), 3.77 (s, 3H, CH_3), 3.70 (s, 3H, CH_3), 1.22 (t, 3H, J = 7.1 Hz, CH_3); ^{13}C NMR ($CDCl_3$): δ 171.4, 154.9, 149.2, 147.8, 145.1, 142.9, 129.8, 127.1, 117.8, 113.9, 110.9, 106.6, 61.8, 56.0, 56.0, 41.9, 14.1; HRMS (ESI) *m/z* found 439.1167; $C_{19}H_{23}N_2O_8S$ (M^+ + H) expected 439.1176.

*1.2.5.7. Ethyl 2-(3-(4-((3,5-dimethoxyphenoxy)sulfonyl)phenyl)ureido)acetate (**27**)*. Flash chromatography (hexanes/ethyl acetate (90:10) to (60:40)). Yield: 34%; white solid; ^{1}H NMR (DMSO-d_6): δ 9.49 (brs, 1H, NH), 7.73-7.62 (m, 4H, Ar), 6.72-6.68 (m, 1H, NH), 6.41 (brs, 1H, Ar), 6.13-6.13 (m, 2H, Ar), 4.10 (q, 2H, J = 7.1 Hz, CH_2), 3.89-3.87 (m, 2H, CH_2), 3.64 (s, 6H, 2x CH_3), 1.18 (t, 3H, J = 7.1 Hz, CH_3); ^{13}C NMR (DMSO-d_6): δ 170.9, 161.2, 155.1, 151.0, 146.7, 130.3, 125.7, 117.6, 101.0, 99.4, 60.9, 55.9, 41.8, 14.5; HRMS (ESI) *m/z* found 439.1168; $C_{19}H_{23}N_2O_8S$ (M^+ + H) expected 439.1176.

*1.2.5.8. Ethyl 2-(3-(4-((3,5-dibromphenoxy)sulfonyl)phenyl)ureido)acetate (**28**)*. Flash chromatography (hexanes/ethyl acetate (80:20) to (50:50)). Yield: 36%; white solid; mp: 210-212 °C; ^{1}H NMR ($CDCl_3$): δ 8.25 (brs, 1H, NH), 7.64-7.61 (m, 2H, Ar), 7.54-7.47 (m, 3H, Ar), 7.15 (brs, 2H, Ar), 6.21 (brs, 1H, NH), 4.23 (q, 2H, J = 7.1 Hz, CH_2), 4.09-4.08 (m, 2H, CH_2), 1.29 (t, 3H, J = 7.1 Hz, CH_3); ^{13}C NMR ($CDCl_3$): δ 172.0, 155.0, 149.8, 145.5, 133.1, 129.8, 126.4, 124.7, 123.0, 118.1, 62.1, 42.1, 14.2; HRMS (ESI) *m/z* found 534.9162; $C_{17}H_{18}Br_2N_2O_6S$ (M^+ + H) expected 534.9175.

*1.2.5.9. Ethyl 2-(3-(4-((3,4,5-trimethoxyphenoxy)sulfonyl)phenyl)ureido)acetate (**29**)*. Flash chromatography (hexanes/ethyl acetate (80:20) to (50:50)). Yield: 71%; colorless oil; ^{1}H NMR ($CDCl_3$): δ 8.12 (brs, 1H, NH), 7.69-7.66 (m, 2H, Ar), 7.51-7.49 (m, 2H, Ar), 6.25 (brs, 2H, Ar), 6.09 (brs, 1H, NH), 4.23 (q, 2H, J = 7.1 Hz, CH_2), 4.06-3.95 (m, 2H, CH_2), 3.81 (s, 3H, CH_3), 3.72 (s, 6H, 2x CH_3), 1.30 (t, 3H, J = 7.1 Hz, CH_3); ^{13}C NMR ($CDCl_3$): δ 171.5, 154.8, 153.3, 145.6, 145.2, 136.4, 129.9, 127.1, 117.8, 100.0, 61.9, 61.0, 56.2, 42.0, 14.1; HRMS (ESI) *m/z* found 469.1273; $C_{20}H_{24}N_2O_9S$ (M^+ + H) expected 469.1282.

*1.2.5.10. Ethyl 2-(3-(4-((4-methoxyphenoxy)sulfonyl)phenyl)ureido)acetate (**30**)*. Flash chromatography (hexanes/ethyl acetate (90:10) to (50:50)). Yield: 22%; white solid; mp: 148-150 °C; ^{1}H NMR ($CDCl_3$): δ 7.98 (brs, 1H, NH), 7.59-7.56 (m, 2H, Ar), 7.44-7.41 (m, 2H, Ar), 6.85 -6.82 (m, 2H, Ar), 6.74-6.71 (m, 2H, Ar), 6.03 (brs, 1H, NH), 4.19 (q, 2H, J = 7.1 Hz, CH_2), 4.03 (brs, 2H, CH_2), 3.72 (s, 3H, CH_3), 1.26 (t, 3H, J = 7.1 Hz, CH_3); ^{13}C NMR ($CDCl_3$): δ 171.6, 158.3, 154.8, 144.9, 142.8, 129.8, 127.2, 123.3, 117.9, 114.5, 61.9, 55.5, 42.0, 14.1; HRMS (ESI) *m/z* found 409.1066; $C_{18}H_{21}N_2O_7S$ (M^+ + H) expected 409.1070.

B.1.2.6. General preparation of PID-SOs 31-37

The relevant EPA-SO (0.2 mmol, **21**, **22**, **24**, **25**, **27**, **28** and **29**) was added to a solution of HCl (6 M, 5.0 mL) and EtOH (5.0 mL). The reaction mixture was heated and stirred at 80 ℃ for 16 h. After completion of the reaction, the mixture was evaporated to dryness under reduced pressure. The residue was purified by flash chromatography on silica gel.

B.1.2.7. Characterisation of PID-SOs 31-37

*1.2.7.1. Phenyl 4-(2,5-dioxoimidazolidin-1-yl)benzenesulfonate (**31**).* Flash chromatography (methylene chloride/ethyl acetate (95:5) to (50:50)). Yield: 52%; white solid; mp: 100-102 °C; ^{1}H NMR (DMSO-d_6): δ 8.56 (s, 1H, NH), 8.04-8.01 (m, 2H, Ar), 7.80-7.77 (m, 2H, Ar), 7.46 -7.33 (m, 3H, Ar), 7.12-7.09 (m, 2H, Ar), 4.12 (s, 2H, CH_2); ^{13}C NMR (DMSO-d_6): δ 171.2, 156.1, 149.5, 138.5, 133.0, 130.6, 129.4, 128.1, 127.1, 122.5, 46.5; HRMS (ESI) *m/z* found 333.0541; $C_{15}H_{13}N_2O_5S$ (M^+ + H) expected 333.0546.

*1.2.7.2. 2-Isopropylphenyl 4-(2,5-dioxoimidazolidin-1-yl)benzenesulfonate (**32**).* Flash chromatography (methylene chloride/ethyl acetate (95:5) to (50:50)). Yield: 4%; white solid; mp: 210-203 °C; ^{1}H NMR (DMSO-d_6): δ 8.50 (s, 1H, NH), 8.01-7.98 (m, 2H, Ar), 7.76-7.73 (m, 2H, Ar), 7.38 -7.19 (m, 3H, Ar), 7.05-7.02 (m, 1H, Ar), 4.08 (s, 2H, CH_2), 3.03-2.94 (m, 1H, CH), 0.99 (d, 6H, J = 6.8 Hz, 2x CH_3); ^{13}C NMR (DMSO-d_6): δ 171.1, 156.0, 146.7, 141.5, 138.5, 133.6, 129.2, 128.2, 127.9, 127.6, 127.2, 122.2, 46.5, 26.7, 23.3; HRMS (ESI) *m/z* found 375.1012; $C_{18}H_{19}N_2O_5S$ (M^+ + H) expected 375.1019.

*1.2.7.3. 3-Chlorophenyl 4-(2,5-dioxoimidazolidin-1-yl)benzenesulfonate (**33**).* Flash chromatography (methylene chloride/ethyl acetate (95:5) to (50:50)). Yield: 20%; colorless oil; ^{1}H NMR (DMSO-d_6): δ 8.56 (s, 1H, NH), 8.08-8.05 (m, 2H, Ar), 7.81-7.79 (m, 2H, Ar), 7.48 -7.46 (m, 2H, Ar), 7.29 (brs, 1H, Ar), 7.12-7.09 (m, 1H, Ar), 4.12 (s, 2H, CH_2); ^{13}C NMR (DMSO-d_6): δ 171.2, 156.0, 149.8, 138.7, 134.3, 132.5, 132.0, 129.5, 128.4, 127.1, 122.9, 121.4, 46.5; HRMS (ESI) *m/z* found 367.0160; $C_{15}H_{12}ClN_2O_5S$ (M^+ + H) expected 367.0156.

*1.2.7.4. 3-Bromophenyl 4-(2,5-dioxoimidazolidin-1-yl)benzenesulfonate (**34**)*. Flash chromatography (methylene chloride/ethyl acetate (95:5) to (50:50)). Yield: 22%; pale yellow oil; ^{1}H NMR (DMSO-d_6): δ 8.51 (s, 1H, NH), 8.03-8.00 (m, 2H, Ar), 7.77-7.74 (m, 2H, Ar), 7.56 -7.54 (m, 1H, Ar), 7.39-7.33 (m, 2H, Ar), 7.11-7.08 (m, 1H, Ar), 4.08 (s, 2H, CH_2); ^{13}C NMR (DMSO-d_6): δ 171.2, 156.0, 149.7, 138.6, 132.5, 132.3, 131.2, 129.5, 127.1, 125.7, 122.3, 121.7, 46.5; HRMS (ESI) *m/z* found 410.9655; $C_{15}H_{12}BrN_2O_5S$ (M^+ + H) expected 410.9651.

*1.2.7.5. 3,5-Dimethoxyphenyl 4-(2,5-dioxoimidazolidin-1-yl)benzenesulfonate (**35**)*. Flash chromatography (methylene chloride/ethyl acetate (95:5) to (50:50)). Yield: 57%; white sticky solid; ^{1}H NMR (DMSO-d_6): δ 8.49 (s, 1H, NH), 8.02-7.99 (m, 2H, Ar), 7.74-7.71 (m, 2H, Ar), 6.43 (brs, 1H, Ar), 6.16-6.15 (m, 2H, Ar), 4.07 (s, 2H, CH_2), 3.63 (s, 6H, 2x CH_3); ^{13}C NMR (DMSO-d_6): δ 171.2, 161.2, 156.0, 150.8, 138.4, 132.8, 129.5, 127.2, 100.9, 99.8, 56.0, 46.5; HRMS (ESI) *m/z* found 393.0752; $C_{17}H_{17}N_2O_7S$ (M^+ + H) expected 393.0757.

*1.2.7.6. 3,5-Dibromophenyl 4-(2,5-dioxoimidazolidin-1-yl)benzenesulfonate (**36**)*, Flash chromatography (methylene chloride/ethyl acetate (95:5) to (70:30)). Yield: 21%; white solid; mp: 135-137 °C; ^{1}H NMR (DMSO-d_6): δ 8.57 (s, 1H, NH), 8.11-8.08 (m, 2H, Ar), 7.91 (brs, 1H, Ar), 7.83-7.81 (m, 2H, Ar), 7.45 (brs, 2H, Ar), 4.12 (s, 2H, CH_2); ^{13}C NMR (DMSO-d_6): δ 171.2, 156.0, 149.9, 138.9, 133.6, 132.1, 129.6, 127.2, 125.2, 123.3, 46.5; HRMS (ESI) *m/z* found 488.8747; $C_{15}H_{11}Br_2N_2O_5S$ (M^+ + H) expected 488.8759.

*1.2.7.7. 3,4,5-Trimethoxyphenyl 4-(2,5-dioxoimidazolidin-1-yl)benzenesulfonate (**37**)*. Flash chromatography (methylene chloride/ethyl acetate (95:5) to (50:50)). Yield: 10%; colorless oil; ^{1}H NMR (DMSO-d_6): δ 9.55 (s, 1H, NH), 7.79-7.68 (m, 4H, Ar), 6.32 (brs, 2H, Ar), 3.86 (s, 2H, CH_2), 3.67-3.65 (m, 9H, 3x CH_3); ^{13}C NMR (DMSO-d_6): δ 172.3, 155.1, 153.5, 146.9, 145.5, 136.7, 130.5, 125.6, 117.6, 100.5, 60.6, 56.5, 41.9; HRMS (ESI) *m/z* found 441.0969; $C_{18}H_{19}N_2O_8S$ ($M^+ + H_3O^+$) expected 441.0962.

B.1.2.8. General preparation of 4-(2,4-dioxoimidazolidin-1-yl)benzene-1-sulfonyl chloride

The preparation of 4-(2,4-dioxoimidazolidin-1-yl)benzene-1-sulfonyl chloride begins with the synthesis of 1-phenylimidazolidin-2,4-dione prepared accordingly to Hirota *et al.* with slight modifications (Hirota, et al., 1985). Briefly, *N*-phenylurea (6.8 g, 1.0 Eq.) was dissolved in THF (75 mL). Chloroacetyl chloride (3.9 mL, 1.0 Eq.) was added and the reaction mixture was stirred for 16 h. Then, the mixture was heated to 70 °C for 2 h. The solvent was removed under reduced pressure and the residue was triturated with water. The resulting product was recrystallised with methanol with a yield of 83%. ^{1}H and ^{13}C NMR were equivalent to the characterisation published by Iyer *et al.* (Iyer et al., 2007). The resulting 2-chloro-*N*-(phenylcarbamoyl)acetamide (5.0 g, 1.0 Eq.) was added to a solution of KOH (17.8 M, 7 mL) and EtOH (80 mL). The mixture was heated at 80 °C for 30 min. After reaching ambient temperature, HCl (12 M) was added until the mixture was acidified (pH < 5) and the mixture was evaporated under reduced pressure. The resulting precipitate was filtered and washed with water (5 × 100 mL). The crude product was recrystallised from EtOH to give 1-phenylimidazolidin-2,4-dione with a yield of 30%. Then 1-phenylimidazolidin-2,4-dione was reacted with chlorosulfonic acid using the method described by Mathieu *et al* (Gagné-Boulet, et al., 2018; Gagné-Boulet, et al., 2015; Turcotte, et al., 2012). Briefly, 1-phenylimidazolidin-2,4-dione (4.0 g, 1.0 Eq.) was dissolved in ice cold chlorosulfonic acid (11.6 mL, 7.7 Eq.) under dry argon atmosphere. The ice bath was removed after 10 min. The reaction mixture was stirred at room temperature for 16 h. After the completion of the reaction, the solution was poured on iced water solution slowly dropwise. The solid was filtered, rinsed with water (150 mL) and dried overnight under vacuum. The resulting white 4-(2,4-dioxoimidazolidin-1-yl)benzene-1-sulfonyl chloride was used without further purification with a quantitative yield.

B.1.3. *In silico* methods

B.1.3.1. Docking studies

Molecular modeling experiments and docking studies were performed using Molecular Operating Environment (MOE) version 2019.01 (Chemical Computing Group, Montreal, QC, Canada). PID-SOs **16**-**18** were drawn with ChemBioDraw 13.0 software and

imported in MOE as SDF file for docking experiments. The X-ray crystallographic structure of the α, β-tubulin heterodimer was obtained from the RCSB protein data bank (PDB ID: 1SA0) and loaded to MOE software (Ravelli et al., 2004). The protein was prepared using the QuickPrep tool with default settings to add hydrogens and partial charges, correct Asn/Gln/His orientations, optimise the H-bond network (protonate 3D), delete water molecules farther than 4.5 Å from the ligand and the receptor, and perform an energy minimisation (RMS gradient of 0.1 kcal/mol/Å). Then, a second energy minimisation was realised prior to the docking of α, β-tubulin heterodimer inhibitors. The default settings were applied to all atoms and included the absence of restriction, a force field Amber10 (ETH; R-Field 1:80; Cutoff [8, 10]), system appearing reasonable for the charges, the rigidity of the water molecules and a gradient of 0.1 RMS kcal/mol/$Å^2$. The surface hydrophobicity (blue), hydrophilicity (brown) of the C-BS was mapped using the Surface and Map tool with default setting. The ligand was isolated and the binding site was created with the amino acids in the vicinity of colchicine and GTP. The binding site was constituted of GTP and 32 amino acids (Gln11, Asn101, Ser178, Thr179, Ala180, Val181, Val215, Tyr224, Val238, Cys241, Leu242, Gln247, Leu248, Asn249, Ala250, Asp251, Lys254, Leu255, Asn258, Met259, Thr314, Val315, Ala316, Ala317, Val318, Asn349, Asn350, Val351, Lys352, Thr353, Ala354 and Ile378, respectively). Selected PID-SOs were docked into the C-BS using the selected atoms from the receptor and the selected residues from the binding site. The different conformations, the interactions with the amino acids of the active site and the energies of the complexes were analysed and recorded. Pictures of the most stable conformers in the C-BS site were taken in the 3D and 2D models.

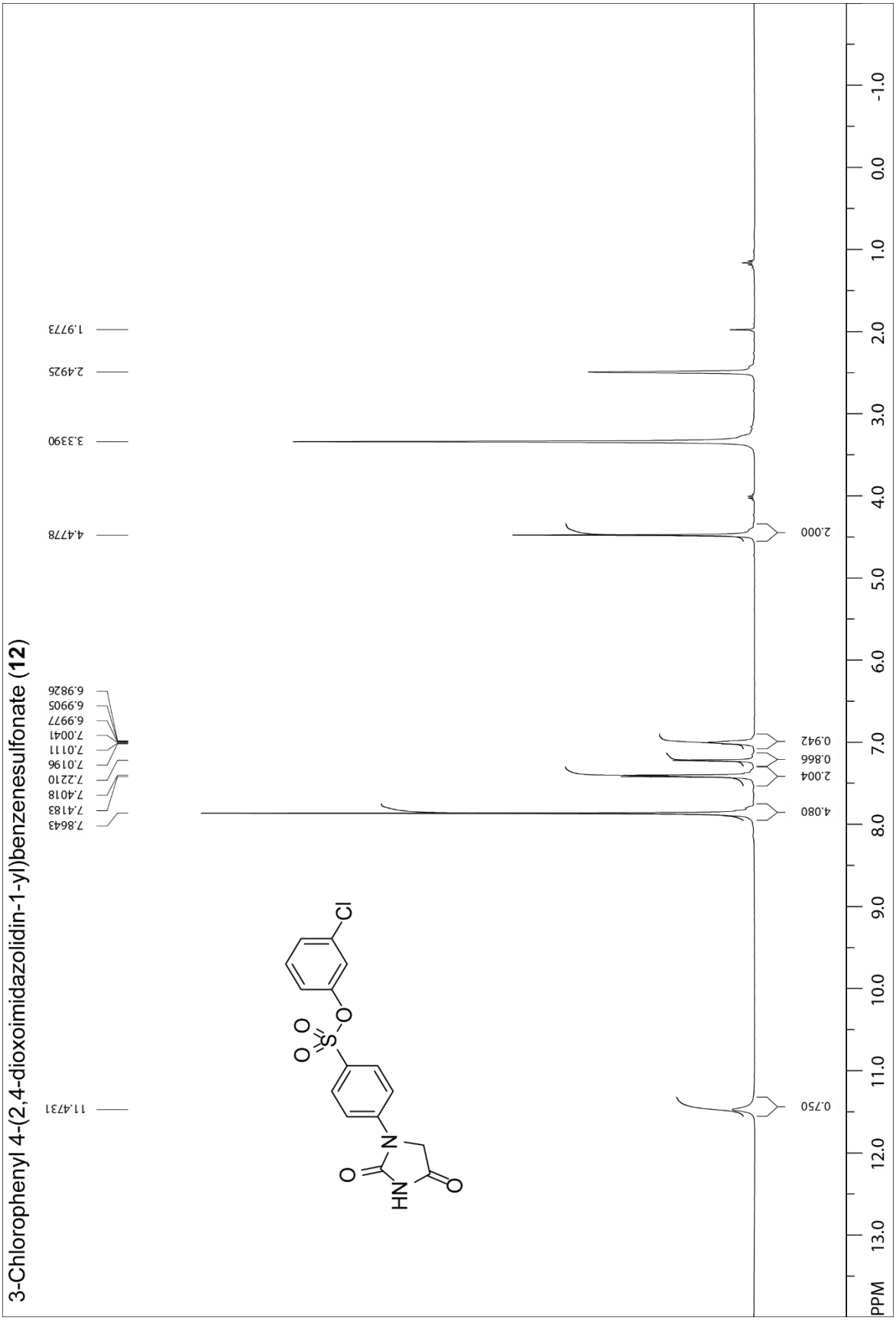
3-Chlorophenyl 4-(2,4-dioxoimidazolidin-1-yl)benzenesulfonate (12)
11.4731
7.8643
7.4183
7.4018
7.2210
7.0196
7.0111
7.0041
6.9977
6.9905
6.9826
4.4778
3.3390
2.4925
1.9773
0.750
4.080
2.004
0.866
0.942
2.000
PPM
13.0
12.0
11.0
10.0
9.0
8.0
7.0
6.0
5.0
4.0
3.0
2.0
1.0
0.0
-1.0
Cl
O
S
O
O
N
HN
O
O

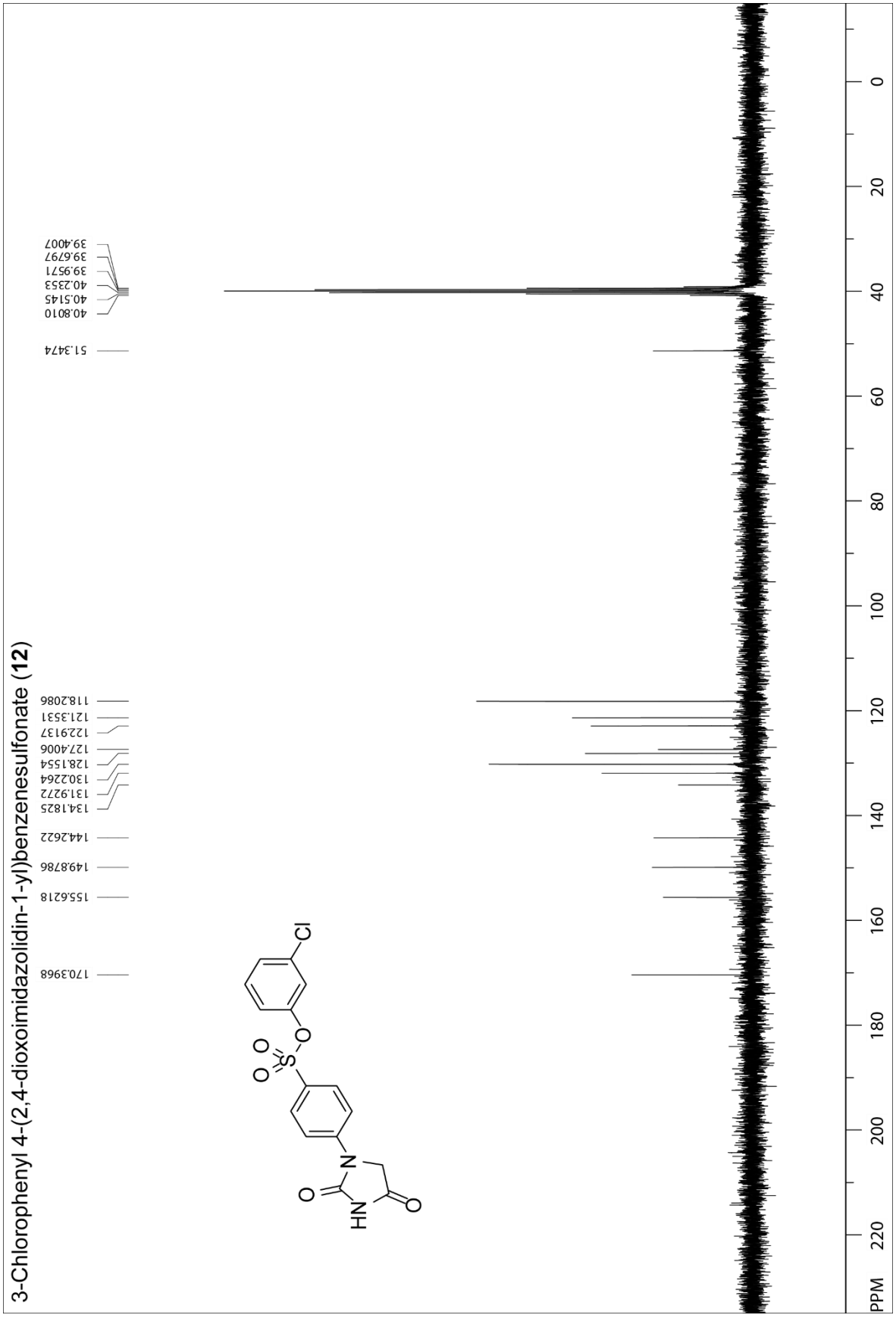
3-Chlorophenyl 4-(2,4-dioxoimidazolidin-1-yl)benzenesulfonate (12)
39.4007
39.6797
39.9571
40.2353
40.5145
40.8010
51.3474
118.2086
121.3531
122.9137
127.4006
128.1554
130.2264
131.9272
134.1825
144.2622
149.8786
155.6218
170.3968
Cl
O
S
O
O
N
O
HN
O
PPM
0
20
40
60
80
100
120
140
160
180
200
220

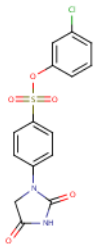

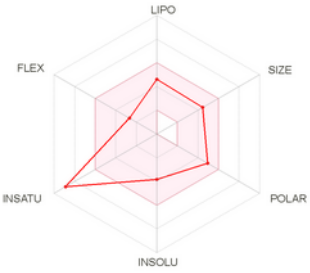

SMILES O=C1NC(=O)N(C1)c1ccc(cc1)S(=O)(=O)Oc1cccc(c1)Cl

Physicochemical Properties	
Formula	C15H11ClN2O5S
Molecular weight	366.78 g/mol
Num. heavy atoms	24
Num. arom. heavy atoms	12
Fraction Csp3	0.07
Num. rotatable bonds	4
Num. H-bond acceptors	5
Num. H-bond donors	1
Molar Refractivity	93.09
TPSA	101.16 Å²

Lipophilicity	
Log $P_{o/w}$ (iLOGP)	2.21
Log $P_{o/w}$ (XLOGP3)	2.56
Log $P_{o/w}$ (WLOGP)	2.48
Log $P_{o/w}$ (MLOGP)	1.96
Log $P_{o/w}$ (SILICOS-IT)	1.24
Consensus Log $P_{o/w}$	2.09

Water Solubility	
Log *S* (ESOL)	-3.83
Solubility	5.39e-02 mg/ml ; 1.47e-04 mol/l
Class	Soluble
Log *S* (Ali)	-4.33
Solubility	1.71e-02 mg/ml ; 4.66e-05 mol/l
Class	Moderately soluble
Log *S* (SILICOS-IT)	-5.14
Solubility	2.65e-03 mg/ml ; 7.23e-06 mol/l
Class	Moderately soluble

Pharmacokinetics	
GI absorption	High
BBB permeant	No
P-gp substrate	No
CYP1A2 inhibitor	Yes
CYP2C19 inhibitor	Yes
CYP2C9 inhibitor	Yes
CYP2D6 inhibitor	No
CYP3A4 inhibitor	No
Log K_p (skin permeation)	-6.72 cm/s

Druglikeness	
Lipinski	Yes; 0 violation
Ghose	Yes
Veber	Yes
Egan	Yes
Muegge	Yes
Bioavailability Score	0.55

Medicinal Chemistry	
PAINS	0 alert
Brenk	2 alerts: hydantoin, sulfonic_acid_1
Leadlikeness	No; 1 violation: MW>350
Synthetic accessibility	2.74

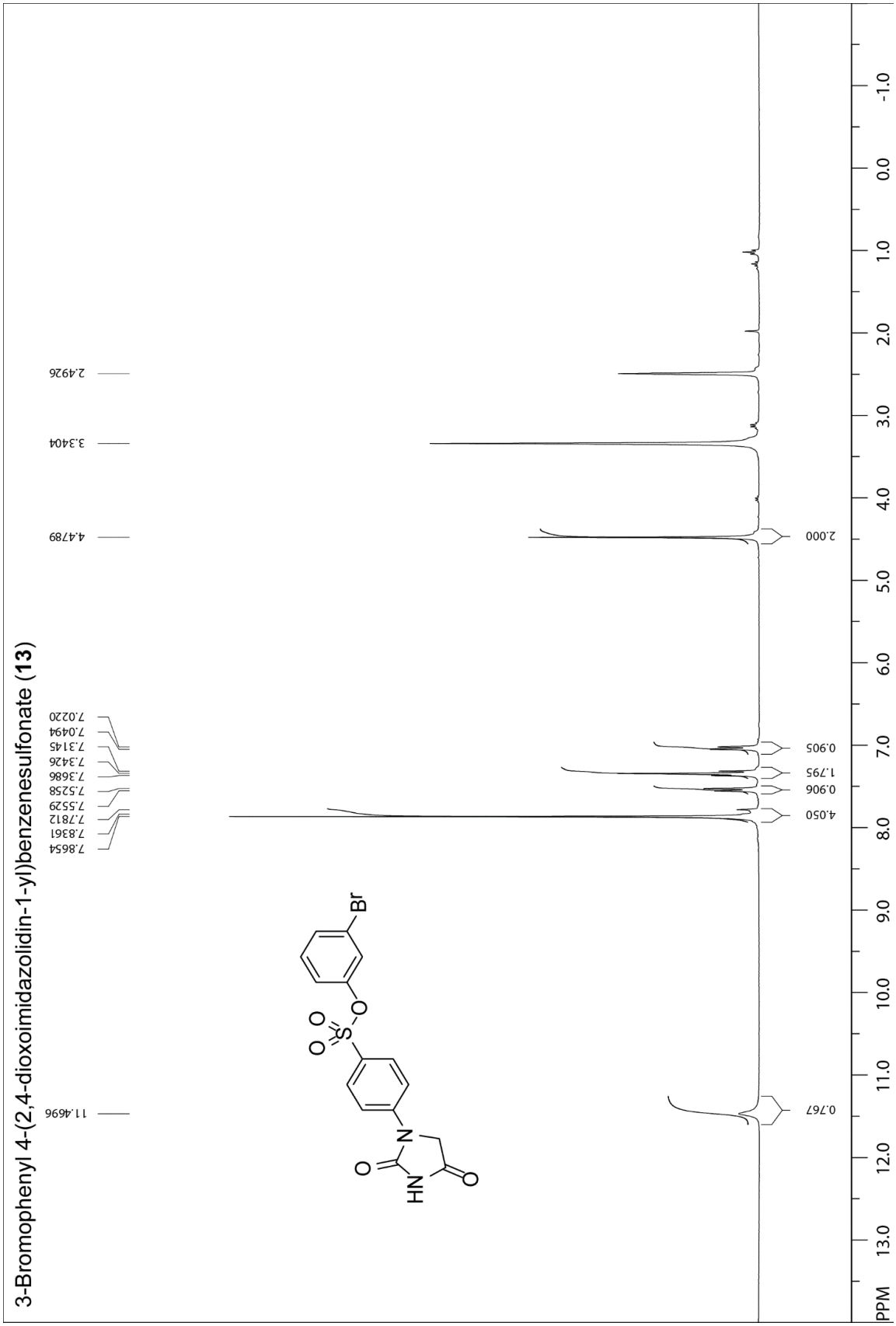
3-Bromophenyl 4-(2,4-dioxoimidazolidin-1-yl)benzenesulfonate (13)
11.4696
7.8654
7.8361
7.7812
7.5529
7.5258
7.3686
7.3426
7.3145
7.0494
7.0220
4.4789
3.3404
2.4926
0.767
4.050
0.906
1.795
0.905
2.000
PPM
13.0
12.0
11.0
10.0
9.0
8.0
7.0
6.0
5.0
4.0
3.0
2.0
1.0
0.0
-1.0
Br
O
O
S
O
N
O
HN
O

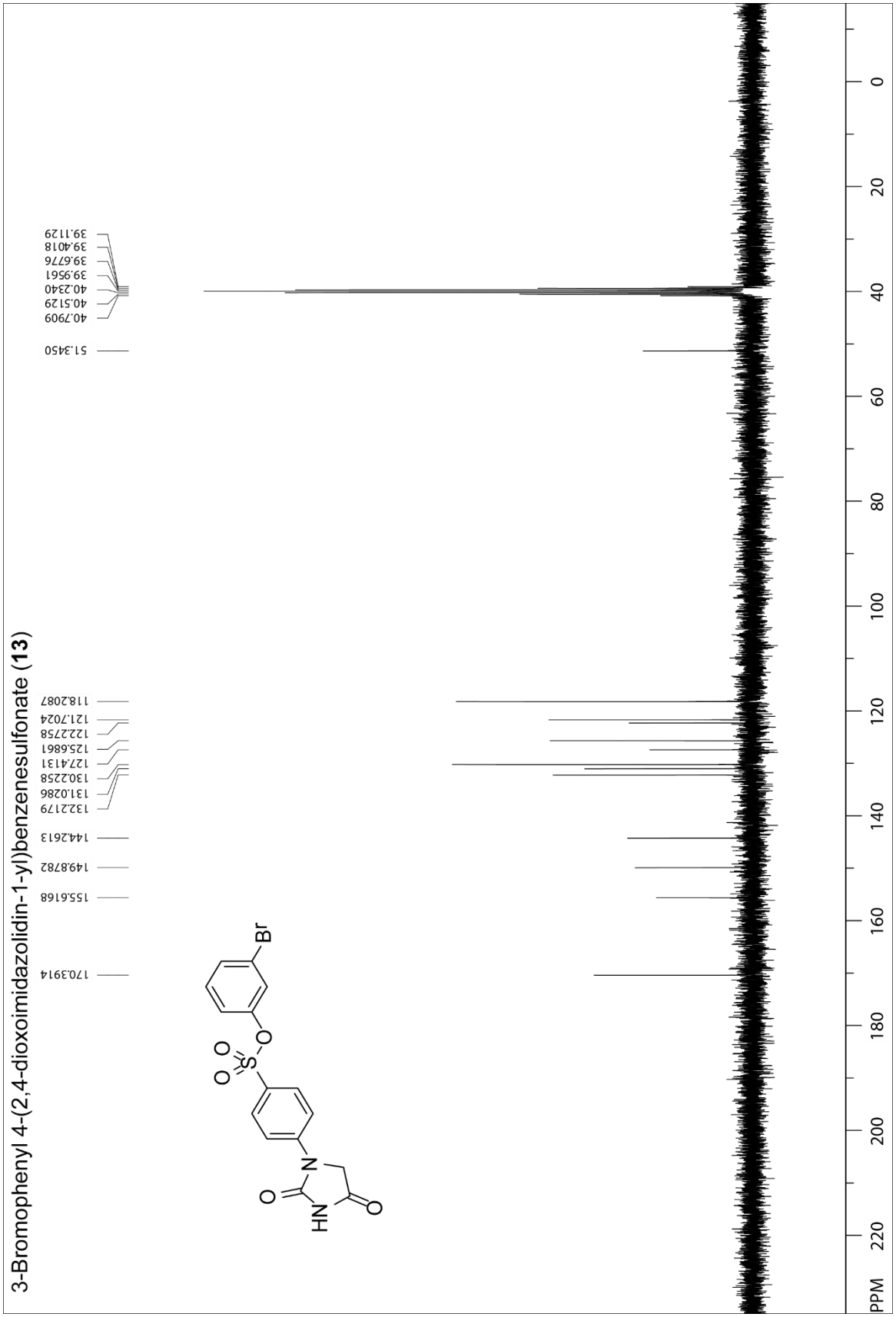
3-Bromophenyl 4-(2,4-dioxoimidazolidin-1-yl)benzenesulfonate (13)
170.3914
155.6168
149.8782
144.2613
132.2179
131.0286
130.2258
127.4131
125.6861
122.2758
121.7024
118.2087
51.3450
40.7909
40.5129
40.2340
39.9561
39.6776
39.4018
39.1129
Br
O
O
S
O
N
HN
O
O
PPM
220
200
180
160
140
120
100
80
60
40
20
0

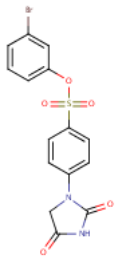

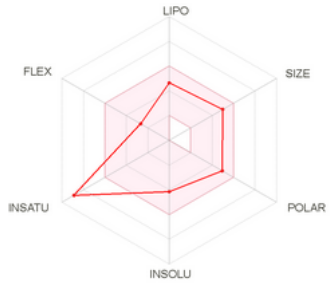

SMILES O=C1NC(=O)N(C1)c1ccc(cc1)S(=O)(=O)Oc1cccc(c1)Br

Physicochemical Properties	
Formula	C15H11BrN2O5S
Molecular weight	411.23 g/mol
Num. heavy atoms	24
Num. arom. heavy atoms	12
Fraction Csp3	0.07
Num. rotatable bonds	4
Num. H-bond acceptors	5
Num. H-bond donors	1
Molar Refractivity	95.78
TPSA	101.16 Å²

Lipophilicity	
Log $P_{o/w}$ (iLOGP)	2.08
Log $P_{o/w}$ (XLOGP3)	2.62
Log $P_{o/w}$ (WLOGP)	2.59
Log $P_{o/w}$ (MLOGP)	2.08
Log $P_{o/w}$ (SILICOS-IT)	1.28
Consensus Log $P_{o/w}$	2.13

Water Solubility	
Log *S* (ESOL)	-4.15
Solubility	2.94e-02 mg/ml ; 7.14e-05 mol/l
Class	Moderately soluble
Log *S* (Ali)	-4.39
Solubility	1.66e-02 mg/ml ; 4.03e-05 mol/l
Class	Moderately soluble
Log *S* (SILICOS-IT)	-5.34
Solubility	1.88e-03 mg/ml ; 4.57e-06 mol/l
Class	Moderately soluble

Pharmacokinetics	
GI absorption	High
BBB permeant	No
P-gp substrate	No
CYP1A2 inhibitor	Yes
CYP2C19 inhibitor	Yes
CYP2C9 inhibitor	Yes
CYP2D6 inhibitor	No
CYP3A4 inhibitor	No
Log K_p (skin permeation)	-6.95 cm/s

Druglikeness	
Lipinski	Yes; 0 violation
Ghose	Yes
Veber	Yes
Egan	Yes
Muegge	Yes
Bioavailability Score	0.55

Medicinal Chemistry	
PAINS	0 alert
Brenk	2 alerts: hydantoin, sulfonic_acid_1
Leadlikeness	No; 1 violation: MW>350
Synthetic accessibility	2.80

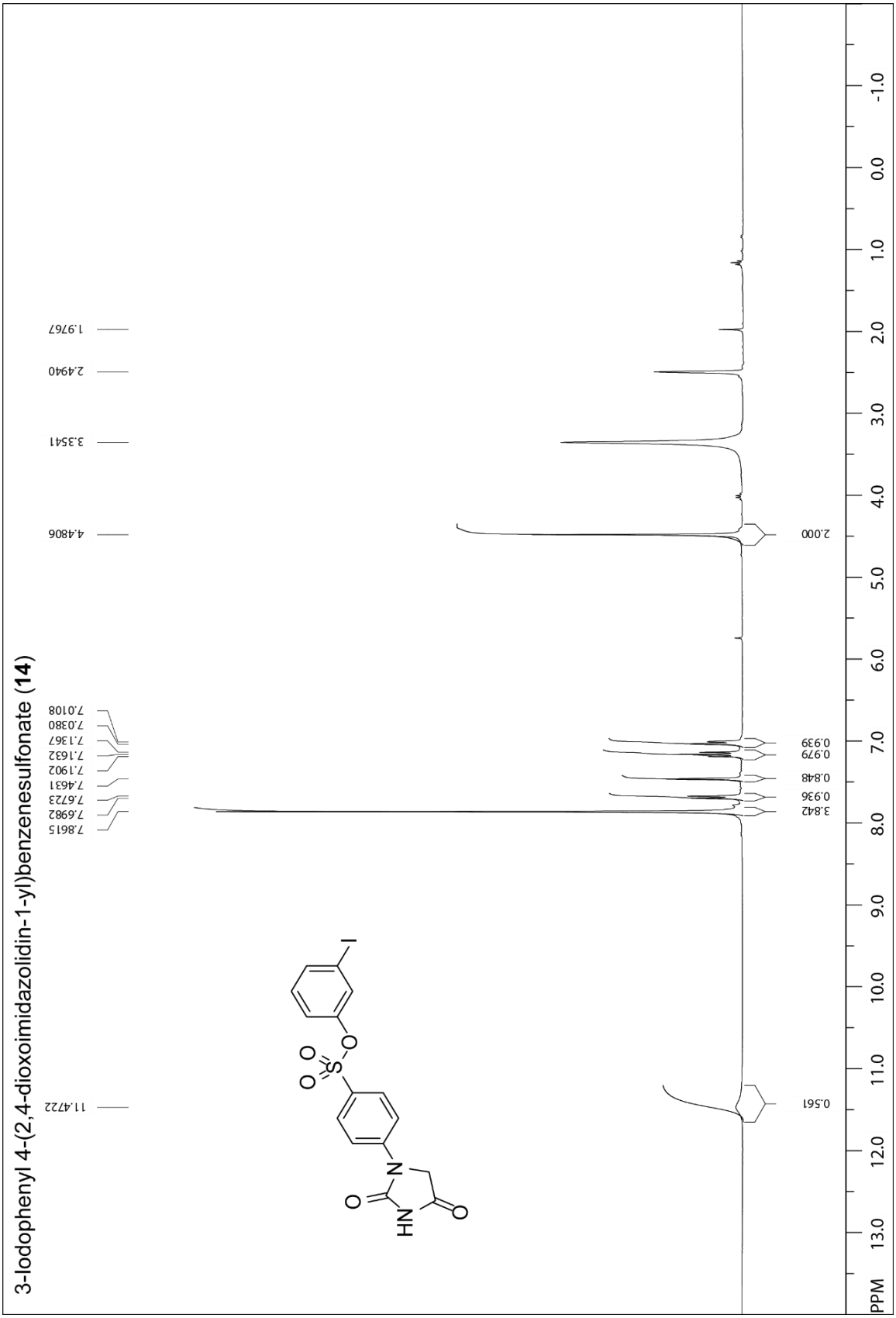
3-Iodophenyl 4-(2,4-dioxoimidazolidin-1-yl)benzenesulfonate (14)
11.4722
7.8615
7.6982
7.6723
7.4631
7.1902
7.1632
7.1367
7.0380
7.0108
4.4806
3.3541
2.4940
1.9767
0.561
3.842
0.936
0.848
0.979
0.939
2.000
PPM
13.0
12.0
11.0
10.0
9.0
8.0
7.0
6.0
5.0
4.0
3.0
2.0
1.0
0.0
-1.0

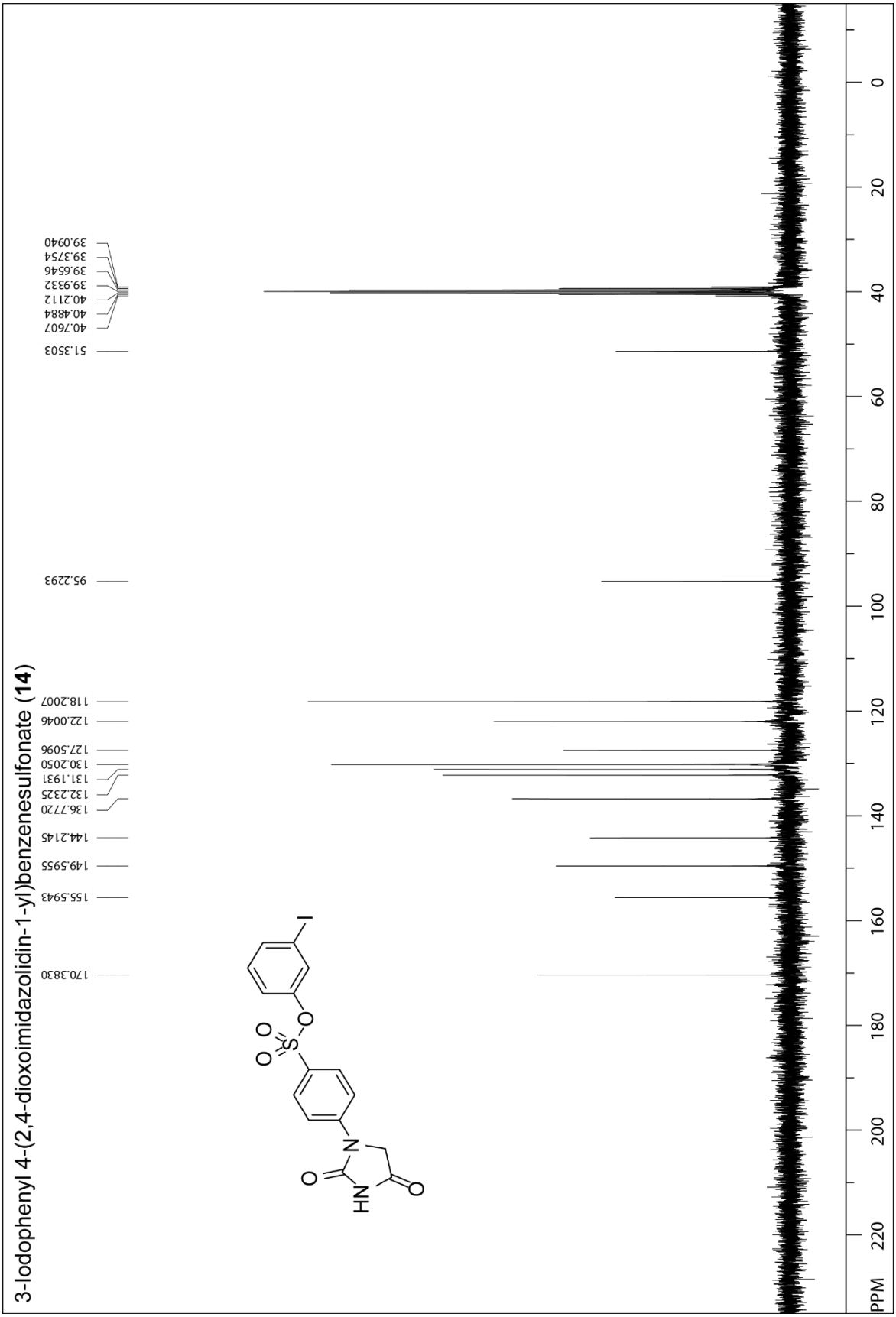
3-Iodophenyl 4-(2,4-dioxoimidazolidin-1-yl)benzenesulfonate (14)
170.3830
155.5943
149.5955
144.2145
136.7720
132.2325
131.1931
130.2050
127.5096
122.0046
118.2007
95.2293
51.3503
40.7607
40.4884
40.2112
39.9332
39.6546
39.3754
39.0940
PPM
220
200
180
160
140
120
100
80
60
40
20
0

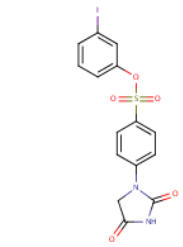

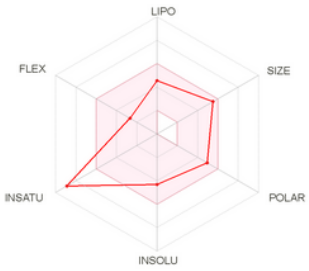

SMILES O=C1NC(=O)N(C1)c1ccc(cc1)S(=O)(=O)Oc1cccc(c1)I

Physicochemical Properties	
Formula	C15H11IN2O5S
Molecular weight	458.23 g/mol
Num. heavy atoms	24
Num. arom. heavy atoms	12
Fraction Csp3	0.07
Num. rotatable bonds	4
Num. H-bond acceptors	5
Num. H-bond donors	1
Molar Refractivity	100.80
TPSA	101.16 Å²

Lipophilicity	
Log $P_{o/w}$ (iLOGP)	1.94
Log $P_{o/w}$ (XLOGP3)	2.44
Log $P_{o/w}$ (WLOGP)	2.43
Log $P_{o/w}$ (MLOGP)	2.20
Log $P_{o/w}$ (SILICOS-IT)	1.57
Consensus Log $P_{o/w}$	2.12

Water Solubility	
Log *S* (ESOL)	-4.32
Solubility	2.17e-02 mg/ml ; 4.74e-05 mol/l
Class	Moderately soluble
Log *S* (Ali)	-4.21
Solubility	2.84e-02 mg/ml ; 6.20e-05 mol/l
Class	Moderately soluble
Log *S* (SILICOS-IT)	-5.39
Solubility	1.85e-03 mg/ml ; 4.05e-06 mol/l
Class	Moderately soluble

Pharmacokinetics	
GI absorption	High
BBB permeant	No
P-gp substrate	No
CYP1A2 inhibitor	Yes
CYP2C19 inhibitor	No
CYP2C9 inhibitor	Yes
CYP2D6 inhibitor	No
CYP3A4 inhibitor	No
Log K_p (skin permeation)	-7.36 cm/s

Druglikeness	
Lipinski	Yes; 0 violation
Ghose	Yes
Veber	Yes
Egan	Yes
Muegge	Yes
Bioavailability Score	0.55

Medicinal Chemistry	
PAINS	0 alert
Brenk	3 alerts: hydantoin, iodine, sulfonic_acid_1
Leadlikeness	No; 1 violation: MW>350
Synthetic accessibility	2.88

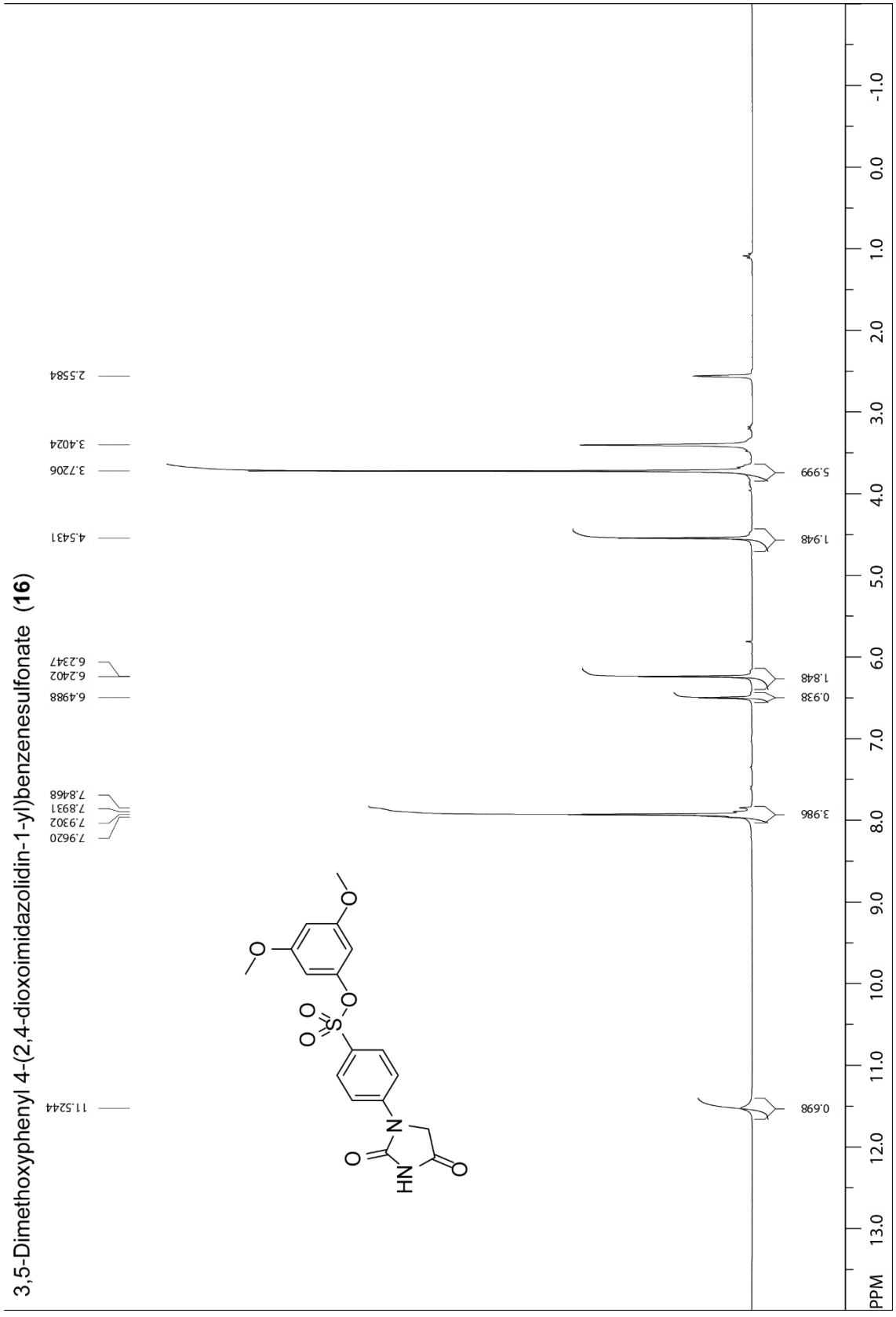
3,5-Dimethoxyphenyl 4-(2,4-dioxoimidazolidin-1-yl)benzenesulfonate (16)
11.5244
7.9620
7.9302
7.8931
7.8468
6.4988
6.2402
6.2347
4.5431
3.7206
3.4024
2.5584
0.698
3.986
0.938
1.848
1.948
5.999
PPM
13.0
12.0
11.0
10.0
9.0
8.0
7.0
6.0
5.0
4.0
3.0
2.0
1.0
0.0
-1.0

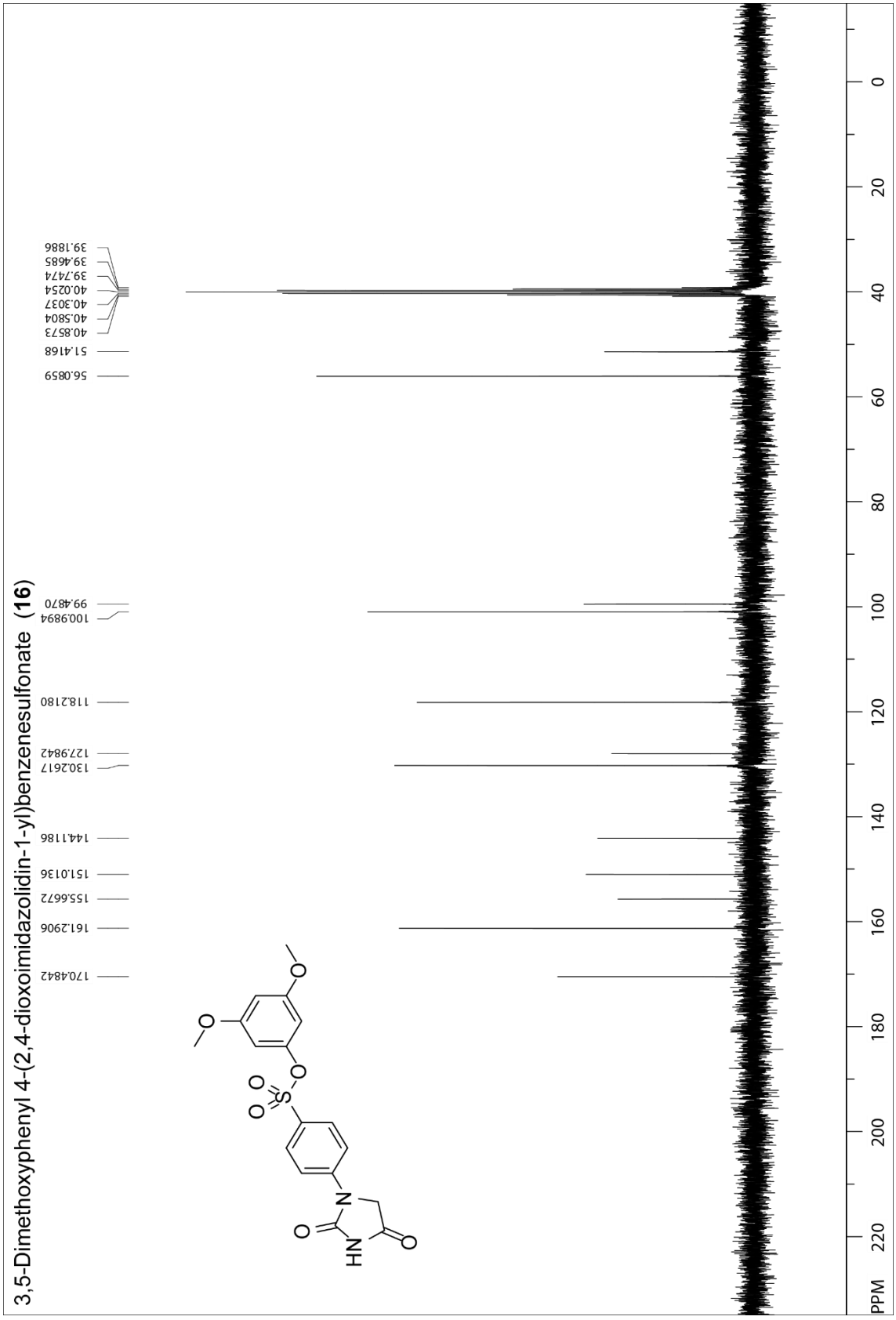
3,5-Dimethoxyphenyl 4-(2,4-dioxoimidazolidin-1-yl)benzenesulfonate (16)
39.1886
39.4685
39.7474
40.0254
40.3037
40.5804
40.8573
51.4168
56.0859
99.4870
100.9894
118.2180
127.9842
130.2617
144.1186
151.0136
155.6672
161.2906
170.4842
PPM
0
20
40
60
80
100
120
140
160
180
200
220
O
O
O
S
O
O
N
HN
O
O

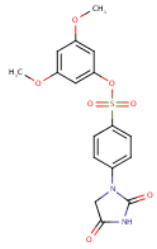

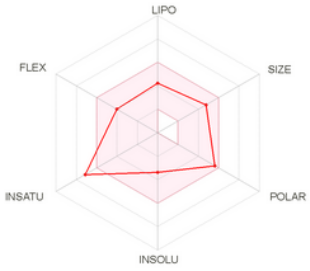

SMILES COc1cc(cc(c1)OC)OS(=O)(=O)c1ccc(cc1)N1CC(=O)NC1=O

Physicochemical Properties	
Formula	C17H16N2O7S
Molecular weight	392.38 g/mol
Num. heavy atoms	27
Num. arom. heavy atoms	12
Fraction Csp3	0.18
Num. rotatable bonds	6
Num. H-bond acceptors	7
Num. H-bond donors	1
Molar Refractivity	101.07
TPSA	119.62 Å²

Lipophilicity	
Log $P_{o/w}$ (iLOGP)	2.16
Log $P_{o/w}$ (XLOGP3)	1.87
Log $P_{o/w}$ (WLOGP)	1.85
Log $P_{o/w}$ (MLOGP)	0.91
Log $P_{o/w}$ (SILICOS-IT)	0.70
Consensus Log $P_{o/w}$	1.50

Water Solubility	
Log *S* (ESOL)	-3.38
Solubility	1.62e-01 mg/ml ; 4.13e-04 mol/l
Class	Soluble
Log *S* (Ali)	-4.00
Solubility	3.89e-02 mg/ml ; 9.91e-05 mol/l
Class	Moderately soluble
Log *S* (SILICOS-IT)	-4.76
Solubility	6.82e-03 mg/ml ; 1.74e-05 mol/l
Class	Moderately soluble

Pharmacokinetics	
GI absorption	High
BBB permeant	No
P-gp substrate	No
CYP1A2 inhibitor	No
CYP2C19 inhibitor	No
CYP2C9 inhibitor	Yes
CYP2D6 inhibitor	No
CYP3A4 inhibitor	Yes
Log K_p (skin permeation)	-7.37 cm/s

Druglikeness	
Lipinski	Yes; 0 violation
Ghose	Yes
Veber	Yes
Egan	Yes
Muegge	Yes
Bioavailability Score	0.55

Medicinal Chemistry	
PAINS	0 alert
Brenk	2 alerts: hydantoin, sulfonic_acid_1
Leadlikeness	No; 1 violation: MW>350
Synthetic accessibility	3.02

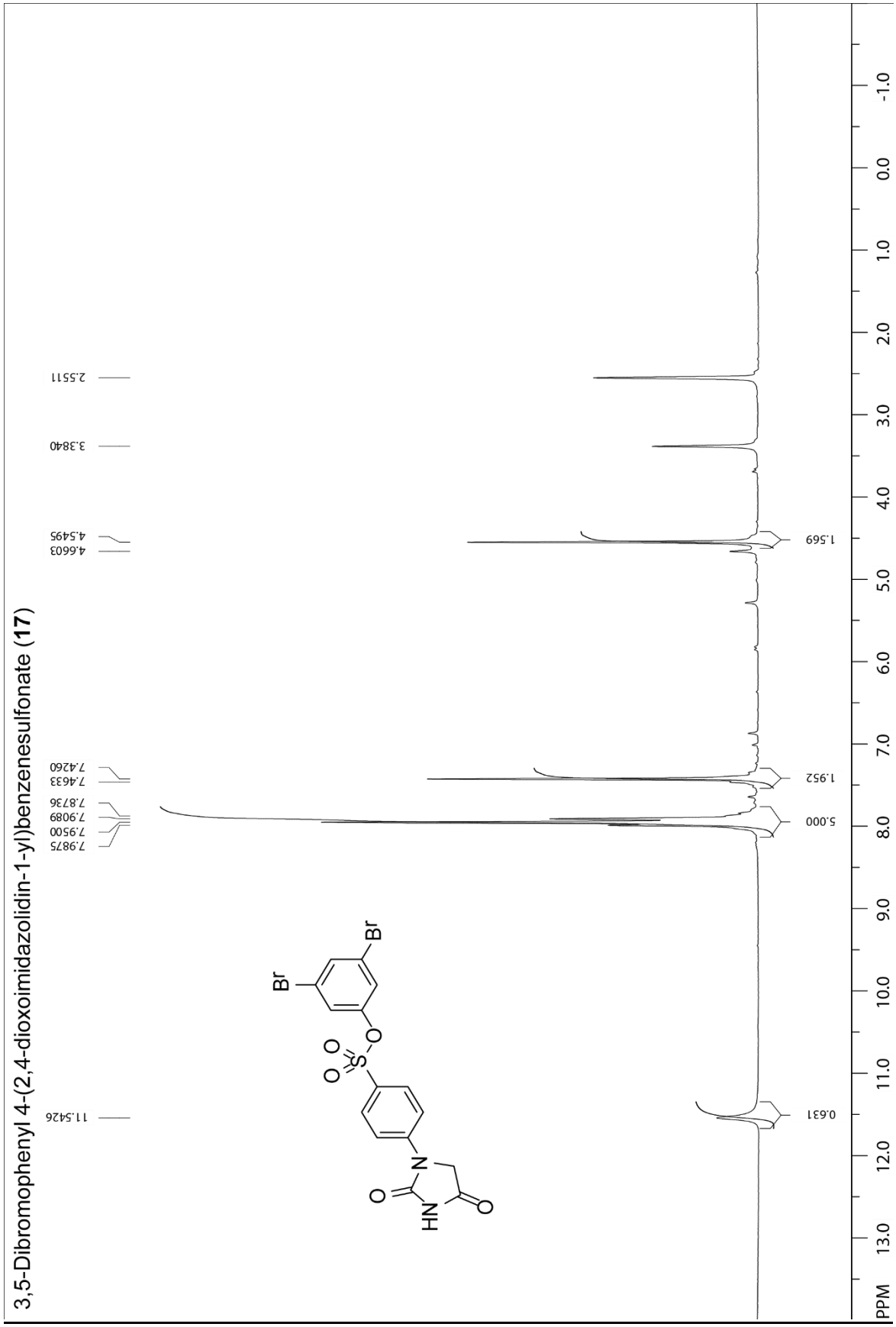
3,5-Dibromophenyl 4-(2,4-dioxoimidazolidin-1-yl)benzenesulfonate (17)
11.5426
7.9875
7.9500
7.9089
7.8736
7.4633
7.4260
4.6603
4.5495
3.3840
2.5511
0.631
5.000
1.952
1.569
Br
Br
O
S
O
O
N
O
HN
O
PPM
13.0
12.0
11.0
10.0
9.0
8.0
7.0
6.0
5.0
4.0
3.0
2.0
1.0
0.0
-1.0

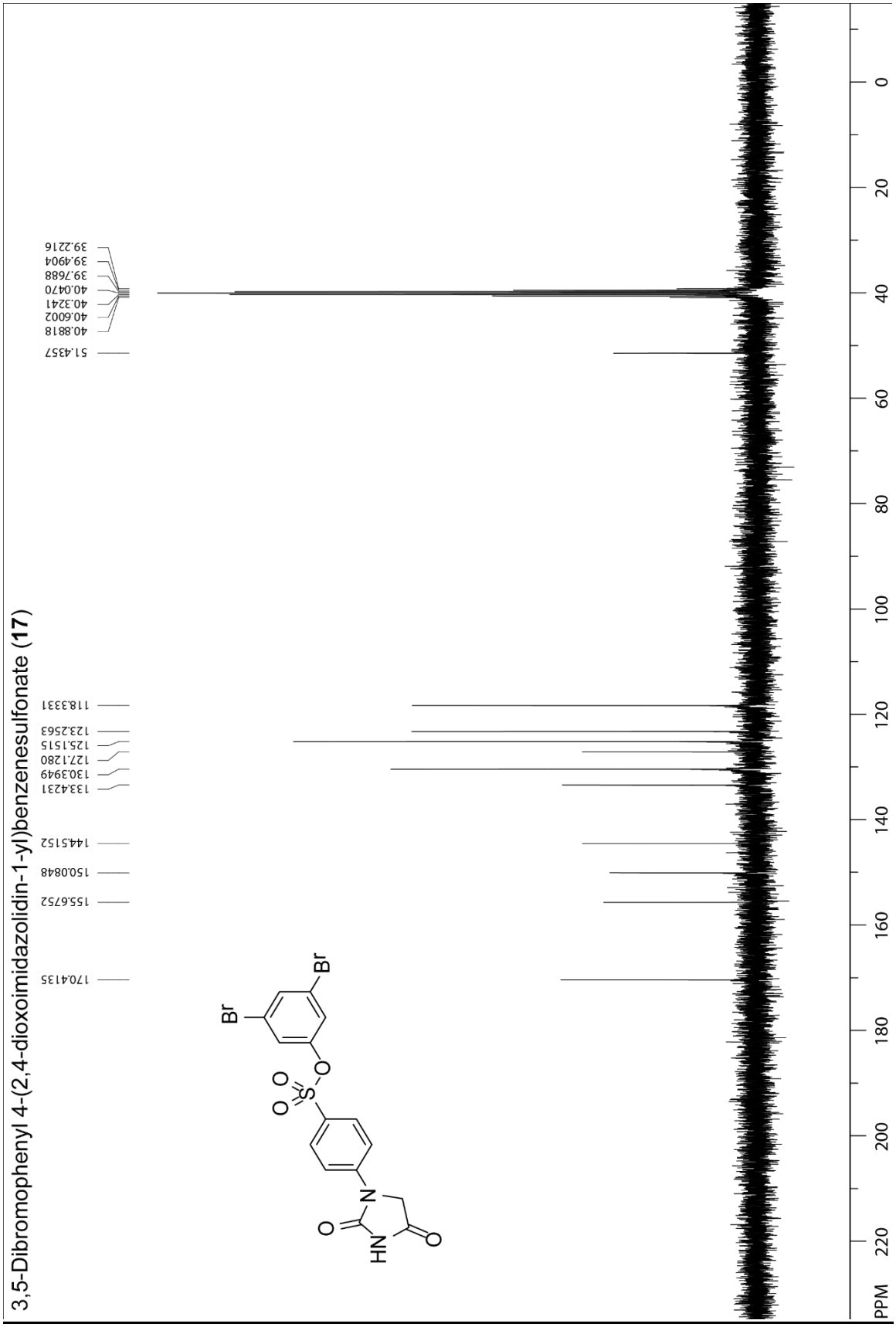
3,5-Dibromophenyl 4-(2,4-dioxoimidazolidin-1-yl)benzenesulfonate (17)
170.4135
155.6752
150.0848
144.5152
133.4231
130.3949
127.1280
125.1515
123.2563
118.3331
51.4357
40.8818
40.6002
40.3241
40.0470
39.7688
39.4904
39.2216
Br
Br
O
O
S
O
N
HN
O
O
PPM
0
20
40
60
80
100
120
140
160
180
200
220

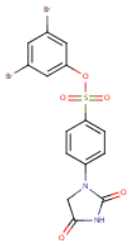

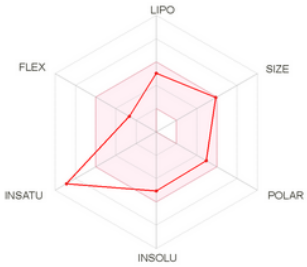

SMILES O=C1NC(=O)CN1c1ccc(cc1)S(=O)(=O)Oc1cc(Br)cc(c1)Br

Physicochemical Properties	
Formula	C15H10Br2N2O5S
Molecular weight	490.12 g/mol
Num. heavy atoms	25
Num. arom. heavy atoms	12
Fraction Csp3	0.07
Num. rotatable bonds	4
Num. H-bond acceptors	5
Num. H-bond donors	1
Molar Refractivity	103.48
TPSA	101.16 Å²

Lipophilicity	
Log $P_{o/w}$ (iLOGP)	2.32
Log $P_{o/w}$ (XLOGP3)	3.31
Log $P_{o/w}$ (WLOGP)	3.35
Log $P_{o/w}$ (MLOGP)	2.71
Log $P_{o/w}$ (SILICOS-IT)	1.96
Consensus Log $P_{o/w}$	2.73

Water Solubility	
Log *S* (ESOL)	-5.06
Solubility	4.32e-03 mg/ml ; 8.81e-06 mol/l
Class	Moderately soluble
Log *S* (Ali)	-5.11
Solubility	3.80e-03 mg/ml ; 7.76e-06 mol/l
Class	Moderately soluble
Log *S* (SILICOS-IT)	-6.11
Solubility	3.78e-04 mg/ml ; 7.71e-07 mol/l
Class	Poorly soluble

Pharmacokinetics	
GI absorption	High
BBB permeant	No
P-gp substrate	No
CYP1A2 inhibitor	Yes
CYP2C19 inhibitor	Yes
CYP2C9 inhibitor	Yes
CYP2D6 inhibitor	No
CYP3A4 inhibitor	Yes
Log K_p (skin permeation)	-6.94 cm/s

Druglikeness	
Lipinski	Yes; 0 violation
Ghose	No; 1 violation: MW>480
Veber	Yes
Egan	Yes
Muegge	Yes
Bioavailability Score	0.55

Medicinal Chemistry	
PAINS	0 alert
Brenk	2 alerts: hydantoin, sulfonic_acid_1
Leadlikeness	No; 1 violation: MW>350
Synthetic accessibility	2.85

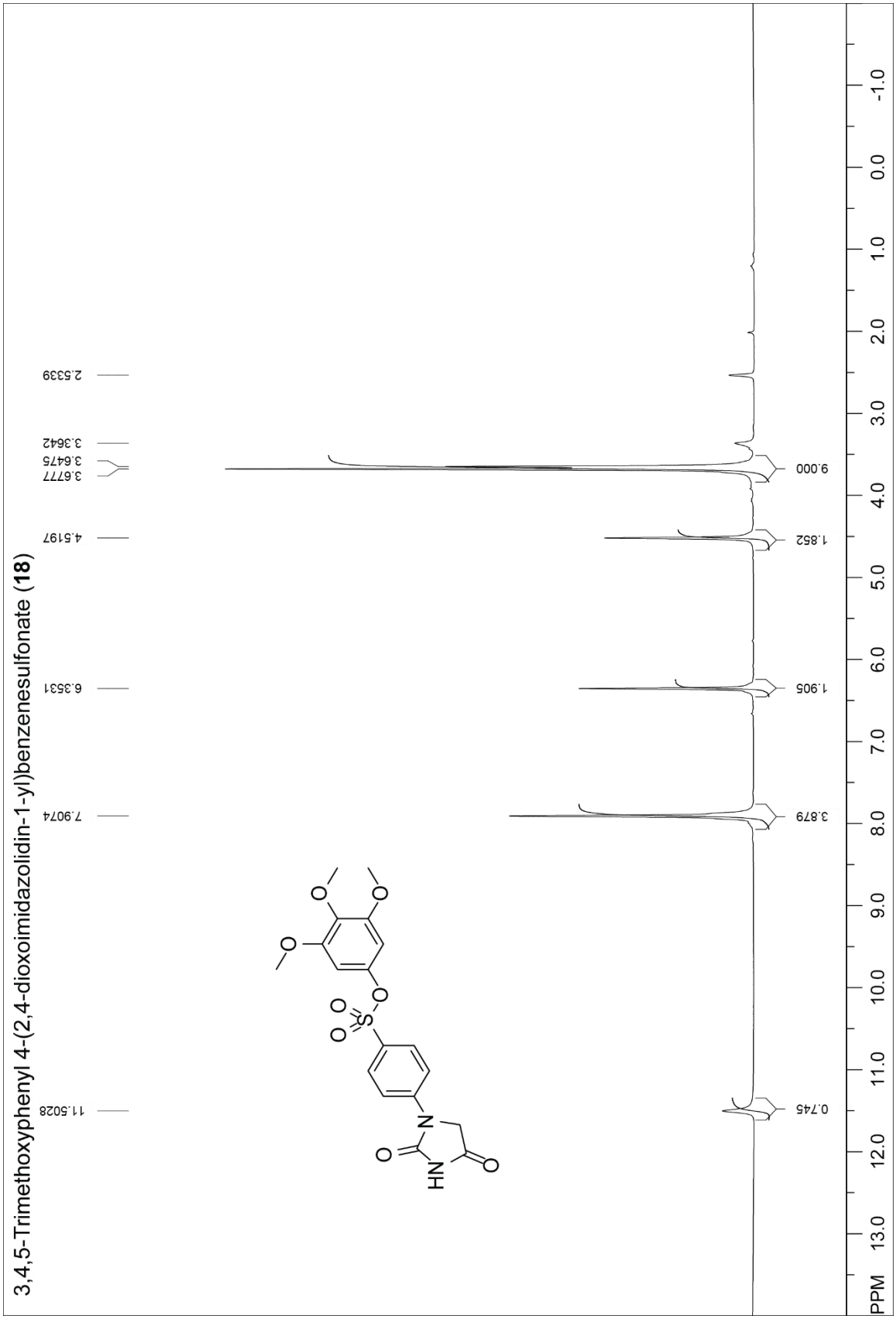
3,4,5-Trimethoxyphenyl 4-(2,4-dioxoimidazolidin-1-yl)benzenesulfonate (18)
11.5028
7.9074
6.3531
4.5197
3.6777
3.6475
3.3642
2.5339
0.745
3.879
1.905
1.852
9.000
PPM
13.0
12.0
11.0
10.0
9.0
8.0
7.0
6.0
5.0
4.0
3.0
2.0
1.0
0.0
-1.0

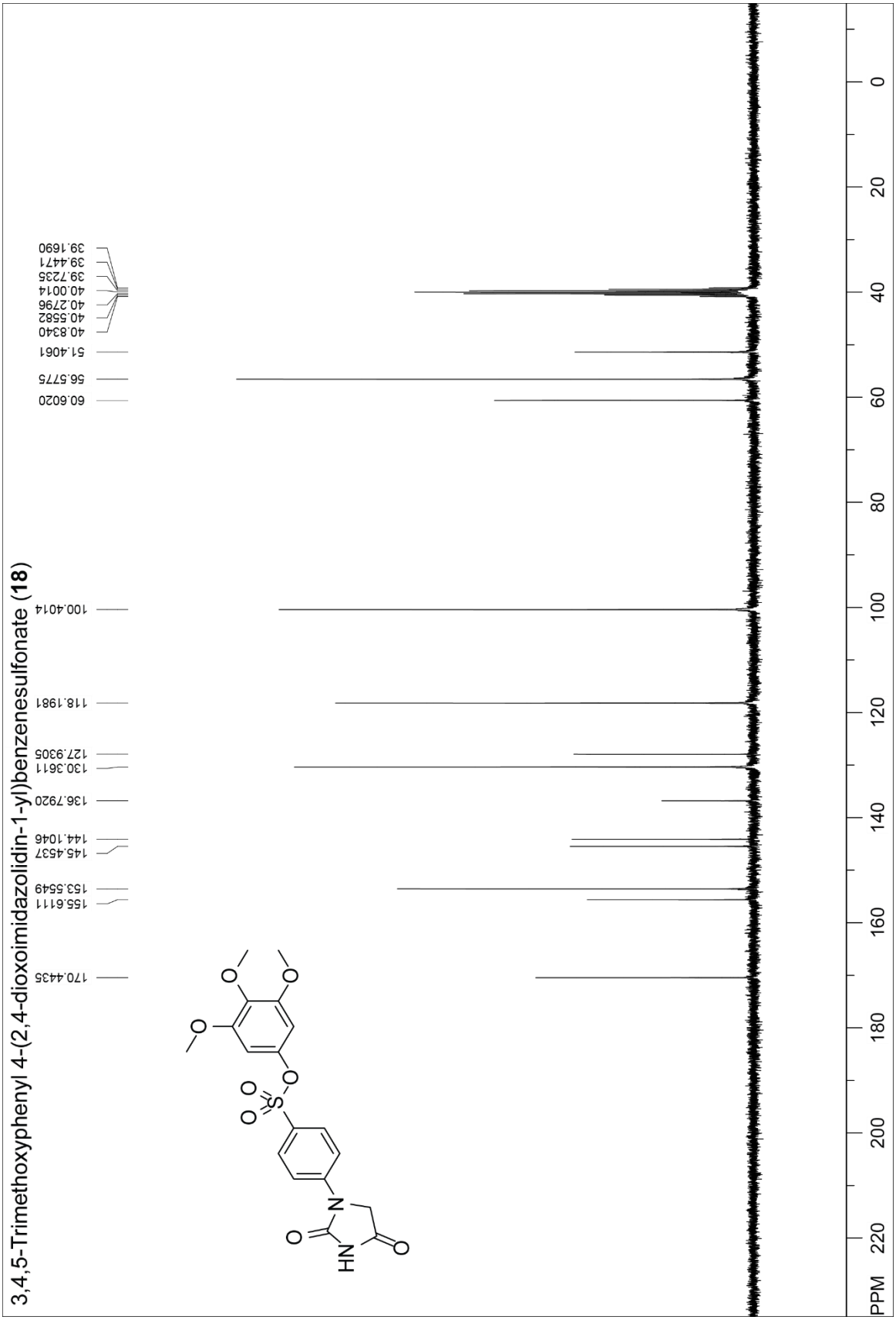
3,4,5-Trimethoxyphenyl 4-(2,4-dioxoimidazolidin-1-yl)benzenesulfonate (18)
170.4435
155.6111
153.5549
145.4537
144.1046
136.7920
130.3611
127.9305
118.1981
100.4014
60.6020
56.5775
51.4061
40.8340
40.5582
40.2796
40.0014
39.7235
39.4471
39.1690
PPM
220
200
180
160
140
120
100
80
60
40
20
0

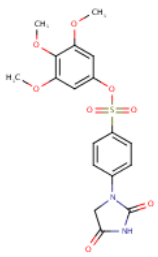

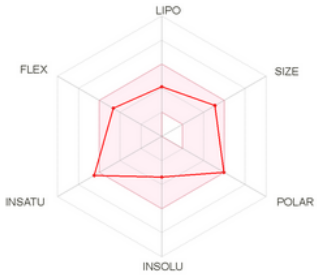

SMILES COc1cc(cc(c1OC)OC)OS(=O)(=O)c1ccc(cc1)N1CC(=O)NC1=O

Physicochemical Properties	
Formula	C18H18N2O8S
Molecular weight	422.41 g/mol
Num. heavy atoms	29
Num. arom. heavy atoms	12
Fraction Csp3	0.22
Num. rotatable bonds	7
Num. H-bond acceptors	8
Num. H-bond donors	1
Molar Refractivity	107.56
TPSA	128.85 Å²

Lipophilicity	
Log $P_{o/w}$ (iLOGP)	2.73
Log $P_{o/w}$ (XLOGP3)	1.71
Log $P_{o/w}$ (WLOGP)	1.86
Log $P_{o/w}$ (MLOGP)	0.64
Log $P_{o/w}$ (SILICOS-IT)	0.77
Consensus Log $P_{o/w}$	1.54

Water Solubility	
Log *S* (ESOL)	-3.38
Solubility	1.76e-01 mg/ml ; 4.16e-04 mol/l
Class	Soluble
Log *S* (Ali)	-4.03
Solubility	3.93e-02 mg/ml ; 9.30e-05 mol/l
Class	Moderately soluble
Log *S* (SILICOS-IT)	-4.86
Solubility	5.82e-03 mg/ml ; 1.38e-05 mol/l
Class	Moderately soluble

Pharmacokinetics	
GI absorption	High
BBB permeant	No
P-gp substrate	Yes
CYP1A2 inhibitor	Yes
CYP2C19 inhibitor	Yes
CYP2C9 inhibitor	Yes
CYP2D6 inhibitor	No
CYP3A4 inhibitor	Yes
Log K_p (skin permeation)	-7.66 cm/s

Druglikeness	
Lipinski	Yes; 0 violation
Ghose	Yes
Veber	Yes
Egan	Yes
Muegge	Yes
Bioavailability Score	0.55

Medicinal Chemistry	
PAINS	0 alert
Brenk	2 alerts: hydantoin, sulfonic_acid_1
Leadlikeness	No; 1 violation: MW>350
Synthetic accessibility	3.20

B.2. References

Beck, W. T., Mueller, T. J., & Tanzer, L. R. (1979). Altered surface membrane glycoproteins in *Vinca* alkaloid-resistant human leukemic lymphoblasts. *Cancer Research, 39*, 2070-2076.

Cabral, F., Sobel, M. E., & Gottesman, M. M. (1980). CHO mutants resistant to colchicine, colcemid or griseofulvin have an altered β-tubulin. *Cell, 20*, 29-36. doi: 10.1016/0092-8674(80)90231-7

Carmichael, J., DeGraff, W. G., Gazdar, A. F., Minna, J. D., & Mitchell, J. B. (1987). Evaluation of a tetrazolium-based semiautomated colorimetric assay: assessment of chemosensitivity testing. *Cancer Research, 47*, 936-942.

Cytoskeleton Inc, Tubulin polymerization assay kit manual. Retrieved from https://www.cytoskeleton.com/pdf-storage/datasheets/bk011p.pdf

Ford, C. H., Richardson, V. J., & Tsaltas, G. (1989). Comparison of tetrazolium colorimetric and [3H]-uridine assays for *in vitro* chemosensitivity testing. *Cancer Chemotherapy and Pharmacology, 24*, 295-301. doi: 10.1007/bf00304761

Fortin, S., Lacroix, J., Côté, M.-F., Moreau, E., Petitclerc, É., & C.-Gaudreault, R. (2010). Quick and simple detection technique to assess the binding of antimicrotubule agents to the colchicine-binding site. *Biological Procedures Online, 12*, 113-117. doi: 10.1007/s12575-010-9029-5

Gagné-Boulet, M., Bouzriba, C., Godard, M., & Fortin, S. (2018). Preparation, characterisation and biological evaluation of new *N*-phenyl amidobenzenesulfonates and *N*-phenyl ureidobenzenesulfonates inducing DNA double-strand breaks. Part 3. Modulation of ring A. *European Journal of Medicinal Chemistry, 155*, 681-694. doi: 10.1016/j.ejmech.2018.06.030

Gagné-Boulet, M., Moussa, H., Lacroix, J., Côté, M.-F., Masson, J.-Y., & Fortin, S. (2015). Synthesis and biological evaluation of novel *N*-phenyl ureidobenzenesulfonate derivatives as potential anticancer agents. Part 2. Modulation of the ring B. *European Journal of Medicinal Chemistry, 103*, 563-573. doi: 10.1016/j.ejmech.2015.09.012

Hirota, K., Banno, K., Yamada, Y., & Senda, S. (1985). Pyrimidines. Part 53. Novel ring transformation induced by the substituent effect of the phenyl group. Reaction of 5-bromo-6-methyl-1-phenyluracil derivatives with amines and hydrazine to give hydantoins and pyrazolones. *Journal of the Chemical Society, Perkin Transactions 1*, 1137-1142. doi: 10.1039/P19850001137

Iyer, P. S., O'Malley, M. M., & Lucas, M. C. (2007). Microwave-enhanced rhodium-catalyzed conjugate-addition of aryl boronic acids to unprotected maleimides. *Tetrahedron Letters, 48*, 4413-4418. doi: 10.1016/j.tetlet.2007.04.084

Laemmli, U. K. (1970). Cleavage of structural proteins during the assembly of the head of bacteriophage T4. *Nature, 227*, 680-685. doi: 10.1038/227680a0

National Cancer Institute (NCI/NIH), Developmental therapeutics program human tumor cell line screen. Retrieved from http://dtp.nci.nih.gov/branches/btb/ivclsp.html

Ravelli, R. B., Gigant, B., Curmi, P. A., Jourdain, I., Lachkar, S., Sobel, A., & Knossow, M. (2004). Insight into tubulin regulation from a complex with colchicine and a stathmin-like domain. *Nature, 428*, 198-202. doi: 10.1038/nature02393

Schibler, M. J., Barlow, S. B., & Cabral, F. (1989). Elimination of permeability mutants from selections for drug resistance in mammalian cells. *The FASEB Journal, 3*, 163-168. doi: 10.1096/fasebj.3.2.2563346

Schibler, M. J., & Cabral, F. (1986). Taxol-dependent mutants of Chinese hamster ovary cells with alterations in α- and β-tubulin. *Journal of Cell Biology, 102*, 1522-1531. doi: 10.1083/jcb.102.4.1522

Turcotte, V., Fortin, S., Vevey, F., Coulombe, Y., Lacroix, J., Côté, M.-F., Masson, J.-Y., & C.-Gaudreault, R. (2012). Synthesis, biological evaluation, and structure-activity relationships of novel substituted *N*-phenyl ureidobenzenesulfonate derivatives blocking cell cycle progression in S-phase and inducing DNA double-strand breaks. *Journal of Medicinal Chemistry, 55*, 6194-6208. doi: 10.1021/jm3006492

Annexe C : Données supplémentaires du chapitre 4

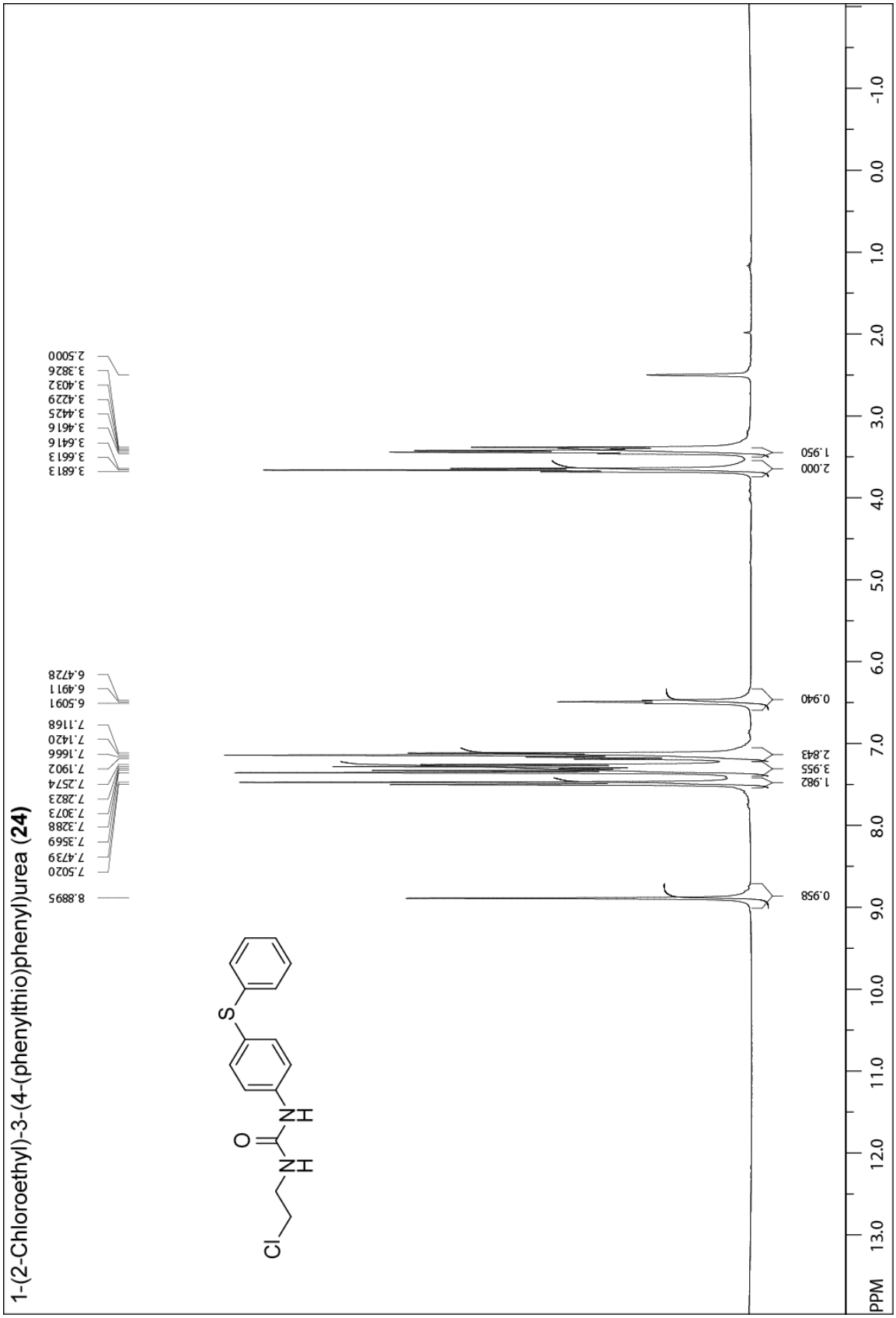
1-(2-Chloroethyl)-3-(4-(phenylthio)phenyl)urea (24)
8.8895
7.5020
7.4739
7.3569
7.3288
7.3073
7.2823
7.2574
7.1902
7.1666
7.1420
7.1168
6.5091
6.4911
6.4728
3.6813
3.6613
3.6416
3.4616
3.4425
3.4229
3.4032
3.3826
2.5000
0.958
1.982
3.955
2.843
0.940
2.000
1.950
PPM
13.0
12.0
11.0
10.0
9.0
8.0
7.0
6.0
5.0
4.0
3.0
2.0
1.0
0.0
-1.0

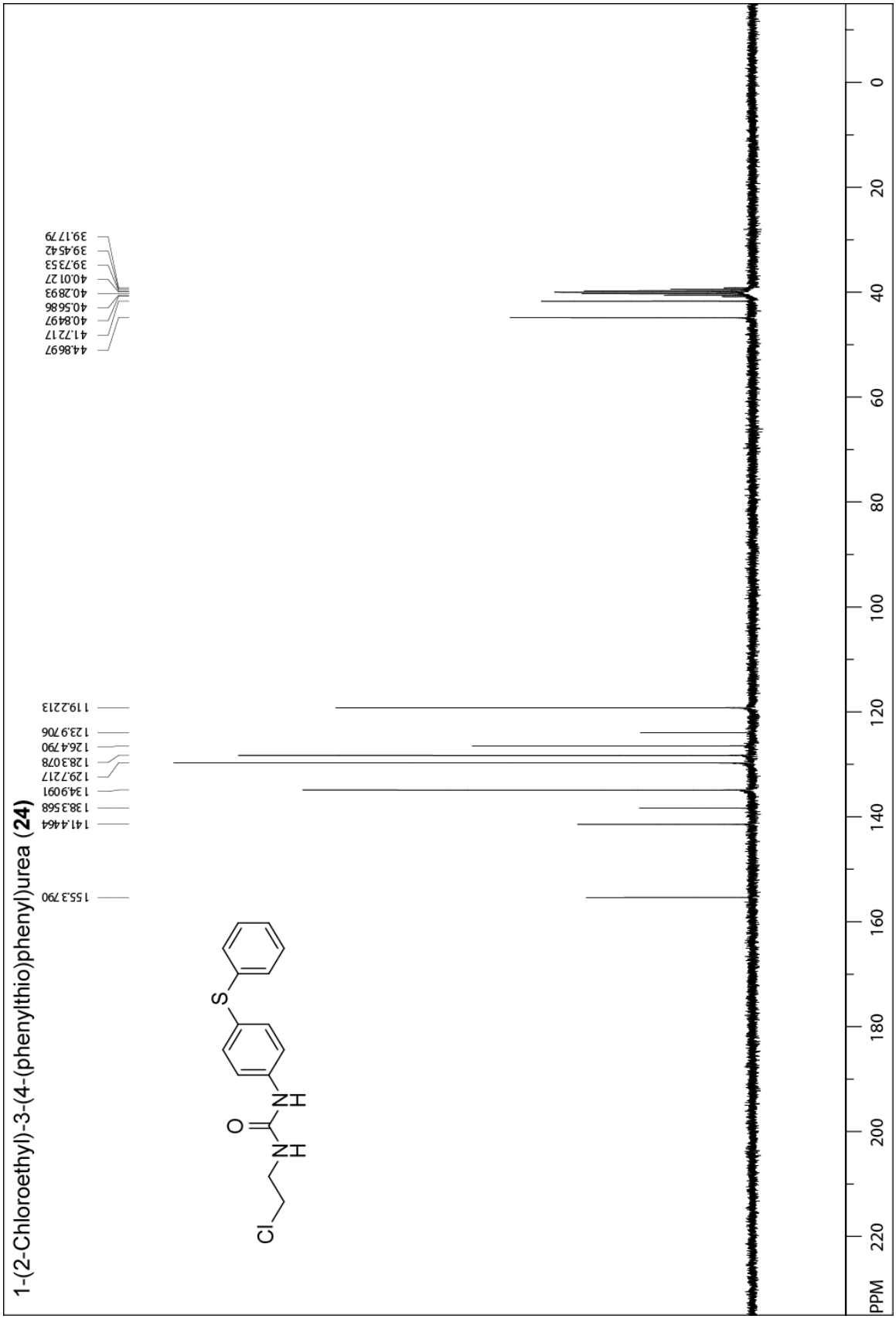
1-(2-Chloroethyl)-3-(4-(phenylthio)phenyl)urea (24)
155.3790
141.4464
138.3568
134.9091
129.7217
128.3078
126.4790
123.9706
119.2213
44.8697
41.7217
40.8497
40.5686
40.2893
40.0127
39.7353
39.4542
39.1779
PPM
0
20
40
60
80
100
120
140
160
180
200
220
S
NH
O
NH
Cl

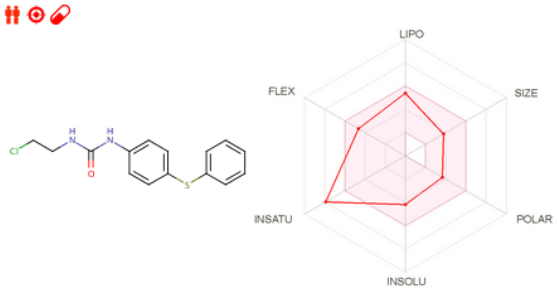

SMILES ClCCNC(=O)Nc1ccc(cc1)Sc1ccccc1

Physicochemical Properties	
Formula	C15H15ClN2OS
Molecular weight	306.81 g/mol
Num. heavy atoms	20
Num. arom. heavy atoms	12
Fraction Csp3	0.13
Num. rotatable bonds	7
Num. H-bond acceptors	1
Num. H-bond donors	2
Molar Refractivity	84.11
TPSA	66.43 Å²

Lipophilicity	
Log $P_{o/w}$ (iLOGP)	2.62
Log $P_{o/w}$ (XLOGP3)	3.93
Log $P_{o/w}$ (WLOGP)	4.01
Log $P_{o/w}$ (MLOGP)	3.98
Log $P_{o/w}$ (SILICOS-IT)	3.27
Consensus Log $P_{o/w}$	3.56

Water Solubility	
Log *S* (ESOL)	-4.20
Solubility	1.94e-02 mg/ml ; 6.31e-05 mol/l
Class	Moderately soluble
Log *S* (Ali)	-5.02
Solubility	2.90e-03 mg/ml ; 9.45e-06 mol/l
Class	Moderately soluble
Log *S* (SILICOS-IT)	-6.49
Solubility	9.97e-05 mg/ml ; 3.25e-07 mol/l
Class	Poorly soluble

Pharmacokinetics	
GI absorption	High
BBB permeant	Yes
P-gp substrate	No
CYP1A2 inhibitor	Yes
CYP2C19 inhibitor	Yes
CYP2C9 inhibitor	Yes
CYP2D6 inhibitor	Yes
CYP3A4 inhibitor	No
Log K_p (skin permeation)	-5.38 cm/s

Druglikeness	
Lipinski	Yes; 0 violation
Ghose	Yes
Veber	Yes
Egan	Yes
Muegge	Yes
Bioavailability Score	0.55

Medicinal Chemistry	
PAINS	0 alert
Brenk	1 alert: alkyl_halide
Leadlikeness	No; 1 violation: XLOGP3>3.5
Synthetic accessibility	2.32

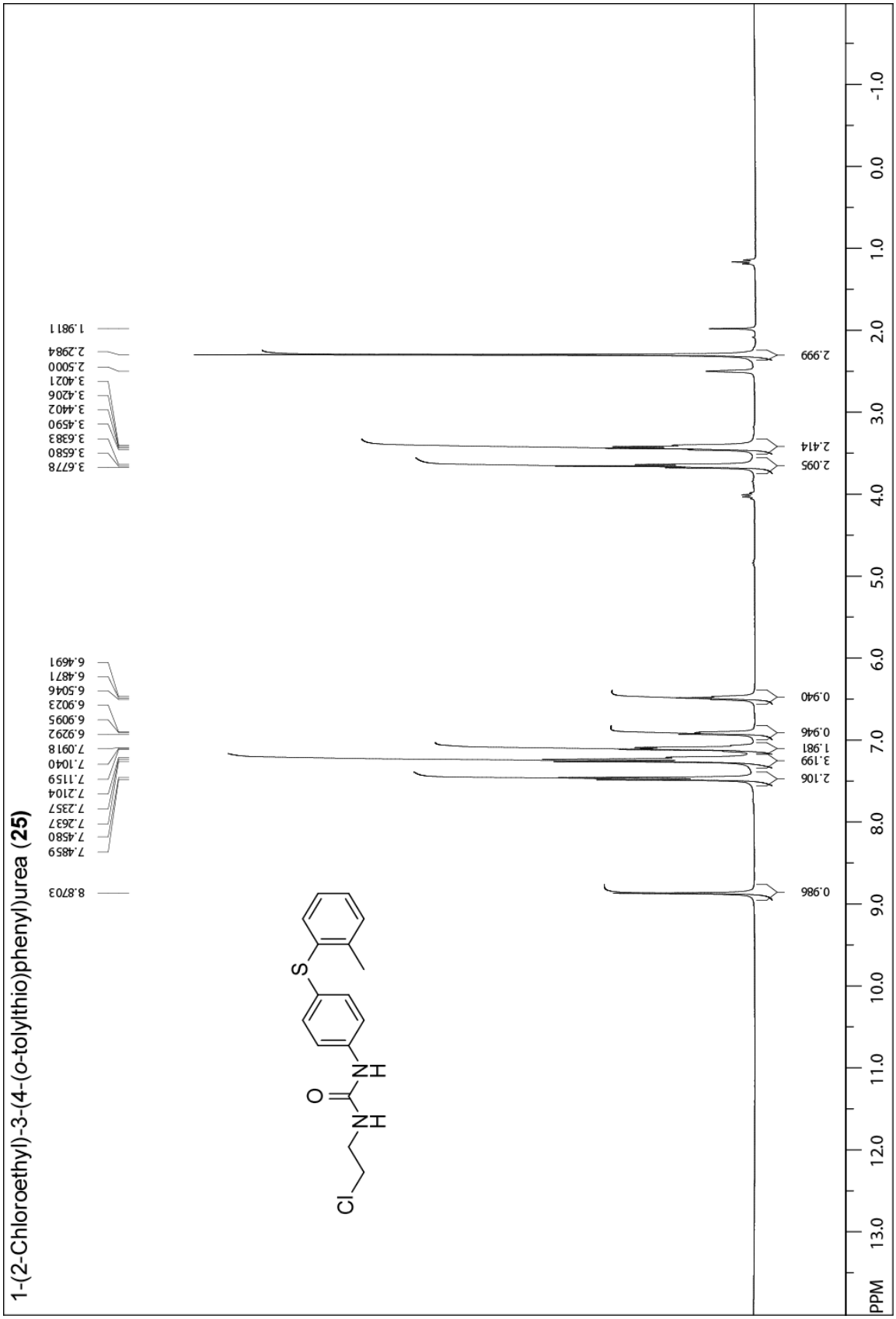
1-(2-Chloroethyl)-3-(4-(o-tolylthio)phenyl)urea (25)
8.8703
7.4859
7.4580
7.2637
7.2357
7.2104
7.1159
7.1040
7.0918
6.9292
6.9095
6.9023
6.5046
6.4871
6.4691
3.6778
3.6580
3.6383
3.4590
3.4402
3.4206
3.4021
2.5000
2.2984
1.9811
0.986
2.106
3.199
1.981
0.946
0.940
2.095
2.414
2.999
PPM
13.0
12.0
11.0
10.0
9.0
8.0
7.0
6.0
5.0
4.0
3.0
2.0
1.0
0.0
-1.0
S
NH
O
NH
Cl

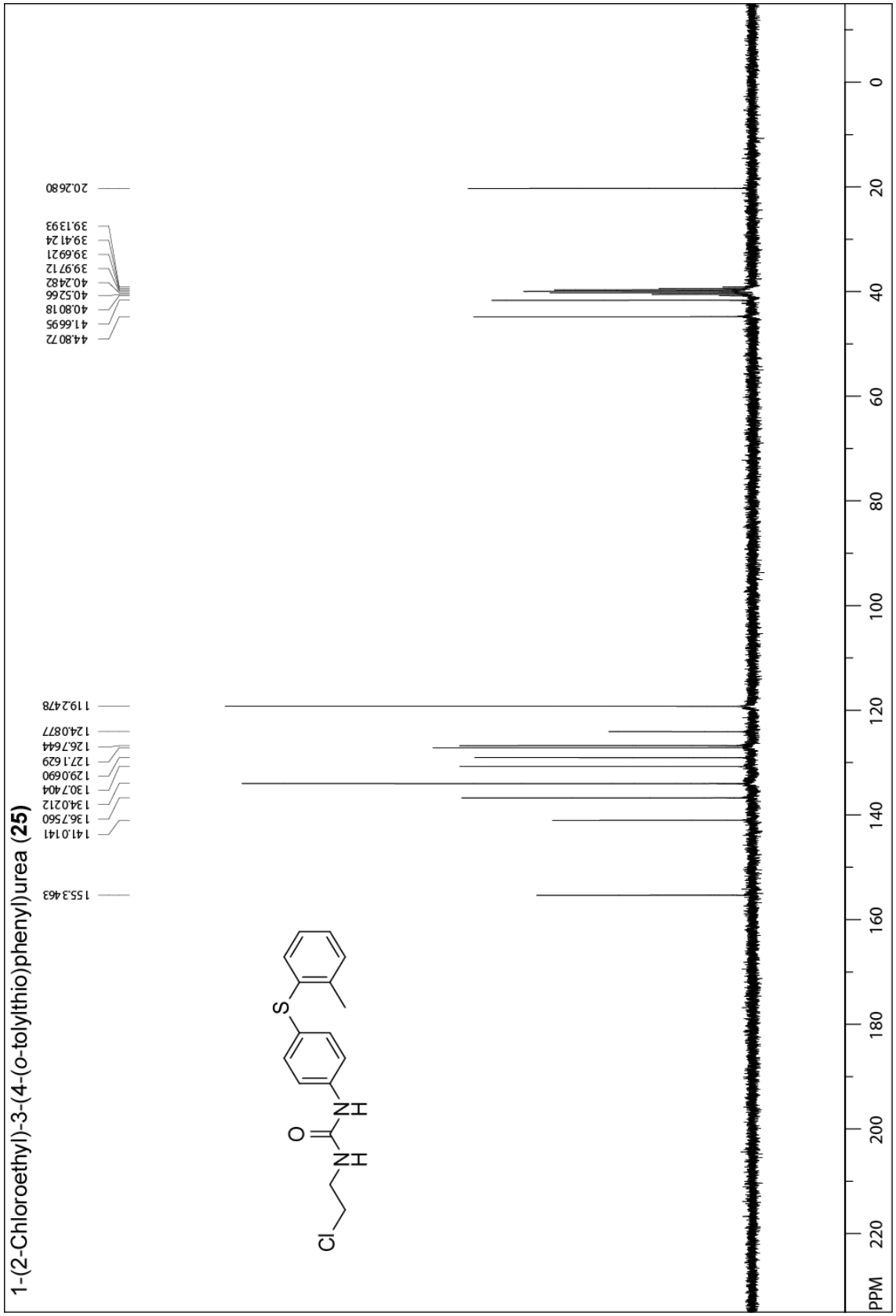
1-(2-Chloroethyl)-3-(4-(o-tolylthio)phenyl)urea (25)
155.3463
141.0141
136.7560
134.0212
130.7404
129.0690
127.1629
126.7644
124.0877
119.2478
44.8072
41.6695
40.8018
40.5266
40.2482
39.9712
39.6921
39.4124
39.1393
20.2680
PPM
220
200
180
160
140
120
100
80
60
40
20
0
O
N
H
N
H
S
Cl

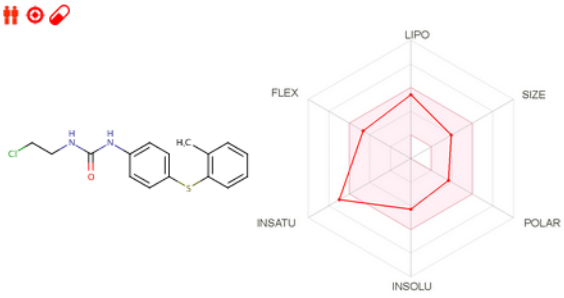

SMILES ClCCNC(=O)Nc1ccc(cc1)Sc1ccccc1C

Physicochemical Properties	
Formula	C16H17ClN2OS
Molecular weight	320.84 g/mol
Num. heavy atoms	21
Num. arom. heavy atoms	12
Fraction Csp3	0.19
Num. rotatable bonds	7
Num. H-bond acceptors	1
Num. H-bond donors	2
Molar Refractivity	89.08
TPSA	66.43 Å²

Lipophilicity	
Log $P_{o/w}$ (iLOGP)	2.49
Log $P_{o/w}$ (XLOGP3)	3.95
Log $P_{o/w}$ (WLOGP)	4.32
Log $P_{o/w}$ (MLOGP)	4.22
Log $P_{o/w}$ (SILICOS-IT)	3.78
Consensus Log $P_{o/w}$	3.75

Water Solubility	
Log *S* (ESOL)	-4.28
Solubility	1.69e-02 mg/ml ; 5.27e-05 mol/l
Class	Moderately soluble
Log *S* (Ali)	-5.05
Solubility	2.89e-03 mg/ml ; 9.01e-06 mol/l
Class	Moderately soluble
Log *S* (SILICOS-IT)	-6.87
Solubility	4.35e-05 mg/ml ; 1.36e-07 mol/l
Class	Poorly soluble

Pharmacokinetics	
GI absorption	High
BBB permeant	Yes
P-gp substrate	No
CYP1A2 inhibitor	Yes
CYP2C19 inhibitor	Yes
CYP2C9 inhibitor	Yes
CYP2D6 inhibitor	Yes
CYP3A4 inhibitor	Yes
Log K_p (skin permeation)	-5.45 cm/s

Druglikeness	
Lipinski	Yes; 1 violation: MLOGP>4.15
Ghose	Yes
Veber	Yes
Egan	Yes
Muegge	Yes
Bioavailability Score	0.55

Medicinal Chemistry	
PAINS	0 alert
Brenk	1 alert: alkyl_halide
Leadlikeness	No; 1 violation: XLOGP3>3.5
Synthetic accessibility	2.37

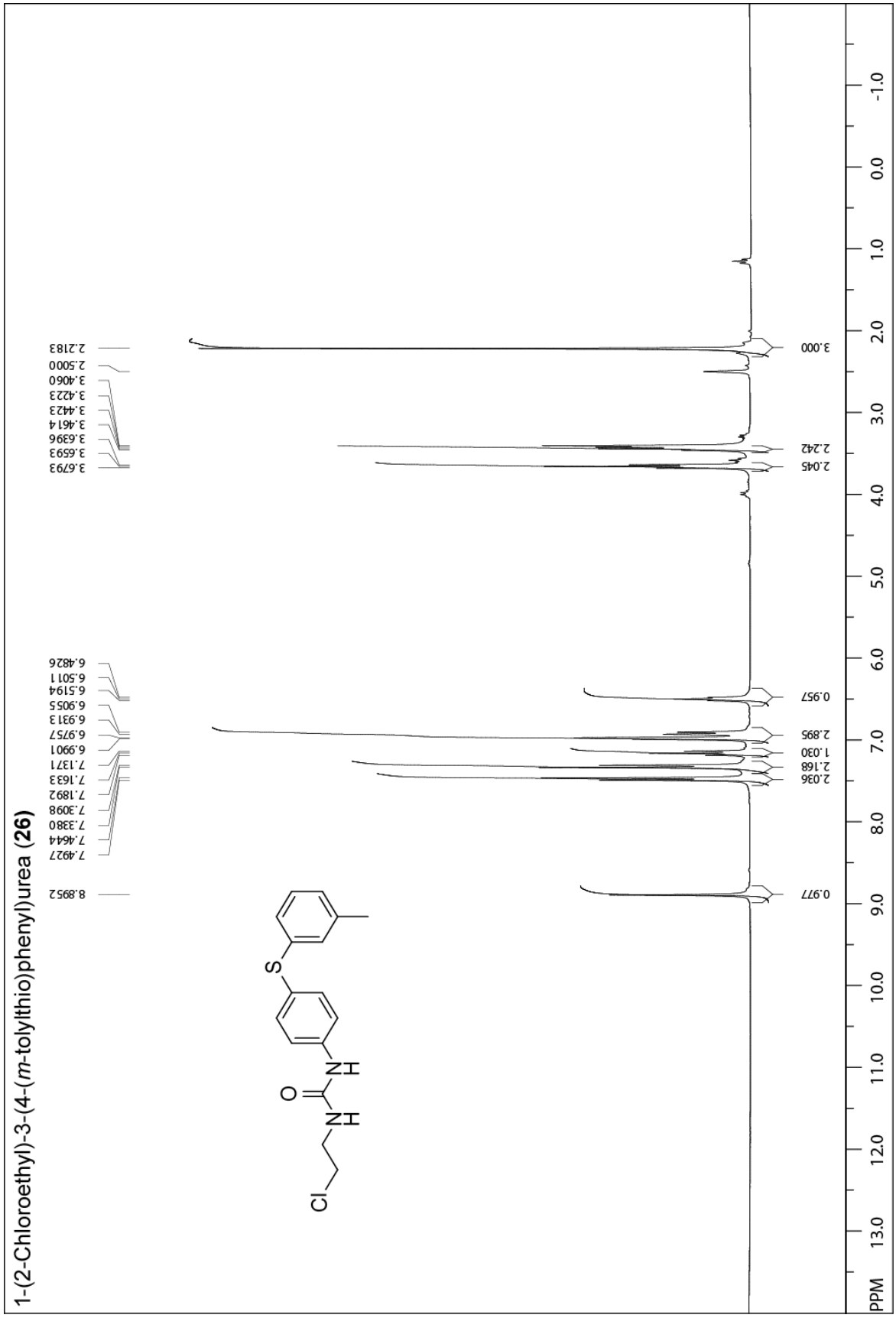
1-(2-Chloroethyl)-3-(4-(m-tolylthio)phenyl)urea (26)
8.8952
7.4927
7.4644
7.3380
7.3098
7.1892
7.1633
7.1371
6.9901
6.9757
6.9313
6.9055
6.5194
6.5011
6.4826
3.6793
3.6593
3.6396
3.4614
3.4423
3.4223
3.4060
2.5000
2.2183
0.977
2.036
2.168
1.030
2.895
0.957
2.045
2.242
3.000
PPM
13.0
12.0
11.0
10.0
9.0
8.0
7.0
6.0
5.0
4.0
3.0
2.0
1.0
0.0
-1.0
S
HN
O
NH
Cl

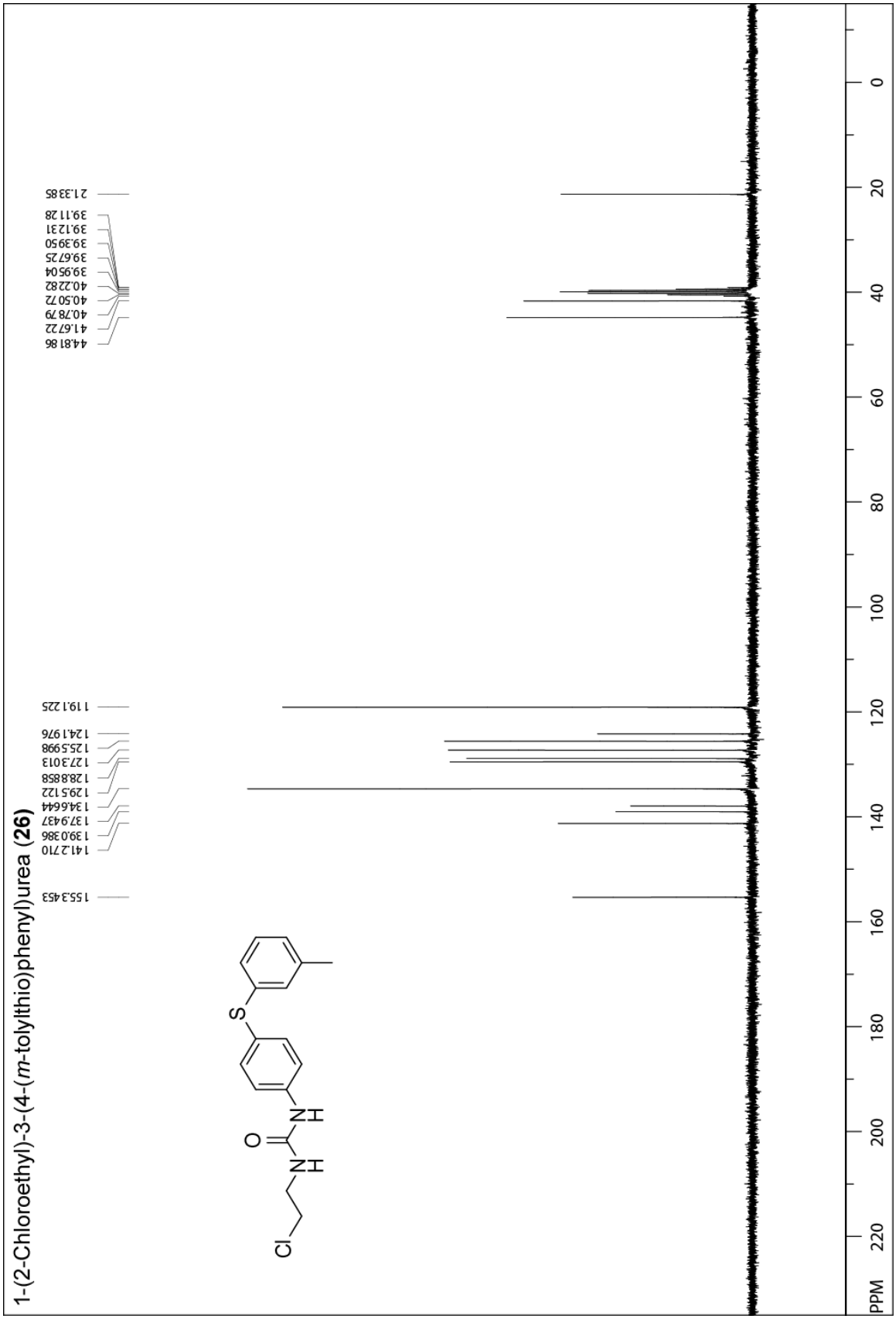
1-(2-Chloroethyl)-3-(4-(m-tolylthio)phenyl)urea (26)
155.3453
141.2710
139.0386
137.9437
134.6644
129.5122
128.8858
127.3013
125.5998
124.1976
119.1225
44.8186
41.6722
40.7879
40.5072
40.2282
39.9504
39.6725
39.3950
39.1231
39.1128
21.3385
PPM
0
20
40
60
80
100
120
140
160
180
200
220

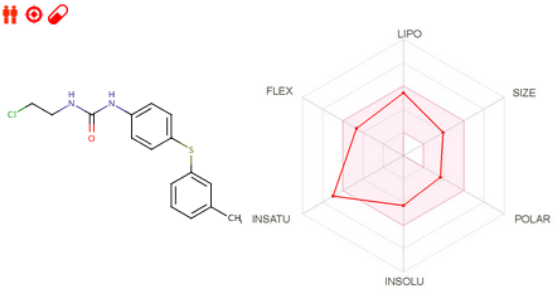

SMILES CICCNC(=O)Nc1ccc(cc1)Sc1cccc(c1)C

Physicochemical Properties	
Formula	C16H17ClN2OS
Molecular weight	320.84 g/mol
Num. heavy atoms	21
Num. arom. heavy atoms	12
Fraction Csp3	0.19
Num. rotatable bonds	7
Num. H-bond acceptors	1
Num. H-bond donors	2
Molar Refractivity	89.08
TPSA	66.43 Å²

Lipophilicity	
Log $P_{o/w}$ (iLOGP)	2.87
Log $P_{o/w}$ (XLOGP3)	3.95
Log $P_{o/w}$ (WLOGP)	4.32
Log $P_{o/w}$ (MLOGP)	4.22
Log $P_{o/w}$ (SILICOS-IT)	3.78
Consensus Log $P_{o/w}$	3.83

Water Solubility	
Log *S* (ESOL)	-4.28
Solubility	1.69e-02 mg/ml ; 5.27e-05 mol/l
Class	Moderately soluble
Log *S* (Ali)	-5.05
Solubility	2.89e-03 mg/ml ; 9.01e-06 mol/l
Class	Moderately soluble
Log *S* (SILICOS-IT)	-6.87
Solubility	4.35e-05 mg/ml ; 1.36e-07 mol/l
Class	Poorly soluble

Pharmacokinetics	
GI absorption	High
BBB permeant	Yes
P-gp substrate	No
CYP1A2 inhibitor	Yes
CYP2C19 inhibitor	Yes
CYP2C9 inhibitor	Yes
CYP2D6 inhibitor	Yes
CYP3A4 inhibitor	Yes
Log K_p (skin permeation)	-5.45 cm/s

Druglikeness	
Lipinski	Yes; 1 violation: MLOGP>4.15
Ghose	Yes
Veber	Yes
Egan	Yes
Muegge	Yes
Bioavailability Score	0.55

Medicinal Chemistry	
PAINS	0 alert
Brenk	1 alert: alkyl_halide
Leadlikeness	No; 1 violation: XLOGP3>3.5
Synthetic accessibility	2.41

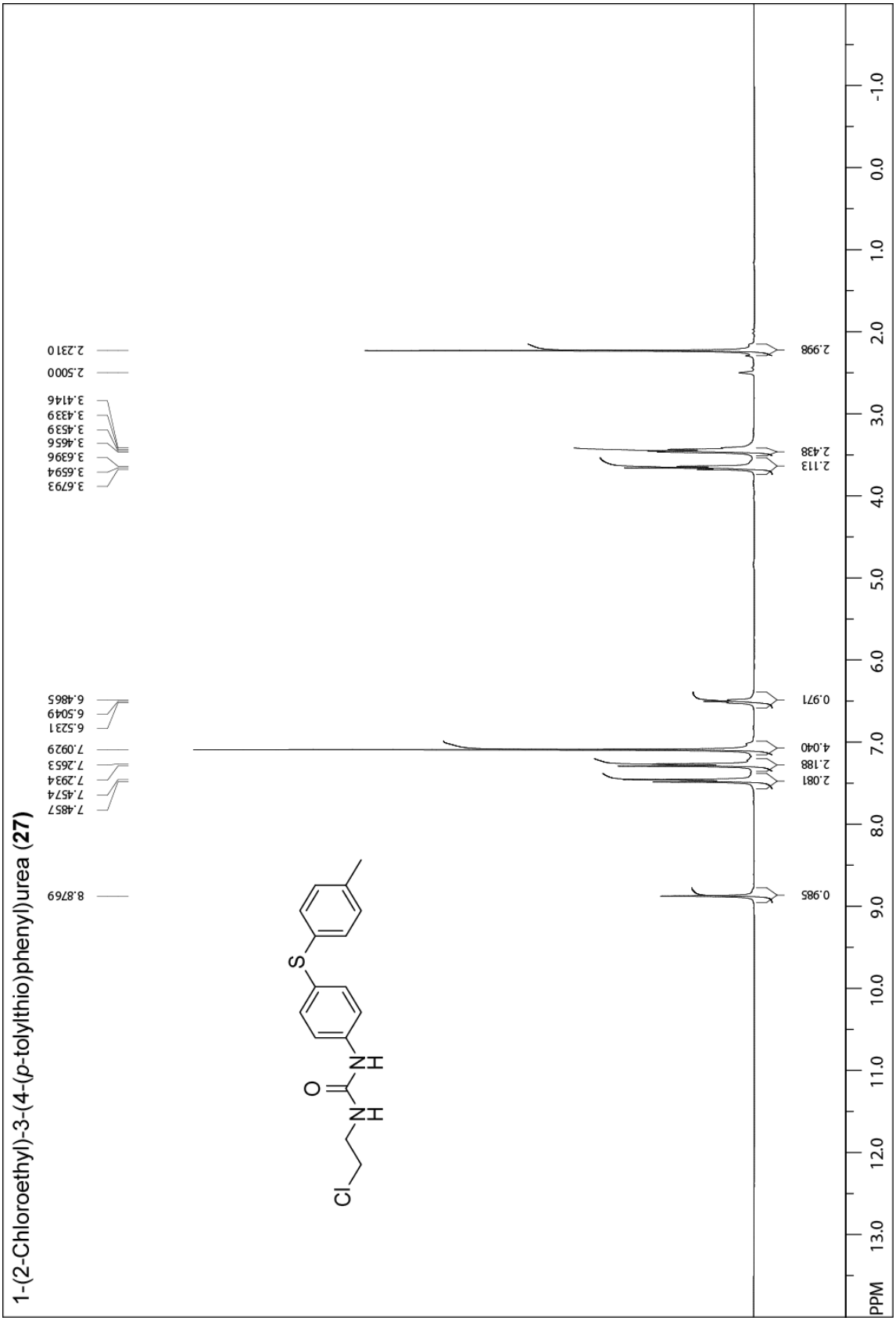
1-(2-Chloroethyl)-3-(4-(p-tolylthio)phenyl)urea (27)
8.8769
7.4857
7.4574
7.2934
7.2653
7.0929
6.5231
6.5049
6.4865
3.6793
3.6594
3.6396
3.4656
3.4539
3.4339
3.4146
2.5000
2.2310
0.985
2.998
2.438
2.113
0.971
4.040
2.188
2.081
PPM
13.0
12.0
11.0
10.0
9.0
8.0
7.0
6.0
5.0
4.0
3.0
2.0
1.0
0.0
-1.0
S
O
NH
NH
Cl

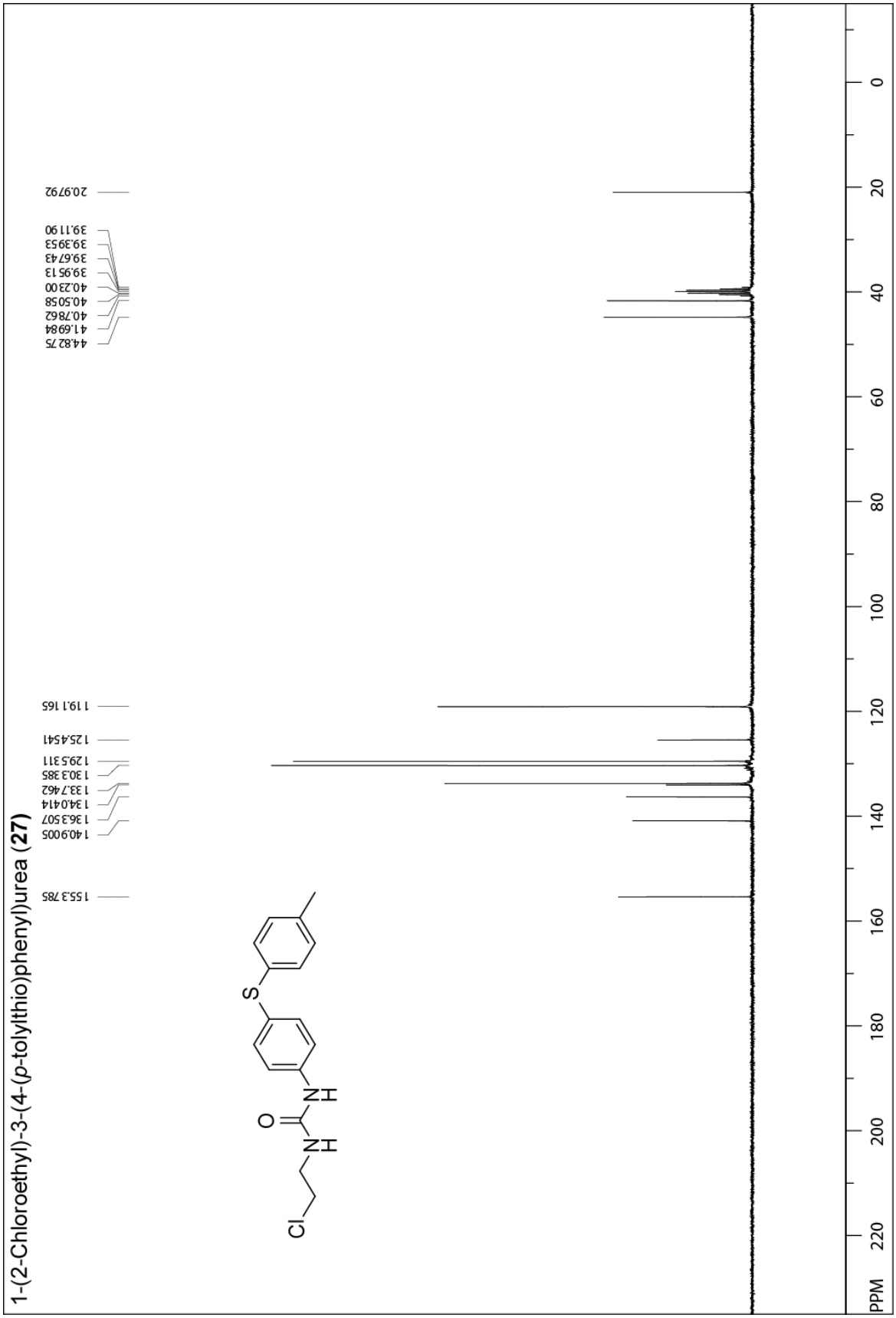
1-(2-Chloroethyl)-3-(4-(p-tolylthio)phenyl)urea (27)
155.3785
140.9005
136.3507
134.0414
133.7462
130.3385
129.5311
125.4541
119.1165
44.8275
41.6984
40.7862
40.5058
40.2300
39.9513
39.6743
39.3953
39.1190
20.9792
PPM
220
200
180
160
140
120
100
80
60
40
20
0

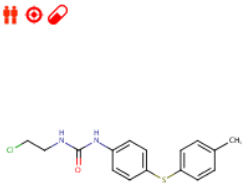

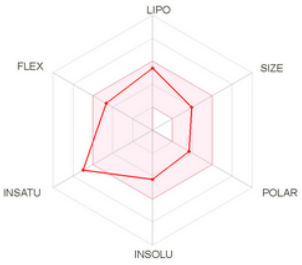

SMILES CICCNC(=O)Nc1ccc(cc1)Sc1ccc(cc1)C

Physicochemical Properties	
Formula	C16H17ClN2OS
Molecular weight	320.84 g/mol
Num. heavy atoms	21
Num. arom. heavy atoms	12
Fraction Csp3	0.19
Num. rotatable bonds	7
Num. H-bond acceptors	1
Num. H-bond donors	2
Molar Refractivity	89.08
TPSA	66.43 Å²

Lipophilicity	
Log $P_{o/w}$ (iLOGP)	2.65
Log $P_{o/w}$ (XLOGP3)	3.95
Log $P_{o/w}$ (WLOGP)	4.32
Log $P_{o/w}$ (MLOGP)	4.22
Log $P_{o/w}$ (SILICOS-IT)	3.78
Consensus Log $P_{o/w}$	3.78

Water Solubility	
Log *S* (ESOL)	-4.28
Solubility	1.69e-02 mg/ml ; 5.27e-05 mol/l
Class	Moderately soluble
Log *S* (Ali)	-5.05
Solubility	2.89e-03 mg/ml ; 9.01e-06 mol/l
Class	Moderately soluble
Log *S* (SILICOS-IT)	-6.87
Solubility	4.35e-05 mg/ml ; 1.36e-07 mol/l
Class	Poorly soluble

Pharmacokinetics	
GI absorption	High
BBB permeant	Yes
P-gp substrate	No
CYP1A2 inhibitor	Yes
CYP2C19 inhibitor	Yes
CYP2C9 inhibitor	Yes
CYP2D6 inhibitor	Yes
CYP3A4 inhibitor	Yes
Log K_p (skin permeation)	-5.45 cm/s

Druglikeness	
Lipinski	Yes; 1 violation: MLOGP>4.15
Ghose	Yes
Veber	Yes
Egan	Yes
Muegge	Yes
Bioavailability Score	0.55

Medicinal Chemistry	
PAINS	0 alert
Brenk	1 alert: alkyl_halide
Leadlikeness	No; 1 violation: XLOGP3>3.5
Synthetic accessibility	2.31

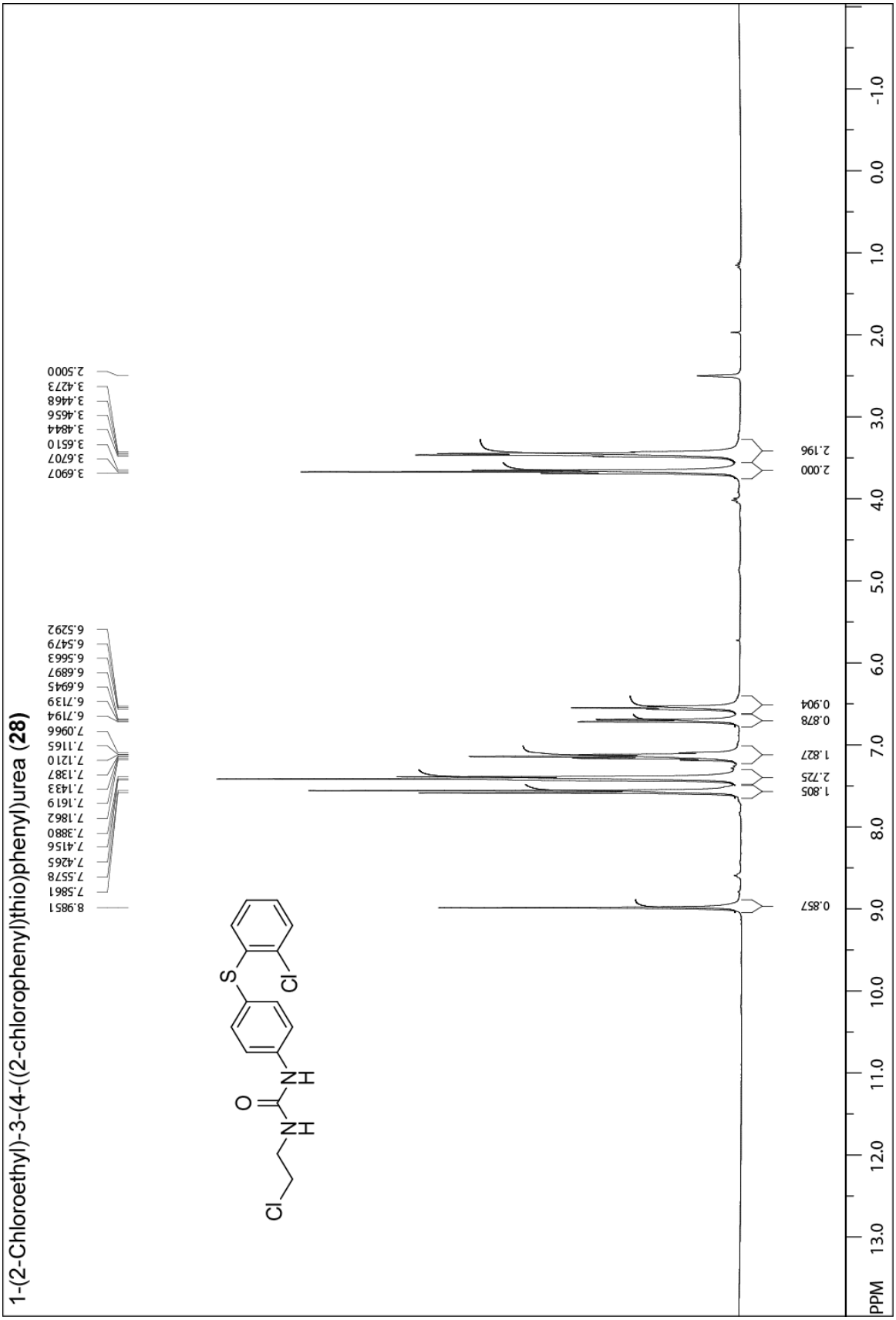
1-(2-Chloroethyl)-3-(4-((2-chlorophenyl)thio)phenyl)urea (28)
8.9851
7.5861
7.5578
7.4265
7.4156
7.3880
7.1862
7.1619
7.1433
7.1387
7.1210
7.1165
7.0966
6.7194
6.7139
6.6945
6.6897
6.5663
6.5479
6.5292
3.6907
3.6707
3.6510
3.4844
3.4656
3.4468
3.4273
2.5000
0.857
1.805
2.725
1.827
0.878
0.904
2.000
2.196
PPM
13.0
12.0
11.0
10.0
9.0
8.0
7.0
6.0
5.0
4.0
3.0
2.0
1.0
0.0
-1.0

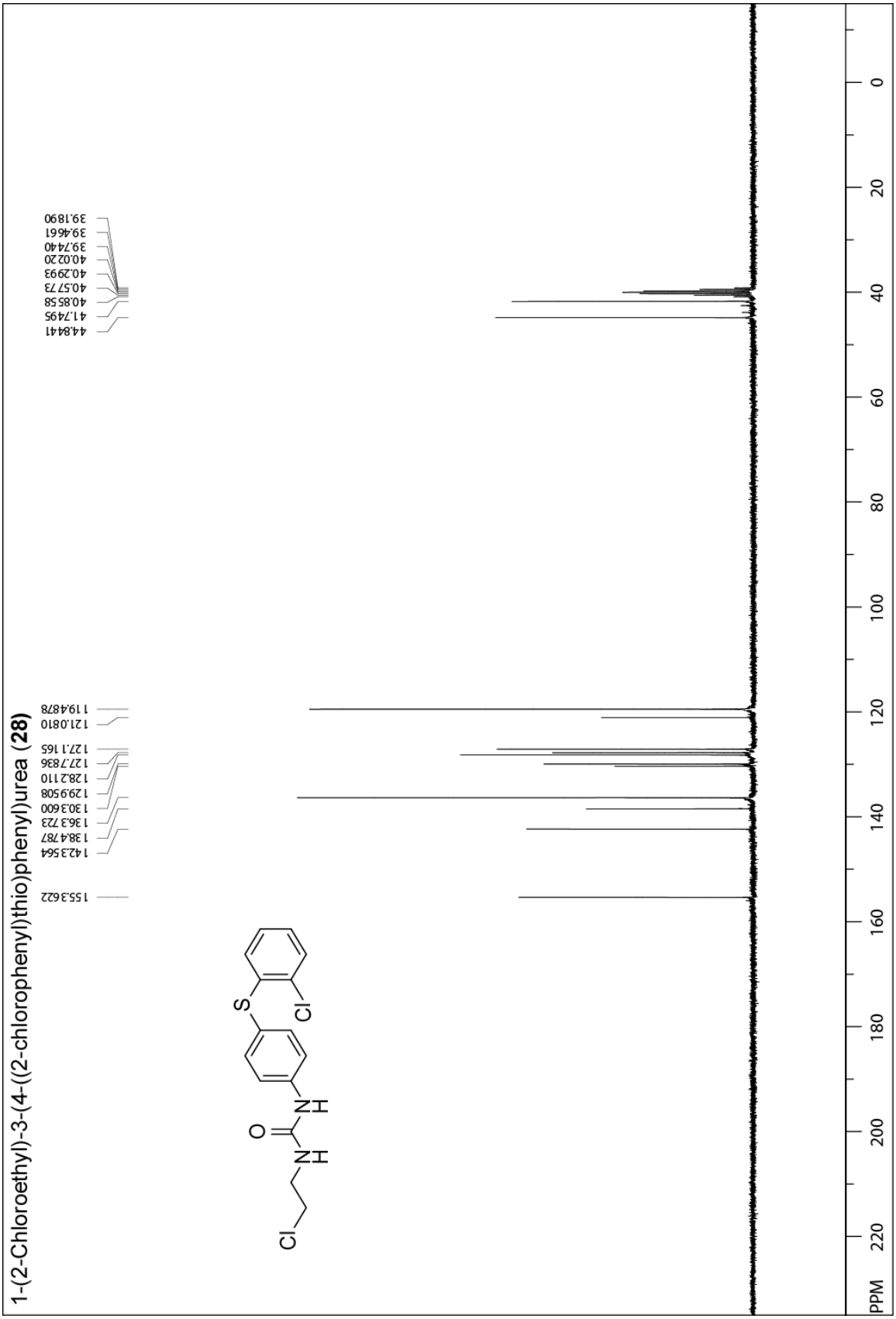
1-(2-Chloroethyl)-3-(4-((2-chlorophenyl)thio)phenyl)urea (28)
155.3622
142.3564
138.4787
136.3723
130.3600
129.9508
128.2110
127.7836
127.1165
121.0810
119.4878
44.8441
41.7495
40.8558
40.5773
40.2993
40.0220
39.7440
39.4661
39.1890
PPM
0
20
40
60
80
100
120
140
160
180
200
220
S
Cl
O
N
H
N
H
Cl

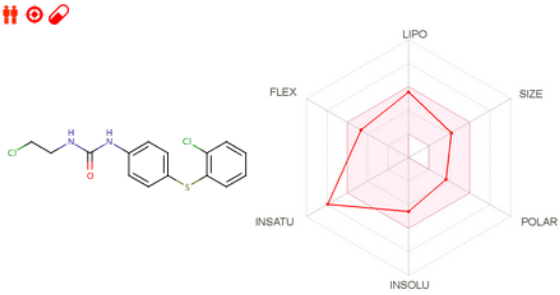

SMILES ClCCNC(=O)Nc1ccc(cc1)Sc1ccccc1Cl

Physicochemical Properties	
Formula	C15H14Cl2N2OS
Molecular weight	341.26 g/mol
Num. heavy atoms	21
Num. arom. heavy atoms	12
Fraction Csp3	0.13
Num. rotatable bonds	7
Num. H-bond acceptors	1
Num. H-bond donors	2
Molar Refractivity	89.12
TPSA	66.43 Å²

Lipophilicity	
Log $P_{o/w}$ (iLOGP)	2.79
Log $P_{o/w}$ (XLOGP3)	4.21
Log $P_{o/w}$ (WLOGP)	4.66
Log $P_{o/w}$ (MLOGP)	4.49
Log $P_{o/w}$ (SILICOS-IT)	3.91
Consensus Log $P_{o/w}$	4.01

Water Solubility	
Log *S* (ESOL)	-4.57
Solubility	9.21e-03 mg/ml ; 2.70e-05 mol/l
Class	Moderately soluble
Log *S* (Ali)	-5.31
Solubility	1.65e-03 mg/ml ; 4.84e-06 mol/l
Class	Moderately soluble
Log *S* (SILICOS-IT)	-7.08
Solubility	2.81e-05 mg/ml ; 8.22e-08 mol/l
Class	Poorly soluble

Pharmacokinetics	
GI absorption	High
BBB permeant	Yes
P-gp substrate	No
CYP1A2 inhibitor	Yes
CYP2C19 inhibitor	Yes
CYP2C9 inhibitor	Yes
CYP2D6 inhibitor	Yes
CYP3A4 inhibitor	Yes
Log K_p (skin permeation)	-5.39 cm/s

Druglikeness	
Lipinski	Yes; 1 violation: MLOGP>4.15
Ghose	Yes
Veber	Yes
Egan	Yes
Muegge	Yes
Bioavailability Score	0.55

Medicinal Chemistry	
PAINS	0 alert
Brenk	1 alert: alkyl_halide
Leadlikeness	No; 1 violation: XLOGP3>3.5
Synthetic accessibility	2.46

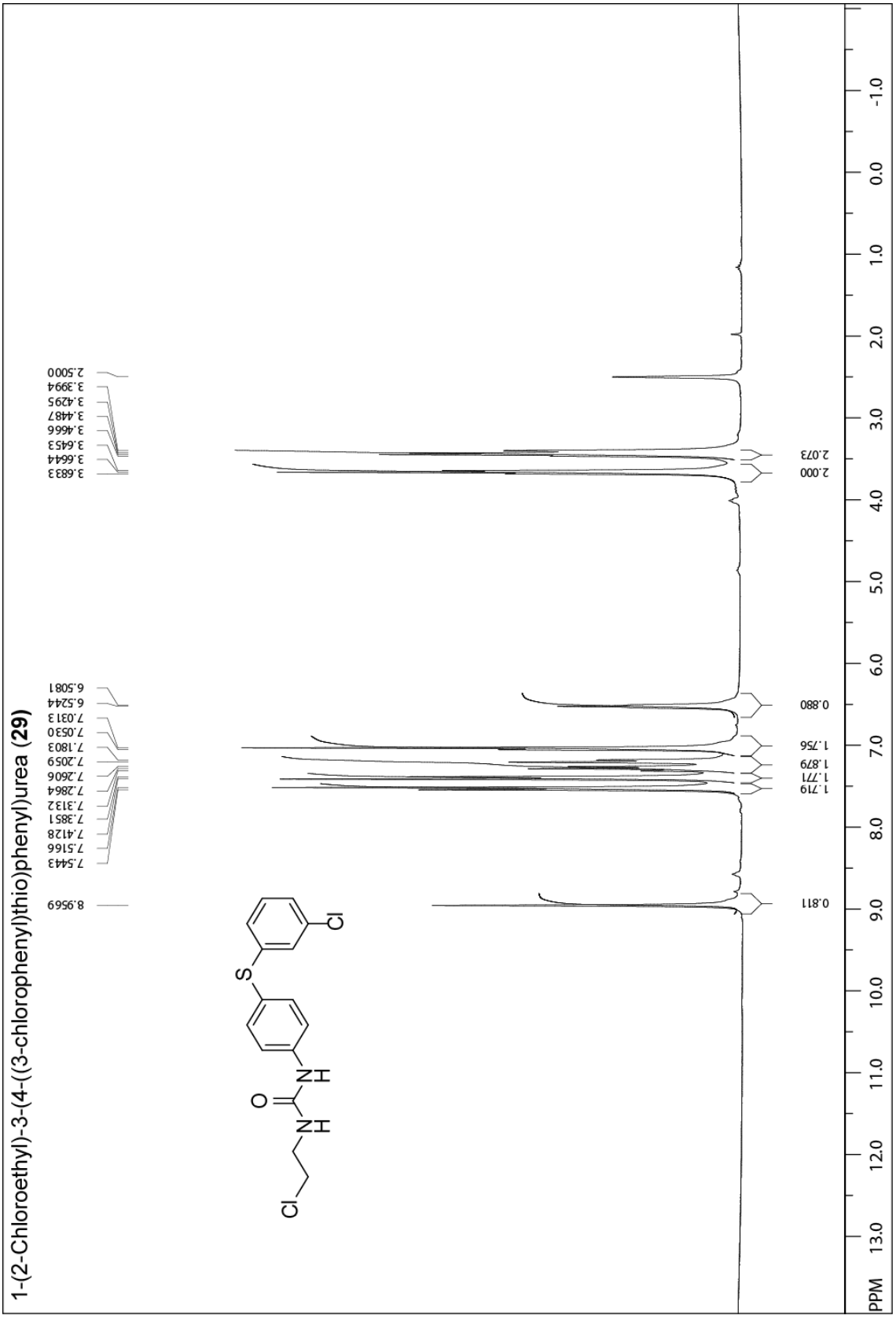
1-(2-Chloroethyl)-3-(4-((3-chlorophenyl)thio)phenyl)urea (29)
8.9569
7.5443
7.5166
7.4128
7.3851
7.3132
7.2864
7.2606
7.2059
7.1803
7.0530
7.0313
6.5244
6.5081
3.6833
3.6644
3.6453
3.4666
3.4487
3.4295
3.3994
2.5000
0.811
0.880
1.756
1.879
1.771
1.719
2.000
2.073
PPM
13.0
12.0
11.0
10.0
9.0
8.0
7.0
6.0
5.0
4.0
3.0
2.0
1.0
0.0
-1.0

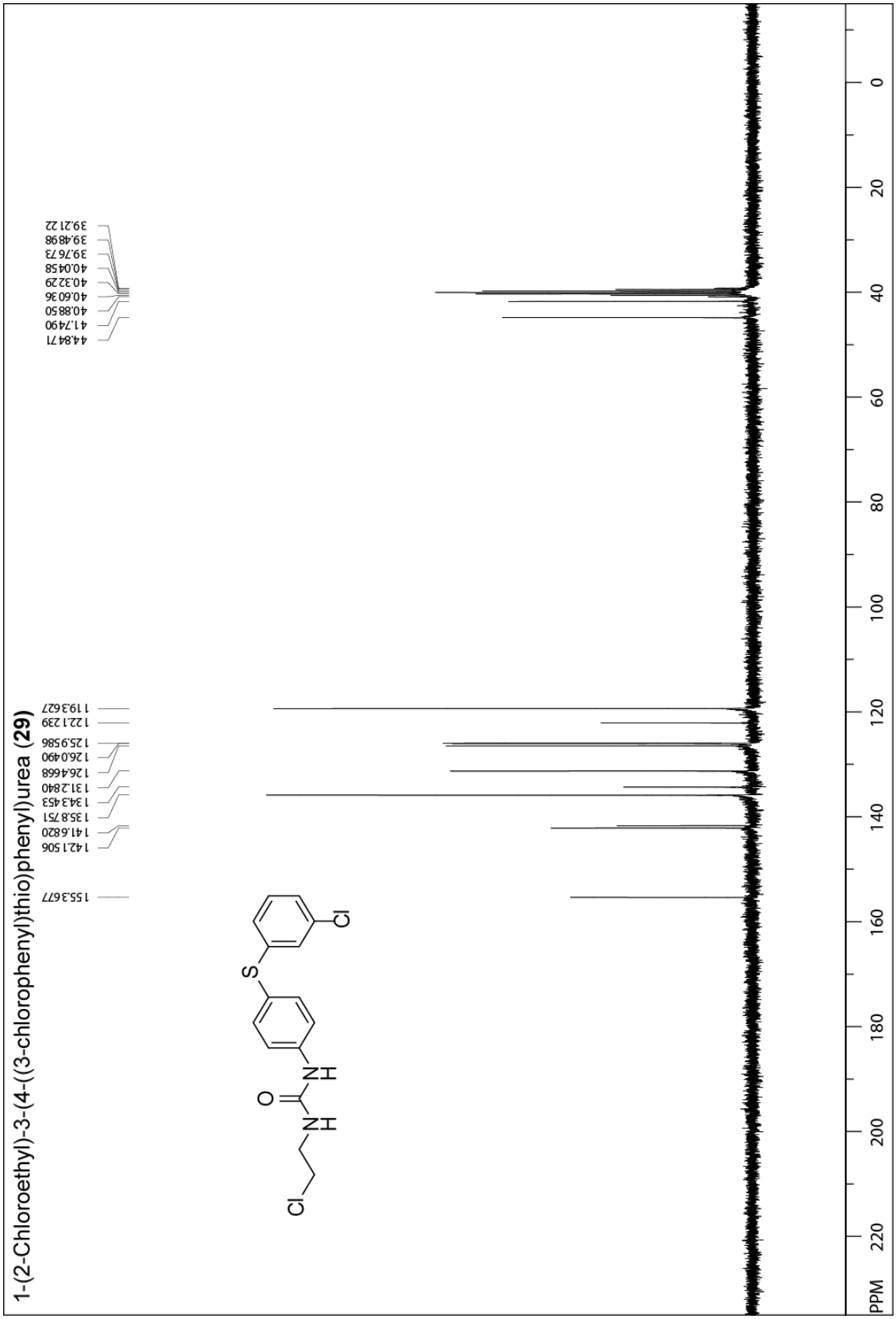
1-(2-Chloroethyl)-3-(4-((3-chlorophenyl)thio)phenyl)urea (29)
155.3677
142.1506
141.6820
135.8751
134.3453
131.2840
126.4668
126.0490
125.9586
122.1239
119.3627
44.8471
41.7490
40.8850
40.6036
40.3229
40.0458
39.7673
39.4898
39.2122
PPM
220
200
180
160
140
120
100
80
60
40
20
0

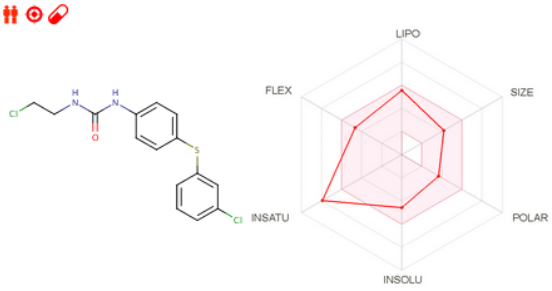

SMILES ClCCNC(=O)Nc1ccc(cc1)Sc1cccc(c1)Cl

Physicochemical Properties	
Formula	C15H14Cl2N2OS
Molecular weight	341.26 g/mol
Num. heavy atoms	21
Num. arom. heavy atoms	12
Fraction Csp3	0.13
Num. rotatable bonds	7
Num. H-bond acceptors	1
Num. H-bond donors	2
Molar Refractivity	89.12
TPSA	66.43 Å²

Lipophilicity	
Log $P_{o/w}$ (iLOGP)	2.86
Log $P_{o/w}$ (XLOGP3)	4.21
Log $P_{o/w}$ (WLOGP)	4.66
Log $P_{o/w}$ (MLOGP)	4.49
Log $P_{o/w}$ (SILICOS-IT)	3.91
Consensus Log $P_{o/w}$	4.03

Water Solubility	
Log *S* (ESOL)	-4.57
Solubility	9.21e-03 mg/ml ; 2.70e-05 mol/l
Class	Moderately soluble
Log *S* (Ali)	-5.31
Solubility	1.65e-03 mg/ml ; 4.84e-06 mol/l
Class	Moderately soluble
Log *S* (SILICOS-IT)	-7.08
Solubility	2.81e-05 mg/ml ; 8.22e-08 mol/l
Class	Poorly soluble

Pharmacokinetics	
GI absorption	High
BBB permeant	Yes
P-gp substrate	No
CYP1A2 inhibitor	Yes
CYP2C19 inhibitor	Yes
CYP2C9 inhibitor	Yes
CYP2D6 inhibitor	Yes
CYP3A4 inhibitor	Yes
Log K_p (skin permeation)	-5.39 cm/s

Druglikeness	
Lipinski	Yes; 1 violation: MLOGP>4.15
Ghose	Yes
Veber	Yes
Egan	Yes
Muegge	Yes
Bioavailability Score	0.55

Medicinal Chemistry	
PAINS	0 alert
Brenk	1 alert: alkyl_halide
Leadlikeness	No; 1 violation: XLOGP3>3.5
Synthetic accessibility	2.45

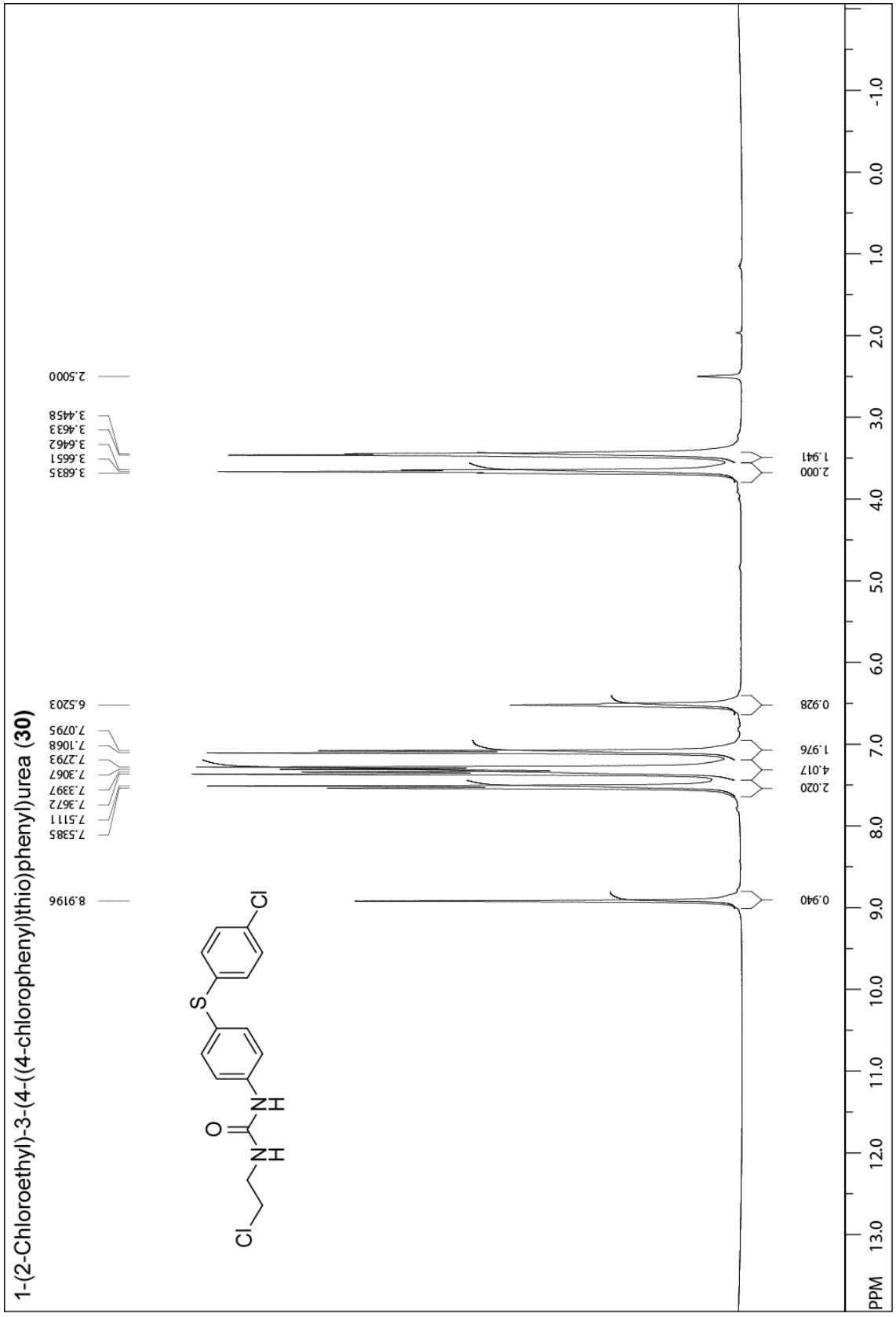
1-(2-Chloroethyl)-3-(4-((4-chlorophenyl)thio)phenyl)urea (30)
8.9196
7.5385
7.5111
7.3672
7.3397
7.3067
7.2793
7.1068
7.0795
6.5203
3.6835
3.6651
3.6462
3.4633
3.4458
2.5000
0.940
2.020
4.017
1.976
0.928
2.000
1.941
PPM
13.0
12.0
11.0
10.0
9.0
8.0
7.0
6.0
5.0
4.0
3.0
2.0
1.0
0.0
-1.0

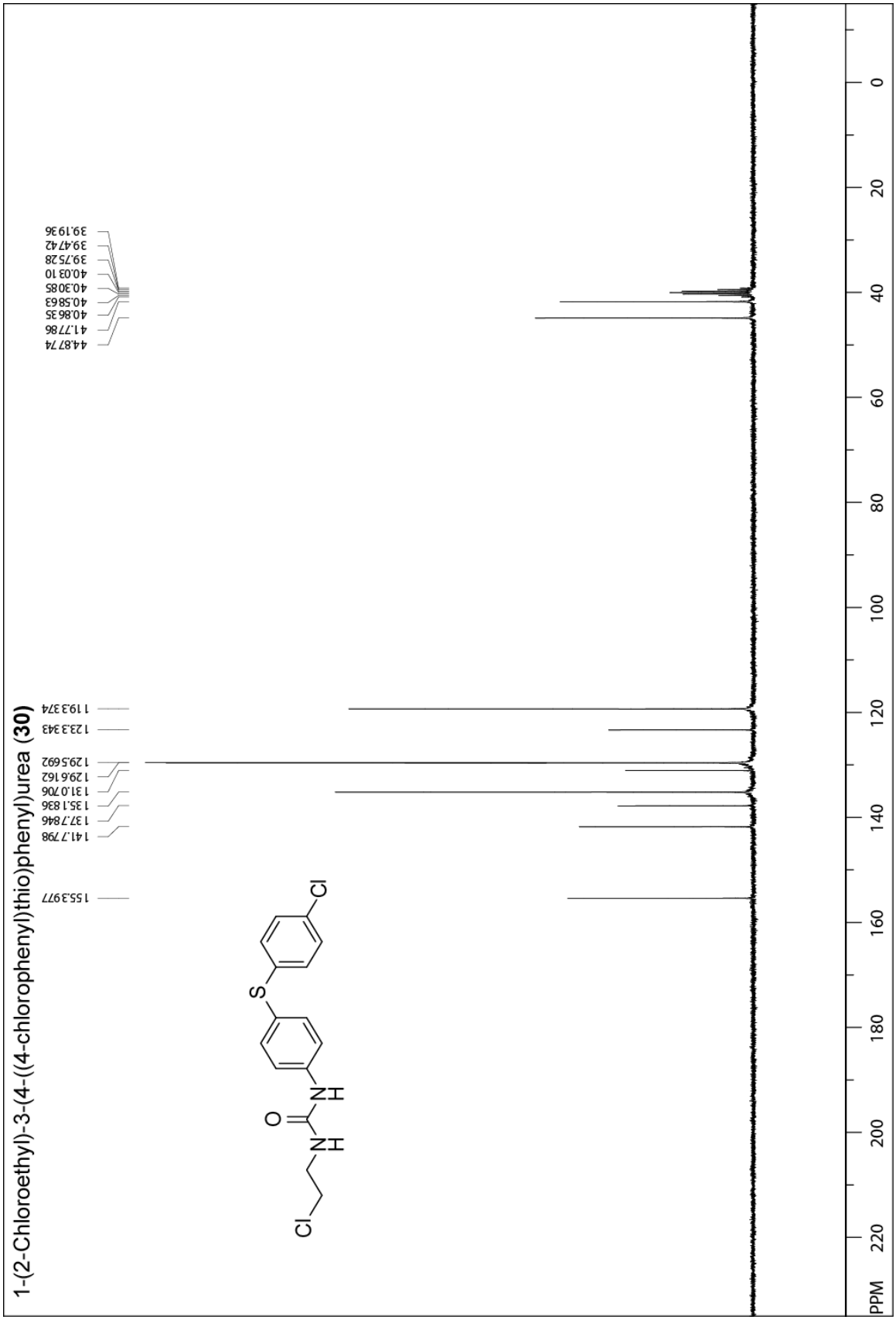
1-(2-Chloroethyl)-3-(4-((4-chlorophenyl)thio)phenyl)urea (30)
155.3977
141.7798
137.7846
135.1836
131.0706
129.6162
129.5692
123.3343
119.3374
44.8774
41.7786
40.8635
40.5863
40.3085
40.0310
39.7528
39.4742
39.1936
PPM
0
20
40
60
80
100
120
140
160
180
200
220

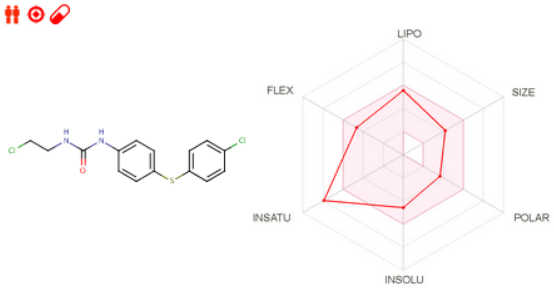

SMILES CICCNC(=O)Nc1ccc(cc1)Sc1ccc(cc1)Cl

Physicochemical Properties	
Formula	C15H14Cl2N2OS
Molecular weight	341.26 g/mol
Num. heavy atoms	21
Num. arom. heavy atoms	12
Fraction Csp3	0.13
Num. rotatable bonds	7
Num. H-bond acceptors	1
Num. H-bond donors	2
Molar Refractivity	89.12
TPSA	66.43 Å²

Lipophilicity	
Log $P_{o/w}$ (iLOGP)	2.88
Log $P_{o/w}$ (XLOGP3)	4.21
Log $P_{o/w}$ (WLOGP)	4.66
Log $P_{o/w}$ (MLOGP)	4.49
Log $P_{o/w}$ (SILICOS-IT)	3.91
Consensus Log $P_{o/w}$	4.03

Water Solubility	
Log *S* (ESOL)	-4.57
Solubility	9.21e-03 mg/ml ; 2.70e-05 mol/l
Class	Moderately soluble
Log *S* (Ali)	-5.31
Solubility	1.65e-03 mg/ml ; 4.84e-06 mol/l
Class	Moderately soluble
Log *S* (SILICOS-IT)	-7.08
Solubility	2.81e-05 mg/ml ; 8.22e-08 mol/l
Class	Poorly soluble

Pharmacokinetics	
GI absorption	High
BBB permeant	Yes
P-gp substrate	No
CYP1A2 inhibitor	Yes
CYP2C19 inhibitor	Yes
CYP2C9 inhibitor	Yes
CYP2D6 inhibitor	Yes
CYP3A4 inhibitor	Yes
Log K_p (skin permeation)	-5.39 cm/s

Druglikeness	
Lipinski	Yes; 1 violation: MLOGP>4.15
Ghose	Yes
Veber	Yes
Egan	Yes
Muegge	Yes
Bioavailability Score	0.55

Medicinal Chemistry	
PAINS	0 alert
Brenk	1 alert: alkyl_halide
Leadlikeness	No; 1 violation: XLOGP3>3.5
Synthetic accessibility	2.38

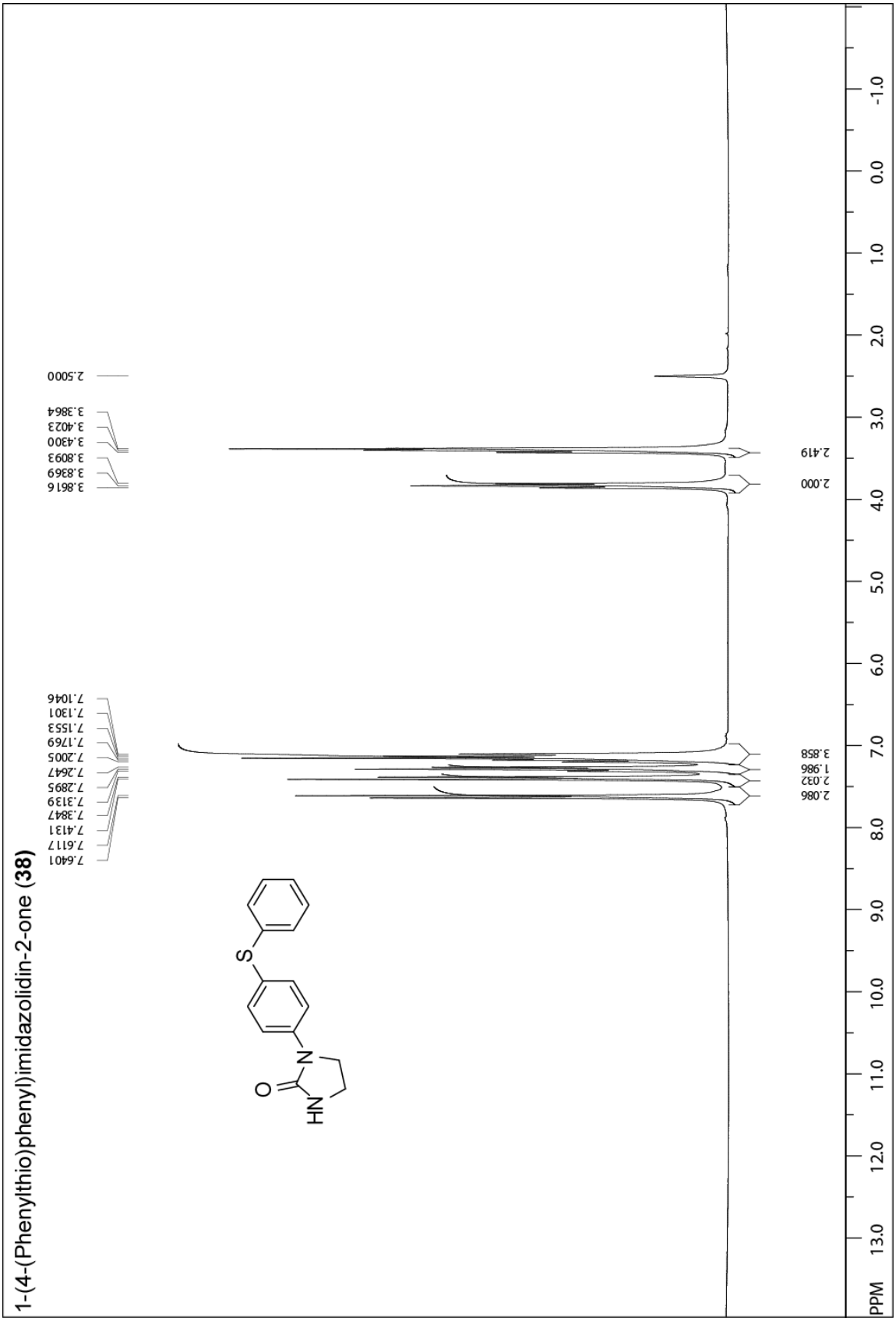
1-(4-(Phenylthio)phenyl)imidazolidin-2-one (38)
7.6401
7.6117
7.4131
7.3847
7.3139
7.2895
7.2647
7.2005
7.1769
7.1553
7.1301
7.1046
3.8616
3.8369
3.8093
3.4300
3.4023
3.3864
2.5000
3.858
2.086
2.032
1.986
2.000
2.419
PPM
13.0
12.0
11.0
10.0
9.0
8.0
7.0
6.0
5.0
4.0
3.0
2.0
1.0
0.0
-1.0
S
N
O
HN

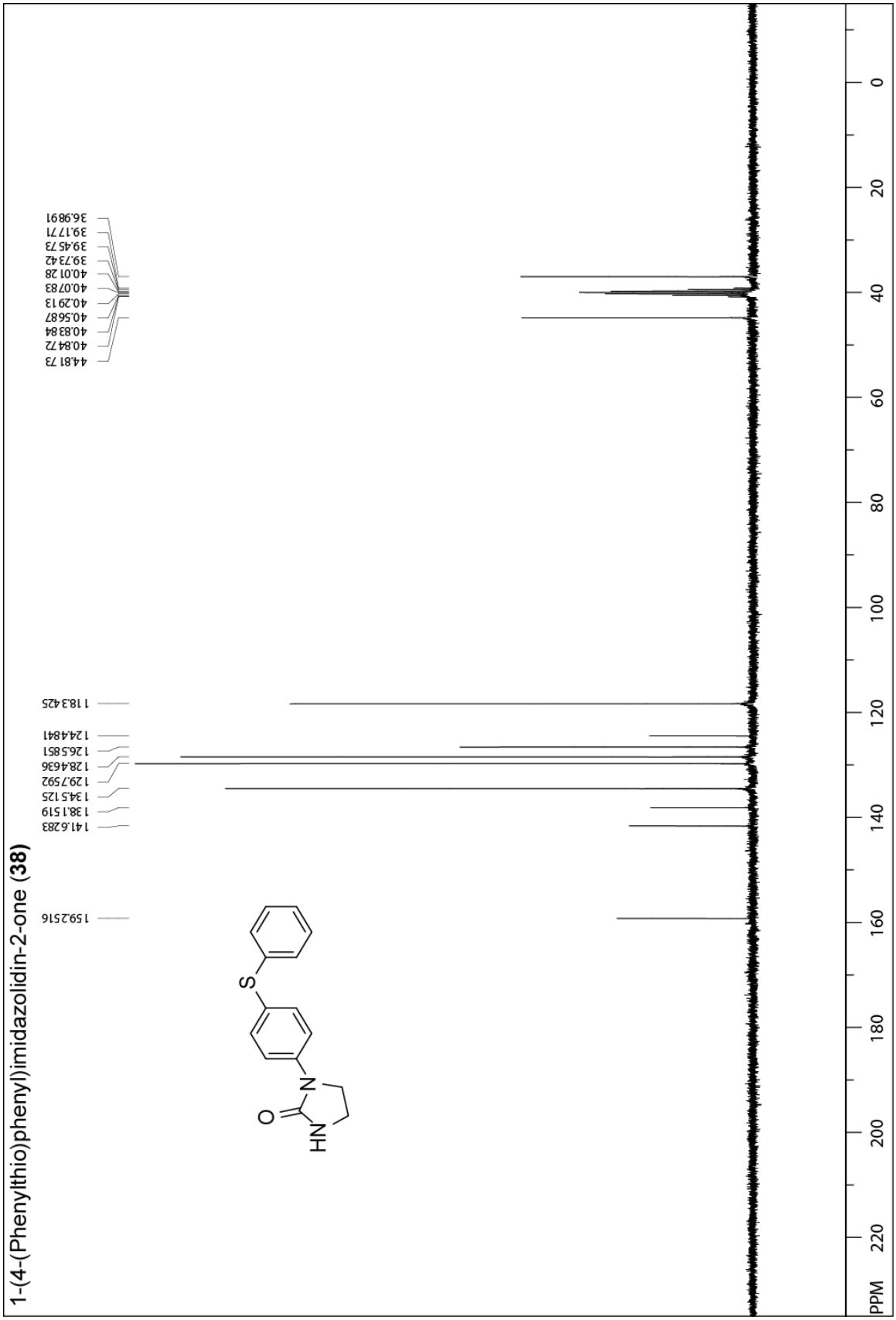
1-(4-(Phenylthio)phenyl)imidazolidin-2-one (38)
159.2516
141.6283
138.1519
134.5125
129.7592
128.4636
126.5851
124.4841
118.3425
44.8173
40.8472
40.8384
40.5687
40.2913
40.0783
40.0128
39.7342
39.4573
39.1771
36.9891
S
N
O
HN
PPM
0
20
40
60
80
100
120
140
160
180
200
220

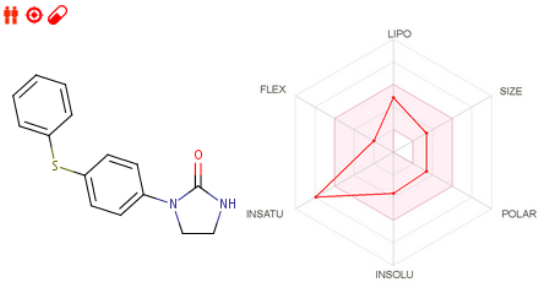

SMILES O=C1NCCN1c1ccc(cc1)Sc1ccccc1

Physicochemical Properties	
Formula	C15H14N2OS
Molecular weight	270.35 g/mol
Num. heavy atoms	19
Num. arom. heavy atoms	12
Fraction Csp3	0.13
Num. rotatable bonds	3
Num. H-bond acceptors	1
Num. H-bond donors	1
Molar Refractivity	84.15
TPSA	57.64 Å²

Lipophilicity	
Log $P_{o/w}$ (iLOGP)	2.61
Log $P_{o/w}$ (XLOGP3)	2.95
Log $P_{o/w}$ (WLOGP)	2.61
Log $P_{o/w}$ (MLOGP)	3.34
Log $P_{o/w}$ (SILICOS-IT)	2.68
Consensus Log $P_{o/w}$	2.84

Water Solubility	
Log *S* (ESOL)	-3.64
Solubility	6.14e-02 mg/ml ; 2.27e-04 mol/l
Class	Soluble
Log *S* (Ali)	-3.82
Solubility	4.07e-02 mg/ml ; 1.50e-04 mol/l
Class	Soluble
Log *S* (SILICOS-IT)	-5.13
Solubility	1.99e-03 mg/ml ; 7.38e-06 mol/l
Class	Moderately soluble

Pharmacokinetics	
GI absorption	High
BBB permeant	Yes
P-gp substrate	Yes
CYP1A2 inhibitor	Yes
CYP2C19 inhibitor	Yes
CYP2C9 inhibitor	Yes
CYP2D6 inhibitor	No
CYP3A4 inhibitor	No
Log K_p (skin permeation)	-5.85 cm/s

Druglikeness	
Lipinski	Yes; 0 violation
Ghose	Yes
Veber	Yes
Egan	Yes
Muegge	Yes
Bioavailability Score	0.55

Medicinal Chemistry	
PAINS	0 alert
Brenk	0 alert
Leadlikeness	Yes
Synthetic accessibility	2.12

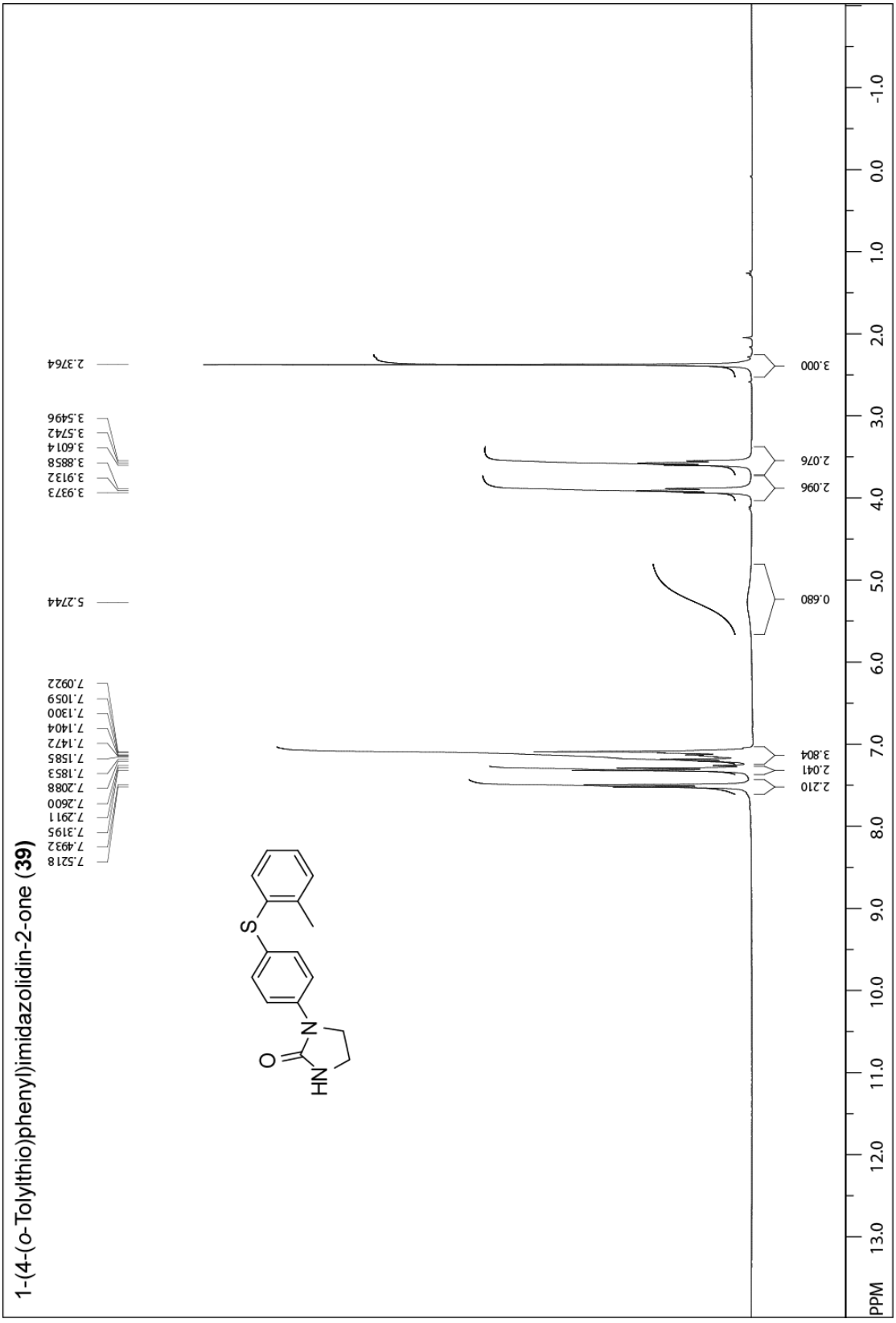
1-(4-(o-Tolylthio)phenyl)imidazolidin-2-one (39)
7.5218
7.4932
7.3195
7.2911
7.2600
7.2088
7.1853
7.1585
7.1472
7.1404
7.1300
7.1059
7.0922
5.2744
3.9373
3.9132
3.8858
3.6014
3.5742
3.5496
2.3764
3.804
2.041
2.210
0.680
2.096
2.076
3.000
PPM
13.0
12.0
11.0
10.0
9.0
8.0
7.0
6.0
5.0
4.0
3.0
2.0
1.0
0.0
-1.0
S
N
O
HN

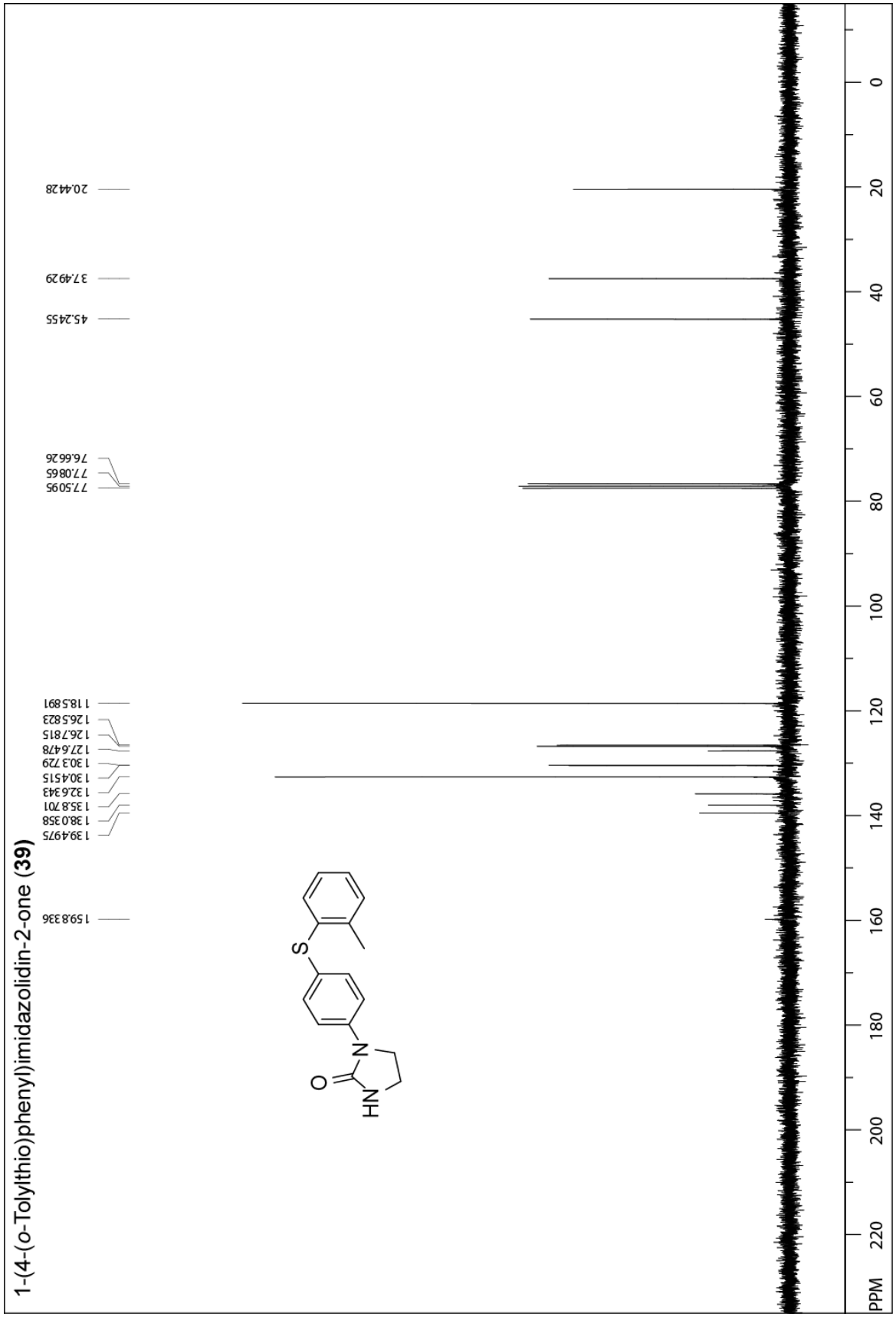
1-(4-(o-Tolylthio)phenyl)imidazolidin-2-one (39)
159.8336
139.4975
138.0358
135.8701
132.6343
130.4515
130.3729
127.6478
126.7815
126.5823
118.5891
77.5095
77.0865
76.6626
45.2455
37.4929
20.4428
PPM
220
200
180
160
140
120
100
80
60
40
20
0
S
N
O
HN

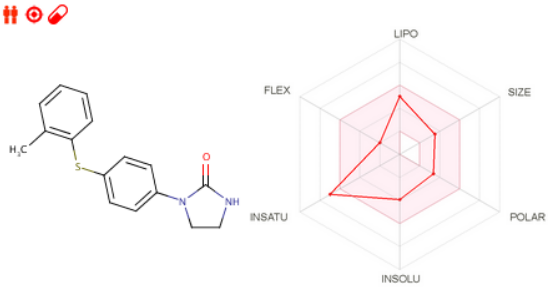

SMILES O=C1NCCN1c1ccc(cc1)Sc1ccccc1C

Physicochemical Properties	
Formula	C16H16N2OS
Molecular weight	284.38 g/mol
Num. heavy atoms	20
Num. arom. heavy atoms	12
Fraction Csp3	0.19
Num. rotatable bonds	3
Num. H-bond acceptors	1
Num. H-bond donors	1
Molar Refractivity	89.11
TPSA	57.64 Å²

Lipophilicity	
Log $P_{o/w}$ (iLOGP)	2.76
Log $P_{o/w}$ (XLOGP3)	3.32
Log $P_{o/w}$ (WLOGP)	2.91
Log $P_{o/w}$ (MLOGP)	3.59
Log $P_{o/w}$ (SILICOS-IT)	3.17
Consensus Log $P_{o/w}$	3.15

Water Solubility	
Log *S* (ESOL)	-3.94
Solubility	3.26e-02 mg/ml ; 1.15e-04 mol/l
Class	Soluble
Log *S* (Ali)	-4.21
Solubility	1.77e-02 mg/ml ; 6.21e-05 mol/l
Class	Moderately soluble
Log *S* (SILICOS-IT)	-5.51
Solubility	8.69e-04 mg/ml ; 3.05e-06 mol/l
Class	Moderately soluble

Pharmacokinetics	
GI absorption	High
BBB permeant	Yes
P-gp substrate	Yes
CYP1A2 inhibitor	Yes
CYP2C19 inhibitor	Yes
CYP2C9 inhibitor	Yes
CYP2D6 inhibitor	Yes
CYP3A4 inhibitor	Yes
Log K_p (skin permeation)	-5.68 cm/s

Druglikeness	
Lipinski	Yes; 0 violation
Ghose	Yes
Veber	Yes
Egan	Yes
Muegge	Yes
Bioavailability Score	0.55

Medicinal Chemistry	
PAINS	0 alert
Brenk	0 alert
Leadlikeness	Yes
Synthetic accessibility	2.19

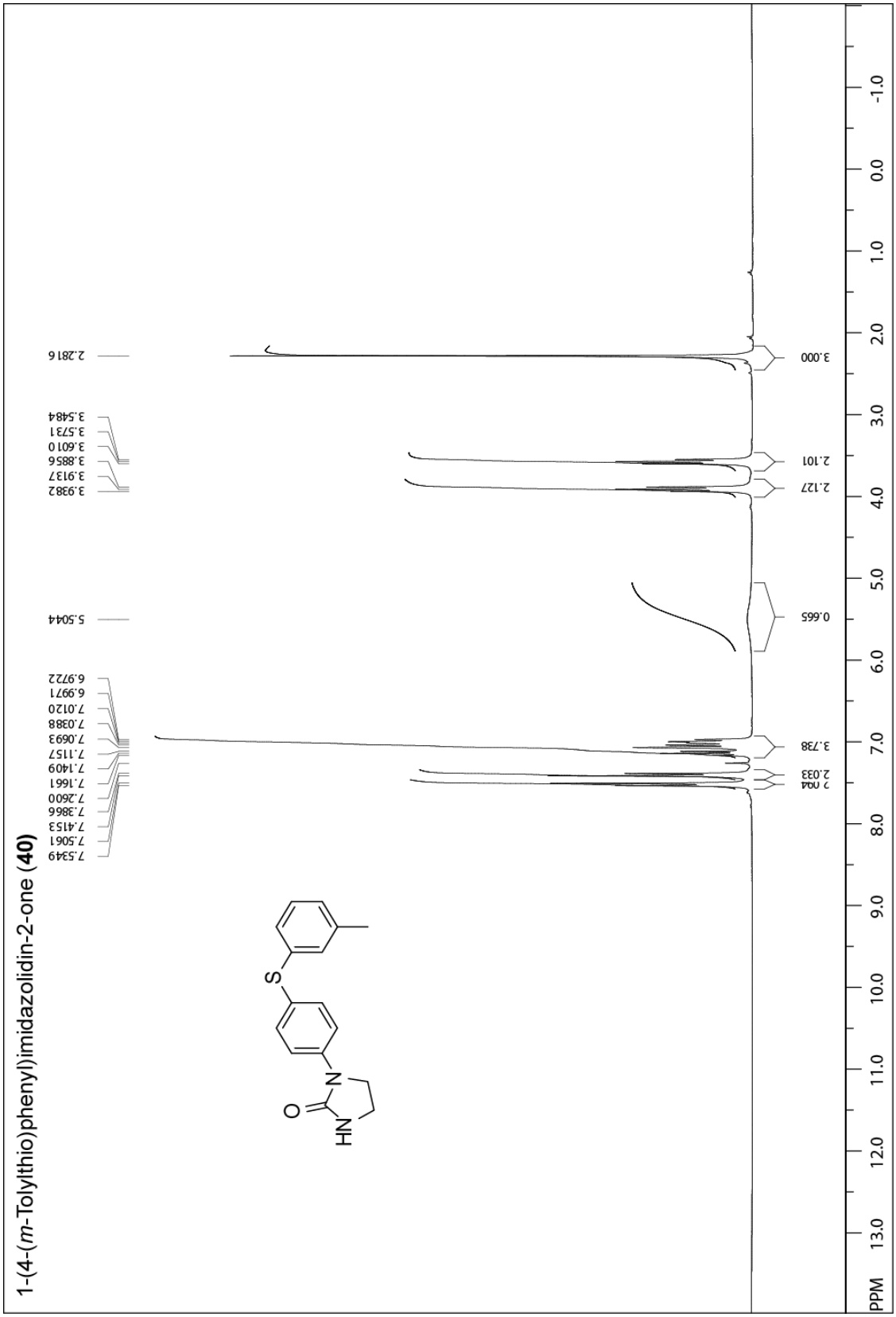
1-(4-(*m*-Tolylthio)phenyl)imidazolidin-2-one (**40**)
7.5349
7.5061
7.4153
7.3866
7.2600
7.1661
7.1409
7.1157
7.0693
7.0388
7.0120
6.9971
6.9722
5.5044
3.9382
3.9137
3.8856
3.6010
3.5731
3.5484
2.2816
3.738
2.033
2.101
2.127
0.665
3.000
PPM
13.0
12.0
11.0
10.0
9.0
8.0
7.0
6.0
5.0
4.0
3.0
2.0
1.0
0.0
-1.0

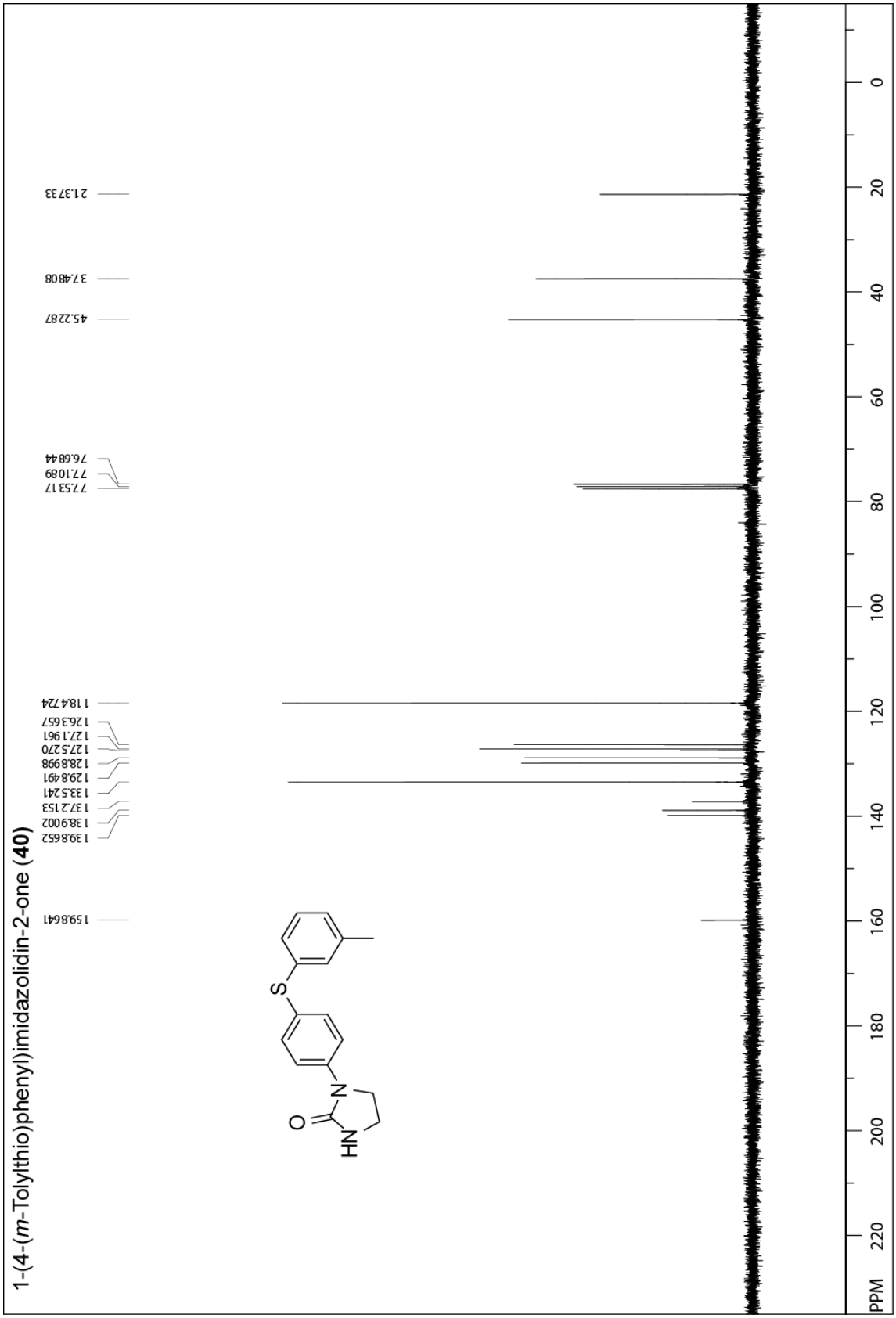
1-(4-(*m*-Tolylthio)phenyl)imidazolidin-2-one (**40**)
159.8641
139.8652
138.9002
137.2153
133.5241
129.8491
128.8998
127.5270
127.1961
126.3657
118.4724
77.5317
77.1089
76.6844
45.2287
37.4808
21.3733
S
N
O
HN
PPM
0
20
40
60
80
100
120
140
160
180
200
220

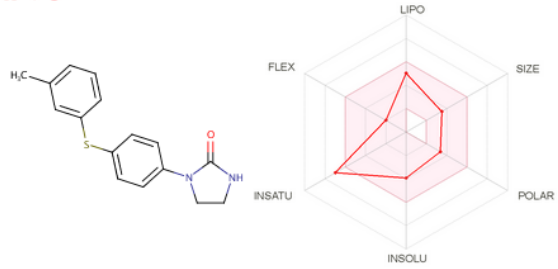

SMILES Cc1cccc(c1)Sc1ccc(cc1)N1CCNC1=O

Physicochemical Properties	
Formula	C16H16N2OS
Molecular weight	284.38 g/mol
Num. heavy atoms	20
Num. arom. heavy atoms	12
Fraction Csp3	0.19
Num. rotatable bonds	3
Num. H-bond acceptors	1
Num. H-bond donors	1
Molar Refractivity	89.11
TPSA	57.64 Å²

Lipophilicity	
Log $P_{o/w}$ (iLOGP)	2.80
Log $P_{o/w}$ (XLOGP3)	3.32
Log $P_{o/w}$ (WLOGP)	2.91
Log $P_{o/w}$ (MLOGP)	3.59
Log $P_{o/w}$ (SILICOS-IT)	3.17
Consensus Log $P_{o/w}$	3.16

Water Solubility	
Log *S* (ESOL)	-3.94
Solubility	3.26e-02 mg/ml ; 1.15e-04 mol/l
Class	Soluble
Log *S* (Ali)	-4.21
Solubility	1.77e-02 mg/ml ; 6.21e-05 mol/l
Class	Moderately soluble
Log *S* (SILICOS-IT)	-5.51
Solubility	8.69e-04 mg/ml ; 3.05e-06 mol/l
Class	Moderately soluble

Pharmacokinetics	
GI absorption	High
BBB permeant	Yes
P-gp substrate	Yes
CYP1A2 inhibitor	Yes
CYP2C19 inhibitor	Yes
CYP2C9 inhibitor	Yes
CYP2D6 inhibitor	Yes
CYP3A4 inhibitor	Yes
Log K_p (skin permeation)	-5.68 cm/s

Druglikeness	
Lipinski	Yes; 0 violation
Ghose	Yes
Veber	Yes
Egan	Yes
Muegge	Yes
Bioavailability Score	0.55

Medicinal Chemistry	
PAINS	0 alert
Brenk	0 alert
Leadlikeness	Yes
Synthetic accessibility	2.22

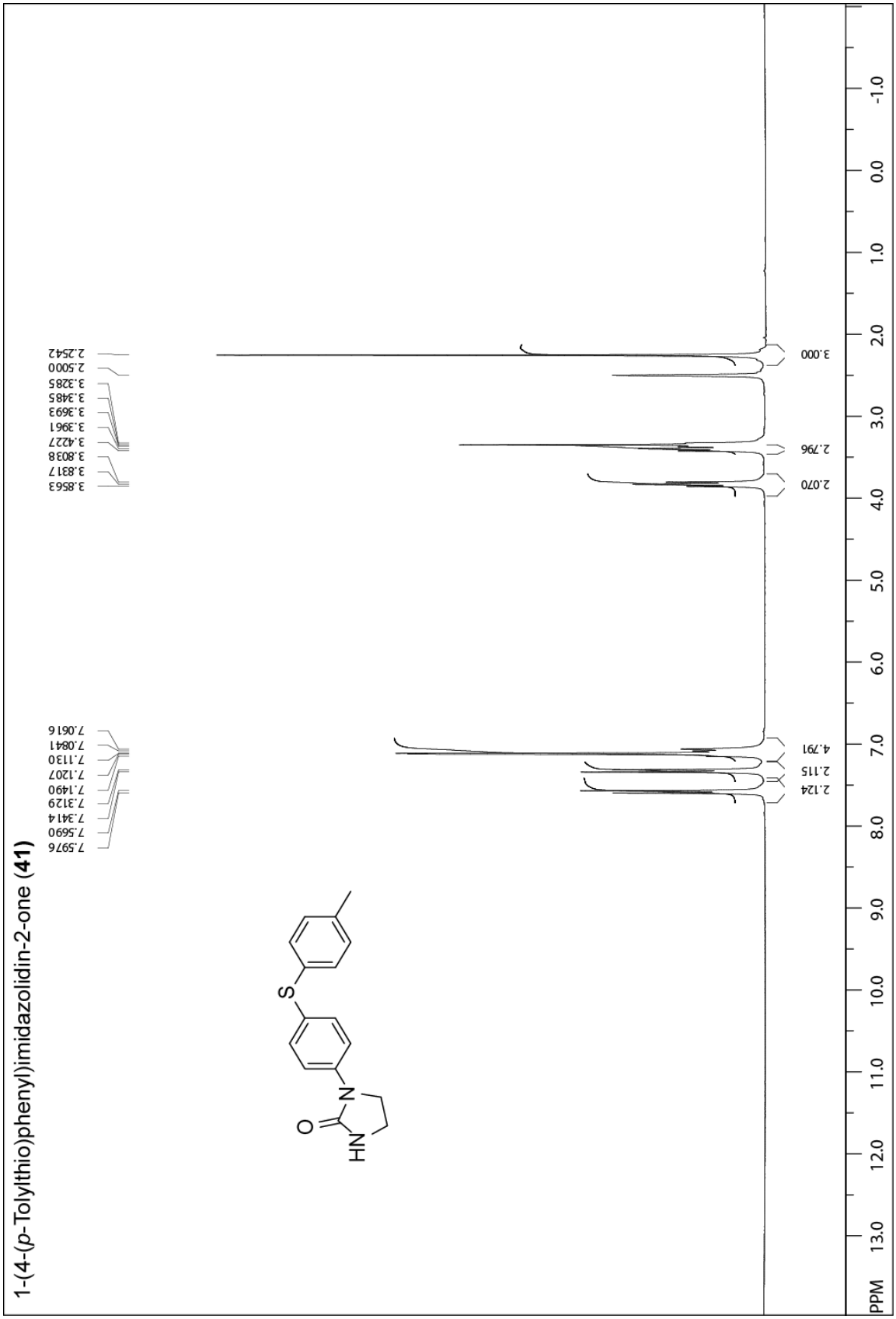
1-(4-(p-Tolylthio)phenyl)imidazolidin-2-one (41)
7.5976
7.5690
7.3414
7.3129
7.1490
7.1207
7.1130
7.0841
7.0616
3.8563
3.8317
3.8038
3.4227
3.3961
3.3693
3.3485
3.3285
2.5000
2.2542
4.791
2.115
2.124
3.000
2.796
2.070
PPM
13.0
12.0
11.0
10.0
9.0
8.0
7.0
6.0
5.0
4.0
3.0
2.0
1.0
0.0
-1.0
S
N
O
HN

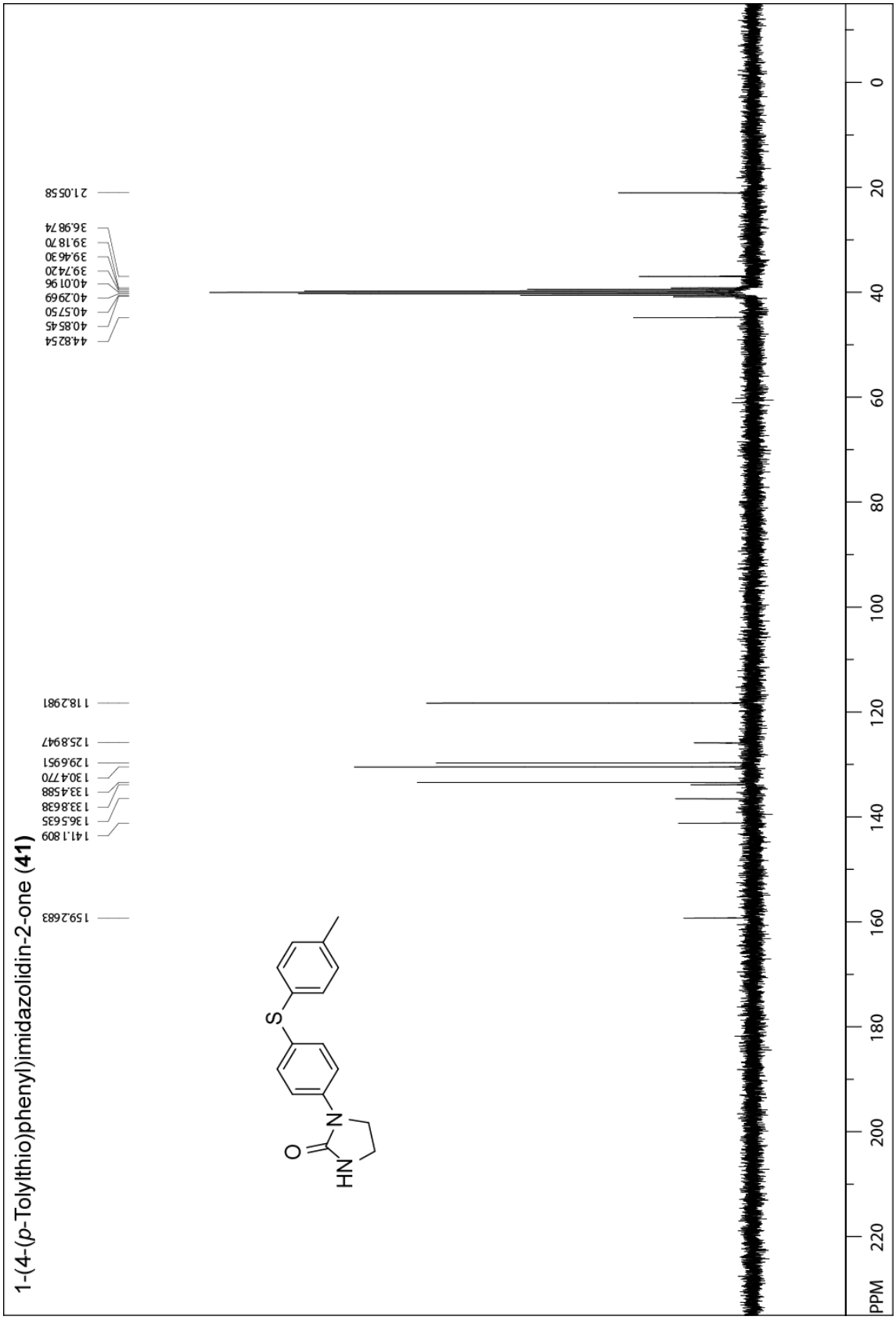
1-(4-(p-Tolylthio)phenyl)imidazolidin-2-one (41)
159.2683
141.1809
136.5635
133.8638
133.4588
130.4770
129.6951
125.8947
118.2981
44.8254
40.8545
40.5750
40.2969
40.0196
39.7420
39.4630
39.1870
36.9874
21.0558
S
N
O
HN
PPM
220
200
180
160
140
120
100
80
60
40
20
0

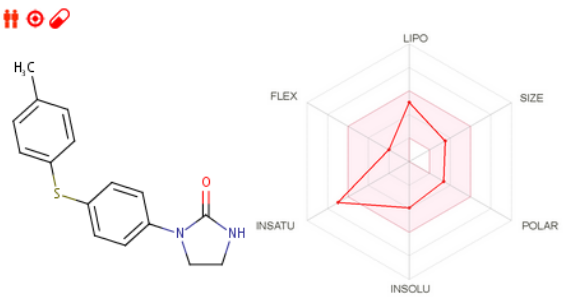

SMILES O=C1NCCN1c1ccc(cc1)Sc1ccc(cc1)C

Physicochemical Properties	
Formula	C16H16N2OS
Molecular weight	284.38 g/mol
Num. heavy atoms	20
Num. arom. heavy atoms	12
Fraction Csp3	0.19
Num. rotatable bonds	3
Num. H-bond acceptors	1
Num. H-bond donors	1
Molar Refractivity	89.11
TPSA	57.64 Å²

Lipophilicity	
Log $P_{o/w}$ (iLOGP)	2.79
Log $P_{o/w}$ (XLOGP3)	3.32
Log $P_{o/w}$ (WLOGP)	2.91
Log $P_{o/w}$ (MLOGP)	3.59
Log $P_{o/w}$ (SILICOS-IT)	3.17
Consensus Log $P_{o/w}$	3.16

Water Solubility	
Log *S* (ESOL)	-3.94
Solubility	3.26e-02 mg/ml ; 1.15e-04 mol/l
Class	Soluble
Log *S* (Ali)	-4.21
Solubility	1.77e-02 mg/ml ; 6.21e-05 mol/l
Class	Moderately soluble
Log *S* (SILICOS-IT)	-5.51
Solubility	8.69e-04 mg/ml ; 3.05e-06 mol/l
Class	Moderately soluble

Pharmacokinetics	
GI absorption	High
BBB permeant	Yes
P-gp substrate	Yes
CYP1A2 inhibitor	Yes
CYP2C19 inhibitor	Yes
CYP2C9 inhibitor	Yes
CYP2D6 inhibitor	Yes
CYP3A4 inhibitor	Yes
Log K_p (skin permeation)	-5.68 cm/s

Druglikeness	
Lipinski	Yes; 0 violation
Ghose	Yes
Veber	Yes
Egan	Yes
Muegge	Yes
Bioavailability Score	0.55

Medicinal Chemistry	
PAINS	0 alert
Brenk	0 alert
Leadlikeness	Yes
Synthetic accessibility	2.13

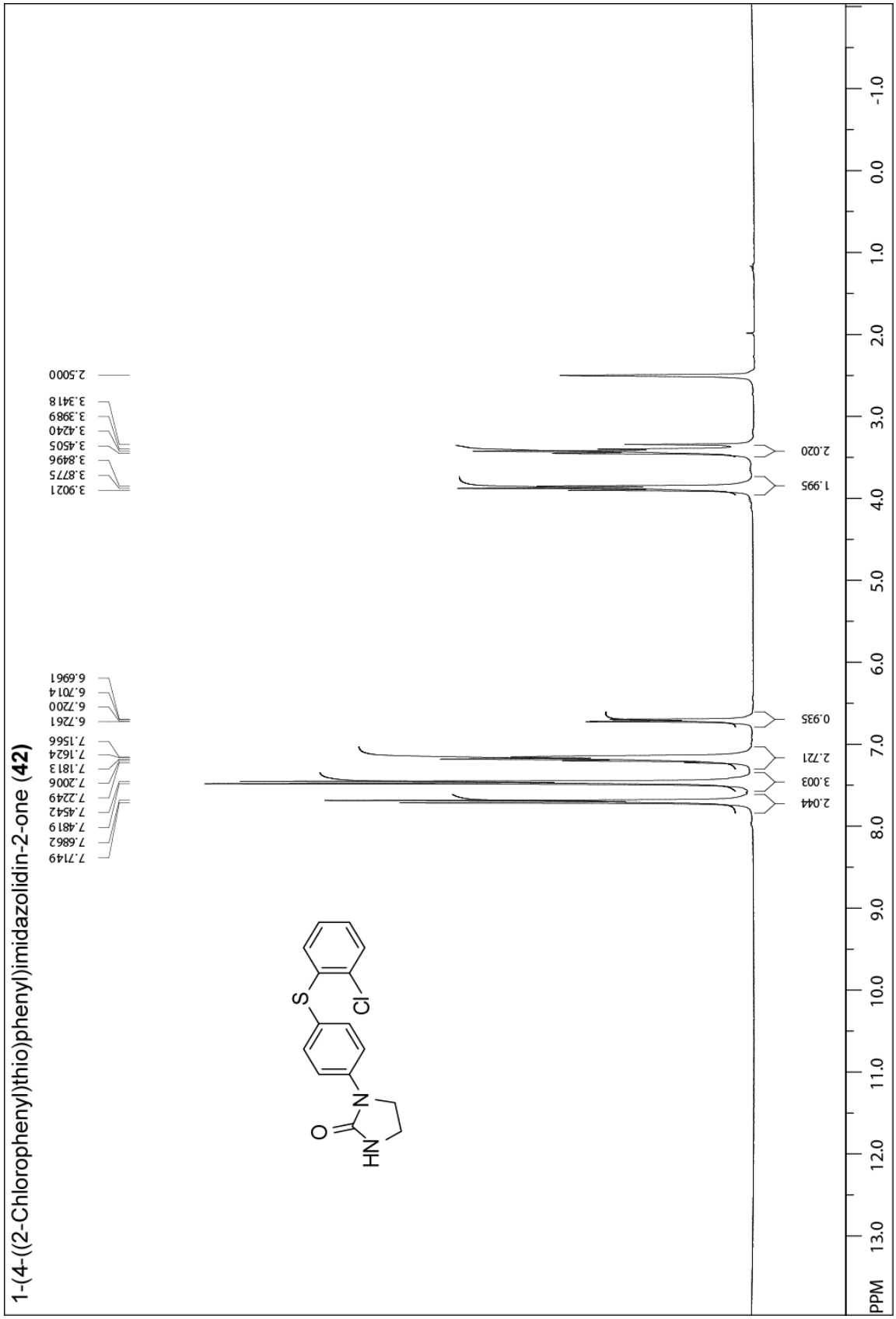
1-(4-((2-Chlorophenyl)thio)phenyl)imidazolidin-2-one (42)
7.7149
7.6862
7.4819
7.4542
7.2249
7.2006
7.1813
7.1624
7.1566
6.7261
6.7200
6.7014
6.6961
3.9021
3.8775
3.8496
3.4505
3.4240
3.3989
3.3418
2.5000
2.044
3.003
2.721
0.935
2.020
1.995
PPM
13.0
12.0
11.0
10.0
9.0
8.0
7.0
6.0
5.0
4.0
3.0
2.0
1.0
0.0
-1.0
S
Cl
N
O
HN

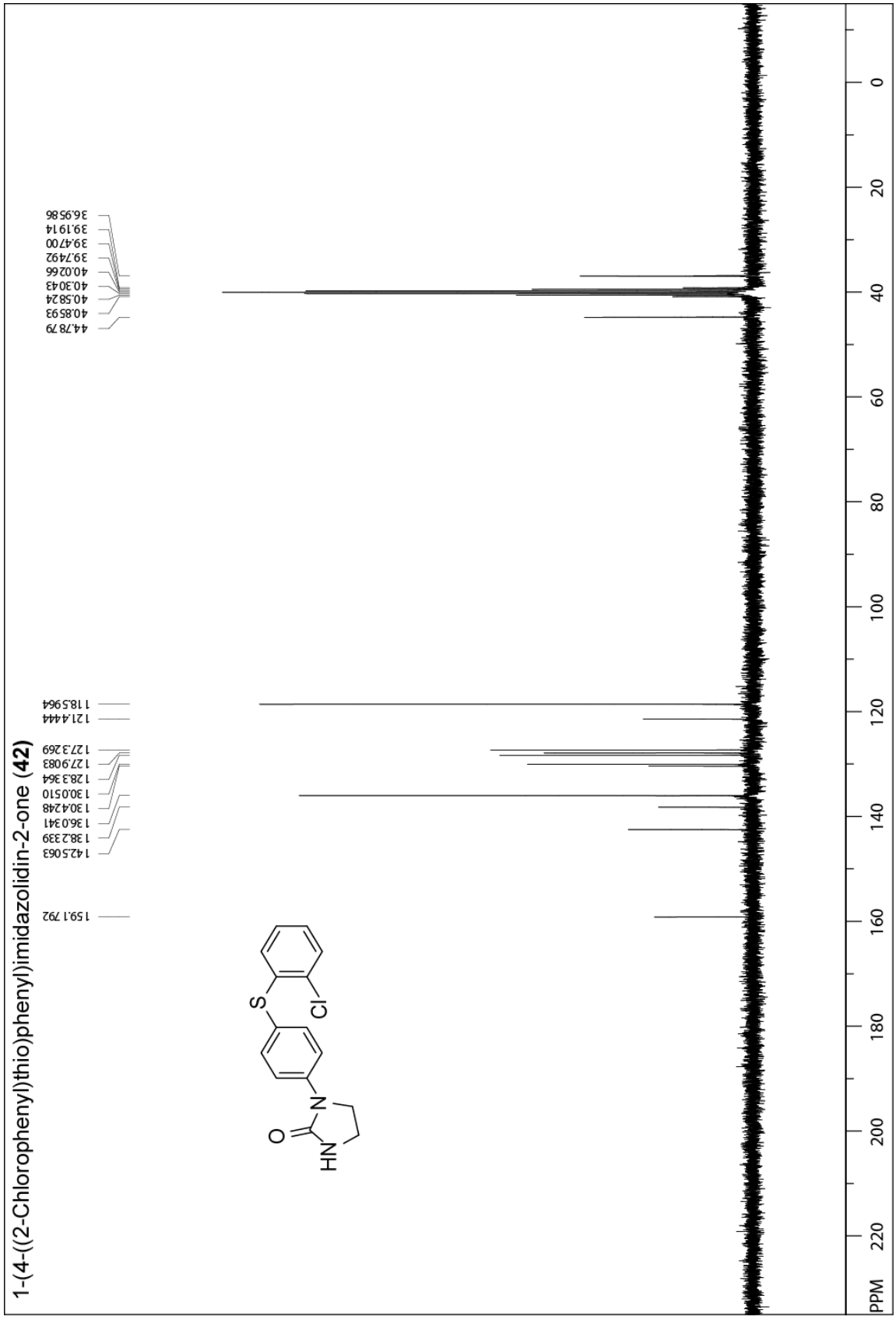
1-(4-((2-Chlorophenyl)thio)phenyl)imidazolidin-2-one (42)
159.1792
142.5063
138.2339
136.0341
130.4248
130.0510
128.3364
127.9083
127.3269
121.4444
118.5964
44.7879
40.8593
40.5824
40.3043
40.0266
39.7492
39.4700
39.1914
36.9586
S
Cl
N
O
HN
PPM
0
20
40
60
80
100
120
140
160
180
200
220

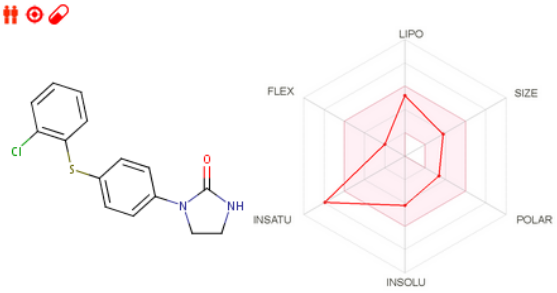

SMILES O=C1NCCN1c1ccc(cc1)Sc1ccccc1Cl

Physicochemical Properties	
Formula	C15H13ClN2OS
Molecular weight	304.79 g/mol
Num. heavy atoms	20
Num. arom. heavy atoms	12
Fraction Csp3	0.13
Num. rotatable bonds	3
Num. H-bond acceptors	1
Num. H-bond donors	1
Molar Refractivity	89.16
TPSA	57.64 Å²

Lipophilicity	
Log $P_{o/w}$ (iLOGP)	2.66
Log $P_{o/w}$ (XLOGP3)	3.58
Log $P_{o/w}$ (WLOGP)	3.26
Log $P_{o/w}$ (MLOGP)	3.86
Log $P_{o/w}$ (SILICOS-IT)	3.30
Consensus Log $P_{o/w}$	3.33

Water Solubility	
Log *S* (ESOL)	-4.23
Solubility	1.79e-02 mg/ml ; 5.87e-05 mol/l
Class	Moderately soluble
Log *S* (Ali)	-4.48
Solubility	1.02e-02 mg/ml ; 3.34e-05 mol/l
Class	Moderately soluble
Log *S* (SILICOS-IT)	-5.74
Solubility	5.61e-04 mg/ml ; 1.84e-06 mol/l
Class	Moderately soluble

Pharmacokinetics	
GI absorption	High
BBB permeant	Yes
P-gp substrate	Yes
CYP1A2 inhibitor	Yes
CYP2C19 inhibitor	Yes
CYP2C9 inhibitor	Yes
CYP2D6 inhibitor	No
CYP3A4 inhibitor	Yes
Log K_p (skin permeation)	-5.62 cm/s

Druglikeness	
Lipinski	Yes; 0 violation
Ghose	Yes
Veber	Yes
Egan	Yes
Muegge	Yes
Bioavailability Score	0.55

Medicinal Chemistry	
PAINS	0 alert
Brenk	0 alert
Leadlikeness	No; 1 violation: XLOGP3>3.5
Synthetic accessibility	2.29

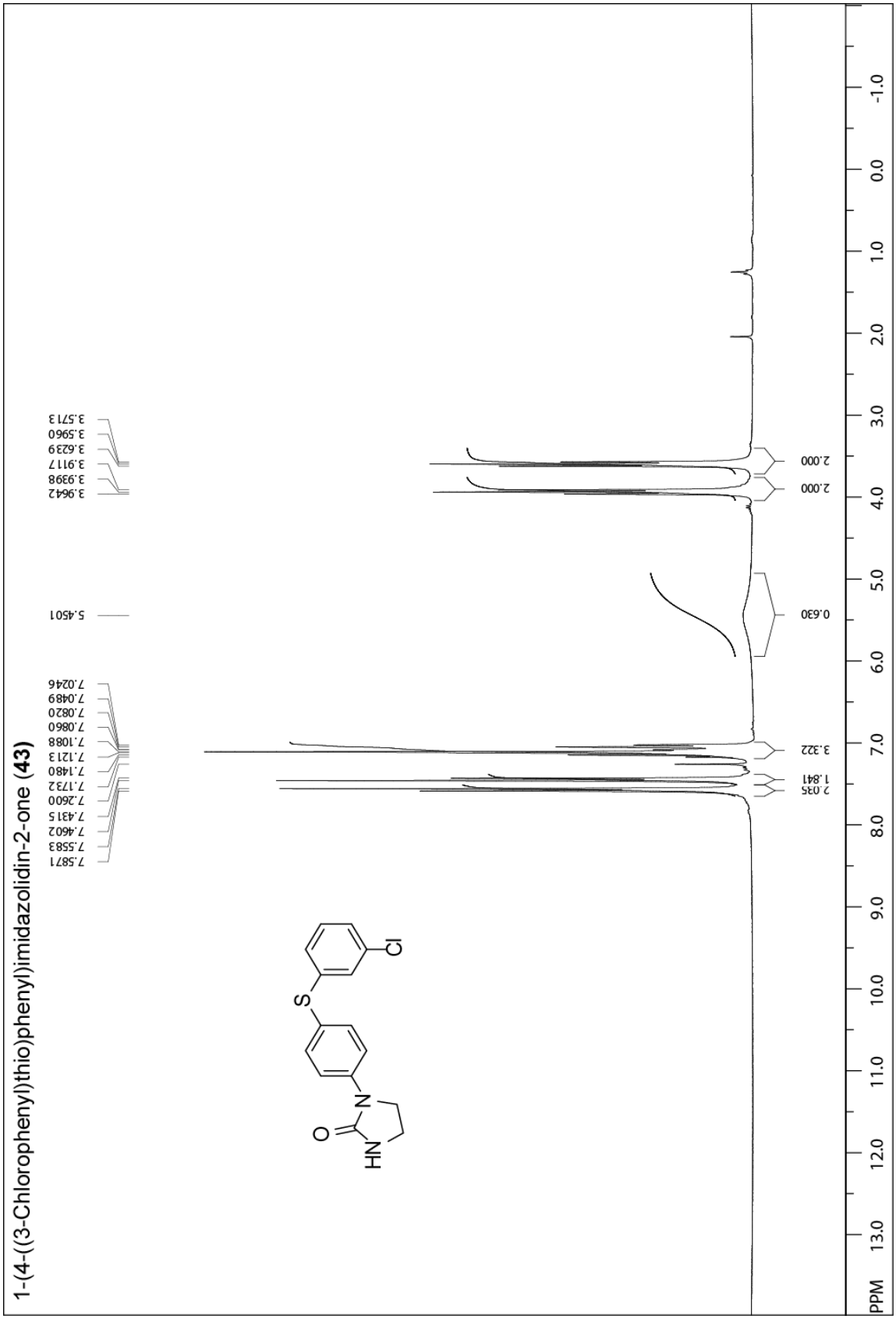
1-(4-((3-Chlorophenyl)thio)phenyl)imidazolidin-2-one (43)
7.5871
7.5583
7.4602
7.4315
7.2600
7.1732
7.1480
7.1213
7.1088
7.0860
7.0820
7.0489
7.0246
5.4501
3.9642
3.9398
3.9117
3.6239
3.5960
3.5713
2.035
1.841
3.322
0.630
2.000
2.000
Cl
S
N
O
HN
PPM
13.0
12.0
11.0
10.0
9.0
8.0
7.0
6.0
5.0
4.0
3.0
2.0
1.0
0.0
-1.0

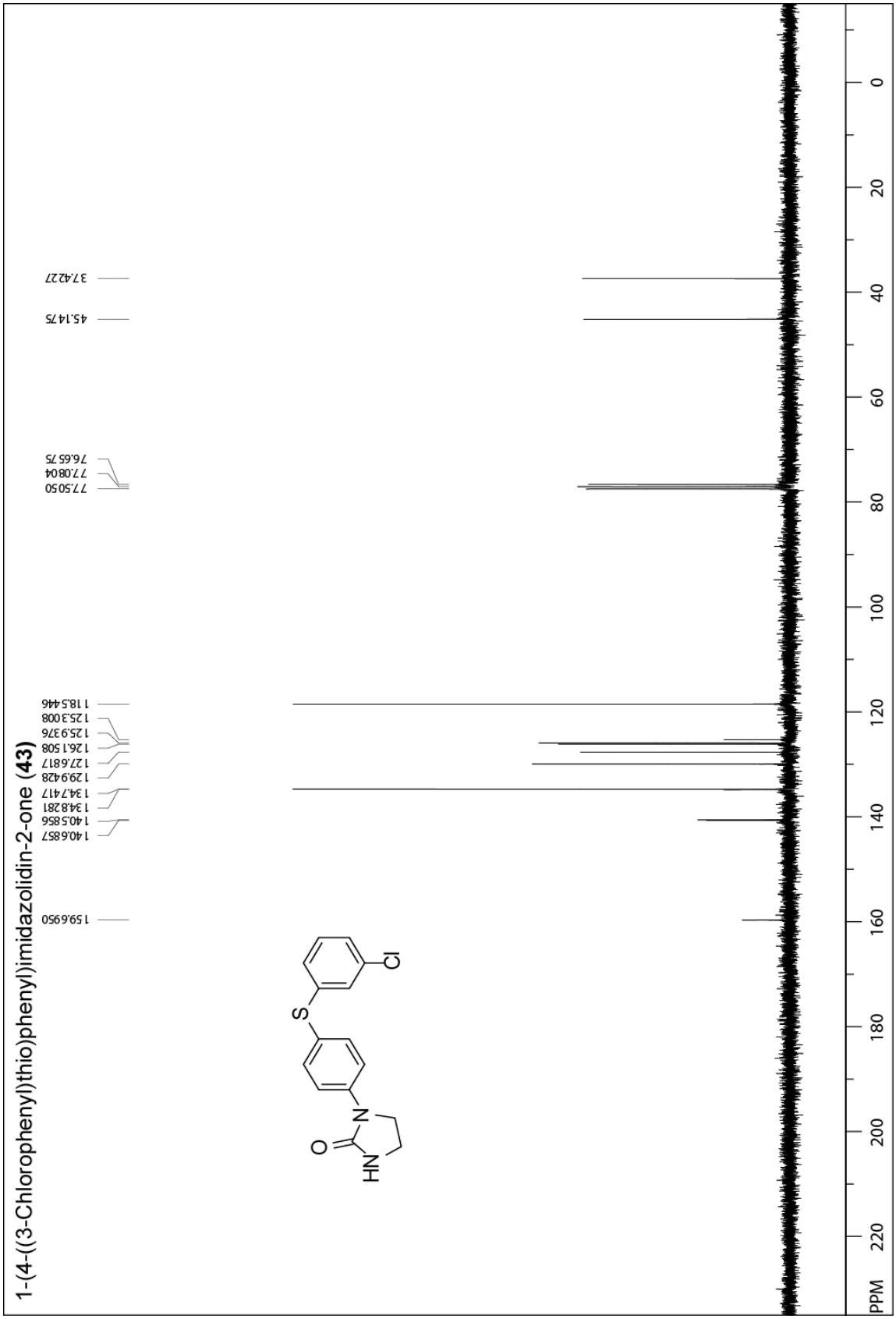
1-(4-((3-Chlorophenyl)thio)phenyl)imidazolidin-2-one (43)
159.6950
140.6857
140.5856
134.8281
134.7417
129.9428
127.6817
126.1508
125.9376
125.3008
118.5446
77.5050
77.0804
76.6575
45.1475
37.4227
Cl
S
N
HN
O
PPM
220
200
180
160
140
120
100
80
60
40
20
0

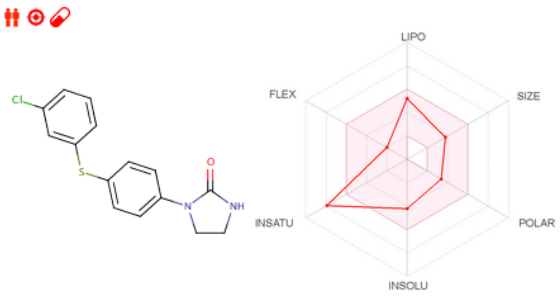

SMILES ClC1cccc(c1)Sc1ccc(cc1)N1CCNC1=O

Physicochemical Properties	
Formula	C15H13ClN2OS
Molecular weight	304.79 g/mol
Num. heavy atoms	20
Num. arom. heavy atoms	12
Fraction Csp3	0.13
Num. rotatable bonds	3
Num. H-bond acceptors	1
Num. H-bond donors	1
Molar Refractivity	89.16
TPSA	57.64 Å²

Lipophilicity	
Log $P_{o/w}$ (iLOGP)	2.95
Log $P_{o/w}$ (XLOGP3)	3.58
Log $P_{o/w}$ (WLOGP)	3.26
Log $P_{o/w}$ (MLOGP)	3.86
Log $P_{o/w}$ (SILICOS-IT)	3.30
Consensus Log $P_{o/w}$	3.39

Water Solubility	
Log *S* (ESOL)	-4.23
Solubility	1.79e-02 mg/ml ; 5.87e-05 mol/l
Class	Moderately soluble
Log *S* (Ali)	-4.48
Solubility	1.02e-02 mg/ml ; 3.34e-05 mol/l
Class	Moderately soluble
Log *S* (SILICOS-IT)	-5.74
Solubility	5.61e-04 mg/ml ; 1.84e-06 mol/l
Class	Moderately soluble

Pharmacokinetics	
GI absorption	High
BBB permeant	Yes
P-gp substrate	No
CYP1A2 inhibitor	Yes
CYP2C19 inhibitor	Yes
CYP2C9 inhibitor	Yes
CYP2D6 inhibitor	No
CYP3A4 inhibitor	Yes
Log K_p (skin permeation)	-5.62 cm/s

Druglikeness	
Lipinski	Yes; 0 violation
Ghose	Yes
Veber	Yes
Egan	Yes
Muegge	Yes
Bioavailability Score	0.55

Medicinal Chemistry	
PAINS	0 alert
Brenk	0 alert
Leadlikeness	No; 1 violation: XLOGP3>3.5
Synthetic accessibility	2.28

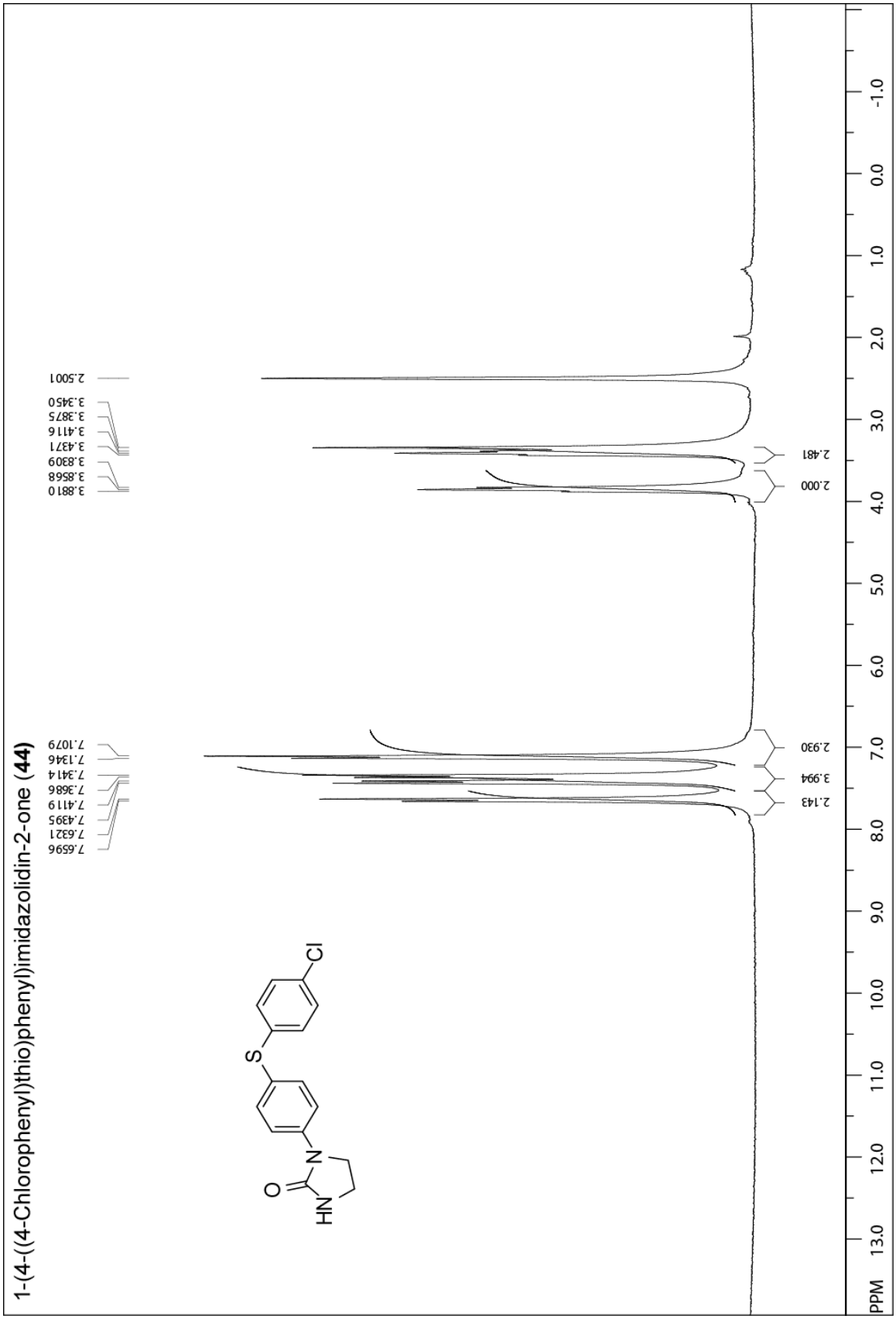
1-(4-((4-Chlorophenyl)thio)phenyl)imidazolidin-2-one (44)
7.6596
7.6321
7.4395
7.4119
7.3686
7.3414
7.1346
7.1079
3.8810
3.8568
3.8309
3.4371
3.4116
3.3875
3.3450
2.5001
2.930
3.994
2.143
2.481
2.000
PPM
13.0
12.0
11.0
10.0
9.0
8.0
7.0
6.0
5.0
4.0
3.0
2.0
1.0
0.0
-1.0
Cl
S
N
O
HN

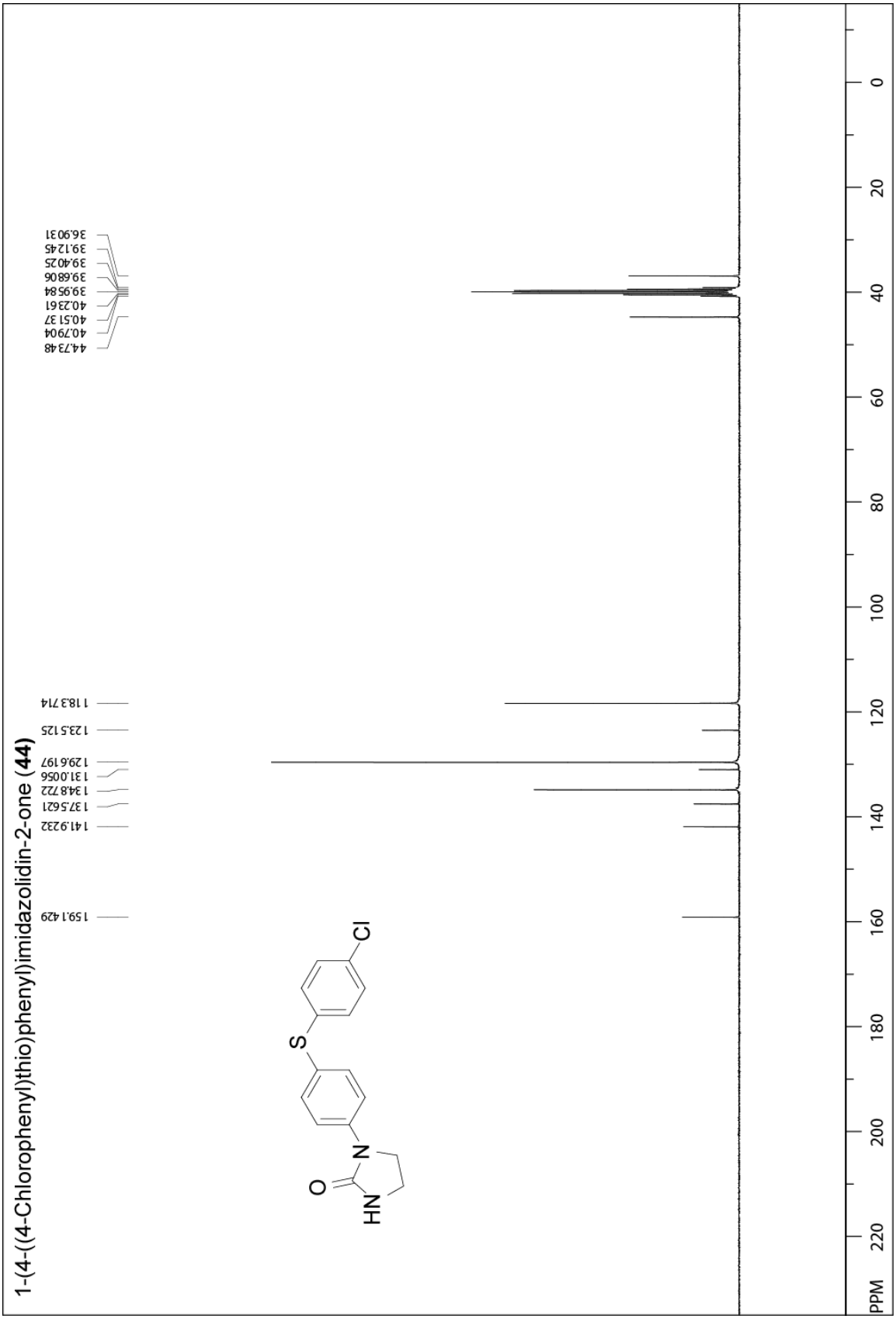
1-(4-((4-Chlorophenyl)thio)phenyl)imidazolidin-2-one (44)
159.1429
141.9232
137.5621
134.8722
131.0056
129.6197
123.5125
118.3714
44.7348
40.7904
40.5137
40.2361
39.9584
39.6806
39.4025
39.1245
36.9031
Cl
S
N
O
HN
PPM
0
20
40
60
80
100
120
140
160
180
200
220

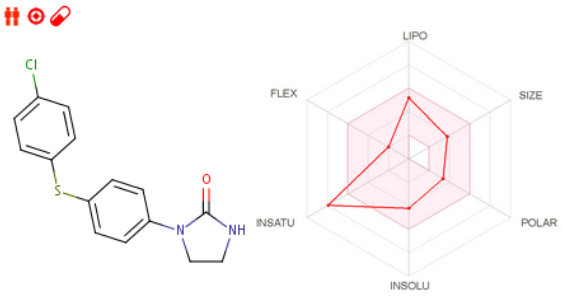

SMILES O=C1NCCN1c1ccc(cc1)Sc1ccc(cc1)Cl

Physicochemical Properties	
Formula	C15H13ClN2OS
Molecular weight	304.79 g/mol
Num. heavy atoms	20
Num. arom. heavy atoms	12
Fraction Csp3	0.13
Num. rotatable bonds	3
Num. H-bond acceptors	1
Num. H-bond donors	1
Molar Refractivity	89.16
TPSA	57.64 Å²

Lipophilicity	
Log $P_{o/w}$ (iLOGP)	2.77
Log $P_{o/w}$ (XLOGP3)	3.58
Log $P_{o/w}$ (WLOGP)	3.26
Log $P_{o/w}$ (MLOGP)	3.86
Log $P_{o/w}$ (SILICOS-IT)	3.30
Consensus Log $P_{o/w}$	3.35

Water Solubility	
Log *S* (ESOL)	-4.23
Solubility	1.79e-02 mg/ml ; 5.87e-05 mol/l
Class	Moderately soluble
Log *S* (Ali)	-4.48
Solubility	1.02e-02 mg/ml ; 3.34e-05 mol/l
Class	Moderately soluble
Log *S* (SILICOS-IT)	-5.74
Solubility	5.61e-04 mg/ml ; 1.84e-06 mol/l
Class	Moderately soluble

Pharmacokinetics	
GI absorption	High
BBB permeant	Yes
P-gp substrate	No
CYP1A2 inhibitor	Yes
CYP2C19 inhibitor	Yes
CYP2C9 inhibitor	Yes
CYP2D6 inhibitor	No
CYP3A4 inhibitor	Yes
Log K_p (skin permeation)	-5.62 cm/s

Druglikeness	
Lipinski	Yes; 0 violation
Ghose	Yes
Veber	Yes
Egan	Yes
Muegge	Yes
Bioavailability Score	0.55

Medicinal Chemistry	
PAINS	0 alert
Brenk	0 alert
Leadlikeness	No; 1 violation: XLOGP3>3.5
Synthetic accessibility	2.21

Annexe D : Données supplémentaires du chapitre 5

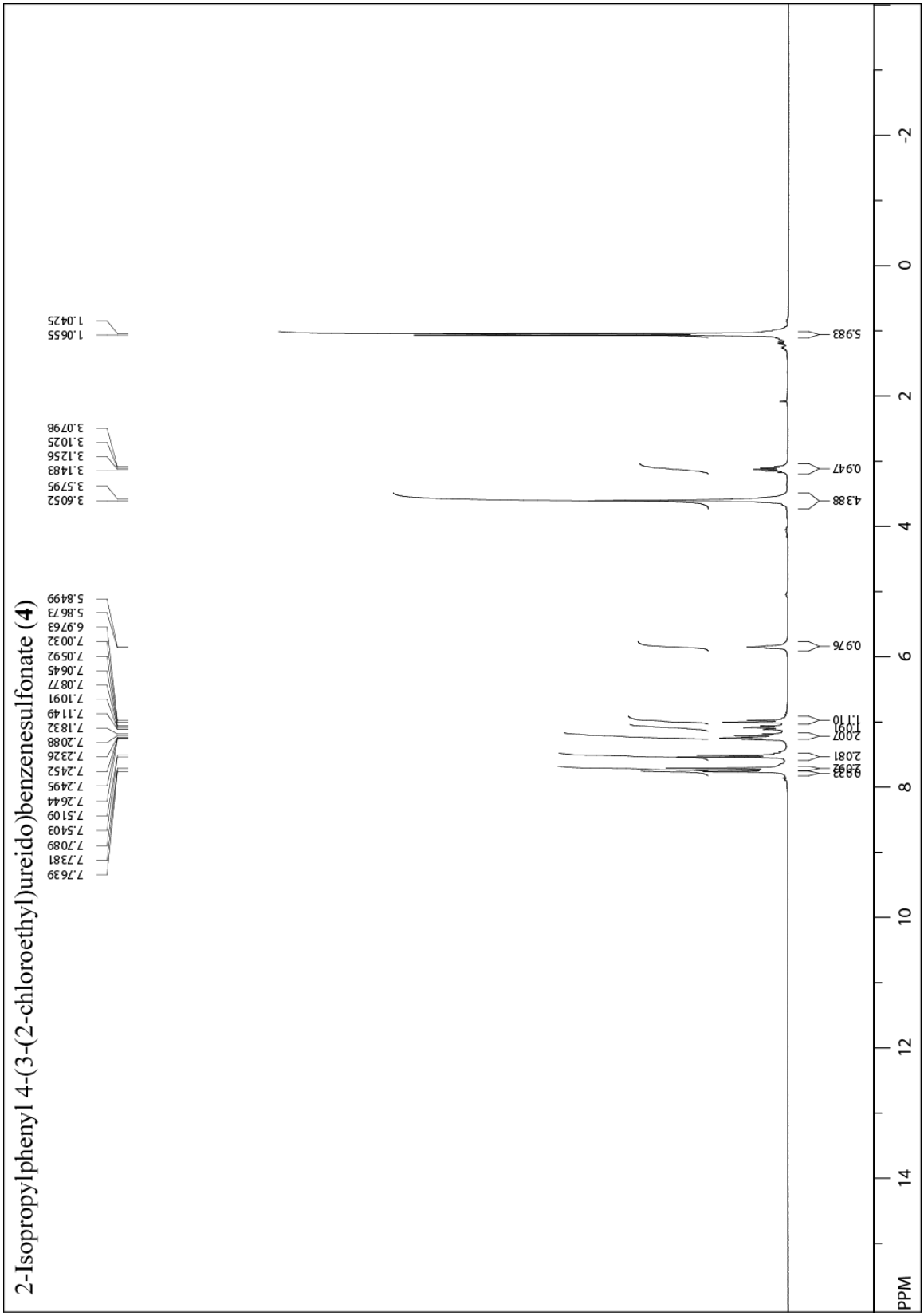
2-Isopropylphenyl 4-(3-(2-chloroethyl)ureido)benzenesulfonate (4)
7.7639
7.7381
7.7089
7.5403
7.5109
7.2644
7.2495
7.2452
7.2326
7.2088
7.1832
7.1149
7.1091
7.0877
7.0645
7.0592
7.0032
6.9763
5.8673
5.8499
3.6052
3.5795
3.1483
3.1256
3.1025
3.0798
1.0655
1.0425
5.983
4.388
0.947
0.976
1.110
1.091
2.007
2.081
PPM

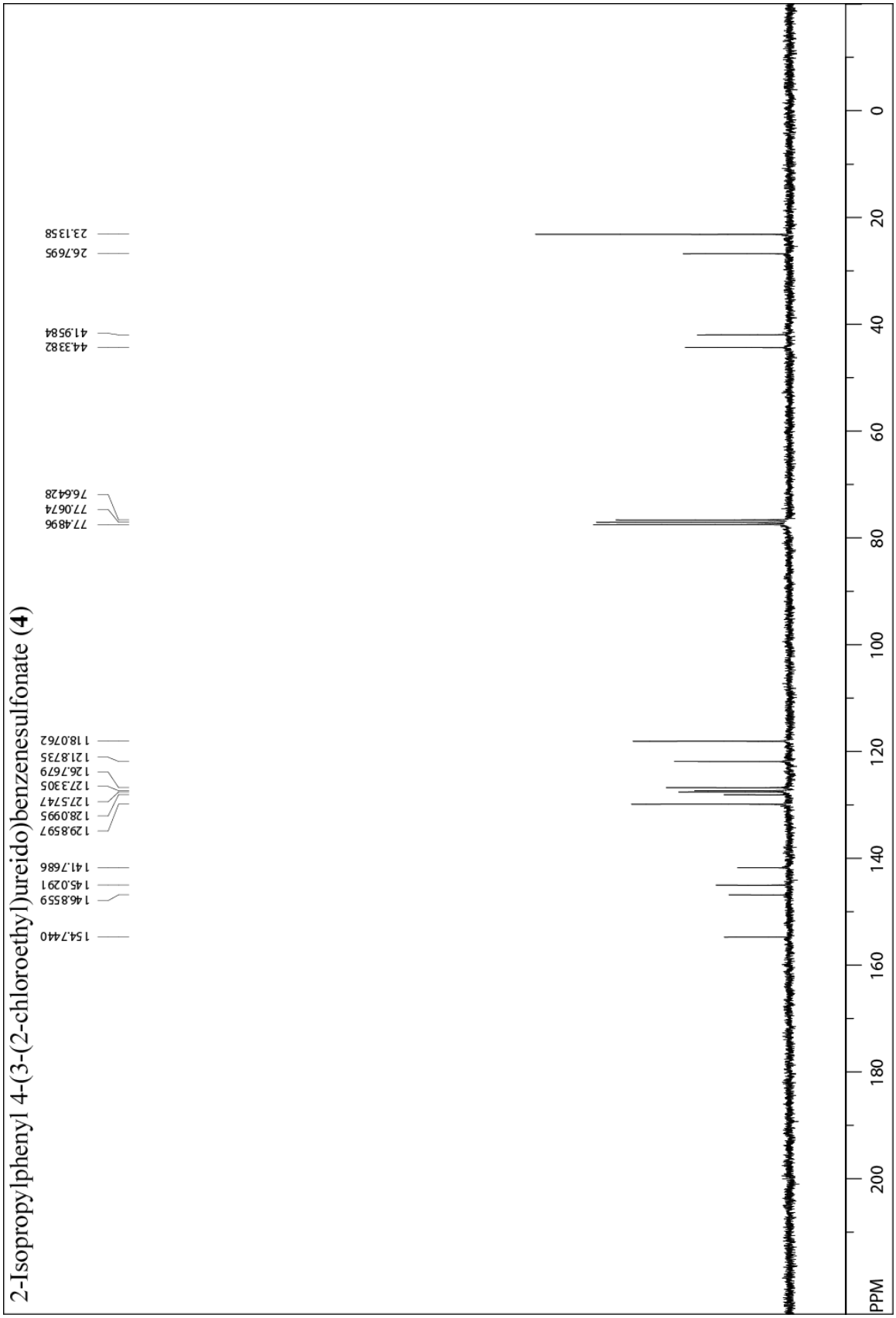
2-Isopropylphenyl 4-(3-(2-chloroethyl)ureido)benzenesulfonate (4)
154.7440
146.8559
145.0291
141.7686
129.8597
128.0995
127.5747
127.3305
126.7679
121.8735
118.0762
77.4896
77.0674
76.6428
44.3382
41.9584
26.7695
23.1358
PPM
200
180
160
140
120
100
80
60
40
20
0

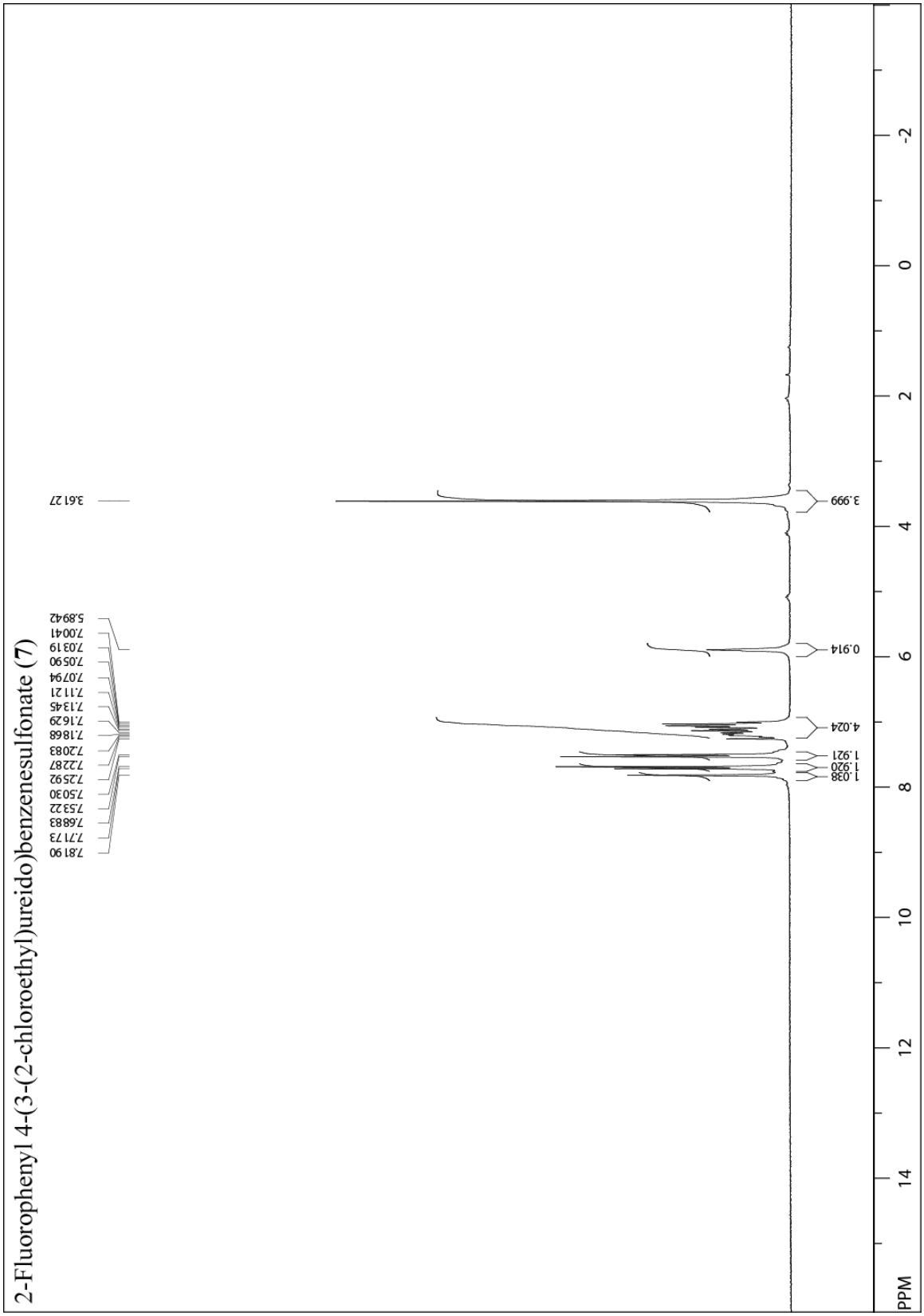
2-Fluorophenyl 4-(3-(2-chloroethyl)ureido)benzenesulfonate (7)
7.8190
7.7173
7.6883
7.5322
7.5030
7.2592
7.2287
7.2083
7.1868
7.1629
7.1345
7.1121
7.0794
7.0590
7.0319
7.0041
5.8942
3.6127
3.999
0.914
4.024
1.921
1.920
1.038
PPM
14
12
10
8
6
4
2
0
-2

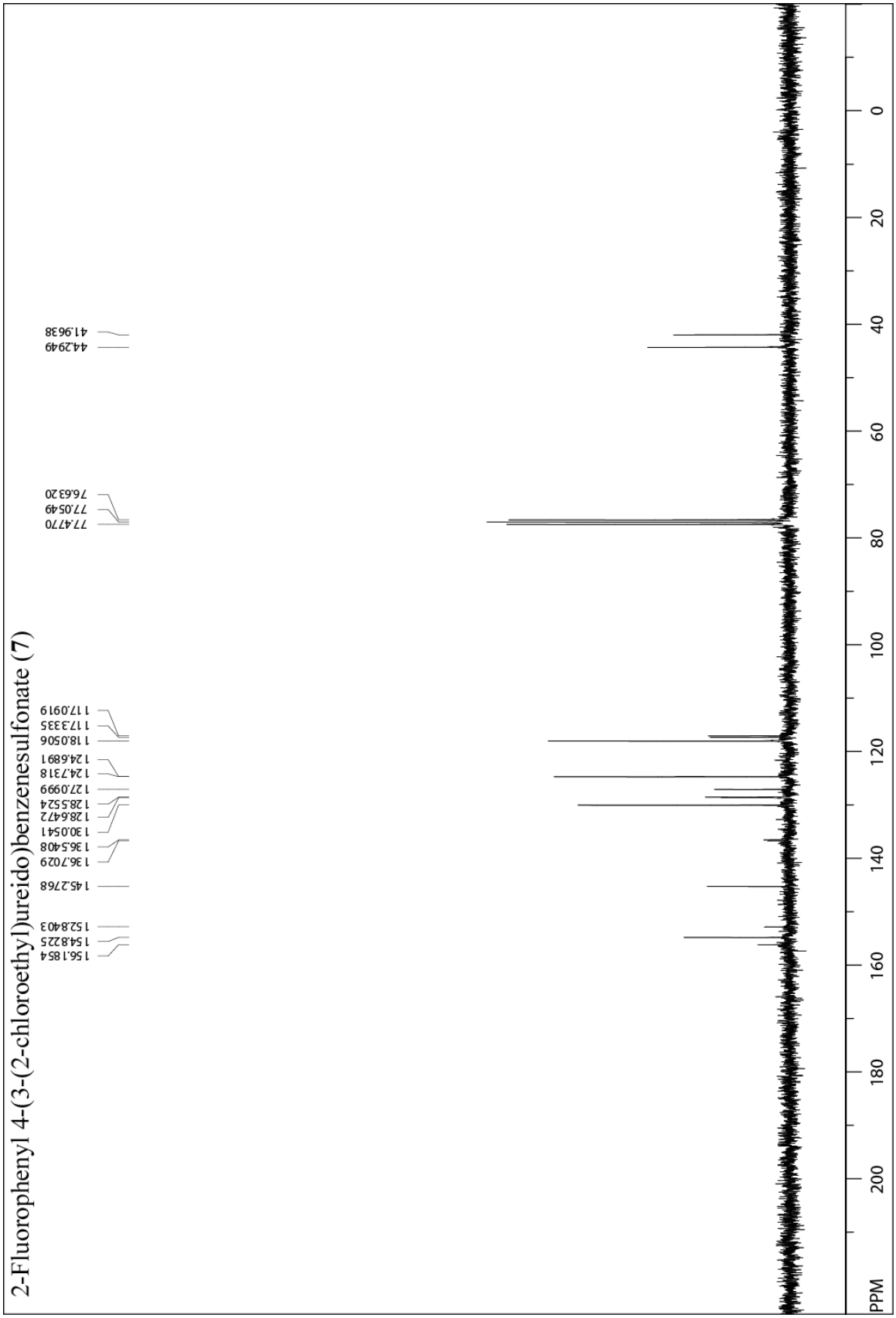
2-Fluorophenyl 4-(3-(2-chloroethyl)ureido)benzenesulfonate (7)
156.1854
154.8225
152.8403
145.2768
136.7029
136.5408
130.0541
128.6472
128.5524
127.0999
124.7318
124.6891
118.0506
117.3335
117.0919
77.4770
77.0549
76.6320
44.2949
41.9638
PPM
200
180
160
140
120
100
80
60
40
20
0

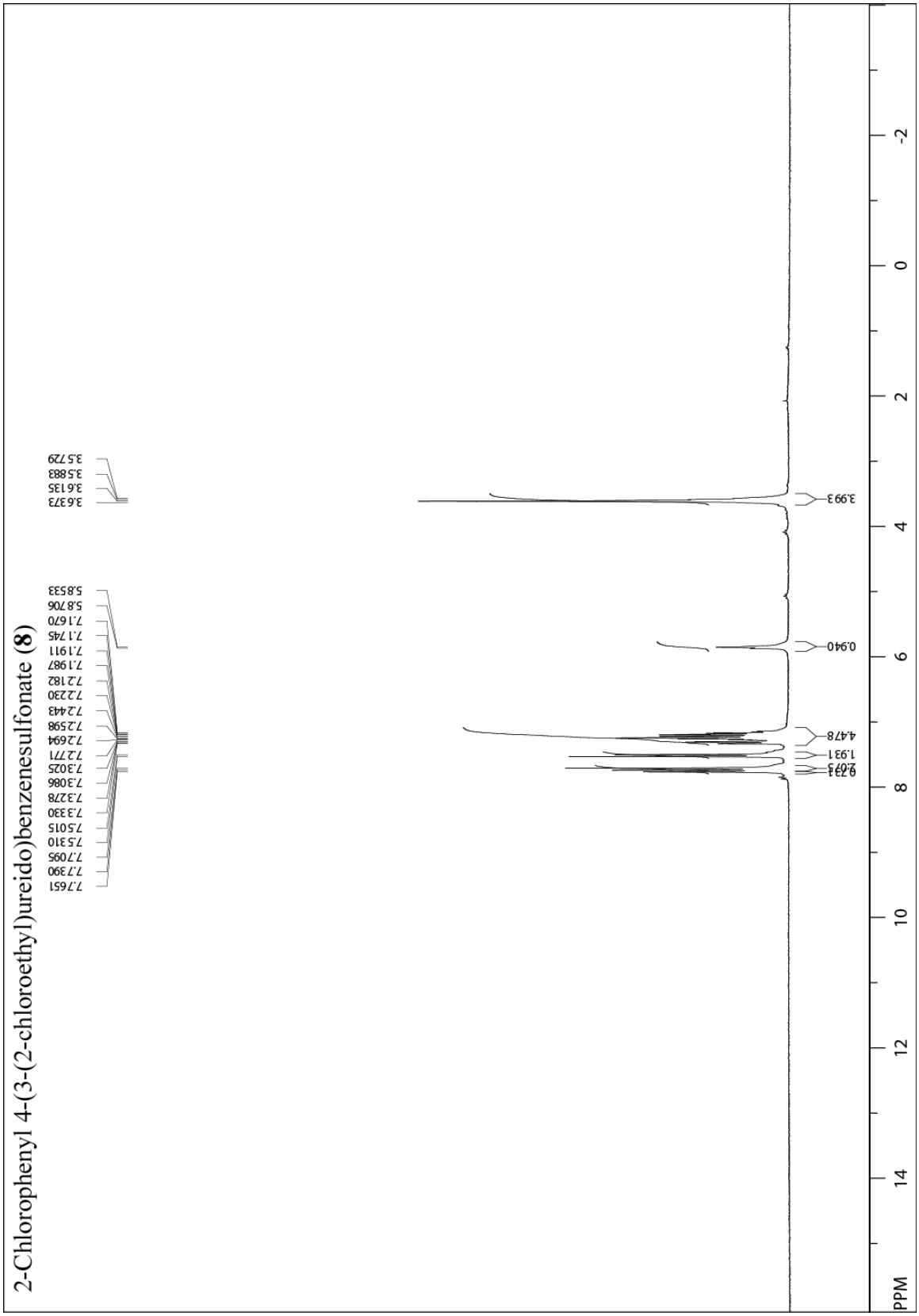
2-Chlorophenyl 4-(3-(2-chloroethyl)ureido)benzenesulfonate (8)
7.7651
7.7390
7.7095
7.5310
7.5015
7.3330
7.3278
7.3086
7.3025
7.2771
7.2694
7.2598
7.2443
7.2230
7.2182
7.1987
7.1911
7.1745
7.1670
5.8706
5.8533
3.6373
3.6135
3.5883
3.5729
3.993
0.940
4.478
1.931
2.073
0.731
PPM
14
12
10
8
6
4
2
0
-2

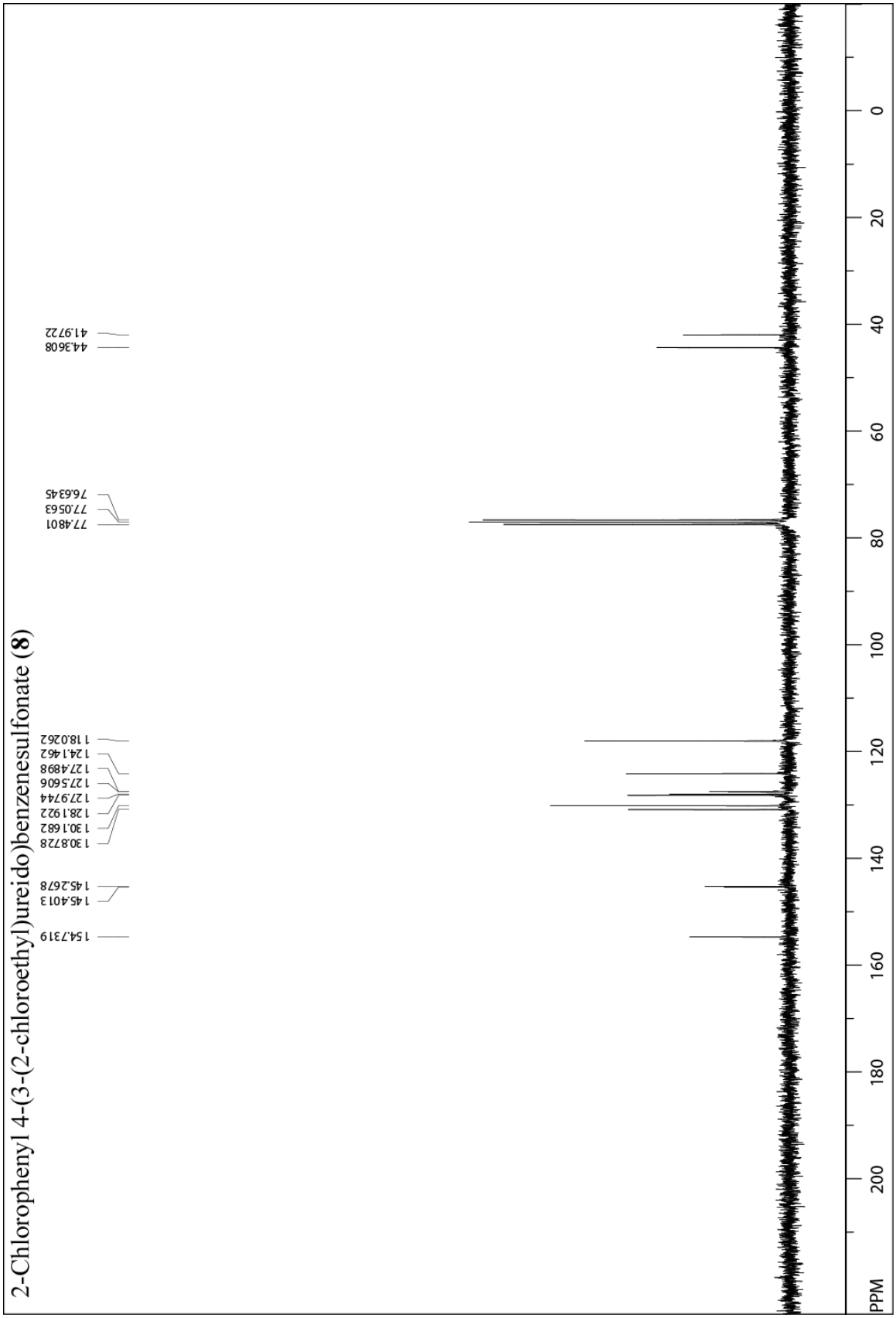
2-Chlorophenyl 4-(3-(2-chloroethyl)ureido)benzenesulfonate (8)
154.7319
145.4013
145.2678
130.8728
130.1682
128.1922
127.9744
127.5606
127.4898
124.1462
118.0262
77.4801
77.0563
76.6345
44.3608
41.9722
PPM
200
180
160
140
120
100
80
60
40
20
0

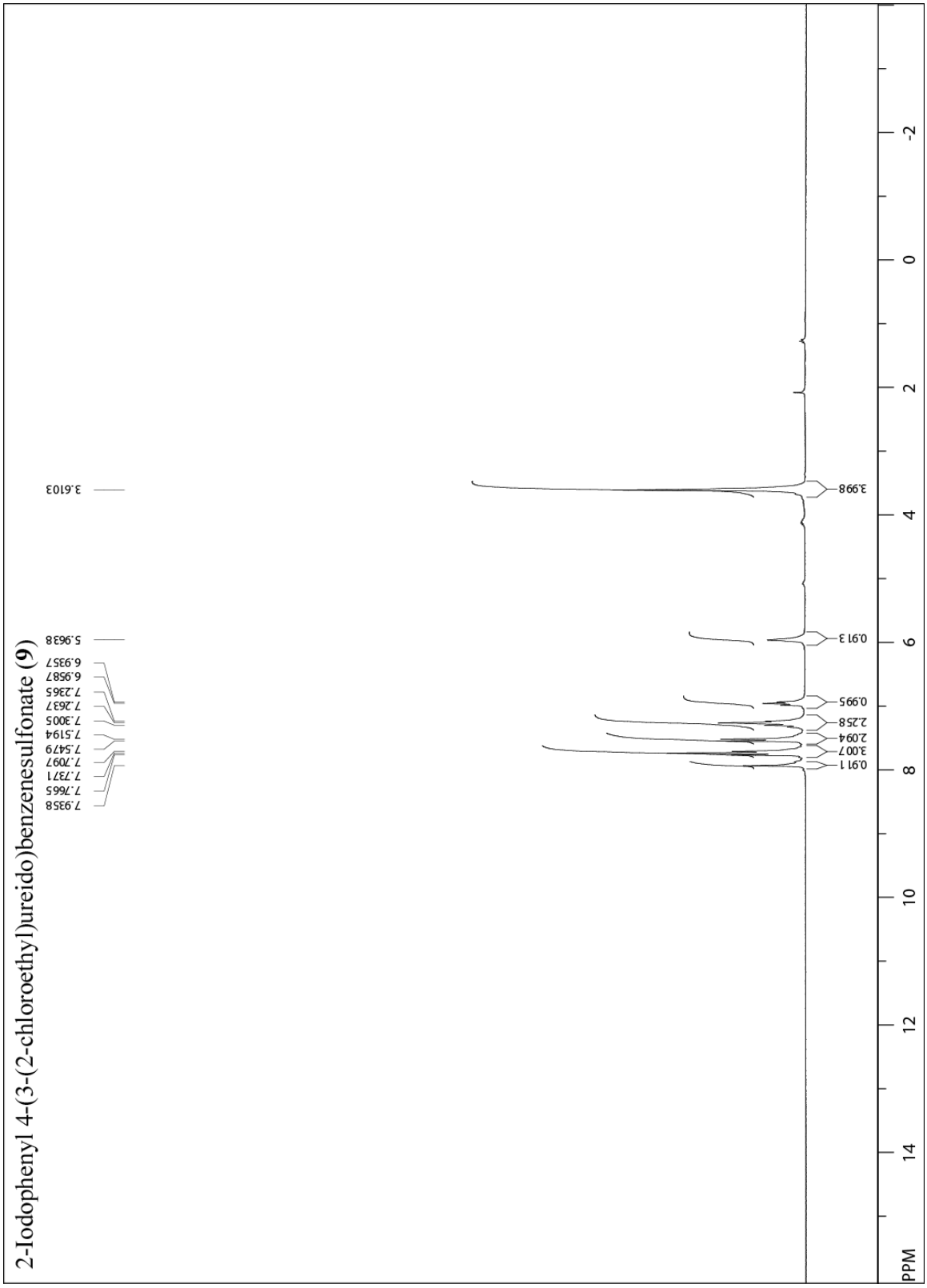
2-Iodophenyl 4-(3-(2-chloroethyl)ureido)benzenesulfonate (9)
7.9358
7.7665
7.7371
7.7097
7.5479
7.5194
7.3005
7.2637
7.2365
6.9587
6.9357
5.9638
3.6103
3.998
0.913
0.995
2.258
2.094
3.007
0.911
PPM
14
12
10
8
6
4
2
0
-2

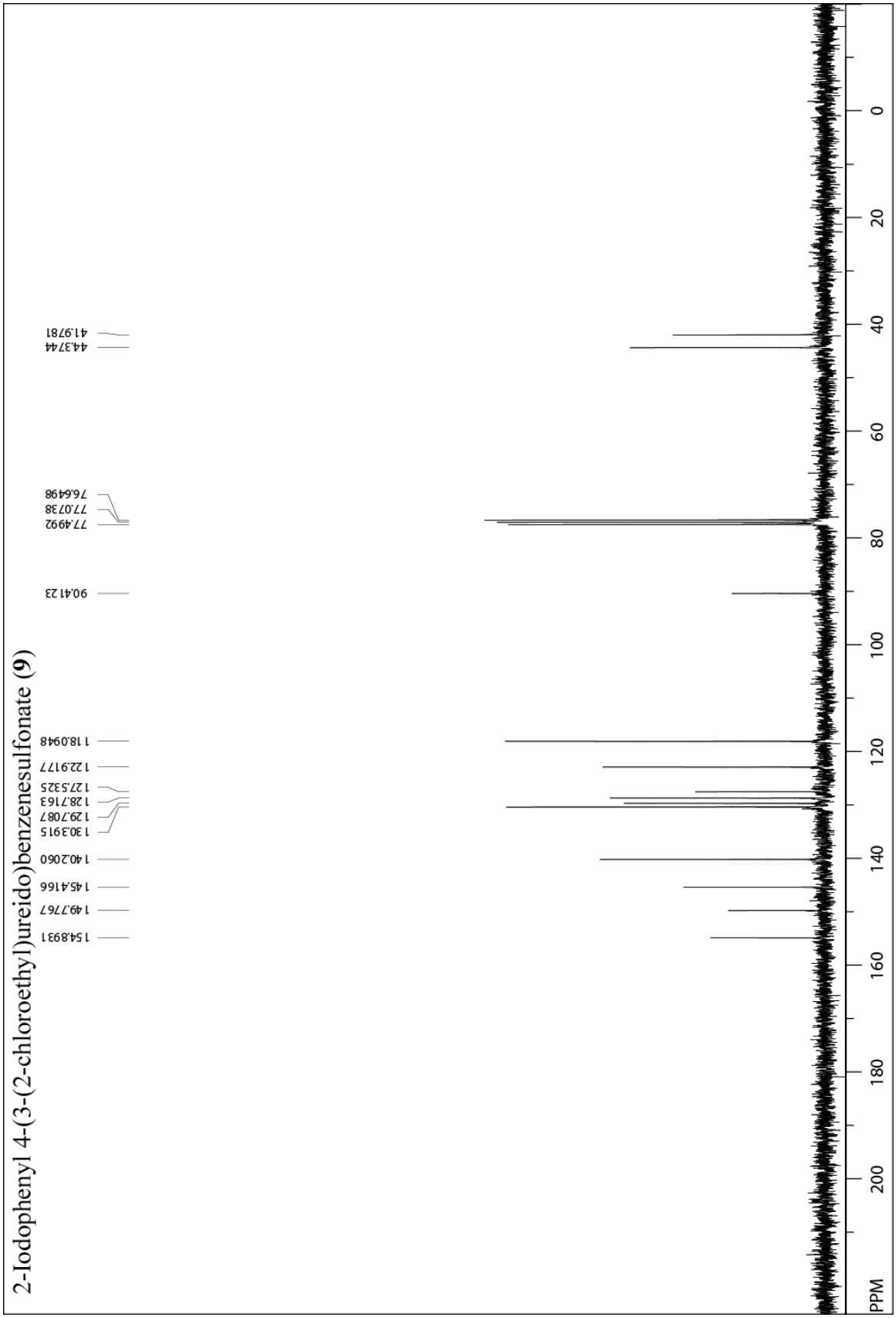
2-Iodophenyl 4-(3-(2-chloroethyl)ureido)benzenesulfonate (9)
154.8931
149.7767
145.4166
140.2060
130.3915
129.7087
128.7763
127.5325
122.9177
118.0948
90.4123
77.4992
77.0738
76.6498
44.3744
41.9781
PPM
200
180
160
140
120
100
80
60
40
20
0

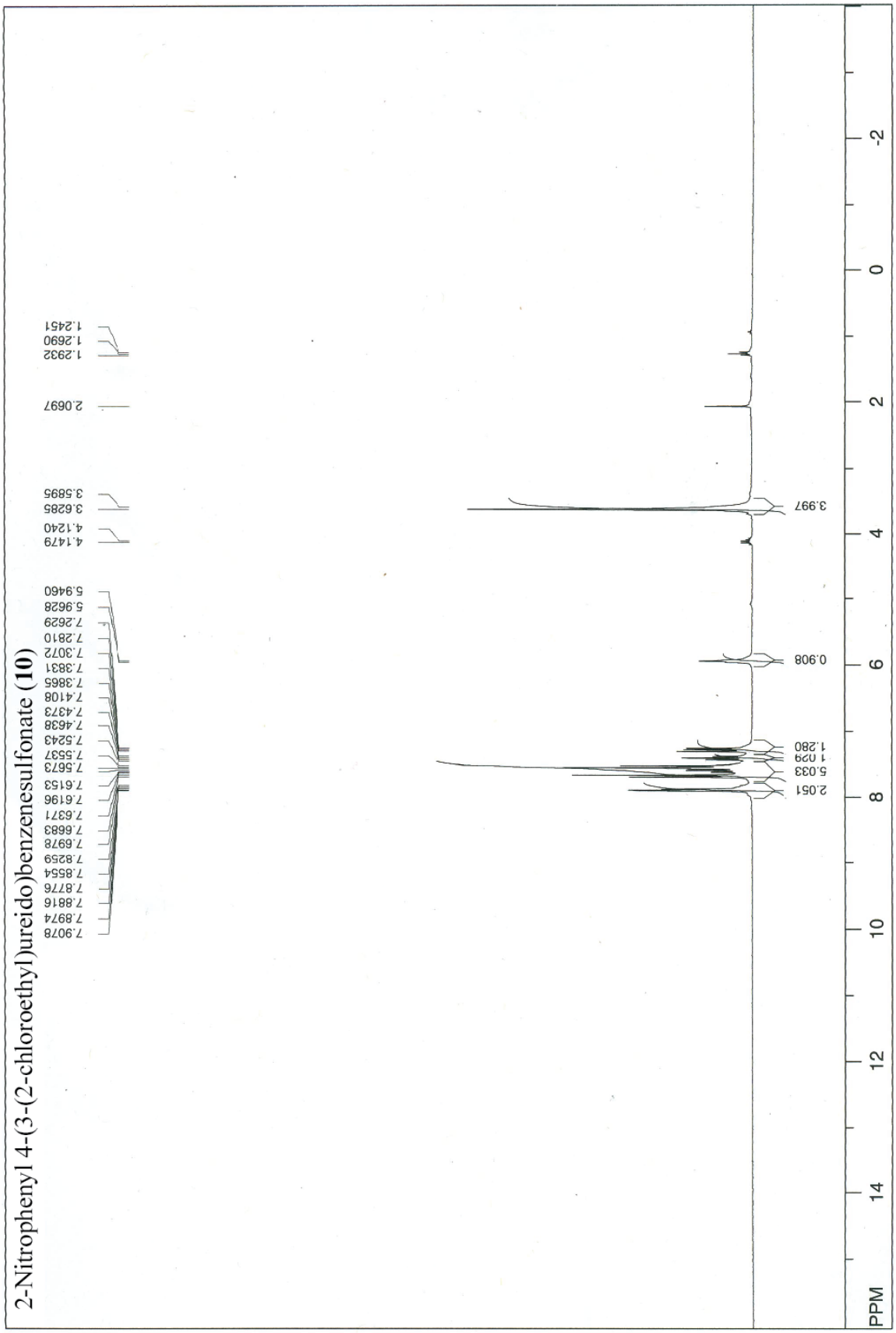
2-Nitrophenyl 4-(3-(2-chloroethyl)ureido)benzenesulfonate (10)
7.9078
7.8974
7.8816
7.8776
7.8554
7.8259
7.6978
7.6683
7.6371
7.6196
7.6153
7.5673
7.5537
7.5243
7.4638
7.4373
7.4108
7.3865
7.3831
7.3072
7.2810
7.2629
5.9628
5.9460
4.1479
4.1240
3.6285
3.5895
2.0697
1.2932
1.2690
1.2451
3.997
0.908
1.280
1.029
5.033
2.051
PPM
14
12
10
8
6
4
2
0
-2

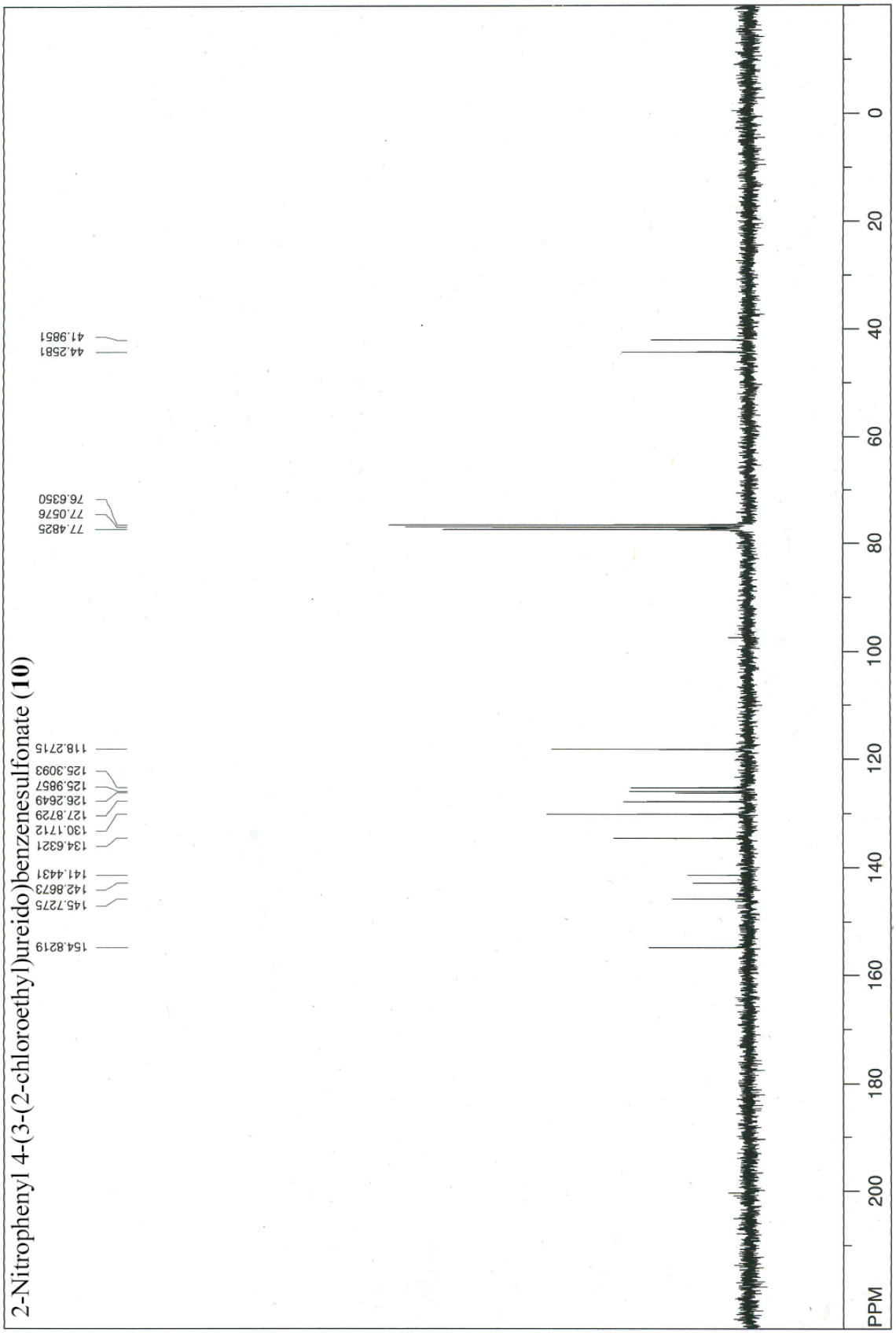
2-Nitrophenyl 4-(3-(2-chloroethyl)ureido)benzenesulfonate (10)
154.8219
145.7275
142.8673
141.4431
134.6321
130.1712
127.8729
126.2649
125.9857
125.3093
118.2715
77.4825
77.0576
76.6350
44.2581
41.9851
PPM
200
180
160
140
120
100
80
60
40
20
0

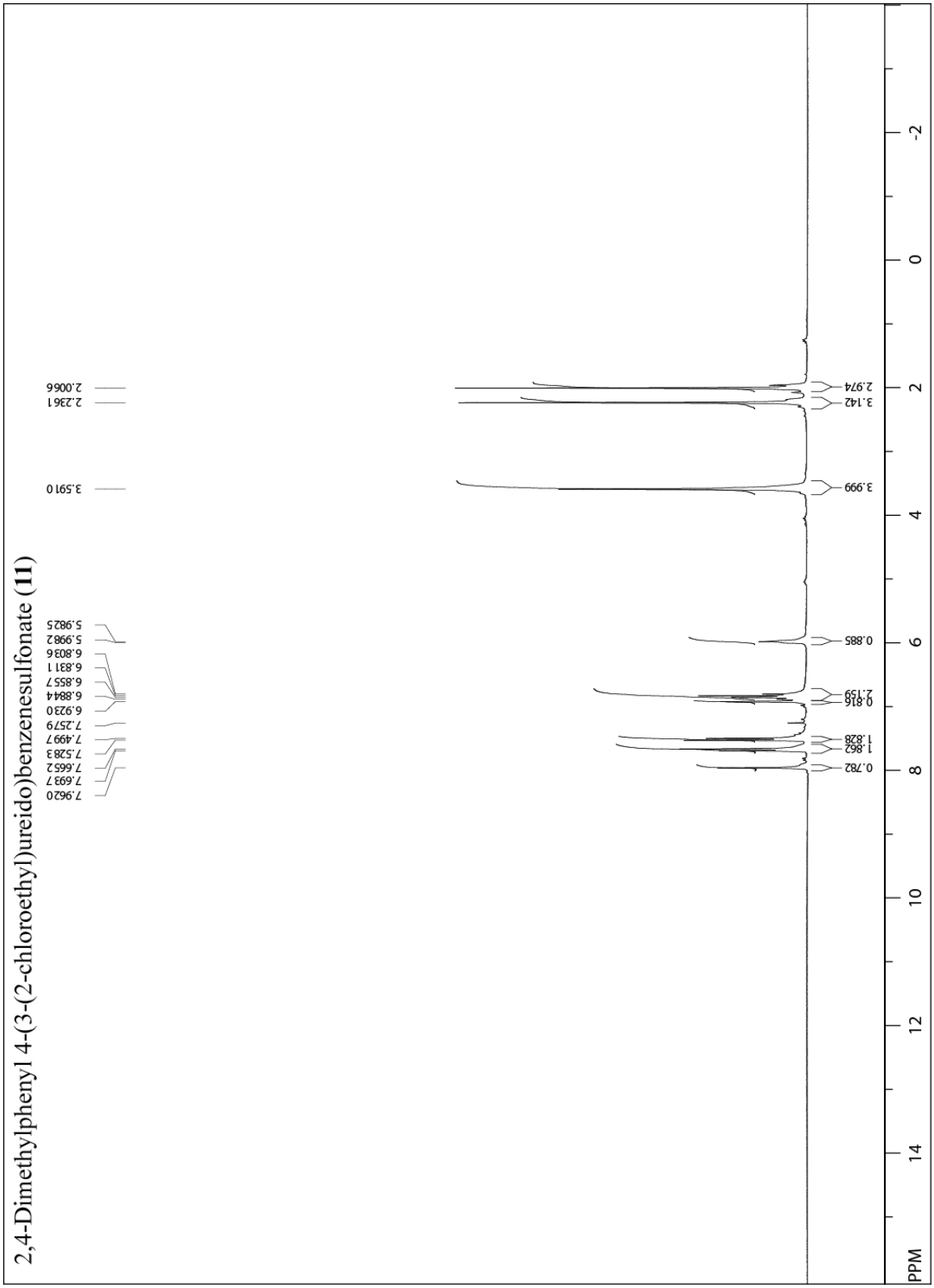
2,4-Dimethylphenyl 4-(3-(2-chloroethyl)ureido)benzenesulfonate (11)
7.9620
7.6937
7.6652
7.5283
7.4997
7.2579
6.9230
6.8844
6.8557
6.8311
6.8036
5.9982
5.9825
3.5910
2.2361
2.0066
0.782
1.862
1.828
0.816
2.159
0.885
3.999
3.142
2.974
PPM
14
12
10
8
6
4
2
0
-2

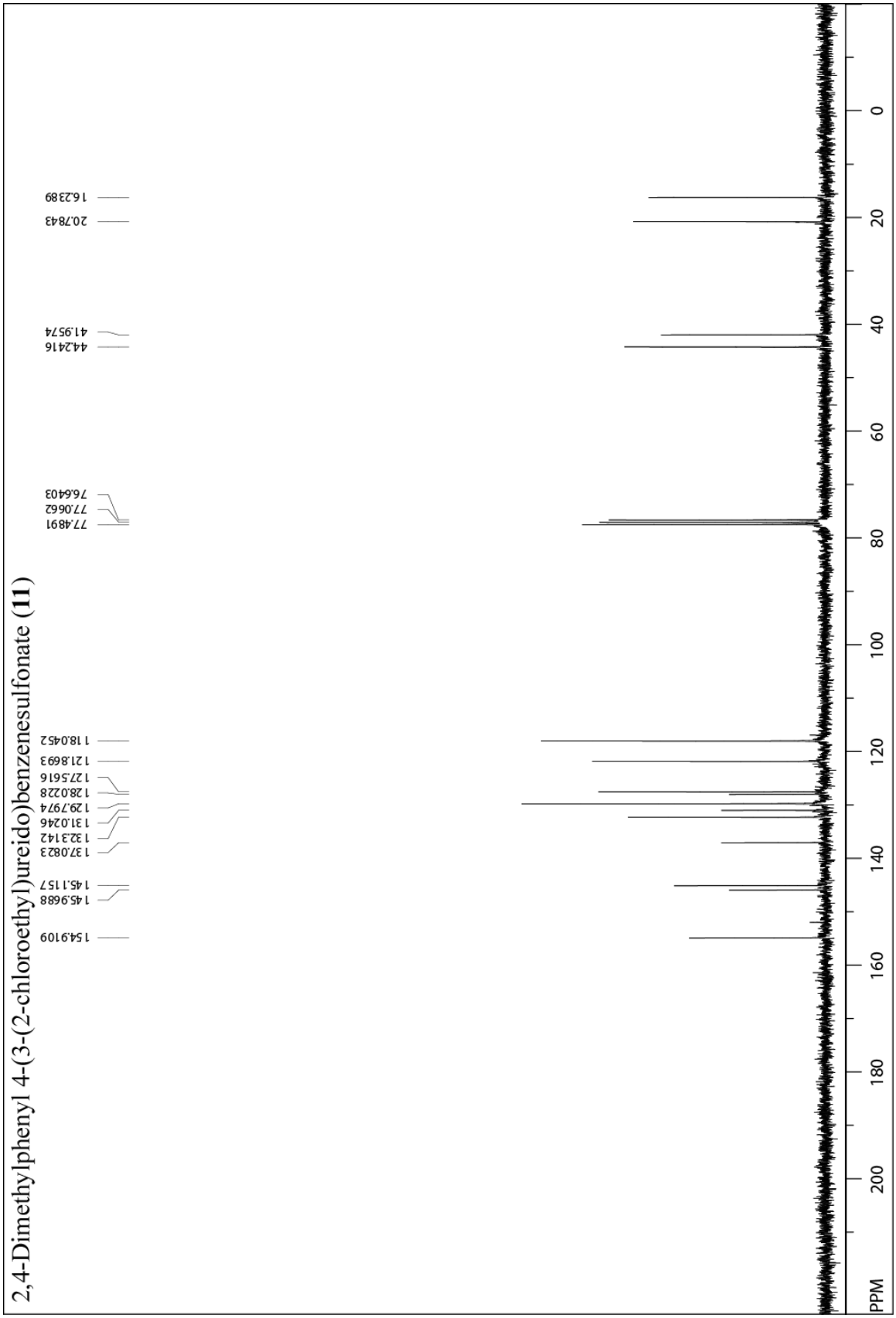
2,4-Dimethylphenyl 4-(3-(2-chloroethyl)ureido)benzenesulfonate (11)
154.9109
145.9688
145.1157
137.0823
132.3142
131.0246
129.7974
128.0228
127.5616
121.8693
118.0452
77.4891
77.0662
76.6403
44.2416
41.9574
20.7843
16.2389
PPM
200
180
160
140
120
100
80
60
40
20
0

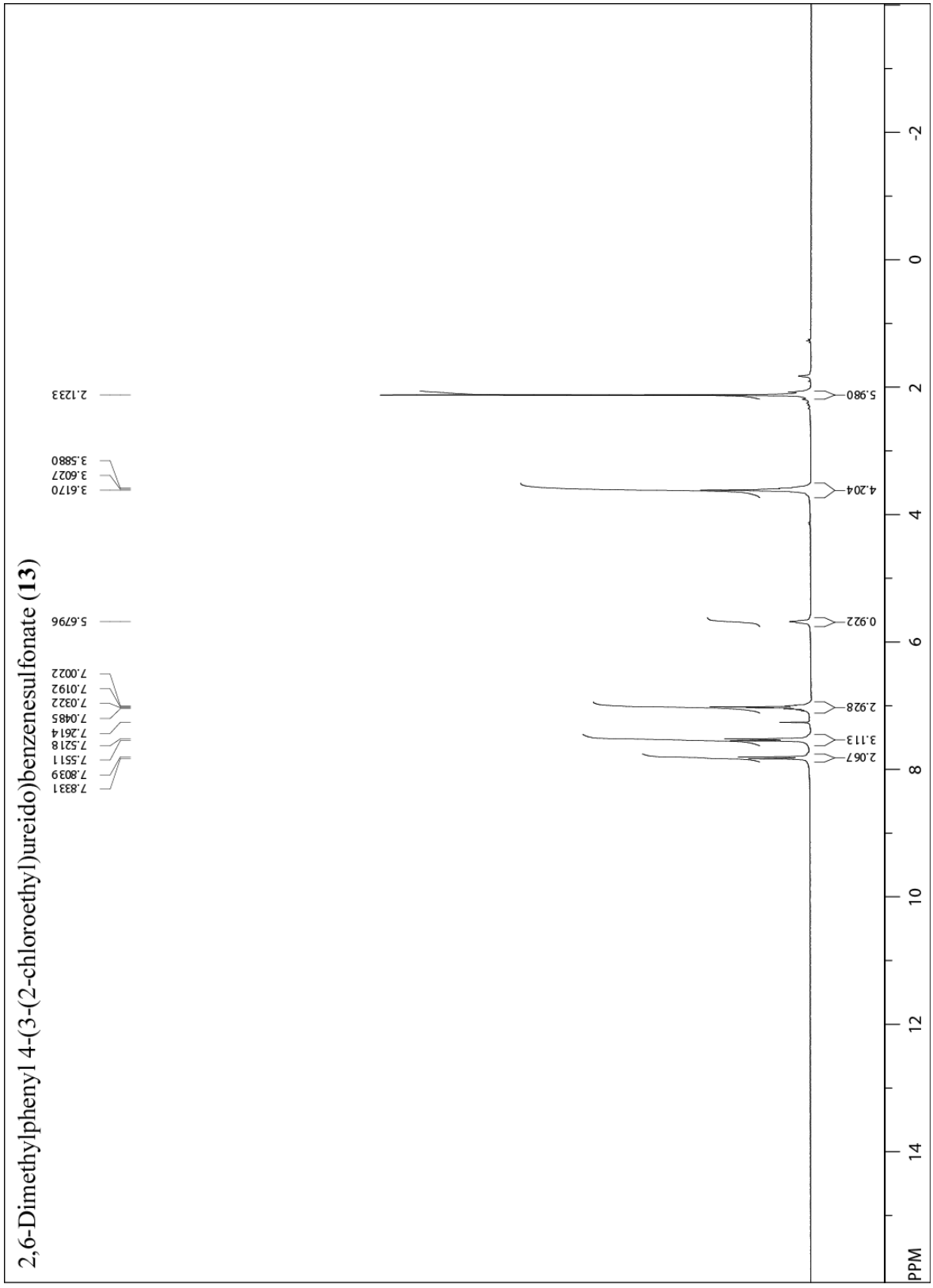
2,6-Dimethylphenyl 4-(3-(2-chloroethyl)ureido)benzenesulfonate (13)
7.8331
7.8039
7.5511
7.5218
7.2614
7.0485
7.0322
7.0192
7.0022
5.6796
3.6170
3.6027
3.5880
2.1233
5.980
4.204
0.922
2.928
3.113
2.067
PPM

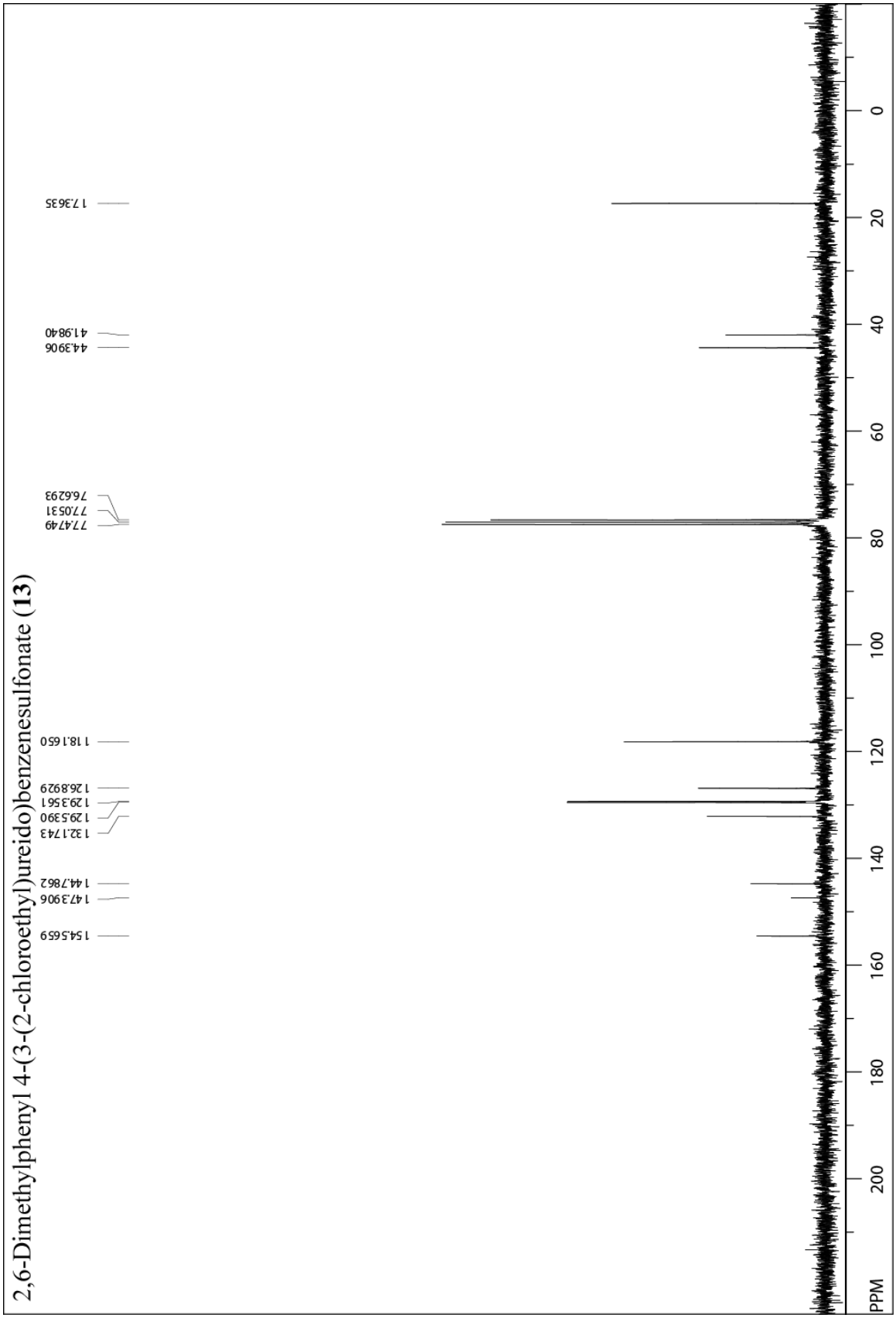
2,6-Dimethylphenyl 4-(3-(2-chloroethyl)ureido)benzenesulfonate (13)
17.3635
41.9840
44.3906
76.6293
77.0531
77.4749
118.1650
126.8929
129.3561
129.5390
132.1743
144.7862
147.3906
154.5659
PPM
200
180
160
140
120
100
80
60
40
20
0

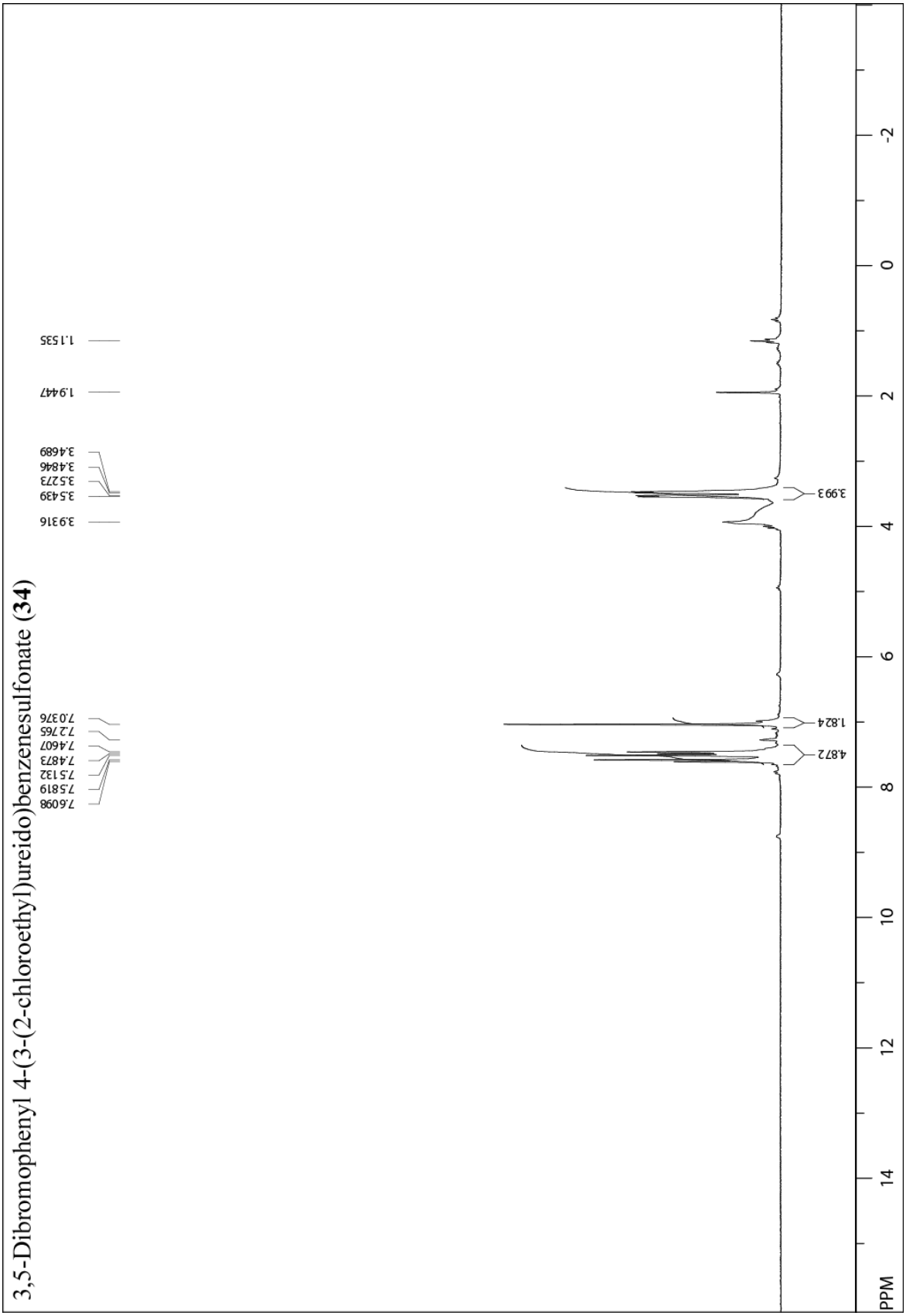
3,5-Dibromophenyl 4-(3-(2-chloroethyl)ureido)benzenesulfonate (34)
7.6098
7.5819
7.5132
7.4873
7.4607
7.2765
7.0376
3.9316
3.5439
3.5273
3.4846
3.4689
1.9447
1.1535
4.872
1.824
3.993
PPM
14
12
10
8
6
4
2
0
-2

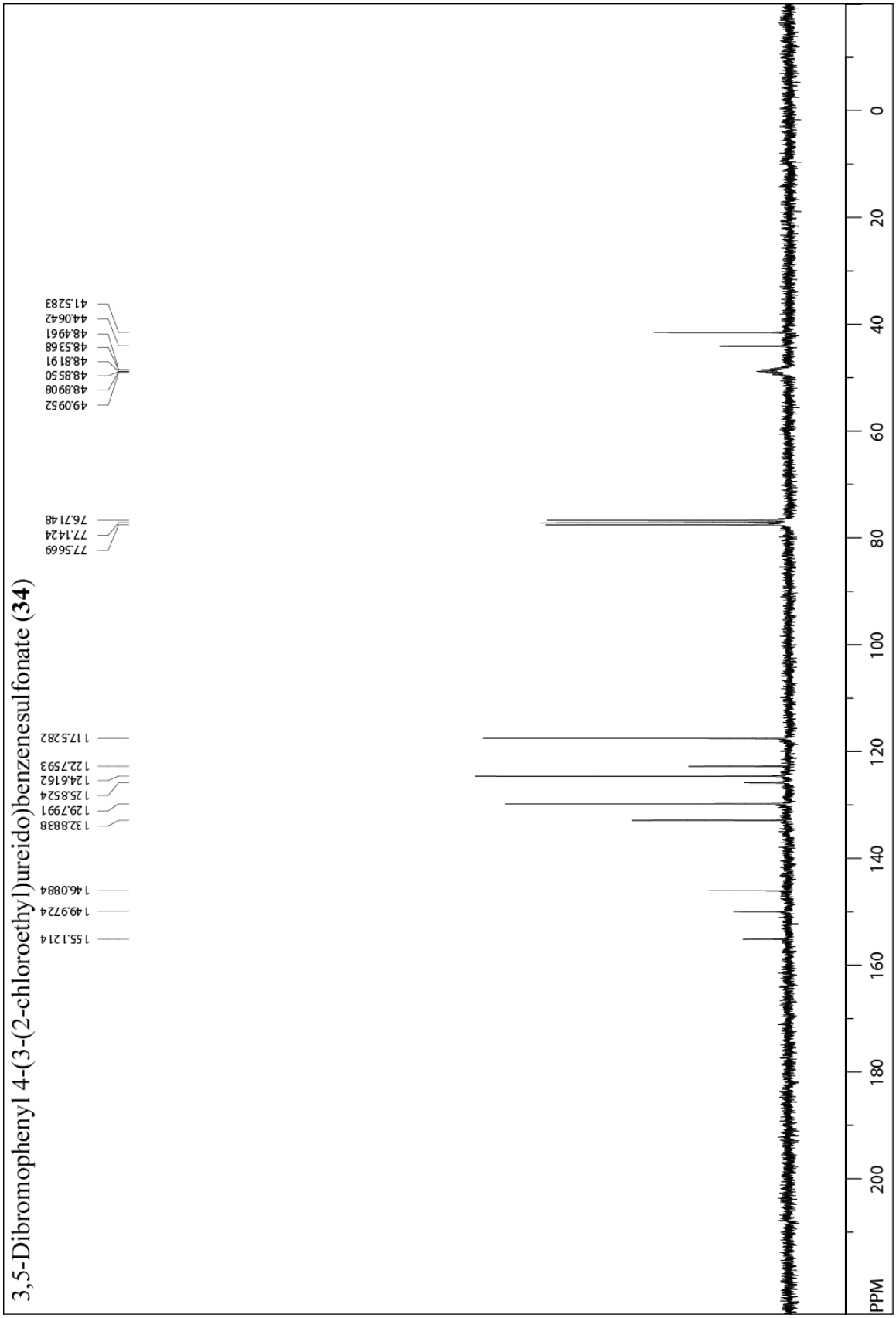
3,5-Dibromophenyl 4-(3-(2-chloroethyl)ureido)benzenesulfonate (34)
155.1214
149.9724
146.0884
132.8838
129.7991
125.8524
124.6162
122.7593
117.5282
77.5669
77.1424
76.7148
49.0952
48.8508
48.8550
48.8191
48.5368
48.4961
44.0642
41.5283
PPM
200
180
160
140
120
100
80
60
40
20
0

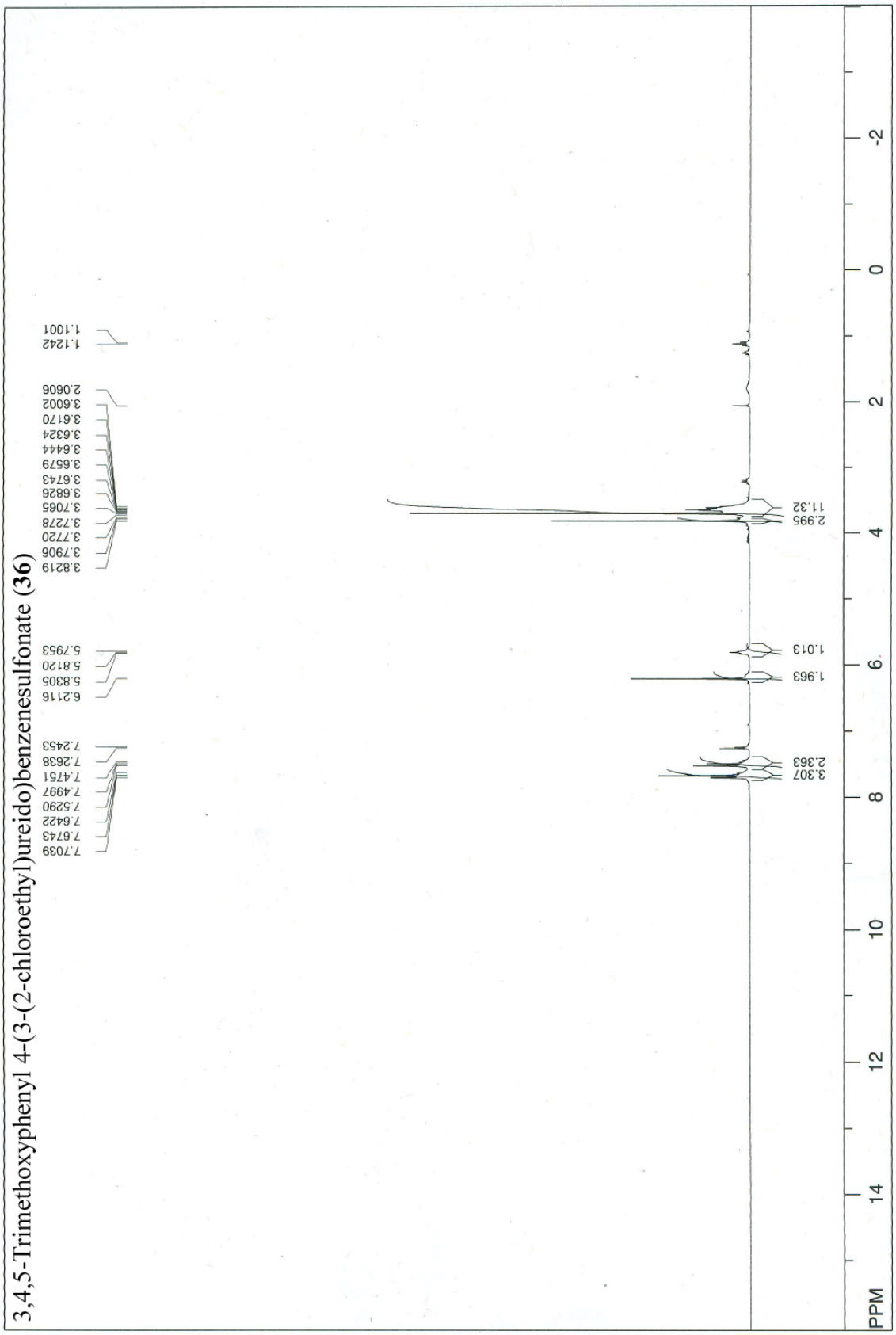
3,4,5-Trimethoxyphenyl 4-(3-(2-chloroethyl)ureido)benzenesulfonate (36)
7.7039
7.6743
7.6422
7.5290
7.4997
7.4751
7.2638
7.2453
6.2116
5.8305
5.8120
5.7953
3.8219
3.7906
3.7720
3.7278
3.7065
3.6826
3.6743
3.6579
3.6444
3.6324
3.6170
3.6002
2.0606
1.1242
1.1001
3.307
2.363
1.963
1.013
2.995
11.32
PPM
14
12
10
8
6
4
2
0
-2

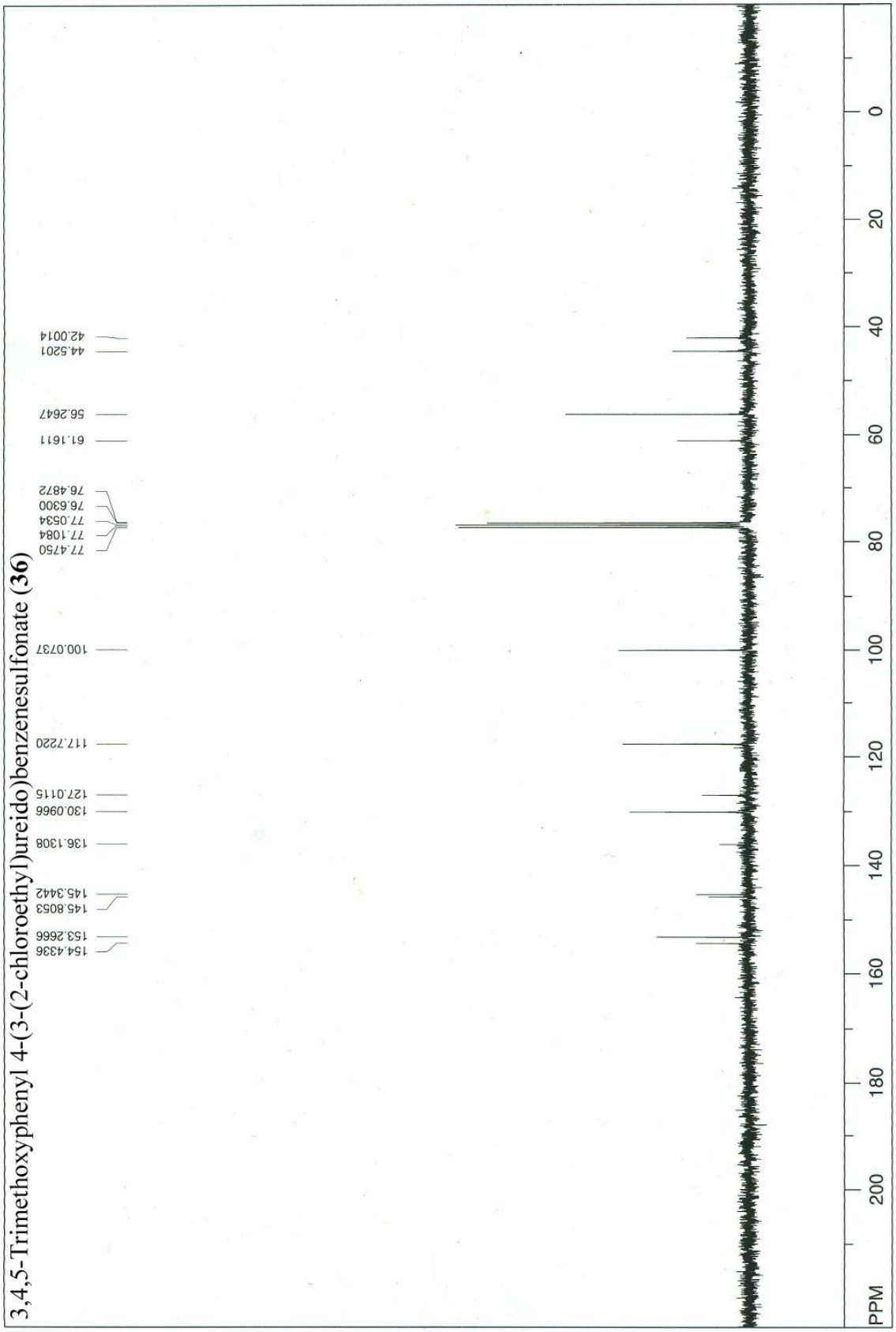
3,4,5-Trimethoxyphenyl 4-(3-(2-chloroethyl)ureido)benzenesulfonate (36)
154.4336
153.2666
145.8053
145.3442
136.1308
130.0966
127.0115
117.7220
100.0737
77.4750
77.1084
77.0534
76.6300
76.4872
61.1611
56.2647
44.5201
42.0014
PPM
200
180
160
140
120
100
80
60
40
20
0

Annexe E : Données supplémentaires du chapitre 6

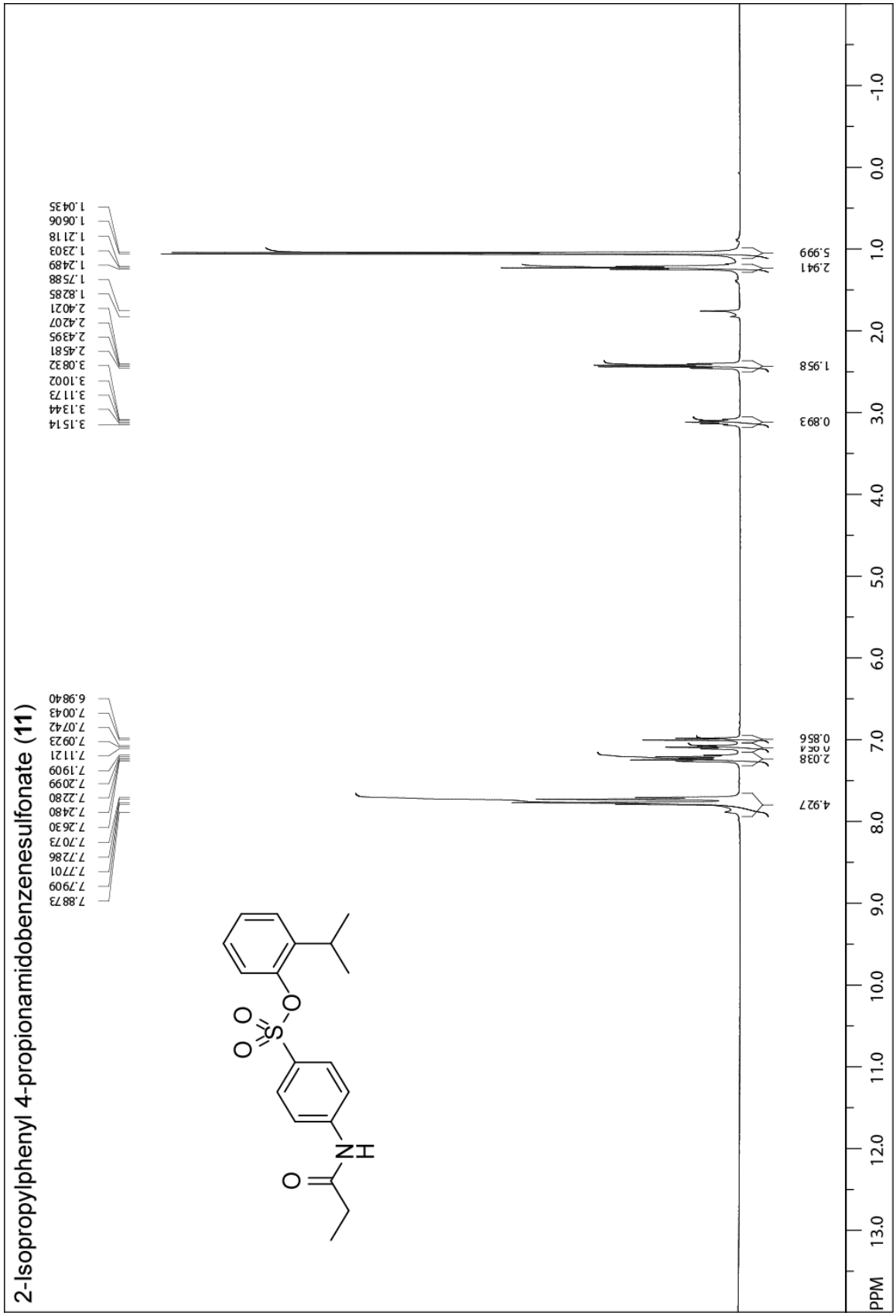
2-Isopropylphenyl 4-propionamidobenzenesulfonate (11)
7.8873
7.7909
7.7701
7.7286
7.7073
7.2630
7.2480
7.2280
7.2099
7.1909
7.1121
7.0923
7.0742
7.0043
6.9840
3.1514
3.1344
3.1173
3.1002
3.0832
2.4581
2.4395
2.4207
2.4021
1.8285
1.7588
1.2489
1.2303
1.2118
1.0606
1.0435
4.927
2.038
2.000
0.856
1.958
0.893
2.941
5.999
PPM
13.0
12.0
11.0
10.0
9.0
8.0
7.0
6.0
5.0
4.0
3.0
2.0
1.0
0.0
-1.0

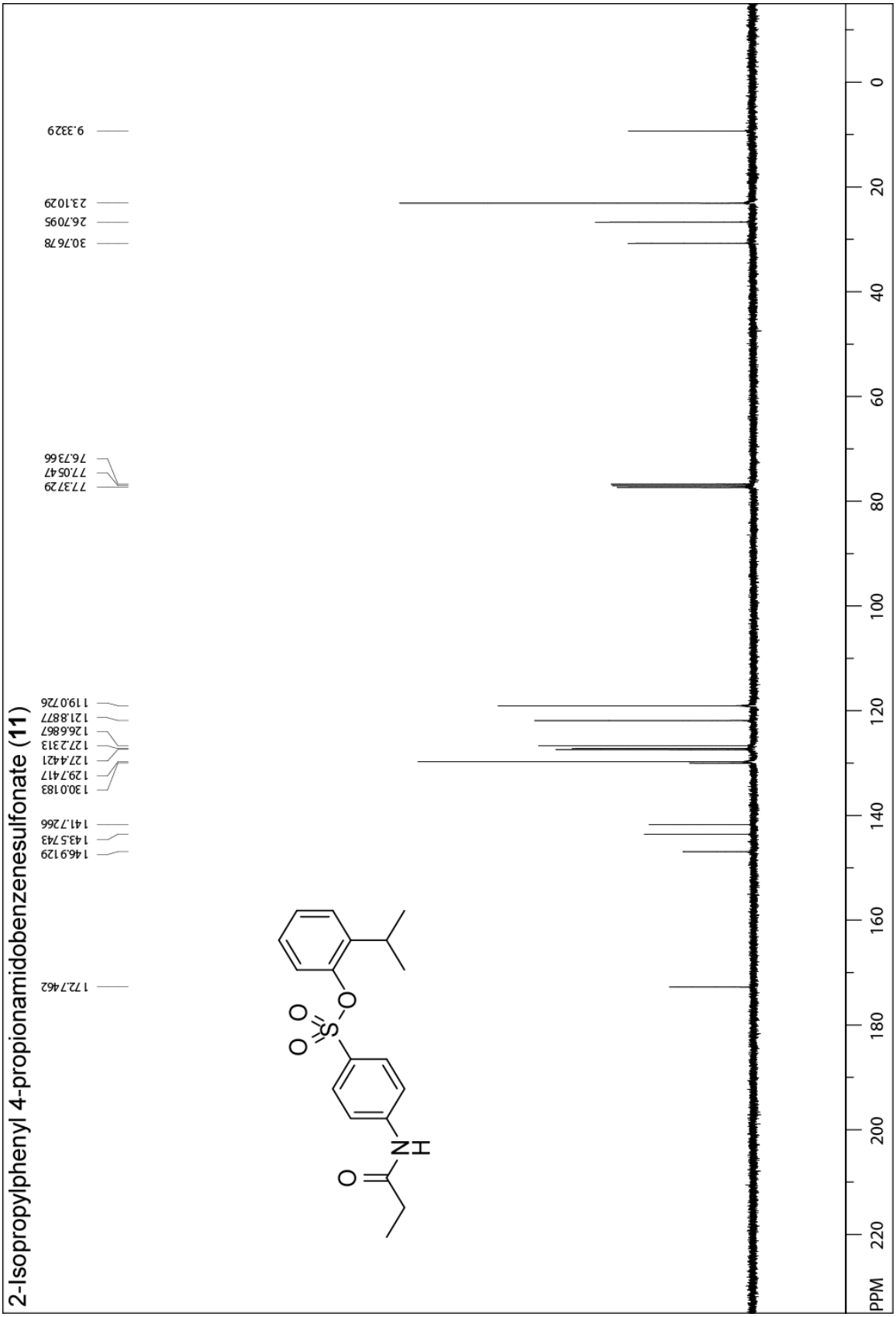
2-Isopropylphenyl 4-propionamidobenzenesulfonate (11)
9.3329
23.1029
26.7095
30.7678
76.7366
77.0547
77.3729
119.0726
121.8877
126.6867
127.2313
127.4421
129.7417
130.0183
141.7266
143.5743
146.9129
172.7462
O
O
S
O
O
N
H
O
PPM
0
20
40
60
80
100
120
140
160
180
200
220

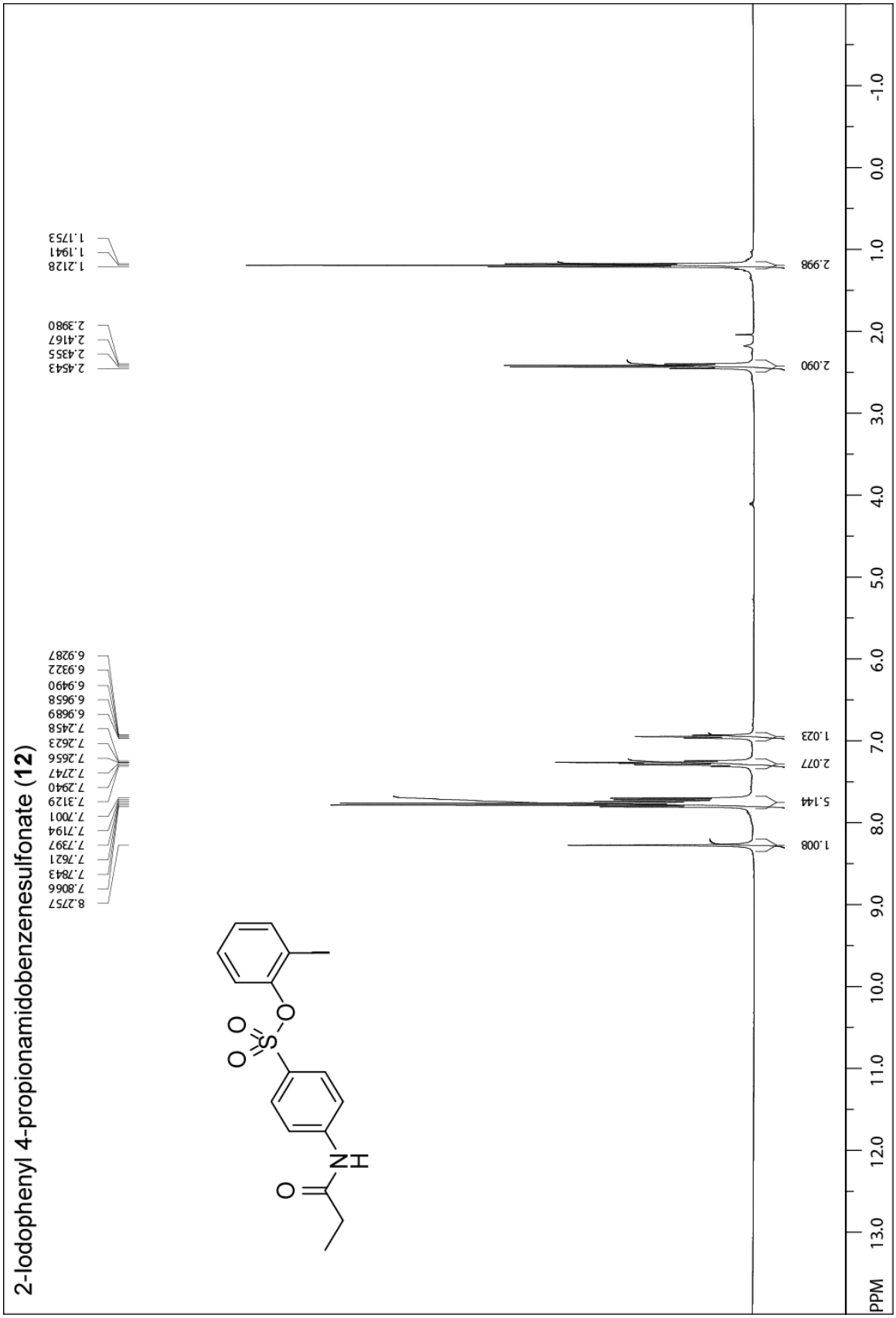
2-Iodophenyl 4-propionamidobenzenesulfonate (12)
8.2757
7.8066
7.7843
7.7621
7.7397
7.7194
7.7001
7.3129
7.2940
7.2747
7.2656
7.2623
7.2458
6.9689
6.9658
6.9490
6.9322
6.9287
2.4543
2.4355
2.4167
2.3980
1.2128
1.1941
1.1753
1.008
5.144
2.077
1.023
2.090
2.998
PPM
13.0
12.0
11.0
10.0
9.0
8.0
7.0
6.0
5.0
4.0
3.0
2.0
1.0
0.0
-1.0

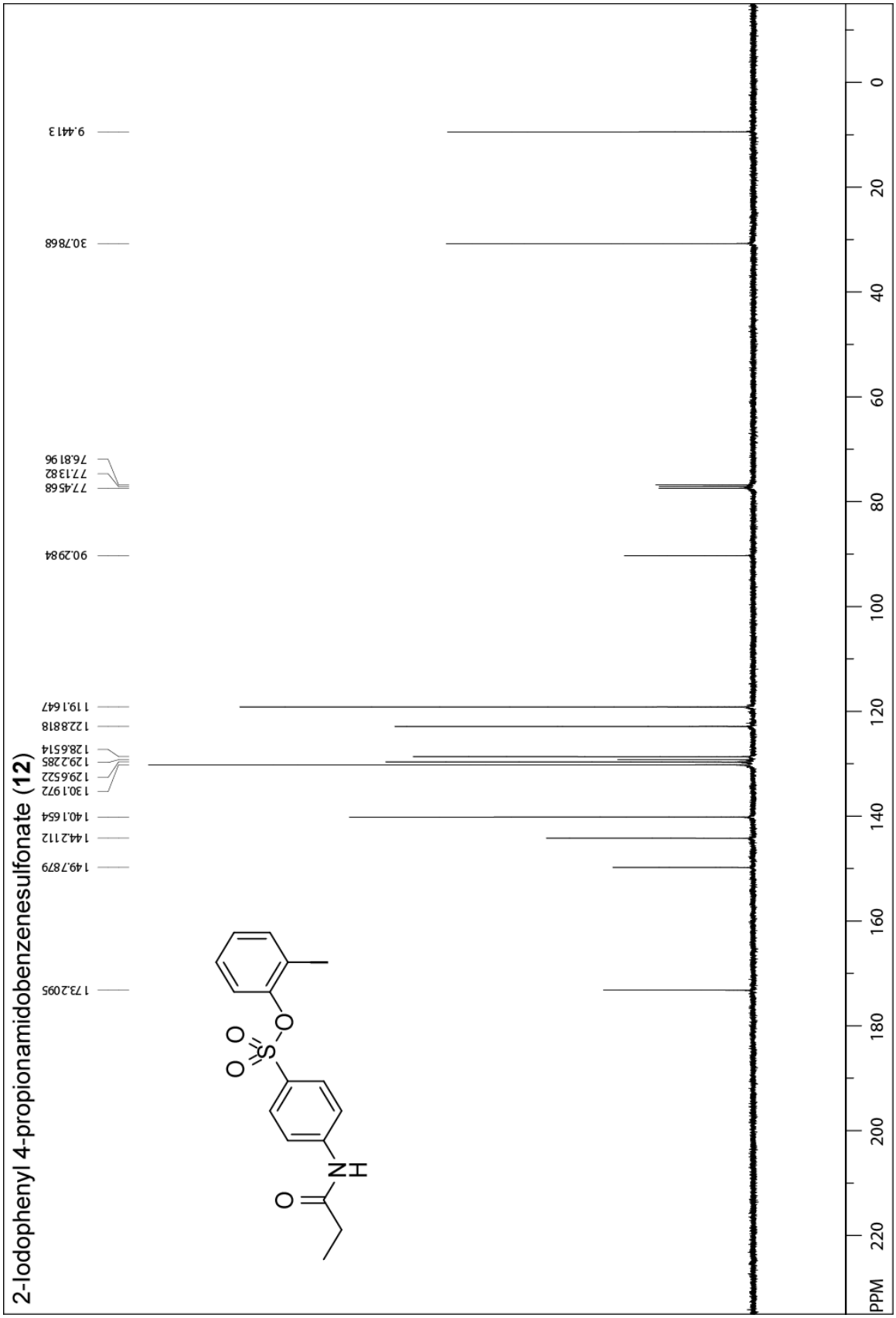
2-Iodophenyl 4-propionamidobenzenesulfonate (12)
9.4413
30.7868
76.8196
77.1382
77.4568
90.2984
119.1647
122.8818
128.6514
129.2285
129.6522
130.1972
140.1654
144.2112
149.7879
173.2095
PPM
0
20
40
60
80
100
120
140
160
180
200
220

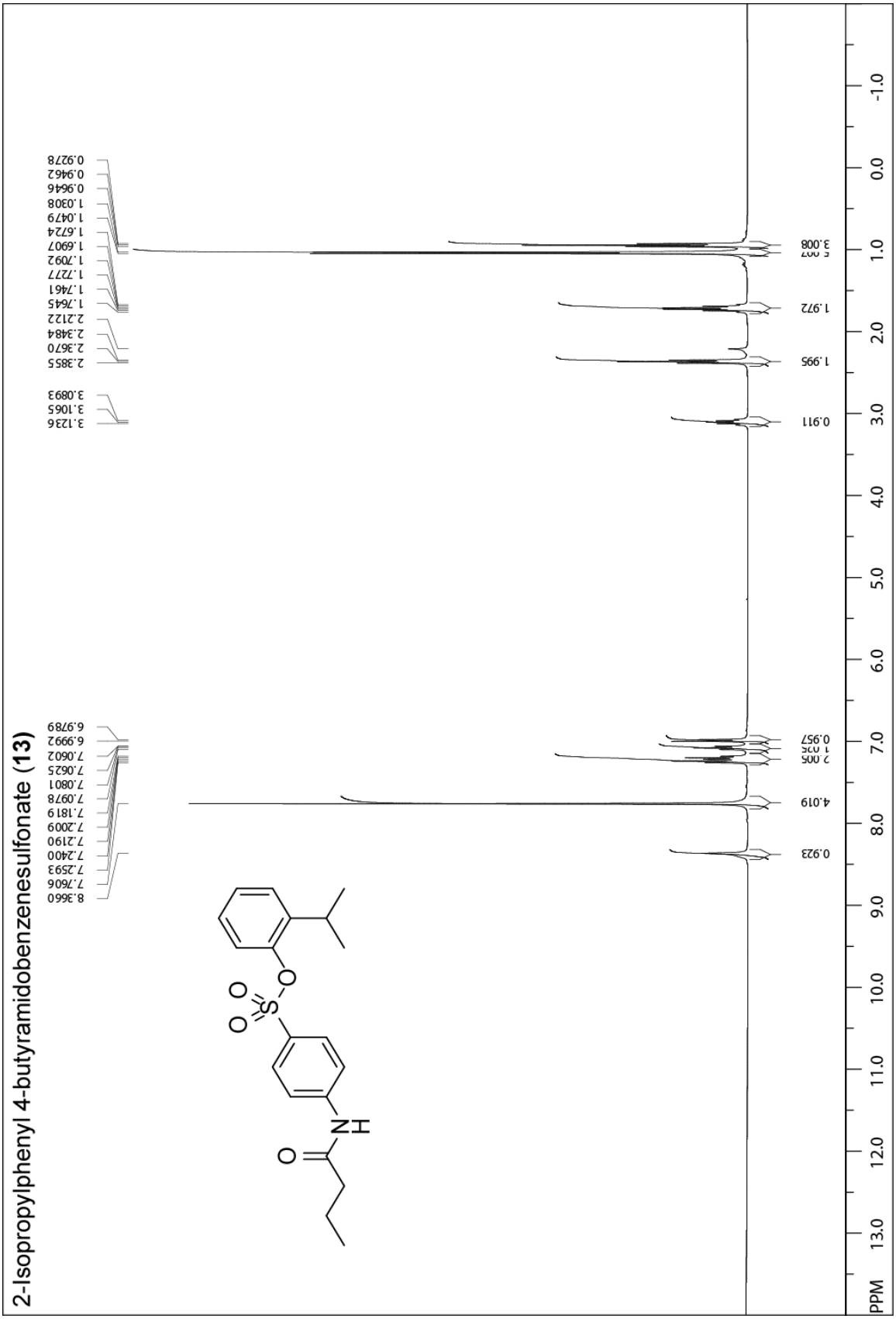
2-Isopropylphenyl 4-butyramidobenzenesulfonate (13)
8.3660
7.7606
7.2593
7.2400
7.2190
7.2009
7.1819
7.0978
7.0801
7.0625
7.0602
6.9992
6.9789
3.1236
3.1065
3.0893
2.3855
2.3670
2.3484
2.2122
1.7645
1.7461
1.7277
1.7092
1.6907
1.6724
1.0479
1.0308
0.9646
0.9462
0.9278
0.923
4.019
0.957
1.995
1.972
0.911
3.008
PPM
13.0
12.0
11.0
10.0
9.0
8.0
7.0
6.0
5.0
4.0
3.0
2.0
1.0
0.0
-1.0

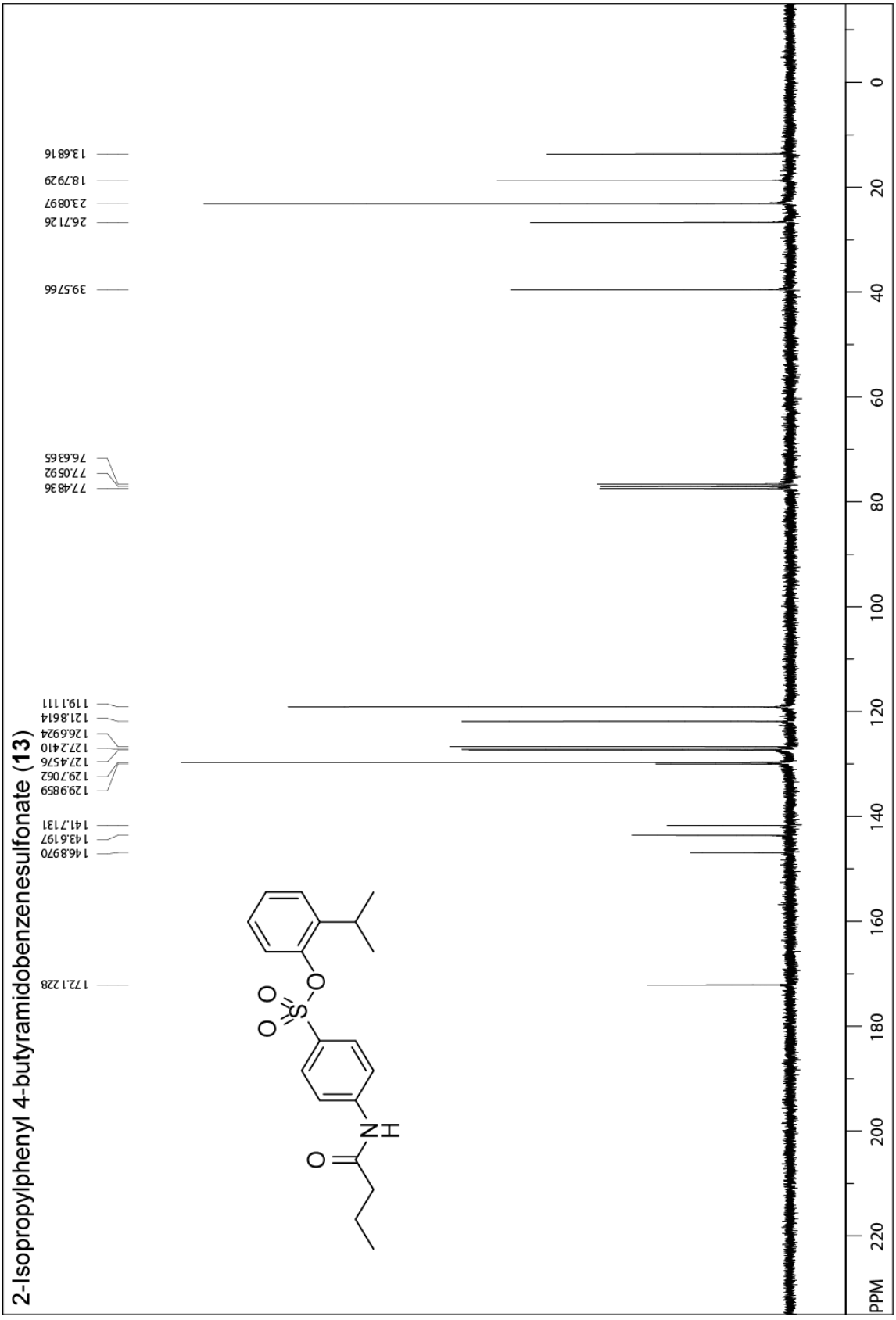
2-Isopropylphenyl 4-butyramidobenzenesulfonate (13)
172.1228
146.8970
143.6197
141.7131
129.9859
129.7062
127.4576
127.2410
126.6924
121.8614
119.1111
77.4836
77.0592
76.6365
39.5766
26.7126
23.0897
18.7929
13.6816
PPM
0
20
40
60
80
100
120
140
160
180
200
220

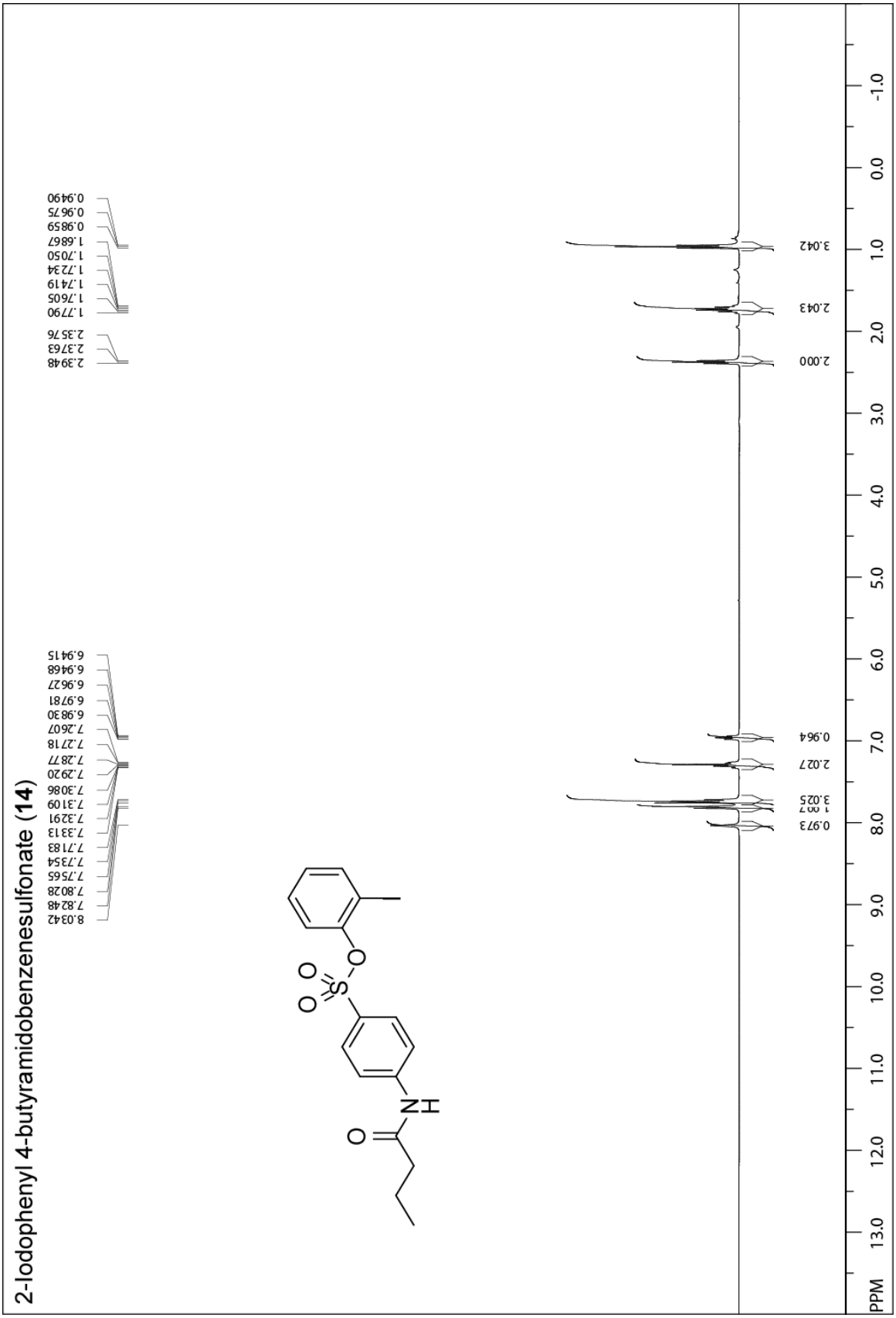
2-Iodophenyl 4-butyramidobenzenesulfonate (14)
8.0342
7.8248
7.8028
7.7565
7.7354
7.7183
7.3313
7.3291
7.3109
7.3086
7.2920
7.2877
7.2718
7.2607
6.9830
6.9781
6.9627
6.9468
6.9415
2.3948
2.3763
2.3576
1.7790
1.7605
1.7419
1.7234
1.7050
1.6867
0.9859
0.9675
0.9490
0.973
1.007
3.025
2.027
0.964
2.000
2.043
3.042
PPM

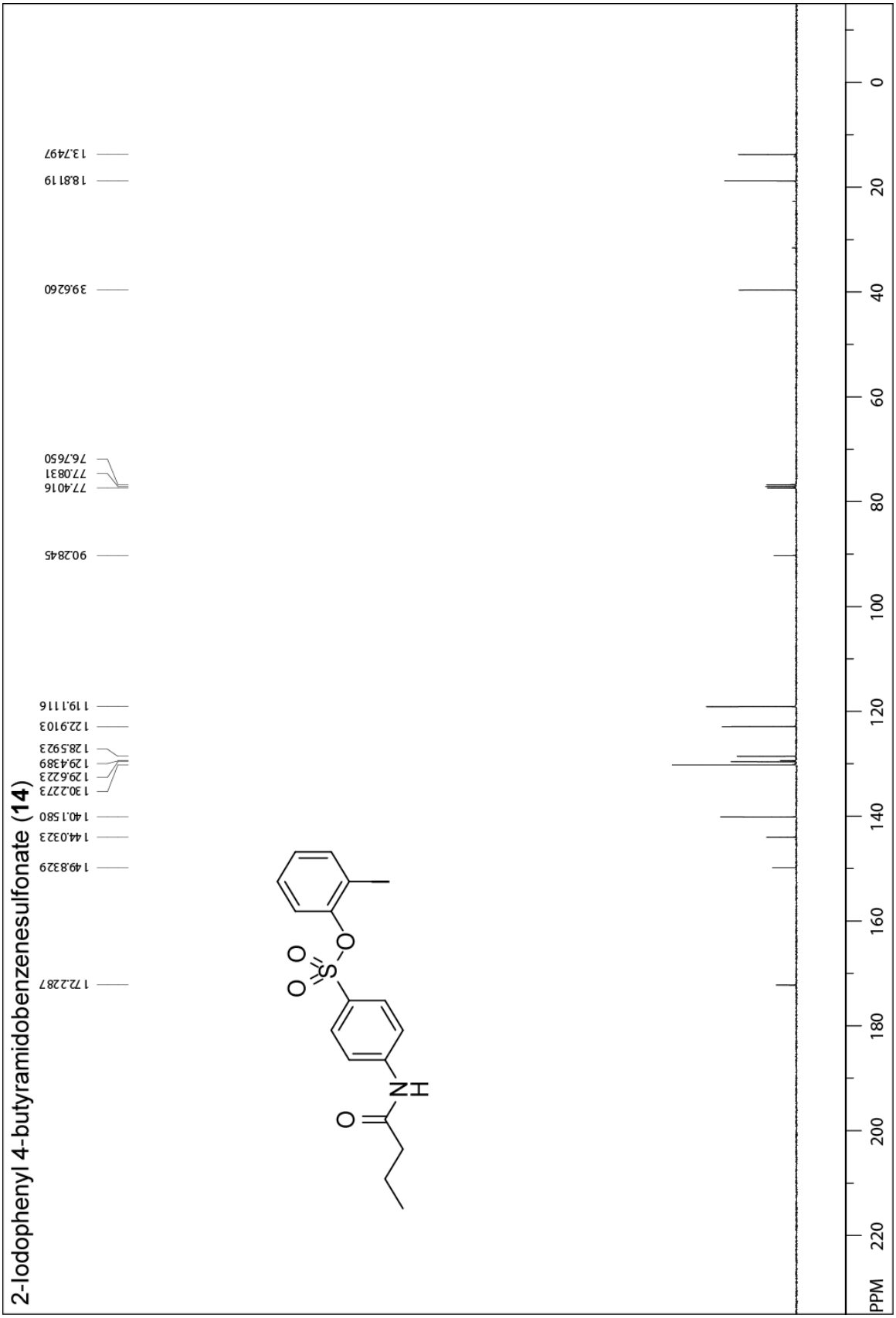
2-Iodophenyl 4-butyramidobenzenesulfonate (14)
172.2287
149.8329
144.0323
140.1580
130.2273
129.6223
129.4389
128.5923
122.9103
119.1116
90.2845
77.4016
77.0831
76.7650
39.6260
18.8119
13.7497
PPM
0
20
40
60
80
100
120
140
160
180
200
220

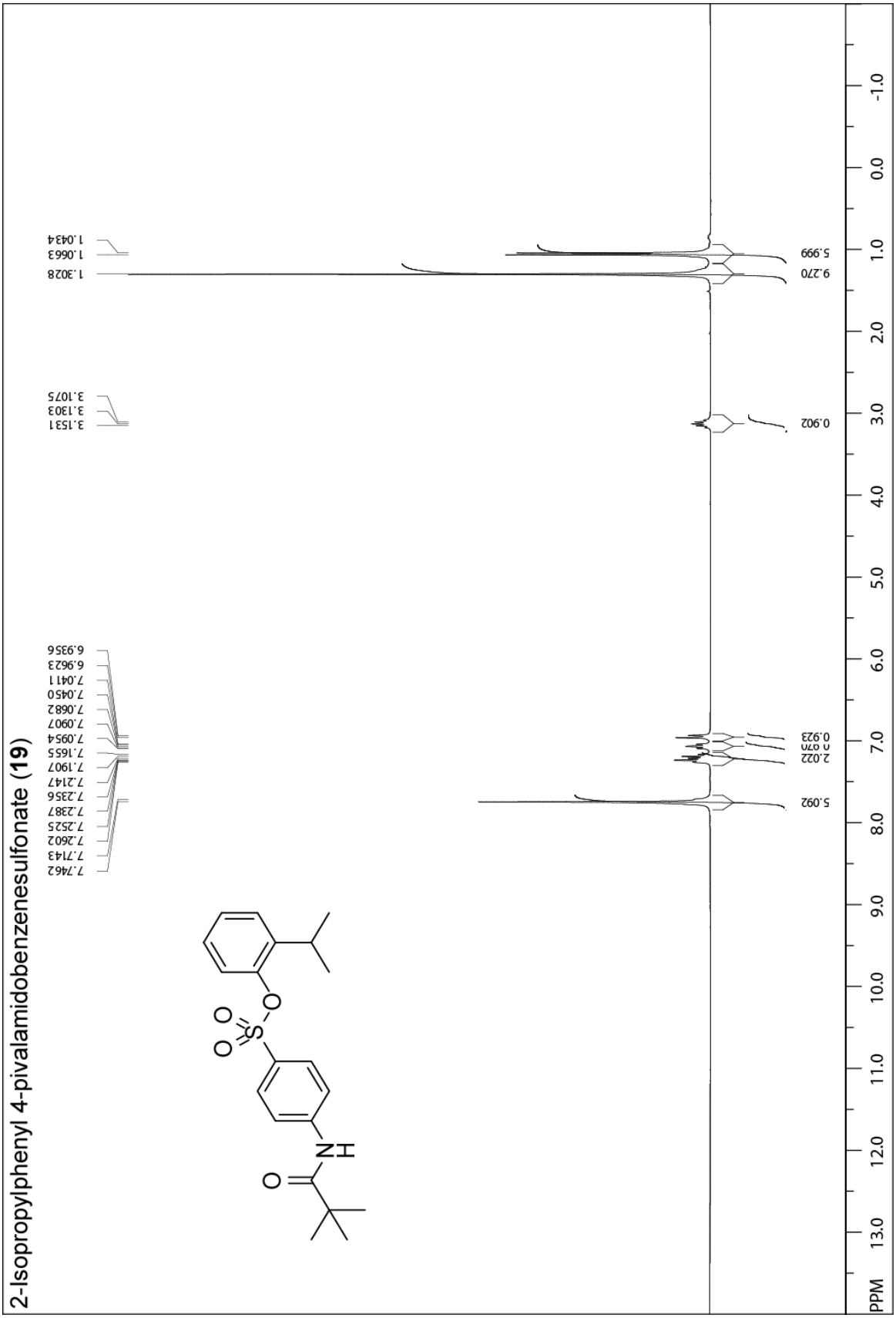
2-Isopropylphenyl 4-pivalamidobenzenesulfonate (19)
7.7462
7.7143
7.2602
7.2525
7.2387
7.2356
7.2147
7.1907
7.1655
7.0954
7.0907
7.0682
7.0450
7.0411
6.9623
6.9356
3.1531
3.1303
3.1075
1.3028
1.0663
1.0434
5.092
2.022
0.973
0.923
0.902
9.270
5.999
PPM
13.0
12.0
11.0
10.0
9.0
8.0
7.0
6.0
5.0
4.0
3.0
2.0
1.0
0.0
-1.0

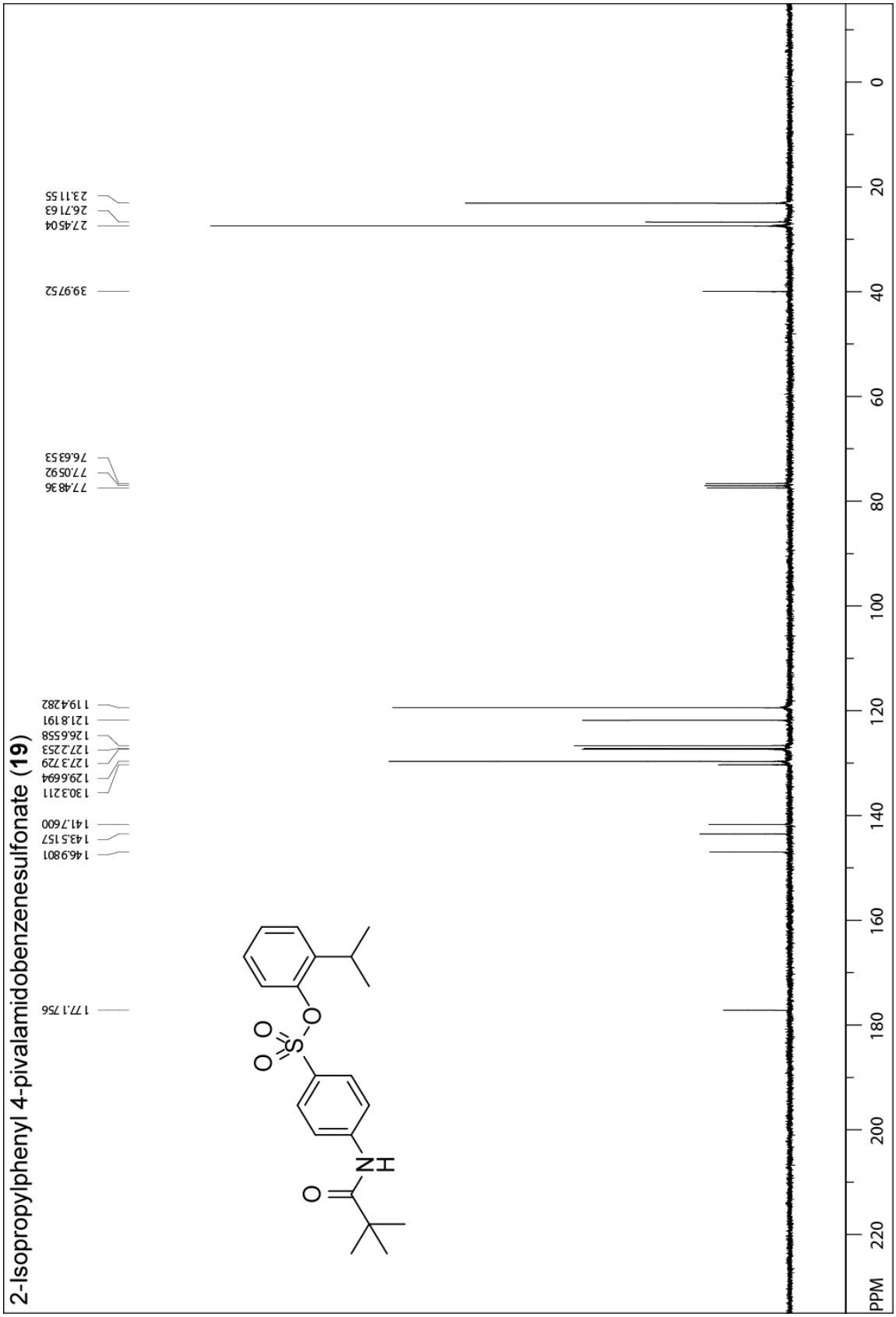
2-Isopropylphenyl 4-pivalamidobenzenesulfonate (19)
177.1756
146.9801
143.5157
141.7600
130.3211
129.6694
127.3729
127.2253
126.6558
121.8191
119.4282
77.4836
77.0592
76.6353
39.9752
27.4504
26.7163
23.1155
PPM
0
20
40
60
80
100
120
140
160
180
200
220

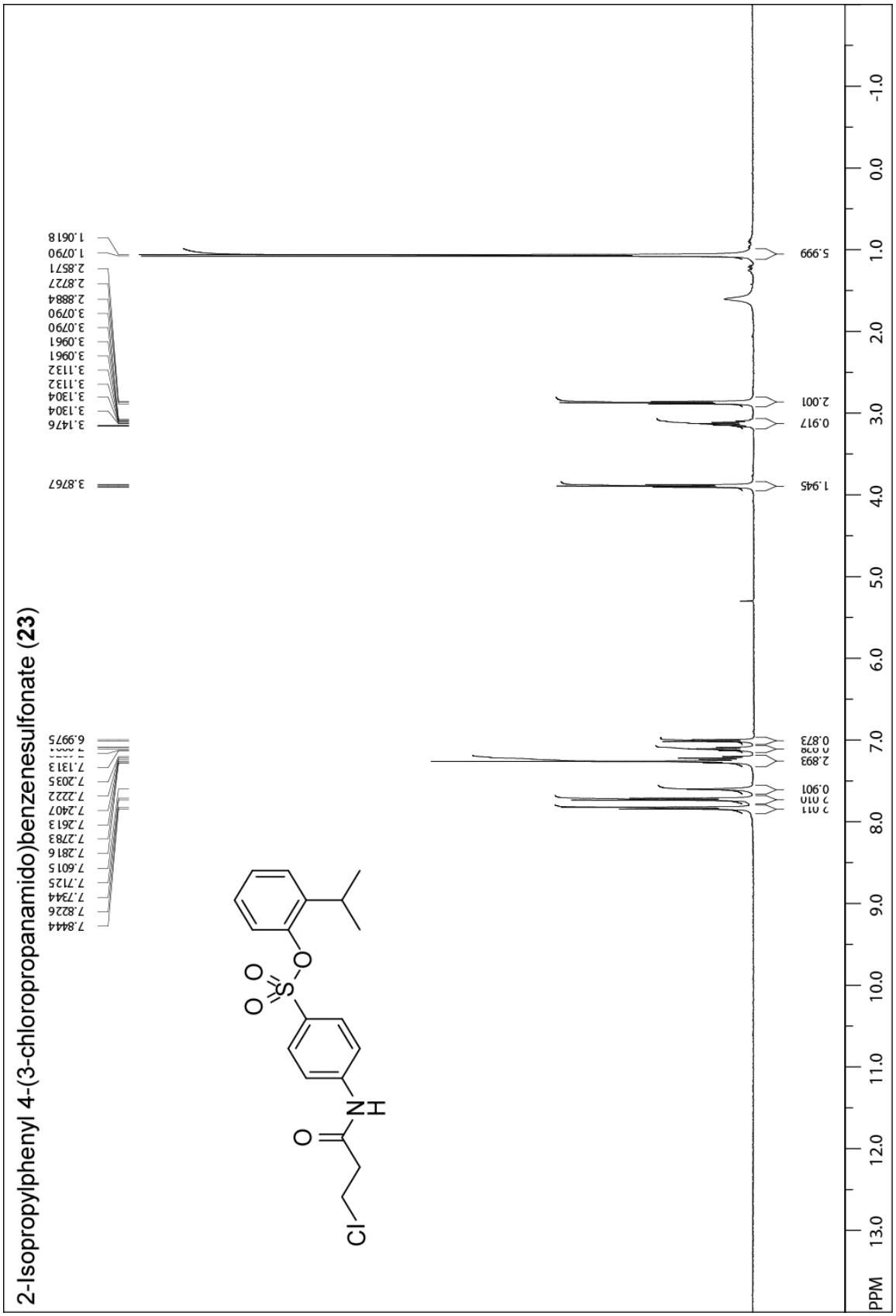
2-Isopropylphenyl 4-(3-chloropropanamido)benzenesulfonate (23)
PPM
13.0
12.0
11.0
10.0
9.0
8.0
7.0
6.0
5.0
4.0
3.0
2.0
1.0
0.0
-1.0
1.0618
1.0790
2.8571
2.8727
2.8884
3.0790
3.0790
3.0961
3.0961
3.1132
3.1132
3.1304
3.1304
3.1476
3.8767
5.999
2.001
0.917
1.945
6.9975
7.1313
7.2035
7.2222
7.2407
7.2613
7.2783
7.2816
7.6015
7.7125
7.7344
7.8226
7.8444
0.873
2.893
0.901
O
O
S
O
O
H
N
O
Cl

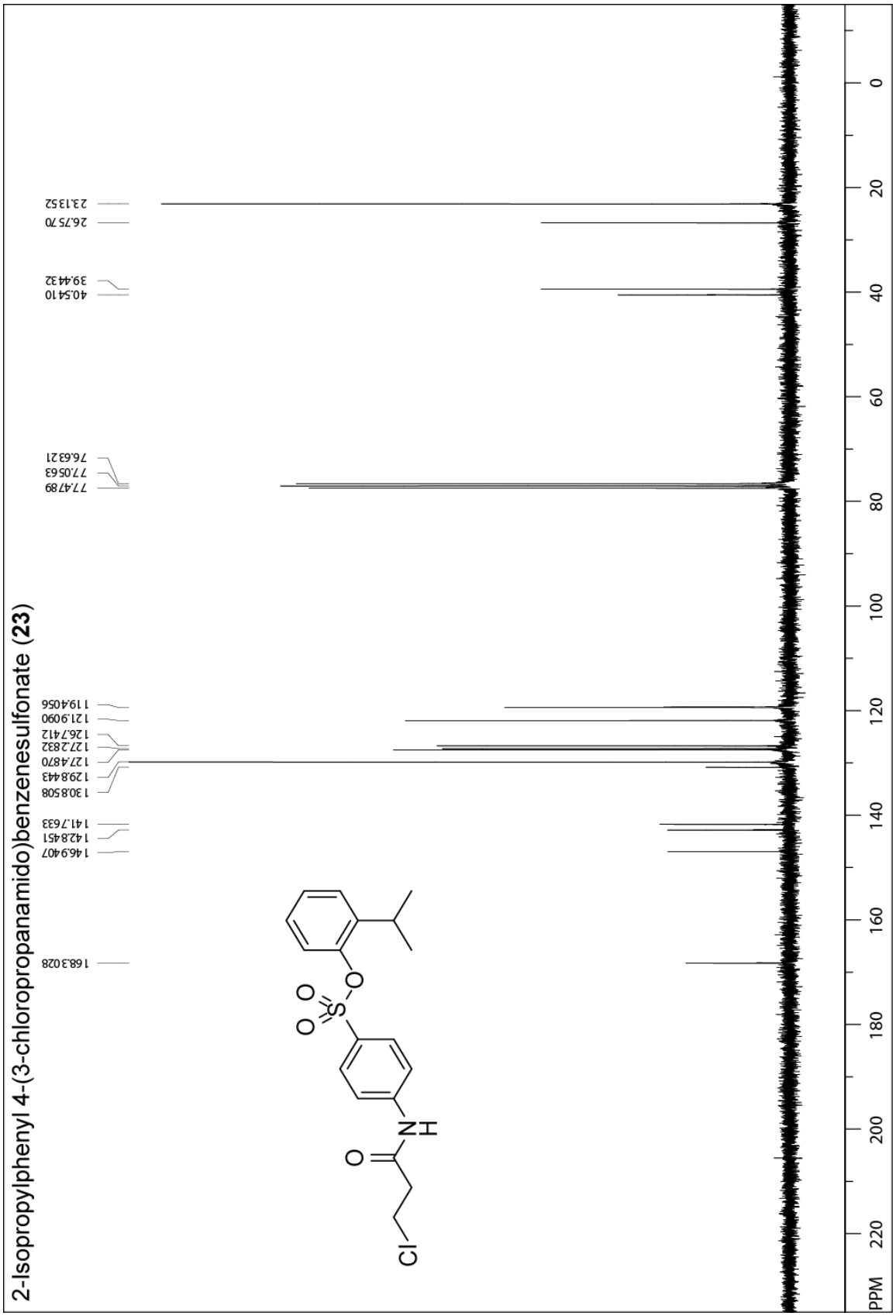
2-Isopropylphenyl 4-(3-chloropropanamido)benzenesulfonate (23)
168.3028
146.9407
142.8451
141.7633
130.8508
129.8443
127.4870
127.2832
126.7412
121.9090
119.4056
77.4789
77.0563
76.6321
40.5410
39.4432
26.7570
23.1352
PPM
0
20
40
60
80
100
120
140
160
180
200
220
O
O
S
O
H
N
O
Cl

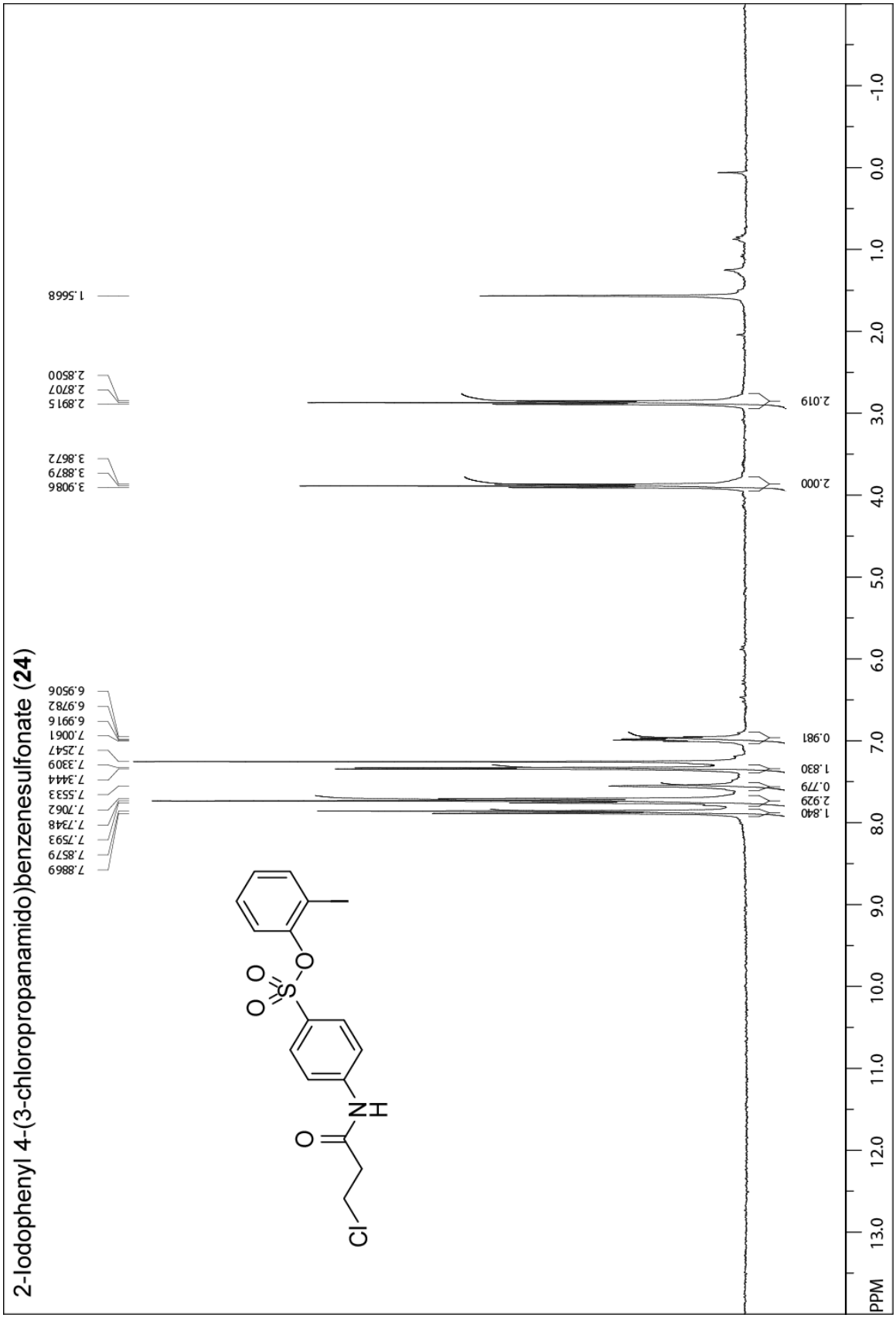
2-Iodophenyl 4-(3-chloropropanamido)benzenesulfonate (24)
7.8869
7.8579
7.7593
7.7348
7.7062
7.5533
7.3444
7.3309
7.2547
7.0061
6.9916
6.9782
6.9506
3.9086
3.8879
3.8672
2.8915
2.8707
2.8500
1.5668
1.840
2.929
0.779
1.830
0.981
2.000
2.019
PPM
13.0
12.0
11.0
10.0
9.0
8.0
7.0
6.0
5.0
4.0
3.0
2.0
1.0
0.0
-1.0

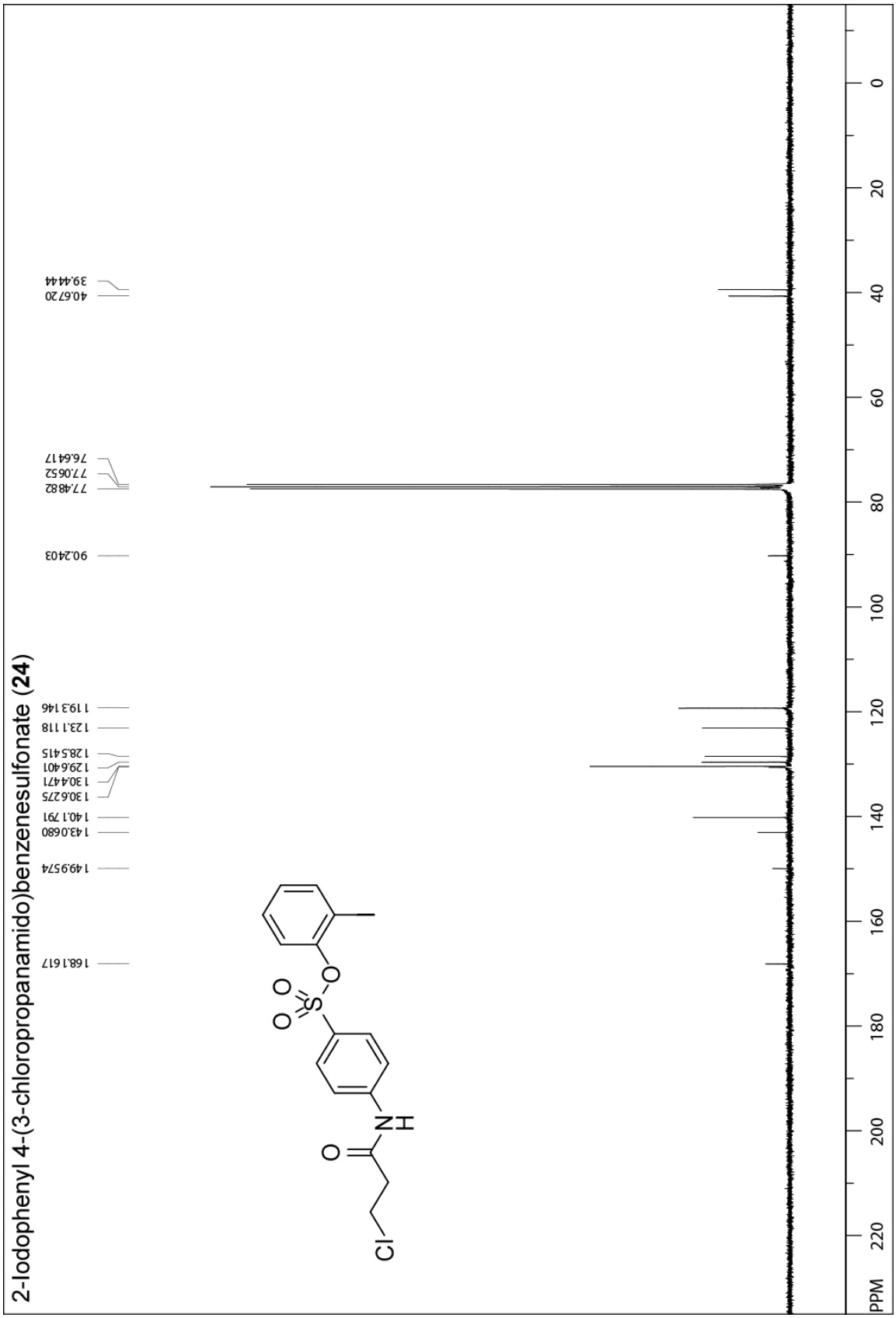
2-Iodophenyl 4-(3-chloropropanamido)benzenesulfonate (24)
168.1617
149.9574
143.0680
140.1791
130.6275
130.4471
129.6401
128.5415
123.1118
119.3146
90.2403
77.4882
77.0652
76.6417
40.6720
39.4444
PPM
0
20
40
60
80
100
120
140
160
180
200
220

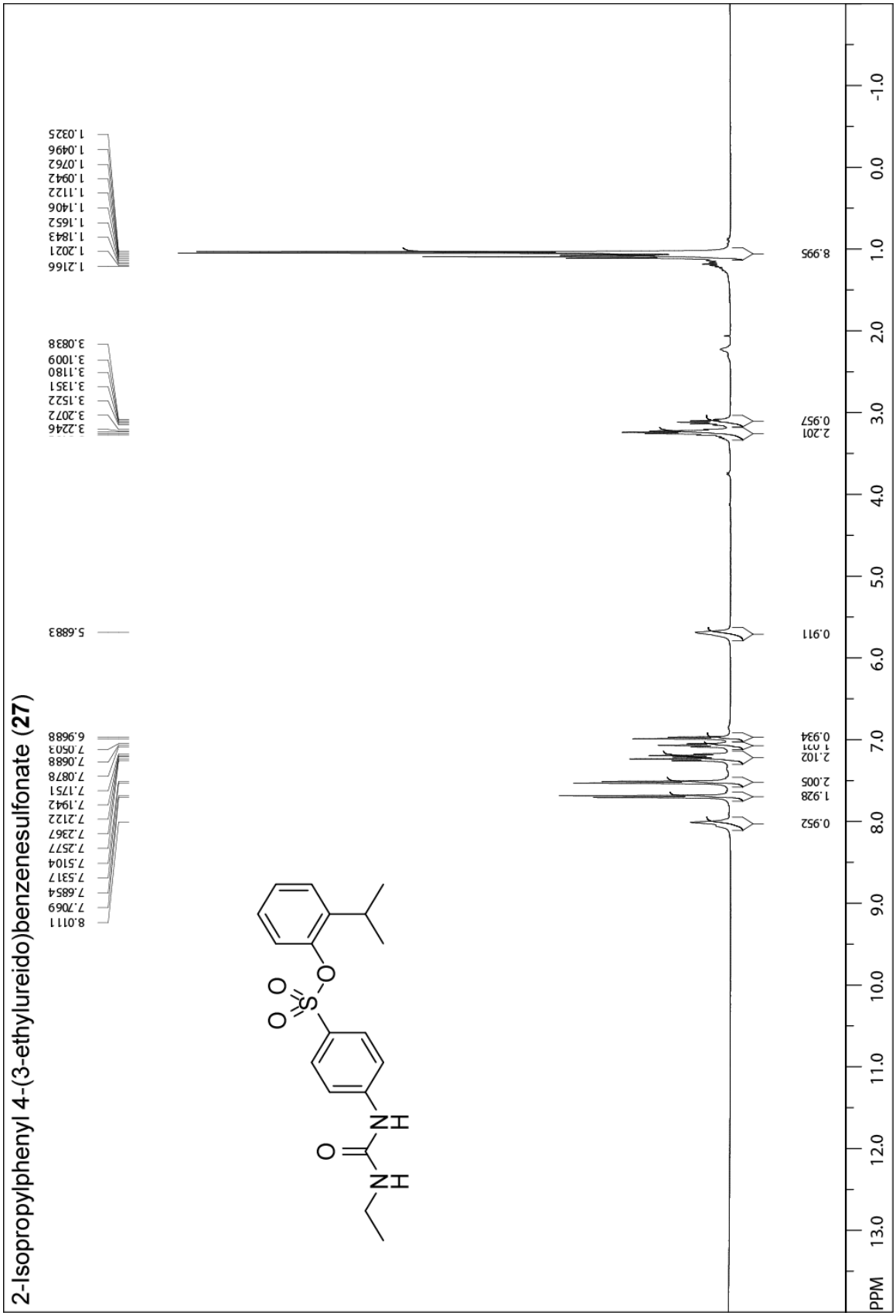
2-Isopropylphenyl 4-(3-ethylureido)benzenesulfonate (27)
PPM
13.0
12.0
11.0
10.0
9.0
8.0
7.0
6.0
5.0
4.0
3.0
2.0
1.0
0.0
-1.0
0.952
1.928
2.005
2.102
1.071
0.934
0.911
2.201
0.957
8.995
5.6883
8.0111
7.7069
7.6854
7.5317
7.5104
7.2577
7.2367
7.2122
7.1942
7.1751
7.0878
7.0688
7.0503
6.9688
3.2246
3.2072
3.1522
3.1351
3.1180
3.1009
3.0838
1.2166
1.2021
1.1843
1.1652
1.1406
1.1122
1.0942
1.0762
1.0496
1.0325

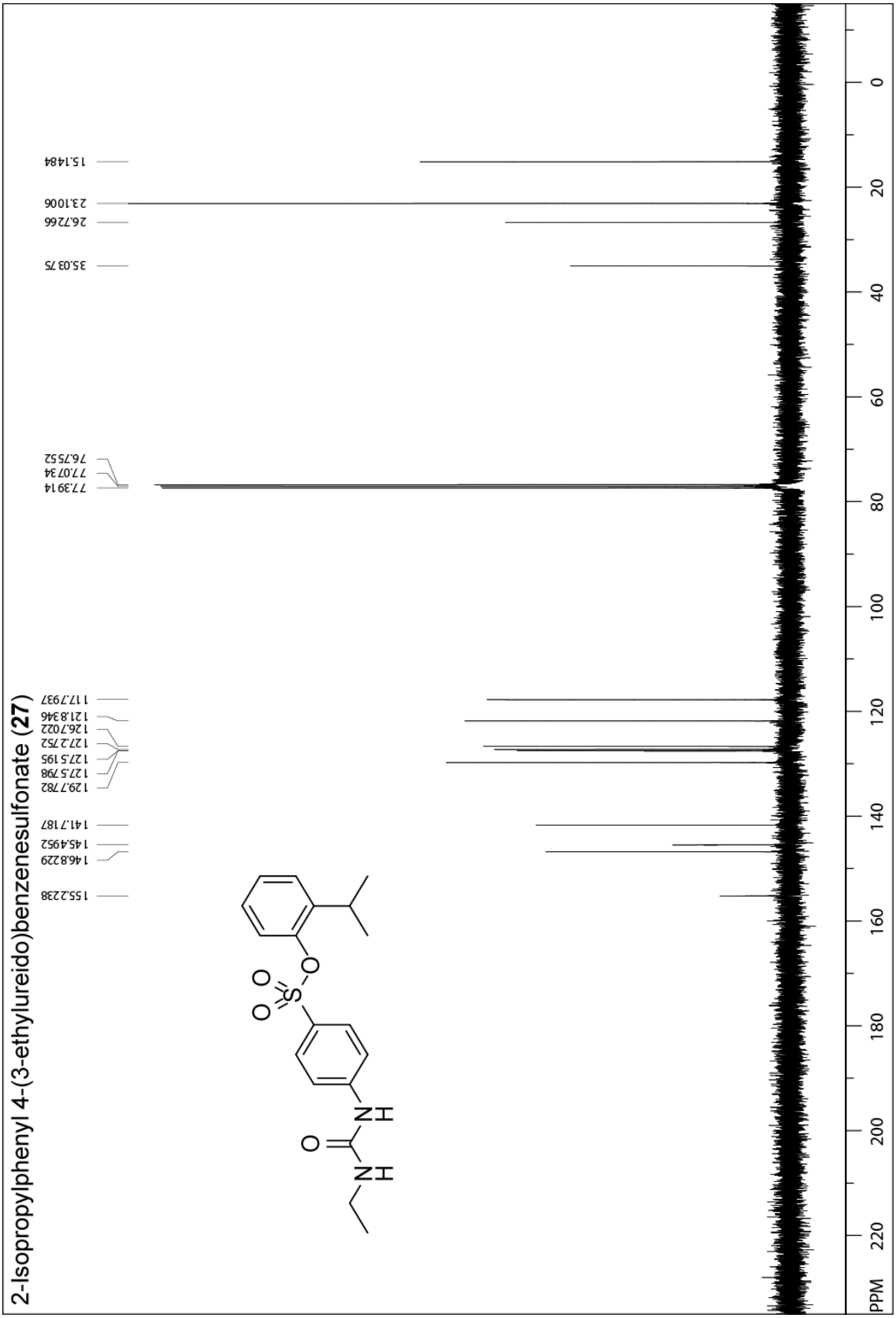
2-Isopropylphenyl 4-(3-ethylureido)benzenesulfonate (27)
155.2238
146.8229
145.4952
141.7187
129.7782
127.5798
127.5195
127.2752
126.7022
121.8346
117.7937
77.3914
77.0734
76.7552
35.0375
26.7266
23.1006
15.1484
PPM
0
20
40
60
80
100
120
140
160
180
200
220

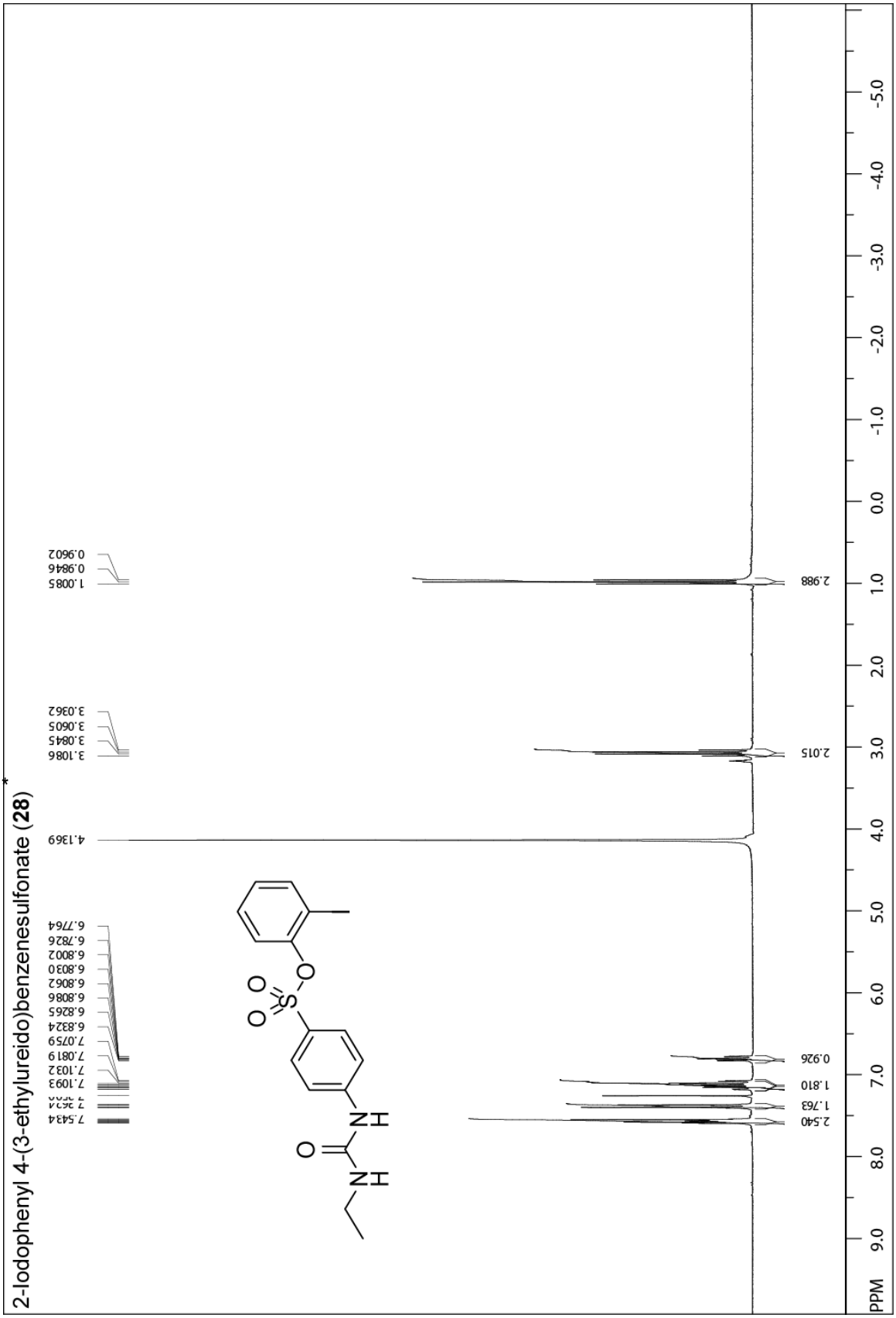
2-Iodophenyl 4-(3-ethylureido)benzenesulfonate (28)
*
7.5434
7.3624
7.3609
7.1093
7.1032
7.0819
7.0759
6.8324
6.8265
6.8086
6.8062
6.8030
6.8002
6.7826
6.7764
4.1369
3.1086
3.0845
3.0605
3.0362
1.0085
0.9846
0.9602
2.540
1.763
1.810
0.926
2.015
2.988
PPM
9.0
8.0
7.0
6.0
5.0
4.0
3.0
2.0
1.0
0.0
-1.0
-2.0
-3.0
-4.0
-5.0

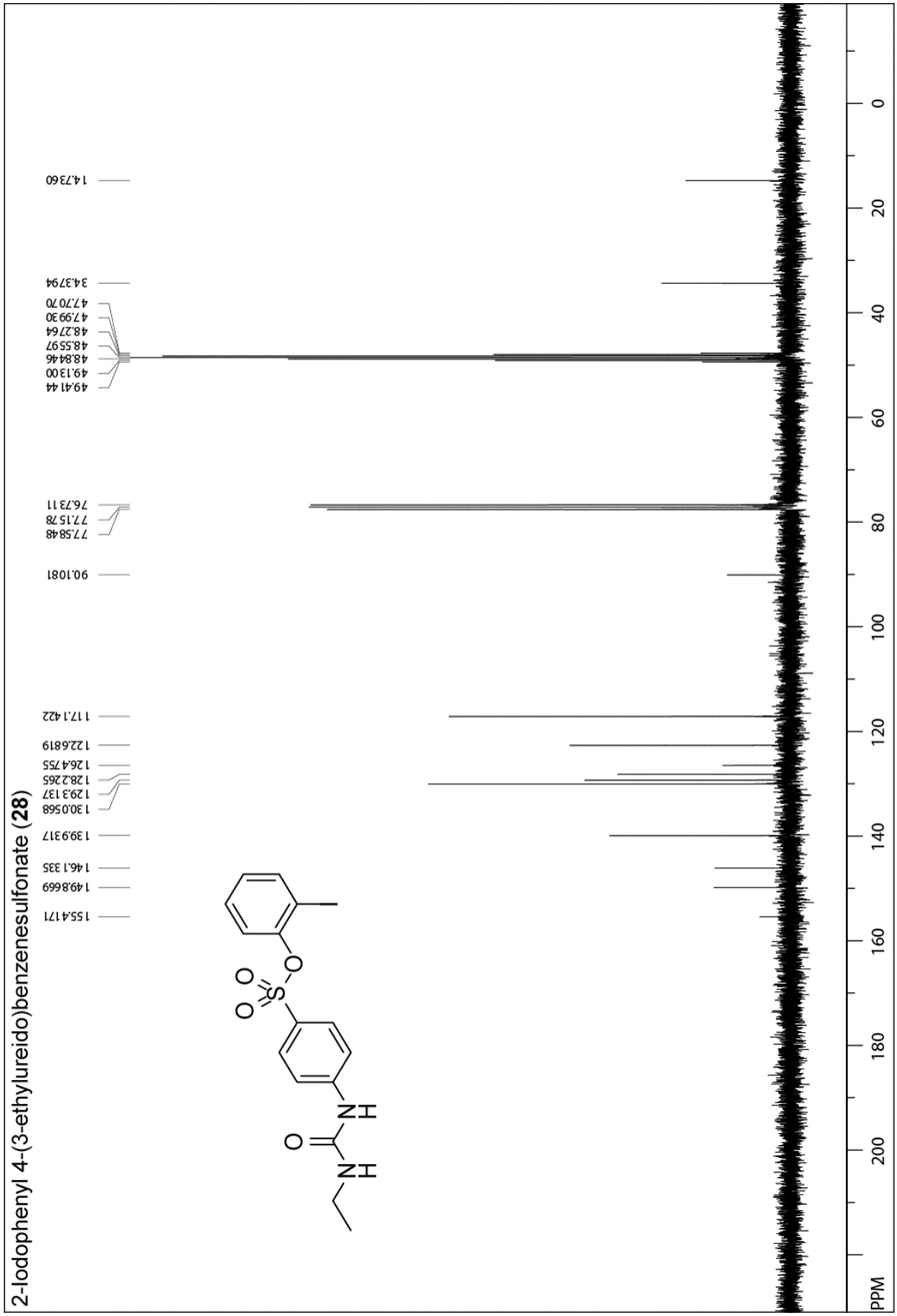
2-Iodophenyl 4-(3-ethylureido)benzenesulfonate (28)
155.4171
149.8669
146.1335
139.9317
130.0568
129.3137
128.2265
126.4755
122.6819
117.1422
90.1081
77.5848
77.1578
76.7311
49.4144
49.1300
48.8446
48.5597
48.2764
47.9930
47.7070
34.3794
14.7360
PPM
0
20
40
60
80
100
120
140
160
180
200

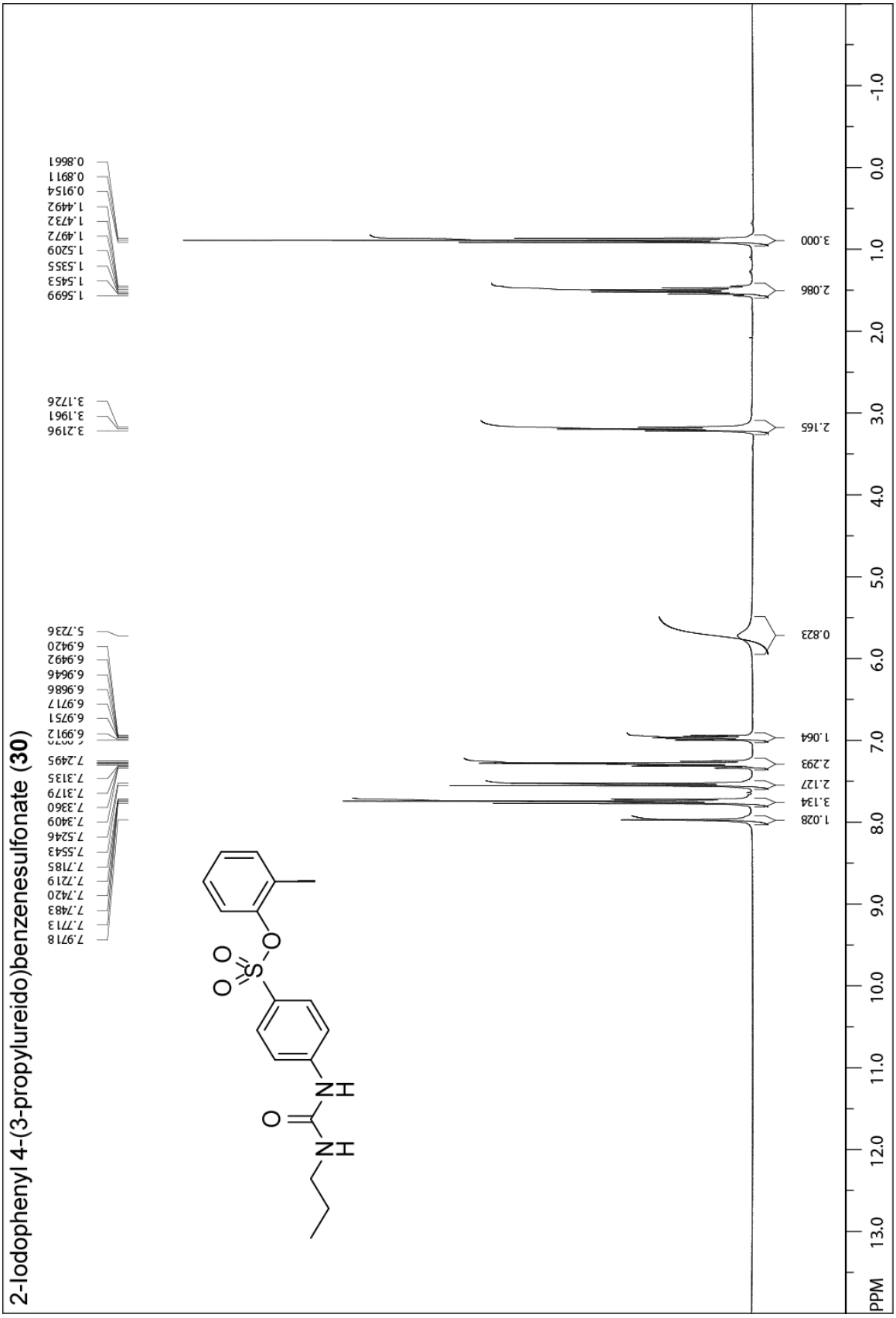
2-Iodophenyl 4-(3-propylureido)benzenesulfonate (30)
7.9718
7.7713
7.7483
7.7420
7.7219
7.7185
7.5543
7.5246
7.3409
7.3360
7.3179
7.3135
7.2495
6.9912
6.9751
6.9717
6.9686
6.9646
6.9492
6.9420
5.7236
3.2196
3.1961
3.1726
1.5699
1.5453
1.5355
1.5209
1.4972
1.4732
1.4492
0.9154
0.8911
0.8661
3.000
2.086
2.165
0.823
1.064
2.293
2.127
3.134
1.028
PPM
13.0
12.0
11.0
10.0
9.0
8.0
7.0
6.0
5.0
4.0
3.0
2.0
1.0
0.0
-1.0

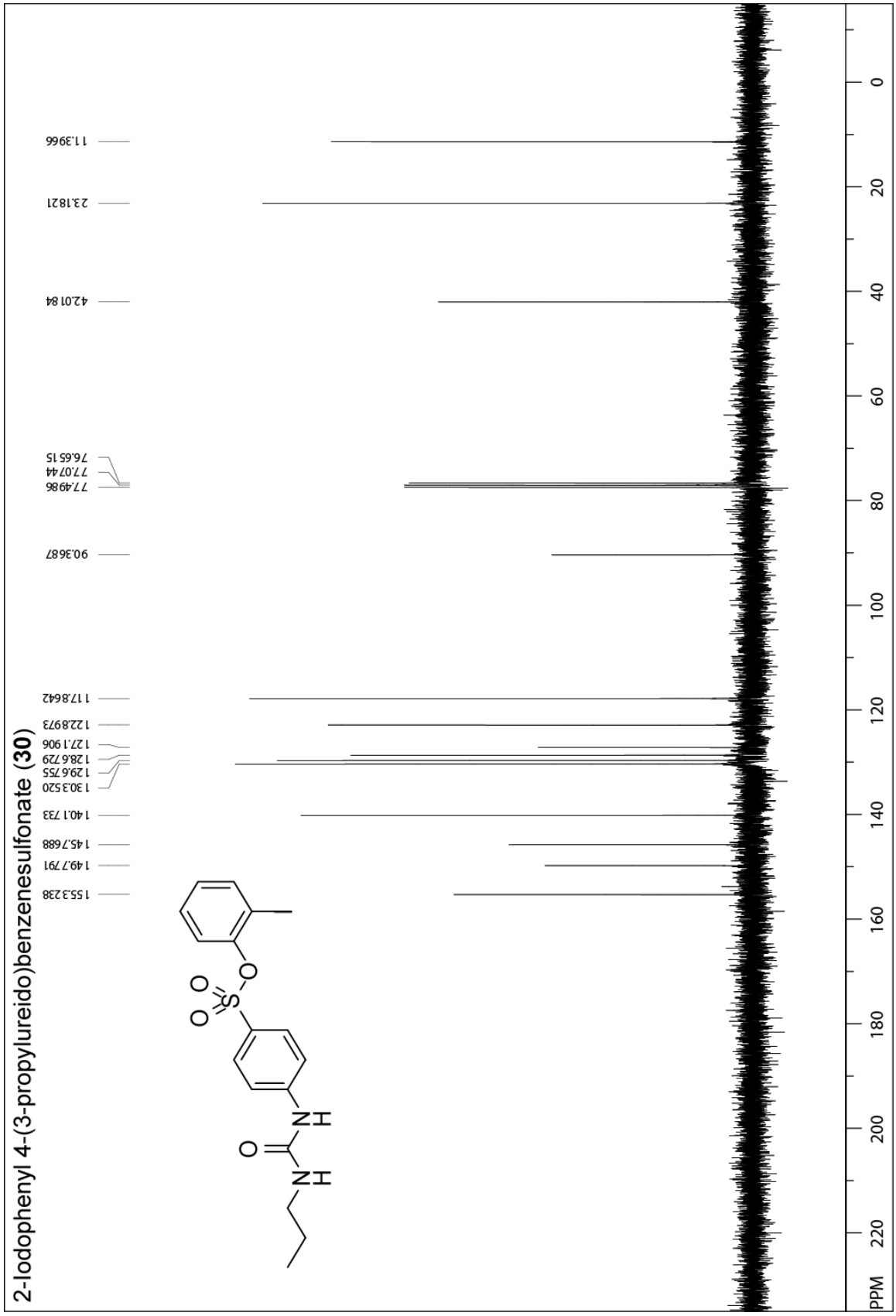
2-Iodophenyl 4-(3-propylureido)benzenesulfonate (30)
155.3238
149.7791
145.7688
140.1733
130.3520
129.6755
128.6729
127.1906
122.8973
117.8642
90.3687
77.4986
77.0744
76.6515
42.0184
23.1821
11.3966
PPM
0
20
40
60
80
100
120
140
160
180
200
220

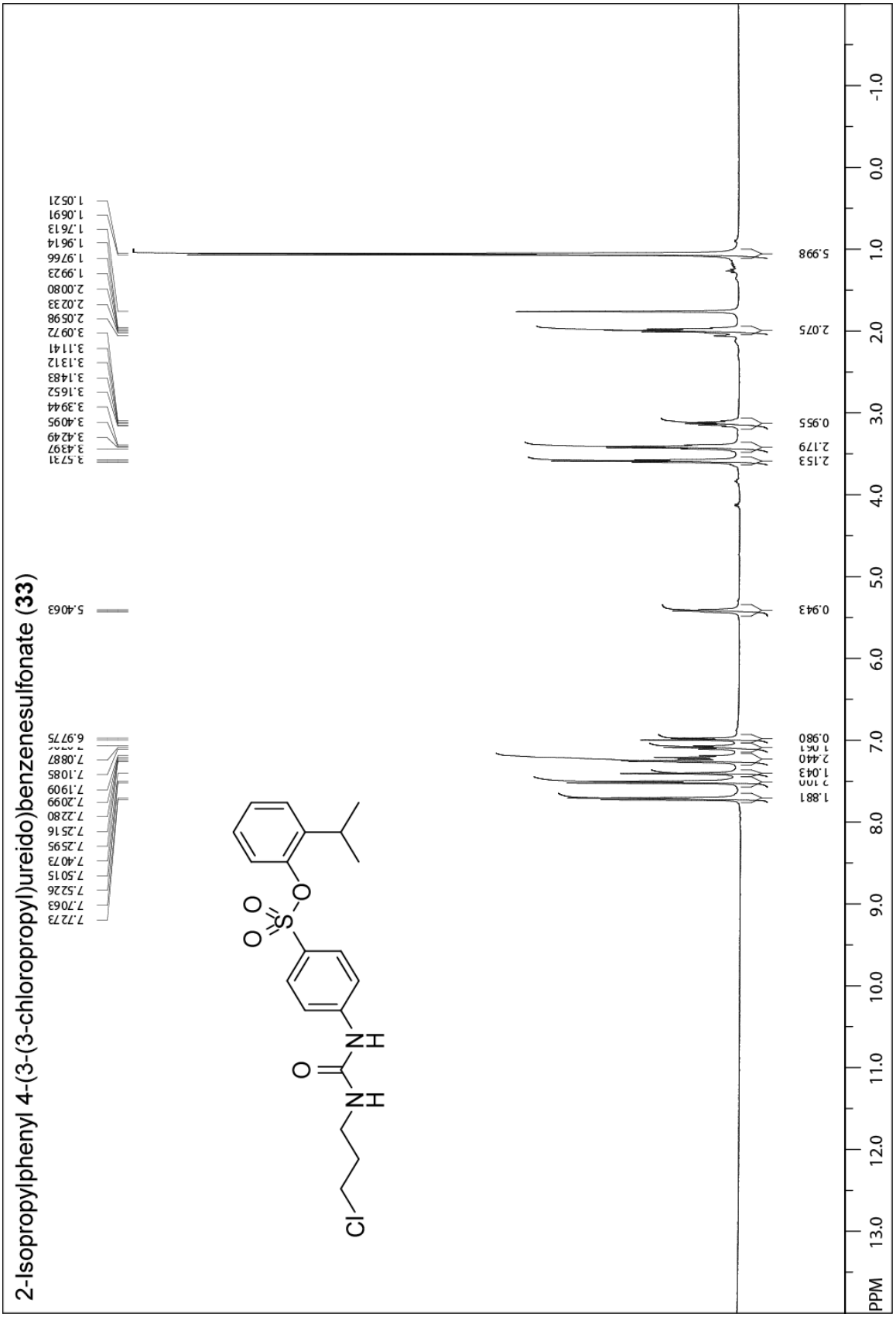
2-Isopropylphenyl 4-(3-(3-chloropropyl)ureido)benzenesulfonate (33)
PPM
13.0
12.0
11.0
10.0
9.0
8.0
7.0
6.0
5.0
4.0
3.0
2.0
1.0
0.0
-1.0
7.7273
7.7063
7.5226
7.5015
7.4073
7.2595
7.2516
7.2280
7.2099
7.1909
7.1085
7.0887
6.9775
5.4063
3.5731
3.4397
3.4249
3.4095
3.3944
3.1652
3.1483
3.1312
3.1141
3.0972
2.0598
2.0233
2.0080
1.9923
1.9766
1.9614
1.7613
1.0691
1.0521
7.881
7.100
7.043
7.440
7.051
0.980
0.943
5.998
2.075
0.955
2.179
2.153
O
O
S
O
O
N
H
O
N
H
Cl

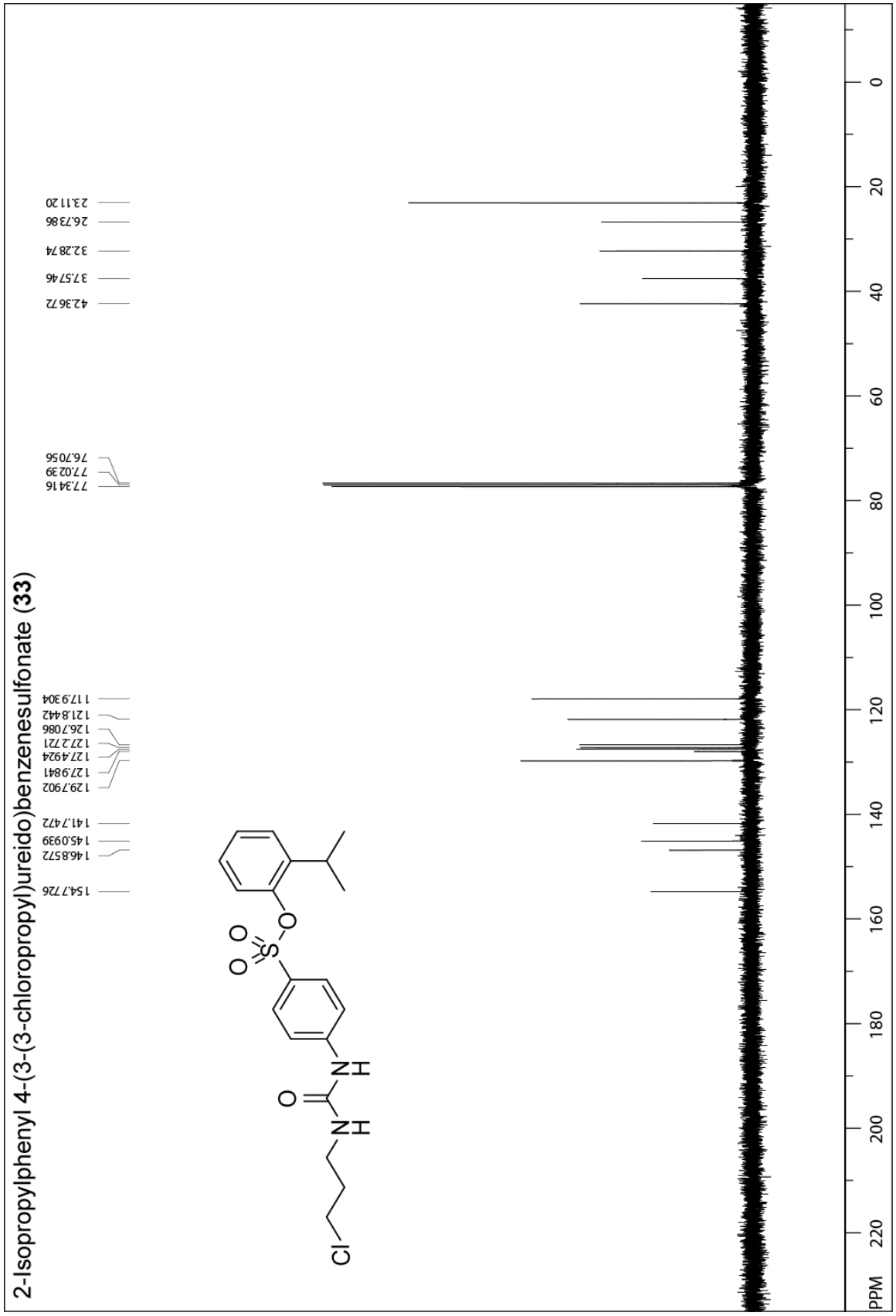
2-Isopropylphenyl 4-(3-(3-chloropropyl)ureido)benzenesulfonate (33)
154.7726
146.8572
145.0939
141.7472
129.7902
127.9841
127.4924
127.2721
126.7086
121.8442
117.9304
77.3416
77.0239
76.7056
42.3672
37.5746
32.2874
26.7386
23.1120
PPM
0
20
40
60
80
100
120
140
160
180
200
220

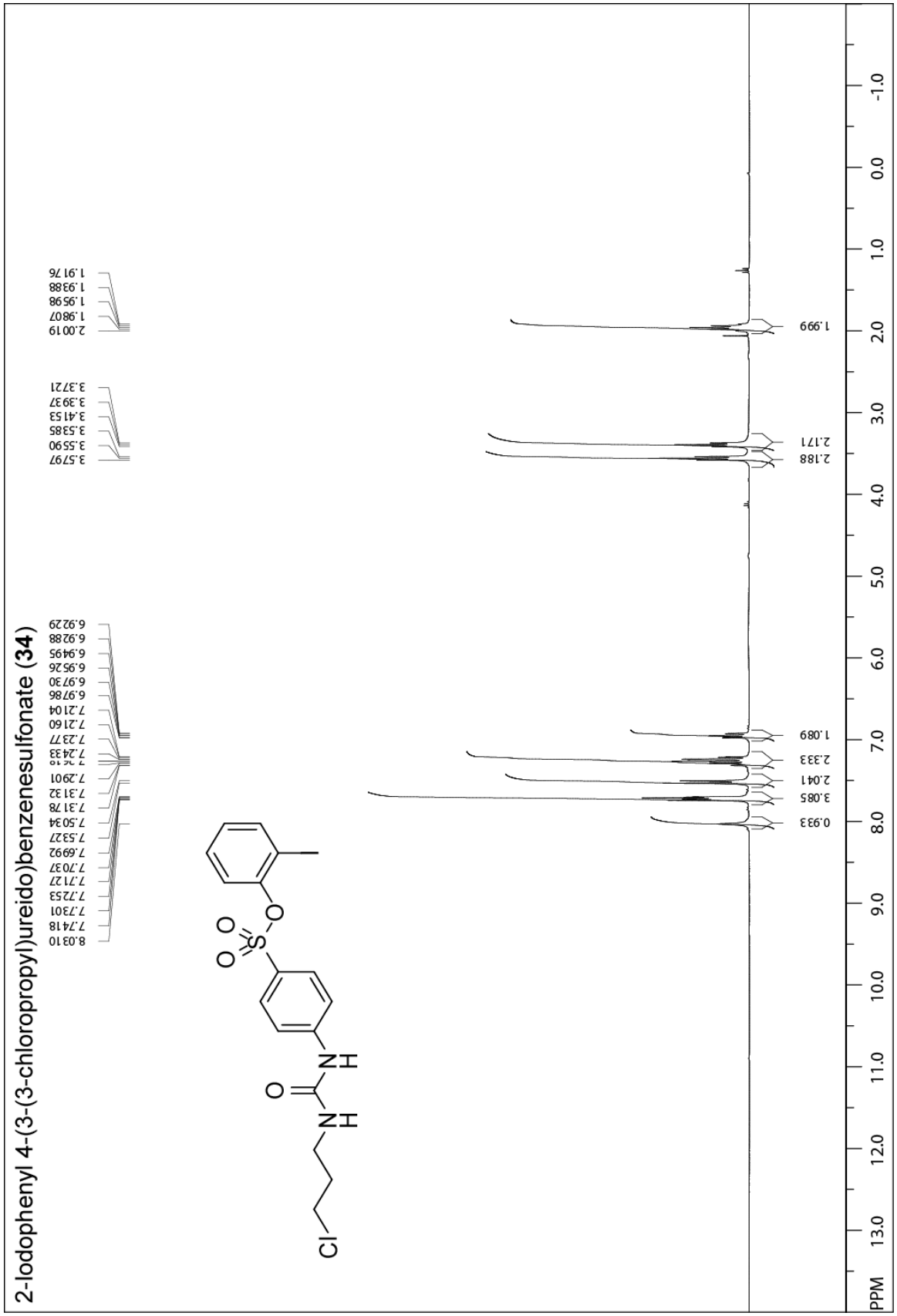
2-Iodophenyl 4-(3-(3-chloropropyl)ureido)benzenesulfonate (34)
8.0310
7.7418
7.7301
7.7253
7.7127
7.7037
7.6992
7.5327
7.5034
7.3178
7.3132
7.2901
7.2433
7.2377
7.2160
7.2104
6.9786
6.9730
6.9526
6.9495
6.9288
6.9229
3.5797
3.5590
3.5385
3.4153
3.3937
3.3721
2.0019
1.9807
1.9598
1.9388
1.9176
0.933
3.085
2.041
2.333
1.089
2.188
2.171
1.999
PPM
13.0
12.0
11.0
10.0
9.0
8.0
7.0
6.0
5.0
4.0
3.0
2.0
1.0
0.0
-1.0

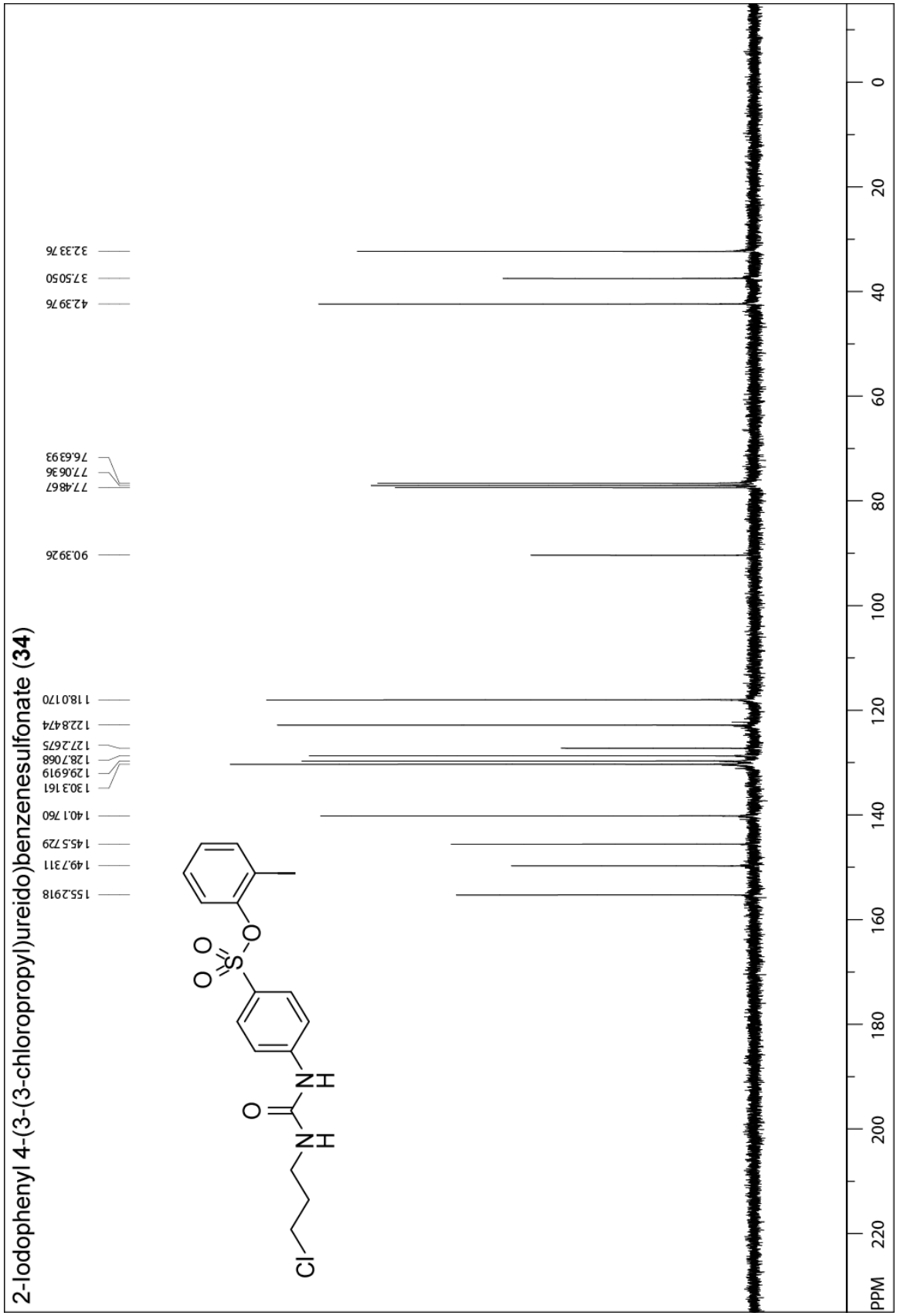
2-Iodophenyl 4-(3-(3-chloropropyl)ureido)benzenesulfonate (34)
155.2918
149.7311
145.5729
140.1760
130.3161
129.6919
128.7068
127.2675
122.8474
118.0170
90.3926
77.4867
77.0636
76.6393
42.3976
37.5050
32.3376
PPM
220
200
180
160
140
120
100
80
60
40
20
0

*The ^{1}H NMR spectrum of compound **28** was shimmed automatically on CD_3OD signal instead of $CDCl_3$ signal. Therefore, we recalibrated this ^{1}H NMR spectrum on $CDCl_3$ signal (7.26 ppm) after the acquisition experiment. For this reason, the ^{1}H NMR spectrum of compound **28** shows a chemical shift interval of -6.0 to 10.0 ppm instead of -2.0 to 14.0 ppm.

Compound 11

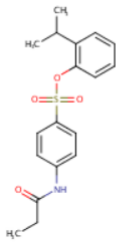

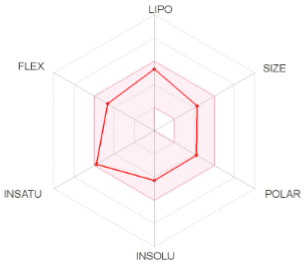

SMILES CCC(=O)Nc1ccc(cc1)S(=O)(=O)Oc1ccccc1C(C)C

Physicochemical Properties	
Formula	C18H21NO4S
Molecular weight	347.43 g/mol
Num. heavy atoms	24
Num. arom. heavy atoms	12
Fraction Csp3	0.28
Num. rotatable bonds	7
Num. H-bond acceptors	4
Num. H-bond donors	1
Molar Refractivity	94.44
TPSA	80.85 Å²
Lipophilicity	
Log $P_{o/w}$ (iLOGP)	2.80
Log $P_{o/w}$ (XLOGP3)	3.79
Log $P_{o/w}$ (WLOGP)	4.82
Log $P_{o/w}$ (MLOGP)	3.44
Log $P_{o/w}$ (SILICOS-IT)	2.95
Consensus Log $P_{o/w}$	3.56

Water Solubility	
Log *S* (ESOL)	-4.29
Solubility	1.78e-02 mg/ml ; 5.13e-05 mol/l
Class	Moderately soluble
Log *S* (Ali)	-5.18
Solubility	2.29e-03 mg/ml ; 6.58e-06 mol/l
Class	Moderately soluble
Log *S* (SILICOS-IT)	-6.16
Solubility	2.41e-04 mg/ml ; 6.95e-07 mol/l
Class	Poorly soluble
Pharmacokinetics	
GI absorption	High
BBB permeant	No
P-gp substrate	No
CYP1A2 inhibitor	Yes
CYP2C19 inhibitor	Yes
CYP2C9 inhibitor	Yes
CYP2D6 inhibitor	No
CYP3A4 inhibitor	Yes
Log K_p (skin permeation)	-5.73 cm/s
Druglikeness	
Lipinski	Yes; 0 violation
Ghose	Yes
Veber	Yes
Egan	Yes
Muegge	Yes
Bioavailability Score	0.55
Medicinal Chemistry	
PAINS	0 alert
Brenk	1 alert: sulfonic_acid_1
Leadlikeness	No; 1 violation: XLOGP3>3.5
Synthetic accessibility	2.80

Compound 12

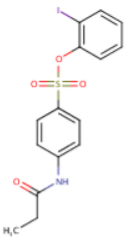

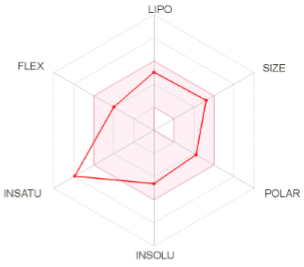

SMILES CCC(=O)Nc1ccc(cc1)S(=O)(=O)Oc1ccccc1I

Physicochemical Properties	
Formula	C15H14INO4S
Molecular weight	431.25 g/mol
Num. heavy atoms	22
Num. arom. heavy atoms	12
Fraction Csp3	0.13
Num. rotatable bonds	6
Num. H-bond acceptors	4
Num. H-bond donors	1
Molar Refractivity	92.58
TPSA	80.85 Å²
Lipophilicity	
Log $P_{o/w}$ (iLOGP)	2.59
Log $P_{o/w}$ (XLOGP3)	3.32
Log $P_{o/w}$ (WLOGP)	4.30
Log $P_{o/w}$ (MLOGP)	3.47
Log $P_{o/w}$ (SILICOS-IT)	2.79
Consensus Log $P_{o/w}$	3.29

Water Solubility	
Log *S* (ESOL)	-4.61
Solubility	1.05e-02 mg/ml ; 2.44e-05 mol/l
Class	Moderately soluble
Log *S* (Ali)	-4.69
Solubility	8.72e-03 mg/ml ; 2.02e-05 mol/l
Class	Moderately soluble
Log *S* (SILICOS-IT)	-6.22
Solubility	2.62e-04 mg/ml ; 6.08e-07 mol/l
Class	Poorly soluble
Pharmacokinetics	
GI absorption	High
BBB permeant	No
P-gp substrate	No
CYP1A2 inhibitor	Yes
CYP2C19 inhibitor	Yes
CYP2C9 inhibitor	Yes
CYP2D6 inhibitor	No
CYP3A4 inhibitor	Yes
Log K_p (skin permeation)	-6.57 cm/s
Druglikeness	
Lipinski	Yes; 0 violation
Ghose	Yes
Veber	Yes
Egan	Yes
Muegge	Yes
Bioavailability Score	0.55
Medicinal Chemistry	
PAINS	0 alert
Brenk	2 alerts: iodine, sulfonic_acid_1
Leadlikeness	No; 1 violation: MW>350
Synthetic accessibility	2.80

Compound 13

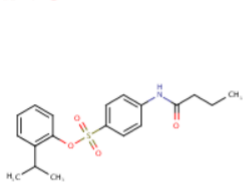

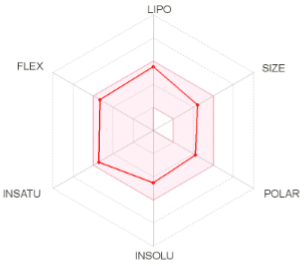

SMILES CCCC(=O)Nc1ccc(cc1)S(=O)(=O)Oc1ccccc1C(C)C

Physicochemical Properties	
Formula	C19H23NO4S
Molecular weight	361.46 g/mol
Num. heavy atoms	25
Num. arom. heavy atoms	12
Fraction Csp3	0.32
Num. rotatable bonds	8
Num. H-bond acceptors	4
Num. H-bond donors	1
Molar Refractivity	99.25
TPSA	80.85 Å²
Lipophilicity	
Log $P_{o/w}$ (iLOGP)	3.17
Log $P_{o/w}$ (XLOGP3)	4.15
Log $P_{o/w}$ (WLOGP)	5.21
Log $P_{o/w}$ (MLOGP)	3.67
Log $P_{o/w}$ (SILICOS-IT)	3.35
Consensus Log $P_{o/w}$	3.91

Water Solubility	
Log *S* (ESOL)	-4.52
Solubility	1.08e-02 mg/ml ; 3.00e-05 mol/l
Class	Moderately soluble
Log *S* (Ali)	-5.56
Solubility	1.01e-03 mg/ml ; 2.78e-06 mol/l
Class	Moderately soluble
Log *S* (SILICOS-IT)	-6.55
Solubility	1.01e-04 mg/ml ; 2.80e-07 mol/l
Class	Poorly soluble
Pharmacokinetics	
GI absorption	High
BBB permeant	No
P-gp substrate	No
CYP1A2 inhibitor	Yes
CYP2C19 inhibitor	Yes
CYP2C9 inhibitor	Yes
CYP2D6 inhibitor	No
CYP3A4 inhibitor	Yes
Log K_p (skin permeation)	-5.56 cm/s
Druglikeness	
Lipinski	Yes; 0 violation
Ghose	Yes
Veber	Yes
Egan	Yes
Muegge	Yes
Bioavailability Score	0.55
Medicinal Chemistry	
PAINS	0 alert
Brenk	1 alert: sulfonic_acid_1
Leadlikeness	No; 3 violations: MW>350, Rotors>7, XLOGP3>3.5
Synthetic accessibility	2.88

Compound 14

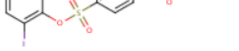

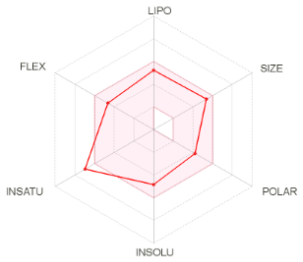

SMILES CCCC(=O)Nc1ccc(cc1)S(=O)(=O)Oc1ccccc1I

Physicochemical Properties	
Formula	C16H16INO4S
Molecular weight	445.27 g/mol
Num. heavy atoms	23
Num. arom. heavy atoms	12
Fraction Csp3	0.19
Num. rotatable bonds	7
Num. H-bond acceptors	4
Num. H-bond donors	1
Molar Refractivity	97.39
TPSA	80.85 Å²
Lipophilicity	
Log $P_{o/w}$ (iLOGP)	2.97
Log $P_{o/w}$ (XLOGP3)	3.67
Log $P_{o/w}$ (WLOGP)	4.69
Log $P_{o/w}$ (MLOGP)	3.71
Log $P_{o/w}$ (SILICOS-IT)	3.18
Consensus Log $P_{o/w}$	3.64

Water Solubility	
Log *S* (ESOL)	-4.84
Solubility	6.48e-03 mg/ml ; 1.46e-05 mol/l
Class	Moderately soluble
Log *S* (Ali)	-5.06
Solubility	3.90e-03 mg/ml ; 8.76e-06 mol/l
Class	Moderately soluble
Log *S* (SILICOS-IT)	-6.61
Solubility	1.10e-04 mg/ml ; 2.47e-07 mol/l
Class	Poorly soluble
Pharmacokinetics	
GI absorption	High
BBB permeant	No
P-gp substrate	No
CYP1A2 inhibitor	Yes
CYP2C19 inhibitor	Yes
CYP2C9 inhibitor	Yes
CYP2D6 inhibitor	No
CYP3A4 inhibitor	Yes
Log K_p (skin permeation)	-6.41 cm/s
Druglikeness	
Lipinski	Yes; 0 violation
Ghose	Yes
Veber	Yes
Egan	Yes
Muegge	Yes
Bioavailability Score	0.55
Medicinal Chemistry	
PAINS	0 alert
Brenk	2 alerts: iodine, sulfonic_acid_1
Leadlikeness	No; 2 violations: MW>350, XLOGP3>3.5
Synthetic accessibility	2.85

Compound 19

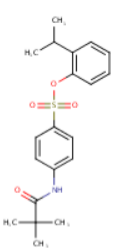

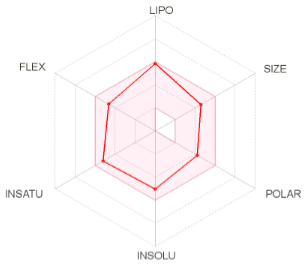

SMILES O=C(C(C)(C)C)Nc1ccc(cc1)S(=O)(=O)Oc1ccccc1C(C)C

Physicochemical Properties	
Formula	C20H25NO4S
Molecular weight	375.48 g/mol
Num. heavy atoms	26
Num. arom. heavy atoms	12
Fraction Csp3	0.35
Num. rotatable bonds	7
Num. H-bond acceptors	4
Num. H-bond donors	1
Molar Refractivity	103.80
TPSA	80.85 Å²
Lipophilicity	
Log $P_{o/w}$ (iLOGP)	3.52
Log $P_{o/w}$ (XLOGP3)	4.72
Log $P_{o/w}$ (WLOGP)	5.45
Log $P_{o/w}$ (MLOGP)	3.90
Log $P_{o/w}$ (SILICOS-IT)	3.42
Consensus Log $P_{o/w}$	4.20

Water Solubility	
Log *S* (ESOL)	-5.02
Solubility	3.58e-03 mg/ml ; 9.53e-06 mol/l
Class	Moderately soluble
Log *S* (Ali)	-6.15
Solubility	2.68e-04 mg/ml ; 7.13e-07 mol/l
Class	Poorly soluble
Log *S* (SILICOS-IT)	-6.56
Solubility	1.04e-04 mg/ml ; 2.78e-07 mol/l
Class	Poorly soluble
Pharmacokinetics	
GI absorption	High
BBB permeant	No
P-gp substrate	No
CYP1A2 inhibitor	No
CYP2C19 inhibitor	Yes
CYP2C9 inhibitor	Yes
CYP2D6 inhibitor	No
CYP3A4 inhibitor	Yes
Log K_p (skin permeation)	-5.24 cm/s
Druglikeness	
Lipinski	Yes; 0 violation
Ghose	Yes
Veber	Yes
Egan	Yes
Muegge	Yes
Bioavailability Score	0.55
Medicinal Chemistry	
PAINS	0 alert
Brenk	1 alert: sulfonic_acid_1
Leadlikeness	No; 2 violations: MW>350, XLOGP3>3.5
Synthetic accessibility	3.02

Compound 23

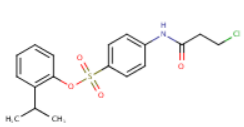

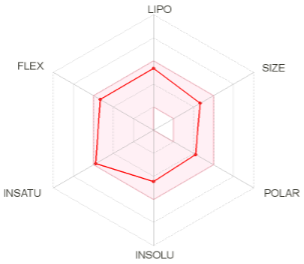

SMILES ClCCC(=O)Nc1ccc(cc1)S(=O)(=O)Oc1ccccc1C(C)C

Physicochemical Properties	
Formula	C18H20ClNO4S
Molecular weight	381.87 g/mol
Num. heavy atoms	25
Num. arom. heavy atoms	12
Fraction Csp3	0.28
Num. rotatable bonds	8
Num. H-bond acceptors	4
Num. H-bond donors	1
Molar Refractivity	99.24
TPSA	80.85 Å²
Lipophilicity	
Log $P_{o/w}$ (iLOGP)	2.96
Log $P_{o/w}$ (XLOGP3)	3.85
Log $P_{o/w}$ (WLOGP)	5.04
Log $P_{o/w}$ (MLOGP)	3.67
Log $P_{o/w}$ (SILICOS-IT)	3.47
Consensus Log $P_{o/w}$	3.80

Water Solubility	
Log *S* (ESOL)	-4.46
Solubility	1.32e-02 mg/ml ; 3.46e-05 mol/l
Class	Moderately soluble
Log *S* (Ali)	-5.24
Solubility	2.18e-03 mg/ml ; 5.70e-06 mol/l
Class	Moderately soluble
Log *S* (SILICOS-IT)	-6.77
Solubility	6.55e-05 mg/ml ; 1.71e-07 mol/l
Class	Poorly soluble
Pharmacokinetics	
GI absorption	High
BBB permeant	No
P-gp substrate	No
CYP1A2 inhibitor	Yes
CYP2C19 inhibitor	Yes
CYP2C9 inhibitor	Yes
CYP2D6 inhibitor	No
CYP3A4 inhibitor	Yes
Log K_p (skin permeation)	-5.90 cm/s
Druglikeness	
Lipinski	Yes; 0 violation
Ghose	Yes
Veber	Yes
Egan	Yes
Muegge	Yes
Bioavailability Score	0.55
Medicinal Chemistry	
PAINS	0 alert
Brenk	2 alerts: alkyl_halide, sulfonic_acid_1
Leadlikeness	No; 3 violations: MW>350, Rotors>7, XLOGP3>3.5
Synthetic accessibility	2.87

Compound 24

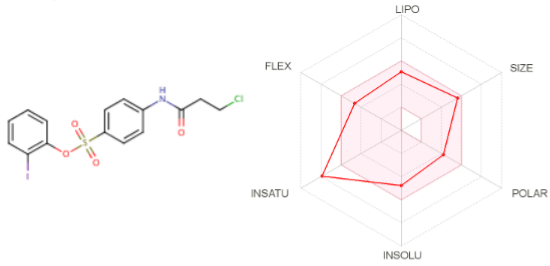

SMILES ClCCC(=O)Nc1ccc(cc1)S(=O)(=O)Oc1ccccc1I

Physicochemical Properties	
Formula	C15H13ClINO4S
Molecular weight	465.69 g/mol
Num. heavy atoms	23
Num. arom. heavy atoms	12
Fraction Csp3	0.13
Num. rotatable bonds	7
Num. H-bond acceptors	4
Num. H-bond donors	1
Molar Refractivity	97.37
TPSA	80.85 Å²
Lipophilicity	
Log $P_{o/w}$ (iLOGP)	2.73
Log $P_{o/w}$ (XLOGP3)	3.37
Log $P_{o/w}$ (WLOGP)	4.52
Log $P_{o/w}$ (MLOGP)	3.71
Log $P_{o/w}$ (SILICOS-IT)	3.32
Consensus Log $P_{o/w}$	3.53

Water Solubility	
Log *S* (ESOL)	-4.77
Solubility	7.83e-03 mg/ml ; 1.68e-05 mol/l
Class	Moderately soluble
Log *S* (Ali)	-4.75
Solubility	8.36e-03 mg/ml ; 1.79e-05 mol/l
Class	Moderately soluble
Log *S* (SILICOS-IT)	-6.82
Solubility	7.13e-05 mg/ml ; 1.53e-07 mol/l
Class	Poorly soluble
Pharmacokinetics	
GI absorption	High
BBB permeant	No
P-gp substrate	No
CYP1A2 inhibitor	Yes
CYP2C19 inhibitor	Yes
CYP2C9 inhibitor	Yes
CYP2D6 inhibitor	No
CYP3A4 inhibitor	Yes
Log K_p (skin permeation)	-6.75 cm/s
Druglikeness	
Lipinski	Yes; 0 violation
Ghose	Yes
Veber	Yes
Egan	Yes
Muegge	Yes
Bioavailability Score	0.55
Medicinal Chemistry	
PAINS	0 alert
Brenk	3 alerts: alkyl_halide, iodine, sulfonic_acid_1
Leadlikeness	No; 1 violation: MW>350
Synthetic accessibility	2.85

Compound 27

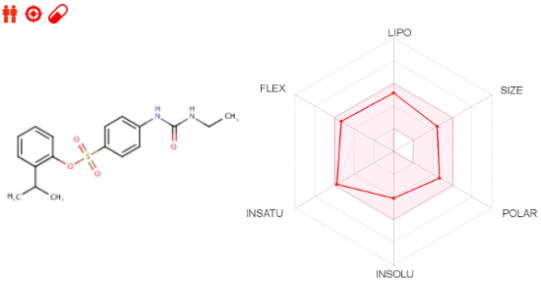

SMILES CCNC(=O)Nc1ccc(cc1)S(=O)(=O)Oc1ccccc1C(C)C

Physicochemical Properties	
Formula	C18H22N2O4S
Molecular weight	362.44 g/mol
Num. heavy atoms	25
Num. arom. heavy atoms	12
Fraction Csp3	0.28
Num. rotatable bonds	8
Num. H-bond acceptors	4
Num. H-bond donors	2
Molar Refractivity	97.63
TPSA	92.88 Å²
Lipophilicity	
Log $P_{o/w}$ (iLOGP)	2.58
Log $P_{o/w}$ (XLOGP3)	3.52
Log $P_{o/w}$ (WLOGP)	4.61
Log $P_{o/w}$ (MLOGP)	3.44
Log $P_{o/w}$ (SILICOS-IT)	2.18
Consensus Log $P_{o/w}$	3.27

Water Solubility	
Log *S* (ESOL)	-4.13
Solubility	2.67e-02 mg/ml ; 7.38e-05 mol/l
Class	Moderately soluble
Log *S* (Ali)	-5.15
Solubility	2.54e-03 mg/ml ; 7.01e-06 mol/l
Class	Moderately soluble
Log *S* (SILICOS-IT)	-6.20
Solubility	2.29e-04 mg/ml ; 6.32e-07 mol/l
Class	Poorly soluble
Pharmacokinetics	
GI absorption	High
BBB permeant	No
P-gp substrate	No
CYP1A2 inhibitor	Yes
CYP2C19 inhibitor	Yes
CYP2C9 inhibitor	Yes
CYP2D6 inhibitor	No
CYP3A4 inhibitor	No
Log K_p (skin permeation)	-6.01 cm/s
Druglikeness	
Lipinski	Yes; 0 violation
Ghose	Yes
Veber	Yes
Egan	Yes
Muegge	Yes
Bioavailability Score	0.55
Medicinal Chemistry	
PAINS	0 alert
Brenk	1 alert: sulfonic_acid_1
Leadlikeness	No; 3 violations: MW>350, Rotors>7, XLOGP3>3.5
Synthetic accessibility	3.05

Compound 28

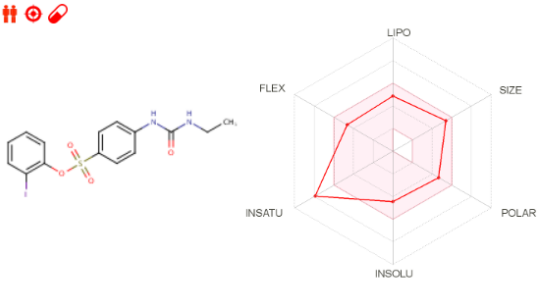

SMILES CCNC(=O)Nc1ccc(cc1)S(=O)(=O)Oc1ccccc1I

Physicochemical Properties	
Formula	C15H15IN2O4S
Molecular weight	446.26 g/mol
Num. heavy atoms	23
Num. arom. heavy atoms	12
Fraction Csp3	0.13
Num. rotatable bonds	7
Num. H-bond acceptors	4
Num. H-bond donors	2
Molar Refractivity	95.77
TPSA	92.88 Å²
Lipophilicity	
Log $P_{o/w}$ (iLOGP)	2.47
Log $P_{o/w}$ (XLOGP3)	3.04
Log $P_{o/w}$ (WLOGP)	4.09
Log $P_{o/w}$ (MLOGP)	3.47
Log $P_{o/w}$ (SILICOS-IT)	2.03
Consensus Log $P_{o/w}$	3.02

Water Solubility	
Log *S* (ESOL)	-4.45
Solubility	1.60e-02 mg/ml ; 3.58e-05 mol/l
Class	Moderately soluble
Log *S* (Ali)	-4.66
Solubility	9.85e-03 mg/ml ; 2.21e-05 mol/l
Class	Moderately soluble
Log *S* (SILICOS-IT)	-6.25
Solubility	2.49e-04 mg/ml ; 5.58e-07 mol/l
Class	Poorly soluble
Pharmacokinetics	
GI absorption	High
BBB permeant	No
P-gp substrate	No
CYP1A2 inhibitor	Yes
CYP2C19 inhibitor	Yes
CYP2C9 inhibitor	Yes
CYP2D6 inhibitor	No
CYP3A4 inhibitor	Yes
Log K_p (skin permeation)	-6.86 cm/s
Druglikeness	
Lipinski	Yes; 0 violation
Ghose	Yes
Veber	Yes
Egan	Yes
Muegge	Yes
Bioavailability Score	0.55
Medicinal Chemistry	
PAINS	0 alert
Brenk	2 alerts: iodine, sulfonic_acid_1
Leadlikeness	No; 1 violation: MW>350
Synthetic accessibility	3.05

Compound 30

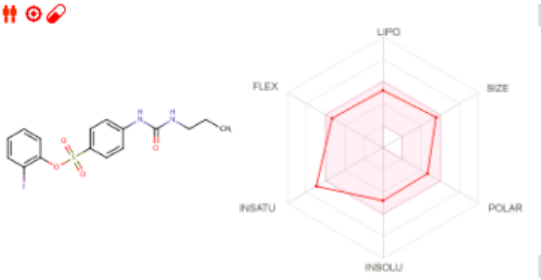

SMILES CCCNC(=O)Nc1ccc(cc1)S(=O)(=O)Oc1ccccc1I

Physicochemical Properties	
Formula	C16H17IN2O4S
Molecular weight	460.29 g/mol
Num. heavy atoms	24
Num. arom. heavy atoms	12
Fraction Csp3	0.19
Num. rotatable bonds	8
Num. H-bond acceptors	4
Num. H-bond donors	2
Molar Refractivity	100.58
TPSA	92.88 Å²
Lipophilicity	
Log $P_{o/w}$ (iLOGP)	2.72
Log $P_{o/w}$ (XLOGP3)	3.57
Log $P_{o/w}$ (WLOGP)	4.48
Log $P_{o/w}$ (MLOGP)	3.71
Log $P_{o/w}$ (SILICOS-IT)	2.42
Consensus Log $P_{o/w}$	3.38

Water Solubility	
Log *S* (ESOL)	-4.78
Solubility	7.55e-03 mg/ml ; 1.64e-05 mol/l
Class	Moderately soluble
Log *S* (Ali)	-5.21
Solubility	2.86e-03 mg/ml ; 6.22e-06 mol/l
Class	Moderately soluble
Log *S* (SILICOS-IT)	-6.64
Solubility	1.04e-04 mg/ml ; 2.27e-07 mol/l
Class	Poorly soluble
Pharmacokinetics	
GI absorption	High
BBB permeant	No
P-gp substrate	No
CYP1A2 inhibitor	Yes
CYP2C19 inhibitor	Yes
CYP2C9 inhibitor	Yes
CYP2D6 inhibitor	No
CYP3A4 inhibitor	Yes
Log K_p (skin permeation)	-6.57 cm/s
Druglikeness	
Lipinski	Yes; 0 violation
Ghose	Yes
Veber	Yes
Egan	Yes
Muegge	Yes
Bioavailability Score	0.55
Medicinal Chemistry	
PAINS	0 alert
Brenk	2 alerts: iodine, sulfonic_acid_1
Leadlikeness	No; 3 violations: MW>350, Rotors>7, XLOGP3>3.5
Synthetic accessibility	3.11

Compound 33

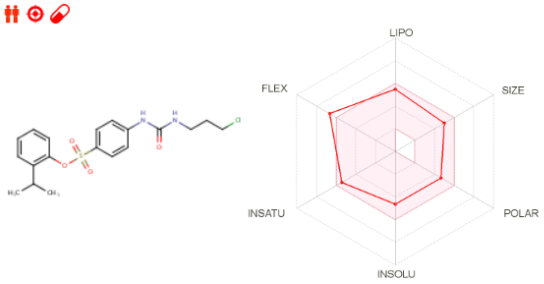

SMILES ClCCCNC(=O)Nc1ccc(cc1)S(=O)(=O)Oc1ccccc1C(C)C

Physicochemical Properties	
Formula	C19H23ClN2O4S
Molecular weight	410.91 g/mol
Num. heavy atoms	27
Num. arom. heavy atoms	12
Fraction Csp3	0.32
Num. rotatable bonds	10
Num. H-bond acceptors	4
Num. H-bond donors	2
Molar Refractivity	107.24
TPSA	92.88 Å²
Lipophilicity	
Log $P_{o/w}$ (iLOGP)	2.86
Log $P_{o/w}$ (XLOGP3)	4.10
Log $P_{o/w}$ (WLOGP)	5.22
Log $P_{o/w}$ (MLOGP)	3.90
Log $P_{o/w}$ (SILICOS-IT)	3.11
Consensus Log $P_{o/w}$	3.84

Water Solubility	
Log *S* (ESOL)	-4.64
Solubility	9.42e-03 mg/ml ; 2.29e-05 mol/l
Class	Moderately soluble
Log *S* (Ali)	-5.76
Solubility	7.20e-04 mg/ml ; 1.75e-06 mol/l
Class	Moderately soluble
Log *S* (SILICOS-IT)	-7.20
Solubility	2.60e-05 mg/ml ; 6.34e-08 mol/l
Class	Poorly soluble
Pharmacokinetics	
GI absorption	High
BBB permeant	No
P-gp substrate	No
CYP1A2 inhibitor	No
CYP2C19 inhibitor	Yes
CYP2C9 inhibitor	Yes
CYP2D6 inhibitor	No
CYP3A4 inhibitor	Yes
Log K_p (skin permeation)	-5.90 cm/s
Druglikeness	
Lipinski	Yes; 0 violation
Ghose	Yes
Veber	Yes
Egan	Yes
Muegge	Yes
Bioavailability Score	0.55
Medicinal Chemistry	
PAINS	0 alert
Brenk	2 alerts: alkyl_halide, sulfonic_acid_1
Leadlikeness	No; 3 violations: MW>350, Rotors>7, XLOGP3>3.5
Synthetic accessibility	3.24

Compound 34

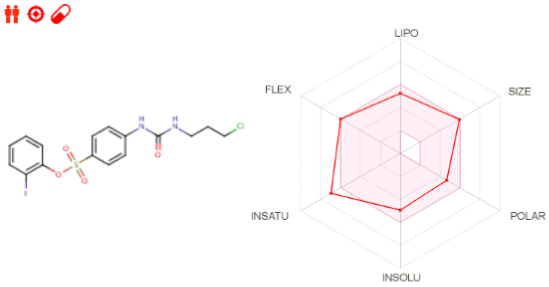

SMILES ClCCCNC(=O)Nc1ccc(cc1)S(=O)(=O)Oc1ccccc1I

Physicochemical Properties	
Formula	C16H16ClIN2O4S
Molecular weight	494.73 g/mol
Num. heavy atoms	25
Num. arom. heavy atoms	12
Fraction Csp3	0.19
Num. rotatable bonds	9
Num. H-bond acceptors	4
Num. H-bond donors	2
Molar Refractivity	105.37
TPSA	92.88 Å²
Lipophilicity	
Log $P_{o/w}$ (iLOGP)	2.78
Log $P_{o/w}$ (XLOGP3)	3.62
Log $P_{o/w}$ (WLOGP)	4.70
Log $P_{o/w}$ (MLOGP)	3.94
Log $P_{o/w}$ (SILICOS-IT)	2.94
Consensus Log $P_{o/w}$	3.60

Water Solubility	
Log *S* (ESOL)	-4.95
Solubility	5.56e-03 mg/ml ; 1.12e-05 mol/l
Class	Moderately soluble
Log *S* (Ali)	-5.26
Solubility	2.73e-03 mg/ml ; 5.52e-06 mol/l
Class	Moderately soluble
Log *S* (SILICOS-IT)	-7.24
Solubility	2.85e-05 mg/ml ; 5.75e-08 mol/l
Class	Poorly soluble
Pharmacokinetics	
GI absorption	High
BBB permeant	No
P-gp substrate	No
CYP1A2 inhibitor	Yes
CYP2C19 inhibitor	Yes
CYP2C9 inhibitor	Yes
CYP2D6 inhibitor	No
CYP3A4 inhibitor	Yes
Log K_p (skin permeation)	-6.75 cm/s
Druglikeness	
Lipinski	Yes; 0 violation
Ghose	No; 1 violation: MW>480
Veber	Yes
Egan	Yes
Muegge	Yes
Bioavailability Score	0.55
Medicinal Chemistry	
PAINS	0 alert
Brenk	3 alerts: alkyl_halide, iodine, sulfonic_acid_1
Leadlikeness	No; 3 violations: MW>350, Rotors>7, XLOGP3>3.5
Synthetic accessibility	3.20

SFOM-0046

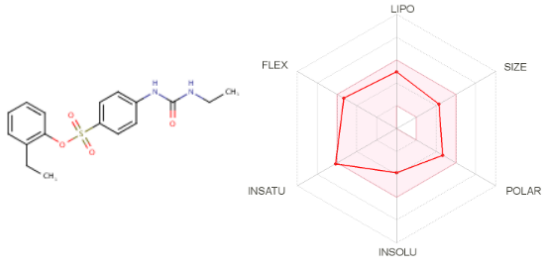

SMILES CCNC(=O)Nc1ccc(cc1)S(=O)(=O)Oc1ccccc1CC

Physicochemical Properties	
Formula	C17H20N2O4S
Molecular weight	348.42 g/mol
Num. heavy atoms	24
Num. arom. heavy atoms	12
Fraction Csp3	0.24
Num. rotatable bonds	8
Num. H-bond acceptors	4
Num. H-bond donors	2
Molar Refractivity	92.83
TPSA	92.88 Å²
Lipophilicity	
Log $P_{o/w}$ (iLOGP)	2.55
Log $P_{o/w}$ (XLOGP3)	3.19
Log $P_{o/w}$ (WLOGP)	4.05
Log $P_{o/w}$ (MLOGP)	3.20
Log $P_{o/w}$ (SILICOS-IT)	1.96
Consensus Log $P_{o/w}$	2.99

Water Solubility	
Log *S* (ESOL)	-3.85
Solubility	4.90e-02 mg/ml ; 1.41e-04 mol/l
Class	Soluble
Log *S* (Ali)	-4.81
Solubility	5.37e-03 mg/ml ; 1.54e-05 mol/l
Class	Moderately soluble
Log *S* (SILICOS-IT)	-6.18
Solubility	2.31e-04 mg/ml ; 6.64e-07 mol/l
Class	Poorly soluble
Pharmacokinetics	
GI absorption	High
BBB permeant	No
P-gp substrate	No
CYP1A2 inhibitor	Yes
CYP2C19 inhibitor	Yes
CYP2C9 inhibitor	Yes
CYP2D6 inhibitor	No
CYP3A4 inhibitor	No
Log K_p (skin permeation)	-6.16 cm/s
Druglikeness	
Lipinski	Yes; 0 violation
Ghose	Yes
Veber	Yes
Egan	Yes
Muegge	Yes
Bioavailability Score	0.55
Medicinal Chemistry	
PAINS	0 alert
Brenk	1 alert: sulfonic_acid_1
Leadlikeness	No; 1 violation: Rotors>7
Synthetic accessibility	2.94

SFOM-0106

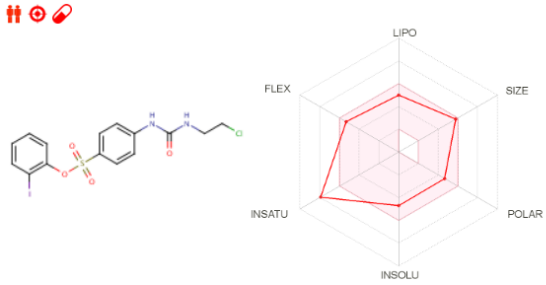

SMILES ClCCNC(=O)Nc1ccc(cc1)S(=O)(=O)Oc1ccccc1I

Physicochemical Properties	
Formula	C15H14ClIN2O4S
Molecular weight	480.71 g/mol
Num. heavy atoms	24
Num. arom. heavy atoms	12
Fraction Csp3	0.13
Num. rotatable bonds	8
Num. H-bond acceptors	4
Num. H-bond donors	2
Molar Refractivity	100.57
TPSA	92.88 Å²
Lipophilicity	
Log $P_{o/w}$ (iLOGP)	2.47
Log $P_{o/w}$ (XLOGP3)	3.27
Log $P_{o/w}$ (WLOGP)	4.31
Log $P_{o/w}$ (MLOGP)	3.71
Log $P_{o/w}$ (SILICOS-IT)	2.55
Consensus Log $P_{o/w}$	3.26

Water Solubility	
Log *S* (ESOL)	-4.72
Solubility	9.11e-03 mg/ml ; 1.89e-05 mol/l
Class	Moderately soluble
Log *S* (Ali)	-4.89
Solubility	6.12e-03 mg/ml ; 1.27e-05 mol/l
Class	Moderately soluble
Log *S* (SILICOS-IT)	-6.85
Solubility	6.77e-05 mg/ml ; 1.41e-07 mol/l
Class	Poorly soluble
Pharmacokinetics	
GI absorption	High
BBB permeant	No
P-gp substrate	No
CYP1A2 inhibitor	Yes
CYP2C19 inhibitor	Yes
CYP2C9 inhibitor	Yes
CYP2D6 inhibitor	No
CYP3A4 inhibitor	Yes
Log K_p (skin permeation)	-6.91 cm/s
Druglikeness	
Lipinski	Yes; 0 violation
Ghose	No; 1 violation: MW>480
Veber	Yes
Egan	Yes
Muegge	Yes
Bioavailability Score	0.55
Medicinal Chemistry	
PAINS	0 alert
Brenk	3 alerts: alkyl_halide, iodine, sulfonic_acid_1
Leadlikeness	No; 2 violations: MW>350, Rotors>7
Synthetic accessibility	3.12

SFOM-0107

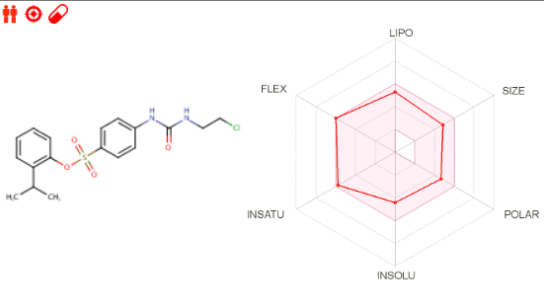

SMILES ClCCNC(=O)Nc1ccc(cc1)S(=O)(=O)Oc1ccccc1C(C)C

Physicochemical Properties	
Formula	C18H21ClN2O4S
Molecular weight	396.89 g/mol
Num. heavy atoms	26
Num. arom. heavy atoms	12
Fraction Csp3	0.28
Num. rotatable bonds	9
Num. H-bond acceptors	4
Num. H-bond donors	2
Molar Refractivity	102.43
TPSA	92.88 Å²
Lipophilicity	
Log $P_{o/w}$ (iLOGP)	2.64
Log $P_{o/w}$ (XLOGP3)	3.74
Log $P_{o/w}$ (WLOGP)	4.83
Log $P_{o/w}$ (MLOGP)	3.67
Log $P_{o/w}$ (SILICOS-IT)	2.71
Consensus Log $P_{o/w}$	3.52

Water Solubility	
Log *S* (ESOL)	-4.40
Solubility	1.56e-02 mg/ml ; 3.94e-05 mol/l
Class	Moderately soluble
Log *S* (Ali)	-5.38
Solubility	1.64e-03 mg/ml ; 4.14e-06 mol/l
Class	Moderately soluble
Log *S* (SILICOS-IT)	-6.80
Solubility	6.22e-05 mg/ml ; 1.57e-07 mol/l
Class	Poorly soluble
Pharmacokinetics	
GI absorption	High
BBB permeant	No
P-gp substrate	No
CYP1A2 inhibitor	Yes
CYP2C19 inhibitor	Yes
CYP2C9 inhibitor	Yes
CYP2D6 inhibitor	No
CYP3A4 inhibitor	Yes
Log K_p (skin permeation)	-6.07 cm/s
Druglikeness	
Lipinski	Yes; 0 violation
Ghose	Yes
Veber	Yes
Egan	Yes
Muegge	Yes
Bioavailability Score	0.55
Medicinal Chemistry	
PAINS	0 alert
Brenk	2 alerts: alkyl_halide, sulfonic_acid_1
Leadlikeness	No; 3 violations: MW>350, Rotors>7, XLOGP3>3.5
Synthetic accessibility	3.14

Topotecan

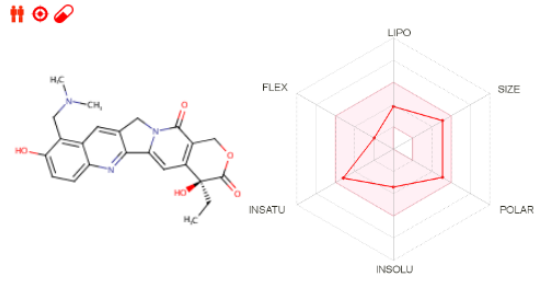

SMILES CC[C@@]1(O)C(=O)OCc2c1cc1c3nc4ccc(c(c4cc3Cn1c2=O)CN(C)C)O

Physicochemical Properties	
Formula	C23H23N3O5
Molecular weight	421.45 g/mol
Num. heavy atoms	31
Num. arom. heavy atoms	16
Fraction Csp3	0.35
Num. rotatable bonds	3
Num. H-bond acceptors	7
Num. H-bond donors	2
Molar Refractivity	114.81
TPSA	104.89 Å²
Lipophilicity	
Log $P_{o/w}$ (iLOGP)	2.79
Log $P_{o/w}$ (XLOGP3)	1.22
Log $P_{o/w}$ (WLOGP)	1.43
Log $P_{o/w}$ (MLOGP)	0.98
Log $P_{o/w}$ (SILICOS-IT)	2.88
Consensus Log $P_{o/w}$	1.86

Water Solubility	
Log *S* (ESOL)	-3.41
Solubility	1.66e-01 mg/ml ; 3.93e-04 mol/l
Class	Soluble
Log *S* (Ali)	-3.02
Solubility	4.03e-01 mg/ml ; 9.55e-04 mol/l
Class	Soluble
Log *S* (SILICOS-IT)	-5.71
Solubility	8.26e-04 mg/ml ; 1.96e-06 mol/l
Class	Moderately soluble
Pharmacokinetics	
GI absorption	High
BBB permeant	No
P-gp substrate	Yes
CYP1A2 inhibitor	No
CYP2C19 inhibitor	No
CYP2C9 inhibitor	Yes
CYP2D6 inhibitor	No
CYP3A4 inhibitor	Yes
Log K_p (skin permeation)	-8.00 cm/s
Druglikeness	
Lipinski	Yes; 0 violation
Ghose	Yes
Veber	Yes
Egan	Yes
Muegge	Yes
Bioavailability Score	0.55
Medicinal Chemistry	
PAINS	1 alert: mannich_A
Brenk	0 alert
Leadlikeness	No; 1 violation: MW>350
Synthetic accessibility	4.23